ΣΧΟΛΗ ΠΟΛΙΤΙΚΩΝ ΜΗΧΑΝΙΚΩΝ

ΤΟΜΕΑΣ ΥΔΑΤΙΚΩΝ ΠΟΡΩΝ ΚΑΙ

ΠΕΡΙΒΑΛΛΟΝΤΟΣ

ΔΙΕΡΕΥΝΗΣΗ ΤΗΣ ΑΝΑΕΡΟΒΙΑΣ ΒΙΟΛΟΓΙΚΗΣ ΕΠΕΞΕΡΓΑΣΙΑΣ ΛΥΜΑΤΩΝ ΜΕ ΧΡΗΣΗ ΜΕΜΒΡΑΝΩΝ

ΔΙΔΑΚΤΟΡΙΚΗ ΔΙΑΤΡΙΒΗ

ΠΛΕΥΡΗ ΑΡΓΥΡΩ

Χημικός Μηχανικός, ΜΔΕ ΕΜΠ

Συμβουλευτική επιτροπή:

1. Δανιήλ Μαμάης, Καθηγητής, ΕΜΠ (Επιβλέπων)

2. Κωνσταντίνος Νουτσόπουλος, Καθηγητής, ΕΜΠ

3. Συμεών Μαλαμής, Αναπληρωτής Καθηγητής, ΕΜΠ

Εξεταστική επιτροπή:

1. Δανιήλ Μαμάης, Καθηγητής, ΕΜΠ (Επιβλέπων)
2. Κωνσταντίνος Νουτσόπουλος, Καθηγητής, ΕΜΠ
3. Συμεών Μαλαμής, Αναπληρωτής Καθηγητής, ΕΜΠ
4. Γεράσιμος Λυμπεράτος, Καθηγητής ΕΜΠ
5. Μελίδης Κωνσταντίνος, Καθηγητής Δ.Π.Θ.
6. Αθανάσιος Στασινάκης, Καθηγητής Πανεπιστημίου Αιγαίου
7. Μιχαήλ Φουντουλάκης, Επίκουρος Καθηγητής Πανεπιστημίου Αιγαίου

Αθήνα, Νοέμβριος 2023

FACULTY OF CIVIL ENGINEERING

DEPARTMENT OF WATER RESOURCES

AND ENVIRONMENTAL ENGINEERING

STUDY OF ANAEROBIC BIOLOGICAL WASTEWATER TREATMENT USING MEMBRANE TECHNOLOGY

DOCTORAL THESIS

PLEVRI ARGYRO

Chemical Engineer, MSc NTUA

Advisory Committee:

1. Daniel Mamais, Professor, NTUA (Supervisor)

2. Konstantinos Noutsopoulos, Professor, NTUA

3. Simeon Malamis, Associate Professor, NTUA

Examination Committee:
1. Daniel Mamais, Professor, NTUA (Supervisor)
2. Constantinos Noutsopoulos, Professor, NTUA
3. Simeon Malamis, Associate Professor, NTUA
4. Gerasimos Lyberatos, Professor. NTUA
5. Paraschos Melidis, Professor, DUTh
6. Athanasios Stasinakis, Professor, University of the Aegean
7. Michael Fountoulakis, Assistant Professor, University of the Aegean

Athens, November 2023

Εἶστε ὑπὲρ ἢ κατά;
Ἔστω ἀπαντεῖστε μ᾽ ἕνα ναὶ ἢ μ᾽ ἕνα ὄχι.
Τὸ ἔχετε τὸ πρόβλημα σκεφτεῖ
Πιστεύω ἀσφαλῶς πὼς σᾶς βασάνισε
Τὰ πάντα βασανίζουν στὴ ζωὴ
Παιδιὰ γυναῖκες ἔντομα
Βλαβερὰ φυτὰ χαμένες ὧρες
Δύσκολα πάθη χαλασμένα δόντια
Μέτρια φίλμς. Κι αὐτὸ σᾶς βασάνισε
ἀσφαλῶς.
Μιλᾶτε ὑπεύθυνα λοιπόν. Ἔστω μὲ ναὶ ἢ ὄχι.
Σὲ σᾶς ἀνήκει ἡ ἀπόφαση.
Δὲ σᾶς ζητοῦμε πιὰ νὰ πάψετε
Τὶς ἀσχολίες σας νὰ διακόψετε τὴ ζωή σας
Τὶς προσφιλεῖς ἐφημερίδες σας· τὶς
συζητήσεις
Στὸ κουρεῖο· τὶς Κυριακές σας στὰ γήπεδα.
Μιὰ λέξη μόνο. Ἐμπρὸς λοιπόν:
Εἶστε ὑπὲρ ἢ κατά;
Σκεφθεῖτε το καλά. Θὰ περιμένω.

Μανόλης Αναγνωστάκης

ΕΥΧΑΡΙΣΤΙΕΣ

Μια διδακτορική διατριβή αποτελεί από μόνη της ένα δύσκολο έργο. Είναι στιγμές που αναρωτιέμαι αν θα το ξαναέκανα. Πέρα από το κομμάτι των γνώσεων, αναλογιζόμενη τους ανθρώπους που συνάντησα, συνειδητοποιώ πόσο πιο πλούσια είναι η ζωή μου τώρα που τους έχω. Επομένως, η απάντησή μου είναι ένα δυναμικό "ναι". Αρκεί να είμαι με τους ίδιους ανθρώπους! Γιατί εκεί και τα πιο δύσκολα πάντα θα φαίνονται παιχνίδι.

ABSTRACT

Amidst the accelerating global urgency for sustainable environmental practices, wastewater treatment techniques, like the Anaerobic Membrane Bioreactor (AnMBR), are rising to the forefront of technological innovations. AnMBR stands out not just for its unmatched energy efficacy in treating wastewater but also for its secondary, yet equally vital, role in generating biogas—a sustainable energy alternative. But like all groundbreaking innovations, the AnMBR too faces its share of challenges. The system's reliance on anaerobic bacteria, which is notorious for its slow growth rate, combined with performance variability due to fluctuating organic loads, poses real-world operational challenges.

A detailed 3.5-year research initiative aimed to dissect these challenges. To investigate the performance of anaerobic wastewater treatment through the incorporation of membrane technology, a 40 L laboratory scale AnMBR with a flat sheet submerged membrane along with a 40 L reservoir for trapping and measuring the biogas produced have been installed and set in operation. Specifically, through long term bench scale experiments, the impact that different temperatures and also different operating conditions have on the efficiency of AnMBR was evaluated. The efficiency of the AnMBR was investigated, in the temperature range 14-26ºC, opeating at four different hydraulic retention times (HRTs) that were 2 d, 1 d, 12 h and 6 h. Each HRT is divided into two different temperature ranges corresponding to winter and summer conditions. With a decrease in HRT, there was a decline in effluent quality and an increase in membrane fouling. During the summer, at an average temperature of 24°C, the AnMBR produced permeate water with an average Chemical Oxygen Demand (COD) of 51 ± 5 mg·L-1 at an HRT of 2 days. The effluent COD increased to 67 ± 6 mg·L^{-1} for an HRT of 1 day and 91 ± 4 mg·L-1 for an HRT of 12 hours, under the same temperature conditions. At an HRT of 6 hours, the COD removal efficiency was further reduced, with values of 177 ± 18 for winter and 121 ± 8 for summer. In general, the findings were multifaceted: while the treatment offered by shorter HRTs is attractive in terms of cost reduction, it occasionally triggered spikes in COD levels, more so during the colder months. Conversely, the balmy Mediterranean summers favored the AnMBR operation, with 12-hour HRTs been sufficient to achieve both short treatment time and efficiency. Yet, the winter season brought its set of challenges, with efficiency metrics sometimes toeing the line of regulatory compliance. To bridge these operational and seasonal inconsistencies, the study investigated performance-enhancing by $FeCl_3$ addition. When administered at a Fe^{+3} dose, within the 25 mg/L to 30 mg/L

concentrations range, this chemical additive showcased a slight enhancement in COD removal efficiencies. Its integration also heralded a substantial reduction in effluent Total Phosphorus (TP) concentrations, effectively sidelining the membrane fouling—an issue that could drastically curtail AnMBR's operational life and efficiency.

Specifically, the addition of 25 mg $FeCl_3$ L^{-1} improved the performance of the AnMBR. Average effluent COD concentrations without $FeCl_3$ addition were 177±21 mg/L, while after the addition of 25 mg $FeCl_3$ L^{-1} and 30 mg $FeCl_3$ L^{-1} COD decreased to 147±8 mg/L and 149±11 mg/L, respectively. Moreover, effluent TP decreased by 75% with the dosage of 25 mg $FeCl_3$ L^{-1} and was almost completely removed with 30 mg $FeCl_3L^{-1}$. The membrane performance was slightly improved by $FeCl_3$ dosing while biogas production was not affected by iron addition.

To further evaluate the energy efficiency of AnMBR, an energy balance was conducted based on the results obtained from the operation of the lab-scale AnMBR throughout this investigation. According to the findings, an energy balance was found favorable for all the scenarios tested. The total electrical energy that can be extracted from AnMBR for the winter and the summer periods was found to be in the range of 0.3 – 0.8 KWh/KgCODrem and 0.4 – 0.9 KWh/KgCODrem, respectively.

Within the context of this research a mathematical model was applied to simulate AnMBR operation. The Anaerobic Digestion Model ADM1, integrated within the versatile Matlab/Simulink platform and a comprehensive Global Sensitivity Analysis (GSA) were undertaken. This analytical approach demystified the complex operational dynamics intrinsic to AnMBR systems. The model was calibrated with real-world experimental data for 2-day winter HRTs, especially in parameters like Qgas. Following model calibration, computational predictions, when evaluated across the five distinct operational scenarios, largely mirrored experimental findings. However, certain runs, such as the 1-day HRT during both seasons, presented notable variations.

Based on the findings of this PhD thesis, a clear narrative emerges: The AnMBR system, while holding immense potential as a dual-purpose solution for wastewater treatment and sustainable energy generation, operates within a complex web of variables. Whether it's the seasonal temperature variations, the fine-tuning of HRTs, or the strategic deployment of additives like $FeCl_3$, achieving optimal performance requires a harmonious alignment of all these factors. This

study, by juxtaposing empirical findings with computational modeling, charts a roadmap for both researchers and practitioners, offering a holistic blueprint for harnessing the full potential of AnMBR systems in varied real-world settings.

ΕΚΤΕΤΑΜΕΝΗ ΠΕΡΙΛΗΨΗ

Εισαγωγή

Στο πλαίσιο της επιταχυνόμενης παγκόσμιας ανάγκης για βιώσιμες περιβαλλοντικές πρακτικές, τεχνικές επεξεργασίας λυμάτων όπως οι Αναερόβιοι Βιοαντιδραστήρες Μεμβρανών (AnMBR) αναδύονται στο προσκήνιο των τεχνολογικών καινοτομιών. Ο AnMBR ξεχωρίζει όχι μόνο για τις χαμηλές ενεργειακές απαιτήσεις στην επεξεργασία των λυμάτων, αλλά και για την παραγωγή βιοαερίου - μιας εναλλακτικής μορφής παραγωγής ενέργειας. Παρόλα αυτά, ο AnMBR αντιμετωπίζει τις δικές του προκλήσεις. Η εξάρτηση του συστήματος από τα αναερόβια βακτήρια, τα οποία είναι γνωστά για το χαμηλό ρυθμό ανάπτυξής τους, σε συνδυασμό με την ποικιλομορφία της απόδοσης λόγω των μεταβλητών οργανικών φορτίων, θέτει πραγματικά προβλήματα λειτουργίας στον πραγματικό κόσμο.

Η αναερόβια επεξεργασία λυμάτων εφαρμόζεται παραδοσιακά σε λύματα υψηλού ορφανικού φορτίου. Τα τελευταία χρόνια, εφαρμόζεται και σε λύματα χαμηλής οργανικής φόρτισης. Η έρευνά της παρούσας διδακτορικής διατριβής επικεντρώθηκε στην αναερόβια βιολογική επεξεργασία λυμάτων με την τεχνολογία μεμβρανών.

Ο γενικός στόχος αυτής της διδακτορικής διατριβής είναι η έρευνα της βιώσιμης λειτουργίας ενός AnMBR στην επεξεργασία των υγρών αποβλήτων, σε συνθήκες περιβάλλοντος. Η προσέγγιση της συγκεκριμένης έρευνας είναι η εφαρμογή του AnMBR στην επεξεργασία πραγματικών αστικών υγρών απόβλητων και την ανάπτυξη πρωτοκόλλων λειτουργίας. Τα δεδομένα που θα προκύψουν από αυτή τη μελέτη προορίζονται να καθοδηγήσουν τους δήμους τόσο στην ενσωμάτωση αυτής της τεχνολογίας, όσο και στην αποτελεσματική λειτουργία και τις πιθανές βελτιώσεις των AnMBR, επικεντρώνοντας στην υψηλή βιωσιμότητα με βάση την ποιότητα του παραγόμενου νερού και τη μείωση της έμφραξης της μεμβράνης.

Στόχοι διδακτορικής διατριβής

Πιο συγκεκριμένα, οι στόχοι της διδακτορικής διατριβής συνοψίζονται στα παρακάτω σημεία:

1. Ανάλυση της Απόδοσης του AnMBR και δημιουργία πρωτοκόλλων για διαφορετικές συνθήκες λειτουργίας: Αξιολόγηση της επίδρασης του Υδραυλικού Χρόνου Παραμονής (HRT), υψηλών οργανικών φορτίων και διακυμάνσεων της θερμοκρασίας στην

αποτελεσματικότητα του AnMBR στην επεξεργασία των αστικών υγρών αποβλήτων. Κύριοι δείκτες απόδοσης γι' αυτόν τον στόχο περιλαμβάνουν:

- o Ποιότητα του νερού εκροής σύμφωνα με τα ελληνικά και ευρωπαϊκά πρότυπα.
- o Παραγωγή βιοαερίου, η ποσόστωση μεθανίου μαζί με την δυνατότητα παραγωγής ενέργειας.
- o Έμφραξη μεμβράνης.

2. Προσθήκη $FeCl_3$ για ενίσχυση της απόδοσης του AnMBR: Αξιολόγηση των επιπτώσεων της προσθήκης $FeCl_3$ στην ενίσχυση των λειτουργικών παραμέτρων του AnMBR, με επίκεντρο τη μείωση της έμφραξης της μεμβράνης σε συνδυασμό με την απομάκρυνση φωσφόρου. Οι παράμετροι απόδοσης περιλαμβάνουν:

- o Δυναμική παραγωγής βιοαερίου και δυνατότητα παραγωγής ενέργειας από το μεθάνιο.
- o Αποτελεσματικότητα απομάκρυνσης οργανικού φορτίου.
- o Αποτελεσματικότητα απομάκρυνσης επιλεγμένων οργανικών μικρορύπων, ιδίως από τις ομάδες μη στεροειδών αντιφλεγμονωδών φάρμακων (NSAID) και ορμονικών διαταρακτών (EDC).

3. Τροποποίηση και Επαλήθευση του Μοντέλου ADM1 για το AnMBR: Προσαρμογή, εφαρμογή και βαθμονόμηση του Μοντέλου Αναερόβιας Χώνευσης 1 (ADM1) για την προσομοίωση της επεξεργασίας αστικών υγρών αποβλήτων μέσω του AnMBR. Ο στόχος των παραπάνω είναι:

- o Η απεικόνιση της συμπεριφοράς του συστήματος AnMBR, στην ποιότητα εξόδου καθώς και την παραγωγή ενέργειας με βάση το μεθάνιο που παράγεται σε διάφορα σενάρια.
- o Η βελτιστοποίηση των λειτουργικών παραμέτρων.
- o Η παροχή ενός πλαισίου για μια ευρύτερη εφαρμογή και κατανόηση του AnMBR σε εγκαταστάσεις επεξεργασίας υγρών αποβλήτων.

Δομή διδακτορικής διατριβής

Η συγκεκριμένη διδακτορική διατριβή περιλαμβάνει έξι κεφάλαια, τα οποία παρουσιάζονται περιληπτικά παρακάτω:

Κεφάλαιο 1: Εισαγωγή Αυτό το κεφάλαιο παρέχει μια επισκόπηση της έρευνας, αναλύοντας το πλαίσιο και τη σημασία της. Επίσης, περιγράφει τη δομή ολόκληρης της διδακτορικής διατριβής.

Κεφάλαιο 2: Θεωρητικό Υπόβαθρο Αυτό το κεφάλαιο εξετάζει τις θεωρητικές βάσεις που υποστηρίζουν την έρευνα. Επικεντρώνεται στη διαδικασία αναερόβιας επεξεργασίας και τους παράγοντες που την επηρεάζουν. Εξετάζονται τα πλεονεκτήματα της αναερόβιας έναντι της αερόβιας επεξεργασίας. Λεπτομερείς πληροφορίες παρέχονται για διάφορα είδη αναερόβιας επεξεργασίας, καταλήγοντας σε μια εκτενή συζήτηση για το AnMBR, τις εφαρμογές του, τις προκλήσεις και τις πιθανές μελλοντικές κατευθύνσεις.

Κεφάλαιο 3: Μεθοδολογία - Πειραματικό Πρωτόκολλο Σε αυτό το κεφάλαιο παρουσιάζεται η μεθοδολογία της έρευνας, αναλύοντας τα πειραματικά πρωτόκολλα και τις αναλυτικές μεθόδους που χρησιμοποιήθηκαν. Προσφέρει μια λεπτομερή ματιά στον αντιδραστήρα AnMBR εργαστηριακής κλίμακας περιγράφοντας τα λειτουργικά πρωτόκολλα για το εργαστηριακό AnMBR και τις τεχνικές παρακολούθησης για την αξιολόγηση της απόδοσής του.

Κεφάλαιο 4: Αποτελέσματα πειραμάτων. Αυτό το κεφάλαιο παρουσιάζει και αναλύει τα ευρήματα των πειραμάτων. Εξετάζει την απόδοση του AnMBR, σε διαφορετικούς Υδραυλικούς Χρόνους Παραμονής (HRT), διαφορετικές θερμοκρασίες και ερευνά τη βελτίωση ή όχι της απόδοσής του μετά την προσθήκη σιδήρου. Πιο συγκεκριμένα, η απόδοση του συστήματος AnMBR ερευνήθηκε για 3,5 χρόνια, μέσα στα θερμοκρασιακά εύρη 16-26°C. Η προσαρμοστικότητα του συστήματος δοκιμάστηκε σε διαφορετικά HRT - από 2 ημέρες έως 6 ώρες-, ενώ λαμβάνονταν υπόψη οι διαφορές λειτουργίας μεταξύ καλοκαιριού και χειμώνα. Ένα καίριο στοιχείο αυτής της έρευνας ήταν η εισαγωγή σιδήρου (σε συγκεντρώσεις 25 και 30 mg FeCl$_3$ L^{-1}), που έπαιξε σημαντικό ρόλο στον προσανατολισμό των αποτελεσμάτων του συστήματος όσον αφορά την ποιότητα του νερού εξόδου την παραγωγή βιοαερίου και τη μείωση της έμφραξης της μεμβράνης.

Κεφάλαιο 5: Αποτελέσματα εφαρμογής μοντέλου ADM1 Αυτό το κεφάλαιο παρουσιάζει ένα τροποποιημένο μοντέλο ADM1 προσαρμοσμένο στο εργαστηριακής κλίμακας σύστημα AnMBR. Το κεφάλαιο υπογραμμίζει την τροποποίηση, βαθμονόμηση και επικύρωση αυτού του μοντέλου για να αντιπροσωπεύσει καλύτερα τις συνθήκες και τη δυναμική των AnMBR σε περιβαλλοντικές θερμοκρασίες. Το προσαρμοσμένο μοντέλο στη Matlab/Simulink υποβλήθηκε σε μια εκτενή Ανάλυση Ευαισθησίας (GSA) με τοπικές αλλά και καθολικές μεθόδους. Συγκεκριμένα, χρησιμοποιήθηκαν τρεις διακριτικές τεχνικές: One At a Time (OAT), Morris και Fourier Amplitude Sensitivity Test (FAST). Αυτή η ανάλυση ευαισθησίας που βασίστηκε σε πειραματικά δεδομένα, οδήγησε σε βαθμονόμηση και επαλήθευση του μοντέλου εξασφαλίζοντας έτσι μεγαλύτερη ακρίβεια και ταύτιση στα πειραματικά αποτελέσματα.

<u>Κεφάλαιο 6: Συμπεράσματα</u>. Το Κεφάλαιο Συμπερασμάτων περιλαμβάνει τα βασικά ευρήματα. Στοχεύει στην παροχή σαφούς εικόνας των πλεονεκτημάτων και των προκλήσεων της τεχνολογίας AnMBR στις Εγκαταστάσεις Επεξεργασίας Λυμάτων, ιδιαίτερα στις Μεσογειακές χώρες που έχουν κατά βάση ψυχροφιλικές θερμοκρασίες.

Περιγραφή αντιδραστήρα εργαστηριακής κλίμακας AnMBR

Για να μελετηθεί η αποτελεσματικότητα της αναερόβιας επεξεργασίας λυμάτων μέσω AnMBR, σχεδιάστηκε και εγκαταστάθηκε ένας αντιδραστήρας εργαστηριακής κλίμακας 40 L εξοπλισμένος με εμβαπτισμένη μεμβράνη επίπεδων φύλλων συνολικής επιφάνειας διήθησης $0.5m^2$. Ακόμη, το σύστημα αποτελούνταν από ένα αεριοφυλάκιο 40 L για τη δέσμευση και τον ποσοτικό προσδιορισμό του βιοαερίου που παράγεται από την αναερόβια επεξεργασία. Το σύστημα εγκαταστάθηκε στο Τμήμα Έρευνας και Ανάπτυξης της Εταιρείας Ύδρευσης και Αποχέτευσης Πρωτευούσης (Ε.ΥΔ.Α.Π), όπως φαίνεται στην Εικόνα 1.
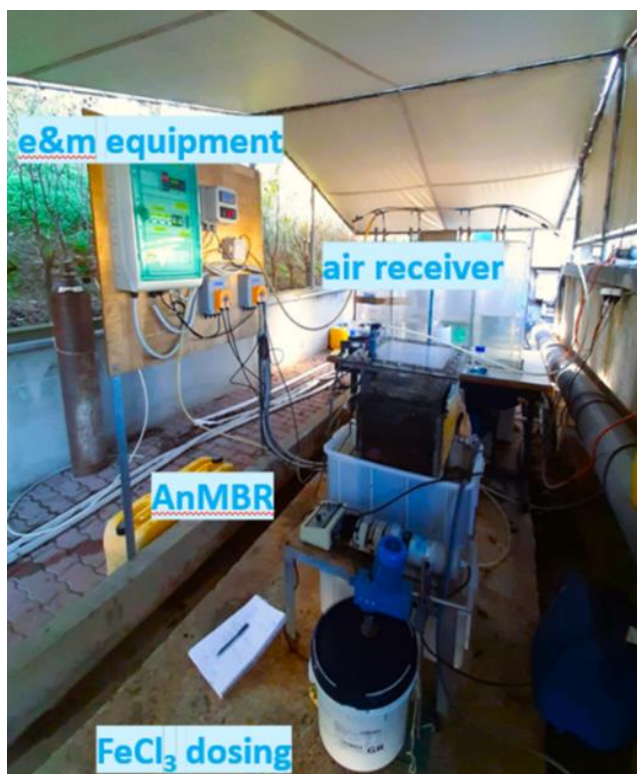
Εικόνα 1: Φωτογραφική αναπαράσταση του συστήματος AnMBR εργαστηριακής κλίμακας

Οι θερμοκρασίες λειτουργίας κυμαίνονταν μεταξύ 15°C και 26°C. Προκειμένου να ευθυγραμμιστεί η θερμοκρασία του αντιδραστήρα με τις τυπικές συνθήκες που αντιμετωπίζουν οι

ελληνικές εγκαταστάσεις επεξεργασίας λυμάτων, χρησιμοποιήθηκε ένα εξωτερικό λουτρό θέρμανσης. Επιπλέον, για να εξασφαλιστεί η σχολαστική παρακολούθηση και έλεγχος των αναερόβιων διεργασιών, στο σύστημα ενσωματώθηκαν αισθητήρες θερμοκρασίας, REDOX και διαμεμβρανικής πίεσης (TMP). Η εκκίνηση λειτουργίας του συστήματος πραγματοποιήθηκε με χρήση βιομάζας από αναερόβιο χωνευτή πλήρους κλίμακας, ο οποίος λειτουργούσε υπό ψυχρόφιλες συνθήκες. Η βιομάζα εκκίνησης είχε pH 7,2 και οι συγκεντρώσεις TSS και VSS καταγράφηκαν στα 18 g/L και 14,3 g/L, αντίστοιχα.

Χρησιμοποιήθηκαν δύο περισταλτικές αντλίες: η μία για την άντληση των εισερχομένων λυμάτων στον αντιδραστήρα, ενώ η άλλη για την εκροή του διηθήματος. Η παραγωγή βιοαερίου πραγματοποιούνταν στην κεφαλή του αντιδραστήρα και στη συνέχεια οδηγούνταν στο αεριοφυλάκιο. Το αποθηκευμένο βιοαέριο επανακυκλοφορούνταν με αντλία βιοαερίου ξανά εντός του αντιδραστήρα για τον καθαρισμό της μεμβράνης και την αποφυγή έμφραξης.

Ένας κύκλος λειτουργίας AnMBR αποτελούνταν από 8 λεπτά διήθησης ακολουθούμενη από ένα διάστημα χαλάρωσης 2 λεπτών. Αυτός ο ρυθμός ήταν απαραίτητος για τη διατήρηση της διαπερατότητας της μεμβράνης. Ο χημικός καθαρισμός των μεμβρανών χρησιμοποιεί υποχλωριώδες νάτριο ως κύριο καθαριστικό μέσο. Μια ολοκληρωμένη σχηματική αναπαράσταση ολόκληρου του συστήματος απεικονίζεται στο Σχήμα 1.
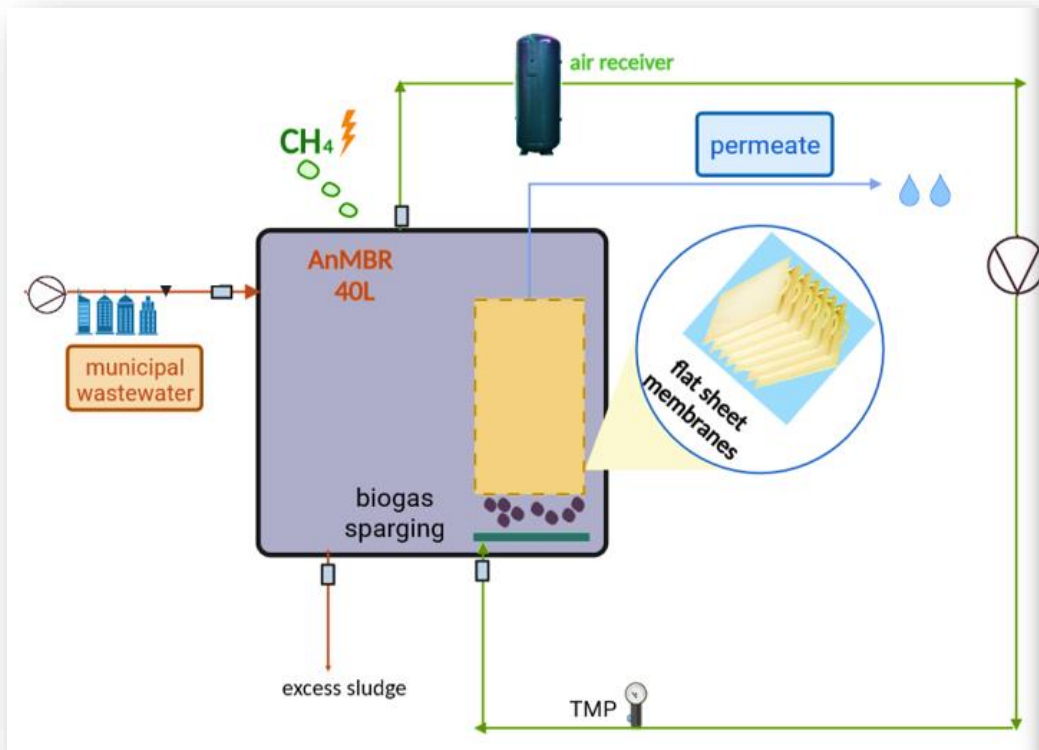
Σχήμα 1 : Διάγραμμα ροής του AnMBR

Συνοπτική παρουσίαση πειραματικών αποτελεσμάτων

Παρακάτω παρουσιάζονται περιληπτικά τα αποτελέσματα του AnMBR για όλες τις συνθήκες λειτουργίας που μελετήθηκαν. Το SRT διατηρήθηκε σταθερά στις 50 ημέρες για όλη την περίοδο λειτουργίας.

Τέσσερα διακριτά HRT μελετήθηκαν- 48 ώρες, 24 ώρες, 12 ώρες και 6 ώρες -. Κάθε HRT αξιολογήθηκε για ένα χρονικό διάστημα έξι μηνών, όπου χωρίστηκε περαιτέρω σε δύο ξεχωριστές φάσεις τριών μηνών για να εξεταστούν οι εποχιακές διακυμάνσεις που αντιστοιχούν σε καλοκαιρινές και χειμερινές συνθήκες. Ο λόγος για την επιλογή του παρόντος διαστήματος των τριών μηνών είναι η τιμή SRT που είχε οριστεί να είναι οι 50 ημέρες. Το σκεπτικό για αυτήν την τρίμηνη υποδιαίρεση είναι για το γεγονός ότι δύο κύκλοι SRT ολοκληρώνονται σε αυτό το διάστημα, ενισχύοντας έτσι την αξιοπιστία των αποτελεσμάτων.

Τα Διαγράμματα 1,2,3,4 παρουσιάζουν συγκεντρωτικά αποτελέσματα και για τα 4 HRT που μελετήθηκαν και για όλα τα θερμοκρασιακά εύρη ανά HRT. Τα γραφήματα αυτά αποτυπώνουν στοιχεία όπως η απομάκρυνση οργανικού φορτίου, οι συγκεντρώσεις των VFAs , η παραγωγή βιοαερίου , κλπ.
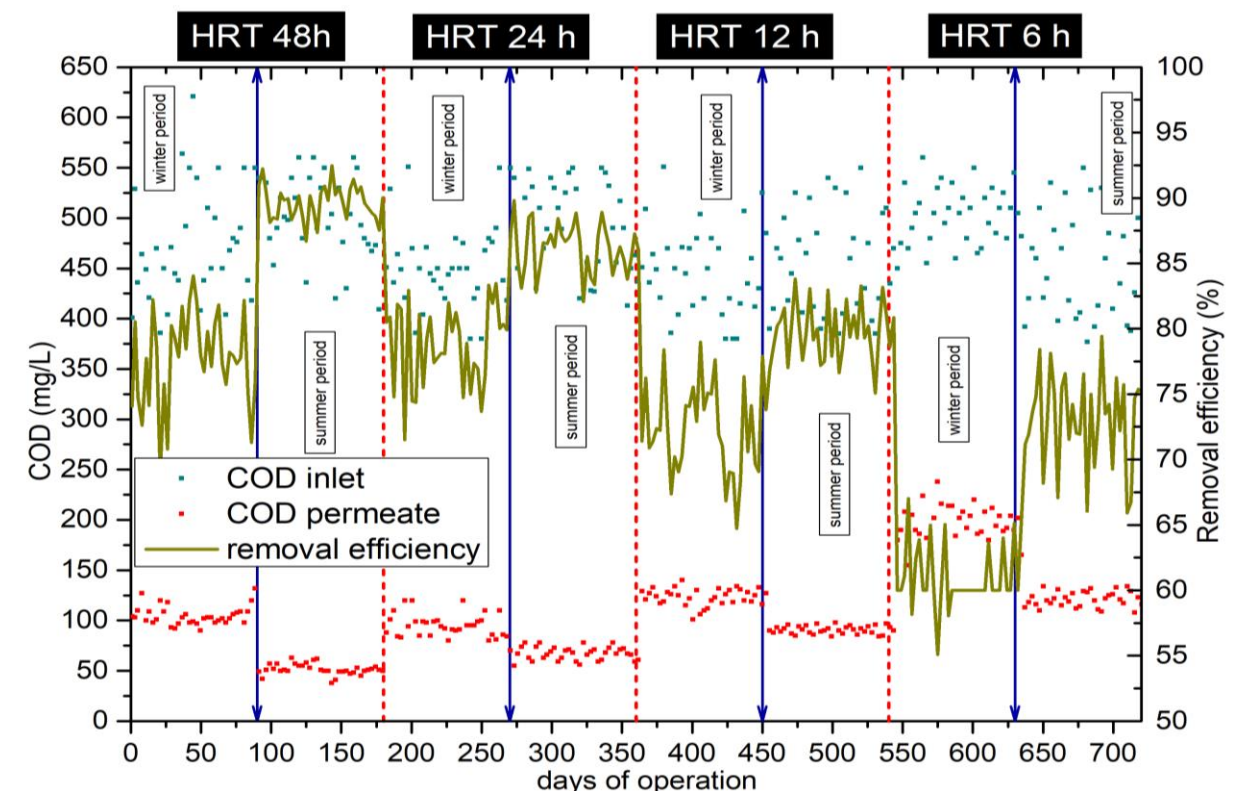
Διάγραμμα 1 Απόδοση AnMBR όσον αφορά την απομάκρυνση οργανικού φορτίου για όλα τα HRT που εξετάστηκαν.
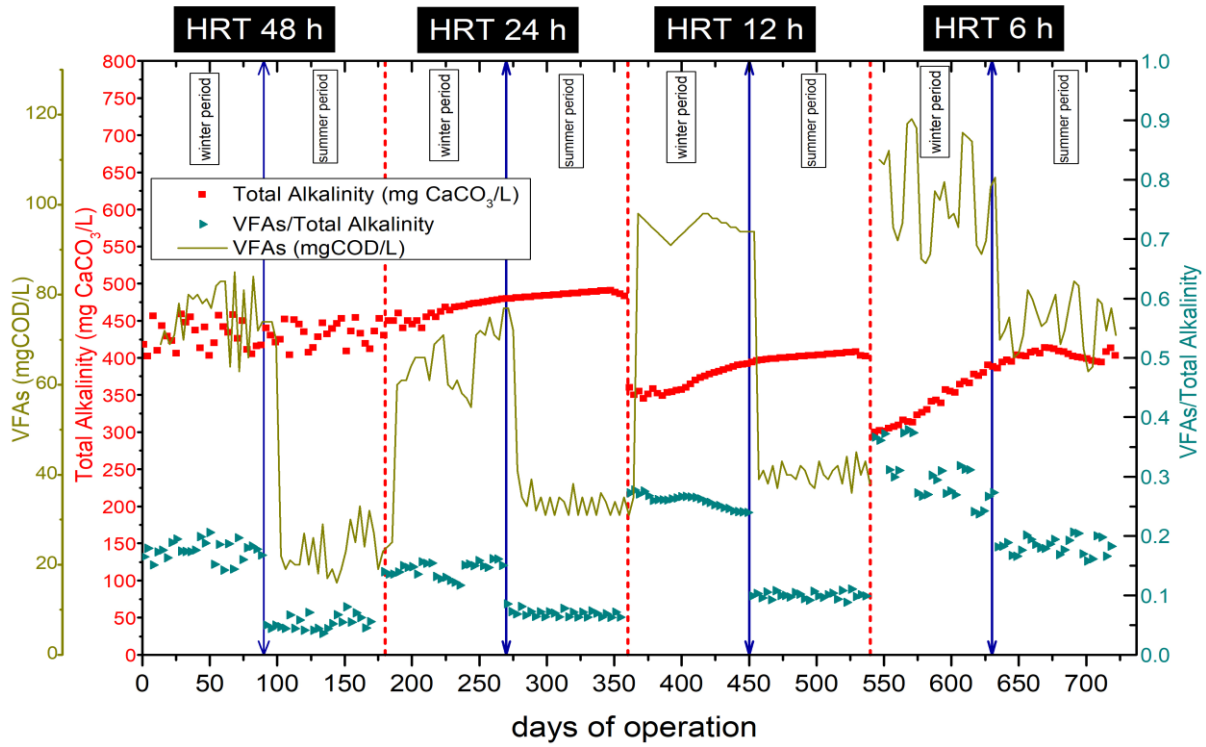
Διάγραμμα 2 Συγκέντρωση VFAs εντός του AnMBR για όλα τα HRT που εξετάστηκαν.
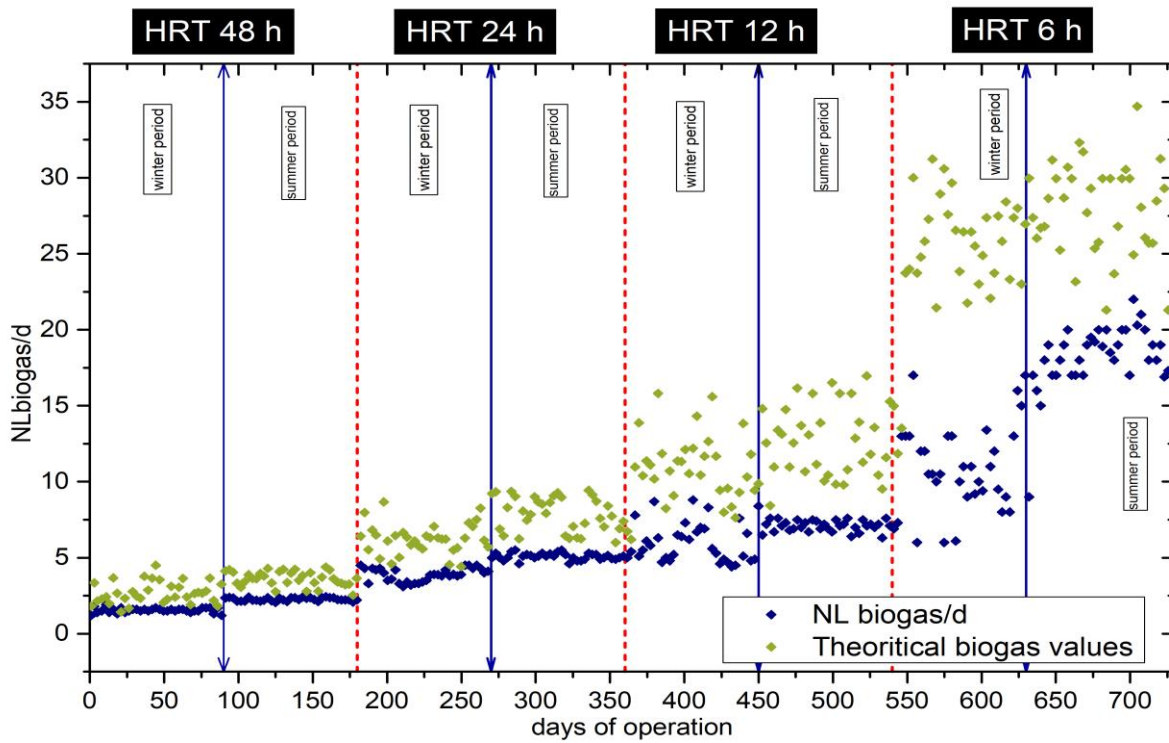
Διάγραμμα 3 Απόδοση AnMBR όσον αφορά την παραγόμενη ποσότητα βιοαερίου για όλα τα HRT που εξετάστηκαν
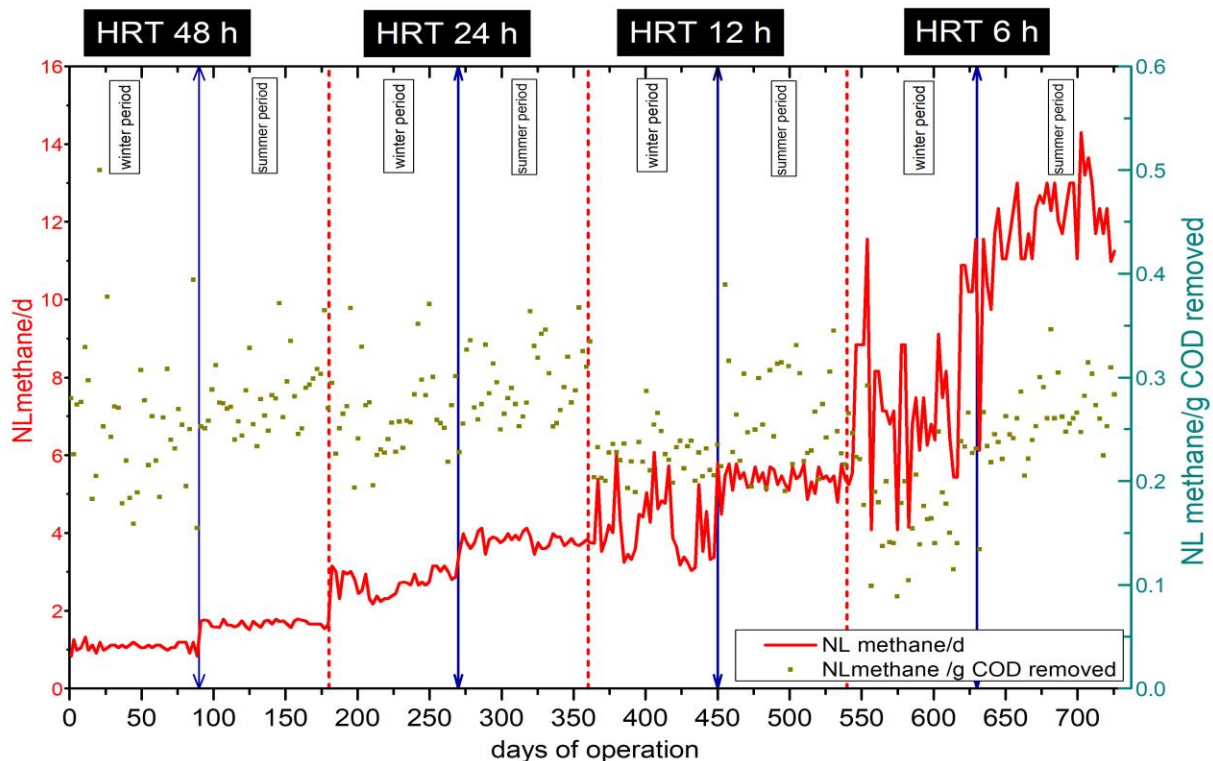
Διάγραμμα 4 Απόδοση AnMBR όσον αφορά την παραγόμενη ποσότητα μεθανίου για όλα τα HRT που εξετάστηκαν

Με βάση τα διαγράμματα 1,2,3,4 γίνεται αντιληπτό ότι με τη μείωση του HRT, παρατηρήθηκε μείωση στην ποιότητα του διηθημένου νερού και αύξηση της έμφραξης της μεμβράνης. Κατά τους καλοκαιρινούς μήνες, με μέση θερμοκρασία 24°C, το AnMBR παρήγαγε νερό με μέσες τιμές COD 51±5 mg·L⁻¹ για HRT 2 ημέρες. Το COD του εξερχόμενου νερού αυξήθηκε σε 67±6 mg·L⁻¹ με HRT 1 ημέρα και 91±4 mg·L⁻¹ για HRT 12 ώρες, υπό τις ίδιες συνθήκες θερμοκρασίας. Σε HRT 6 ωρών, η απόδοση αφαίρεσης COD μειώθηκε περαιτέρω, με τιμές 177±18 mg·L⁻¹ για το χειμώνα και 121±8 mg·L⁻¹ για το καλοκαίρι. Γενικά, τα ευρήματα είχαν πολλές αναγνώσεις: ενώ η επεξεργασία με μικρούς χρόνους HRT είναι ελκυστική από άποψη μείωσης του κόστους, περιοδικά προκαλούσε αυξήσεις στα επίπεδα COD, ιδίως κατά τους χειμερινούς μήνες. Αντίστροφα, σε υψηλότερες θερμοκρασίες ευνοούνταν η λειτουργία του AnMBR, με το HRT 12 ωρών να είναι αρκετό για να επιτευχθεί η αποτελεσματικότητα λειτουργίας και επίτευξη των ορίων. Ωστόσο, σε χαμηλές θερμοκρασίες σε συνδυασμό με χαμηλό HRT, δεν επιτυγχάνει τα όρια που έχουν τεθεί από τους Ευρωπαϊκούς κανονισμούς.

Το Διάγραμμα 5 απεικονίζει τις μεταβολές της διαμεμβρανικής πίεσης για όλο το εξεταζόμενο διάστημα και για όλα τα HRT που εξετάστηκαν.
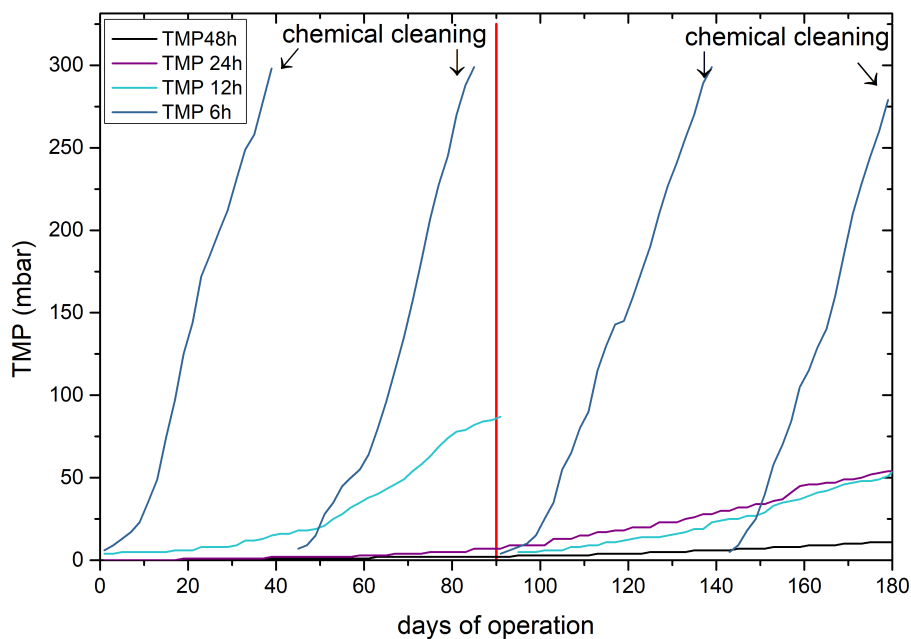
Διάγραμμα 5 Απόδοση AnMBR όσον αφορά την έμφραξη της μεμβράνης για όλα τα εξεταζόμενα HRT

Από το Διάγραμμα 5, είναι σαφές ότι κατά τη διάρκεια των δύο πρώτων HRT που εξετάστηκαν, δεν απαιτήθηκε χημικός καθαρισμός. Συγκεκριμένα, σε HRT 2 ημερών, η αύξηση της TMP ήταν αμελητέα, ενώ στο HRT 1 ημέρας, η TMP αυξήθηκε μόνο στα 50 mbar, πολύ κάτω από την τιμή των 300 mbar που έχει τεθεί από τον κατασκευαστή ως το ανώτατο όριο. Λόγω της ελάχιστης αύξησης, δεν ήταν δυνατό να αξιολογηθούν οι εποχικές διακυμάνσεις της θερμοκρασίας μεταξύ καλοκαιριού και χειμώνα. Αντίθετα, όταν το HRT ρυθμίστηκε στις 12 ώρες, η TMP έφτασε τα 80 mbar κατά τις πρώτες 90 ημέρες λειτουργίας και οδήγησε σε χημικό καθαρισμό πριν από την καλοκαιρινή περίοδο. Κατά την επόμενη καλοκαιρινή περίοδο, η TMP αυξήθηκε μόλις στα 50 mbar, παρουσιάζοντας καλύτερη απόδοση. Ωστόσο, μετά την περαιτέρω μείωση του HRT, το TMP παρουσίασε ταχεία αύξηση, φτάνοντας το όριο των 300 mbar σε περίπου ένα μήνα. Το καλοκαίρι, η μεμβράνη λειτούργησε χωρίς καθαρισμό περίπου 45 ημέρες.

Για να γεφυρώσει αυτές τις λειτουργικές και εποχικές αντιφάσεις, η μελέτη εξέτασε την ενίσχυση της βελτίωσης της απόδοσης με την προσθήκη $FeCl_3$. Όταν χορηγήθηκε σε συγκεκριμένες συγκεντρώσεις Fe^{+3}, στο εύρος 25 mg/L και 30 mg/L, έδειξε μια ελαφρά βελτίωση στις απομακρύνσεις COD (Διάγραμμα 6). Επίσης, παρουσίασε σημαντική μείωση στις συγκεντρώσεις εξερχόμενου φωσφόρου αλλά και βελτίωσε το φαινόμενο της μεμβρανικής έμφραξης(Διάγραμμα 7).
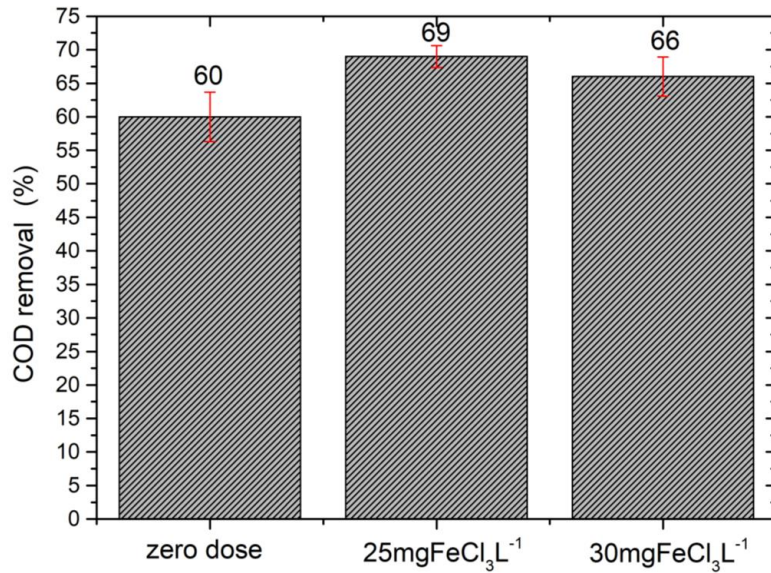
Διάγραμμα 6: Απομάκρυνση COD με την προσθήκη δύο δόσεων σιδήρου
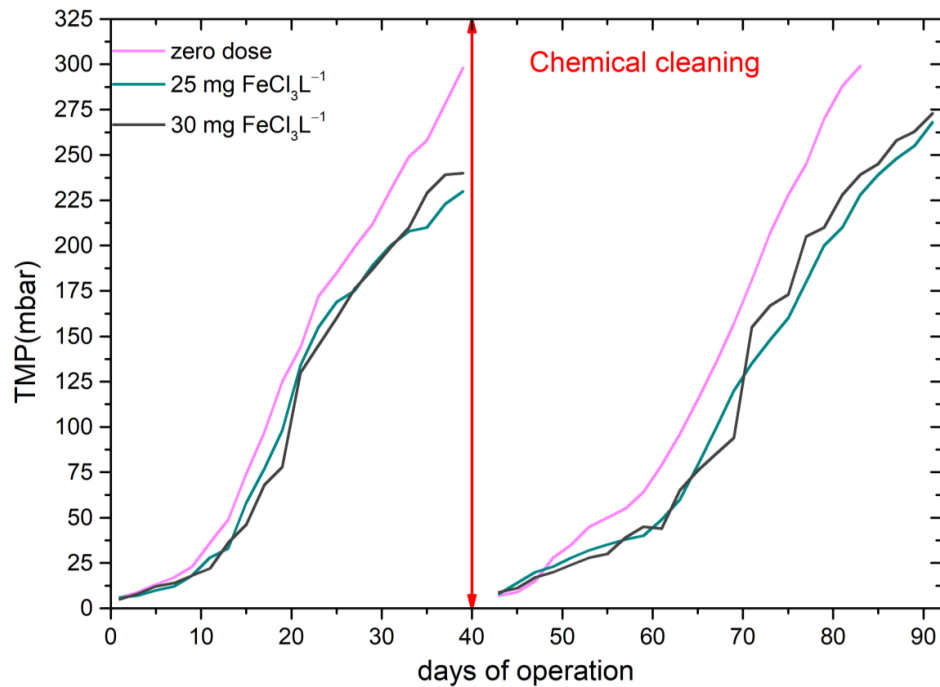
Διάγραμμα 7: Τιμές διαμεμβρανικής πίεσης χωρίς και με τις δύο δόσεις σιδήρου

Προκειμένου να αξιολογηθεί περαιτέρω η ενεργειακή απόδοση του AnMBR, πραγματοποιήθηκε ένα ενεργειακό ισοζύγιο σύμφωνα με τα αποτελέσματα που προέκυψαν από τη λειτουργία του AnMBR εργαστηριακής κλίμακας. Το Διάγραμμα 8 απεικονίζει την παραγωγή

ενέργειας που προέρχεται από την παραγωγή μεθανίου σε όλα τα HRT που εξετάστηκαν. Το συνολικό ενεργειακό περιεχόμενο του CH_4 (τόσο θερμικό όσο και ηλεκτρικό) υπολογίστηκε χρησιμοποιώντας έναν συντελεστή μετατροπής 0,222 kWh ανά mole CH_4.
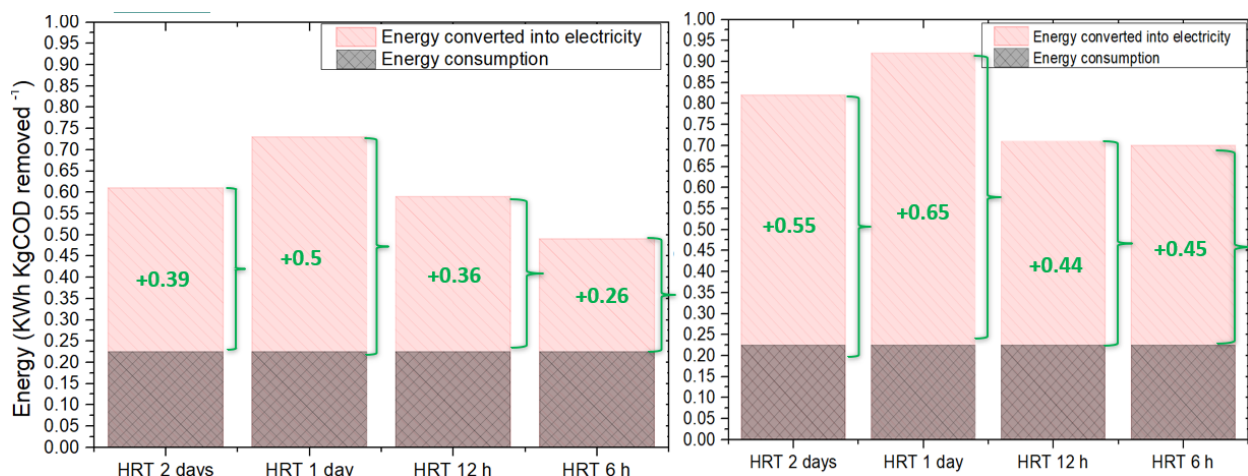
Διάγραμμα 8: Ενεργειακό ισοζύγιο για όλα τα εξεταζόμενα σενάρια.

Όπως παρατηρείται στο Διάγραμμα 8, το ενεργειακό ισοζύγιο είναι ευνοϊκό για όλα τα εξεταζόμενα σενάρια. Είναι σημαντικό να σημειωθεί ότι τα δεδομένα συνολικής κατανάλωσης ενέργειας που έχει το Διάγραμμα 6 προέρχονται από τη βιβλιογραφία, καθώς ο υπολογισμός αυτών των καταναλώσεων για το εργαστηριακό μας σύστημα δεν θα ήταν ακριβής λόγω της μικρής του κλίμακας. Ακόμη και αν εξαιρέσουμε τη θερμική ενέργεια, η ηλεκτρική ενέργεια δίνει ένα θετικό ισοζύγιο. Οι τιμές κυμαίνονται από 0.26 έως και 0.65 KWh/KgCODrem. Κάνοντας σύγκριση με το συμβατικό σύστημα CAS, εκεί είναι αδύνατο να υπάρξει θετικό ισοζύγιο. Εκτός από τον μετριασμό της κλιματικής αλλαγής, αυτό το θετικό ενεργειακό αποτέλεσμα ευθυγραμμίζεται με τα αυστηρότερα ενεργειακά κριτήρια που υπάρχουν ήδη σε διαβούλευση στη νέα οδηγία που έχει προγραμματιστεί να εφαρμοστεί το 2023 και θα αφορά ενεργειακή ουδετερότητα.

Μοντελοποίηση AnMBR μέσω προσαρμογής του μοντέλου αναερόβιας χώνευσης ADM1

Το μοντέλο αναερόβιας χώνευσης ADM1 τροποποιήθηκε και εφαρμόστηκε στο Matlab/Simulink, συγκρίνοντας τρεις μεθόδους ανάλυσης ευαισθησίας: Μίας παραμέτρου τη φορά (OAT), Morris και Fourier Amplitude Sensitivity Test (FAST). Τα πειραματικά δεδομένα που

χρησιμοποιήθηκαν για βαθμονόμηση και επαλήθευση του μοντέλου ήταν αυτά από τον AnMBR εργαστηριακής κλίμακας. Η αξιολόγηση της απόδοσης περιλάμβανε παραμέτρους όπως COD εκροής, ολική εκροή αζώτου, παραγωγή βιοαερίου και συγκεντρώσεις πτητικών αιωρούμενων στερεών. Ο πρωταρχικός στόχος ήταν να συγκριθεί η αποτελεσματικότητα των μεθόδων ανάλυσης ευαισθησίας OAT Morris και FAST στην αποτύπωση της ευαισθησίας του μοντέλου στις παραμέτρους εισόδου. Αυτή η συνολική ανάλυση ευαισθησίας ενισχύει την κατανόησή μας για τη συμπεριφορά του μοντέλου και τη δυνατότητα εφαρμογής του στο σχεδιασμό και τη λειτουργία AnMBR για την επεξεργασία αστικών λυμάτων.

Τα Διαγράμματα 9 και 10 δείχνουν πώς επηρεάζει το HRT τόσο την απομάκρυνση COD όσο και την παραγωγή βιοαερίου (Qgas) για το χειμώνα και το καλοκαίρι αντίστοιχα.
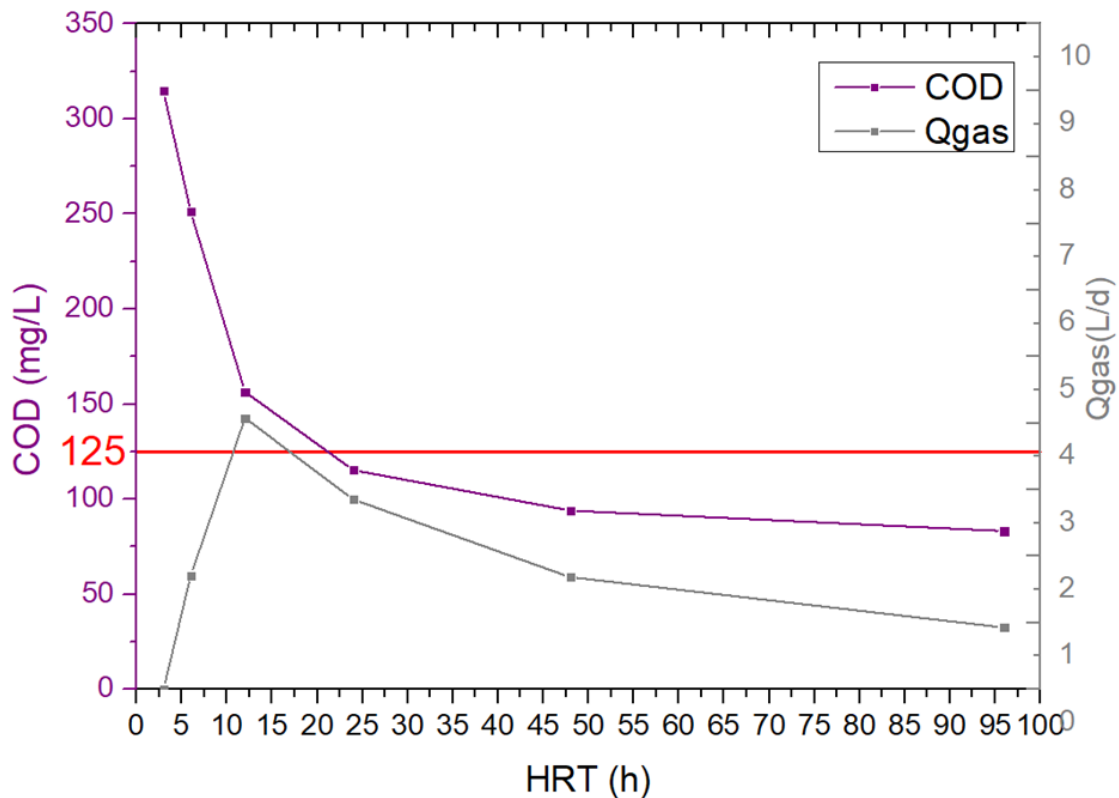
Διάγραμμα 9: Μεταβολές στις τιμές COD εξόδου και στην παραγωγή βιοαερίου για διαφορετικές τιμές HRT κατά τη διάρκεια της χειμερινής περιόδου

Όπως φαίνεται από το Διάγραμμα 9, παρατηρείται σημαντική πτώση στο COD καθώς αυξάνεται το HRT, με μια απότομη μείωση εμφανή από όταν το HRT είχε τιμές από 0 έως 15 ώρες. Παράλληλα, το Qgas παρουσιάζει επίσης πτωτική τάση, αν και λιγότερο έντονη από αυτή του

COD. Για HRT κάτω από 10 ώρες εμφανίζεται μία τιμή πέρα από τις συνηθισμένες. Αυτό θα μπορούσε να οφείλεται στον βραδύτερο ρυθμό ανάπτυξης των μεθανογόνων που ενδεχομένως δεν επιτρέπει την πλήρη έναρξη της μεθανογένεσης. Είναι ενδιαφέρον ότι αυτό το μοτίβο απουσίαζε στα πειραματικά αποτελέσματα στο HRT 6 ωρών, αν και δεν υπήρχαν διαθέσιμα δεδομένα για ένα διάστημα 3 ωρών. Η κόκκινη γραμμή στο γράφημα αντιπροσωπεύει το νομοθετικό όριο για το COD, που έχει οριστεί στα 125 mg/L, υπογραμμίζοντας τη ρυθμιστική αναγκαιότητα διατήρησης των επιπέδων COD κάτω από αυτό το σημείο αναφοράς. Ο συνδυασμός του μοντέλου και των πειραματικών ευρημάτων προσφέρει κρίσιμες γνώσεις σχετικά με την αποτελεσματικότητα της επεξεργασίας αποβλήτων, την παραγωγή αερίου και τη συμμόρφωση, υπογραμμίζοντας τη σημασία της επιβεβαίωσης των προβλέψεων του μοντέλου με πραγματικά δεδομένα.
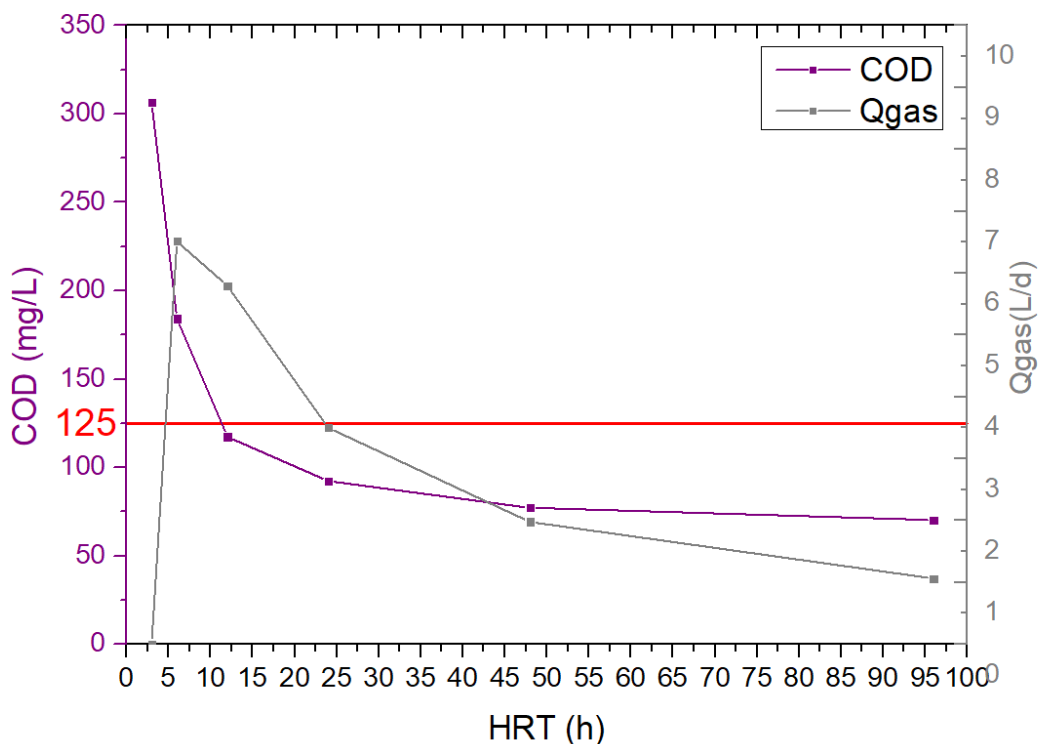
Διάγραμμα 10: Μεταβολές στις τιμές COD εξόδου και στην παραγωγή βιοαερίου για διαφορετικές τιμές HRT κατά τη διάρκεια της καλοκαιρινής περιόδου

Με βάση τα δεδομένα του χειμώνα, το Διάγραμμα 10 απεικονίζει την απόδοση του αντιδραστήρα σε καλοκαιρινές συνθήκες. Όπως και με το χειμερινό γράφημα, μια αύξηση στο HRT σχετίζεται με μείωση των επιπέδων COD. Το Qgas μειώνεται ομοίως, αλλά με πιο σταδιακό

ρυθμό. Μια βασική διαφορά μεταξύ των καλοκαιρινών και χειμερινών γραφημάτων είναι η συμπεριφορά Qgas. Κατά τη διάρκεια του καλοκαιριού, το Qgas παρουσιάζει μια ανωμαλία σε τιμές HRT 6 ωρών, ενώ το χειμώνα, αυτό το ασυνήθιστο μοτίβο εμφανίζεται στις 12 ώρες. Αυτή η διακύμανση θα μπορούσε να επηρεαστεί από τις θερμότερες θερμοκρασίες του καλοκαιριού που επηρεάζουν τα μεθανογόνα.

Συμπερασματικά, με βάση τα παραπάνω γραφήματα, οι βέλτιστες συνθήκες λειτουργίας ορίζονται στις 12 ώρες για τις καλοκαιρινές περιόδους και κυμαίνονται από 20 έως 24 ώρες για τις χειμερινές.

Γενικά συμπεράσματα διδακτορικής διατριβής

Παρακάτω, συγκεντρώνονται τα ευρήματα της διατριβής, υπογραμμίζοντας τις δυνατότητες και τους περιορισμούς της τεχνολογίας AnMBR για την εφαρμογή τους σε εγκαταστάσεις επεξεργασίας λυμάτων με μεσογειακά κλίματα.

Συνολική απόδοση AnMBR:

Το καλοκαίρι με μέση θερμοκρασία λειτουργίας 23±1 °C, 24 ± 2 °C, 24 ±3 °C και 23 ±2 °C, επιτεύχθηκαν ποσοστά απομάκρυνσης COD 89%±1, 85%±2, 78%±3 και 73±4. , με αποτέλεσμα οι μέσες συγκεντρώσεις COD διηθήματος να έχουν τιμές 51±5 mg/L, 67±6 mg/L, 91±4 mg/L και 121±8 mg/L για HRT 2 ημερών, 1 ημέρας, 12 ωρών και 6ωρών, αντίστοιχα. Το χειμώνα (με Τ=18±4°C, 19 ± 2 °C, 19 ± 3 °C και 18 ±3 °C), τα ποσοστά αφαίρεσης καταγράφηκαν σε 76%±4, 77%±4, 69%±5 και 60%±3, με αντίστοιχες μέσες συγκεντρώσεις COD διηθήματος 105±9 mg/L, 95±12 mg/L, 123±9 mg/L και 177±8 mg/L, αντίστοιχα. Καθ' όλη τη διάρκεια της μελέτης, διατηρήθηκε η σταθερότητα της λειτουργίας AnMBR. Οι τιμές TMP παρατηρήθηκαν να είναι χαμηλές στις 2 ημέρες HRT αλλά αυξήθηκαν όταν το HRT ρυθμίστηκε σε 1 ημέρα και μια πιο σημαντική αύξηση παρατηρήθηκε στις 12 ώρες HRT. Όταν το HRT ρυθμίστηκε στις 6 ώρες, σημειώθηκε έντονος ρυθμός ανάπτυξης TMP κατά τη διάρκεια του χειμώνα, οδηγώντας σε χημικό καθαρισμό κάθε 38 ημέρες, ενώ το καλοκαίρι, αυτό το διάστημα καθαρισμού επεκτάθηκε σε 50 ημέρες. Διαπιστώθηκε ότι η απόδοση του AnMBR επηρεάστηκε περισσότερο από τις θερμοκρασίες στις 12 ώρες και 6 ώρες HRT.

Βελτίωση της λειτουργίας AnMBR με προσθήκη σιδήρου:

Κατά τη χειμερινή περίοδο και όταν το HRT είχε ρυθμιστεί στις 6 ώρες, πραγματοποιήθηκε προσθήκη $FeCl_3$. Με την προσθήκη σιδήρου σε συγκεντρώσεις 25 mg $FeCl_3$/L και 30 mg $FeCl_3$/L, παρατηρήθηκαν μειώσεις στις μέσες τιμές COD διηθήματος σε 147 mg/L και 149 mg/L, από 177 mg/L χωρίς $FeCl_3$. Αυτό υποδηλώνει μεγαλύτερη αποτελεσματικότητα στην απομάκρυνση του οργανικού φορτίου. Το ποσοστό απομάκρυνσης φωσφόρου για τις δύο συγκεντρώσεις $FeCl_3$που εξετάστηκαν έφτασε το 75% και 100%. Η απόδοση μεθανίου παρέμεινε αμετάβλητη. Κατά τη διάρκεια του χειμώνα παρήχθη κατά μέσο όρο 0,37 L βιοαερίου/g COD που αφαιρέθηκε. Το διαλυτό μεθάνιο στο διήθημα βρέθηκε να είναι σε επίπεδα κορεσμού, αντιπροσωπεύοντας το 20,6% και το 43,8% του συνολικού μεθανίου το καλοκαίρι και το χειμώνα, αντίστοιχα. Για εφαρμογές μεγάλης κλίμακας του AnMBR, κρίνεται απαραίτητη μια αποτελεσματική διαδικασία ανάκτησης διαλυμένου μεθανίου.

Όταν προστέθηκαν 25 mg $FeCl_3$/L, ελέγχθηκε η πιθανή βελτίωση της απομάκρυνσης μικρορύπων. Εκτός από την Εννευλοφαινόλη (NP), το AnMBR βρέθηκε να έχει περιορισμένη αποτελεσματικότητα στην απομάκρυνση μικρορύπων. Με ή χωρίς σίδηρο, επιτεύχθηκαν ποσοστά αφαίρεσης NP άνω του 70%. Ωστόσο, άλλοι μικρορύποι όπως Τρικλοζάνη (TCS), Βισφαινόλη (BPA), Ιβουπροφένη (IBU), Ναπροξένη (NPX), Δικλοφαινάκη (DCF) και Κετοπροφαίνη (KTP) παρουσίασαν ποσοστά απομάκρυνσης μεταξύ 10% και 40%. Από αυτές τις παρατηρήσεις, συνήχθη το συμπέρασμα ότι οι αναερόβιες συνθήκες δεν ευνοούν την απομάκρυνση μικρορύπων.

<u>Συμμόρφωση με τους κανονισμούς και πιθανή επαναχρησιμοποίηση:</u>

Από τα αποτελέσματα της παρούσας διδακτορικής διατριβής μπορεί να συναχθεί ότι τα συστήματα AnMBR που λειτουργούν σε ψυχρόφιλες θερμοκρασίες που συνηθίζονται στη Νότια Ευρώπη κατά τη διάρκεια του χειμώνα, φαίνεται να πληρούν τα πρότυπα της Οδηγίας 91/271/EEC όταν λειτουργούν με HRT 2 ημερών, 1 ημέρας και 12 ωρών. Η απόδοση του αντιδραστήρα όταν το HRT είχε ρυθμιστεί στις 12 ώρες ήταν κοντά στο καθορισμένο όριο που καθορίζει η οδηγία UWWTD, με μερικές τιμές να ήταν εκτός ορίων. Παρόλο που η προσθήκη σιδήρου βελτίωσε τη διαδικασία, δεν πέτυχε σταθερές τιμές εκροής, κάτω από τα όρια που έχουν τεθεί. Παρά τις δυσκολίες, τα AnMBR θεωρούνται μια αρκετά υποσχόμενη τεχνολογία για την επεξεργασία αστικών λυμάτων, προσφέροντας τόσο παραγωγή ενέργειας όσο και νερό κατάλληλο για άρδευση.

Παραγωγή ενέργειας

Η παρούσα διδακτορική διατριβή έδειξε ότι το σύστημα AnMBR εργαστηριακής κλίμακας πέτυχε σταθερά μια ισορροπημένη παραγωγή ενέργειας σε όλα τα εξεταζόμενα σενάρια. Συγκεκριμένα, οι καταγεγραμμένες ενεργειακές παραγωγές κυμαίνονταν από 0,3 – 0,9 KWh/KgCODrem τόσο τη χειμερινή όσο και την καλοκαιρινή περίοδο. Σε σύγκριση με τα συμβατικά αερόβια συστήματα ενεργού ιλύος, το σύστημα AnMBR ευθυγραμμίζεται με το πρότυπο ενεργειακής ουδετερότητας. Δεδομένης της πρόσφατης πρότασης της Ευρωπαϊκής Επιτροπής για την αναθεώρηση της Οδηγίας για την Επεξεργασία Αστικών Λυμάτων (UWWTD) 91/271/EEC, η οποία τονίζει την ανάγκη για ενεργειακά ουδέτερες εγκαταστάσεις επεξεργασίας αστικών λυμάτων, η βελτιστοποίηση του AnMBR γίνεται ακόμη πιο σημαντική, όχι μόνο για την Ευρώπη αλλά παγκοσμίως.(https://environment.ec.europa.eu/publications/proposal-revised-urban-wastewater-treatment-directive)

Μοντελοποίηση AnMBR

Το μοντέλο της IWA για την αναερόβια χώνευση (ADM1) τροποποιήθηκε και προσαρμόστηκε για την προσομοίωση του αντιδραστήρα AnMBR χρησιμοποιώντας πειραματικά δεδομένα από τον AnMBR εργαστηριακής κλίμακας. Η ανάλυση ευαισθησίας πραγματοποιήθηκε χρησιμοποιώντας τις μεθόδους Morris, Fast και One-at-a-Time (OAT). Στη συνέχεια, πραγματοποιήθηκε βαθμονόμηση του μοντέλου με βάση τα εμπειρικά δεδομένα. Κατά την επικύρωση, επιβεβαιώθηκε η αξιοπιστία του μοντέλου. Ο κώδικας τροποποιήθηκε με σκοπό την ταύτιση με την τεχνολογία AnMBR και παρατηρήθηκε ότι οι τιμές πολλών απαιτούμενων κινητικών παραμέτρων ήταν σημαντικά υψηλότερες από ότι στο αρχικό μοντέλο που αφορούσε την αναερόβια χώνευση. Αυτό δείχνει ότι οι διαδικασίες εντός του αντιδραστήρα ήταν ταχύτερες απ' ότι αναμενόταν. Σε πέντε διαφορετικά σενάρια, βρέθηκε στενή ευθυγράμμιση μεταξύ των προβλέψεων του μοντέλου και των πειραματικών αποτελεσμάτων. Το μοντέλο χρησιμοποιήθηκε περαιτέρω για να εξεταστεί η βέλτιστη λειτουργία AnMBR όσον αφορά την ποιότητα των λυμάτων και την παραγωγή βιοαερίου. Τα αποτελέσματα του μοντέλου, επαλήθευσαν τα πειραματικά αποτελέσματα και προέβλεψαν το βέλτιστο HRT για χειμώνα 24 ώρες και για καλοκαίρι 12 ώρες.

TABLE OF CONTENTS

List of Figures

Chapter 2

Chapter 3

Chapter 4

Chapter 5

List of Tables

Chapter 2

Chapter 3

Chapter 4

Chapter 5

List of abbreviations

ACP	Anaerobic Contact Process
AAT	All at a time
ABR	Anaerobic baffled reactor
AD	Anaerobic Digestion
ADM1	Anaerobic Digestion Model No1
AFMBR	Anaerobic Fluidized Membrane Bioreactor
AnDMBR	Anaerobic Dynamic Membrane Bioreactors
AnMBR	Anaerobic Membrane Reactors
AnWT	Anaerobic Wastewater Treatment
ASM	Activated Sludge Model
BOD$_5$	Biochemical Oxygen Demand
BSM2	Benchmark Simulation Model 2
CFV	Cross-flow velocity
CHP	Combined heat and Power
COD	Chemical Oxygen Demand
CSTR	Completely Stirred Tank Reactor
DAE	Differential-Algebraic Equations
DE	Differential Equations
EDCs	Endocrine Disrupting Chemicals
EET	Elementary Effect Test
EGSB	Expanded Granular Sludge Bed
EPS	Extracellular Polymeric Substances
FB	Fluidized Bed
FO	Forward Osmosis
FS	Flat Sheet
GAC	Granular Activated Carbon
GSA	Global Sensitivity Analysis
HF	Hollow Fiber
HRARs	High-Rate Anaerobic Reactors
HRT	Hydraulic Retention Time

IA	Intermediate Alkalinity
IAFMBR	Integrated Anaerobic Fluidized Bed Membrane Bioreactor
LCFA	Long-Chain Fatty Acids
LSA	Local Sensitivity Analysis
MLSS	Mixed liquor Suspended Solids
MPB	Methane Producing Bacteria
MSW	Municipal Solid Waste
MT	Multi-Tubular
MWW	Municipal Wastewater Treatment
NF	Nanofiltration
nZVI,	nano ZVI
OAT	One at a time
OFMSW	Organic Fraction of Municipal Solid Waste
OLR	Organic Loading Rate
PA	Partial Alkalinity
PAC	Powdered Activated Carbon
PE	Polyethylene
PES	Polyethersulfone
PhACs	Pharmaceutically Active Compounds
PP	Polypropylene
PSD	Particle Size Distribution
PSF	Polysulfone
PVDF	Polyvinylidene Fluoride
RO	Reverse Osmosis
RSA	Regional Sensitivity Analysis
SAnMBR	Submerged Anaerobic Membrane Bioreactor
SCFAs	Short-Chain Fatty Acids
SMP	Soluble Microbial Products
SRB	Sulfate-Reducing Bacteria
SRT	Solids Retention Time
SS	Suspended Solids

TA	Total Alkalinity
TMP	Trans membrane pressure
TN	Total Nitrogen
TOC	Total Organic Carbon
TP	Total Phosphorus
TSS	Total Suspended solids
UASB	Upflow Anaerobic Sludge Blanket
VFAs	Volatile Fatty Acids
VSS	Volatile fatty acids
WWTP	Wastewater Treatment Plant
ZVI	Zero Valent Iron

Chapter 1 Introduction

1.1 Introduction

With the escalating urban population density globally, there's a mounting pressure on wastewater management systems. Traditional aerobic processes, once the stalwart of urban wastewater treatment, are now being critically evaluated for their economic and environmental constraints. An emerging alternative that's drawing significant attention in scientific and policy circles is the anaerobic treatment process.

Historically, the application of anaerobic treatment was mostly relegated to high-strength wastewaters and municipal sludge treatment due to its perceived inefficiencies with low-strength wastewaters. However, this perception has been challenged by research which successfully demonstrated the efficacy of anaerobic treatments for even low-strength municipal wastewaters.

Economically speaking, anaerobic treatments appear to be more viable in the long run. The operational costs associated with these systems are generally lower. This is attributed to the fact that anaerobic treatments require less energy input and yield a lesser volume of residual sludge. The reduced sludge output not only translates to lower disposal costs but is also environmentally advantageous as it's significantly more stabilized, implying a reduced environmental footprint both in terms of disposal and associated greenhouse gas emissions.

Perhaps one of the standout features of the anaerobic treatment process is its capacity for energy recovery. Methane, a by-product of this treatment, can be harnessed and utilized as a potent energy source. To provide some perspective, research by Shizas and Bagley (2004) showcased that the energy inherent in wastewater is roughly six to nine times greater than the electricity required for its treatment.

However, like all technologies, anaerobic treatments are not devoid of challenges. The inherent slow growth rate of anaerobic bacteria implies that extended hydraulic and solid retention times are required. This often necessitates larger reactor volumes, which can be a limitation in urban settings where space is at a premium. In response to this, the wastewater treatment industry has seen the emergence of innovative reactor designs. Notable mentions include the Upflow Anaerobic Sludge Blanket (UASB) and the Anaerobic Baffled Reactor (ABR). Both are engineered to optimize bacterial activity and mitigate the need for expansive reactor volumes. Another

promising process is the AnMBR method, which merges biological treatment with membrane filtration, promising enhanced biomass retention and minimized effluent suspended solids.

In summation, as urban centers globally grapple with the intricate challenges of wastewater management, the anaerobic treatment process is steadily emerging as a compelling solution. While certain challenges remain to be addressed, the overarching benefits of efficient waste treatment combined with energy recovery make it a promising candidate in the roadmap towards sustainable urban wastewater management.

1.2 Research Objectives

Given the outlined context, the overarching aim of this doctoral dissertation is to systematically probe the sustainable operation of an Anaerobic Membrane Bioreactor (AnMBR) in treating wastewater, under ambient environmental conditions. The specificity and novelty of this research lie in its application of AnMBR for real municipal wastewater treatment and the consequent development of operation protocols. The knowledge extracted from this study is intended to guide municipalities in both the integration of this technology, effective functioning and potential enhancements of full-scale AnMBRs, emphasizing heightened sustainability in terms of superior effluent quality and mitigated membrane fouling. The detailed objectives are delineated as follows:

➢ <u>Performance Analysis of AnMBR under Varied Conditions</u>: *To evaluate the influence of Hydraulic Retention Time (HRT), elevated organic loadings, and ambient temperature fluctuations on the AnMBR's efficacy in treating municipal wastewater.* Key performance indicators for this objective include:
  ✓ Quality of the effluent water in alignment with Greek and European regulatory standards.
  ✓ Biogas yield, its methane fraction, and the associated energy production potential.
  ✓ Insights into membrane fouling dynamics.

➢ <u>FeCl$_3$ Addition for Enhanced AnMBR Performance</u>: *To systematically assess the implications of FeCl3 addition in bolstering AnMBR's operational metrics, specifically focusing on curtailing membrane fouling and enhancing phosphorus removal.* Performance metrics to be considered under this objective comprise:

- ✓ Biogas production dynamics and the resultant energy generation from methane.
- ✓ Organic Load removal efficiency.
- ✓ Removal efficiency of select organic micropollutants, particularly from the NSAID and EDC groups.
- ✓

➤ <u>Modification and Validation of the ADM1 Model for AnMBR:</u> *To adapt, apply, and authenticate the Anaerobic Digestion Model No. 1 (ADM1) for simulating the municipal wastewater treatment via AnMBR.* This endeavor aims to:
- ✓ Accurately depict the AnMBR system's behavior, output, and its methane-based energy production across different scenarios.
- ✓ Optimize operational parameters through predictive modeling.
- ✓ Provide a framework for a wider application and understanding of AnMBR in wastewater treatment plants.

1.3 Structure of the Doctoral Dissertation

This doctoral dissertation is structured into six chapters, in alignment with the set research objectives and the conducted research:

<u>Chapter 1: Introduction</u>

This chapter provides an overview of the research, elucidating its context and significance. It also outlines the structure of the entire doctoral dissertation.

<u>Chapter 2: Theoretical Background</u>

This chapter delves into the theoretical foundations underpinning the research. It emphasizes the anaerobic treatment process and the factors influencing it. The advantages of anaerobic over aerobic treatment are explored. Different types of anaerobic treatments are detailed, culminating in an in-depth discussion on AnMBR, its applications, challenges, and potential future directions.

<u>Chapter 3: Methodology - Experimental Protocol</u>

Here, the research methodology is laid out, detailing the experimental protocols and analytical methods employed. This chapter provides an in-depth look at the AnMBR laboratory system,

describing the operational protocols for the lab-scale AnMBR and monitoring techniques to assess its performance.

Chapter 4: Results

This chapter presents and discusses the findings of the experiments. It showcases the performance metrics of the AnMBR, highlighting its behavior with variations in hydraulic retention time (HRT), temperature, and the inclusion of ferric iron.

Chapter 5: AnMBR System Simulation Model

This chapter introduces a simulation model tailored for the AnMBR system. Comprehensive sensitivity analyses, along with calibration and validation processes, are conducted. The chapter also explores the influence of various parameters on the AnMBR system, with some scenarios investigated that extend beyond the experimental results.

Chapter 6: Conclusions and Recommendations

The dissertation concludes by summarizing the key findings and drawing overarching conclusions. This chapter also puts forth suggestions for potential avenues of future research in the domain

Chapter 2: Theoretical Background

Chapter 2 provides an extensive theoretical background about anaerobic treatment processes. The chapter begins with a comprehensive introduction to anaerobic treatment, detailing its process, environmental and operational factors, benefits compared to aerobic treatment, and various reactor types (Section 2.1). It then delves into the specifics of Anaerobic Membrane Reactors (AnMBR), including a thorough description of their functioning, operating parameters, advantages, disadvantages, economic aspects, and comparison with aerobic membrane bioreactors, among other topics (Section 2.2). Following this, the chapter explores different anaerobic digestion models, such as the ADM1 model by IWA, and sensitivity analysis methodologies (Section 2.3). Finally, the chapter concludes with the objectives of the doctoral thesis, setting the stage for the research and analysis to follow (Section 2.4).

2.1 Anaerobic Processes: Definition and Environmental Benefits

Anaerobic digestion (AD) is a process where organic material is broken down and converted into biogas, consisting mainly of methane and carbon dioxide. This process occurs in areas with no oxygen, such as the stomachs of ruminants, marshes, lakes and ditches, landfills, and sewers. AD is an effective method for removing biodegradable organic compounds, leaving mineralized compounds in the solution. It can be performed in simple systems and at any scale, producing only a small amount of excess sludge that has a market value when produced in a bioreactor. Additionally, biogas is generated during the process, providing useful energy without requiring high-grade energy consumption.

In contrast, aerobic treatment is characterized by high operational costs and the conversion of a large portion of waste into another type of waste, sludge. Aerobic treatment in a conventional activated sludge process typically yields about 50% or more new sludge from the chemical oxygen demand (COD) converted, which requires further treatment before it can be reused, disposed of, or incinerated (Figure. 2.1). The carbon/energy flow principles of aerobic and anaerobic bioconversion affect the design of wastewater treatment systems. Anaerobic digestion has become a competitive wastewater treatment technology, and many types of organically polluted wastewaters that were once believed to be unsuitable for it are now treated using high-rate anaerobic conversion processes.
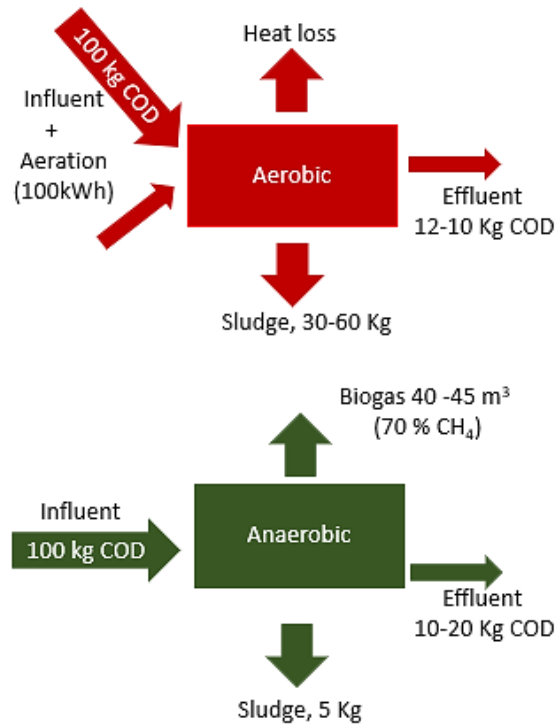
Figure 2. 1: : Carbon and energy in aerobic and anaerobic wastewater treatment processes[1]

Anaerobic reactor systems are widely used for the treatment of agro-industrial wastewaters in countries like the Netherlands, and their potential applications in industries such as petro-chemicals are increasing rapidly. The number of anaerobic high-rate reactors has gradually increased since the mid-seventies, with a total of 2,266 registered full-scale installations currently in operation, constructed by reputable companies, as well as many local companies (Figure 2.2). Additionally, there are an estimated 500 "homemade" reactors constructed by small local companies or industries themselves, which are not included in the statistics. The reasons for selecting Anaerobic Wastewater Treatment (AnWT) over conventional aerobic treatment systems include several significant advantages.

- ➢ Excess sludge production can be reduced by up to 90%.
- ➢ The use of expanded sludge bed systems can reduce space requirements by up to 90%.
- ➢ High applicable COD loading rates of 20-35 kg COD per m^3 of reactor per day are possible, requiring smaller reactor volumes.

- ➢ Treatment does not require the use of fossil fuels, saving about 1 kWh/kgCOD removed (depending on aeration efficiency).
- ➢ About 13.5 MJ of CH_4 energy is produced per kgCOD removed, which can generate 1.5 kWh of electricity (assuming 40% electric conversion efficiency).
- ➢ The system can be rapidly started up (<1 week) using granular anaerobic sludge as seed material.
- ➢ The technology does not require the use of chemicals or requires very little use.
- ➢ The system has high treatment efficiency and is easy to operate.
- ➢ Anaerobic sludge can be stored unfed, allowing reactors to be operated during agricultural campaigns only (e.g., 4 months per year in the sugar industry).
- ➢ Excess sludge produced can have a market value.
- ➢ High-rate systems facilitate water recycling in factories towards closed loops.
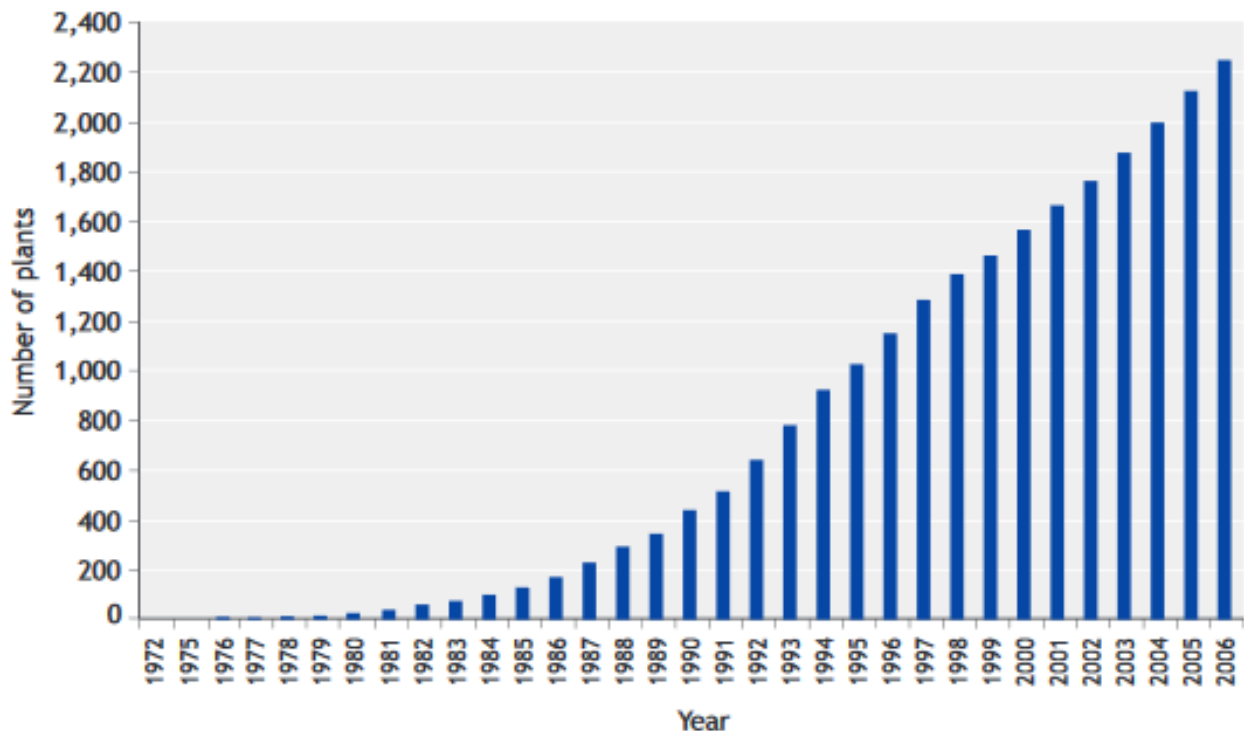
Figure 2. 2 The number of anaerobic high-rate reactors installed globally showed a gradual increase from 1972 to 2006[1]

The advantages listed above may vary in their significance depending on local economic and societal conditions. In the Netherlands, for instance, the cost of handling excess sludge is a major factor in wastewater treatment operations. Given that landfills are not an option for excess sewage

sludge and biowastes, and the prices for incineration are high, the low sludge production in anaerobic reactors provides an immediate economic benefit. Additionally, the compactness of AnWT is exemplified by a full-scale reactor with a diameter of 6 m and a height of 25 m, which can treat up to 25 tons of COD per day and produce less than 1 ton of dry matter sludge per day that is not a waste product but can be marketed as seed sludge for new reactors. This compactness makes it possible to implement the system on industrial premises or even inside factory buildings, which is particularly useful in densely populated areas and for industries seeking to use anaerobic treatment as the first step in a treatment process for reclaiming process water.

The increasing focus on the energy benefits of AnWT is a direct result of the rising energy costs and growing concerns about global warming. By converting 25 tons of agro-industrial waste per day, approximately 7,000 m^3 of CH_4 per day can be produced, with an energy equivalent of around 250 GJ per day. Using a modern CHP gas engine with 40% efficiency, a useful 1.2 MW of electric power output can be obtained. The overall energy recovery could be even higher if excess heat is utilized on the industry premises or nearby. In comparison, full aerobic treatment would require about 1 kWh/kgCOD removed, or 1 MW installed electric power in this case, making the total energy benefit of using AnWT over the activated sludge process 2.2 MW.

Carbon credits can also be earned by generating renewable energy using AnWT. The predicted CO_2 emission reduction of an anaerobic reactor, operated at commercially available organic loading rates, is summarized in Table 2.1. This provides a real incentive for implementing AnWT systems in developing countries to protect the local environment, and the carbon credit policy can be seen as a Western subsidy for this purpose.

Table 2. 1: Predicted CO_2 emission reduction by applying a high-rate anaerobic reacto[1]

Loading Capacity (KgCOD /m^3 d	5-35
Energy output (Mj/m^3 reactor installed per d)	55-390
Electric power output (kW/m^3 reactor installed)	0.25-1.7
CO_2 emission reduction (tonCO_2 /m^3, based on coal driven power plant)	1.9-13

*Assumptions: 80% recovery of CH_4 compared to the influent COD load and 40% efficiency in electric conversion using a modern combined heat power generator.

2.2 Process description and microbiology

The breakdown of organic material into methane involves a complex, multi-step process consisting of four stages: hydrolysis, acidogenesis, acetogenesis, and methanogenesis. These stages occur in a sequential and parallel manner, resulting in the gradual degradation of the organic matter and the eventual production of methane gas. A brief explanation of each stage is described below. Also, Table 2.2 provides information on the chemical reactions and bacteria that are associated with each of the four stages. Additionally, Figures. 2.3 and 2.4 illustrate the process flow chart[2,3].

Table 2. 2: The chemical reactions and bacteria involved in AD [4,5]

Stage	Type of conversion	Bacteria involved
Stage-I Hydrolysis $(C_6H_{10}O_5)$ n + nH2O = $n(C_6H_{12}O_6)$	Proteins to soluble peptides and amino acids	*Clostridium, Proteus vulgaris, Vibrio, Bacillus, Peptococcus, Bacteriodes,*
	Carbohydrates to soluble sugars	*Clostridium, Acetovibrio celluliticus, Staphylococcus, Bacteriodes*
	Lipids to fatty acids or alcohols	*Clostridium, Micrococcus, Staphylococcus*
Stage-II Acidogenesis $C_6H_{12}O_6 + 2H_2O \rightarrow 2CH_3COOH + 4H_2+CO_2$ $C_6H_{12}O_6 + 2H_2 \rightarrow$ $2CH_3CH_2COOH + 2H_2O$ $C_6H_{12}O_6 \rightarrow CH_3CH_2CH_2COOH + 2H_2+2CO_2$ $C_6H_{12}O_6$ $\rightarrow 2CH_3CH_2OH +2CO_2$ $C_6H_{12}O_6 \rightarrow 2CH_3CHOHCOOH$	Amino acids to fatty acids, acetate and NH_3	*Lactobacillus, Escherichia, Bacillus, Staphylococcus,Pseudomonas, Sarcina, Desulfovibrio, Selenomonas, Streptococcus,Veollonella, Desulfobacter, Desulforomonas*
	Sugars to intermediary fermentation products	*Clostridium, Eubacterium limosum, Streptococcus*
Stage III Acetogenesis $CH_3CH_2OH + H_2O \rightarrow CH_3COOH + 2H_2$ $2CH_3CH2OH + 2CO_2 \rightarrow CH_4 + 2CH_3COOH$ $CH_3CH2COOH + 2H_2O \rightarrow CH_3COOH + 3H2 + CO_2$ $CH_3CH_2CH2COOH + 2H_2O \rightarrow 2CH_3COOH + 2H_2$ $CH_3CHOHCOOH + H_2O \rightarrow CH_3COOH + CO_2 + 2H_2$	Higher fatty acids or alcohols to hydrogen and acetate	*Clostridium, Syntrophomonas wolfeii*
	Volatile fatty acids and alcohols to acetate or hydrogen	*Syntrophomonas wolfei, Syntrophomonas wolinii*
Stage IV Methanogenesis $CH_3COOH \rightarrow CH_4 + CO_2$ $CO_2 + 4 H_2 \rightarrow CH_4 + 2H_2O$	Acetate to methane and carbondioxide	*Methanosaeta, Methanosarcina*
	Hydrogen and carbondioxide to methane	*Methanobacterium formicicum, Methanobrevibacterium, Methanoplanus, Methanospirilum*

Hydrolysis

Hydrolysis plays a vital role in the anaerobic biodegradation process, specifically during the initial stage of anaerobic digestion. In this stage, bacteria facilitate the conversion of complex organic substrates such as carbohydrates, proteins, lipids, and others, which are initially insoluble, into soluble monomers and polymers. This transformation is made possible through the action of exoenzymes like cellulase, protease, and lipase, which are excreted by the microorganisms responsible for fermentation. These enzymes break down proteins into amino acids, lipids into long-chain fatty acids (LCFA), and polysaccharides into simple sugars.[6,7]. Fermenting microorganisms are classified as a diverse group of bacteria that have the ability to survive and thrive in the presence or absence of oxygen[8,9]. In the digestion of substrates with a high ratio of suspended solids (SS) to COD, the hydrolysis process tends to be the bottleneck. The limitation is typically not caused by insufficient enzyme activity, but rather by the presence of a limited surface area that is accessible to free hydrolytic action, as well as the overall structure of the solid substrate[10,11].

Furthermore, when operating at low temperatures, hydrolysis can become the limiting factor in the overall process, as demonstrated by Lew et al. (2011). This limitation plays a crucial role in determining the necessary design of the reactor. The breakdown products of hydrolysis serve as substrates for acidogenic bacteria. Equation (2.1), provided by Ostrem et al. (2004), presents an illustrative example of a hydrolysis reaction wherein organic waste is converted into a simple sugar, specifically glucose.

$$C_6 H_{10} O_4 + 2H_2O \rightarrow C_6 H_{12} O_6 + 2H_2 \qquad\qquad Eq\ (2.1)$$
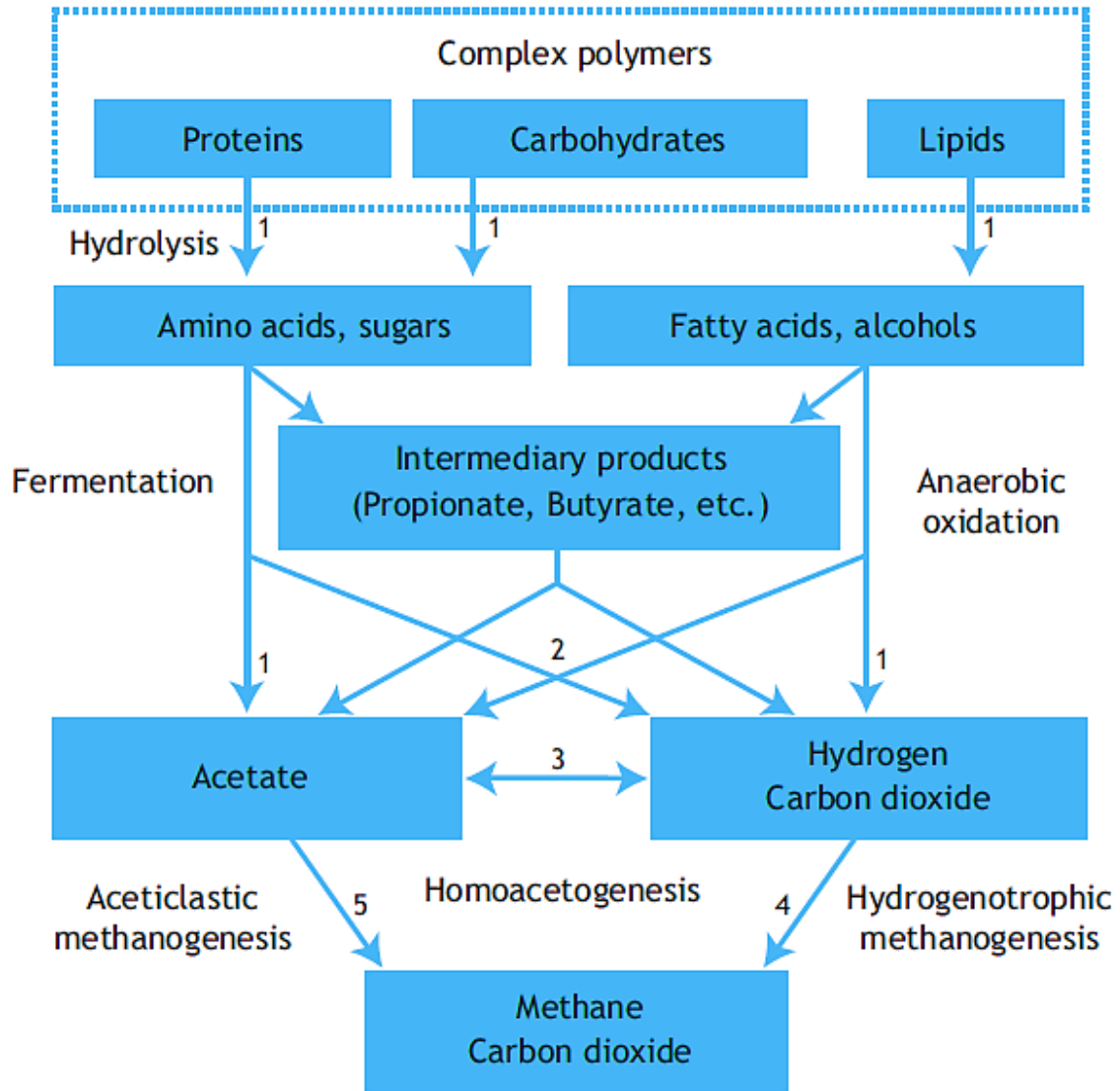
Figure 2. 3: The anaerobic digestion of polymeric materials involves a series of reactions performed by different groups of bacteria. The bacterial groups mentioned (1) hydrolytic and fermentative bacteria, (2) acetogenic bacteria, (3) homo-acetogenic bacteria, (4)) hydrogenotrophic methanogens, and (5) aceticlastic methanogens, play distinct roles in this process. [12]
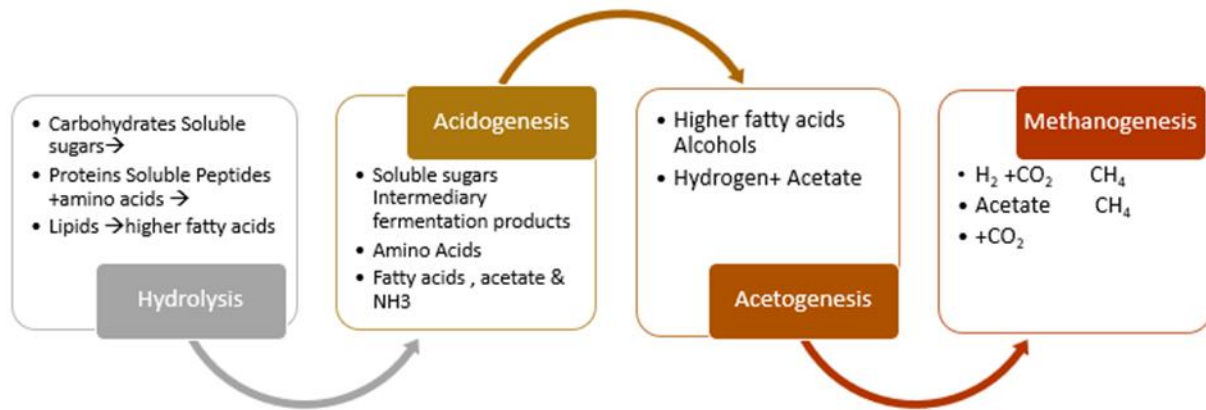
Figure 2. 4: Anaerobic Digestion Process[12]

Acidogenesis

During the second stage of AD, the hydrolysis products, including amino acids, LCFA, and simple sugars, which are relatively soluble compounds, undergo a conversion process resulting in the formation of various small organic compounds. The primary products of this stage are volatile fatty acids (VFAs), notably acetate (CH_3COOH), along with other organic acids such as propionate (CH_3CH_2COOH), butyrate ($CH_3CH_2CH_2COOH$), valeric ($CH_3CH_2CH_2CH_2COOH$), formic (HCOOH), lactic ($C_3H_6O_3$), as well as hydrogen gas (H_2), carbon dioxide (CO_2), and ammonia (NH_3)[7]. The conversion process described above is primarily carried out by fermentative microorganisms. The specific end products resulting from this process are influenced by the conditions present in the reactor medium. For example, if hydrogen gas (H_2) is effectively removed from the system by organisms known as H_2-scavenging organisms, such as methanogens, acetate will be the predominant end product.[1]. In situations where the process of methanogenesis is hindered and hydrogen gas (H_2) starts to accumulate, the formation of more reduced end products, such as propionate and butyrate, becomes more likely. This occurs when the conversion of intermediates is affected, resulting in the production of acidic byproducts. Consequently, when anaerobic reactors are overloaded or experience disturbances, the effluents may contain these more reduced intermediate compounds and exhibit increased acidity.[1]. Among the products of acidogenesis, namely hydrogen, carbon dioxide, and acetic acid, some bypass the acetogenesis process and are directly utilized by the methanogenic microorganisms in the final stage, as illustrated in Figure 2.3. Equations (2.2) and (2.3) depict common acidogenic reactions in which glucose is converted into acetic acid and propionate, respectively [7,13].

$$C_6H_{12}O_6 + 2H_2O \rightarrow 2CH_3COOH + 2CO_2 + 4H_2 \qquad\qquad \text{Eq (2.2)}$$
$$C_6H_{12}O6 + 2H_2 \rightarrow 2CH_3CH_2COOH + 2H_2O \qquad\qquad \text{Eq (2.3)}$$

During the third stage of AD, the short-chain fatty acids (SCFAs), excluding acetate produced in the acidogenesis steps, undergo further conversion by acetogenic bacteria. As depicted in Figure. 2.3, these bacteria transform SCFAs into acetic acid, carbon dioxide, and hydrogen. There are two types of acetogenic bacteria involved in this process: hydrogen-producing acetogens and homoacetogens.[6]. Equations (2.4) and (2.5) demonstrate the generation of acetic acid from butyrate and propionate, respectively, through the involvement of hydrogen-producing bacteria. These reactions showcase the conversion of these specific compounds into acetic acid with the assistance of bacteria capable of producing hydrogen[7]. Homoacetogenesis refers to the process where acetic acid is produced from dissolved hydrogen (H_2) and carbon dioxide (CO_2) by homoacetogens, as illustrated in Equation (2.6).

$$CH_3CH_2CH_2COOH + 4H_2O \rightarrow CH_3COOH + 2CO_2 + 6H_2 \qquad\qquad \text{Eq (2.4)}$$
$$CH_3CH_2COOH + 2H_2O \rightarrow CH_3COOH + CO_2 + 3H_2 \qquad\qquad \text{Eq (2.5)}$$
$$2CO_2 + 4H_2 \rightarrow CH_3COOH + 2H_2O \qquad\qquad \text{Eq (2.6)}$$
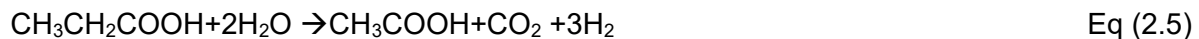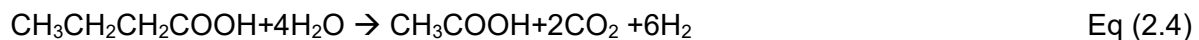
Methanogenesis

During the ultimate phase of anaerobic breakdown of organic material, methanogenic bacteria facilitate the production of methane and carbon dioxide. In this final step, a set of methanogenic archaea utilize hydrogen as an electron donor to reduce carbon dioxide and also convert acetate into CH_4 through decarboxylation.[6]. In this phase, the incoming COD transforms into a gaseous state, which naturally exits the reactor system. Methanogens are strictly anaerobic, possessing a limited range of substrates they can utilize. Some are specific to particular substrates like acetate, methylamines, methanol, formate, and H_2/CO_2 or CO[1].

For engineering purposes, methanogens are classified into two major groups: the acetate converting or aceticlastic methanogens and the hydrogen utilising or hydrogenotrophic

methanogens (Table 2.3). The conclusive phase of AD is acetoclastic methanogenesis, where acetic acid undergoes conversion into CH_4 and CO_2 through the action of a group of archaea referred to as acetoclastic methanogens. These methanogens are responsible for approximately two-thirds of methane production, as demonstrated in Equation (2.7)[7]. The growth rate of the aceticlastic methanogens is very low, resulting in doubling times of several days or even more. The extremely low growth rates explain why anaerobic reactors require a very longstart-up time with unadapted seed material and why high sludge concentrations are pursued. Hydrogenotrophic bacteria have a much higher maximum growth rate than the acetoclastic bacteria with doubling times of 4 to12 hours. Because of this feature and despite the very delicate acetogenic reaction step discussed in the previous section, anaerobic high-rate reactor systems exert a remarkable stability under varying conditions[1].

The remaining one-third of methane is produced through hydrogenotrophic methanogenesis, where a group of slow-growing hydrogenotrophic methanogens convert dissolved H_2 and CO_2 into CH_4. This process, as illustrated in Equation (2.8), involves the utilization of hydrogen by the methanogens to generate methane[7].

Table 2.3 lists two types of aceticlastic methanogens with very different kinetic characteristics

Table 2. 3: Most important methanogenic reactions, the corresponding free energy change and some kinetic properties[1]

Functional step	Reaction	ΔG Kj/mol	μmax 1/d	Td d	Ks mgCOD/l	Eq
Acetotrophic methanogenesis	$CH_3COOH \rightarrow CH_4 + CO_2$	-31	0.12[a] 0.71[b]	5.8[a] 1.0[b]	30[a] 300[b]	(2.7)
Hydrogenotrophic methanogenesis	$CO_2 + 4H_2 \rightarrow CH_4 + 2H_2O$	-131	2.85	0.2	0.06	(2.8)

[a]Methanosarcina spec. and [b]Methanosaeta spec.

Also, the morphological characteristics of both methanogenic genera are very different as indicated by Figure 2.5.
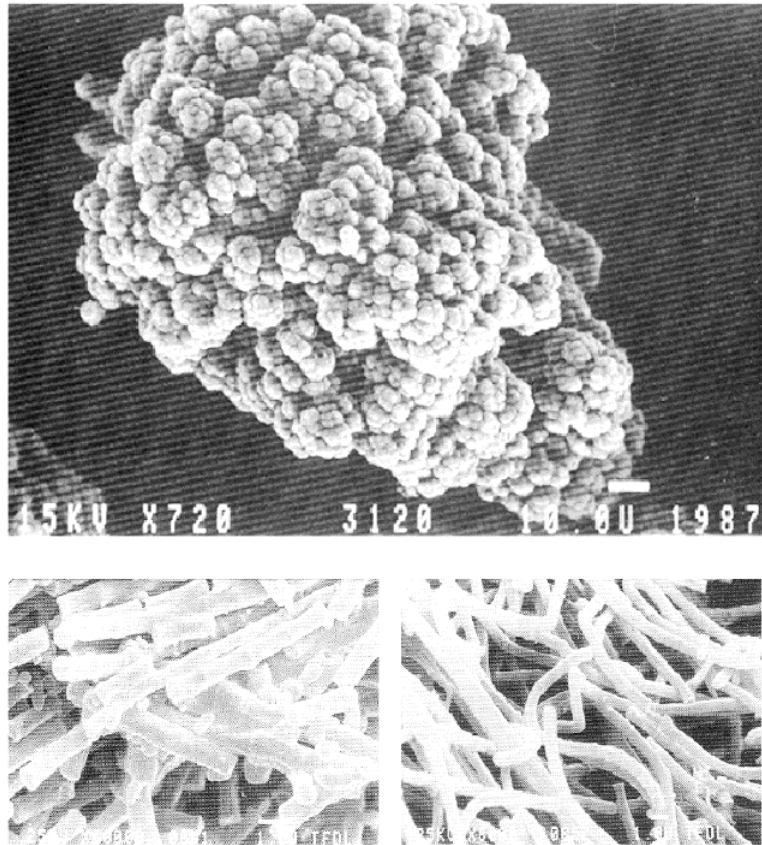
Figure 2. 5: Morphology and appearance of the most important acetotrophic methanogens belonging to the genera Methanosarcina (above) and Methanosaeta (below) [1]

Methanosarcina species have a coccoid shape, forming small grape-like clusters. They can process a variety of substrates including acetate, H_2/CO_2, methylamines, methanol, and formate, and exhibit a high maximum growth rate ('max) but low substrate affinity. In contrast, Methanosaeta species are filamentous, resembling large spaghetti-like aggregates. Their primary substrate is acetate, and they demonstrate a low 'max but very high substrate affinity. Even though Methanosaeta species grow slower, they dominate in anaerobic high-rate systems like sludge bed systems and anaerobic filters. This prevalence is because wastewater treatments prioritize low effluent concentrations. When concentrations inside biofilms or granules drop, Methanosaeta species have a kinetic advantage over Methanosarcina due to their high substrate affinity[1](Figure 2.6).
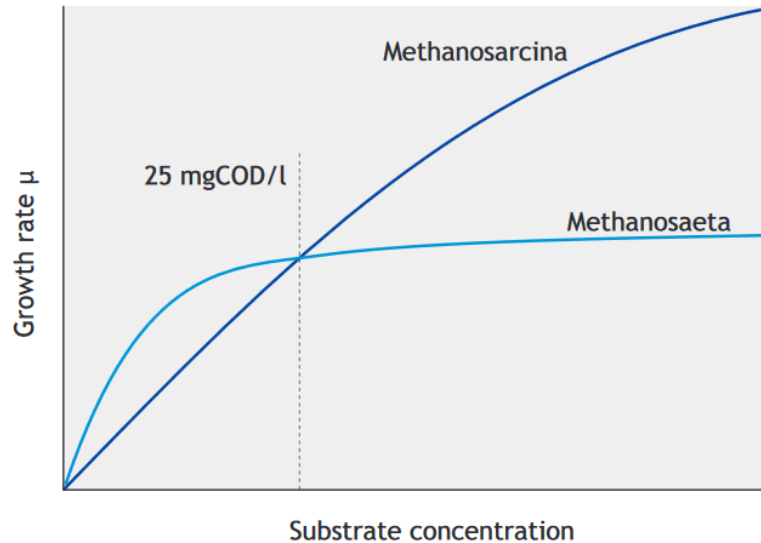
Figure 2. 6 Monod growth curves of the acetotrophic methanogens Methanosarcina spp. and Methanosaeta spp. Both 'max and the Monod half saturation constant (Ks) of both genera [1]

In the presence of elevated concentrations of sulphate, methanogenic microorganisms can engage in competition with sulphate-reducing microorganisms[14].

2.3 Environmental factors affecting anaerobic processes.

The rates of the four sub-processes within the system vary depending on the operating conditions and substrate concentration. As a result, the overall rate of stabilization is constrained by the slowest step, also known as the rate-limiting step. This rate-limiting step can shift from one sub-process to another over time, depending on the characteristics of the substrate being processed[15,16]. When dealing with wastewater with a high concentration of solid content, it becomes necessary to initiate an initial hydrolysis step to transform particulate matter into a soluble substrate, which is crucial for achieving efficient AD. The effectiveness of this hydrolysis step is significantly influenced by temperature, particularly in conditions where low temperatures prevail. As a result, the hydrolysis step often serves as the rate-limiting step under such low-temperature circumstances[17,18].

In cases where the waste consists primarily of dissolved organic matter, the rate-limiting steps are typically acetogenesis and methanogenesis. The groups of bacteria involved, exhibit slower growth rates compared to other AD processes. Consequently, the acetogenesis and methanogenesis stages become the key limiting factors in the overall rate of stabilization within

the system[12,17]. Microorganisms themselves largely govern the control of AD processes. They possess the ability to regulate and adjust their activities based on the prevailing environmental conditions. Factors such as temperature, pH levels, availability of essential trace nutrients, and the presence of toxic substances significantly impact the reaction rates of individual sub-processes. Therefore, these environmental conditions play a crucial role in modifying and influencing the overall rates of the AD reactions[17,19]. The International Water Association (IWA) task group responsible for the mathematical modeling of AD processes has established two distinct categories of inhibition concerning microorganisms: biocidal and biostatic inhibition. Biocidal inhibition refers to the toxic effects that irreversibly harm microorganisms, preventing their survival or growth under the given conditions. On the other hand, biostatic inhibition occurs when the growth of microbes temporarily ceases when exposed to inhibitory conditions but resumes once the conditions improve or return to normal[20].

2.3.1 Thermodynamic Reactions

Thermodynamics play a vital role in comprehending the dynamics of anaerobic metabolism. It is important to note that reactions with a positive net free energy change (ΔG) are not feasible. Figure 2.7 illustrates the free energy changes associated with various fermentation reactions. In the absence of nitrate and sulfate, which is typical in most anaerobic digesters, the only respiratory reactions observed involve the conversion of bicarbonate to methane or acetate. Among these reactions, the reduction of glucose to propionate exhibits the most negative value in terms of free energy change. However, it is worth noting that the conversion of propionate to acetate and hydrogen is considered the most challenging reaction [21]. Hydrogen, acting as a crucial intermediate in the AD process, necessitates low partial pressure to proceed in several reactions where it is produced. To ensure the thermodynamic feasibility and completion of reactions producing hydrogen, the presence of hydrogen scavengers like HMB (hydrogen-consuming microorganisms) becomes indispensable.

If inorganic oxidants, such as Fe^{3+} salts, are present in the medium, they can also contribute to the removal of hydrogen. Furthermore, the partial pressure of hydrogen plays a significant role in the process of anaerobic degradation. Thermodynamically, the ΔG value is directly related to the activities of the species involved in the reaction (Eq. 2.9).

$$\Delta G = \Delta Go + RT \ln [\text{'Equilibrium-constant-like expression'}] \qquad \text{Eq (2.9)}$$

Where:

ΔGo = free energy /mole of species at standard state conditions,

T= absolute temperature (°K),

The expression resembling an equilibrium constant involves the present activities of the reaction products, each raised to the power corresponding to its stoichiometric coefficient, in the numerator. Conversely, the present activities of the reactants, raised to the appropriate powers, are found in the denominator. In the case of gaseous components, their activity is quantified by their partial pressure in the reaction medium.

When plotting the ΔG values of oxidations 1–4 and respirative reactions 13–15 (Table 2.4) against the logarithm of the partial hydrogen pressure on a logarithmic scale, a series of linear plots is observed, as demonstrated in Figure 2.7. Reactions 1–4 exhibit a negative slope in the graph, while reactions 13–15 display a positive slope (Table 2.3).

Consequently, the region where the reactions are thermodynamically feasible, indicated by negative ΔG values, is limited to a narrow range of low hydrogen partial pressure values. Therefore, monitoring hydrogen partial pressure becomes an essential indicator of the status and effectiveness of the AD process.
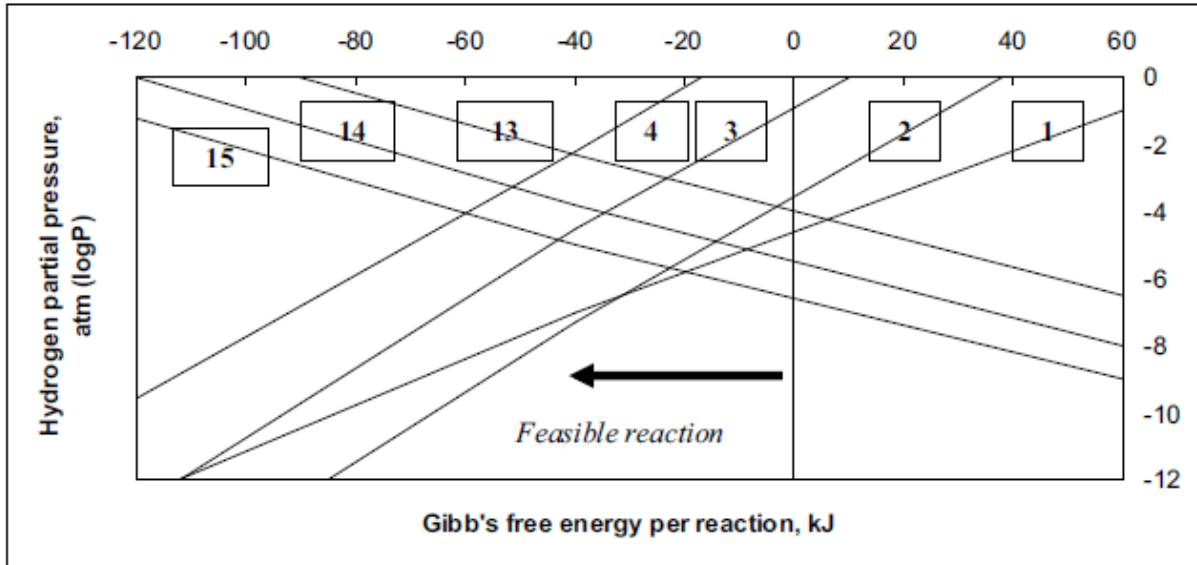
Figure 2. 7:The thermodynamic feasibility of various reactions within the anaerobic digestion process is influenced by hydrogen partial pressure 24These reactions include: (1) Oxidation of propionic acid to acetic acid. (2) Oxidation of butyric acid to acetic acid. (3) Oxidation of ethanol to acetic acid. (4) Oxidation of lactic acid to acetic acid. (13) Acetogenic respiration of bicarbonate. (14) Methanogenic respiration of bicarbonate. (15) Respiration of sulfate to sulfide.[22]

Table 2. 4 :Free energy values for some key AD bioreactions[22]

	Reaction	ΔG_o, kJ
Oxidations (electron-donating reactions)		
1 Propionate → Acetate	$CH_3CH_2COO^- + 3H_2O \rightarrow CH_3COO^- + H^+ + HCO_3^- + 3H_2$	+76.1
2 Butyrate → Acetate	$CH_3CH_2CH_2COO^- + 2H_2O \rightarrow 2CH_3COO^- + H^+ + 2H_2$	+48.1
3 Ethanol →Acetate	$CH_3CH_2OH + H_2O \rightarrow CH_3COO^- + H^+ + 2H_2$	+9.6
4 Lactate →Acetate	$CHCHOHCOO^- + 2H_2O \rightarrow CH_3COO^- + HCO_3 + H^+ + 2H_2$	-4.2
5 Lactate →Propionate	$3CHCHOHCOO^- \rightarrow 2CH_3CH_2COO^- + CH_3COO^- + H^+ + HCO_3^-$	-165
6 Lactate →Butyrate	$2CHCHOHCOO^- + 2H_2O \rightarrow CH_3CH_2CH_2COO^- + 2HCO_3^- + 2H_2$	-56
7 Acetate → Methane	$CH_3COO^- + H_2O \rightarrow HCO_3^- + CH_4$	-31
8 Glucose → Acetate	$C_6H_{12}O_6 + 4H_2O \rightarrow 2CH_3COO^- + 2HCO_3^- + 4H^+ + 4H_2$	-206
9 Glucose → Ethanol	$C_6H_{12}O_6 + 2H_2O \rightarrow 2CH_3CH_2OH + 2HCO_3^- + 2H^+$	-226
10 Glucose →Lactate	$C_6H_{12}O_6 \rightarrow 2CHCHOHCOO- + 2H^+$	-198
11 Glucose →Propionate	$C_6H_{12}O_6 + 2H_2 \rightarrow 2CH_3CH_2COO^- + 2H_2O + 2H^+$	-358
Respirative (electron-accepting reactions)		
12 HCO_3^- →Acetate	$2HCO_3^- + 4H_2 + H^+ \rightarrow CH_3COO^- + 4H_2O$	-104.6
13 HCO_3^- → Methane	$HCO_3^- + 4H_2 + H^+ \rightarrow CH_4 + 3H_2O$	-135.6
14 Sulphate →Sulfide	$SO_4^{2-} + 4H_2 + H^+ \rightarrow HS^- + 4H_2O$	-151.9
	$CH_3COO^- + SO_4^{2-} + H^+ \rightarrow 2HCO_3^- + H_2S$	-59.9
15 Nitrate →Ammonia	$NO_3^- + 4H_2 + 2H^+ \rightarrow NH_4^+ + 3H_2O$	-599.6
	$CH_3COO^- + NO^- + H^+ + H_2O \rightarrow 2HCO_3^- + NH_4^+$	-511.4
16 Nitrate →Nitrogen gas	$2NO_3^- + 5H_2 + 2H^+ \rightarrow N_2 + 6H_2O$	-1120.5

Below, the factors that can cause inhibition in anaerobic digestion are discussed:

Volatile Fatty Acids, Alkalinity, and pH

The buffering capacity and pH values of an anaerobic system are influenced by the concentrations of volatile fatty acids, alkalinity, and ammonia, making them dependent variables. However, among these variables, pH holds utmost significance in anaerobic digesters. It is considered the most crucial parameter to regulate and control as it directly reflects the stability of the system. Monitoring and maintaining the appropriate pH level serves as an essential indicator for assessing the overall health and operational performance of the anaerobic digestion process[23,24]. The optimum pH for anaerobic digestion is typically reported to be around neutral. This neutral pH range is favored as it promotes higher yields in most biochemical processes. By maintaining a neutral pH level, the conditions are optimized for the efficient performance of anaerobic digestion.[25]

Acetoclastic methanogenesis, a key process in anaerobic digestion, is highly sensitive to low-pH conditions. If the pH drops below 6.5, it quickly becomes inhibited, jeopardizing the overall efficiency of the process[1]. This inhibition hinders the removal of acids from the system, interrupting the overall process. Souring occurs when there is an elevation in the rate of acid production, typically caused by a high organic loading rate, coupled with a decrease in the rate of acid removal due to a reduction in buffering capacity. This imbalance between acid production and removal results in a decrease in pH, leading to the occurrence of souring. Souring arises when the acid-producing rate exceeds the system's ability to effectively remove acids, leading to a pH drop below the desired range. This condition adversely affects acetoclastic methanogenesis and disrupts the overall anaerobic digestion process. To prevent souring, it is crucial to manage and balance the acid-producing and acid-removing rates, ensuring sufficient buffering capacity to maintain a stable and favorable pH level. In the process of biogas production, three primary types of bacteria are involved: hydrolytic bacteria, fermentative bacteria, and methane-producing archaea. The fermentative bacteria, specifically, are capable of functioning within a pH range of 8.5 to 4, with their optimal pH range being 5.0 to 6.0 [26]. On the contrary, methanogenic archaea are capable of functioning within a pH range spanning from 5.5 to 8.5, with their optimal range falling between 6.5 and 8.0. Inhibition of pH occurs when homeostasis is disrupted, leading to elevated levels of

non-dissociated volatile fatty acids (VFA) [20]. Under normal conditions, methane-producing bacteria generate bicarbonate, which helps neutralize the pH decrease caused by acid-producing bacteria[20,27].

While pH is an important parameter in anaerobic digestion, its value is primarily influenced by the buffering capacity of the system. The pH is not solely determined by the anaerobic digestion process itself but is affected by various other reactions occurring within the system. Therefore, it cannot be solely relied upon as the sole indicator of process stability. The buffering capacity of the system, which is influenced by factors such as the concentrations of volatile fatty acids, alkalinity, and ammonia, plays a crucial role in maintaining a stable pH. Hence, a comprehensive assessment of multiple parameters is necessary to evaluate the stability and performance of the anaerobic digestion process.

The primary risk leading to digester failure is the accumulation of acids, which can occur when there is a sudden increase in the loading of volatile solids into the digester. This increase promotes the growth of acidogenic bacteria, causing them to produce large quantities of organic acids and further lowering the pH below 5.0, which is detrimental to methanogens. Conversely, pH values above 8 are toxic to most anaerobic organisms, inhibiting their biological functions. High pH levels may arise from excessive methanogenesis, which leads to a higher concentration of ammonia that hampers acidogenesis. This issue can be mitigated by introducing a larger quantity of fresh feedstock, which can counterbalance the acid accumulation.

The alkalinity of the medium, which determines its capacity to withstand pH changes, is influenced by the presence of hydroxides, carbonates, and bicarbonates.

In an imbalanced system where, VFAs accumulate due to the limited growth capacity of methanogens, the alkalinity of the medium becomes crucial for maintaining pH values close to neutral and preventing potential system failure. The concentration of VFAs is commonly regarded as a process indicator since it serves as the primary pre-methanogenic intermediate[28,29].

During an imbalanced development of the trophic chain, volatile fatty acids, acting as the primary intermediate compounds preceding methanogenesis, tend to accumulate. This accumulation eventually results in a pH decrease, influenced by both the concentrations of volatile fatty acids and the alkalinity of the system. VFAs can exert a toxic effect on microorganisms, with undissociated species being particularly reported as more harmful. This increased toxicity is

attributed to their ability to diffuse into the inner regions of the cell. Among the volatile fatty acids, propionic and butyric acid are identified as the most inhibitory.

During an imbalanced development of the trophic chain, VFAS, acting as the primary intermediate compounds preceding methanogenesis, tend to accumulate. This accumulation eventually results in a pH decrease, influenced by both the concentrations of volatile fatty acids and the alkalinity of the system. VFAs can exert a toxic effect on microorganisms, with undissociated species being particularly reported as more harmful. This increased toxicity is attributed to their ability to diffuse into the inner regions of the cell. Among the volatile fatty acids, propionic and butyric acid are identified as the most inhibitory[22]. In this perspective, the VFAs to alkalinity ratio is frequently regarded as a reliable indicator of process stability, with values ranging between 0.4 and 0.8 considered favorable[30,31].

Temperature

Anaerobic digestion can operate within a wide temperature range, spanning from psychrophilic temperatures around 10 °C to extreme thermophilic temperatures exceeding 70 °C [32,33].

The temperature exerts significant influence on anaerobic reactions, impacting both their kinetics and thermodynamics. Specifically, the process of methanogenesis is highly sensitive to temperature, with degradation rates and yields typically increasing as temperature rises. Figure. 2.8 illustrates a diagram correlating the rate of the anaerobic digestion process with temperature. As depicted, the relative growth rates of thermophilic methanogens surpass those of psychrophilic and mesophilic strains by a significant margin. As a result, two optimal temperature ranges with maximum activity have been identified: mesophilic (approximately 35 °C) and thermophilic (around 55 °C)
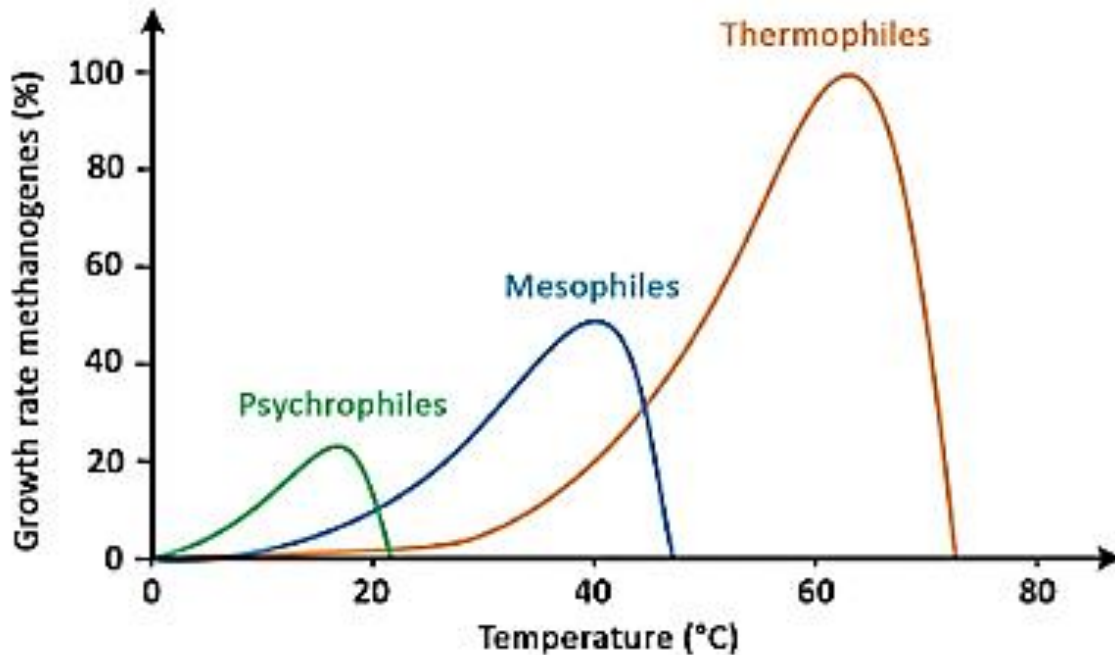
Figure 2. 8 :The temperature ranges for optimal anaerobic digestion are generally observed at mesophilic temperatures, typically around 30-35 °C, and thermophilic temperatures, ranging from 55-60 °C[34]

Industrial AD installations typically operate within the temperature range of 30-42°C. Mesophilic digestion is favored due to its ability to achieve high biogas production while maintaining process stability. It is crucial to maintain a consistent temperature level in the reactors to ensure a stable AD process, as methanogens are highly sensitive to temperature fluctuations[35].

It is crucial to control temperature fluctuations within the digestion chamber to ensure maximum biogas production. Ideally, the daily temperature variations should not exceed 2°C, as higher fluctuations can lead to a significant decrease of up to 30% in biogas production. In the case of thermophilic anaerobic digestion, which operates at temperatures between 50-55°C, there is a heightened sensitivity to changes in operating parameters. It is well established that biochemical processes exhibit enhanced speed and efficiency at elevated temperatures[36]. The relationship between higher temperatures and increased reaction rates can be mathematically expressed using an Arrhenius type equation (Equation 2.10):

$$r_T = r_{20 * \theta^{(T-20)}}$$ Eq (2.10)

Where:

T=temperature (°C),

r=reaction rate at T,

r_{20}=reaction rate at 20°C, and

θ=temperature-activity coefficient.

Table 2.5 provides a comparison of the maximum growth rates of various mesophiles and thermophiles, revealing that the values are typically higher for thermophiles compared to mesophiles.

Table 2. 5 :Comparison of maximum growth rates of mesophiles and thermophiles[1]

Substrate	Genus	Mesophiles (μmax/day)	Thermophiles (μmax/day)
H_2/CO_2	Methanobacerium	0.26	4.80-16.6
	Methanococcus	2.16-5.52	18.2-51.1
	Methanosarcina	0.48-1.44	NA
	Methanobrevibacter	1.44-4.08	NA
Formate	Methanobacerium	1.44-1.92	13.4
Acetate	Methanothrix	0.10-0.22	0.48-0.72
	Methanosarcina	0.24-0.67	1.27-2.04
Propionate	Syntrophobacter	0.10-0.14	0.14-0.31
Butyrate	Syntrophomonas	0.36	0.48-0.77

Elevated temperatures also contribute to the reduction in parameters such as viscosity and surface tension of liquids, facilitating easier mass transport within the bioreactor and promoting enhanced degradation of organic compounds[37] . However, it is essential to recognize that the temperature within the digestion chamber cannot be increased indefinitely, as there is a limit to the biodegradation capacity of organic matter. Excessive temperatures can lead to the denaturation of biologically active protein structures. Considering these limitations imposed by biological processes, it is advisable to maintain the temperature below 55°C. However, it should be noted that for hydrolytic bacteria involved in acid production, temperature is not a significant constraint as these bacteria possess the ability to adapt to new conditions quite readily. In contrast, temperature is a critical parameter for methanogenic bacteria, as their enzymes are

highly sensitive to temperature fluctuations and generally exhibit lower tolerance to high temperatures.

The effect of low temperature on anaerobic biological conversion is significant. Microorganisms are categorized into temperature classes based on their optimal temperature and the range within which they can grow and metabolize. The overlapping temperature ranges in Figure 2.8 indicate that there is no clear distinction between psychrophilic, mesophilic, and thermophilic microorganisms. While the growth rates of methanogenic thermophiles and mesophiles in anaerobic reactors are well-established, only a few psychrophilic methanogenic bacteria from specific cold environments and psychrotrophic acetogenic bacteria from natural sediments have been isolated. This scarcity of knowledge about anaerobic reactors operating under psychrophilic conditions highlights the limited understanding in this area.

Under psychrophilic conditions, both chemical and biological reactions occur at a much slower pace compared to mesophilic conditions. Most reactions involved in the biodegradation of organic matter require more energy to proceed at low temperatures than at the optimal temperature of 37°C. However, there are a few exceptions, such as hydrogenotrophic sulfate reduction, hydrogenotrophic methane production, and acetate formation from hydrogen and bicarbonate, which require less energy at lower temperatures.

Multiple researchers have observed a significant influence of temperature on the maximum rates at which microorganisms utilize substrates[38–47]. Generally, reducing the operational temperature results in a decline in the maximum specific growth and substrate utilization rates. However, it can also lead to an augmented net biomass yield (grams of biomass per gram of substrate converted) for methanogenic populations or acidogenic sludge[48,49].

Solid waste digestion, the process of breaking down waste materials, is commonly done at two temperature ranges: mesophilic (around 30-35 ºC) and thermophilic (around 55-60 ºC). Thermophilic temperatures are known to result in higher yields and increased production of biogas. However, it's important to consider the trade-off between this energy surplus and the additional energy required for heating the feed. Before deciding on the temperature range, factors such as substrate concentration, yields, and kinetics should be carefully evaluated to make an informed decision[22].

In conclusion, it can be stated that while thermophilic temperatures generally offer more favorable biogas production yields and bioreaction kinetics, the optimal conditions for anaerobic digestion

depend on factors such as substrate type, concentration, biodegradability, and the specific system utilized.

Carbon and nutrients

Vitamins, macro- and micro-nutrients are essential for optimal functioning of anaerobic microorganisms in degradative processes. While most substrates contain enough necessary nutrients, long-term operation of anaerobic digesters with the same feedstock, particularly energy crops or vegetable residues, may result in a deficiency of essential micronutrients [50]. The fundamental nutrient requirements include carbon, phosphorous, and nitrogen, with nitrogen being the most crucial and potentially limiting element for bacterial growth and reproduction. Additionally, microorganisms rely on trace amounts of light metals like potassium, calcium, and magnesium to maintain cell membrane integrity and regulate osmotic pressure [51]. Healthy digesters typically contain traces of heavy metals such as iron, zinc, cobalt, nickel, or tungsten, which sustain microbial metabolism [52,53]. Other essential components, such as vitamins, amino acids, purines, and pyrimidines, may also be required to enhance microbial activity [51].

Organic carbon and nitrogen serve as the basis of biodegradable substrates. However, certain microelements necessary for digestion may not be present in sufficient quantities when a single source of feedstock is used. Therefore, these missing microelements are added as process additives. However, the addition of nutrients should be carefully planned due to the costs involved and the potential toxicity of additives beyond a certain threshold level, which may not necessarily improve system efficiency [22,54].

Anaerobic digestion processes require various substances, both organic and inorganic, for optimal operation. Apart from the obvious presence of organic carbon for degradation, nutrients such as phosphorus, nitrogen, sulfur, vitamins, and traces of minerals (such as iron, nickel, magnesium, calcium, sodium, barium, tungsten, molybdenum, selenium, and cobalt) are necessary. These micronutrients, when present in small quantities, can stimulate microbial growth, but exceeding a certain threshold level can become inhibitory.

While the low biomass production yield of anaerobic processes is generally sustained by the nutrients and micronutrients present in the waste, it is crucial to assess their availability, as deficits in these compounds can occur. As nutrients and micronutrients are necessary for synthesizing cellular matter, their quantitative requirement depends on the operating conditions of the digester.

Empirically, based on the representative formula $C_5H_9O_3N$ for proteinic matter, the COD/N ratio is estimated to be 11/4. Similarly, the P/N ratio for cellular matter ranges from 1/5 to 1/7. Considering cellular matter production yields and digester load, COD/N ratios between 400/7 (high load) and 1000/7 (low load) have been reported. Consequently, an average ratio of COD/N/P around 600/7/1 is recommended for substrates undergoing anaerobic digestion. [22,55,56]

Toxic compounds

A vast array of substances can hinder the effectiveness of anaerobic digestion by exerting a negative impact on the microbial community when their concentrations surpass a certain threshold. The literature extensively reports a variety of common inhibitors in this context, including ammonia, sulfide, long chain fatty acids, salts, heavy metals, phenolic compounds, and xenobiotics.[22,57]

The compounds can be categorized into two groups: toxic substances (toxicants) that have a negative impact on microorganisms without necessarily causing lethality, and inhibitors that impair bacterial function by affecting specific targets or overall cellular kinetics and functions. Examples of toxicants include long chain fatty acids, nitro-compounds, and antibiotics, while inhibitors encompass hydrogen sulfide, ammonia, and volatile fatty acids[20].

At lower concentrations, most inhibitors typically exert a stimulating influence on the overall biodegradation process. However, as their concentration increases, these substances reach a toxic level that depends on environmental factors, operational parameters, and the adaptation capacity of the biomass.

The phenomenon of inhibition is represented by different phases in Figure 2.9. However, there are certain compounds that exhibit an immediate and irreversible lethal effect on a wide range of microorganisms, categorizing them as biocides. Within this classification, xenobiotics and specific phenolic compounds are included due to their utilization for antiseptic and disinfectant purposes[58]. To mitigate the impact of inhibitors, various strategies can be employed. One approach involves adapting the microbial consortium to enhance its tolerance towards the inhibitors. Another strategy is co-digestion, which involves diluting the substrate to reduce the concentration of inhibitors introduced into the system. By implementing these measures, the overall effect of inhibitors can be minimized[59].
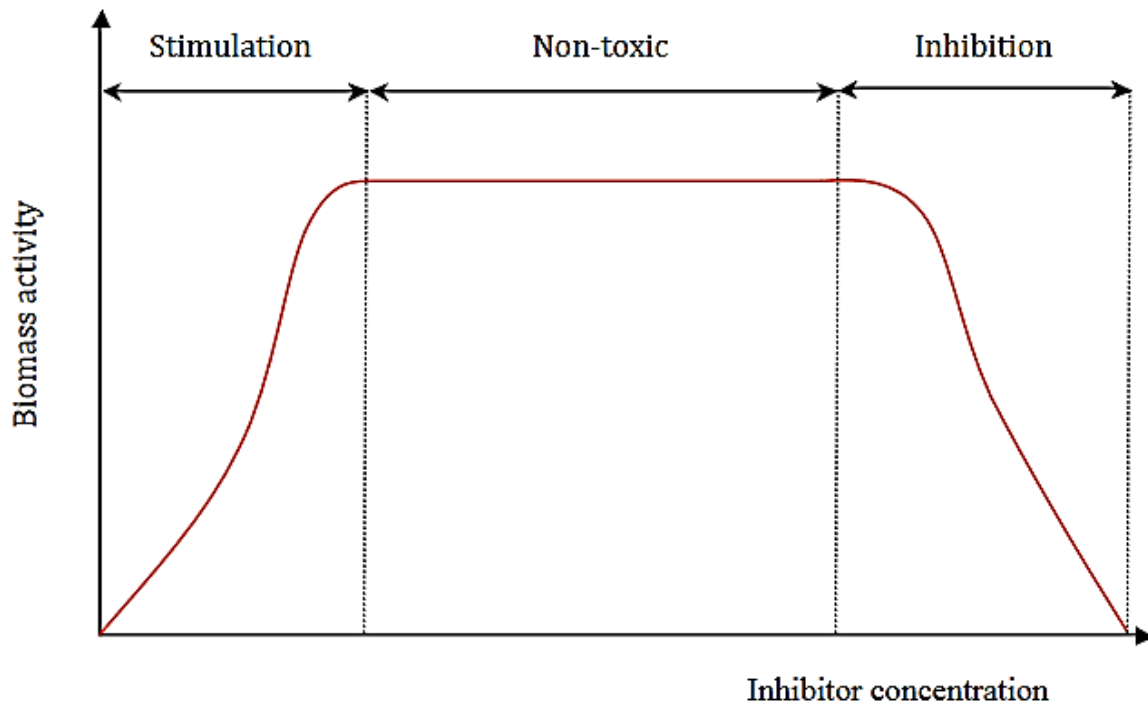
Figure 2. 9: Schematic representation of the inhibition phenomenon[60]

Ammonia and ammonium are naturally present in anaerobic digesters as byproducts of the biological breakdown of nitrogen-containing substances. The non-ionized form of ammonia (NH_3) is generally regarded as more toxic compared to the ammonium ion (NH_4^+), primarily because NH_3 can freely permeate cell membranes[57,61].

The concentration of ammonia is influenced by the pH of the system, as the abundance of hydrogen ions determines the predominant form it takes. Additionally, temperature plays a role in ammonia concentration due to its effect on gas solubility coefficients, considering that ammonia is also present in gaseous form. It is commonly understood that anaerobic digestion benefits from lower levels of ammonia, as nitrogen is an essential nutrient for microorganisms involved in the process. Nevertheless, when ammonia concentrations reach high levels, it starts to inhibit microbial growth, with methanogens being particularly vulnerable to its detrimental effects[31,62–66]. More specifically, Table 2.6 summarizes the concentrations at which ammonia are beneficial, inhibitory or toxic to the AD process

Table 2. 6: Effect of ammonia levels on the anaerobic digestion process.

Effect on AD process	Ammonia (mg NH₄-N/L)	References
Beneficial	50–200	[67]
No antagonistic effect (especially at higher pH values)	200–1000	[68]
Inhibition (especially at higher pH values)	1500–3000	[69]
Complete inhibition or toxic at any pH	>3000	[70]

The methanogenic bacteria that utilize acetate display higher sensitivity to ammonia compared to those that utilize hydrogen[71]. Ammonia inhibition operates through two distinct mechanisms. Firstly, methanogens are directly impeded by the presence of free ammonia. Secondly, free ammonia rapidly converts into ammonium ions within the bacterial cell wall, as depicted in Equation (2.11) [72]

$$NH_3 + H_2O \rightarrow NH_4^+ + H_2O \hspace{3cm} Eq\ (2.11)$$

When sulphur-rich substrates are degraded in an anaerobic digester, the resulting sulphides can reach inhibitory concentrations. The inhibitory effect of sulphides is typically observed in two stages. In the primary stage, sulphate-reducing bacteria and methanogens compete for carbonaceous substrates, affecting both methane production and the sulphide concentration in the system [57]. The outcome of this competition determines the second stage, characterized by sulphide toxicity towards a wide range of microorganisms [20]. Among the various forms, hydrogen sulphide (H_2S) is the most toxic to the microbial consortium and can also exist in the gas phase.

Sulfide tolerance varies considerably among different microbial groups involved in anaerobic digestion. It is reported that sulfate-reducing bacteria (SRB) growing on acetate and ethanol remained unaffected by sulfide levels as high as approximately 1300 mg/L H_2S[73]. Furthermore, it is also observed that sulfate removal rates even increased with total sulfide concentrations, reaching up to 1424 mg/L, when ethanol and sugar were used as substrates[73].

Conversely, methanogens displayed a marked sensitivity to sulfide. Parkin et al. (1983) highlighted that sulfide concentrations as low as 50 mg/L were toxic to unacclimated methanogens[74]. In line with this, Yamaguchi et al. (1999) determined the IC50 values for H_2S with acetotrophic methanogens at 160 mg/L and for hydrogenotrophic methanogens at 220 mg/L, respectively[75].

Light metal salts, such as sodium, calcium, potassium, and magnesium, are commonly present in anaerobic digesters. They can originate from the decomposition of organic matter or be intentionally added for pH regulation purposes [57]. In anaerobic systems, small amounts of these light metals are necessary to stimulate bacterial growth and optimize the process[22]. However, excessive levels of these metals can lead to significant inhibition of microbial activity [76].

The buildup of salts in anaerobic digesters has a detrimental effect on microorganisms. This is primarily due to the significant elevation of osmotic pressure, which disrupts the regulation of water flow across the cell membrane and can ultimately result in cell death. The levels at which salts become inhibitory depend on the ability of the bacterial consortium to adapt and the synergistic effects resulting from the presence of other cations [77–79].

Similarly, certain heavy metals such as chromium, cobalt, iron, zinc, or nickel can be found in substrates at concentrations that can have toxic effects due to their interference with enzyme function and structural integrity [57]. Table 2.7 illustrates the trace heavy metals that can promote biogas and methane production, while excessive amounts can cause inhibition.

Table 2. 7: Effects and mechanisms of heavy metals on anaerobic digestion

Heavy metals	Influencing Factors	Biogas yield		Methane content		Reference
		Promoting concentration	Inhibitory concentration	Promoting concentration	Inhibitory concentration	
Cu	methanogenic activity, cellulase activity, microbial community and VFA concentration	0-100 mg/L	500 mg/L	5 mg/L	130 mg/L	80,81
Ni	cellulase activity and methanogenic activity	0.8-50 mg/L	100 mg/L	0-20 mg/L	32 mg/L	82,83
Fe	cellulase activity	50-4000 mg/L	20000mg/L	0-1000 mg/L	20000 mg/L	84
Cd	methanogenic activity	0.1-0.3 mg/L	1.2 mg/L	-	1 mg/L	85,86
Zn	methanogenic activity	5mg/L	50 mg/L	0-100 mg/L	-	87

Phenolic compounds and long chain fatty acids belong to a group of organic substances that have the potential to inhibit microbial activity. Their inhibitory effects on microorganisms are attributed to their ability to interact with cell membranes, causing the leakage of intracellular components [58]. High molecular weight phenols inhibit extracellular microbial enzymes, disrupt microbial metabolism, or deplete essential substrates necessary for microbial growth [88]. Furthermore, there are other organic compounds with potential toxicity, including halogenated benzenes, chlorophenols, and N-substituted aromatics. These substances possess the ability to exert toxic effects on microorganisms.

Denitrification

In anaerobic treatment, the growth yield of denitrifying microorganisms per unit of substrate consumed surpasses that of methanogenic microorganisms. Moreover, these microorganisms compete for the same carbon and electron sources, such as acetate or H_2. Consequently, the presence of nitrate has a significant impact on microbial competition, leading to the inhibition of CH_4 production. The overall reduction of nitrate by acetic acid to produce N_2, as illustrated in Equation (2.12), as discussed by [20,89].

$$5CH_3COOH + 8NO_3^- + 8H_2 \rightarrow 4N_2 + 10CO_2 + 19H_2O \qquad \text{Eq (2.12)}$$

However, nitrates are seldom found in anaerobic treatment. This is primarily because nitrogen in untreated waste typically exists as ammonium or organic nitrogen. Additionally, there are no anaerobic processes known to produce nitrates.

Sulphate reduction

Sulphate-reducing bacteria (SRB) play a pivotal role in anaerobic systems, particularly in the sulphur cycle (Figure 2.10). Their primary function involves using sulphate (SO_4^{2-}) as a terminal electron acceptor in the degradation of organic matter[20]. This metabolic activity results in the formation of hydrogen sulphide (H_2S) as shown in Equations 2.13 and 2.14 [90]:

$$SO_4^- + 4H_2 \rightarrow H_2S + 2H_2O + 2OH^- \qquad \text{Eq (2.13)}$$

$$SO_4^- + CH_3COOH \rightarrow H_2S + 2HCO_3^- \qquad \text{Eq (2.14)}$$

This hydrogen sulphide can subsequently be oxidized in various manners:

1. Aerobically by chemolithotrophic sulphur-oxidizing bacteria (e.g., Thiobacillus or Beggiatoa spp.)
2. Anaerobically by phototrophic sulphur bacteria (e.g., Chlorobium spp.) to elemental sulphur $(S°)$ and SO_4^{2-}.

Other specialized microbial groups also conduct unique transformations in the sulfur cycle:

1. Sulphur reduction by species like Desulfuromonas spp.
2. Sulphur disproportionation via Desulfovibrio sulfodismutans.
3. Conversion of organic sulphur compounds, such as dimethylsulphoxide (DMSO) into dimethylsulphide (DMS) and vice versa.[91]
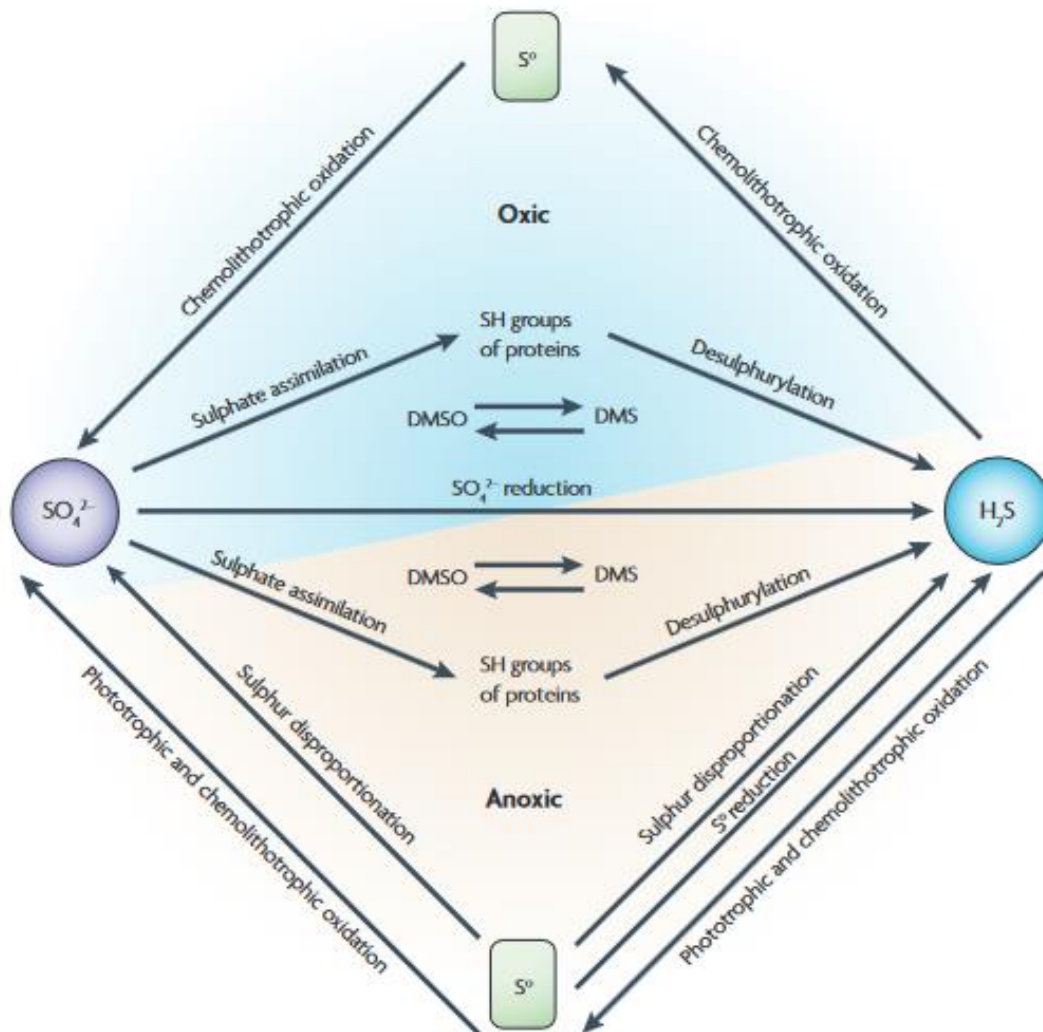
Figure 2. 10:Sulphur transformations[92].

The presence of SRB in anaerobic systems is complex due to the potential inhibitory effects of H_2S on various microbial groups and the competitive relationship between SRB and methanogens over common substrates. Typically, in environments with a high concentration of organic carbon but limited by sulphur, SRBs have an advantage and can outcompete methanogens. Conversely, in environments rich in sulphate, the metabolic pathways shift. The degradation of organic matter in such conditions differs substantially from methanogenic environments. It's crucial to note that methanogens, in comparison to SRB, utilize a limited range of substrates, with hydrogen, carbon dioxide, and acetate being the most significant.[91]

In diverse microbial communities, SRBs are often found near oxygen-consuming microbes. This proximity establishes niches where strict anaerobes, including SRBs, can thrive, further highlighting the interconnectedness of microbial metabolic pathways in anaerobic systems[93].

Organic loading rate and hydraulic retention time

The Organic Loading Rate (OLR) quantifies the influx of organic material per unit volume in the digester. It can be expressed using the equation: $OLR = \frac{Q*COD}{V}$

Here, Q represents the flow rate of the feed in cubic meters per day, COD represents the chemical oxygen demand in kilograms of COD per cubic meter (a measure of the organic material content in the substrate), and V denotes the volume of the reactor in cubic meters.

The OLR is influenced by the concentration of organic matter in the substrate, and its optimal value is determined through experimental investigation. If the OLR exceeds the optimal range, it can induce toxicity within the digester, resulting in a decline in methanogenic activity, as discussed later. Conversely, maintaining an OLR below the optimum level reduces the production of biogas.

HRT is a measure of the average duration that the substrate resides within the digester. It is crucial to allow sufficient time for the complete conversion of organic materials into biogas. However, a longer HRT necessitates a larger digester volume, as demonstrated by Equation (2.15):

  Digester volume (m^3) = HRT (day) × substrate input flow rate (m^3/day)   Eq (2.15)

This larger digester size results in increased capital costs associated with its construction[94].

The quantity of substrate being introduced in an anaerobic reactor during a given period of time is defined as the OLR of the system. It is mainly dependent on the type of substrate, but also on the reactor size, hydraulic retention time, and temperature. Careful consideration must be given to the amount of organic matter loaded into the system to maintain its stability. A rapid increase in the OLR is likely to result in the build-up of VFAs, which in turn might lead to process failure.

During the design phase of an anaerobic system, the organic loading rate and hydraulic retention time are defined as key parameters for determining the volume of a digester [95]. The HRT measures the period that a fluid element spends in an anaerobic digester. Its value should be a

compromise between the time necessary for the microbial consortium to degrade most of the organic matter and a period that should be short enough to guarantee a limited reactor volume and hence, reduce construction and maintenance costs. HRT should also be high enough to allow the active microbial populations to remain in the reactor, especially the slow-growing methanogens [96–98]. Therefore, the retention time is sometimes considered to be an indication of reactor efficiency [99].

The impact of a given inhibitory compound concentration applied at a low HRT would hence be greater when compared to the same concentration applied at high retention times due to the detrimental effect of most inhibitors on the growth rate of microorganisms [100].

2.4 Anaerobic Treatment Compared to Aerobic Treatment

2.4.1 Current technologies in WWTPs

The traditional activated sludge (CAS) method has been utilized for over a century to treat domestic wastewater, primarily transforming organic substances into biomass and carbon dioxide. Over time, adaptations and modifications to the CAS process have been made to address soluble nutrients like nitrogen and phosphorus in domestic wastewater. One notable example is the evolution of CAS into various biological nitrogen removal (BNR) techniques, with the most recent being the combination of short-cut nitrification and anaerobic ammonium oxidation (anammox) processes[101,102].

Recent advances suggest more efficient methods for nutrient removal. However, the CAS process's energy efficiency is a concern. For example, Singapore's Jurong Water Reclamation Plant reached only 35% efficiency, and China's Gaobeidian Plant achieved 31%[103]. Notably, the US uses about 3% of its annual electricity on wastewater treatment. In the USA, major wastewater plants have energy usage ranging from 0.086 to 1.19 kWh/m^3.[104]. In Europe, particularly in 11 WWTPs in Portugal, energy consumption ranged between 0.9 and 1.1 kWh/m3.[105]. In Italy, a study conducted across 251 WWTPs found that energy consumption below 23 kWh /PE/y is the target for large plants serving more than 100,000 PE. For smaller plants, a higher benchmark of 76 kWh/PE/y is considered reasonable. For plants in the intermediate range of 2,000–100,000

PE, the benchmark is set between 42–48 kWh /PE/y.[106]. In Germany, the average energy consumption from 5,668 WWTPs is 0.43 kWh/m³.[104]. In Greece, for biological nutrient removal WWTPs, the average energy consumption is approximately 38 kWh/PE, with a range from 15 to 86 kWh/PE. [107]. This energy is mostly due to the aeration system in more than 50 % (Figure 2.11)[108],[107].
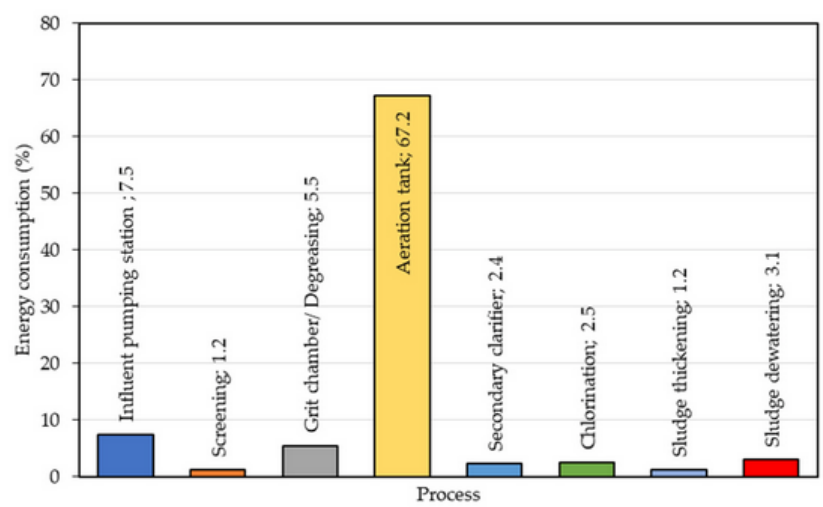
Figure 2. 11: Energy distribution in the main processes of conventional activated sludge systems (influent pumping station; screening; grit chamber/degreasing; aeration tank; secondary clarifier; chlorination; sludge thickening; sludge dewatering).[108]

Additionally, as effluent discharge standards become stricter worldwide because of heightened public health and environmental concerns, there's an inevitable uptick in in-plant energy use. This suggests that energy-demanding treatment methods might be essential to meet these standards. The significant energy consumption of today's wastewater treatment plants (WWTPs) undoubtedly poses a challenge to global wastewater treatment, especially in the context of environmental sustainability[109].

Wastewater treatment plants (WWTPs) consume significant amounts of electricity, often derived from fossil fuels, to facilitate the treatment process. This consumption is directly tied to global climate change concerns. For instance, in China, the electricity used by WWTPs leads to the annual emission of around 114 million metric tons of carbon dioxide. Moreover, during the biological breakdown of organic and nitrogen-rich substances in wastewater, a sizable quantity of greenhouse gases, including carbon dioxide, methane, and nitrogen oxide, is emitted. The high energy usage within these plants underscores the urgency to address its environmental

implications, especially in light of global climate change[103]. In Greece, the annual average GHG emissions in Greek WWTPs is of the order of 94 kCO_{2e}/PE, ranging from 61 to 161 $kgCO_{2e}$ /PE[107].

In wastewater treatment plants using the CAS method, for every gram of COD removed, 0.3 to 0.5 g of dry biomass are produced. This translates to a significant amount of waste sludge globally from wastewater treatment. To cut down on electricity consumption, current practices aim to extract energy from this waste sludge via anaerobic digestion. However, with the current advancements in this technology, only around 30-50% of the total COD or volatile solids are transformed into biogas, showcasing its limited energy efficiency. One of the reasons for this inefficiency is that microorganisms in the digestion process can't directly use the waste sludge. Instead, the sludge needs to be broken down into soluble COD before digestion can occur. A fundamental limitation of current wastewater treatment setups is the indirect pathway of energy recovery: first converting soluble COD to biomass and then deriving energy from that biomass through anaerobic digestion with a notably low efficiency. This has resulted in overall energy efficiencies between 20-50% in wastewater treatment plants across various countries[110–113]

Based on the above, there's a pressing global demand to enhance the energy efficiency of WWTPs by implementing innovative process designs. A shift to anaerobic wastewater treatment technologies could redefine the current model of WWTPs, offering advantages like increased energy recovery, lowered energy usage for aeration, and reduced sludge output.

2.4.2 Comparing anaerobic and aerobic wastewater treatment alternatives

Modern domestic wastewater shouldn't be viewed as "waste." Instead, it's a resource rich in energy, valuable materials, and clean water. Traditional wastewater treatment processes, like the CAS method explained in the previous subchapter, typically consume about 0.45 kWh for every cubic meter of water treated, equating to 1620 kJ/m^3[110,114]. Given that the average COD (a measure of organic matter) in wastewater is around 500 mg/L, the energy used in CAS processes equates to 3.20 kJ for every gram of CO. However, the potential energy in typical wastewater is estimated at 16.2 kJ/g of COD, which is almost five times the electrical energy used in CAS treatment[115,116]. This implies that wastewater treatment plants could be self-sustaining if just 20% of the energy in wastewater could be turned into electricity. Currently, most of the recoverable energy in these plants comes from anaerobic digestion of primary and secondary sludges.

An innovative way to treat wastewater and produce energy at the same time is anaerobic treatment. Anaerobic processes are traditionally used for high-strength wastewater or municipal sludge treatment [117]. Recently, it has been efficiently applied for the treatment of low strength municipal wastewaters as well [118]. The main advantages of the anaerobic treatment compared to the conventional aerobic treatment methods are: a) the low structural and operational cost, b) the production of small volumes of well stabilized excess sludge and c) the production of methane which is a useful source of energy[119] (Show and Lee, 2016). Table 2.1 in previous subchapter illustrates the energy output and CO_2 emission reduction achieved by using anaerobic wastewater treatment systems.

Table 2.8 below compare the two treatment systems.

Table 2. 8: Comparison of aerobic and anaerobic treatment [120]

Feature	Aerobic	Anaerobic
Organic removal efficiency	High	High
Nutrient removal	High	Low
Effluent quality	Excellent	Moderate
Organic loading rate	Moderate	High
Sludge production	High	Low
Nutrient requirement	High	Low
Alkalinity requirement	Low	High for certain industrial waste
Energy requirement	High	Low to moderate
Temperature sensitivity	Low	High
Startup time	2-4 weeks	2-4 months
Odor	Less opportunity for odors	Potential odor problems
Bioenergy and nutrient recovery	No	Yes
Mode of treatment	Total (Depending on feedstock characteristics)	Essentially pretreatment

Anaerobic treatment processes offer several advantages over aerobic treatment processes:

➢ Anaerobic treatment processes have lower energy requirements compared to aerobic processes, resulting in reduced operational costs.

➢ The generation of biomass in anaerobic processes is significantly lower, around six to eight times less, than that in aerobic processes. As a result, the costs associated with sludge treatment and disposal are greatly reduced.

- Due to the lower biomass production, anaerobic treatment requires fewer nutrients. This translates into lower costs for nutrient supplementation, if needed, in comparison to aerobic treatment.
- Anaerobic processes can achieve higher volumetric loading rates, allowing for smaller reactor volumes and space requirements.
- Methane, a potent source of energy, is produced in anaerobic processes, offering potential energy recovery opportunities.
- Anaerobic processes exhibit favorable responses to various wastewater characteristics and can effectively treat a wide range of organic compounds.

Overall, the advantages of anaerobic treatment processes include energy efficiency, reduced sludge-related costs, lower nutrient requirements, compact reactor design, potential energy generation, and versatility in treating diverse wastewater compositions.

Anaerobic treatment processes do have certain drawbacks compared to aerobic treatment processes:

- Anaerobic processes typically require a prolonged start-up period to establish and develop the appropriate biomass for efficient treatment.
- Anaerobic treatment cannot meet effluent nutrient limits
- Maintaining suitable pH levels in anaerobic processes necessitates the addition of alkalinity, which can impact the cost-effectiveness of anaerobic treatment. Methanogenic bacteria, crucial for methane production, are sensitive to pH and function optimally within a narrow range of 6.5-7.5. Deviating from this range can significantly impact their metabolic rates and impede methane production.
- Anaerobic processes can be sensitive to toxic compounds such as heavy metals, chlorinated compounds, and detergents. Pretreatment may be necessary for wastewater with high concentrations of these toxic compounds.
- There is the potential for odor and corrosive gas generation in anaerobic treatment processes.
- Anaerobic treatment is more vulnerable to the adverse effects of lower operating temperatures. Maintaining a stable and optimal operating temperature is critical as anaerobic bacteria, particularly methanogens, are sensitive to temperature fluctuations.

➢ Depending on the desired effluent quality and regulatory requirements, anaerobic treatment may require further polishing through additional aerobic treatment to meet discharge standards.

To sum up, the disadvantages of anaerobic treatment processes include extended start-up periods, the need for pH control, sensitivity to toxic compounds, the possibility of odor and corrosive gas production, susceptibility to lower temperatures, and potential requirements for additional aerobic treatment to achieve desired effluent quality.

2.5 Anaerobic Reactors

2.5.1 High-Rate anaerobic systems

A significant milestone in the development of anaerobic wastewater treatment was the introduction of high-rate reactors, which separate biomass retention from liquid retention. Unlike aerobic processes, where the maximum load is determined by the supply of necessary reactants like oxygen, anaerobic process has a different limiting factor. In anaerobic processes, the maximum permissible load is not governed by the availability of a specific reactant, but rather by the quantity of viable anaerobic biocatalysts or bacteria capable of directly interacting with the constituents in the wastewater.

In anaerobic high-rate systems, elevated sludge concentrations are achieved through physical retention and/or immobilization of anaerobic sludge. This allows for the application of high COD loading rates while maintaining long SRT with relatively short HRTs. Over the past three decades, various high-rate systems have been developed, including the anaerobic contact process (ACP), anaerobic filters, upflow anaerobic sludge blanket (UASB) reactors, fluidized bed (FB) reactors, expanded granular sludge bed (EGSB) reactors, and baffled reactors.

To facilitate the effective treatment of a specific wastewater with high organic loading rates in an anaerobic reactor system, the following requirements must be fulfilled:

1. *Effective Sludge Retention*: It is vital to retain a substantial amount of viable sludge within the reactor during operation. The greater the sludge retention, the higher the system's loading

potential. Therefore, cultivating a biomass that settles well or can be immobilized is crucial. Moreover, the sludge should not deteriorate in terms of settling characteristics.

2. *Optimal Biomass-Wastewater Contact*: Sufficient contact between the viable bacterial biomass and the wastewater is essential. If any portion of the retained sludge lacks access to adequate substrate, its value in the system diminishes. Ensuring consistent and thorough contact between biomass and wastewater is critical for efficient treatment.

3. *Enhanced Reaction Rates and Minimized Transport Limitations*: The kinetics of degradation processes play a significant role. It is important that metabolic end-products can readily diffuse out of the biofilm or aggregate. Maintaining relatively small biofilm sizes and high accessibility of organisms within the biofilm contribute to efficient reaction rates. By minimizing transport limitations, optimal degradation can be achieved.

4. *Adapted and Acclimatized Biomass*: The viable biomass should be suitably adapted and acclimatized to the specific characteristics of the wastewater being treated. This allows for effective degradation of contaminants present in the wastewater. The biomass's ability to thrive under the given conditions is crucial for successful treatment.

5. *Favorable Environmental Conditions*: The reactor should provide favorable environmental conditions for all necessary organisms, focusing on the rate-limiting steps of the degradation processes. It is important to note that conditions may vary spatially and temporally within the reactor. The existence of micro-niches within the system is essential to accommodate the diverse range of organisms involved in the degradation of complex compounds. It is important to observe that within the biofilms and granules, the substrate and metabolite concentrations are sufficiently low to enable even highly endergonic acetogenic reactions to occur. For example, the oxidation of propionate can proceed despite the very low hydrogen concentrations present in these environments.

Figure 2.12 depicts the evolution of high-rate reactor systems, showcasing the influence of improved sludge retention and enhanced contact on the achievable organic loading rates.

Although the initial attempts by Buswell did not reach loading rates of 1 kgCOD/m^3.d, modern anaerobic wastewater treatment (AnWT) systems available on the market now guarantee loading rates surpassing 40 kgCOD/m^3.d.
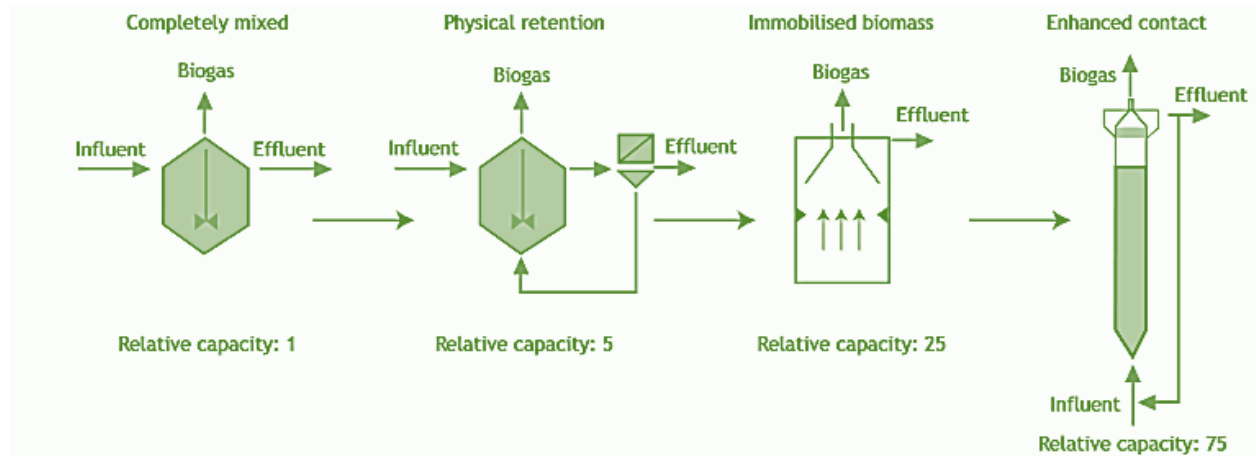
Figure 2. 12 Different AnWT systems exhibit varying loading capacities. Full-scale conditions with enhanced contact in EGSB reactors can achieve maximum loading rates of about 45 kgCOD/m3.d.[1]

AnWT is commonly employed as a treatment technology for wastewater originating from food processing and agro-industrial sectors.

In a recent development, high-rate AnWT systems have been designed to effectively treat cold and extremely low strength wastewaters. This includes not only municipal sewage but also industrial wastewater streams, such as those from beer industries, which are commonly discharged at low temperatures. Remarkably, full-scale results have demonstrated the successful anaerobic treatment of these diverse wastewaters using common seed materials. This underscores the resilience and flexibility of the anaerobic process. The most commonly applied high-rate AnWT systems are:

➢ The Anaerobic Contact Process (ACP)
➢ The Anaerobic Filters (AF)
➢ The Anaerobic Sludge Bed Reactors (ASBR)
➢ The Anaerobic expanded and fluidized bed systems (EGSB and FB)
➢ The Anaerobic membrane bioreactors (AnMBR)
➢ Other anaerobic high-rate systems

The following subparagraphs include a brief description of these alternative high-rate anaerobic wastewater treatment technologies that can effectively achieve organic carbon removal. The state of the art on AnMBR technology, which is the subject of this PhD research is described in detail in paragraph 2.6.

2.5.2 The Anaerobic Contact Process (ACP)

ACP refers to processes that utilize external settlers and sludge return mechanisms, as depicted in Figure 2.13.
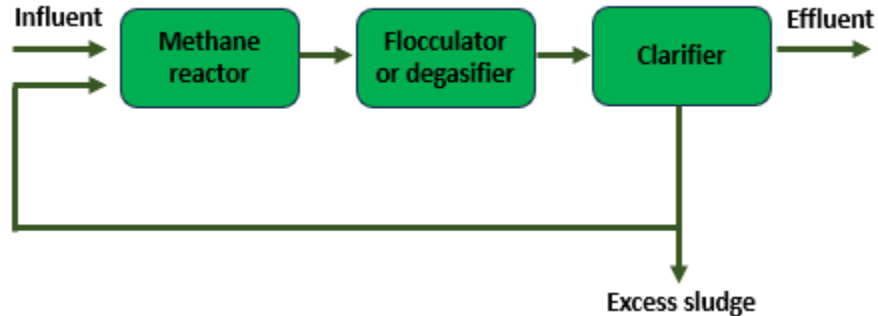
Figure 2. 13 ACP, equipped with flocculator or a degasifier unit to enhance sludge sedimentation in the secondary clarifier.

The initial versions of the first-generation "high-rate" anaerobic treatment systems for medium-strength wastewaters faced significant challenges. The main difficulty encountered in practice was the separation of sludge from the treated water. The prevailing belief at the time was that intense agitation in the bioreactor would improve the contact between the sludge and wastewater. However, little consideration was given to the detrimental effects of intensive mixing on sludge structures, such as settleability and the disruption of balanced micro-ecosystems.

Various methods were tested and employed in the different versions of the ACP to address sludge separation. These included vacuum degasification with sedimentation, the use of organic polymers and inorganic flocculants, centrifugation, and even aeration to halt digestion. However, these approaches yielded unsatisfactory results.

With the current knowledge on anaerobic digestion technologies, a more gentle and intermittent mode of mixing is now applied. This approach ensures that the sludge maintains excellent sedimentation properties. The modern ACP can significantly contribute to environmental protection and energy recovery, particularly for wastewaters containing high levels of suspended solids and semi-liquid wastes. Well-designed ACP systems can achieve organic loading rates of up to 10 kgCOD/m^3. d

2.5.3 Anaerobic Filters (AF)

In the late sixties, Young and McCarty in the USA developed the Upflow Anaerobic Filter (UAF) (1964, 1982). The UAF employs various methods for sludge retention, including the attachment of a biofilm to the solid carrier material, the entrapment and sedimentation of sludge particles within the interstices of the packing material, and the formation of compact and easily settling sludge aggregates. A schematic of AF is presented in Figure 2.14.
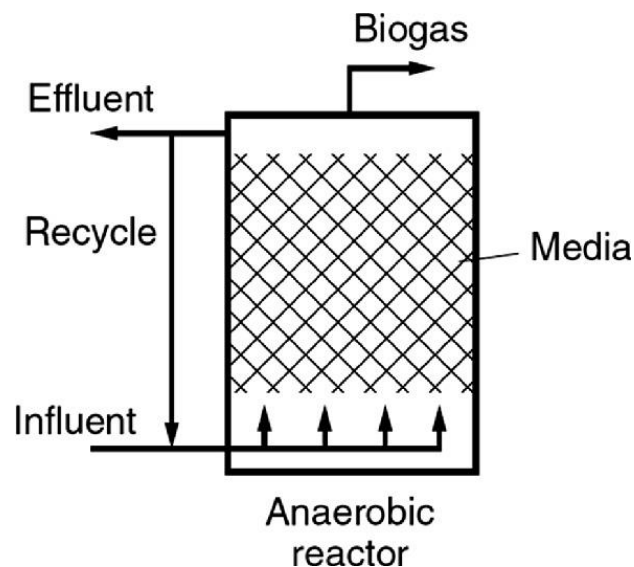
Figure 2. 14:Anaerobic filter configuration [121]

In the early stages, finding a suitable carrier material for these systems posed a challenge [122]. Researchers explored various options, including synthetic packings and natural materials like gravel, coke, and bamboo segments. The shape, size, and weight of the packing material were found to be crucial factors. Surface characteristics also played a significant role in facilitating

bacterial attachment. Additionally, it was discovered that maintaining an open and structurally sound bed with a large void fraction was essential. By utilizing appropriate support materials, AF systems could be quickly established, thanks to the efficient adherence of anaerobic organisms to the inert carrier. The ease of system start-up greatly contributed to the popularity of AF systems during the 1980s and 1990s.

Long-term operation of UAF systems can present challenges. The primary disadvantage of the UAF concept is the difficulty in maintaining the required contact between sludge and wastewater due to the propensity for bed clogging. This issue is especially prominent when dealing with partially soluble wastewater. While the inclusion of a primary settler and/or a pre-acidification step can partially address these clogging problems, implementing such measures necessitates additional units, leading to higher costs. Moreover, despite these interventions, the problem of short-circuiting flows and reduced treatment efficiencies resulting from bed clogging may persist, leaving room for improvement in system performance.

Since 1981, approximately 140 full-scale UAF installations have been operational for treating various wastewater types, accounting for around 6% of the total installed high-rate reactors (Figure. 2.15). The overall experience with UAF systems has been satisfactory, achieving modest to relatively high loading rates of up to 10 kgCOD/m^3. d. The UAF system remains appealing for treating primarily soluble wastewaters, particularly when sludge granulation is not feasible.

However, long-term issues related to system clogging and filter material stability have resulted in a decline in the number of installed full-scale AF systems. In the past five years, only six new and registered AF systems have been constructed, representing approximately 1% of the total number of newly installed AnWT systems.

To minimize clogging and sludge accumulation within the filter material interstices, anaerobic filters have been operated in a downflow mode, known as downflow fixed-film reactors. Despite investigations into various operational modes and filter materials, the practical application of these approaches has been disappointing. The limiting factor lies in the low applicable OLR due to the limited biomass retention capacity within such systems, primarily relying on the attachment of biomass to the packing material surface. In UAF filters, most of the anaerobic activity occurs in the non-attached biomass.
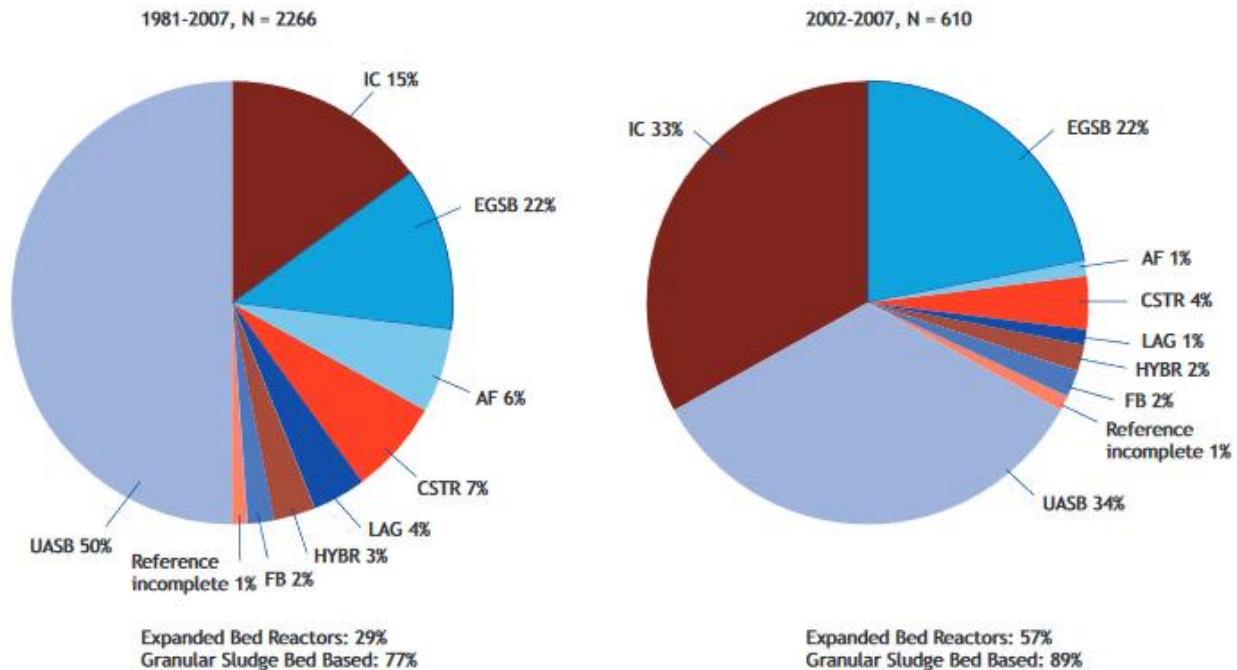
Figure 2. 15: Implemented anaerobic technologies for industrial wastewater pictured for the period 1981-2007 (left) and the period 2002-2007 (right). UASB: upflow anaerobic sludge blanket, EGSB: expanded granular sludge bed, IC internal circulation reactor, type of EGSB system with biogas-driven hydrodynamics, AF: anaerobic filter, CSTR: continuous stirred tank reactor, Lag.: anaerobic lagoon, Hybr.: combined hybrid system with sludge bed at the bottom section and a filter in top, FB: fluidized bed reactor.[1]

2.5.4 Anaerobic Sludge Bed Reactors (ASBR)

ASBRs, have gained significant popularity as the prevailing choice for AnWT systems. Sludge retention in ASBRs is achieved through the formation of easily settling sludge aggregates, such as flocs or granules, and the utilization of an internal gas-liquid-solids separation system (GLSS device). The upflow anaerobic sludge bed reactor (UASB) stands as the most well-known and widely utilized example of this concept. Originating in the Netherlands during the early 1970s [123], the UASB process has shown tremendous potential . UASB reactors are by far the most robust high-rate anaerobic reactors for sewage treatment and there have been more than 1000 UASB reactors installed worldwide[124]. While the primary application remains the treatment of agro-industrial wastewater, there is a growing trend of adopting UASB for wastewater treatment from chemical industries and sewage. Figure 2.16 presents a schematic representation of a UASB reactor.
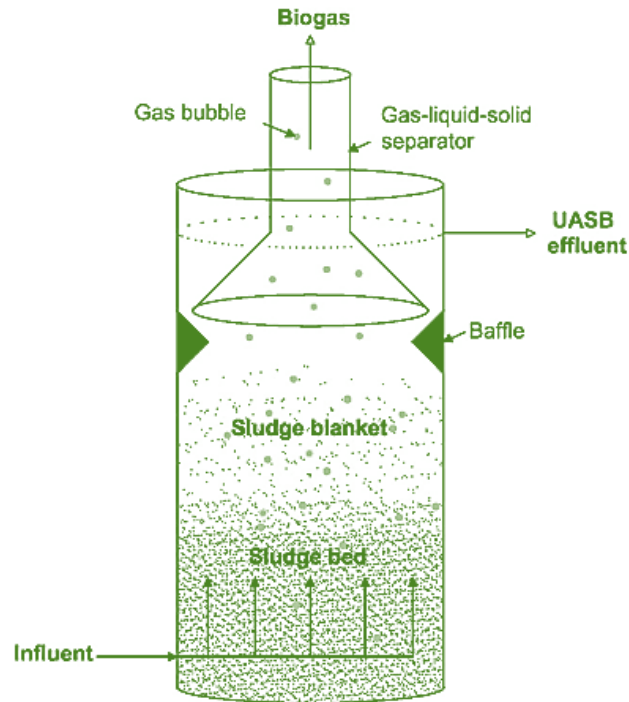
Figure 2. 16 Schematic of a UASB reactor[125]

Similar to the UAF system, the wastewater flows upward through the reactor in the sludge bed reactor. However, unlike the AF system, there is typically no packing material in the reactor vessel. The concept of the sludge bed reactor is founded on the following principles:

UASB reactors rely on the inherent sedimentation properties of anaerobic granular sludge, which are either present or developed during operation. This allows for gentle mechanical mixing, eliminating the need for additional mixing mechanisms and reducing investment and maintenance costs. The excellent settling characteristics of the granular sludge enable the application of high superficial liquid velocities without the risk of significant sludge washout.

Effective contact between the sludge and wastewater in UASB systems is achieved through two methods. First, wastewater is evenly distributed over the bottom of the reactor to ensure uniform contact. Alternatively, agitation caused by the production of biogas and the upflow velocity within the reactor promote contact between the sludge and wastewater.

A low surface area design of the reactor facilitates the feeding process, while the accumulation of biogas production along the height of the tower reactor creates a turbulent flow. The increased upflow velocity enhances the contact between the sludge and pollutants present in the

wastewater. For wastewaters containing biodegradable compounds, a liquid recirculation flow can be employed to further improve mixing and minimize stratification of substrates and intermediate products along the reactor's height, thereby reducing the risk of inhibition[124,126–130].

To prevent the washout of sludge aggregates, the UASB reactor incorporates a gas collection dome at the top, creating a zone with reduced turbulence. This design feature effectively serves as an in-built secondary clarifier within the reactor.

Table 2.9 presents a comprehensive overview of the distinctive characteristics and challenges associated with UASB reactors. The key feature that makes UASB reactors popular as high-rate anaerobic reactors globally, particularly in tropical countries, is their ability to achieve high removal efficiencies of COD without the need for support materials, thanks to the presence of granular or flocculent sludge. Moreover, the natural turbulence generated by rising gas bubbles facilitates efficient contact between wastewater and biomass, eliminating the need for mechanical mixing and significantly reducing energy requirements and associated costs. Most notably, the granulation/blanketing process in UASB reactors enables independent and effective manipulation of solids and HRTs, allowing the design to be tailored based on the degradative capacity of the biomass and resulting in considerably shorter treatment times compared to conventional digesters[131].

Table 2. 9 Challenges and distinctiveness of UASB reactor

Distinctiveness	Challenges
➢ Utilization of granular or flocculent sludge, eliminating the need for a support medium[132,133] ➢ High biomass concentration, enabling effective COD removal and accommodating diverse loading rates[131,132] ➢ Sludge blanketing, allowing for shorter hydraulic retention time and extended solids retention time. ➢ Generation of rising gas bubbles, obviating the need for mechanical mixing and reducing energy consumption ➢ Extensive practical expertise in implementation[132]	➢ Start-up susceptibility to temperature and organic shock loads[132]. ➢ Difficulties in controlling bed expansions, limiting organic loading rates[132,134]. ➢ Wash-out, flotation, and disintegration of granular sludge. ➢ Performance deterioration at low temperatures[135]. ➢ High sulphate concentration[136]. ➢ Necessity of post-treatment to meet discharge standards for organic matter, nutrients, and pathogens.[137] ➢ Purification of biogas.

Start- up.

The successful operation and stability of a UASB reactor heavily rely on the initial start-up phase, which is influenced by various physical, chemical, and biological factors [138]. These factors encompass the nature of the wastewater, operating conditions, and the presence and growth of active microbial populations in the seed sludge or inoculum. An essential requirement is the acclimatization period during which the seed sludge is gradually adapted to the specific operating conditions. Typically lasting between 2 to 8 months [128], this period has posed significant challenges for the practical implementation of UASB reactors.

Different inoculum sources can be used for UASB reactors, including granules from full-scale UASB reactors treating brewery wastewater, as well as non-granular sources such as anaerobic digested sludge and waste activated sludge. The selection of the most suitable inoculum source for a specific wastewater type can be determined through toxicity and biodegradability tests [138,139]. While UASB reactors can function efficiently without granules, the formation of granules during start-up offers advantages by enabling high COD removal efficiency in a shorter time frame and allowing treatment of larger wastewater volumes. The significance of granules in UASB reactor operation has spurred research on the theories and mechanisms of anaerobic granulation [140,141]

The initial development of granules involves four steps: (1) Transport of cells to a substratum, (2) Initial reversible adsorption to the substratum, (3) Irreversible adhesion of cells to the substratum through microbial appendages and/or polymers, and (4) Cell multiplication and granule formation.

2.5.5 Anaerobic expanded and fluidized bed systems (EGSB and FB)

The presence of sulfate-reducing bacteria (SRB) in anaerobic digestion of organic wastewater can negatively impact methane-producing bacteria (MPB) and hinder treatment efficiency. Additionally, the toxic effect of sulfides produced by SRB affects anaerobic bacteria in the reactor. To overcome these challenges, a two-phase process has been employed to separate sulfate reduction from methane production, but it can be complex and costly. As research on SRB and anaerobic reactors advances, there is growing interest in utilizing modern, high-efficiency anaerobic reactors to treat high-sulfate wastewater [142–151].

EGSB and FB systems represent the second generation of sludge bed reactors, capable of handling high organic loading rates exceeding 30 to 40 kgCOD/m^3. d. In the FB process, bacteria attach to mobile carrier particles such as fine sand, basalt, pumice, or plastic. The FB system is considered an advanced anaerobic technology with potential loading rates of 50-60 kgCOD/m^3. d. However, maintaining long-term stable operation has proven to be challenging.

The system relies on the development of a uniform and stable attached biofilm or particles in terms of thickness, density, and strength. To achieve stable biofilm growth, extensive pre-acidification, and the absence of dispersed matter in the feed are necessary. Despite these efforts, controlling the film thickness evenly throughout the reactor is difficult, often resulting in the segregation of different biofilm types along the reactor height. In full-scale reactors, carrier particles tend to segregate from the biofilms, causing operational issues. Flow adjustments are required to retain the biofilm particles in the reactor, leading to the accumulation of support material in the lower section and the presence of detached biofilms in the upper section. Achieving this separation requires maintaining a relatively low superficial velocity, which contradicts the primary objective of a FB system.

FB systems have evolved in recent years, with the Anaflux system[152] representing a modern approach. Unlike traditional FB systems, the Anaflux system emphasizes bed expansion rather than bed fluidization for improved operational ease. It employs an inert porous carrier material (such as particles <0.5 mm in size with a density of around 2) to facilitate bacterial attachment.

At the top of the reactor, a triple-phase separator, like the gas-liquid-solids separation (GLSS) device found in UASB and EGSB reactors, is incorporated. When the biofilm layer on the media becomes excessively thick, causing lighter aggregates to accumulate in the separator, periodic extraction takes place using an external pump. The extracted material undergoes shear forces to remove a portion of the biofilm. Subsequently, both the media and detached biomass are reintroduced into the reactor, allowing the free biomass to be rinsed out of the system. This controlled process ensures a more homogeneous reactor bed and enables the retention of a substantial biomass concentration (up to 30-90 kgVSS/m^3 reactor) while facilitating excellent liquid-biomass contact through high liquid upflow velocities (up to 10 m/h)

The EGSB system utilizes granular sludge, which possesses excellent settling characteristics and high methanogenic activity. Under high sludge loading rates, the settleability may be affected by biogas accumulation in the granules. However, the system allows for the application of high superficial liquid velocities exceeding 6 m/h. These velocities, combined with gas lifting within the

bed, lead to a slight expansion of the sludge bed. This facilitates efficient contact between the sludge and wastewater, resulting in significantly higher loading potentials compared to conventional UASB installations.

In certain expanded bed systems, the combined hydraulic and gas flows generate net liquid flow velocities of 25-30 m/h, promoting extensive mixing of the reactor medium with the available biomass. Unlike the Anaflux FB system, controlling the size of the biomass is generally not required, although oversized granules have been observed in specific cases. EGSB systems rely on complete retention of the granular sludge and have demonstrated exceptional performance in full-scale installations treating various types of wastewaters, achieving organic loading rates up to 40-45 kgCOD/m3. d.

Importantly, EGSB reactor systems offer the ability to effectively treat challenging wastewater that conventional UASB systems may struggle with.

➢ Wastewater containing biodegradable organic chemicals: Full-scale reactors demonstrate stable performance over extended periods when treating wastewaters with high concentrations of formaldehyde, such as 10 g/l formaldehyde [153].

➢ Cold and dilute wastewater: EGSB reactors excel in treating low-temperature (even below 10°C) and low-concentration (COD << 1 g/l) wastewaters, where biogas production and mixing are limited [154]. The enhanced hydraulic mixing in EGSB systems is independent of biogas production.

➢ Wastewater containing long-chain fatty acids: In UASB systems, long-chain fatty acids tend to accumulate and form inaccessible clumps on the sludge. EGSB systems, with higher upflow velocities, allow for better distribution and utilization of the substrate by the biomass [155].

➢ Wastewater with foaming issues in UASB systems: EGSB systems offer a solution for wastewater prone to foaming problems in UASB systems.

Due to the exceptional performance of these "super" high-rate anaerobic systems, large companies currently tend to install more EGSB systems than UASB system (Figure. 2.17)
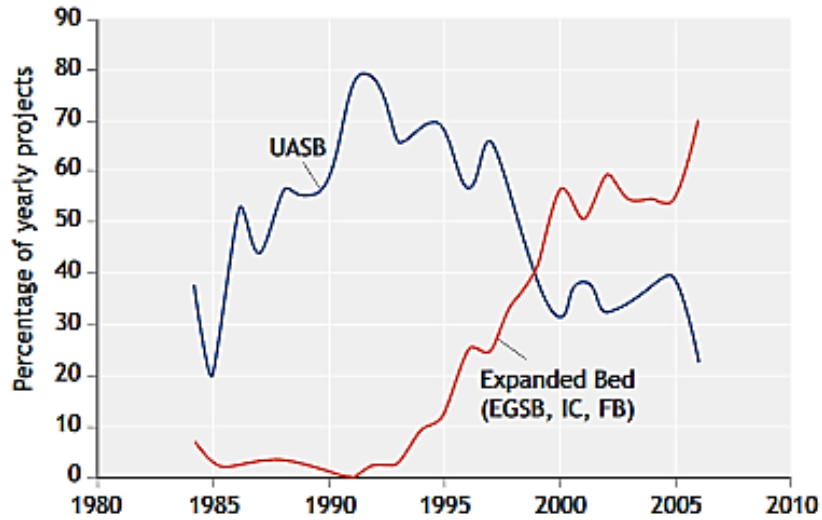
Figure 2. 17: UASB and EGSB systems in full-scale anaerobic treatment installations (1984-2007).

A schematic presentation of EGSB reactor is illustrated in Figure 2.18.
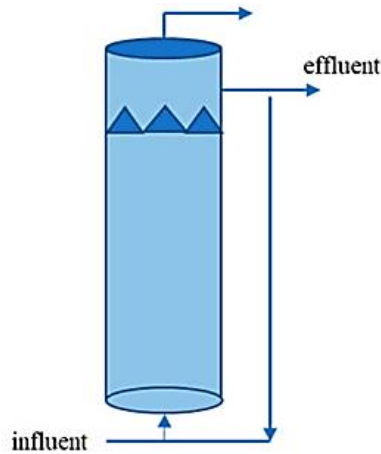
Figure 2. 18 Schematic diagram of EGSB reactors [156].

2.5.6 Other anaerobic high-rate systems

Different designs have been tested to introduce staging in the various phases of anaerobic treatment, offering alternatives to ACP, UASB, and EGSB reactors [157]. A prominent example is the two-stage process, where the acidification step is fully separated from the methanogenic step. Additionally, anaerobic baffled reactors (ABR) provide horizontal staging by operating as a series

of UASB units in sequence. These innovative approaches offer potential advancements in anaerobic treatment strategies.

Large-scale applications of the baffled reactor on domestic sewage have not progressed further due to hydrodynamic limitations and constraints on achieving the desired solid retention time (SRT). In a baffled system, the superficial liquid velocity is significantly higher than in a single-step sludge bed reactor, causing most of the sludge to be carried along with the liquid through various compartments. This necessitates separation of the sludge after the last compartment in a settler and its return to the reactor. For high-temperature treatment, vertically staged reactors like the upflow staged sludge bed system[158,159] have been specifically developed. Although the staged reactor concept has shown promising results on a pilot scale, no full-scale reactors have been developed thus far.

The anaerobic sequencing batch reactor (ASBR) offers interesting possibilities as a set of anaerobic reactors operated in a batch mode using a 'fill and draw' method. In this system, a specific amount of raw wastewater is introduced into the anaerobic reactor after the supernatant from the previous batch has been discharged. The gentle mixing of the reactor contents facilitates the contact between settled viable sludge and the wastewater, leading to the elimination of biodegradable organics. After an appropriate reaction time, the sludge is allowed to settle, and the supernatant solution is discharged before starting the next cycle. ASBR has demonstrated successful granulation on dilute wastewaters, even at lower ambient temperatures [160]. It has also shown effectiveness in treating wastewaters containing LCFAs [161]. During the filling period, LCFAs are absorbed by the anaerobic sludge, followed by a gentle digestion phase that stabilizes and regenerates the absorbed sludge into highly active methanogenic biomass. Another high-rate system that has garnered increased attention over the past decade is the AnMBR. This reactor type is the focus of this PhD thesis and will be analyzed in-depth in subchapter 2.6.

2.5.7 Types of anaerobic high-rate reactors installed until 2015

Sludge bed systems dominate the market among high-rate reactors. Van Lier (2008) highlighted that between 1981 and 2007, around 77% of all installed reactors were sludge bed systems, predominantly UASB and EGSB/IC types. The study also noted a decline in the sales of traditional UASB reactors, with a rising preference for EGSB types. This shift has persisted, with leading

contractors like Paques BV and Biothane-Veolia reporting minimal sales of conventional UASB reactors, as seen in Figures 2.19 and 2.20[162].
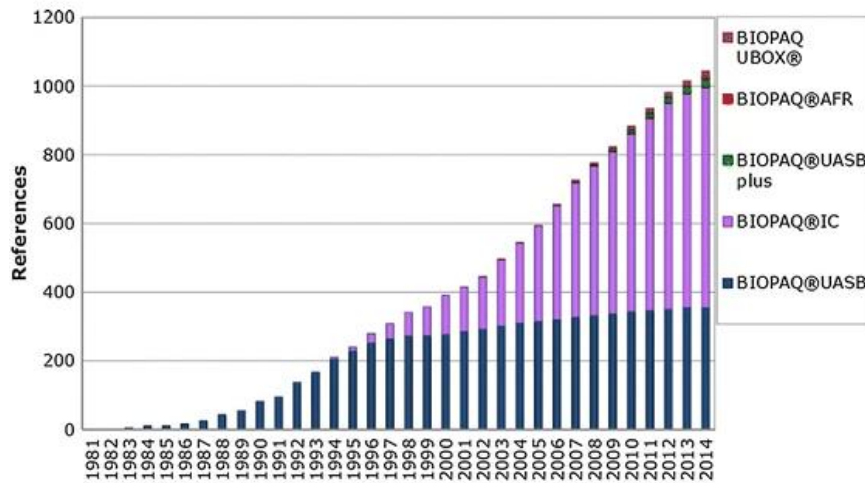
Figure 2. 19: Sales of anaerobic high-rate reactors by Paques BV since the company's start-up (1981)
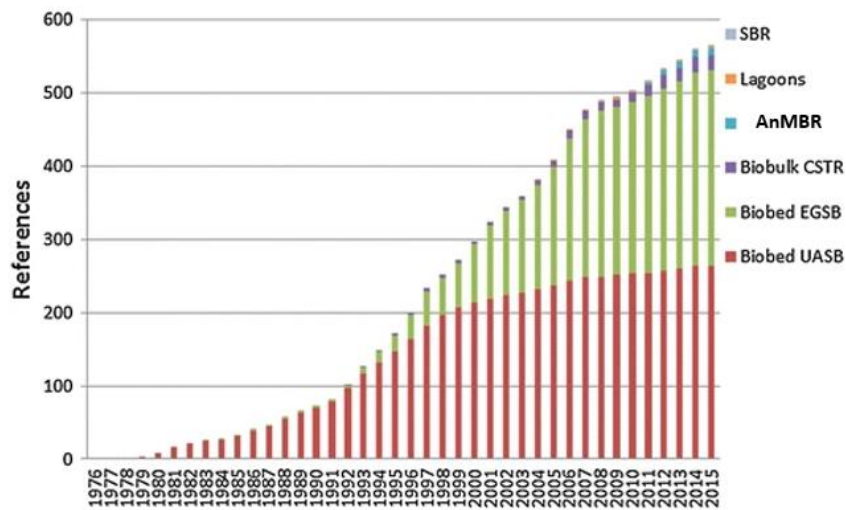
Figure 2. 20: Sales of anaerobic high-rate reactors by Biothane-Veolia since the company's start-up (1976)[162]

From the two figures, it's evident that AnMBR began to emerge after 2008. However, there were very few installations up until 2015.

2.6 Anaerobic membrane bioreactors (AnMBR)

2.6.1. Introduction

Previous chapters discussed various high-rate anaerobic systems. A primary limitation of anaerobic treatment is the slow growth rate of anaerobic bacteria, leading to an extended HRT and, consequently, large reactor volumes. Several schemes proposed in the previous chapter address this challenge by adopting high-rate systems that retain active bacterial biomass. The most prevalent anaerobic reactor types are the UASB reactor and the ABR. However, when using UASB technology to treat partially soluble wastewaters, such as domestic wastewater, there's a challenge: the washout of un-hydrolyzed fine particulate matter due to high upward liquid velocities, resulting in reduced organic matter removal [126]. Conversely, the ABR isn't apt for treating high-strength wastewaters (e.g., industrial wastewater with a COD exceeding 1000 mg/L) over extended periods due to biomass washout from elevated gas production.

Another emerging technology that can potentially increase the efficiency of the anaerobic processes is AnMBR. AnMBRs combine anaerobic treatment with membrane filtration, offering efficient wastewater treatment, high biomass retention time and energy recovery [163,164].MBRs that combine biological treatment and membrane filtration for the secondary treatment of wastewater have been applied successfully for aerobic wastewater treatment in many full scale WWTPs [163,164]. Conventional aerobic/anoxic processes are usually used for the treatment of municipal wastewater. A key advantage of MBR is the complete retention of biomass leading to higher mixed liquor suspended solids concentrations and zero effluent suspended solids concentrations [119]. This characteristic allows for long SRTs and a corresponding decrease in HRT; SRTs of 150 d to >200 d have been reported [165] and sludge production is up to 20 times lower compared with that in aerobic processes [166].

AnMBRs are effective in treating wastewater with high COD, BOD, salinity, and SS [167]. Industrial wastewater (from the pharmaceutical [168], brewery [169], textile[170], dairy [171], pulp and paper , and food [172], etc.) are all treated using this method. The last decade, it has been efficiently applied for the treatment of low strength municipal wastewaters (e.g., municipal wastewater with COD in the 400-700 mg/L range).as well[118].

Energy recovery is a key benefit of AnMBRs. Biogas is produced, primarily methane, which can be utilized as a valuable energy source [115]. This biogas can cover a significant portion of the

energy demand for the wastewater treatment process, reducing reliance on external energy sources and promoting sustainability. AnMBRs align with the principles of the circular economy by maximizing resource utilization and minimizing waste.

It should be underlined that AnMBR is being in line with the new package that European Commission is piloting since 2018 and is called "Innovation Deals for the Circular Economy". This package promotes AnMBR as an innovation towards sustainable wastewater treatment. On the report of EU, AnMBR promotes the extraction of energy and nutrients, and accelerates treated water re-use for irrigation to overcome challenges of water scarcity [173].

However, AnMBRs face challenges that need to be addressed for successful implementation. Competition between methanogenic bacteria and SRB, membrane biofouling, and efficient operation at low ambient temperatures are among the challenges that need to be overcome [174]. High sulfate concentrations can hinder biogas production, while sulfate-reducing bacteria can cause odor issues, outcompete methanogens, and lead to corrosion. Membrane biofouling reduces filtration efficiency and increases operational costs [175]. Operating AnMBRs at low temperatures poses challenges related to lower treatment efficiency, methane solubility and biogas retrieval [176].

In conclusion, AnMBRs offer a sustainable and efficient approach to wastewater treatment and energy recovery. By combining anaerobic treatment with membrane filtration, they achieve enhanced solids removal, reduced sludge production, and the production of valuable methane gas. Addressing challenges related to bacterial competition, membrane fouling, and low-temperature operation will further improve the performance and feasibility of AnMBRs for sustainable wastewater treatment and energy recovery.

2.6.2 History and commercial development

The concept of AnMBR was first introduced by Grethlein[177], who utilized an external cross-flow membrane to treat the effluent from a septic tank. This process resulted in an increased biomass concentration, an 85-95% reduction in biochemical oxygen demand (BOD), and 72% nitrate removal. Over the last three decades, AnMBR's advantages have been extensively established in academic literature.

Realizing AnMBR's potential, both industry and government sectors have invested significantly to promote AnMBR systems. The most significant advancements include the creation of commercially viable AnMBR systems, notably "Membrane Anaerobic Reactor System (MARS)" and "Anaerobic Digestion Ultrafiltration (ADUF)"in the 1980s. These systems underwent extensive testing and operation on both pilot- and full-scale levels, primarily for industrial wastewater treatment. Concurrently, the Japanese government launched a national project, "Aqua-Renaissance '90", leading to the creation of numerous AnMBR systems [178–180]. Most of these commercial AnMBR systems relied on an external configuration.

By the 2000s, research on AnMBR pivoted towards system performance, filtration characteristics, membrane foulant characterization, and membrane fouling control. The successful implementation of submerged aerobic MBRs in the early 2000s fueled the exploration of submerged AnMBRs (SAnMBRs) for wastewater treatment. In the recent decade, the Kubota Corporation designed a SAnMBR process called "KSAMBR", which found successful application in multiple full-scale food and beverage industries [181]. ADI Systems Inc., using similar technology, developed the ADI-AnMBR system, specifically for food wastewater treatment. The most extensive AnMBR installation globally, completed by ADI, delivered an effluent devoid of SS, with 99.4% COD removal, enabling 100,000 gallons/day of wastewater to be conveniently discharged into the municipal system. The 2010s witnessed a significant amount of research dedicated to submerged AnMBR treatment, with efforts made to enhance energy efficiency, widen application scope, and tackle technical issues such as membrane fouling.

2.6.3 Research trends in AnMBR since 2006

In recent years, there has been a significant increase in research dedicated to the application of AnMBRs for treating various types of wastewater. Numerous articles have been published that delve into different aspects of anaerobic MBR, including its configuration, operational methods, a critical comparison with other existing reactors, membrane configuration, strategies for mitigating fouling, and the performance of the reactor when treating both municipal and industrial wastewater. These scholarly publications aim to establish a solid foundation and provide general insights into the topic.

From 2006 onwards, there has been a significant surge in global research focused on AnMBRs, as depicted in Figure 2.21. As of the time of writing this thesis, Scopus has documented 715

research publications dedicated to AnMBR studies. These publications cover a diverse range of topics, including membrane fouling, membrane cleaning techniques, treatment of residential or municipal wastewater, industrial wastewater treatment, modeling approaches, economical design considerations, and microbial community analysis, among others. It is evident from this extensive body of research that AnMBR systems represent a cutting-edge technology with a broad spectrum of applications.
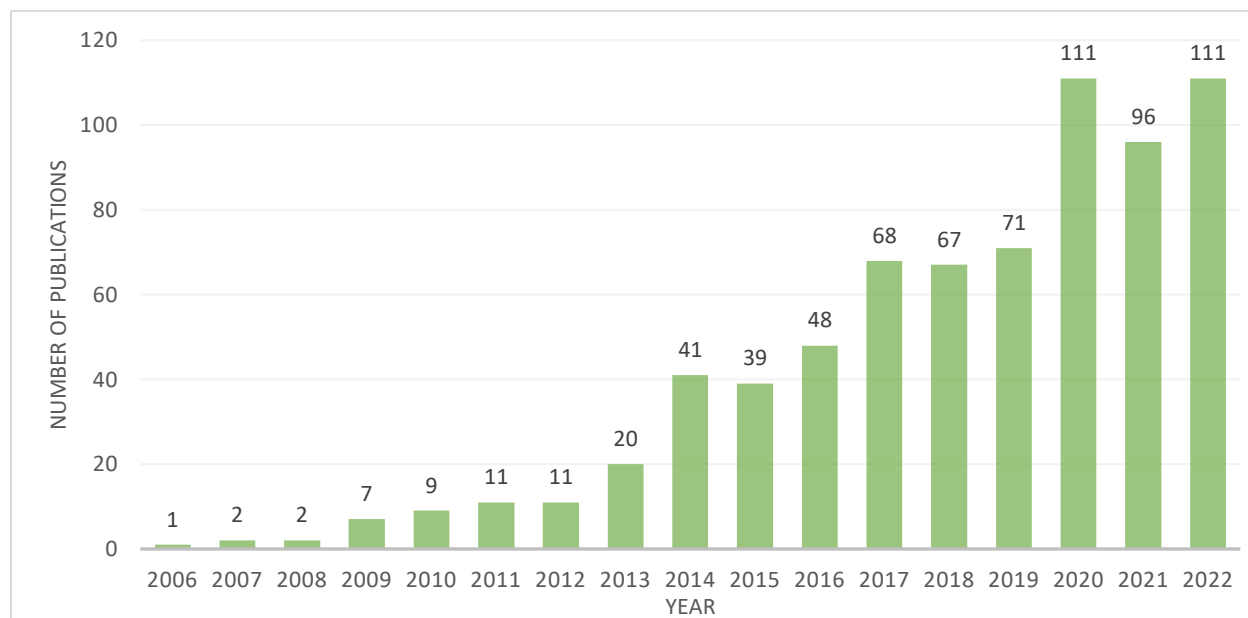
Figure 2. 21 :Number of AnMBR research articles published since 2006 retrieved from Scopus.

AnMBR-related articles have been published across 48 different journals. In 2006, there was only 1 publication that specifically explored AnMBR and its procedures. Except for slight increments in 2013 and 2014, the number of publications remained relatively stable until 2016. However, starting from that point, there was a substantial annual growth, leading to 111 articles being published in 2020.

The accompanying pie chart in Figure 2.22 indicates the prominence of Bioresource Technology (26%), Water Research (10%), Journal of Membrane Science (8%), and Chemical Engineering Journal (7%) as the top publishing journals. These four journals collectively account for over 60% of all AnMBR-related articles, while the remaining papers are distributed among an additional 44 journals.
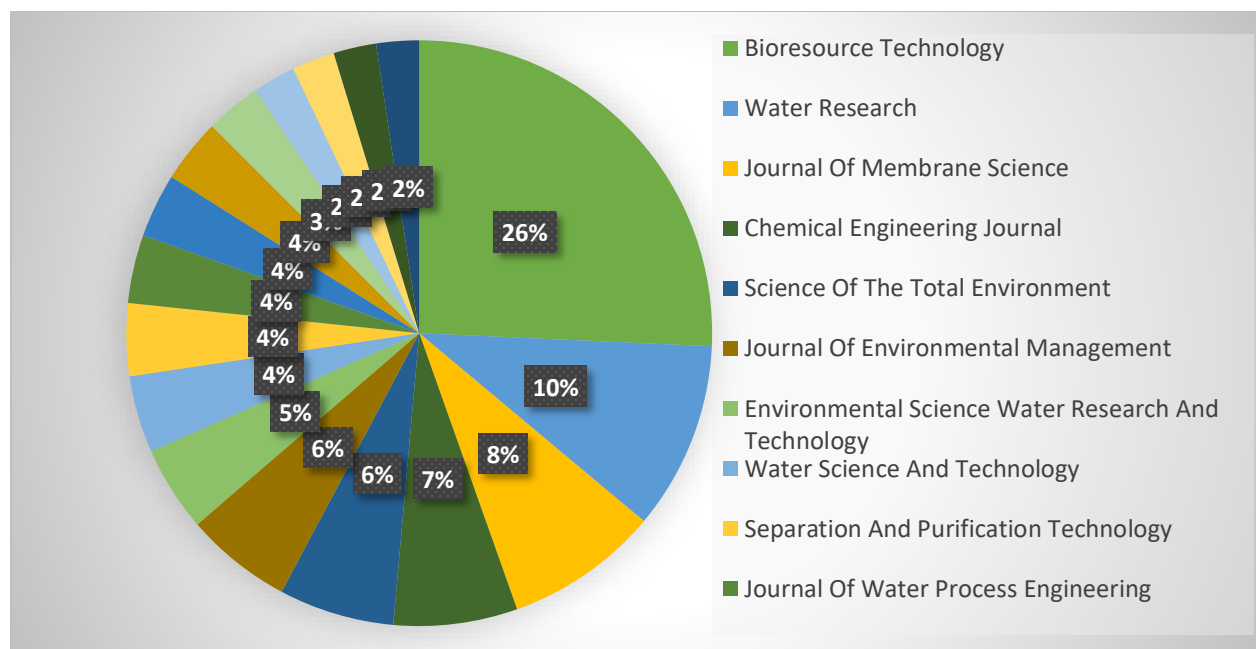
Figure 2. 22: Major journals publishing articles related to AnMBR retrieved from Scopus.

The research reviewed encompasses various areas, with the highest proportion (18.07%) dedicated to other applications. These applications cover a wide range of topics, including activated sludge treatment, removal of trace organic contaminants, anammox process, landfill leachate, food waste, HRT impact, comparative performance of UASB reactor with AnMBR, biogas production, dissolved gas transfer, and energy recovery, among others. These topics are collectively classified as "other topics."

Around 12.84% of the studies investigated the microbial community. The remaining research themes are as follows: fouling studies (12.52%), municipal wastewater (11.89%), wastewater treatment (10.62%), temperature studies (7.13%), combined aerobic and anaerobic membrane bioreactor systems (6.34%), industrial wastewater (4.62%), sewage treatment (3.33%), forward osmosis (FO) (3.17%), pharmaceuticals (3.17%), modeling (2.85%), design and economics (1.90%), and membrane cleaning (1.58%). All the remaining percent is dedicated to other applications which cover a wide range of topics, including activated sludge treatment, removal of trace organic contaminants, anammox process, landfill leachate, food waste, HRT impact, comparative performance of UASB reactor with AnMBR, biogas production, dissolved gas transfer, and energy recovery.

2.6.4 Advantages and Disadvantages of AnMBR technology

In its simplest terms, an AnMBR is a process of biological treatment that operates in an oxygen-deprived environment and uses a membrane to facilitate the separation of solids and liquids. Its benefits, when compared to traditional anaerobic systems and aerobic MBRs, have been widely acknowledged in scientific literature[182–185].

A comparison of conventional aerobic treatment, anaerobic treatment, aerobic MBR, and AnMBR is encapsulated in Table 2.10. Evidently, AnMBR technology merges the benefits of both anaerobic treatment and MBR technology. Some of the key advantages often highlighted include: the complete retention of biomass, superior quality of the resulting effluent, reduced sludge output, smaller spatial requirements, and the production of net energy.

There are predominantly two design layouts employed in the deployment of AnMBR systems: the external, or side-stream configuration, and the submerged, or immersed configuration. The external design allows for more immediate and direct management of fouling, delivering benefits such as simplified membrane replacement and high fluxes. However, these come with the trade-offs of more frequent cleaning needs and high energy usage (approximately 10 kWh/m^3 product) [186]. Additionally, it has been found that elevated cross-flow velocities can detrimentally affect the activities of the biomass in AnMBR systems [187–189].

In contrast, the submerged configuration involves the direct placement of the membrane within the liquid medium, utilizing a pump or gravity to draw the permeate through the membrane. This setup boasts several unique advantages over its external counterpart. These include significantly reduced energy demands and less stringent cleaning protocols, as well as gentler operating conditions, due to the lower tangential velocities.

Table 2. 10: Comparative analysis of aerobic treatment, anaerobic treatment, aerobic MBR and AnMBR.[117]

Feature	Conventional aerobic treatment	Conventional anaerobic treatment	Aerobic MBR	Anaerobic MBR
Organic Removal Efficiency	High	High	High	High
Effluent quality	High	Moderate to poor	Excellent	High
Nutrient Removal	High	Low	High	Low
Organic Loading Rate	Moderate	High	High to Moderate	High
Sludge production	High	Low	High to moderate	Low
Footprint	High	High to moderate	Low	Low
Biomass retention	Low to moderate	Low	Total	Total
Nutrient requirement	High	Low	High	Low
Alkalinity requirement	Low	High for certain industrial Stream	Low	High to moderate
Energy requirement	High	Low	High	Low
Temperature sensitivity	Low	Low to moderate	Low	Low to moderate
Startup time	2-4 weeks	2-4 months	<1 week	<2 weeks
Bioenergy recovery	No	Yes	No	Yes
Mode of treatment	Total	Essentially pretreatment	Total	Total or pretreatment

2.6.5 Implementations of AnMBR in different wastewater treatment scenarios.

A thorough examination reveals a growing focus on AnMBR research by individuals and research institutions, particularly over the last six years. This trend can be attributed to two main factors in wastewater treatment. On one hand, industrial sectors are confronted with increasingly strict demands for improving water use efficiency and closing their process water cycles, a trend set to continue into the future. Furthermore, the likelihood of dealing with extreme wastewater conditions is expected to rise in the coming years.

On the other hand, while the expenses associated with traditional technologies are gradually increasing due to labor costs and inflation, the prices for all membrane equipment have been consistently decreasing over the past decade. In addition, the opportunity to recover biogas during AnMBR treatment can provide significant benefits that can substantially reduce operational costs.

When assessing the financial outlay, both in terms of setup and running costs for a project, AnMBR is progressively becoming a more appealing choice. In this section, we will examine the various applications of AnMBR and their cutting-edge implementations in wastewater treatment.

2.6.5.1 Synthetic wastewater

Treating synthetic wastewater is a standard procedure to trial novel ideas or investigate membrane fouling's broad aspects [182]. Many recent investigations involving AnMBR have used synthetic wastewater as the feed, which makes sense given that AnMBR, particularly SAnMBR, is a relatively new approach for wastewater treatment, and membrane fouling is a significant concern. Table 2.11 showcases several recent studies about AnMBR systems treating synthetic wastewater. Various materials, including glucose, starch, molasses, peptone, yeast, and volatile fatty acids, have been used to create feed.

Since there are no persistent compounds, AnMBR typically achieves over 95% COD removal. OLR depends on the purpose of the research and is generally high when synthetic wastewater is used to measure the removal efficiency or processing capacity of an AnMBR. Theoretically, AnMBR can reach high OLRs (usually >10 kg COD/m^3/d) like High-Rate Anaerobic Reactors (HRARs), such as UASB reactors, hybrid UASB reactors, and EGSB reactors.

However, most studies applied an OLR of less than 10 kg COD/m^3/d. This can be traced back to several factors associated with AnMBR operation. Many studies have used a completely stirred tank reactor (CSTR) configuration due to its simplicity in use and construction. This setup typically operates at a lower biomass concentration compared to HRARs, translating to a lower OLR. Additionally, for research purposes, high biomass concentration and OLR may not be necessary, as membrane fouling is the primary research focus, and high biomass concentration or OLR could obstruct sustainable AnMBR operation. Based on these studies, it's safe to conclude that AnMBR holds promise as a technology capable of achieving high organic degradation.

Table 2. 11: Studies on AnMBRs employed for treating synthetic wastewater .

Type of wastewater	Scale [a]	Configuration	Characteristics of membrane [b]	Type of reactor	Reactor volume (L)	Operating condition	Influent [d]	Effluent [e]	Reference
Tapioca starch wastewater	L	External	Hollow fiber UF membrane Pore size: 0.03–0.15 μm	AF+M	1	HRT=10 d Temp=30 °C OLR=1.76 kg COD/m³/d	COD=20.15	COD=675–780 (>95%)	190
Meat extract+peptone	L	Submerged	Flat-sheet PE membrane, Pore size: 0.4 μm	CSTR+M	3	HRT=6 h SRT=150 MLVSS=2.62±0.13 g/L Temp=35±1 °C Flux=10 LMH	COD=0.45 ± 0.02	CODs=18±9 (95%)	183
Whey +sucrose	L	Submerged	Flat-sheet membrane, Pore size: 0.4 μm	CSTR+M	11	SRT=30–40 d MLVSS=5.5–20.4 g/L OLR=1.5–13 kg COD/m³/d Temp=35±1 °C Flux=2–5 LMH	-	-	191
Glucose+peptone+yeast extract	L	External	Tubular MF membrane Zirconia pore size: 0.14 μm PP pore size: 0.2 μm	CSTR+M	4.5	HRT=6.5 h Temp=54–56 °C OLR=4 kg COD/m³/d	COD=27 Kj-N=1.288	CODt=-(79–84%)	190
Glucose	L	External	Hollow fiber PE membrane Pore size: 0.4 μm	CSTR+M	2.5	MLSS=3.5 g/L	COD=0.8	-	192
Glucose	L	External	Flat-sheet membrane, Pore size: 0.45 μm	CSTR+M	5	HRT=12 h SRT=30 d Flux=5.3 LMH OLR=1.1 kg COD/m3/d pH=6.8–7.0 MLVSS=5.132 g/L Temp=25–30 °C	COD=0.55	COD=– (99.1%)	193
Volatile fatty acid	L	External	Tubular ceramic aluminum oxide (Al₂O₃) membrane Pore size: 0.2 μm	CSTR+M	2	SRT=120 d MLVSS<21 g/L OLR=10–55 kg COD/m³/d Temp=55 °C Flux=20–40 LMH	COD=10	-	194
Maltose +glucose + volatile fatty acid	L	Submerged	Hollow fiber PP membrane Pore size: 0.45 μm	CSTR+M	0.6	HRT=14 d MLVSS=19.5 g/L OLR=2.5 kg COD/m³/d Temp=35 ° C	COD=25	COD=95±9(99.6%)	195
Molasses	L	External	Tubular ceramic membrane, Pore size: 0.1 μm	CSTR/ CSTR+M	3/6	HRT=16/32 h MLVSS=1.8/10 g/L OLR=14.9/5.6 kg COD/m³/d	COD=10/8	COD=- (78–81%)	196

						Temp=55/55 °C pH=5.5/7.2			

a L=laboratory/bench scale.

b PE=polythylene and PP=polypropylene.

c CSTR=completely stirred tank reactor and AF=anaerobic filter.

d The concentration unit is g/L if not specified and – indicates value not reported.

e The concentration unit is mg/L; removal efficiency is presented in parentheses; CODs=soluble COD, and CODt=total COD.

2.6.5.2 Industrial wastewater treatment

The upswing in industrial activities has generated substantial industrial wastewater, predominantly coming from a wide array of sectors like food processing, paper and pulp, textiles, chemicals, pharmaceuticals, petroleum, tanneries, and manufacturing. Industrial wastewater typically features high organic density and/or extreme physical and chemical properties such as pH, temperature, and salinity. Additionally, it may contain synthetic and natural elements that could be detrimental to or hinder biological treatment procedures.

Table 2.12 provides a snapshot of notable recent cases where AnMBR was utilized to process different types of industrial wastewater. The principal area of application seems to be wastewater from the food industry. A review of relevant literature indicates that this wastewater is usually biodegradable and non-hazardous, containing high amounts of COD and SS[197] . As pointed out by Liao et al. [182], AnMBR has vast potential for treating wastewater that's high in organic strength and particulate content. Such characteristics make wastewater from the food industry especially compatible with AnMBR treatment.

In general, the COD removal efficiency achieved was above 90%, with the applied OLR typically falling within the 2-15 kg COD/m^3/d range. Since the majority of AnMBRs used CSTR configurations, the achievable OLR would be less than that of HRAR, but more than conventional CSTR digesters. For instance, Kubota Corporation developed a SAnMBR system known as the "KSAMBR" process, which has been successfully deployed in numerous full-scale food and beverage industries [181]. This process can reduce the volume to about a third or a fifth of conventional digesters if the biomass is concentrated three to five times, resulting in three to five times the volume based OLR, assuming the same flow rate is maintained.

Table 2. 12: AnMBR performance in treating industrial wastewater summarized.

Type of Wastewater	Scale [a]	Configuration	Characteristics of membrane [b]	Type of reactor [c]	Reactor volume (L) [d]	Operating condition	Influent [e]	Effluent [f]	Reference
Cheese whey	L	External	MF pore size: 0.2 µm	CSTR/ CSTR+M	5/15	HRT=1 d/4 d SRT=–/29.7–78.6 d MLVSS=–/6.4–10 g/L OLR=–/19.78 kg COD/m³/d Temp=37±2/37 °C Flux=139.5 LMH	COD=68.6±3.3 BOD₅=37.71±2.84 Kj–N=1.12±0.01 TP=0.5±1.8×10–3 TSS=1.35±0.06 pH=6.5	COD=– (98.5%) BOD₅<100 (99.2%) TSS=– (100%)	[198]
Diluted tofu processing waste	L	External	Hollow fiber MF membrane	CSTR+M	5	HRT=4h RNA concentration= 150–200 mg/L Temp=60±0.1 °C pH=5.5±0.1 Flux=4.32 LMH	COD=26.5±2.2 NH₄⁺-N=0.86±0.12 PO₄³⁻–P=0.58±0.06 TSS=23.5±3.5 pH=1.0	Carbohydrate Content<2 g/L	[199]
Olive-mill wastewater	L	External	Ceramic tubular UF 25 kDa MWCO	PABR+M	15	HRT=16.67 h MLSS=1.05–2.41 g/L Temp=35±2 °C Flux=80–450 LMH	COD=350–500 NH₄⁺–N=15–21 PO₄³⁻–P=3–4.5 SS=1–1.5 pH=6.5–7.8	COD<30 (>95%) TN=9–9.85 (15–20%) PO₄³⁻-P<1 (81%) pH=6.9–7.3	[200]
Brewery wastewater+surplus yeast	L	External	Ceramic tubular; Pore size: 0.2 µm	CSTR+M	4.5	OLR=12 kg COD/m3/d MLVSS=12 g/L Flux=4–20 LMH Temp=30 °C pH=6.9	CODs=21 Particulate COD= 45–50	COD=190 (99%) TSS=0 (100%)	[201]
High-concentration food wastewater	P	External	Flat-sheet PES 20–70 kDa MWCO	CSTR+M	400	HRT=60 h SRT=50 d pH=7.0±0.2 OLR<4.5 kg COD/m³/d MLSS=6–8 g/L Temp=37±0.5 °C	COD=2–15 SS=0.6–1.0 Chromaticity color=6000–1000 pH=5–6	COD=141–2388 (81.3–94.2%)	[185]
Distilley produces wastewater	F	Submerged	Kubota flat-sheet membrane	CSTR+M	-	Thermophilic range	COD=101.3 TN=3.72 TS=6 % pH=4.11	COD=– (75–92%)	[181]
Kraft evaporator condensate	L	Submerged	Flat-sheet PVDF membrane 140 kDa MWCO	UASB+M	10	HRT=5.8 d SRT=230 d MLSS=8.3±1.6 g/L OLR=3.1±0.8 kg COD/m³/d Temp=55±1 °C Flux=2.4±0.6 LMH	CODt=10	CODs=– (97–99%)	[184]
Kraft evaporator condensate	L	Submerged	Flat-sheet PVDF membrane 140 kDa MWCO	UASB+M	10	HRT=1.93 d SRT=230 d MLSS=8.2±1.5 g/L OLR=12.2±1.1 kg COD/m³/d	CODt=10	CODs=– (97–99%)	[184]

Type of Wastewater	Scale [a]	Configuration	Characteristics of membrane [b]	Type of reactor [c]	Reactor volume (L) [d]	Operating condition	Influent [e]	Effluent [f]	Reference
						Temp=35±1 °C Flux=7.2±0.9 LMH			
TMP whitewater	L	Submerged	Flat-sheet PVDF membrane 140 kDa MWCO	UASB+M	10	MLSS=5.7±0.8 g/L OLR=2.4±0.4 kg COD/m³/d Temp=35±1 °C Flux=5.2±0.5 LMH	CODs=2.78–3.35	CODs<300 (90%)	202
Petrochemical wastewater	L	Submerged	Kubota flat panel membrane Pore size: 0.45 µm	CSTR+M	23	HRT=31.5 h SRT=175 d MLSS>30 g/L OLR=14.6 kg COD/m³/d Temp=37 °C Flux=8.5–16 LMH	COD=19 pH=7.2	COD=612 (98%)	203
Textile wastewater	L	Submerged	Hollow fiber MF membrane Pore size: 0.40 µm	CSTR+M	3.25	HRT=24 h pH=6.8–7.2 Temp=35 °C Flux=1.8–14.4 LMH PAC dose=1.7 g/L	COD=730–1100	COD=– (90%) Color=– (94%) Turbidity=8 NTU	204

a L=laboratory/bench scale, P=pilot scale, and F=full scale.

b PVDF=polyvinylidine fluoride and PES=polyethersulfone.

c CSTR=completely stirred tank reactor, UASB=upflow anaerobic sludge blanket, and PABR=periodic anaerobic baffled reactor.

d – indicates value not reported.

e The concentration unit is mg/L if not specified; CODs=soluble COD, and CODt=total COD.

f The concentration unit is mg/L and removal efficiency is presented in parentheses

2.6.5.3 Municipal wastewater

The primary use of anaerobic methodologies has historically been focused on industrial or high strength wastewater treatment. Its use in municipal wastewater treatment has been comparatively less, a trend that can be attributed to two major factors. Firstly, retaining slow-growth anaerobic microorganisms within the short HRT needed for treatment of low strength, or municipal wastewater has proven to be a challenge [205]. Secondly, the slower kinetic rates of anaerobic metabolism often result in effluents that do not meet the required standards for wastewater disposal or reuse [206].

However, a promising solution for sustainable municipal wastewater treatment could come from integrating membrane separation technology with anaerobic bioreactors. This combination ensures total biomass retention and provides several benefits, including reduced sludge production, improved effluent quality, the potential for net energy production, and the elimination of additional costs linked to aeration in aerobic treatment processes [207–209].

The use of AnMBRs in municipal wastewater treatment has gained significant recognition in recent years [118,207,209]. Several studies attest to the effectiveness of this technology. For instance, AnMBRs have been found to typically eliminate >85% of COD and >99% of TSS under selected operational conditions, irrespective of system design[210]. This level of performance notably exceeds that of conventional UASB treatments and is comparable with aerobic MBR procedures.

The high efficiency of AnMBRs is largely due to the employment of membranes with pore sizes ranging from 0.01–0.45 μm, which allow for effective retention of SS, most colloids, and some organic materials. Moreover, the full capture of sludge by the membrane and the use of extended SRT ensure effective pollutant removal [208].

Nevertheless, it is important to note that increasing the pore size of the membrane can lead to a decrease in the efficiency of COD removal. This was apparent in a study by Zhang et al., which reported a reduction in COD removal to 57.3±6.1% due to the use of a dynamic membrane for separation [211].

Despite the high efficacy of AnMBR systems in the removal of COD and TSS, the effectiveness in eliminating total nitrogen (TN) and total phosphorus (TP) tends to be minimal [210] (Table 2.13). This is anticipated as the removal processes of TN and TP typically require the presence of anoxic or aerobic conditions. While this characteristic could prove beneficial if the effluent is destined for

applications such as irrigation or agriculture, it usually necessitates an additional downstream treatment phase for effluent reclamation.

The integration of AnMBR technology with traditional biological nutrient removal methods can present challenges due to the low COD:N and COD:P ratios common in AnMBR effluents. A potentially promising solution for nutrient removal lies in the process of partial nitritation/nitrification, with ammonium serving as the electron donor, thus decreasing the need for additional carbon sources or electron donors [212]. The Forward Osmosis (FO) membrane process provides an alternate approach, with its capability to reject almost all N and P contaminants. Albeit more energy-intensive, physical, or chemical nutrient removal processes also offer potential solutions.

A recent and significant concern in the realm of environmental health is the occurrence of trace contaminants, such as endocrine disrupting chemicals (EDCs) and pharmaceutically active compounds (PhACs), in both treated and untreated municipal wastewater [213]. Studies suggest that the efficacy of removing EDCs and PhACs during anaerobic digestion is subpar [214,215]. As reported by Ifelebuegu [214], the anaerobic digestion process witnesses a persisting presence of EDCs, with removal percentages varying between 21–24% for steroidal estrogens (E1), 18–32% for 17β-estradiol (E2), 10–15% for 17α-ethynylestradiol (EE2) and 44–48% for nonylphenol (NP).

It's important to note that the removal efficiency could be improved by prolonging the HRT and utilizing bioaugmentation. Under anaerobic conditions and with a relatively extended HRT can be substantial degradation of certain PhACs, including acetylsalicilic acid (ASA), ibuprofen (IBU), and fenofibrate (FNF). An AnMBR system implemented by Saravanane and Sundararaman [216] to treat wastewater containing a cephalosporin derivative achieved a considerable degradation enhancement, with a removal rate of 81% at a maximum cephalosporin concentration of 175 mg/L, through the process of bioaugmentation. The primary means of removing these trace contaminants during the sludge process appears to be biodegradation facilitated by microorganisms and sorption onto biomass [214].

Regarding operational parameters, AnMBR systems usually maintain a HRT longer than 8 hours, which compares favorably with traditional anaerobic systems [182], and surpasses the typical 4–8 hours seen in aerobic MBRs. This corresponds to a lower OLR of less than 3 kg COD/m^3/day compared to aerobic MBRs. The membrane flux used in most AnMBR studies seems to be under 15 LMH, which is less than the 25-140 LMH and 3.7–85 LMH for external and submerged

configurations respectively in aerobic MBRs [217]. This lower sustainable membrane flux could present a challenge for the practical engineering application of AnMBR.

In a study examining the creation of a dynamic membrane on Dacron mesh (pore size=61 μm), a high flux of about 65 LMH was attained in anaerobic dynamic membrane bioreactors (AnDMBR) [211]. Considering the relatively high cost of ultrafiltration (UF) or microfiltration (MF) membranes, coupled with their low sustainable flux, AnDMBR seems to be a promising solution for municipal wastewater treatment.

The capital costs for SAnMBR systems treating municipal wastewater were found to be approximately 800 US$/m^3/day capacity [197], which is competitive when compared to literature values for full-scale aerobic MBRs [218]. The total operational costs were only a third of the aerobic counterpart of a similar capacity [219]. Additionally, the operational costs can be fully compensated by the benefits of biogas recovery. A cost-sensitive analysis demonstrated that membrane parameters, including flux, price, and lifespan, have decisive roles in determining the total life cycle costs of the SAnMBR [197]. SAnMBR could be a promising technology for municipal wastewater treatment, provided that significant improvements can be made to membrane performance.

Table 2. 13: AnMBR performance in treating municipal wastewater summarized.

Type of wastewater	Scale [a]	Configuration	Characteristics of membrane [b]	Type of reactor [c]	Reactor volume (L)	Operating condition	Influent [d]	Effluent [e]	Reference
Municipal wastewater	L	Submerged	Flat-sheet MF PVDF 140 kDa MWCO	CSTR	60	HRT=10 h MLSS=6.4–9.3 g/L OLR=~1.0 kg COD/m3/d Temp=30±3 °C Flux=11 LMH	COD=425±47 NH4+ –N=32.4±11.6 NO$_3$ – N=1.3±0.4 TP=4.3±0.5 SS=294±33 pH=7.6±0.3	COD=51±10 (88±2%) NH$_4^+$–N=31.1±12.3 (~0%) NO$_3^-$–N=1.1±0.6 (~0%) TP=3.8±0.7 (~0%) SS<0.8 (>99.5%) pH=7.0±0.2	[197]
Municipal wastewater	L	Submerged	Flat-sheet dynamic membrane, Dacron mesh	UASB	45	HRT=8 h MLSS=5.9–19.8 g/L OLR=~0.9 kg COD/m3/d Temp=10–15 °C Flux=65 LMH	COD=302.1±87 9 NH4 + N=37.9±8.6 TN=58.8±10.2 SS=120±23 pH=7.3±0.3	COD=121±34 (57.7±4.6%) SS=0–15 pH=7.2–7.6	[211]
Municipal wastewater	L	External	Tubular UF membrane 40 kDa MWCO	UASB	1	HRT=3 h SRT=100 d Temp=25 °C Fluxb7 LMH	CODt=646±103 CODs=385±63 TSS=140±18 MPNFecal coliforms=106/ 100 ml	CODt=104±12 (87%) CODs=104±12 (73%) BOD=32±5 TSS<1 MPN $_{Fecal\ coliforms}$=0 (100%)	[206]
Dilute Municipal wastewater	L	External	PVDF; pore size: 0.1 µm, 200 kDaMWCO	CSTR	10	HRT=3 h SRT=100 d Temp=25 °C Fluxb7 LMH	CODs=38–131 pH=7.5	CODs=18–37 (55–69%) NH$_4^+$–N=8.9–51.8 NO^{3-}N<0.4 (0%) NO$_2^-$N<0.4 (0%) pH=6.6±0.1	[208]
Domestic wastewater	L	External	Hollow fiber, MF, Pore size: 0.2 µm	CSTR	180	HRT=6 h MLSS=14–80 g/L OLR=2.16 kg COD/m^3/d Temp=25 °C Flux=7.5 LMH	CODt=540	CODs=65 (88%)	[207]
Municipal wastewater	L	Submerged	Non-woven fabric, PET, pore size: 0.64 µm	UASB	12.9	HRT=2.6 h OLR=2.36 kg COD/m^3/d Temp=15–20 °C Flux=5 LMH	COD=259.5±343.8 NH$_4$ + N=27.5±13.6 TP=4.2±1.4	COD=77.5±29.5 NH$_4^+$–N=27.6±12.5 TP=3.2±1.3	[118]
Domestic wastewater	L	External	UF membrane 100 kDa MWCO	CSTR	50	HRT=15 h SRT>140 d MLVSS=0.5–10 g/L OLR=2.0 kg COD/m^3/d Temp=37 °C Flux=3.5–13 LMH	COD=685±46.4 TOC=157±8.6 BOD5=356±18.5 Kj–N=156±7.8 TP=11.5±0.6 SS=380±9.3	COD=87.8±6.2 (88%) TOC=19±1 BOD5=31.2±2.2 (90%) Kj–N=38.8±2 TP=11±0.55 SS=0 pH=7.7±0.2	[209]
Municipal wastewater	L	External	Flat-sheet, CA, Pore size: 0.2 µm	CSTR	15	HRT=16.67 h	COD=350–500 NH4 + –N=15–21	CODb30 (>95%) TN=9–9.85 (15–20%)	[197]

Type of wastewater	Scale [a]	Configuration	Characteristics of membrane [b]	Type of reactor [c]	Reactor volume (L)	Operating condition	Influent [d]	Effluent [e]	Reference
						MLSS=1.05–2.41 g/L Temp=35±2 °C Flux=80–450 LMH	PO4 3−–P=3–4.5 SS=1–1.5 pH=6.5–7.8	PO_4^{3-}–Pb1 (81%) pH=6.9–7.3	
Domestic wastewater	L	External	PTFE Teflon membrane pore size: 0.45 µm	CSTR	850	HRT=14.4 h OLR=0.8 kg COD/m³/d Temp=22 °C	CODt=620–650 (637) TOC=180–230 (207) NH_4 +–N=56–61 (58) Kj–N=70–78 (74) TP=10–12 (11)	TOC=17 (>90%) Kj–N=67 TP=10	[220]
Municipal wastewater	L	External	PVDF; pore size: 0.1 µm, 200 kDa MWCO	CSTR	10	HRT=48 h MLSS=1.01±0.29 OLR=0.03±0.01 kg COD/m³/d SRT=19 d Temp=32 °C	CODs=84±21 NH_4+–N=27.3±13.5 PO_4^{3-}–P=6±2.3 NO_3^-–N=0.3±0.2 TSS=120±60 pH=7.5±0.1	CODs=25±12 (58±14%) NH_4+–N=8.9–51.8 NO_3^-–Nb0.4 (0%) NO_2^-–Nb0.4 (0%) pH=6.6±0.1	[221]

a L=laboratory/bench scale.

b PVDF=polyvinylidine fluoride, PET=polythylene terephthalate, CA=cellulose acetate, and PTFE=polytetrafluoroethylene.

c CSTR=completely stirred tank reactor and UASB=upflow anaerobic sludge blanket.

d The concentration unit is mg/L if not specified; CODs=soluble COD, and CODt=total COD.

e The concentration unit is mg/L; and removal efficiency is presented in parentheses.

2.6.6 Membrane system

The performance and efficiency of AnMBR systems are directly influenced by the choice of membrane module [222]. Among the modules available, the most widely marketed and utilized options are hollow fiber (HF), flat sheet (FS), and multi-tubular (MT) membranes, primarily due to their favorable quality-to-price ratio. Submerged processes, such as those involving vacuum-driven membranes in anaerobic reactors, often employ HF or FS membranes [223,224]. On the other hand, MT membranes are commonly used in side-stream configurations, where they operate as cross-flow membranes driven by external pressure [225].

Choosing the appropriate module and its material is crucial for achieving optimal process performance. Membranes in AnMBR systems are typically constructed using materials such as polymers, ceramics, and metals. The selection of the module and its specific material composition plays a significant role in determining the overall efficiency and effectiveness of the AnMBR process.

Polymeric membranes are widely utilized in practical membrane separation processes, in contrast to metal and ceramic membranes, which tend to be costly and have limited applications [222]. Among the polymeric membrane options, materials such as polyvinylidene fluoride (PVDF), polysulfone (PSF), polypropylene (PP), polyethylene (PE), and polyethersulfone (PES) are commonly employed in AnMBR systems [222,224,226–228]

There are several reasons why organic polymer membranes are well-suited for AnMBR applications. Firstly, they offer a more cost-effective solution compared to ceramic membranes. Moreover, organic polymer membranes exhibit higher packing density and enjoy widespread availability in the commercial market. These advantages make organic polymer membranes the preferred choice for AnMBR systems, owing to their lower cost, higher packing density, and greater commercial accessibility compared to alternatives such as ceramic membranes[229].

Only few research studies have explored the use of inorganic ceramic membranes, by conducting laboratory scale experiments. These ceramic membranes, typically composed of aluminum oxide, have wide pore sizes ranging from 0.05 to 0.5 μm [230]. Integrating ceramic membranes into AnMBRs could be a strategic choice for treating wastewater under challenging conditions, such as high temperatures and pressures, handling substantial organic loads with short HRTs, while minimizing excessive sludge production. This integration allows for direct and efficient capture of COD and improved biogas production [231].

Ceramic membranes exhibit impressive resistance to temperatures up to 350 °C, pressures up to 4 bars, and a wide pH range of 0–14, making them highly durable against corrosive chemicals and cleaning agents [232]. One study, [233] demonstrated that a bench-scale AnMBR system using ceramic flat-sheet membranes effectively treated domestic wastewater supplemented with food waste recycling wastewater, achieving impressive COD and Total Organic Carbon (TOC) removal efficiencies of 98.3% and 97.9%, respectively. The system operated at a target HRT of 12 hours, corresponding to an OLR of 3.0 kg COD/m^3/d. During operation, the average methane production was 0.21 L CH_4/g COD removed [233].

Ceramic flat-sheet membranes have a double-layer structure with a coated layer on the porous support layer, facilitating permeate draw and maintaining the target flux for extended periods, up to approximately 200 days, without the need for chemical cleaning. Furthermore, these membranes effectively eliminate biopolymers and low molecular weight substances, major fouling precursors[231,233]. By utilizing ceramic membranes, clogging frequency is reduced due to their high hydrophilicity, leading to improved fouling efficiency. The negatively charged surface of ceramic membranes at neutral pH enhances electrostatic repulsion forces with most foulants, further contributing to effective fouling prevention [233].

In comparison to polymeric membranes, ceramic membranes have demonstrated superior performance in filtering solutions with varying ionic strength, requiring less frequent cleaning and withstanding more aggressive cleaning agents. Physically and chemically, ceramic membranes are more efficiently cleaned, surpassing polymeric membranes by 70% and 25%, respectively [232].

However, the cost of ceramic membranes remains a significant concern, constituting a considerable portion of the total investment cost for implementing large-scale AnMBRs for MWW [197]. Researchers are continuously working on improving the permeability and antifouling properties of filtration membranes to make the application of membrane filtration in AnMBRs more technically and economically viable, given the rapid advancements in materials science [234].

Among the promising membrane processes, FO stands out as an osmosis process utilizing semipermeable membranes to efficiently separate water from solvents through highly concentrated draw solutions. FO systems rely on osmotic pressure differentials rather than hydraulic pressure differences, enabling operation at low or no hydraulic pressure and exhibiting high contaminant removal and low membrane fouling tendencies [235].

The analysis above highlights the potential benefits of combining various configurations of anaerobic bioreactors with membrane filtration to create an efficient AnMBR system. These high retention systems are specifically designed to meet stringent standards for eliminating certain pollutants and adhering to strict regulations. They utilize bioreactors with membranes of even higher porosity, such as the anaerobic osmotic membrane bioreactor and anaerobic membrane distillation bioreactors. Integrating forward osmosis or membrane distillation processes into these setups can enhance the removal of contaminants and germs in specific water reuse applications [229,235,236].

Compared to conventional microfiltration and ultrafiltration membranes, FO membranes offer distinct advantages, including higher selectivity, reduced fouling tendencies, and better fouling reversibility [237]. However, the choice of using these membranes depends on the vision and scale of the water reuse projects, considering that they can be quite expensive. To make an informed decision and find the optimal AnMBR configuration, a comparative study involving long-term full-scale operation is crucial to serve as a valuable reference [224].

Table 2.14 provides a summary of the principal membrane materials and modules utilized in AnMBR research. As indicated, most of the membranes deployed feature pore sizes spanning from 0.03 to 1.0 µm. This range is notably smaller than the size of most flocs or microorganisms found in AnMBR systems, thereby facilitating almost total biomass retention.

Table 2. 14: Principal materials and modules of the membrane employed in AnMBR research.

Membrane material	Module configuration	Nominal pore size/µm	Manufacturer	Reference
PVDF	Hollow Fiber	0.04	GE, USA	[238]
PVDF	Hollow Fiber	100kDa	Koch, USA	[239]
PVDF	Flat sheet	70kDa 140 kDa	SINAP, China	[197,240]
PVDF	Tubular	0.03	Norit X-Flow, Inc. Netherlands	[241]
PVDF	Tubular	0.1	PCI Membrane Systems, Inc. USA	[221]
PES	Flat sheet	20-70 kDa	SINAP, China	[185]
PES	Tubular	20kDa	Weir Envig, Paarl, South Africa	[242]
PE	Flat sheet	0.4	Kubota Corporation,Japan	[243]

Membrane material	Module configuration	Nominal pore size/μm	Manufacturer	Reference
PE	Hollow Fiber	0.4	Mitsubishi Rayon, Japan	[244]
PP	Hollow fiber	0.45	Sumitomo Electric Fine Polymer Inc., Japan	[195]
PSF	Tubular	0.2	Triqua, Netherlands	[245,246]
Ceramic	Tubular	40kDa	Aquatech Memtuf©, Korea	[206]
Ceramic	Tubular	0.2	Atech Innovations, Germany	[194]
Metal	Tubular	1.0	Fibertech Co., Ltd, Korea	[247]

Typically, the membrane accounts for a significant portion, up to 72.3%, of the total capital cost in AnMBR systems used for MWWT[248] To address this cost challenge, researchers have explored the possibility of using low-cost filters as an alternative to reduce the expenses associated with membranes, considering that membranes are primarily employed for liquid-solid separation.[249,250] These low-cost filters have been modified by incorporating anti-fouling functional groups on their surfaces to mitigate membrane fouling.[251]. However, it's worth noting that while these filters achieve high water flux due to their high permeability and larger pore size, they are not suitable for long-term operation due to their low shear and tensile strength. In light of this, investigations have been conducted on more economical pore-sized materials, such as non-woven filter media and stainless steel mesh, which exhibit self-forming dynamic membrane properties[252].

The membrane pore size plays a crucial role in AnMBRs, impacting the retention rate, energy consumption, and filtration resistance. Additionally, the membrane pore size significantly influences membrane fouling.[253]. Consequently, selecting the appropriate membrane pore size in AnMBRs depends on the type of mixed liquor suspended solids.

Table 2.15 provides a summary of various AnMBRs with different membrane pore sizes and configurations and their respective influence on COD removal. The range of pore sizes between 0.1–10 μm is typically associated with microfiltration (MF), while pore sizes of 0.002–0.1 μm are related to ultrafiltration (UF). These membrane options enable longer SRT or better biomass retention in the AnMBR system[254,255]. Previous research has demonstrated that using smaller membrane pore sizes can mitigate surface clogging and improve the retention rate[256].

Table 2. 15: Membrane materials and module configuration of AnMBR technology

Membrane material	Module	Membrane pore size	Surface area (m²)	Operational conditions	Reference
PTFE [a]	Hollow fiber	0.3 µm	0.2	Municipal wastewater; flux: 12 LMH; pH: 7.5; COD (g L^{-1}): 72.9; TS (g L^{-1}): 44.7	[257]
PVDF [b]	Hollow fiber	0.05 µm	30	Urban wastewater; removal efficiency: 87%; HRT (h): 6–21; SGD: 0.23	[258]
Metallic	Flat sheet	0.2 µm	0.1	Distillery wastewater; removal efficiency: 94.7%; pH: 4–5; COD (g L^{-1}): 0.7–1.5; HRT (h): 10–30; SS (g L^{-1}): 3–8	[259]
PE [c]	Flat sheet	0.2 µm	0.122	Synthetic industrial wastewater; removal efficiency: 97%; pH: 7; COD (g L^{-1}): 3–4; HRT (h): 24–6	[260]
PTFE [a]	Flat sheet	0.45 µm	1.59	Municipal wastewater; removal efficiency: 92%; COD (g L^{-1}): 0.637; TOC (g L^{-1}): 0.207	[222]
PVDF [b]	Flat sheet	0.1 µm	0.33	Synthesized wastewater; removal efficiency: 84%; pH: 4–5; HRT (h): 36; SS (g L^{-1}): 1.9	[261]
Ceramic	Flat tubular	0.1 µm	0.08	Synthesized wastewater; removal efficiency: 88%; pH: 6.8–7.2; HRT (h): 7; COD (g L^{-1}): 0.35–0.5; SS (g L^{-1}) 10	[262]
PES [d]	Flat sheet	0.038 µm	3.5	Synthesized wastewater; removal efficiency: 82.7%; pH: 6.8; COD (g L^{-1}): 0.630	[263]

[a] PTFE, polytetrafluoroethylene. [b] PVDF, polyvinylidene difluoride. [c] PE, polyethylene. [d] PES, polyethersulfone

The pore sizes of membranes mentioned in Table 2.15 typically range from <0.001 to 1 µm, which is generally smaller than the size of microorganisms and flocs, allowing them to effectively retain almost all biomass. Figure 2.23 illustrates the different membrane separation capacities.
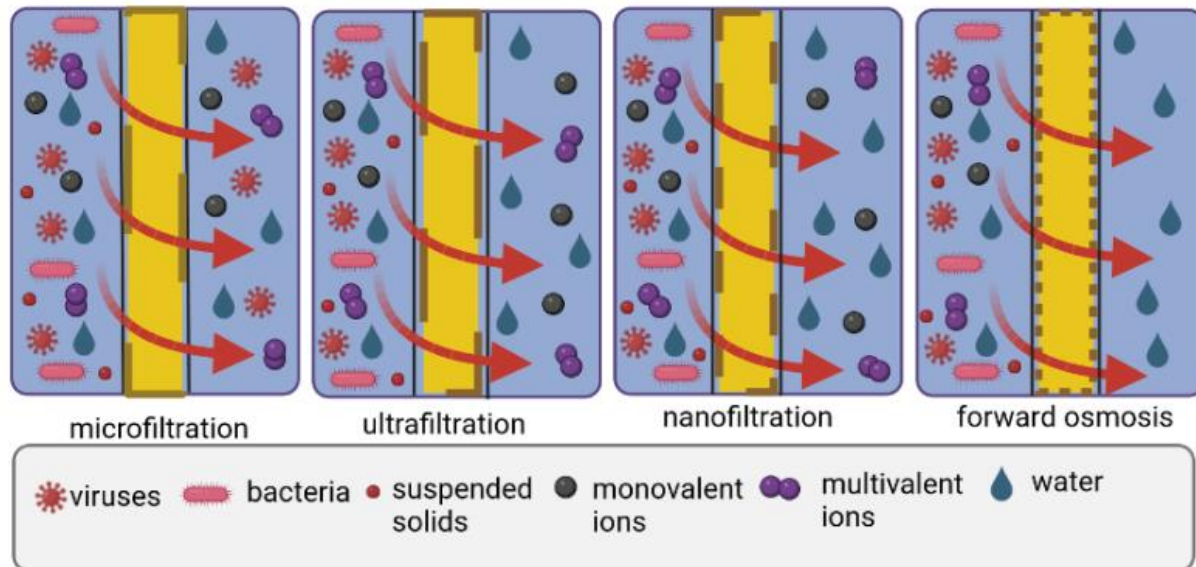
Figure 2. 23 Types of membrane separation capacities[264]

In general, AnMBRs commonly employ three types of membrane configurations: hollow-fiber, tubular, and flat sheet membranes (Figure. 2.24). The hollow-fiber membranes have garnered significant interest in the scientific community for treating bio-waste due to their advantages, such as a higher surface area per unit volume (1200 m^2 m^{-3}), cost-effectiveness, and capability to withstand heavy backwashing. However, they are prone to rapid fouling, necessitating more frequent cleaning cycles [265].

On the other hand, tubular membranes exhibit higher resilience to harsh operating conditions, greater mechanical strength, longer lifespan, and lower fouling propensity, making them an attractive option. Despite these benefits, tubular membranes have some drawbacks, including lower packing density, reduced surface area per unit volume (100 m^2 m^{-3}), and relatively higher operational costs, which somewhat limit their practicality[266] .In contrast, flat sheet membranes show great promise for commercial applications in AnMBRs due to their enhanced stability, higher effective flux, longer lifespan, and ease of replacement and cleaning [197]. These features position flat sheet membranes as an appealing choice for a wide range of AnMBR applications.
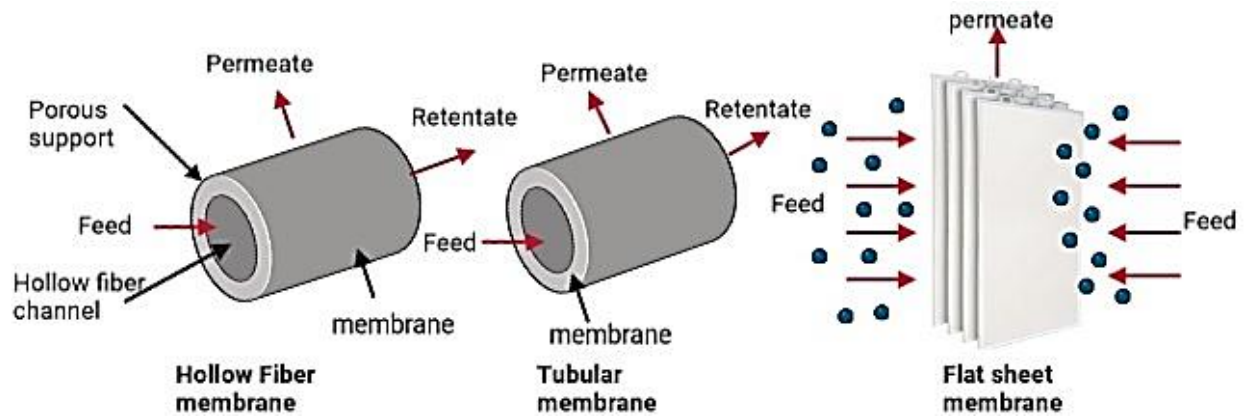
Figure 2. 24: Different membrane configurations of AnMBR [264]

2.6.7. Operating parameters and conditions affecting AnMBR performance

When considering the key operational parameters that influence the efficiency of AnMBRs, the primary operating parameters include: (1) sludge retention time (SRT), (2) hydraulic retention time (HRT), (3) organic loading rate (OLR), and (4) temperature, The influence of these parameters on the AnMBR system's performance is evident in terms of organic removal (like COD and/or BOD removal) and reactor stability, characterized by volatile fatty acids (VFAs) content and alkalinity.

➢ Sludge Retention Time (SRT)

The SRT which corresponds to the period the sludge remains in the AnMBR is one of the most important operational parameters that affects the following: (1) effluent characteristics; (2) concentration of suspended solids in the reactor; (3) biogas production; (4) microbial community and (5) degree of sludge stabilization[223]. It's noteworthy that, unlike an UASB reactor, an AnMBR has the capacity for complete biomass retention, which facilitates a more straightforward control over the SRT.

To minimize sludge wasting, the use of long SRT is desired [267]. It results in higher digestion efficiency lower sludge production and increased methane recovery [268,269,270]. Longer SRT retains the organic matter longer, allowing more time for degradation of slowly biodegradable-organic compounds that leads to higher quality of the permeate [269,271].

Methane yield is lower at shorter SRT because more carbon is utilized for cellular growth rather than methane production [267,269]. In terms of methane solubility in the permeate, Yeo and Lee (2013) demonstrate that longer SRT decreases the amount of dissolved methane by over 50% specifically when the SRT is extended from 20 to 40 days[272]. This is potentially due to the reduction in active methanogens as indicated by slower substrate utilization and endogenous decay at SRT of 40 days. At longer SRT, sludge production decreases due to the increased hydrolysis of volatile suspended solids (VSS)) and greater proportion of available carbon is utilized for methanogenesis rather than cellular growth [220].

A study conducted by Trzcinski and Stuckey (2010) involving two SAnMBRs treating municipal solid waste leachate at psychrophilic temperatures - with SRTs set at 300 and 30 days, respectively - discovered a correlation between extended SRT and increased soluble COD removal[243]. On the other hand, Baek et al. (2010) reported that a substantial reduction in SRT, from 213 to 40 days, did not yield any significant effects on the performance of the treatment or the incidence of membrane fouling[208]. This observation underlines the intricate nature of the relationship between SRT, treatment efficiency, and membrane fouling. The relationship seems to depend heavily on the chosen HRT and the characteristics of the feed being treated. As a general rule, AnMBR operations employing relatively prolonged HRTs and SRTs tend to be beneficial, as they lead to enhanced methane recovery, improved overall treatment performance, and diminished sludge production[273] .

➢ pH

The majority of AnMBR systems are known to operate within a nearly neutral pH range, given that anaerobic digestion typically occurs within a pH spectrum of 6.5-8.5, with the optimal range being between 7.0 and 8.0 [274]. Attaining such a pH range usually necessitates neutralization, which may lead to excessive use of chemicals, especially in instances where the feeds have extreme pH values or when the hydrolysis and acidogenesis phases result in a decrease in pH values. From this perspective, achieving equilibrium at a desirable pH seems to be a promising strategy, though the relevant research in the context of AnMBR systems remains notably limited.

➢ OLR

Controlling OLR in an AnMBR system is vital as excessively high value results in its failure while extremely low values do not maximize its capacity [275]. Changes in OLR may be obtained either by increasing the influent flow rate, the influent pollutant concentration or by shortening HRT.

A rise in OLR leads to better COD removal rates and boosts biogas output due to greater methane generation[269,276–278]. As an example, a 400% OLR increase results in around 600% and 625% surge in biogas and methane outputs respectively [278]. This surge can be attributed to the positive effects on microbial communities [279]. For instance, in AnMBRs treating different wastes, the primary methanogens shift, indicating changes in microbial compositions [242,277]. This shift seems to enhance certain microbial functions, like hydrolytic enzyme activities, which can increase significantly with rising OLR [277].

However, there are downsides to high OLR. It might cause a dip in methane's proportion in biogas due to the rising CO_2 levels [280]. The reason could be the growth of CO2-producing bacteria promoted by elevated OLR and the negative effects of accumulating VFAs [280]. For example, a study observed reduced biogas production when OLR was ramped up [167].

Despite this, the ability to handle varying (and particularly higher) OLRs showcases AnMBR's operational stability. This adaptability, coupled with potential benefits like more biogas output and cost savings, makes high OLR operation of AnMBR economically favorable [277,281].

➢ Temperature

AD is profoundly affected by temperature. AD processes can be categorized into three temperature groups: psychrophilic (0-20°C), mesophilic (20-42°C), and thermophilic (42-75°C). Elevated temperatures notably enhance methanogenesis, with the thermophilic range (50–60°C) being particularly effective in degrading carbohydrates (97% degradation), lipids (95% degradation), and proteins (75% degradation) [282]. The increased removal efficiency leads to improved methanogenic activity, methane production, and recovery[283].

Operating within the mesophilic range (25–35°C) can achieve a net energy recovery. However, to reduce operational costs, especially for AnMBR, temperatures below 15°C are more economical[34,284]. One drawback of lower temperatures is the decline in removal efficiency[285,286].

In AnMBR treating concentrated sewage, COD removal efficiency varies between 76–95% for temperatures ranging from 17–34°C but drops to 67% at 15°C[285]. Likewise, the Annamox-FMBR from Kwak et al. (2019) showed a decrease in TN removal efficiency from 85% to below 30% when temperatures went from 25°C to 15°C. Subsequent increases in temperature led to improvements in removal efficiency[285,287]. Contrarily, a study by Lim et al. 2019 found little difference in COD and BOD_5 removal efficiencies across temperatures ranging from 31.5°C to 12.7°C, suggesting that AnMBRs can still function effectively even below 20°C. Reduced removal efficiency at lower temperatures stems from slowed microbial activity, which correlates with higher VFAs levels in the permeate[276,285].

Additionally, decreased temperatures impact biogas production. Biogas and methane outputs decline at cooler temperatures with methane being more soluble in liquid phases in colder conditions[285,286,288] . Shifts in the archaeal community can occur due to temperature changes, potentially causing reduced methane yields from lowered methanogenic activity[286]. Significant temperature drops might even halt biological processes in AnMBRs, evident by stopped biogas production and VFA accumulation [289].

From the perspective of industries like pulp and paper or textiles that produce high-temperature wastewater, AnMBRs operating at thermophilic temperatures can negate the need for temperature moderation methods common in mesophilic treatments[184,196,290]. Yet, higher temperatures can cause reduced membrane flux due to sludge deflocculation and Extracellular Polymeric Substances (EPS) release. Finding the optimal operational temperature is crucial.

Yet, for many streams, including municipal wastewater, operation at ambient or lower temperatures is a practical necessity for cost-effective implementation of AnMBRs. The treatment by psychrophilic AnMBRs has recently garnered substantial interest [291]. It has been discovered that both psychrophilic and mesophilic treatments achieved similar COD removal efficiency, nearing 90%, although the former showed a slightly higher rate of membrane fouling due to the accumulation of VFAs [292]. This outcome underscores the potential role of membrane filtration in maintaining performance stability amidst temperature variations.

Temperature also influences membrane fouling, as evidenced by multiple studies [288,293]. Generally, sludge becomes denser and smaller at higher temperatures. As a result, it is less influenced by cross-flow forces and is more likely to deposit on the membrane surface, forming a cake layer[184]. Specifically, the fouling layer on the membrane surface of an AnMBR operated at 65°C is thicker than that at 45°C. This identifies 45°C as the optimum temperature that balances both biogas production and sustained membrane use. The thicker fouling layer and resultant flux decline observed by Yao et al. (2019) might also be attributed to the enhanced microbial activity at elevated temperatures, leading to increased production of SMP and EPS [217]. Conversely, the reduced cake layer at lower temperatures results in more significant pore blocking, as noted by Watanabe et al. (2017) at 10–15°C[286]. This phenomenon is likely due to the increased SMP and EPS production at these cooler temperature ranges. Such an uptick in SMP and EPS production is often a microbial defensive response against environmental stresses like temperature fluctuations [286]. Between cake layer fouling and pore blocking, the former is considered more manageable because of its reversible nature. Other AnMBRs operated within the 15–35°C temperature range also demonstrate more severe fouling at lower temperatures, as marked by flux reduction [288].

To broaden the application of AnMBR technology, a key challenge lies in overcoming the issues caused by local climate change conditions within the 0 to 25°C range. However, up until now, no studies have evaluated the treatment performance of AnMBRs on psychrophiles at ambient temperatures.

> ### Hydraulic Retention Time (HRT)

In contrast to SRT, HRT refers to the duration wastewater (specifically, soluble compounds) remains in the bioreactor. Extending the HRT offers several benefits: it enhances treatment performance, diminishes sludge production, and augments methane recovery [294,295].

Yang et al. (2019) found that when HRT is reduced to just 1 hour, there's a roughly 60% drop in COD removal. This dip leads to a poorer effluent quality (meaning a higher COD in the effluent). Such an outcome might arise from incomplete pollutant degradation at these brief HRTs [266,296]. Additionally, reductions in nitrogen and volatile solids removal have been observed with decreasing HRT [287,297].

Interestingly, a shorter HRT intensifies the process (that is, leads to a higher OLR). This intensified environment fosters faster microbial growth, as evidenced by increases in metrics like MLSS and MLVSS [298]. One might expect this to yield more biogas. However, Santos et al. (2017) found no notable difference in methane production between HRTs of 127 hours and 74 hours[299]. This lack of significant change could be because 74 hours, in this context, is still a relatively lengthy HRT compared to other studies. As an illustration, Yang et al. (2019) reported a 90% surge in biogas production (from 0.21 to 0.40 L/g COD removed) when HRT was cut from 24 to 8 hours[300]. Yet, when HRT was further shortened to just 1 hour, methane production plummeted by about 60%, going from 0.12 to 0.05 L CH_4/g COD removed. This drastic HRT cutback can curb specific methanogenic activity, resulting in an accumulation of VFAs instead of the more desired methane output [301]. This methane reduction might also stem from decreased recovery opportunities, given the insufficient time at shorter HRTs for dissolved methane to transition to the gas phase.

Another consequence of a low HRT is the potential destabilization of the AnMBR system due to increased VFA production. While VFAs are vital intermediate products in anaerobic digestion and play a role in green fuel production [302–304], their abundance in an AnMBR system can signal instability [278,303,305,306]. Elevated VFAs at lower HRTs can cause a pH drop, leading to acidogenesis. This acidic environment inhibits methane-producing microorganisms [57,306,307]. Consequently, the VFA-to-alkalinity ratio of the system is often employed as an overarching stability metric. A system is deemed stable (and primed to handle higher OLR) when this ratio is below 0.3–0.4, but it's seen as verging on acidification when the ratio exceeds 0.5 [308–310]

2.6.8 Important references on AnMBR treating Municipal Wastewater Treatment

Based on the previously discussed literature, AnMBR is emerging as a viable solution for treating municipal wastewater when the appropriate HRT and SRT settings are applied. Its adoption has expanded since 2008. Yet, there are discrepancies in the data, with some studies presenting conflicting results. Many of these investigations use synthetic wastewater and are conducted at specific temperatures. This raises questions about how temperature, SRT, and HRT impact AnMBR's efficiency in processing real municipal wastewater. There's a pressing need to delve deeper into these variables to determine the optimal operating conditions and assess if AnMBR can operate in an energy-positive manner. Tables 2.16 and 2.17 catalog AnMBR studies that focus

on treating municipal wastewater under various conditions. The studies have been categorized by temperature range and span from 2009 to 2022.

Table 2. 16:References regarding AnMBR treating synthetic municipal wastewater

Synthetic wastewater Year of references	Operating Temperature			
	0-15ºC	16-20 ºC	21-42 ºC	43-55 ºC
2009			273,311,312	194
2010			191,195,240	
2011	313		269,314	196
2012				
2013	175		315	
2014		316	316–321	
2015	284	322	284,323	
2016	324,325	324,325	324,325	326
2017	286	289,327,328	277,286,289,329–331	
2018				
2019			282,304,332–336	
2020			230,337,338	
2021			339	
2022			340,341	

Table 2.16 presents references related to the treatment of synthetic municipal wastewater using AnMBR from 2009 to 2022, organized by operating temperature ranges. Notably, the 21-42°C range has garnered the most attention, evidenced by the majority of references. On the other hand, the 0-15°C and 16-20°C intervals have seen less research focus. It's also observed that COD removal rates from synthetic wastewater consistently show efficiencies exceeding 90%. This highlights the importance of examining real wastewater to obtain more authentic data

Table 2. 17: References regarding AnMBR treating real municipal wastewater

Real wastewater Year of references	Operating Temperature			
	0-15ºC	16-20 ºC	21-42 ºC	43-55 ºC
2009		118	207	
2010			206,208,342	
2011		343	197,343,344	
2012		345	345,346	
2013	175			
2014	49,350	347,348	49,350	
2015	349	225,350	231,351	
2016			352	

Real wastewater	Operating Temperature			
Year of references	0-15°C	16-20 °C	21-42 °C	43-55 °C
2017		353,354	355,356	
2018		357–359	359,360	
2019	361	361	361	
2020			337,362,363	364
2021	365	366,365	365–368	
2022	369–371	369,370	369,370,372–375	

Table 2.17 illustrates that, once again, there are more references associated with mesophilic temperatures. However, the difference is not as pronounced as in the case of synthetic wastewater, which is understandable given that we are dealing with real wastewater here. As for the references related to psychrophilic temperatures, only a few of them pertain to ambient temperatures and are presented in detail in the Table 2.18.

Table 2. 18: AnMBR treating municipal wastewater at ambient temperatures

	Reactor Type/Membrane configuration	Type of membrane	Type of wastewater	Inlet COD (mg/L)	Operating Conditions T, HRT	Outlet COD	Ref
1	UASB External	Tubular Area 0.2 m^2	Municipal Wastewater	186.5	Ambient HRT 5.5-10h	-	376
2	UASB Submerged	Tubular Polyethylene Area 0.98m^2	Municipal wastewater	259.5	15-20°C HRT 2.6	77.5 ±29.5	118
3	Gas sparging AnMBR submerged	Hollow Fibre Area 30m^2	Municipal wastewater	-	17-33°C HRT=6-26h	-	345
4	Submerged UASB	Tubular Polyvinylidene fluoride Area 0.2375 m^2	Municipal wastewater	525 ± 174	18-21 °C HRT 8 h	222±61	353
5	Gas sparged AnMBR submerged	Hollow fiber	Municipal wastewater after screening	620 ± 240	13 -32 °C HRT 11h	58 ±27	361
6	Granular activated carbon synergized anaerobic membrane bioreactor	Hollow Fiber Area 20 m^2	Municipal wastewater	277-348	5- 35 °C HRT 6-24 h	<50	365
7	Submerged AnMBR	UF membrane system 41 m^2	Effluent from the pre-treatment step (sand and grease removal)	905 ±429	18-27 °C SRT 70 d HRT 41, 25	80 ,116 mg /L	370

	Reactor Type/Membrane configuration	Type of membrane	Type of wastewater	Inlet COD (mg/L)	Operating Conditions T, HRT	Outlet COD	Ref
8	submerged AnMBR	PVDF hollow-fiber membrane module 72 m^2	Municipal wastewater	400mg/l	15, 20, 25 ^{o}C (simulate ambient temperatures)	50 mg/L	[369]

Most of the current research primarily focuses on a single HRT, with only a few studies examining multiple HRTs. However, the relationship between temperature variations and the performance of the AnMBR is not well-researched. This thesis aims to address this gap by investigating the effects of different HRT variations on AnMBR's performance under the ambient (psychrophilic) conditions typical of the Mediterranean climate in Greece.

Additionally, it's important to note that until 2021, all references were limited to pilot and laboratory studies. The introduction of a full-scale AnMBR treating municipal/domestic wastewater is first appeared in 2022[370]. This indicates a significant need for further research on AnMBR for further integration.

2.6.9 AnMBR different Configurations

Three distinct configurations can be utilized when integrating a membrane model with an anaerobic bioreactor, as illustrated in Figure. 2.25:

➤ The Side-stream AnMBR configuration positions the membrane module externally to the bioreactor tank, setting them up in parallel.
➤ The Internal Submerged AnMBR layout submerges the membrane within the main body of the bioreactor tank, ensuring a more direct interaction between the process and the membrane.
➤ The External Submerged AnMBR configuration, by contrast, immerses the membrane module in a separate chamber, distinct from the primary bioreactor vessel.
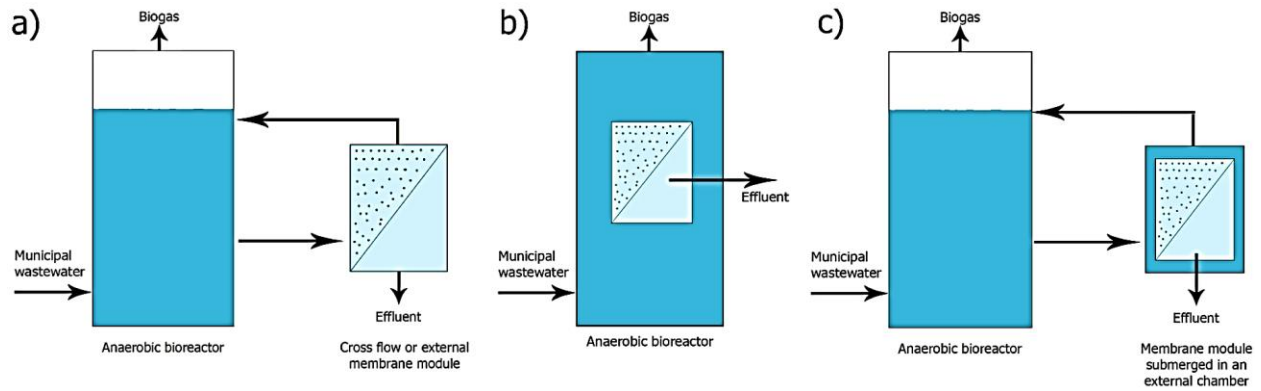
Figure 2. 25 Schematic presentation of (a) an external/pressurized AnMBR; (b) a submerged AnMBR; and (c) externally submerged AnMBR

The first variant of the anaerobic reactor configuration involves an external membrane unit, referred to as a crossflow AnMBR or external AnMBR (Figure 2.25a). In this setup, the membrane module remains separate from the reactor itself, with the mixed liquor pumped under pressure from the bioreactor to the membrane unit. Operating under pressure and with a tangential flow, the membranes facilitate the generation of permeate, which is essentially the treated effluent. The concentrated retentate is then recycled back into the anaerobic bioreactor[377].

The second configuration is termed the submerged AnMBR, where the membrane module is directly placed within the anaerobic bioreactor (Figure 2.25b). This immersion facilitates a direct contact between the membranes and the dissolved anaerobic biomass. The filtration process is driven by a pressure difference generated by applying low negative pressure inside the membranes.

The third setup involves an external tank anaerobic reactor with a submerged membrane unit, also known as the externally submerged AnMBR (Figure 2.25c). Here, the membrane system is placed in an external setup, separate from the main bioreactor, submerged in a tank filled with biomass and functioning under low negative pressure. The biomass is pumped from the bioreactor to the external setup while the surplus mixed liquor is recycled back to the bioreactor.

One notable advantage of external membrane configurations is the ease of membrane cleaning or replacement without disturbing the operational conditions of the anaerobic reactor. Specifically, in the external AnMBR, the use of pumps for retentate recycling creates a high shear rate that can disrupt cells and flocs, mitigating membrane fouling [378].

However, submerged systems have gained popularity in recent years due to economic considerations. Compared to external systems, these setups have lower energy requirements as the filtration occurs at reduced pressures. External systems, on the other hand, demand more space and have more expensive infrastructural requirements, including the need for additional tanks.

2.6.10 Membrane fouling

AnMBRs have become a significant technology in wastewater treatment, but they face a critical problem known as membrane fouling. This phenomenon leads to reduced efficiency, necessitates frequent cleaning, shortens the membrane's life, and increases both costs and energy consumption for processes like sludge recirculation or gas scouring.

While membranes from aerobic systems can sometimes be used in AnMBR, the interaction between the membrane and the materials in the sludge suspension is different in the anaerobic environment. This difference results in unique challenges regarding fouling characteristics in AnMBR systems.

In recent years, a variety of methods to study membrane fouling has been developed, enhancing our understanding of how fouling occurs specifically in AnMBR systems [379]. Although there is a considerable amount of research on AnMBR, there appears to be a lack of a thorough review that focuses solely on membrane fouling within this system.

2.6.10.1 Membrane fouling classification.

Membrane fouling is usually divided into reversible and irreversible types, based on how it can be cleaned. Reversible fouling pertains to fouling that can be cleared by physical methods such as backflushing or relaxation under cross-flow conditions, while irreversible fouling requires chemical cleaning for removal. On the other hand, irreversible fouling is a type of permanent fouling that can't be eradicated by any cleaning techniques.

Typically, reversible fouling is associated with the loose external deposition of material, whereas irreversible fouling is often the result of pore blocking and foulants that become strongly attached

during the filtration process. Over time, as the fouling layer forms a robust matrix with the solute, removable fouling may transform into an irremovable layer.

In studying the characteristics and origins of irreversible fouling, significant attention has been paid to the investigation of cake layer formation. In extended SAnMBR operations, researchers noticed that the mechanism of membrane fouling was predominantly due to cake formation and consolidation, which couldn't be removed through back-flush cycles or relaxation. This differed from internal pore fouling.

Comparatively, Di Bella et al.(2007) found that the cake layer in an aerobic MBR was primarily removable[380]. Cake formation is indeed a multifaceted process affected by numerous factors, but it can be concluded that, on average, the cake layer in AnMBR generally exhibits lower removability than that in the aerobic compartment. This difference in removability is likely due to the distinct sludge properties between the two systems.

Membrane fouling can be further differentiated into biological, organic, and inorganic categories, depending on the components causing the fouling [182,251]. Biological fouling is linked to how biomass interacts with the membrane. This form of fouling often begins with pore clogging, initiated by cell debris and colloidal particles. Interestingly, passive adhesion of colloids and organic matter has been observed even in zero-flux operation scenarios, before the commencement of biomass deposition [380].

Gao et al.(2010) noted that in a SAnMBR, about 65% of the particles in the top cake layer were smaller than 0.3 μm, coinciding with the pore size of the used membrane[240]. These small particles or flocs could easily penetrate and obstruct the membrane pores. Additionally, biological fouling encompasses the gathering and adhesion of extracellular polymeric substances (EPS) and soluble microbial products (SMP) on the membrane and pore surfaces since these substances are biologically excreted.

Some research has also delved into the investigation of the microbial community and its contribution to membrane fouling in AnMBRs. For example, Gao et al. (2010) and Lin et al. (2011) discovered differences in the microbial communities found on membrane surfaces versus those in bulk sludge in both external and submerged AnMBRs. These findings suggest that specific bacteria might selectively adhere to and proliferate on the membrane surface, further complicating the understanding and mitigation of fouling in these systems.

Organic fouling is mainly linked to macromolecular species like biopolymers. An analysis in SAnMBR revealed that foulants were rich in proteins and polysaccharides. Inorganic fouling involves substances such as struvite ($MgNH_4PO_4·6H_2O$), $K_2NH_4PO_4$, and $CaCO_3$. The cake layer in a SAnMBR may consist of various organic and inorganic elements [188,190,209,381,382].

Biological, organic, and inorganic fouling occur simultaneously, often increasing filtration resistance. For example, microbial cells' deposition with struvite contributes to the formation of a firmly attached cake layer. Membrane fouling generally starts with pore clogging, followed by biocake formation [383,384]. In SAnMBR, cake thickness and maximum sustainable membrane flux have been found to vary greatly compared to aerobic MBR systems. Additionally, AnMBRs might be more prone to inorganic fouling due to higher concentrations of specific substances[385]. These unique characteristics of membrane fouling indicate that controlling it in AnMBR requires special attention.

Membrane fouling is a complex phenomenon that can result from various contributing factors, and several mechanisms have been proposed to elucidate this [386,387]. These include pore obstruction by microscopic particles known as colloids, adsorption of soluble compounds onto the membrane, biofouling caused by microbial growth on the membrane, and solids deposition on the membrane's surface, forming a layer that can harden over time. Furthermore, the composition of these fouling substances can change over a prolonged operational period.

In the current design trend of AnMBRs, a consistent flow rate is maintained [184,246,388–390]. Operating in this mode, a three-stage pressure profile across the membrane is observed, characterized by an initial quick increase in pressure (stage 1 Figure. 2.26), a prolonged slow rise (stage 2 Figure. 2.26), and then a swift escalation again (stage 3 Figure. 2.25). This pressure profile is also seen in aerobic Membrane Bioreactors (MBRs)[391].
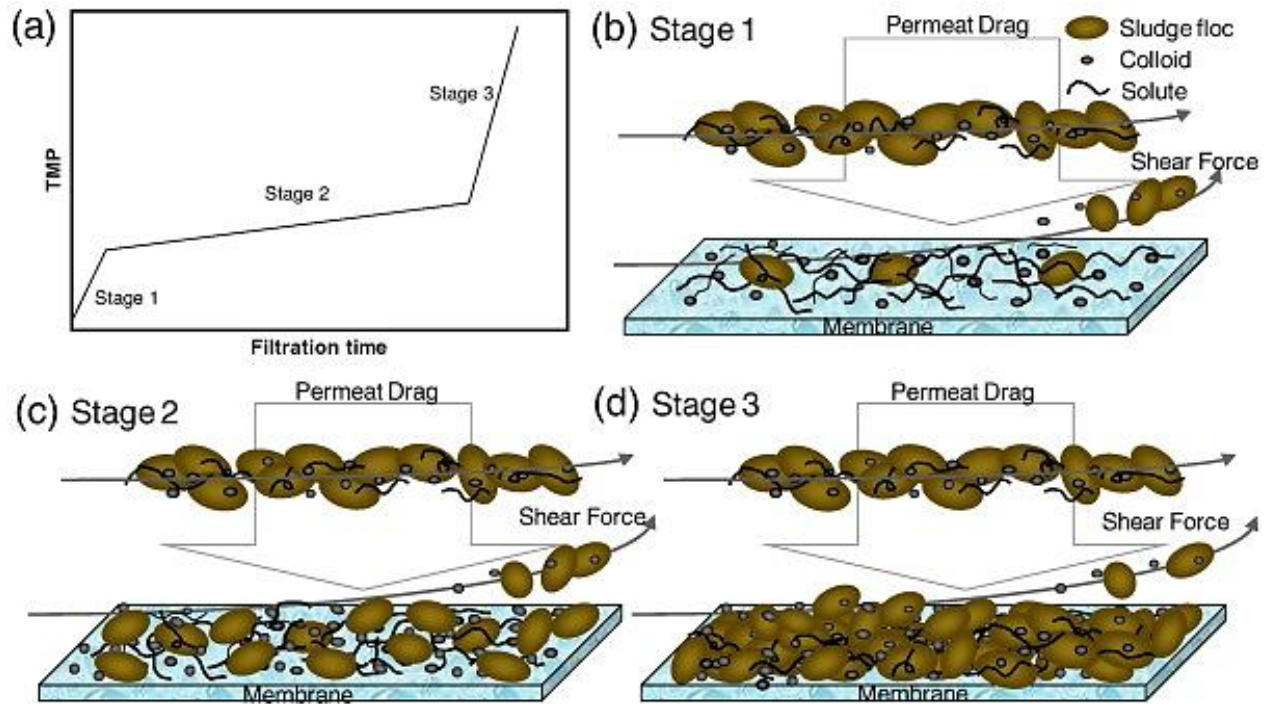
Figure 2. 26 Diagrammatic representation of the three-stage TMP (Transmembrane Pressure) profile, along with the associated fouling mechanisms.[284]

The interplay of forces in these processes is complex. On one hand, there's permeation drag, which draws substances onto the membrane and intensifies with increasing pressure. On the other hand, back transport exists, which involves forces that can push particles away from the membrane. Initially, colloids and soluble products are easily drawn into the membrane pores and can block them, causing the first quick surge in pressure. These substances also condition the membrane surface, promoting the subsequent formation of a solids layer, known as cake[184,186].

As the cake layer thickens, it prevents more particles from penetrating and clogging the membrane pores, leading to the slow rise in pressure. The cause of the second sudden jump in pressure is still up for debate. Some suggest it could be due to an uneven distribution of fouling materials and changes in local flow rates, while others link it to a sudden surge in certain compounds at the bottom of the cake layer, possibly due to bacterial death within the cake layer. It's likely that both these explanations have merit[387,388].

Lastly, the cake on the membrane surface undergoes a process referred to as consolidation or compression, where it becomes denser as pressure rises. This process can create an osmotic gradient or a difference in salt concentration across the membrane. Recent studies suggest this

osmotic pressure might be a significant factor in membrane fouling once a cake layer has formed[392].

To summarize, membrane fouling in AnMBR systems is multifaceted, potentially involving pore obstruction, compound adsorption, biofouling, as well as the creation and consolidation of cake layers. Understanding these processes demands consideration of both physical forces and chemical interactions. Continued research is necessary to fully comprehend and manage these complex mechanisms [388,393,394].

2.6.10.2 Parameters Affecting Membrane Fouling

Membrane fouling in AnMBR stems from the interplay between the membrane and the sludge suspension, and it's influenced by various factors. These can be grouped into four main categories:

➢ Feed Characteristics: The nature of the material being treated, such as solids and chemicals like Mg, Al, Ca, Si, and Fe, can cause fouling. Pretreatment methods like filtration, pH adjustment , and specific removal of elements (e.g., using a dialyzer/zeolite unit to remove NH_4^+) can help reduce fouling [190,198,220].

➢ Broth Characteristics: These include aspects like SMP, EPS, and particle size distribution (PSD). Extreme conditions like pH and temperature can change the PSD of the sludge, which affects fouling. For example, Martin-Garcia et al. found that SMP in AnMBR was 500% higher than in aerobic MBR [395].

➢ Membrane Characteristics: The specific properties of the membrane itself, such as its composition and structure.

➢ Operational Conditions: Operational aspects like flow rates, HRT, OLR, SRT, and pH can either directly or indirectly affect fouling. For instance, increasing gas scouring can improve conditions but may also disrupt sludge, leading to more fouling. The concept of the "shear rate dilemma" describes this dual effect. Optimizing operational conditions requires careful balancing and often pilot testing to find the right setup[194].

Generally, higher MLSS, OLR, residual COD, and SMP in AnMBR are likely to cause more serious fouling. As a result, membrane fouling control should receive more focus in AnMBR systems.

2.6.10.3 Membrane Fouling Control

Addressing membrane fouling is crucial for efficient system operation, and strategies can be divided into five areas:

> Pretreatment of Feed: Removing trash or adjusting extreme pH levels in the feed can prevent fouling. Certain elements originating from inorganic matters can also be managed through wastewater pretreatment programs [188,198,220,390].

> Optimization of Operational Conditions: Proper adjustments to parameters like flux, HRT, SRT, biomass concentration, pH, and temperature can control fouling. Strategies like operating at sustainable flux are well-known, and the connection between these parameters and broth properties is summarized in Table 2.19[396].

> More specifically, Table 2.19 systematically details how various factors impact the fouling parameters in anaerobic membrane bioreactors (AnMBR). Operational conditions, like Hydraulic Retention Time (HRT), directly influence specific biomass concentrations, whereas Substrate Retention Time (SRT) can affect membrane fouling with specific wastewater types. Temperature shifts are seen to modify COD supply and flux behaviors. Biomass characteristics, such as Mixed Liquor Suspended Solids (MLSS), are linked to both initial and stabilized flux changes. On the microbial front, certain bacteria play a decisive role in cake layer formation on the membrane. The membrane's inherent properties, like its surface roughness or type (e.g., PEI or PVDF), are also shown to exhibit particular fouling trends.

> Modifying Activated Sludge: Altering the composition of the sludge to minimize its fouling potential.

> Modification of Membrane and Optimal Design of Membrane Module: Adjusting the membrane's design and characteristics to reduce its susceptibility to fouling.

> Membrane Cleaning: Regular maintenance and cleaning to remove fouling substances from the membrane's surface.

In conclusion, membrane fouling is a multi-dimensional issue that requires attention to a range of factors, from the nature of the feed and the properties of the sludge to the operational conditions and the membrane's own characteristics. By understanding these aspects and implementing control strategies, more effective and efficient AnMBR operation can be achieved.

Table 2. 19 :The influence of fouling parameters on AnMBRs operation

Parameter	Effect on Membrane Fouling	Wastewater Type	Ref.
Operational conditions			
HRT	HRT↓→ biomass concentration↑, PN/PS in SMP↑ → dTMP/dt↑	Synthetic low-strength wastewater	269
	HRT↓→EPS↑, SMP↑ →cake resistance↑	Acidified wastewater	195
	HRT↓→biopolymers↑, floc size↓ → specific cake resistance↑	Synthetic municipal wastewater	397]
OLR	OLR↑→VFA concentration↑, predominant VFA type changed	Synthetic coke wastewater	196
SRT	SRT↑→sludge activity↓, SMP→ dTMP/dt↑	Synthetic low-strength wastewater	269
	SRT↑→MLVSS↑, floc size↓ →irreversible fouling↑	Synthetic low-strength wastewater	193
Hydrodynamic conditions	Gas sparging rate↑→ critical flux↑	Kraft evaporator condensate	398
	Gas sparging time↓→TMP↑	Saline sewage	311
	CFV↑→shear force↑, floc size↓ →critical flux firstly↑ then↓	Acidified synthetic wastewater	399
	Gas sparging was ineffective in increasing the critical flux	Acidified wastewater	386
	CFV↑→SMP↑, floc size↓ → flux↓	Diluted anaerobic sludge	295
Permeate flux	Permeate flux↑ →long-term operation period↓	Swine wastewater	291
	Permeate flux↑ →cake formation rate↑	Kraft evaporator condensate	400
	Permeate flux↑ →fouling rate↑	Domestic wastewater	256
Temperature	Temperature↓ →COD sup↑ →stable flux↓	Municipal solid waste leachate	291
	Temperature↑ →COD sup↑, floc size↓, PN/PS of EPS↑ →filtration resistance↑	Kraft evaporator condensate	184
	Temperature↑ →viscosity↓, COD removal↑ → flux↑	Food wastewater	185
Biomass characteristics			
MLSS	MLSS↑→initial and stabilized flux↓, optimal MLSS = 15–18 g/L	Diluted anaerobic sludge	295
	MLSS↑→TMP↑	Food industry wastewater	183
	MLSS↓→solids deposition rate↓	Dilute municipal wastewater	208
PSD	Number of small flocs↑ → filtration resistance↑	Kraft evaporator condensate	184
	Floc size↓ →specific cake resistance↑	Synthetic municipal wastewater	401
	D 0.1↑→cake formation rate↓	Kraft evaporator condensate	400
SMP	SMP↑ → filtration resistance↑	Kraft evaporator condensate	184
	High-MW protein and carbohydrate material↑ → internal fouling↑	Low-strength synthetic feed	183
	Low flux was attributed to high amounts of SMP	Medium strength wastewater	402
EPS	PN/PS ratio↑ →fouling rate↓	TMP whitewater	202
	EPS↑ → cake resistance↑	Acidified wastewater	195
	EPS the foulant layer contributed to membrane fouling	Particulate artificial sewage	240
Microbial community	Some bacteria play a pioneering role in cake formation	TMP whitewater	403
	Relative abundance of bacteria was different in cake layer and suspension	Artificial sewage	240
Membrane characteristics	MWCO↑, surface roughness↑ → flux decline↑, recoverable flux rate↓	Food wastewater	185
	Pore size↑ →attainable flux↓	Synthetic wastewater	404
	Fouling of PEI membrane was faster than PVDF membrane coated with PEBAX	Artificial sewage	240

2.6.11 Materials utilized for optimizing AnMBR performance: a look into their various types and distinguishing features.

Enhancing performance in AnMBRs, specifically digestion improvement and fouling mitigation, can be achieved through the implementation of various materials with distinct characteristics. Among various techniques like scouring, cross-flow filtration, and parameter optimization, the addition of cost-effective and accessible additives in AnMBRs stands out as an efficient way to alleviate membrane fouling[405].

Some of these additives include carbon-based materials such as activated carbon, biochar, and carbon nanomaterials, have been extensively studied for their effectiveness. Flocculants, both organic and inorganic, are also used in wastewater treatment for COD removal, suspended solids reduction, and color elimination. Inorganic flocculants are favored for their non-toxicity, ease of availability, and rapid global development due to low cost and high efficiency. Organic polymer flocculants are divided into natural forms, like chitosan and modified starch, and synthetic varieties like polyacrylamide and phenolic condensates[406,407]

Another innovative method is the application of carriers like porous suspended biofilm carriers in submerged ceramic membrane bioreactors, which have proven effective in alleviating fouling. Other materials such as PAC, GAC, biochar, zeolite, and waste yeast have also been employed to effectively reduce membrane fouling.

In summary, the performance enhancement of AnMBRs is closely tied to the characteristics of various materials utilized within the system, from carbon-based substances to diverse flocculants and specialized carriers. These materials not only assist in improving digestion but play a significant role in mitigating fouling, an essential aspect of efficient AnMBR operation [408].

2.6.11.1 Carbon based materials.

Carbon-based materials are known to significantly enhance interspecies electron transfer within the microbial communities of anaerobic digestion systems. The improvement in anaerobic digestion using these materials is ascribed to their conductivity, biocompatibility, chemical stability, lightweight composition, and porous structure. Such materials, including activated carbon, biochar, and carbon cloth, are highly conductive, enabling an efficient increase in direct interspecies electron transfer (DIET) between acetogens and methanogens. Within the DIET

microbial framework, electrons are directly relayed from exoelectrogenic microbes to electron-trapping microbes at a rate that is 106 times faster than indirect interspecies electron transfer (IIET). This leads to the effective biodegradation of organics [409].

Activated carbon is a widely used additive in AnMBRs, effective in treating various types of wastewater ranging from high-strength industrial waste to low-strength municipal waste. The efficiency of AnMBR varies with the substrate concentration and type of wastewater; for example, a high OLR may cause VFA accumulation and hamper system performance.

Activated carbon can be prepared through different methods, including microwave pyrolysis (MP), hydrothermal carbonization, and the two-step activation method. Each method has its advantages and drawbacks. For instance, MP offers uniform pore volume but suffers from large-scale reproducibility issues [410]. The two-step activation process allows for higher surface areas but consumes more energy and time [411].

Some studies have experimented with different raw materials, such as sawdust and corn cob, to create activated carbon with specific surface areas that support microbial colonization, thereby promoting anaerobic processes [412]. A comparison with biochar, a more economical option [413], reveals that biochar's low-temperature production preserves pore structure but results in a less efficient specific surface area compared to activated carbon.

Activated carbon, known for its rich porosity, large surface area, and high electric conductivity, has become a popular additive in AnMBRs due to its efficiency? and unique properties. Recent studies have examined different forms and sizes of activated carbon to control membrane fouling. Zhang et al. (2017) found that certain powdered activated carbons (PACs) reduced fouling effectively, though over-dosage of PAC might lead to blockage. A study by Ng et al. (2017) revealed that smaller-sized PAC (100 µm) improved flux and produced cleaner permeate, enhancing biogas production. Charfi et al. (2017) further emphasized the importance of GAC size, with larger particles being more efficient in fouling mitigation but needing more energy for fluidization. Future research is needed to optimize particle size to minimize both energy consumption and membrane surface accumulation. Though adding activated carbon raises the operating cost compared to biochar, its retention for reuse can significantly cut costs[414,415].

2.6.11.2 Iron based and other potential materials.

Iron-based materials can replace parts in anaerobic digestion systems, making a connection between different microbes to complete a complex reaction. Zero valent iron (ZVI) is useful and affordable in reducing clogs in the system[416]. Research showed that ZVI in wastewater treatment could reduce clogging by 20%. It also helps group waste particles together[417,418]. Nano ZVI (nZVI), a smaller version of ZVI, can reduce concentrations in the system and aid in methane production.

Zeolite, a mineral, helps remove nitrogen and phosphorous and allows bacteria to cling to it, improving the process.

Other chemicals like $FeCl_3$, $CaCl_2$, and PACl have been used to control clogs [351,419].They work by grouping waste particles, making them easier to remove. A study found that adding $FeCl_3$ improved waste breakdown and prevented further clogging). $FeCl_3$ could be a good long-term choice.

Researchers have tried to find the right amount of chemicals like PACl and $FeCl_3$ to use. While there are promising results, there's still uncertainty about how $FeCl_3$ works over the long term. If it keeps working well, it could be great for large-scale, ongoing waste treatment.

Some studies have focused on combining carbon-based and iron-based materials to enhance the breakdown of organic substances and improve the overall performance of anaerobic digestion, a process used to decompose waste materials [420,421]

Zhao et al. (2017) explored the combination of granular activated carbon (GAC) and magnetite (Fe_3O4) in anaerobic digestion. They found that adding Fe_3O4 to the system significantly enhanced the removal of organic substances in a subsequent reactor containing GAC. This improvement was linked to the growth of special bacteria that reduce iron, encouraged by the presence of ferric oxides[422].

Wang et al. (2021) developed a new material by combining iron-rich Fenton sludge with biochar. When applied to an anaerobic digestion system, this novel material aided in breaking down wastewater's organic matter, increasing the rate of a specific COD removal by 3.7–7.2%.

Carbon-based and iron-based materials also influence the production of EPS, which are compounds produced by microbes. In a study by Sun et al. (2021), researchers created GAC loaded with nZVI, finding that the iron ions released by nZVI contributed to the formation of EPS. These iron ions (Fe^{2+}) can interact with proteins in bacteria, creating a stable three-dimensional

structure. The interaction between EPS and metal ions can form a gel-like network on the surface of sludge, strengthening the connection between microbes and resulting in a stable granular sludge. This structure enhances the overall efficiency of the anaerobic digestion process[423].

Previous research has demonstrated the effectiveness of using beads, such as polyethylene terephthalate beads and glass beads, to prevent clogging) in certain systems. These beads are used in a process called granular media fluidization.

This approach works in two primary ways. First, the movement and mixing of the beads create turbulence within the fluid, reducing what is known as concentration polarization, a condition that can lead to fouling. Second, the beads have a scouring effect, rubbing against surfaces and removing previously deposited materials that can cause clogging [424]. Together, these actions by the beads effectively mitigate membrane fouling, enhancing the overall efficiency of the system.

In conclusion, various additives have proven effective in reducing membrane fouling. However, further research is needed to understand the long-term effects of different types of additives. For larger particles, such as GAC, an examination of potential wear and tear on membranes is necessary. For smaller particles like Poly-Aluminium Chloride (PAC), careful determination of the optimal dosage is required to prevent clogging of pores. Lastly, exploring the use of waste materials as additives could provide meaningful insights and advantages.

2.6.12 Economic aspects of AnMBR

As we delve into the detailed economic assessment of AnMBR plants, Table 2.20 presents a comprehensive outlook, dividing the costs into capital and operational ones. The capital expenditure primarily encompasses the procurement and setup of anaerobic reactors, filtration tanks, pumps, compressors and blowers, screeners, pipelines, control systems, as well as the acquisition of land and construction. On the other hand, operational costs are those related to energy, chemicals, labor and maintenance. Despite the extensive list of cost components, this review will confine itself to the critical cost variables, focusing specifically on costs associated with membranes and energy.

Table 2. 20: Breakdown of Capital and Operating Costs for an AnMBR Plant

Category	Item	Cost Description
Capital Costs	Bioreactor and Filtration Tank	Expenditure associated with the acquisition of bioreactor and filtration tanks
	Anaerobic Digestors (CSTR, UASB, EGSB, etc.)	Costs for various anaerobic digestors and accompanying filtration tanks
	Membrane Cost	Procurement of hollow fiber or flat-sheet membranes
	Pump Cost	Investment in permeation, backpulse, and sludge recirculation pumps
	Screener Cost	Expenditure for screeners utilized in the pretreatment of influent
	Compressor and Blower Cost	Costs associated with submerged AnMBR compressors and blowers for biogas scouring for fouling control
	Piping Cost	Investment in influent, permeation, and sludge recirculation piping
	Control System	Expenditure related to the process control system
	Land Cost	Cost of land procurement for the AnMBR facility
	Construction Cost	Overall construction expenditure for the AnMBR facility
Operating Costs	Energy Cost	Ongoing energy consumption costs for pumps, compressors, and blowers
	Chemical Cost	Recurring costs for chemicals utilized in membrane fouling treatment
	Labor Cost	Labor expenses for staff including operators, technical personnel, and managerial staff
	Maintenace Cost	This refers to the regular expenses associated with the upkeep, repair, and replacement of equipment and parts to ensure the AnMBR facility's optimal performance.

It's essential to underline that the adoption of any novel technology pivots largely on cost considerations. A key breakthrough, in this respect, was the inclusion of membrane modules into anaerobic processes. This innovation led to a substantial cutback in operating expenses by 50%, compared to the anaerobic processes that existed before the upgrade[425] . This economic advantage can be attributed to an amplified system capacity, the ability? to process wastewater with a higher biomass concentration, and the elimination of the need for dewatering and solids disposal.

To illustrate the distribution of costs within an AnMBR system, it's useful to segment them into three categories: a) capital costs, involving aspects such as reactor design and construction,

membrane, and equipment installation; b) operational costs, which include energy consumption, sludge disposal, and the usage of chemicals; and c) maintenance costs, which cover the cleaning and replacement of membranes, and the replacement of electrical equipment.

Of these, the membrane-related costs are particularly significant. They are a function of the membrane price, the applicable flux, and the lifespan of the membrane, and they represent the most substantial part of the expenses tied to the full-scale application of AnMBRs Studies have shown that the cost of the membrane in an AnMBR accounts for a massive 72.3% of the total capital cost at a design flux of 10 L/m^2 h and a membrane price of US $50/m^2$ for a flat-sheet PVDF membrane[390]. This is ten times the cost associated with the energy required for biogas sparging per m^3 of treated wastewater [245].

Although there is a significant decrease in membrane cost over the past decade [426,427], the overall lifecycle capital costs are still highly affected by membrane cost due to their relatively short lifespan, typically between 3–11 years[219,245]. To decrease AnMBR capital cost dynamic membranes have been introduced. These dynamic membranes are seen as a cost-efficient replacement for traditional membranes in AnMBRs for wastewater treatment. Encouragingly, research indicates that the production cost of a nanocomposite nonwoven membrane for dynamic membrane bioreactors is roughly one-third the price of a commercial PVDF membrane. Therefore, the development of efficacious strategies for controlling cake layer thickness in dynamic AnMBRs could be pivotal in substantially reducing AnMBR capital costs.

The operational expenditures linked with AnMBRs comprise costs associated with energy consumption, particularly biogas scouring on the membrane surface, sludge disposal, and chemical usage, including the addition of nutrients. The energy required for biogas scouring constitutes a significant segment of the total operational costs. This cost factor is particularly crucial in side-stream AnMBRs, which demand a high cross-flow velocity to mitigate membrane fouling.

Upon comparison of energy and membrane costs for a specific flux and membrane price, submerged AnMBRs present a more economical option, with expenses being several times lower than their side-stream counterparts. This finding is reinforced by research conducted by Lin, Chen, et al. (2011), and Lin, Liao, et al. (2011), which showed that the operational cost of a submerged AnMBR utilized for municipal wastewater treatment was significantly less than that of an aerobic submerged MBR. This discrepancy in cost is attributable to the reduced expenses related to biogas scouring energy and sludge disposal in the case of submerged AnMBRs. Similar

results were reported in a study by Martin et al. (2011), which modelled the energy demand of aerobic and anaerobic MBRs for wastewater treatment[428]. The results revealed that the energy required for fouling control in AnMBRs had a value of 0.8 kWh/m^3. Hence, the examination of these operational costs suggests a clear economic advantage for submerged AnMBRs in wastewater treatment applications.

Relative to aerobic MBRs, AnMBRs hold a distinct advantage in the form of biogas recovery, which has the potential to offset operational costs. A striking illustration of this advantage is the successful operation of an anaerobic reactor integrated with ultrafiltration membranes at Tenstar for over a decade. This system, employed for the treatment of soluble wheat starch, led to substantial financial savings. These savings included a significant reduction in effluent charges, amounting to over £100k (US$161k), coupled with a biogas benefit of £30k (US$48.3k) per year [429].

Furthermore, AnMBRs facilitate significant cost reductions in aeration and sludge disposal due to their low sludge yield and oxygen-free environment. While direct cost comparisons between aerobic and anaerobic MBRs are not widespread, noteworthy observations have been made. For instance, the total costs for treating evaporator condensate, a byproduct of the kraft pulp production process, were found to be lower when an AnMBR was used prior to a conventional aerobic process, compared to using a standalone aerobic process.

Maintenance costs for AnMBRs include expenses related to membrane cleaning and replacement, as well as electrical equipment replacement. The information available on the chemical cleaning of fouled membranes in AnMBRs is somewhat limited due to the small number of pilot-scale studies and full-scale AnMBR applications. Nevertheless, the data garnered from a few pilot-scale studies [174,343,430,431] suggests that the membrane maintenance cost of AnMBRs is expected to align with the performance of aerobic hollow-fiber membranes used in full-scale MBR plants.

In terms of membrane fouling, it is anticipated that the protocols and frequency of membrane cleaning used in full-scale aerobic MBR plants could be applied to AnMBR plants [219,390]. Research concluded that the cost of chemicals consumed for membrane cleaning accounts for approximately 33% of the operational cost in an AnMBR plant for municipal wastewater treatment with a capacity of 20,000 m^3/day.

2.7 Anaerobic Digestion models

2.7.1 Introduction

Anaerobic digestion (AD) is renowned as a pivotal technology, specializing in the microbial treatment of organic wastes and byproducts to produce biomethane, a substantial source of renewable energy. This technology aligns with the goals of the Circular Economy Action Plan, a cornerstone of the European Green Deal, which aspires to steer the EU towards a sustainable transformation, aiming for climate neutrality by 2050 [432].

It is crucial to note the specific energy consumption in Greek WWTPs averages around 38 kWh/PE annually, with a range between 15 to 86 kWh/PE. Concurrently, the average annual GHG emissions from Greek WWTPs stand at approximately 94 kCO2e/PE, with variations between 61 to 161 kgCO2e/PE. Notably, a significant portion of a WWTP's total energy consumption, between 40-70%, is attributed to the energy demands for aeration [107,433].

There are multiple discussions today regarding the integration of AD plants into the future energy system and circular bioeconomy, aimed at supplying biomethane or electricity tailored to demand [434]. Depending on specific objectives, proper methods for process design, monitoring, and control are essential to accommodate flexible plant management amidst varying substrate qualities and quantities. When paired with pertinent sensor data and laboratory analyses, dynamic process models form a solid foundation for the highly automated and efficient operation of future plant concepts [435].

Anaerobic process models can be leveraged for 1) pragmatic plant design and efficiency appraisal, 2) thorough state analysis and process optimization, 3) model-based process control and surveillance, 4) parameter approximation and system identification, 5) investigation of biochemical and physicochemical correlations, 6) benchmarking of operating systems, or 7) devising experiments for cost-intensive test series [436,437].

Since the late 1960s, a plethora of dynamic models for simulating the characteristic variables of AD processes have been established. The structures of individual models exhibit substantial variability in the number and kind of components considered, the phases of the process, and the physicochemical dependencies. Initial models typically delineated the anaerobic breakdown of simple monomers or organic acids, while later models integrated substrate characterization by

organic compounds or specific nutrients (such as carbohydrates, proteins, and lipids), enabling a comprehensive representation of the entire AD process [438].

By combining relevant model approaches, the Anaerobic Digestion Model No. 1 (ADM1) presented by [20] has established itself as the standard for modelling of AD processes. Typically applied to Continuous Stirred-Tank Reactors (CSTR), the ADM1 outlines 19 biochemical processes, including reactions of disintegration, hydrolysis, acidogenesis, acetogenesis, and methanogenesis, along with three gas-liquid transfer processes and six acid-base kinetic processes. These processes facilitate conversions between 36 state variables.

Building on Batstone et al. (2002) study, Rosen and Jeppsson in 2006 integrated the ADM1 with the Activated Sludge Model (ASM) under the IWA Benchmark Simulation Model 2 (BSM2) framework, forming a comprehensive plant-wide model suitable for wastewater treatment plants. BSM2, with its detailed depiction of AD acid-base processes and recommended values for model stoichiometric and kinetic parameters, has since become a standard for studies utilizing ADM1.

2.7.2 Brief Description of the ADM1 anaerobic digestion model by IWA

ADM1 serves as a structured model delineating the biochemical and physicochemical procedures inherent to AD. The model is elaborated comprehensively in the pertinent scientific document by Batstone et al., (2002). It primarily encompasses components, processes, stoichiometric coefficients, kinetic expressions, and relevant parameters as its major elements. All these components are integrated within a Petersen matrix to facilitate the quantitative depiction of the AD process.

In the case of the majority of mechanistic biochemical models, intensive state variables are employed. Soluble components, denoted as S in the model, and particulate components, represented as X in the model, include microbial biomass, categorized by functional clades, and substrate particulates. These components are illustrated by state variables, with biochemical and chemical processes serving as source/sink elements within the overall mass balance. The model encompasses the biochemical processes of Anaerobic Digestion (AD), outlining five integral steps: disintegration, hydrolysis, acidogenesis, acetogenesis, and methanogenesis.

The model provides a comprehensive overview of the components and bioconversion processes, as depicted in Figure. 2.27. As originally outlined, the ADM1 proposed a two-phase solubilization

process, where composite particulates (XC) undergo disintegration into particulate proteins (Xpr), carbohydrates (Xch), lipids (Xli), and inert substances (Xi and Si). Subsequently, degradable disintegration products are hydrolyzed into amino acids (Saa), sugars (Ssu), and long-chain fatty acids (LCFAs, represented as Sfa in the model).
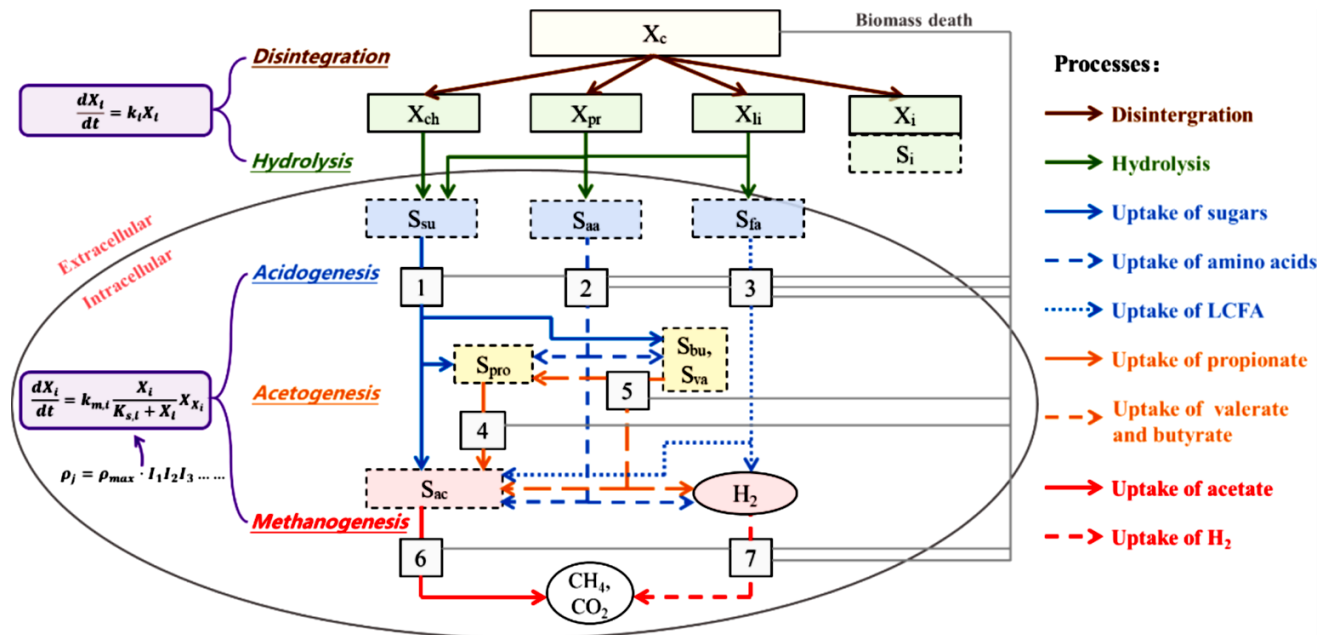
Figure 2. 27 The conceptual model for ADM1: (1) sugar degraders (Xsu), (2) amino acid degraders (Xaa), (3) LCFAs degraders (Xfa), (4) propionate degraders (Xpro), (5) butyrate and valerate degraders (Xc4), (6) acetate degraders (Xac), and (7) hydrogen degraders (Xh2).[439].

Following this, the acidogenesis process ensues, where sugars and amino acids are fermented into VFAs, hydrogen, and carbon dioxide by varied degraders, while LCFAs are oxidized to yield acetate and hydrogen. Additionally, propionic acid (Spro), butyric acid (Sbu), and valeric acid (Sva) undergo anaerobic conversion into acetate (Sac), carbon dioxide (Sco2), and hydrogen (Sh2). The concluding step, methanogenesis, encompasses aceticlastic methanogenesis, resulting in methane production through acetate cleavage, and hydrogenotrophic methanogenesis, where carbon dioxide is converted into methane (SCh4) by hydrogen-utilizing methanogenic bacteria.

Biomass growth is inherently connected to substrate uptake, correlated via a yield coefficient. The decayed biomass reverts to the complex organics fraction and undergoes further disintegration

and hydrolysis. Besides the organic species, the model includes inorganic carbon (SIC) and nitrogenous species (SIN) as acid-base active compounds, serving as elemental balance closures. The Chemical Oxygen Demand (COD) is employed as the primary unit, with zero-COD nitrogenous and inorganic carbon species represented in their molar concentrations.

The conversion rates of substrates are represented through a variety of process kinetics. The disintegration and hydrolysis of intricate organic materials—being extracellular processes—are characterized by first-order kinetics, dependent on substrate concentration. The decay of biomass is similarly depicted by first-order kinetics. This model is empirical, presumed to mirror the accumulative impacts of extracellular processes while omitting microbial effects [440].

For all intracellular biochemical processes, including acidogenesis, acetogenesis, and methanogenesis, Monod-type kinetic expressions are employed. Intracellular conversion processes can experience inhibition due to unsuitable pH levels or the buildup of intermediate products like inorganic nitrogen, free ammonia [441,442] among others. The impacts of such inhibitions are quantified through inhibition functions (I) and incorporated into the kinetics as follows (Eq 2.16):

$$\rho j = \rho \max * I_1 I_2 I_3$$
<div align="right">Eq (2.16)</div>

where ρmax is the Monod-type kinetic equation without inhibitions and Ii are inhibition functions.

Stoichiometric coefficients serve as a quantitative representation of the formation and conversion of components in AD, maintaining the element mass balance in reaction processes and reflecting microbial growth in respective uptake processes.

In ADM1, the physicochemical processes entail six acid/base equilibria, which are related to pH and are resolved through a charge balance method, along with three gas-liquid transfer processes for methane (CH4), carbon dioxide (CO2), and hydrogen (H2). The acid-base reactions involved in the liquid-phase physicochemical reactions can be expressed either as differential-algebraic equations (DAE) or differential equations (DE). When integrated as a DAE system, the acid/base pairs are typically aggregated as a unified dynamic state variable. Subsequently, the concentration of each individual acid or base is deduced from the ensuing acid-base equilibrium equation (Eq 2.17).

$$S_{i-} - \frac{KaS_i}{Ka + S_{H-}} = 0 \qquad\qquad\qquad \text{Eq (2.17)}$$

In this context, Ka represents the acid-base equilibrium constant, and SH+ denotes the variable for the concentration of hydrogen ions. The pH is ascertained by the concentration of protons, which is directly resolved by solving the aforementioned implicit algebraic set.

If the liquid phase equations are incorporated as differential equations (DE), the acid-base transfer is articulated by an additional dynamic rate equation, as demonstrated below in Eq 2.3:

$$\rho_{A|B,H\iota} = K_{A|B}(S_{liq,H}S_{liq,i} - K_{a,Hi}S_{liq,Hi}) \qquad\qquad \text{Eq (2.18)}$$

Where Sliq,j represents the dynamic state variable for soluble gas, Pgas,j stands for the pressure of the gas, kLaj is the gas-liquid transfer coefficient, and KH,j denotes the coefficient based on Henry's law. The process of gas-liquid transfer is governed by the dual-film theory, where both the liquid film and the gas film control mass transfer, with the liquid film being the controlling factor.

2.7.3 Practical applications of ADM1.

As already mentioned before, the ADM1 was originally formulated as a generalized model with a primary focus on sewage sludge [20]. However, by modifying the model, its applicability can be expanded for use in various Anaerobic Digestion (AD) systems, dealing with complex substrates including food waste, agricultural waste, or other co-substrates combined with sewage sludge. To date, the refined ADM1 has been employed to simulate both lab-scale and full-scale anaerobic digestion (AD) processes in reactors. These include the Continuously Stirred Tank Reactor (CSTR), Upflow Anaerobic Sludge Bed Reactor (UASB), Anaerobic Baffled Reactors (ARB), Two-Phase Anaerobic Digestion, Temperature-Phase Anaerobic Digestion, and Anaerobic Membrane Bioreactor (AnMBR). The modified model has yielded positive simulation outcomes on various output indexes, as depicted in Table 2.21.

Table 2. 21 Application of the ADM1 to different anaerobic digestion scenario for urban applications related to wastewater.

Substrates	Conditions	Scale and Reactor	Simulation items	Simulation results and analysis	References
PS + WAS	Part of a WTTP Mesophilic	Full-scale CSTR	Biogas, Ch4 %, TS, VS,	The differences between the ADM1 results are all within 2%.	[443]
Sewage, grey water, black water and faeces	Part of urban sanitation Low and high temperature (14-35 oC)	Full scale UASB +UASB septic tank	Ch4 flow, CH4 %, COD, COD removal	Determination of a suitable design for each system	[444]
OFMSW +WAS	Mesophilic	Full-scale	Biogas flow, CH4%, CO2%, pH, COD, TVFA, IN, IC	Acceptable simulating results	[445]
Domestic Wastewater	Mesophilic	Pilot -scale UASB	Biogas flow, pH, TCOD, sCOD	With average experimental values within 10% of the simulated results	[446]
Municipal wastewater	Mesophilic	Full-scale	Ch4, flow, COD, alkalinity, pH	Acceptable simulating results	[447]
Urban wastewater	Part of a WRRF Mesophilic	Full-scale	Biogas flow, CH4 %, COD, TSS, VSS, N, P	Acceptable simulating results	[448]

PS: primary sludge;.OFMSW: organic fraction of municipal solid waste;. PAD: temperature-phased anaerobic digestion;.EGSBR: Expanded granular sludge bed reactor;.ADR: advective-diffusive reactor.

As it is evident from Table 2.21, for urban applications, ADM1 has been employed to simulate and design AD systems for urban organic wastes. This includes wastes such as municipal wastewater, grey water, black water, and faeces. Additionally, it has been used for primary or waste activated sludges originating from Water Resource Recovery Facilities (WRRFs).

The ADM1 serves as a practical management tool for designing and operating engineered AD processes. Initiating the AD process is critical when establishing or restarting a new biogas plant [449]. This process can become unstable or fail due to inferior inoculum [450] or excessive organic

loading rate (OLR) [451]. The enhanced ADM1 can offer more accurate predictions of the start-up process, such as microbial activity [452] and the dynamic fluctuations of VFAs [453]. Additionally, it can guide the development of a start-up procedure, incorporating dynamic control.

The range of applications for the modified ADM1 has seen considerable expansion. Beyond its traditional utilization in the AD process, the refined models can provide critical insights into optimizing processes, utilizing substrates, and forming products during the fermentation processes. Anaerobic fermentation can produce various valuable by-products, such as lactate, VFAs, and H_2. The modified ADM1 is capable of predicting the production of these compounds and can help in determining the optimal conditions for fermentation [453,454].

Moreover, processes to upgrade biogas are vital for improving the quality and enhancing the possible uses of biogas. The ADM1 model has been developed further and adjusted to enable the simulation of biogas upgrading, such as biogas desulfurization. In a research conducted by [455], the adapted ADM1 was employed to fine-tune microaeration conditions, discovering that the ideal start time for microaeration was day 11, with the digester having a dissolved oxygen concentration of 1.936×10^{-4} ppm. Nonetheless, the application of ADM1 in biogas upgrading procedures is still comparatively constrained. Looking ahead, the model has the potential to be a beneficial instrument for examining more biogas upgrading processes, like CO_2 removal and CH_4 enrichment.[439]

2.7.4 Sensitivity analysis methodologies

2.7.4.1 Introduction to Sensitivity Analysis

Sensitivity analysis serves as a robust instrument within the realm of mathematical modeling and manifests its relevance across a multitude of scientific disciplines. It primarily endeavors to establish a correlation between variations in the output magnitudes of a computational model and the corresponding alterations in the input magnitudes, a concept supported by [456]. Such analytical approaches enable the evaluation and quantification of the ramifications of perturbations in a model's input parameters on its subsequent outcomes, a notion articulated by [457].

The overarching objective of conducting sensitivity analysis is to discern the paramount parameters of the model and to appraise the significance attributed to them in the accurate

emulation of natural phenomena. This generalized definition implicates a vast spectrum of practical applications, implying the existence of diverse methods, each tailored to the intricacies of the processes and the goals of each respective study and application.

The classification of these methods is congruent with the principles previously outlined and will be delineated in the subsequent sections of this thesis. Furthermore, the application of sensitivity analysis is also prevalent in other domains, including risk computation, model stratification, assessment of the reliability and validity of models, and performing uncertainty analyses in issues that are more intricate and demanding [458,459].

This section seeks to elucidate the essence of sensitivity analysis and its multifaceted applications, illustrating its indispensable role in enhancing the precision and reliability of mathematical models in diverse scientific investigations. By exploring various methodologies and applications, this discourse aims to furnish a comprehensive understanding of sensitivity analysis, paving the way for its adept incorporation in subsequent research endeavors.

2.7.4.2 Classification of Sensitivity analysis methods

Sensitivity analysis methods can fundamentally be segregated into local and global methods. The distinction between them arises from the delineation of intervals and values for the input quantities (parameters), upon which depend the variations in the output quantities (variables). In local methods, parameters are chosen around a specific value, typically sourced from literature. Contrarily, in global methods, parameters are usually selected in a random manner, spanning their entire possible range.

This foundational difference dictates the divergence in appropriate applications for which each method is employed. Specifically, local methods prove effective in assessing the validity of a model when the parameters acquire values distant from their proposed ones. This evaluation is executed through indicators with partial derivatives or finite differences

Global methods, conversely, are deemed effective across a broad spectrum of applications such as: model calibration [460–464], uncertainty reduction [465], analysis of significant control systems [466], and support for adequate decision-making [467–469].

These methods, based on their respective characteristics and applications, aid in developing a holistic understanding and addressing the various aspects and complexities involved in sensitivity

analysis, thus providing comprehensive insights into the significant elements affecting model outcomes. By integrating these methods aptly, one can enhance the model's reliability and predictive accuracy, reinforcing the decision-making process in various scientific fields.

Additionally, methods are distinguished into qualitative and quantitative, according to the manner of calculation and presentation of sensitivity for each respective parameter. In quantitative methods, an index is defined for every parameter, which has arisen from estimates of its relative significance to the model's outcome. Conversely, qualitative methods represent this significance through diagrams and visualization of results and model predictions. Some of these diagrams include tornado plots [470,471] and scatter plots [472,473].

Typically, the use of qualitative methods is recommended as complementary to quantitative ones. They offer visual insights and a more tangible representation of the model's sensitivities and dependencies, enhancing the interpretative understanding of the analyzed system. By utilizing both qualitative and quantitative methods, researchers can obtain a comprehensive view of the variables' importance, gaining more profound insights into the intricate dynamics governing the model. This amalgamation facilitates a robust analysis, allowing for the refinement and optimization of models, essential for reinforcing the accuracy and reliability of predictions and decision-making processes in various domains.

An additional categorization in the methods is the way of constructing the sample of values for the parameters, which is needed for the calculation of sensitivity indices. Two methods stand out: 1) the "one-at-a-time" (OAT), in which only one of the parameters is varied, while all the others remain constant, and 2) the "all-at-a-time" (AAT), where all the parameters are varied simultaneously. As expected, the second method, besides the direct impact of each parameter on the result, allows for the calculation of their interactions. In local methods, OAT is usually chosen for creating the parameter sample, while in global methods, either of the two can be chosen. Practically with AAT, the interactions are quantified, something which OAT does not allow; however, it is computationally and consequently more time-consuming.

2.7.4.3. Goal of sensitivity analysis

At this point, it would be useful to present the main goals for which sensitivity analysis is performed on a numerical model. According to Saltelli et al (2008), they consist of three: 1) the ranking of parameters, 2) their screening into significant and non-significant, and 3) the mapping of their ranges. More specifically, ranking is achieved by classifying the importance of each parameter, with the final result and its variations. Screening identifies the parameters that have minimal contribution to the variability of the output sizes. Finally, the space from which values of parameters that produce extreme results for the variables of our model are obtained is practically calculated by mapping. Consequently, the appropriate method needs to be selected based on the purposes for which sensitivity analyses are performed, as each one has different capabilities.

2.7.4.4 Sensitivity Analysis and Uncertainty Analysis

As already mentioned, sensitivity analysis is used in conjunction with other types of analyses, with the most significant ones being uncertainty analysis and model grading. It has been proposed that sensitivity analysis, and more specifically global methods (GSA), have significant correlation with uncertainty analysis[474]. The latter quantifies the overall uncertainty of the model, which is ultimately allocated by the former to different input sizes with the corresponding uncertainty they contain and introduce into the model. In accordance with the above, Pianosi et al., (2016), argue that it is wise to use these two analyses complementarily. When performing GSA, the uncertainty analysis provides confirmation that the results of the GSA are within acceptable limits regarding the behavior of our model. Similarly, after performing uncertainty analysis, sensitivity indices offer valuable additional details, without significant extra cost or time.

2.7.4.5. Sensitivity Analysis and Model Calibration

The process of calibrating a model is described as the process of estimating the parameters in such a way that the results of the model are in the best possible agreement with corresponding natural observations [456]. Sensitivity analysis contributes to identifying the correlation between the variability of input parameters and the results of the model. Through this, this agreement with natural observations is also quantified. Local methods are used once the accepted value of the parameters has been found, and through the analysis, their uncertainty is investigated [475]. Global methods are used after calibration, aiming to reduce the range of values for the parameters to

that where the more correct behavior of the model is observed. Conversely, for a more complex model, GSA contributes to the elimination of non-significant parameters regarding calibration [476], in the selection of better value ranges for further investigation about them with local methods [477], while it also examines other parameters of the overall problem such as the way and accuracy of physical measurements [478].

2.7.4.6 Methods of Analysis for Constant Disturbances

According to all the above, there are many different methods by which sensitivity analysis is performed. Each has its appropriate field of application, and their choice should be made once their purpose has been fully defined but also taking into account their computational cost. Subsequently, some of the most famous and widely used methods, according to the literature in the broader science of water quality, will be presented.

Initially, there are methods with the introduction of constant disturbances in all parameters, while sensitivity is quantified with numerical indices that use partial derivatives. The disturbance of the parameters is usually carried out in a "one-at-a-time" (OAT) manner and represents the simplest method of sensitivity analysis. The numerical indices are calculated with the partial derivative of the variation of the model's output quantities y, in relation to the variation of each input quantity x[456]. The basis of these derivatives are the Taylor series and have been analyzed and explained by [479,480]. The general formula for the numerical indices is presented below in Eq 2.19:

$$Spy_{ji} = \frac{\frac{\Delta yi}{yi,o}}{\frac{\Delta pj}{pj,o}} \qquad \text{Eq (2.19)}$$

Where:

- Δyi represents the difference between the value of the output variable in the reference state and its corresponding value due to the disturbance of the input parameter pj.
- Δpj denotes the difference between the value of the input parameter in the reference state and its corresponding value after its disturbance.
- yi,0 is the value of the output variable in the reference state.
- pj,0 is the value of the input parameter in the reference state.

In general, these methods are the simplest and the least costly in terms of computational expense. However, it must be highlighted that they only depict sensitivity locally and do not illustrate any potential interactions between the parameters. They are deemed ideal for an initial estimation of the importance of input quantities in a model, facilitating preliminary sorting for further, more demanding analyses, without forgetting the constraints regarding interactions.

By using these methods, researchers can make preliminary evaluations and understandings of the system's response to changes in input parameters, which is crucial for refining models and developing robust, reliable simulations. However, the simplicity of these methods also implies the possibility of missing nuanced interactions between parameters and potential nonlinearities in system behavior, which might necessitate more sophisticated approaches to thoroughly understand the complexities involved in the system. Nonetheless, these methods serve as an essential step in the initial stages of sensitivity analysis, laying down the groundwork for more comprehensive studies and allowing for focused, more intricate investigations in later stages.

2.7.4.7 Methods of Multiple Initial Point Disturbance Analysis

Subsequently, the methods of multiple initial points of parameter disturbances are encountered, which are constituted as a hybrid between local and global methods. To elaborate, the disturbances of the variables are calculated from numerous diverse points—values of the parameters, and the global sensitivity is accumulated from these disturbances at all the chosen points. These particular methods differ regarding whether they use finite differences or another quantity (their absolute values, squares) for the indicators, in the way they choose the initial points—values, and the magnitude of the disturbances Δi, and in how they assess the final indicator for the sensitivity of each parameter [456]. The most renowned method is Morris [481], which is also recognized by Saltelli et al., 2008 as the Elementary Effect Test (EET). It takes as quantity r the average of the finite differences EEs, through which the sensitivity is also gauged with the subsequent index in Eq 2.20:

$$Si = \frac{1}{r}\sum_{j=1}^{r} EE^j \qquad\qquad \text{Eq (2.20)}$$

The method constitutes a hybrid between local and global ones, as the magnitude of the standard deviation of the EEs illustrates the interaction of parameter i with the others. Specifically, the larger

the standard deviation, the greater the feedback existing between them. Therefore, without additional simulations, information is also provided about the interaction of the parameters, something that previous methods did not allow.[482] proposed the use of absolute values to avoid issues with any negative values canceling each other out.

Concerning the choice of initial points – values for the sample, as well as the magnitude of the disturbances Δi, Morris (1991) proposed the construction of r trajectories with M+1 elements, where M is the number of input parameters of our model. The starting point of each trajectory is chosen randomly, and points are selected with the disturbance of one parameter at a time for the interval Δ. The user defines the size L, from which derive the size of the space from which the values are selected (equals to 1/(L-1) from the possible range of values of each parameter) and the size of the disturbance Δ = L/(2*L-1). Typical values for L are 4 to 8, hence for Δ, they are 0.76 to 0.57. According to this sampling method, only local behaviors of the model are avoided in the description, however, the results become unacceptable if the model is characterized by high non-smoothness.

Methods of similar logic utilize squared finite differences, which allows their association with the dispersion methods that will be mentioned subsequently. [483] suggest the usage of the mean value of the squared differences and demonstrate its ability to provide an upper limit for the values of the total effect indicators. This feature makes this approach ideal for the parameter screening process, as smaller values of the upper limits mean that the parameter is also non-significant for the model. Conversely, they argue that the ranking is not carried out satisfactorily through this approach. [484] propose a different but closely related approach using squared finite differences as indicators of significance, the DELSA (Distributed Evaluation of Local Sensitivity Analysis). The significance values are not aggregated, but their entire density function is explored, and the final aggregation is realized using the median value, not the mean.

2.7.4.8 Correlation or Regression Analysis Methods

The following methods for estimating model sensitivity are based on the statistical analysis of the input and output data of the model, which are generated by random Monte Carlo type simulations. These statistical analyses are conducted either through correlation methods with proponents like [474], or through regression analyses by [485]. Correlation methods use the correlation index between input and output sizes as a sensitivity indicator. Correlation indices used are the Pearson

coefficient (CC) and the partial Pearson (PCC), which are used when the model is linear, and the Spearman coefficient (SRCC) or partial rank coefficient (PRCC) for non-linear but relatively monotonic models [466]. Pianosi et al., (2016), argue that the choice among these coefficients depends on the degree of linearity and monotony of the model, which can be assessed from scatter plots of parameters and model variables. For more complex studies, where multiple variables must be evaluated simultaneously, [486] utilize canonical correlation analysis (CCA).

Regarding regression methods, sensitivity indices are estimated by applying regression to the sample of input-output sizes. The simplest and most common method is linear regression with a relation of the type, $y = \alpha_i + b_i \cdot x_i$. The estimation of the least squares of the regression coefficient b_i constitutes the measure of sensitivity. Many of the sizes for which their sensitivity is measured have different units of measurement, therefore a normalized index (SRC) is used as shown in Eq 2.21[456]

$$Si = bi \frac{SD(xi)}{SD(y)}$$

Eq (2.21)

where SD is defined as the standard deviation of the size.

Linear regression is simple to use and can be utilized in multiple forms to calculate the sensitivities for all parameters simultaneously.

2.7.4.9 Regional Sensitivity Analysis Methods (RSA)

Regional Sensitivity Analysis (RSA), also known as Monte Carlo filtering, consists of various methods that explore areas of these parameter values which produce specific values for the model variables. They are mainly used for mapping the value ranges for the input sizes, but also for the analysis of system control [456]Various methodologies, which are presented below, exist for the application of RSA. Initially, the parameters can be divided into two subsets (behavioral and non-behavioral), based on the behavior of the model and the results of its variables. [487]. A different methodology involves separating the parameter samples, according to a predetermined limit of the variable values, resulting from them. Subsequently, the two subsets of input sizes are compared with the aim of understanding the complete behavior of the model. The next methodology involves constructing the graphical representation of the probability density

functions for the parameters (behavioral and non-behavioral). Qualitative information about the parameter ranges, i.e., the mapping process, is obtained from these representations. Additionally, the divergence between the two samples can be calculated using the Kolmogorov-Smirnov index as presented in Eq 2.22.

$$Si = _{xi}^{max} |FXi|yb \cdot (xi|y \epsilon Yb) - FXi|ynb \cdot (xi|y \epsilon Ynb)| \qquad\qquad Eq\ (2.22)$$

Where F_{Xilyb} and F_{Xilynb} are the empirical cumulative distribution functions of xi of the sample with behavioral parameters and respectively with non-behavioral. The use of empirical distribution functions results in the good performance of the method even in models with small samples, as analyzed by [488]. However, it should be mentioned that the aforementioned index cannot be used for sorting the parameters. As supported by Saltelli et al., (2008) if the Kolmogorov-Smirnov index has a zero value, this is a necessary but not sufficient condition to consider the sensitivity also zero. This is due to the fact that parameters that contribute to the variability of output sizes only due to interactions among them, may have the same behavioral and non-behavioral distribution functions. The main advantage of RSA is found in the ease of applying the method to any model, even with non-numeric output sizes, provided that the criterion for separating the parameters is correctly structured and verified and by some qualitative analysis of the model. Conversely, when there is no clear definition of the separation criterion, the method has problems. [475,489,490] studied ways to bypass the separation criterion so that RSA can be applied without specific limits. Specifically, they examined the grouping of output sizes into sets of predetermined size and equal spatial interval and the comparison of the distribution functions of the output sizes with those of the input sizes.

2.7.4.10. Variance Analysis Methods

Sensitivity analyses which are based on variances have three basic principles:

1) parameters are considered as stochastic type sizes and introduce a distribution function to the output sizes,
2) the variability of the distribution function of the output sizes is a satisfactory representation of their uncertainty and
3) the contribution to the variability of the output sizes of each parameter has a satisfactory correlation with the sensitivity of the latter[456].

There are several sensitivity indicators based on variances such as the first order effects index Si. Through this, the direct contribution of each parameter to the model variables or more specifically, the expected reduction in the variability of the output sizes is measured, if one of the input sizes is determined. The formula, is in the following form as shown in Eq 2.23 [491]:

$$Si_i^F = \frac{V_{xi}\ (E_{x \sim i}(Y|x_i))}{V(y)}$$
Eq (2.23)

where E is the expected value, V is the variance, and X~I refers to a matrix with all parameters except the i-th one. Similarly, in the same article, the total effects index is proposed (Eq 2.24), which calculates the overall contribution of each parameter, taking into account its interactions with the rest.

$$S_i^T = \frac{E_{x \sim i}\ (V_{x i}(Y|x \sim_i))}{V(y)} = 1 - \frac{V_{x \sim i}\ (E_{x i}(Y|x \sim_i))}{V(y)}$$
Eq (2.24)

Total effect indices are used in the sorting of parameters, as their zero value is a sufficient and necessary condition to prove that they do not affect the model. Main effect indices are used for ranking, especially when significant interactions among parameters are not observed. Additionally, second-order, third-order, etc. indices can be defined, which measure the contribution of parameters in pairs, triples, etc. This allows for the analysis of parameters and their interactions in smaller subsets.

Sobol' (1993) showed that first-order and higher-order indices are related to the terms of the variance of the above types. They also maintain this relationship for different types of models, as they are based on assumptions that the parameters are independent. However, if the parameters are correlated, illogical results are observed e.g., the total effect indices may be smaller than the main effect indices or tend to zero [492]. Concurrently, these indices have algebraic types, easy to construct and use, for their estimation. However, it should be mentioned that to achieve a good estimation of the indices, a sufficiently large initial sample is required, which makes the method computationally and temporally demanding. Some variations that have been proposed to reduce time are:

1) the use of Fourier series for the calculation of the main effect indices, Fourier Amplitude Sensitivity Test (FAST) [493] and its extension, extended FAST for the total effect indices [457]

2) the use of simulators as in [494]

The methods that utilize the expansions of Fourier series (FAST and extended FAST) constitute very good alternatives to the classic variance methods. Specifically, they calculate the significance indicators for the model's parameters with a significantly smaller sample of values. This is achieved because, in contrast to the classic Sobol, the FAST technique varies all the parameters in their corresponding range simultaneously, using a common variable s for all, thus saving much more time[488]

The sensitivity indices are calculated based on the formulas proposed by Saltelli, (1999), which use the ωj, as well as the Fourier coefficients (Aj, Bj) to calculate the variances of the output variables for the model, from which, ultimately, the indices for the parameters are derived. Below are presented all the formulas that were used for the FAST method (Eq 2.25 – Eq 2.29).

$$A_j = \frac{1}{2\pi}\int_{-\pi}^{\pi} f(s)Cos\,(js)ds \qquad\qquad \text{Eq (2.25)}$$

$$B_j = \frac{1}{2\pi}\int_{-\pi}^{\pi} f(s)Sin\,(js)ds \qquad\qquad \text{Eq (2.26)}$$

$$\bar{V}ar\,(Y) = 2\sum_{j=1}^{\infty}(A_{jwi}^2 + B_{jwi}^2) \qquad\qquad \text{Eq (2.27)}$$

$$\bar{V}ar\,(Y) = 2\sum_{j=1}^{\infty}(A_j^2 + B_j^2) \qquad\qquad \text{Eq (2.28)}$$

$$Si = \bar{V}ar\,(Y)/\bar{V}ar\,(Y) \qquad\qquad \text{Eq (2.29)}$$

The limitation of this technique lies in the fact that it cannot calculate the total effect indices and, therefore, it does not provide information about the interactions among the parameters. [457,495], developed the extended FAST technique, which allows for the calculation of total effect indices without significant additional iterations compared to the simple FAST.

2.8 Opportunities and Challenges of AnMBR – PhD objectives

Over the last couple of decades, AnMBRs have emerged as an innovative technology in the field of wastewater treatment. By merging the advantages of anaerobic biological treatment and membrane filtration, AnMBRs facilitate high organic matter removal, energy recovery in the form of biogas, and excellent effluent quality. These characteristics make AnMBRs an attractive option for sustainable wastewater treatment. However, challenges remain, such as efficient operation at high organic loadings and ambient temperature, membrane fouling and nutrient removal, which lead to reduced efficiency and increased operation and maintenance costs.

Therefore, in order to address these challenges, the scope of this doctoral dissertation is to systematically evaluate the operation of Anaerobic Membrane Bioreactor (AnMBR) in treating real wastewater, under ambient environmental conditions. Specifically, the research conducted within the context of this PhD thesis has the following objectives:

a) To evaluate the influence of Hydraulic Retention Time (HRT), elevated organic loadings, and ambient temperature fluctuations on the AnMBR efficacy in treating municipal wastewater.

b) To systematically assess the implications of $FeCl_3$ addition in bolstering AnMBR operational metrics, specifically focusing on curtailing membrane fouling and enhancing phosphorus removal.

c) To adapt, apply, and authenticate the Anaerobic Digestion Model No. 1 (ADM1) for simulating the municipal wastewater treatment via AnMBR, in order to provide a mathematical tool for the optimization of AnMBR operation.

Chapter 3. Materials and Methods

3.1. Description of the AnMBR reactor

To study the efficacy of anaerobic wastewater treatment via AnMBR, a 40 L laboratory-scale reactor equipped with a flat-sheet submerged membrane was set up. Accompanying this, a 40 L reservoir was designated for the capture and quantification of the resultant biogas. This system was placed within the R&D Department of the Athens Water Supply and Sewerage Company (EYDAP), as depicted in Figure 3.1. Pertinent specifications of the membrane can be perused in Table 3.1.

According to operational monitoring, temperatures were fluctuating between 15°C and 26°C. In order to align the reactor's temperature with the typical conditions experienced at Greek WWTPs, an external heating bath was employed. Furthermore, to ensure meticulous monitoring and control over the anaerobic processes, sensors for temperature, REDOX, and TMP were integrated within the system. Start-up was performed using biomass from a full-scale anaerobic digester, which was operating under psychrophilic conditions at that time. The employed inoculum exhibited a pH of 7.2, and TSS and VSS concentrations were recorded at 18 g/L and 14.3 g/L, respectively.

Two peristaltic pumps were deployed: one catered to the influx of screened wastewater into the reactor, while the other managed the efflux of filtrate. Biogas generation was monitored within the AnMBR's headspace, which was directed to the 40 L reservoir. An auxiliary pump was employed for biogas recirculating, contributing to membrane cleaning.

The operation of the AnMBR consisted of an 8-minute filtration phase followed by a 1-minute relaxation interval. This rhythm was essential for maintaining the membrane's permeability. Biogas-induced cleaning was facilitated by a dedicated pump, which redistributed the stored biogas from the reservoir. The biogas aeration rate was standardized at 12 L/min per membrane. The chemical cleaning of membranes utilizes sodium hypochlorite as the primary cleaning agent. A comprehensive schematic representation of the entire system is depicted in Figure 3.2. The characteristics of the membrane are outlined in Table 3.1.
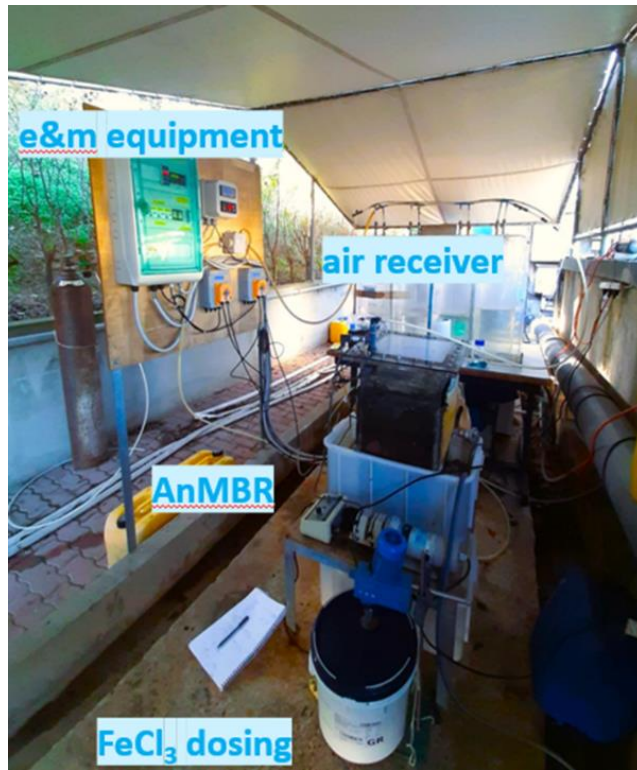
Figure 3. 1: Photographic representation of the Lab scale AnMBR system
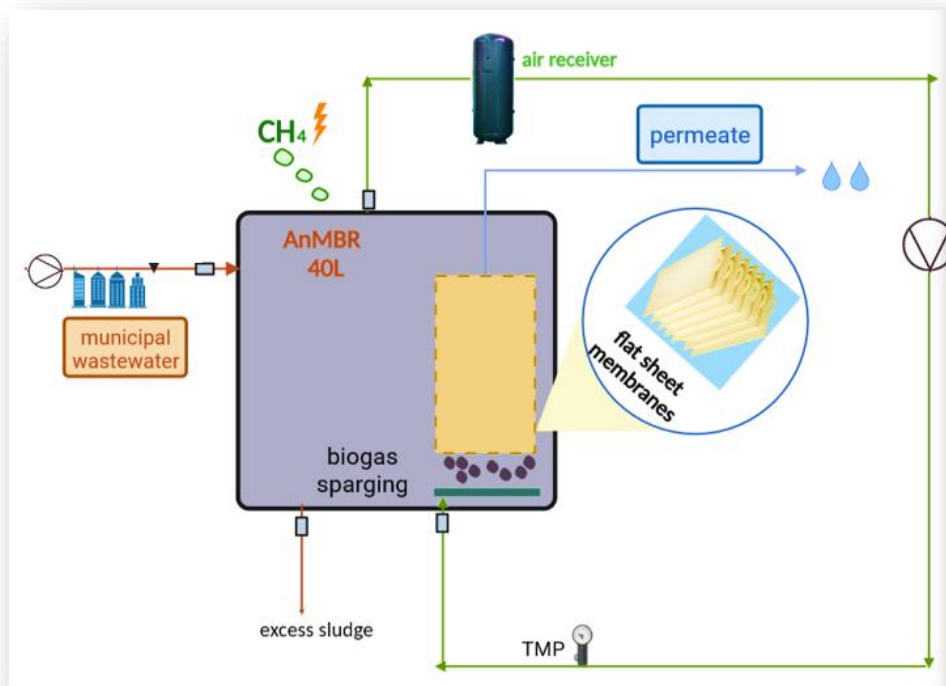
Figure 3. 2: Schematic presentation of the AnMBR reactor

Table 3. 1: Membrane characteristics

Manufacturer	SINAP
Membrane type	Flat sheet
Membrane model	SINAP 10 (5x0.1 m^2)
Pore size	<0,1µm
Membrane surface	0,1m^2
Material	PVDF
Specific air demand based on membrane area (SADm)	0.36 m^{3}air/m^{2}membrane area/ h

3.2 AnMBR operation

Throughout the study the reactor SRT was maintained at 50 d by daily wasting of the required mass of solids from the reactor. Following the initial start-up phase, four distinct HRTs—48 hours, 24 hours, 12 hours, and 6 hours—were systematically studied. Each HRT underwent an exhaustive six-month evaluation period, further divided into two separate three-month phases to mimic seasonal variations corresponding to summer and winter conditions. The detailed operation of each phase is shown in Table 3.2.

Table 3. 2: Operating characteristics of lab-scale AnMBR

Parameters	Winter/ Summer	Winter/ Summer	Winter/ Summer	Winter/ Summer
Days of operation	1-90/ 90-180	180-270/ 270 -360	360-450/ 450-540	540-630/ 630-720
Operating temperature	18±4/23 ±1	19±2/24±2	19±3/24±3	
Q(L·d^{-1})	20	40	80	160
HRT(h)	48	24	12	6
SRT(d)	50	50	50	50
Flux (L/m^2 h)	1.6±0.2	3.3±0.4	6.6±0.7	13 ±0.7
OLR (KgCOD/m^3/d)	0.24 ±0.3/ 0.23 ± 0.02	0.45±0.04/ 0.49 ± 0.05	0.9±0.09/ 0.91±0.1	2 ±0.11/ 1.8 ±0.22

Parameters	Winter/ Summer	Winter/ Summer	Winter/ Summer	Winter/ Summer
Waste Activated Sludge (L·d^{-1})	0.8	0.8	0.8	0.8

The laboratory-scale AnMBR, was fed with screened municipal wastewater from the Metamorfosis WWTP (Athens, Greece). The reactor operated at the R&D department of Athens Water Supply and Sewerage Company (E.YD.A. P S.A) continuously for 3.5 years. Physicochemical characteristics of the screened municipal wastewater are presented in Table 3.3.

Table 3. 3: Characteristics of the influent screened municipal wastewater.

Parameter	winter period (T=18°C ±3)	summer period (T=23 °C ±2)
TSS (mg/L)	107 ±12	120 ±15
VSS (mg/L	97 ±8	99 ± 6
COD (mg/L)	439±34	453±26
CODs (mg/L)	171±25	185±30
NH$_4$-N (mg/L)	63±9	67±5
TN (mgP/L)	55 ± 17	53±13
TP (mg/L)	8.5±3.2	8.3±2.9
Conductivity (µS cm^{-1})	1450 ± 130	1530 ± 170
Cl (mg/L)	170±30	167±25

3.3 Experimental design

The study employed a systematic monitoring process targeting various parameters within the lab-scale unit.

Sampling Process:

Samples were collected from three distinct points:

1. Pretreated wastewater influent
2. AnMBR permeate
3. Excess sludge

For conventional parameters such as COD, TSS, TN, and others, composite samples were acquired thrice weekly. On the other hand, some parameters including biogas production, reactor temperature, ambient temperature, pH, TMP, and effluent flow were scrutinized on a daily basis.

Biogas Collection:

The biogas was amassed in a specialized reservoir. This reservoir featured four inverted cylinders, housed within partitioned tanks filled with acidified water. The rate of biogas production was gauged using the water displacement technique. For precise assessments, samples were extracted from this reservoir into a 200 mL gasbag.

Table 3.4 summarizes the frequency and objective for each parameter, ensuring a holistic understanding of the AnMBR system's operation.

Table 3. 4: Laboratory Measurements Schedule After System Stabilization

Parameter	Frequency	Objective
Temperature and pH	3 times/week	Monitor conditions
Biogas	Daily	Ensure proper system operation and record production
TMP	Daily	Examine membrane performance
COD	3 times/week	Monitor operations
TSS, VSS	3 times/week for supernatant, 1 time/week for reactors	Count solids and calculate volume removal per sampling
Soluble methane	1 time/2 weeks	Destruction of organic load
Sulphates	1-2 times/week	Compare sulfates in reactors with control reactors
TN	1 time/week	checking for possible accumulation
TP	1 time /week	checking for possible accumulation/removal when iron was added
VFAs	1-2 times/week	Monitor concentration of volatile fatty acids
Alkalinity	1 time/2 weeks	Ensure proper system operation
Biogas productions	Daily	Examine system performance
Biogas composition	1 time/week	Examine system performance

3.1 Analytical methods

3.3.1 Conventional parameters

3.3.1.1 Analysis of COD

Analysis of soluble chemically required oxygen (COD) was performed according to the 5220 D "Closed Reflux Colorimetric Method" of Standard Methods for the Examination of Water and Wastewater, 22nd Edition, 2012.

COD is defined as the chemically required oxygen for the oxidation of organic and inorganic compounds in a sample. It is essentially the amount of potassium dichromate ($Kr_2Cr_2O_7$) consumed during this oxidation. Through its measurement, the biodegradable or non-biodegradable organic load of the wastewater is determined.

A strongly acidic environment (50% H_2SO_4) is required to measure COD. A sample is digested with a strong acid solution and a quantity of potassium dichromate at a temperature of 150oC for a period of 2 hours, while Ag_2SO_4 is added as a catalyst for the more efficient oxidation of some organic compounds, such as volatile organic acids which, due to their volatility, are not oxidized as efficiently. The organic compounds under these conditions are oxidized to CO_2, H_2O, NH_4^+, PO_4^{-3}, $SO_4^{-2,}$ while the Cr (VI) dichromate anion is reduced to Cr (III). These two oxidation states of chromium are characterized by orange and green colors respectively, and are absorbed at specific wavelengths (400 nm for Cr (VI) and 600 nm for Cr (III)).

For the application of the method, ready-made reagents of the company HACH were used. These reagents are contained in vials depending on the measuring range. HACH LCK314 vials are used for a measuring range of 15-150 mg / L and HACH LCK114 vials are used for a measuring range of 150-1000 mg / L. The digestion at 150oC was carried out in a compatible digester device of the same company (Figure 3.3). The measurement of the wavelength was done in a spectrophotometer of visible light type HACH DR2800.

Figure 3. 3: COD digester

3.3.1.2 Analysis of total and volatile suspended solids (TSS – VSS)

Determination of TSS and VSS was performed according to method 2540 D of Standard Methods for the Examination of Water and Wastewater, 22nd Edition, 2012. This method is applicable for water and treated or untreated wastewater.

The basic techniques for solids determination are separation by filtration, evaporation, combustion and weighing. Initially, during filtration, a separation is made between the suspended, non-permeable solids and the dissolved, permeable solids. Whatman GF / C layered filters with a pore size of 1.2 μm were used for this application. These filters hold the particles along their mattress, trapping them in a mesh of inorganic fibers. The filter is first placed in an oven at 550°C (Figure 3.4B) for at least 15 minutes in order to completely remove possible moisture, whereafter it is left to cool in a dryer and is weighed on a precision scale prior to filtration. The sample is stirred effectively in order to homogenize its content and is applied to the filter under vacuum. The selected volume of the sample depends on the density of the liquor.

Following filtration, the filter is placed in an oven, that is maintained at 103-105°C (Figure 3.4A), for at least 1 hour, for the complete removal of moisture (evaporation stage). After it is left briefly to cool in the dryer, the filter is then weighed once again. With this, the TSS concentration of the sample may be determined as:

$$TSS\left(\frac{mg}{L}\right) = \frac{M_{s1} - M_f}{V_{sample}}$$
<div align="right">Eq (3.3)</div>

where:

Ms$_1$: the filter's weight after the evaporation process

Mf: the filter's weight prior to filtration

Vsample: the volume of the filtered sample

After determining the TSS of the sample, the filter may be then placed in the oven set to 550°C for a period of at least 15 minutes, for the removal of the volatile solids (combustion stage) (Figure 3.4B). After allowing the filter to return to room temperature in the dryer, the filter is once again weighed and the VSS concentration of the sample may be determined as:

$$VSS \left(\frac{mg}{L}\right) = \frac{M_{s1} - M_f}{V_{sample}}$$

Eq (3.4)

where:

Ms1: the filter's weight after the evaporation process

Ms2: the filter's weight after the combustion process

V sample: the volume of the filtered sample
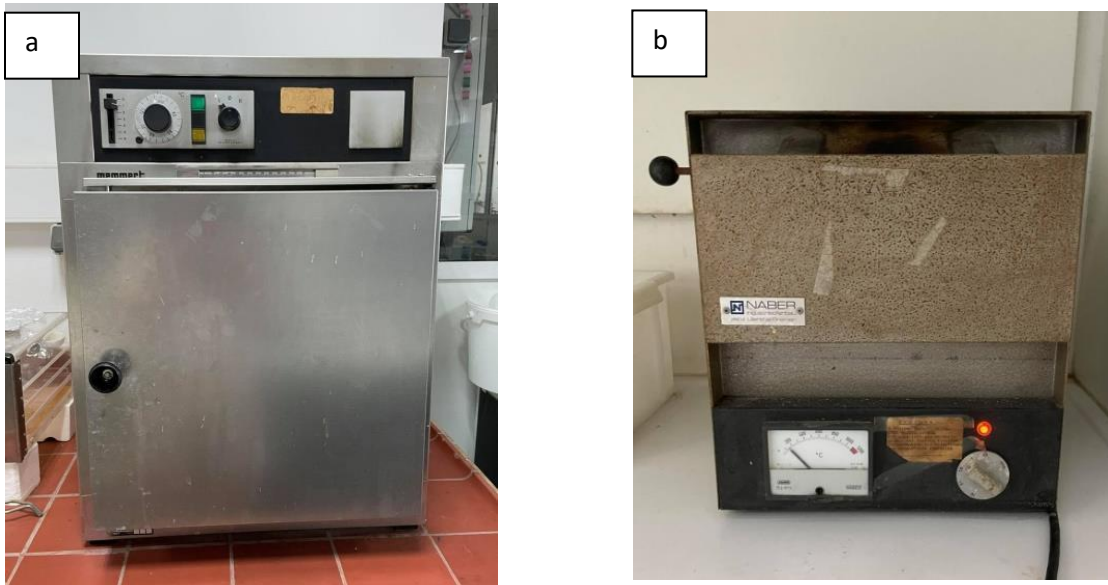
Figure 3. 4: Appliances for TSS and VSS analysis: evaporation oven (a), combustion oven (b)

3.3.1.3 Analysis of phosphorus

The method for the determination of total phosphorus and its various fractions was performed based on the standard method 4500-P E. Ascorbic Acid of Standard Methods for the Examination of Water and Wastewater, 22nd Edition, 2012.

Phosphorus in urban wastewater is found either in inorganic form as orthophosphate radicals (PO_4^{-3}, HPO_4^{-2}, $H_2PO_4^-$) and polyphosphate chains or in organic form. The determination of organic phosphorus and polyphosphates first requires their hydrolysis to orthophosphates. For this reason, the determination of total phosphorus that includes all three forms of phosphorus (orthophosphate, polyphosphate and organic phosphorus) is performed in two stages. In the first stage, organic phosphorus and polyphosphates are digested with the aim of converting them into

orthophosphate radicals and in the second stage, the total phosphorus is determined as orthophosphates (PO_4-P).

The amount of organic phosphorus can be determined in most samples, where chemical precipitation is not expected to occur, as the difference between the total phosphorus of an unfiltered sample and the total phosphorus concentration of the same sample after filtration through membrane type filters (0.45 μm). By bypassing the digestion step and directly filtrating a sample through a 0.45 μm membrane, it is possible to determine the orthophosphate radicals in the sample by applying the ascorbic acid method. By digestion of a filtered sample and then application of the ascorbic acid method, the total of orthophosphate radicals and polyphosphate chains is determined.

During the digestion step, the sample is heated to boiling point in the presence of sulfuric acid and a catalyst (ammonium persulfate). Under these conditions the organic matter is oxidized to CO_2 and H_2O, while the phosphorus contained in the organic matter and in the polyphosphate chains is hydrolyzed to orthophosphates. The orthophosphate concentration can then be determined by various spectroscopic methods.

The concentration of orthophosphates was determined according to the ascorbic acid method. A mixture of ammonium molybdate $((NH_4)6Mo_7O_{24})$ and potassium-antimony tartrate $(K(Sb)C_4H_4O_6)$ is used, which reacts with the orthophosphates under acidic conditions, producing ammonium phosphomolybdate according to the following reaction:

$$PO_4^{-3} + 12(NH_4)2MoO_4 + 24H^+ \rightarrow (NH_4)3PO_4.12MoO_3 + 21NH_4^+ + 12H_2O$$

Then, in the presence of ascorbic acid, the molybdenum contained in the ammonium phosphomolybdate complex is reduced to free molybdenum, giving a strong blue tint to the solution. The hue of the solution is proportional to the orthophosphate concentration (for values between 0.1 and 1.0 mg P/L) which may be determined spectrophotometrically at a wavelength of 890 nm.

Following their filtration, samples were diluted appropriately in 50 mL volumetric flasks, based on the expected phosphorus concentration (within the respective limits) and transferred to conical flasks. Then, 8 mL of mixed reagents (mix) were added to each flask and allowed to react for a period of 10 minutes, in which the reaction becomes complete. The mix consists of 50 mL 5N

sulfuric acid, 5 60ypothesiium antimonyl tatrate, 15 mL ammonium molybdate and 30 mL ascorbic acid. The samples would undergo spectral analysis within the following 20-minute period as to not allow discoloration.

3.3.1.4 Analysis of ammoniacal nitrogen

The process for the determination of ammoniacal nitrogen (NH4-N + NH3-N) is based on the 4500-NH3 C. Nesslerization Method (Direct and Following Distillation) of the Standard Methods for the Examination of Water and Wastewater, 18th Edition, 1992.

The method involves distillation in a BUCHI K-314 apparatus (Figure 3.5), where under alkaline conditions water vapor is introduced into the sample. Under these conditions the ammonia is released as follows:

$NH_4 \rightarrow$ (heat) $NH_3 \uparrow + H^+$
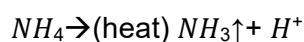
A concentrated NaOH solution is first added to the sample in order to raise pH close to 9.5, while the ammonia gas is collected in an acidic boric acid solution, where it retakes the form of ammonium.

$NH_3 \uparrow + H_3BO_3 \rightarrow NH_4^+ + H_2BO_3^-$
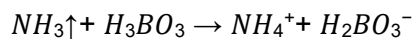
Upon completion of the distillation, the distilled solution is transferred to a 50 mL volumetric flask, after appropriate dilution, where 2 mL of the Nessler reagent are added. The Nessler reagent is a mixture of potassium iodide and mercuric iodide, which react with ammoniacal nitrogen under alkaline conditions to give a brownish-yellow colloidal solution according to the following reaction:

$2K_2HgI_4 + NH_3 + 3KOH \rightarrow Hg_2IONH_2 + 7KI + 2H_2O$
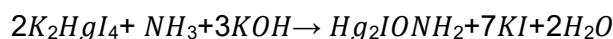
The reaction of the diluted sample with the Nessler reagent requires around 10 minutes to be complete. Upon completion, the concentration of the ammoniacal nitrogen may be determined using a spectrophotometer at 425 nm, as the hue of the solution is proportional to the concentration of ammonium. Analysis was performed within 30 minutes from the completion of the reaction to avoid discolouration of the samples.

Figure 3. 5: BUCHI K-314 distillation apparatus

3.3.1.5 Analysis of nitrate nitrogen and nitrite nitrogen

Analysis for nitrate nitrogen was performed by the HACK LCK339 method, which is based on the reaction of nitrate anions with 2,6-dimethylphenol to form 4-nitro-2,6-dimethylphenol, in a solution containing sulfuric and phosphoric acid. Following filtration and appropriate dilution, 1 mL of the diluted sample was added to a vial of LANGE LCK 339 reagent along with 0.2 ml of the accompanying reagent supplied with the vial. After 15 minutes the reaction is complete, and the nitrate concentration is measured using a spectrophotometer at a wavelength of 345 nm. The range of measurement is within 0.–3 - 13.50 mg NO_3-N / L.

Analysis for nitrite nitrogen was performed with the HACK 5807 Nitrite method, which is based on the reaction of nitrite with sulfanilic acid to form a nitrogenated sulfanilic salt, which reacts with chromotropic acid to produce a pinkish color. Following filtration and appropriate dilution of the sample, a HACK Nitriver 3 reagent is added to 10 mL of the diluted sample. The sample is then stirred lightly and left over a period of 20 minutes for the completion of the reaction. Following this, the sample is analyzed spectrophotometrically at a wavelength of 507 nm. The range of measurement is within 0.002 and 0.300 mg NO_2-N / L.

3.3.1.6 Measurement of Alkalinity

The alkalinity was measured using the titration method, as recommended by the Standard Methods for Examination of Water and Wastewater (APHA, 1997). Alkalinity represents the ability of a sample to neutralize acids, effectively acting as a buffer. Various compounds, such as phosphates, sulfates, and ammonia, can contribute to this alkalinity. However, the primary components are bicarbonates, carbonates, and hydroxides. The mathematical expression for alkalinity is given by:

Alk=[HCO_3^-] +2[CO_3^{2-}] + [OH^-]−[H^+] in terms of g.eq/L

Alkalinity is often represented in terms of calcium carbonate concentration. In anaerobic systems, alkalinity is predominantly in the form of bicarbonates. The apparatus required for the measurement included:

➢ 50 ml burette
➢ 50 ml beaker
➢ Stirrer
➢ Portable pH meter

Initially, 5 ml of the sample was diluted with 25 ml of deionized water in the beaker. The solution was titrated with 0.05N sulfuric acid, with continuous pH measurement and stirring. Both total and partial alkalinity (TA, PA) were measured. The former encompasses both volatile fatty acids (VFAs) and bicarbonate alkalinity, while the latter is primarily associated with bicarbonate alkalinity. The titration was initially halted when the pH reached 5.7 (partial alkalinity) and finally at 4.5 (total alkalinity). Alkalinity was calculated in terms of $CaCO_3$ using the following equation:

$$alk \ (CaCO_3 \ mg/L) = \frac{V_{H2SO4} * (0.1 \ N \ H_2SO_4) * (eq.wt.CaCO_3) * 1000 \ mg}{V_{\delta\varepsilon\iota\gamma\mu\alpha\sigma\varsigma}} \pi r^2 \qquad \text{Eq (3.5)}$$

Where:

VH_2SO_4 is the volume of sulfuric acid consumed (ml).

N H_2SO_4 is the normality (equivalent sulfuric acid per liter of titration solution).

Eq. wt. CaCO$_3$:50

Vsample is the sample volume measured (typically 5ml).

3.3.1.7 Sulfide Measurement

Sulfide measurement was carried out 1-2 times a week depending on the results of the previous cycle and to determine the sulfide salts in each reactor, as the presence of ferric trichloride theoretically leads to the consumption of sulfides by the SRBs and the formation of S-2 anions without consuming organic load. The difference in the concentration of the S-2 anions in the reactors fed with ferric trichloride compared to the control reactors indicates the role of iron in the growth of SRBs and the consumption of organic food.

The method followed for the measurement of sulfides is the spectrophotometric method of Hach 8131 (program 690) or otherwise the methylene blue method. The process is based on the Standard Methods for the Examination of Water and Wastewater (APHA, 1997) and has a measuring range of 0-800µl S-2.

The method relies on the ability of sulfide anions to convert the substance N,N-dimethyl-p-phenylenediamine sulfate into methylene blue. The intensity of the color is proportional to the concentration of anions present in the solution.

For the analysis of the samples, the initial preparation of the blank sample was necessary, consisting of 10 ml deionized water, 0.5 ml of sulfide reagent (Sulfide Reagent) 1, and 0.5 ml of sulfide reagent (Sulfide Reagent) 2. Measurement is carried out at a wavelength of 665 nm.

After zeroing the spectrophotometer with the blank, 10 ml of the sample is placed in a cell that is properly sealed, and 0.5 ml of sulfide reagent (Sulfide Reagent) 1 is added. The sample is stirred, and then 0.5 ml of sulfide reagent (Sulfide Reagent) 2 is added. The cell is inverted to mix the reagents with the sample. Initially, the mixture has a pink color that turns blue. The reaction takes 5 minutes to complete. After 5 minutes, the cell, once cleaned externally, is placed for measurement.

It should be noted that for the accuracy of the method, it is essential that the samples are measured immediately after collection and cannot be preserved for later analysis. Stirring the samples should not be excessive, as over-stirring leads to a reduction in sulfide concentration. Also, dilution of the samples can result in a loss of S-2, resulting in inaccurate results.

3.3.2 Volatile Fatty Acids (VFAs)

The volatile fatty acids (VFAs), butyric (Butyric acid; But), isobutyric (iso-Butyric acid; isoBut), propionic (Propionic acid; Pr), and acetic acid (Acetic acid; Ac), are analyzed using a gas chromatograph Autosystem XL Perkin Elmer (Gas Chromatography; GC), equipped with a flame ionization detector (FID).

More specifically, about 200 μL of the permeate effluent, after being doubly filtered through a membrane with a pore diameter of 0.45 μm, was stored in the freezer at -20 °C until measurement. Before analysis, the samples were thawed and acidified with the addition of 2% v/v HCl (2N). They were then placed in special containers to inject 0.5 μL into the instrument through an automated sampling system (Autosampler XL PerkinElmer). The temperature of the injector and the detector was 220 °C, while the column (Nukol; 15 m, 0.53 mm; by Supelco company) was adjusted according to the substance being quantified as follows: for the volatile fatty acids at 90 °C, for propanol at 40 °C, and for benzoic acid at 180 °C.

The VFAs are measured to ensure the proper operation of the system. Comparing the concentration of the VFAs in COD terms in relation to the soluble COD of each reactor can give an indication of its operating efficiency and the possible accumulation.

3.3.3. Biogas Measurement

3.3.3.1 Biogas production

The daily produced biogas was measured just before sample collection. For the measurement of biogas, the difference in the water level created by the produced biogas displacing the water

within the cylinders was initially noted using a scale. Subsequently, the dailli biogas production was calculated based on the following equation 2.1:

$$Produced\ biogas\ (\frac{L}{d}) = \frac{3.14 * R * (Level\ before - Level\ after\ )}{\Delta t} \qquad \text{Eq (3.6)}$$

Where:

R: The radius of the inverted cylinder used for biogas collection, Δt: The time elapsed

Next, the standard biogas production was calculated based on the daily barometric pressure and the standard atmospheric pressure using the equation 2.2:

$$Standard\ Biogas\ Production\ (\frac{L}{d})$$
$$= \frac{Produced\ Biogas\ (\frac{l}{d}) * barometric\ Pressure}{Standard\ atmospheric\ pressure} \qquad \text{Eq (3.7)}$$

Where:

Produced Biogas (L/d)): as calculated from (3.1)
Barometric Pressure: The measured pressure in hPa.
Standard Atmospheric Pressure: 1013.25 hPa.

3.3.3.2 Methane measurement /Analysis of Headspace Phase - Nominal Concentration

Volatile compounds, such as chlorinated ethenes, ethane, acetylene, and sulfides, can be measured in the gaseous phase of the experiments by taking a gas sample. This specific method is called Static Headspace Analysis (SHA) and has the ability to extract volatile substances with relative ease and without particular interferences from a mixture with many components (Figure 3.6).

The headspace is considered as the gaseous phase above a liquid or solid sample, enclosed in a sealed bottle. After a reasonable amount of time has passed, the concentrations of a compound between the two phases will stabilize, meaning equilibrium will be achieved. The proportion of the mass of the volatile compound that has transferred to the headspace depends on the relationships between the phases and the interaction of the substance with the mixture. For more information on headspace analysis, readers can refer to the books by [496].
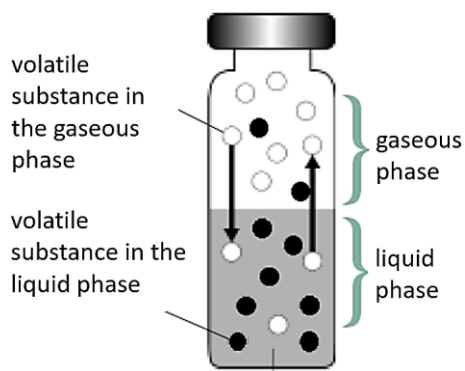
Figure 3. 6: Distribution of volatile and non-volatile substances in the two phases.

Consequently, the distribution between the gaseous and liquid phase can be calculated via the Henry coefficient (H), according to the following equations [497]:

$$M = C_l * V_l + C_g * V_g$$

$$C_g = H_c * C_l$$

$$M = C_l * (V_l + H_c * V_g)$$

Where,

M: total mass of the substance, mole

C_l: concentration of the substance in the liquid phase, M

V_l: volume of the liquid phase, L

C_g: concentration of the substance in the gaseous phase, M

V_g: volume of the gaseous phase, L

H_c: dimensionless Henry constant.

This approach was employed to calculate the amount of dissolved methane in the permeate. Specifically, a 100 ml sample was taken from the AnMBR permeate. Upon collection, samples were promptly sealed using rubber stoppers and aluminum caps. To ensure equilibrium between the liquid and gaseous phases, the samples were mixed with magnetic stirrers for 15 minutes.

A 50 μL sample was extracted from the gaseous phase and manually introduced into the PerkinElmer Autosystem XL Gas Chromatograph (GC). To extract samples from the overlying gaseous phase, a specialized gas collection syringe, the Hamilton gas-tight syringe equipped with a valve, was utilized. This ensured that the sample was securely contained and prevented any leakage.

The sample was then introduced into the gas chromatograph's inlet system (specifically, the Programmed-temperature Split/Splitless inlet system, or PSS, by PerkinElmer). The sample was vented and directed towards the instrument's analytical column (GS-GasPro; 30 m, 0.32 mm in dimensions, produced by J&W). Within this column, a separation process occurred, differentiating substances based on their distribution between the stationary and mobile phases. The stationary phase consists of a non-volatile, high molecular weight liquid secured to the column walls. The mobile phase, conversely, is an inert carrier gas – in this instance, helium (with a purity of 99.999%).

Operational conditions for the Gas Chromatograph were set as follows: the injector and detector temperatures were maintained at 220°C and 250°C, respectively, while the oven housing the column was kept at a consistent 50°C.

3.3.4 Methodology for assessing the COD mass balance and methane yield coefficient.

The application of a COD balance that reflects the operation of the reactors is essential in order to compare methane production to the theoretical yield and to evaluate the performance of the system. For these reasons, the COD balance was based on the method of Giménez et al. (2012), in which the COD considered in methane production is that which remains available to methanogenic bacteria. The dissolved CH4 that is lost in the effluent is calculated. In this way, methane production performance is calculated based on the removed COD (otherwise known as COD_{REM}). The COD removed during the process can be calculated using the mean data gathered during the experimental period according to the COD mass balance:

$$COD\text{-}_{REM} = COD_{INF} * Q_{INF} - COD_W * Q_W - COD_{EF} * Q_{EF}$$ Eq (3.8)

Where:

Q_{INF}, Q_W, and Q_{EF} are the flow rates of the influent,

purged sludge and effluent of the AnMBR, respectively

To accurately determine the methane yield coefficient, it's crucial to precisely measure the total COD removed during the process. In addition, during the acid digestion process used for COD determination, sulfide is completely oxidized to sulfate. Thus, it becomes necessary to define the remaining COD in the effluent, which we'll term as COD_RES-EF, in a specific manner.

$$COD_{RES-EF} = COD_{EF} - COD_{S^{2-}}$$ Eq (3.9)

To properly account for the residual COD, it's important to exclude the COD used up by the oxidation of sulfide during the testing phase. Specifically, 2 kg of O_2 is needed to oxidize 1 kg of S^{2-}. As a result, knowing the remaining sulfide concentration in the effluent is essential. To ensure accurate measurements, samples of the effluent were carefully preserved to prevent any loss of sulfide during transportation and handling of the samples.

Additionally, to avoid underestimating the amount of COD removed from the system, the actual COD reduction, which we'll call COD_TREM, is calculated based on the residual COD in the effluent.

Eq (3.10)
$$COD_{TREM} = COD_{INF} * Q_{INF} - COD_W * Q_W - COD_{RES-EF} * Q_{EF}$$

The methane yield coefficient $Y\frac{CH4}{Obs}$ observed was calculated from the volume of methane produced in the biogas $V\frac{CH4}{BG}$ thus:

$$Y_{Obs}^{CH_4} = \frac{V_{BG}^{CH_4}}{COD_{REM}}$$

Eq (3.11)

The amount of COD used by Sulphate-Reducing Bacteria (abbreviated as CODREM SRB) can be estimated based on the depletion of sulfate concentration during the treatment process. It's important to consider that 2 kg of COD is required by SRB to reduce 1 kg of sulfate sulfur (SO_4-S), as outlined in the work by Lens et al. (1998). By removing the COD used up by SRB from the total COD eliminated in the system, we can then define what's known as the biomethanation yield. This yield specifically accounts for the COD that was removed solely by Methanogenic Archaea (MA).

$$COD_{REM,SRB} = 2 * [(SO_4 - S)_{INF} - (SO_4 - S)_{EF}] * Q_{INF}$$

Eq (3.12)

$$COD_{REMMA} = COD_{REM} - COD_{REM,SRB}$$

Eq (3.13)

$$Y_{BM}^{CH_4} = \frac{V_{BG}^{CH_4}}{COD_{REMMA}}$$

Eq (3.14)

Another important consideration when evaluating the COD mass balance is that some of the methane generated during the process remains dissolved in the wastewater and is consequently lost in the effluent. To quantify this lost methane, the concentration of dissolved CH_4 in the permeate was taken weekly, using a methodology suggested by Souza et al. (2011). To gauge the degree of saturation, this measured methane concentration was then compared to the theoretical saturation concentration. The saturation concentration was calculated using Henry's Law, taking into account the concentration of methane in the biogas present in the headspace of the AnMBR under conditions of 1 atm pressure and a temperature of 273K. Henry's constant for methane in pure water was determined using a specific equation, as cited in the work by Tchobanoglous et al. (2003).

$$\log_{10} K_H = -\frac{675.74}{T\,(K)} + 6.88$$

Eq (3.15)

It has been observed that the concentration of dissolved methane in the effluent increases at low temperatures. The concentration of methane is determined for deionized water because there are no available data for determining it in solutions (whether municipal or otherwise). Methane production is then calculated based on Henry's Law accordingly.

$$X_{CH_4}^{ΔIAΛ} = \frac{P_g^{CH_4}}{K_H}$$

Eq (3.16)

Where $P_g^{CH_4}$ is the partial pressure of methane and K_H^- is the temperature-dependent constant.

Once the dissolved CH_4 is quantified, $Y\frac{CH4}{BM}$ should be corrected, $Y\frac{CH4}{BM}$ considering the total CH_4 produced (i.e., CH_4 in the biogas + CH_4 dissolved in the effluent).

3.3.5: Analysis of Pharmaceuticals and EDCs

➤ <u>Sampling</u>

During the experiments, sampling was carried out in 50 mL glass vials, and the following procedure was followed for each sample:

1. Measurement of pH, dissolved oxygen (DO), and temperature (T).
2. Filtration of the sample.
3. Volumetric measurement of 20 mL of the filtered sample and its placement in a 50 mL glass vial.
4. Addition of 16 μL of methanol using a pipette to halt the action of free radicals. This was only done for samples originating from experiments with hyperthiol.
5. Dilution of the sample with deionized water up to 50 mL.
6. Acidification of the solution using 2N HCl (pH 2.5).
7. Addition of 60 μL from the mixture of internal standards of 600 ppb.
8. Sealing the vial with parafilm, stirring, and refrigeration for up to 24 hours until solid phase extraction.

➢ Solid Phase Extraction (SPE)

SPE achieves the isolation of the substances under examination from the liquid phase. This method involves the use of an appropriate vacuum device, C18 cartridges (500 mg-6mL), plastic syringes, and a pump. This device includes valves at each cartridge inlet to regulate the flow. According to Theodoridis et al. (2015α), the SPE method briefly consists of the following stages• Activation of the adsorbent medium • Sample loading • Rinsing to remove undesirable polar constituents of the substrate • Elution of the solution with the appropriate solvent or solvent mixture • Evaporation of the solvent

For the achievement of the above, the following procedure was carried out for the samples:

1. For the activation of the active groups of the adsorbent medium contained in the cartridges, the following solvents were introduced using a pipette: • 6 mL ethyl acetate (3 x 2mL), • 6 mL methanol (3 x 2mL), and • 6 mL ultrapure water (3 x 2mL) The solvents were allowed to pass through each cartridge filter with a natural flow rate (0.5 mL*min−1) with the valve fully open, always making sure the filter did not dry out. Subsequently, with the valve closed, 4 mL of acidified ultrapure water (pH 2.5) was added to each cartridge, which remained inside until the sample was introduced.

2. For the introduction of the sample, a suitable plastic adapter was placed over each cartridge onto which a 50 mL plastic syringe was placed containing the sample. Immediately after, the valve was fully opened at each cartridge inlet, and the acidified ultrapure water from the previous step and the sample were allowed to flow naturally (0.5 mL*min−1), ensuring sufficient contact time of the sample with the adsorbent medium for the retention of the desired substances.

3. Subsequently, the cartridges were rinsed by passing 2 mL of acidified ultrapure water (pH 2.5) through each one to remove undesirable retained impurities. The valves were fully open.

4. With the valves fully open, the device was connected to a pump that operated for one hour at the maximum permissible pressure to dry the cartridge filters.

5. Subsequently, the elution of the substances under examination from the adsorbent medium was carried out by passing 6 mL of ethyl acetate (3 x 2 mL) through each cartridge with natural flow. The eluate from each medium was collected in a 15 mL dark bottle, and all the bottles were stored in the freezer until the solvent was evaporated.

6. Finally, the solvent, which is the 6 mL of ethyl acetate in each sample, was evaporated using nitrogen gas (Figure 3.7).

Figure 3. 7:solvent evaporation using nitrogen gas, immediately after the collection of the eluates in dark-colored vials from solid-phase extraction

The final stage of the analysis for the qualitative and quantitative determination of the substances under examination is gas chromatography-mass spectrometry (GC-MS).. For each conical vial, once it reached room temperature, an injection of 1 μL was made into the appropriate GC port, and the duration of the analysis via GC-MS was about 18 minutes, using the ChemStation software.

The gas chromatograph used in this thesis is the 7890A and was connected to the 5975C mass spectrometer from Agilent Technologies (Figure 3.8).

For the quantification of the pharmaceutical substances, the internal standard meclofenamic acid (MCF) was used, while for the endocrine disruptors, the deuterated bisphenol A (BPA-d16) was used, according to the determination method developed by Samaras et al,(2011)[498].
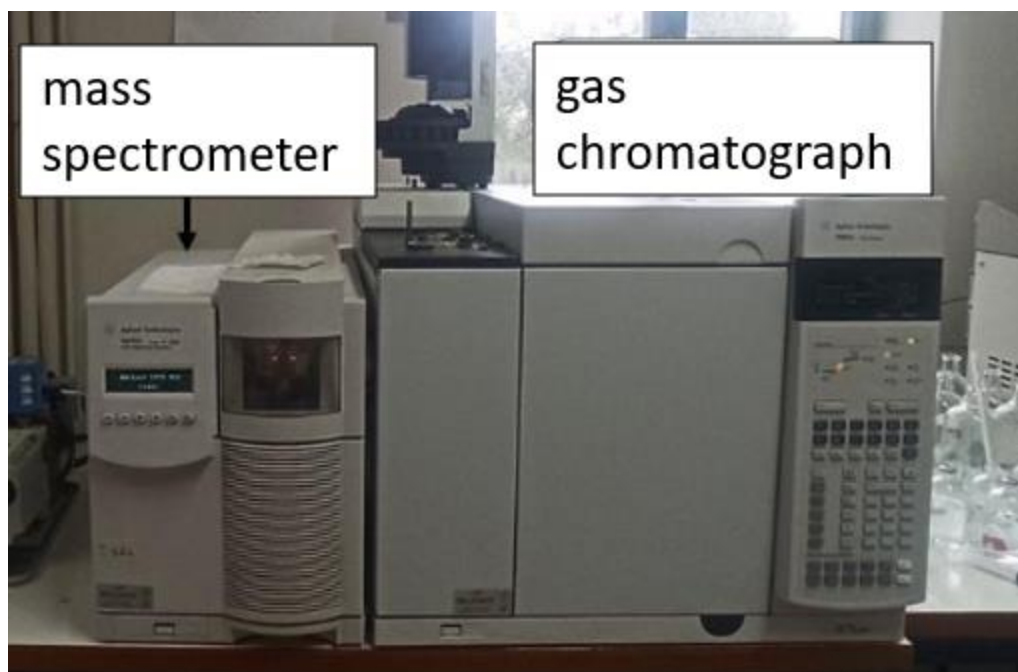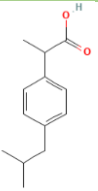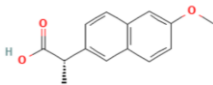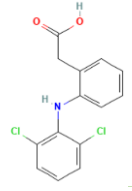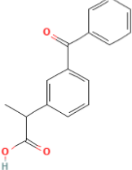
Figure 3. 8:Photographic representation of the gas chromatography-mass spectrometry system (GC-MS)
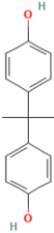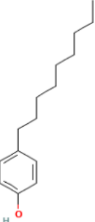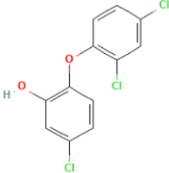
The temperature control of both the sample injection area and the column, as well as in many cases the detector, ranges from 0 to 300°C and takes place either for all components together or individually. Reducing the temperature results in increased separation efficiency but also an increase in retention time tR, leading to longer analysis time. Keeping the column at a constant temperature throughout the analysis hinders the complete separation and detection of mixture components when their boiling points or polarities vary widely. Components with higher volatility and thus low boiling points show peaks that are close to each other or overlapping, resulting in poor separation. On the other hand, less volatile components display broad and low-height peaks, which may be far apart, leading to their non-detection. This problem is solved by using temperature-programmed gas chromatography, where the temperature change follows a specific program.

In the current dissertation, the column temperature change program was set in specific steps as follows: I. from 80°C to 248°C at a rate of 15°Cmin-1, II. maintaining the temperature at 248°C for 1 min, III. from 248°C to 280°C at a rate of 3°Cmin-1, IV. maintaining the temperature at 280°C for the last 5 minutes of the analysis. The transfer temperature was kept at 280°C.

Ibuprofen (IBU), naproxen (NPX), diclofenac (DCF), and ketoprofen (KFN) are the NSAIDs investigated and more frequently detected in the literature among some others, so they were selected as representatives from the NSAID category. Bisphenol A (BPA), nonylphenol (NP), and triclosan (TCS) were selected as the representative compounds from the EDC group. BPA is one of the most frequently detected endocrine-disrupting phenols in soil, surface water, and groundwater because of its release during the manufacture of plastics/resins [499,500]. NP is mainly used as an intermediate in the chemical manufacturing industry to produce NP polyethoxylates (NPnEO) which are used as emulsifiers and dispersing, wetting, and foaming agents [501], while their partial biodegradation is the primary source of NP in the environment [502]. TCS is a highly used antiseptic agent due to its antimicrobial action. The main physicochemical properties and the chemical structure of the target compounds which are important influencing factors for the fate of these substances during the AnMBR treatment are presented in Table 3.5.

Table 3. 5 Main physicochemical properties and chemical structure of the target compounds. [501,503–505]

Target Compound	Category	Molecular Formula	Chemical Structure	Water Solubility (mg/L)	pKa	Log K_{ow}
Ibuprofen (IBU)	NSAID	$C_{13}H_{18}O_2$		21.0 (25 °C)	4.91	3.97
Naproxen (NPX)	NSAID	$C_{14}H_{14}O_3$		15.9 (25 °C)	4.15	3.18
Diclofenac (DCF)	NSAID	$C_{16}H_{14}O_3$		2.37 (25 °C)	4.15	4.51
Ketoprofen (KFN)	NSAID	$C_{16}H_{14}O_3$		51 (22 °C)	4.5	3.12

Target Compound	Category	Molecular Formula	Chemical Structure	Water Solubility (mg/L)	pKa	Log K_{ow}
Bisphenol A (BPA)	EDC	$C_{15}H_{16}O_2$		120 (25 °C)	10.3	3.43
Nonylphenol (NP)	EDC	$C_{15}H_{24}O$		7 (25 °C)	10.28	5.76
Triclosan (TCS)	EDC	$C_{12}H_7Cl_3O_2$		10 (20 °C)	7.9	4.8

3.3.6 Application Protocol for the Fluorescent In Situ Hybridization Method (FISH)

3.3.6.1 Introduction

The FISH method is ideal for the selective identification of a specific group within a set of microorganisms. It relies on analyses of ribosomal ribonucleic acid (16S rRNA) conducted using electronic computers, which revealed short oligonucleotide sequences unique to certain groups of microorganisms, certain genera, or even specific species. This led to the construction of molecular tools and allowed for the study of environmental samples based on their genotype rather than their phenotype. These molecular tools will hereafter be referred to as probes.

The principle of the method can be summarized as follows: The probes, which consist of single-stranded oligonucleotides of a known sequence, enter the cells and hybridize with their complementary ribonucleic acid (RNA) sequences in the ribosomes. If a complementary RNA sequence is not found, then hybridization does not occur, and the added probes are removed in a subsequent purification stage. Thus, only the cells targeted by the molecular tools retain the

oligonucleotide sequences and, since these are labeled with fluorescent substances, the hybridized cells can be observed under a fluorescence microscope due to the natural amplification of the fluorescent signal by the large number of ribosomes in each cell (Figure 3.9).
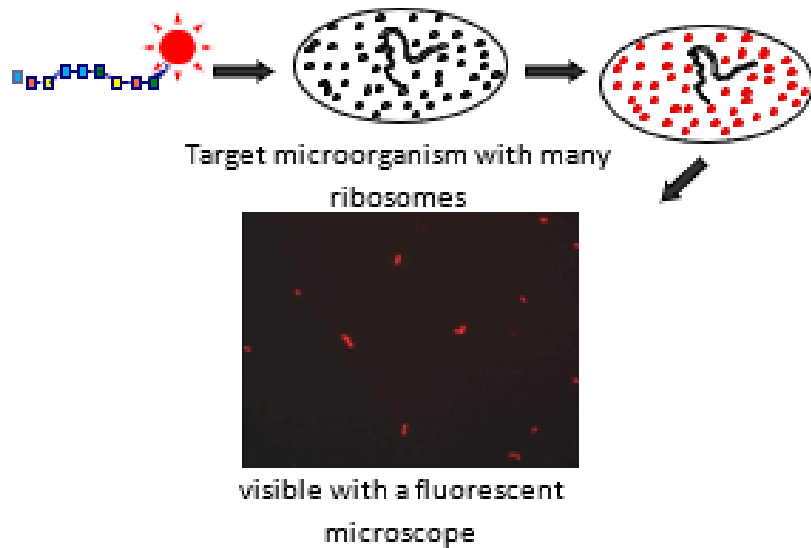
Figure 3. 9:Flow diagram of the FISH method

3.3.6.2 Fish Analysis Protocol

Preparation of 4% w/v PFA/PBS Solution Under the hood, add 4 grams of paraformaldehyde (PFA) to 80 ml of ultrapure water and heat to 60°C for about 10 minutes. Then, add 3 drops of 1M NaCl to clarify and allow it to cool. Afterward, add 10 mL of 1M phosphate-buffered saline (PBS) solution (1/10 dilution of concentrated 10M PBS), a small amount of 5M sulfuric acid until the pH reaches 7.2, and the necessary volume of ultrapure water to reach a final volume of 100 mL. Store the solution at 4°C for less than 24 hours or at -20°C.

Sample Stabilization Collect two samples of 0.4 mL for Gram-negative microorganisms and 0.6 mL for Gram-positive from each culture and transfer them to a 1.5 mL tube. For optimal fluorescence, stabilize the Gram-negative microorganisms by adding 0.8 mL of paraformaldehyde solution and phosphate-buffered saline (4% w/v PFA/PBS), while the Gram-positive ones with 0.6 mL of pure ethanol (98%). Store the samples at 4°C for 4-16 hours. Then, centrifuge at 10,000

rpm for 5-10 minutes and remove the supernatant. To resuspend the samples, add 1.2 mL of 1M PBS. Repeat the centrifugation and supernatant removal processes and resuspend in a 1.2 mL mixture of 50%/50% v/v 1M PBS/ethanol. Store the sample at -20°C for up to 3 months.

Slide Mounting Allow the sample to liquify and shake to resuspend. Place 10 µL onto a spot of the microscope slide and spread with the pipette tip across the surface. Once the 12 spots on the slide are filled, place it in an oven at 46°C until the samples dry.

Dehydration The slides are placed vertically in a special container (Coplin jar), in which a quantity of ethanol solution, concentration 50% v/v, has been added, so that the area of the slides with the sample is fully covered, for 3 minutes. Subsequently, the slides are successively transferred to a second and third container with ethanol solutions of concentrations 80% v/v and 98% v/v for 3 minutes each and are left to dry.

Hybridization In a 2 mL tube, the hybridization solution is prepared in the dark by adding 360 µL NaCl (5M), 40 µL Tris-HCl (1 M) and formamide depending on the probe that will be used . Finally, on the tube cap, 2 µL SDS (10% v/v) are added to avoid sedimentation. To each position of the slide, 8 µL of hybridization solution, 1 µL of probe, and 1 µL 4',6-Diamidino-2-phenylindole dihydrochloride (DAPI) are added, or otherwise prepared in a 500 µL tube, the quantity required according to the number of samples and a ratio of 80%:10%:10% hybridization solution/DAPI/probe. Then, the slides are inserted into a wet and dark chamber and left for 2 hours at 46°C.

Rinsing In a 50 mL corning tube, 1000 mL Tris-HCl (1M), NaCl, and EDTA are added according to the concentration of formamide introduced in the hybridization step. Then, add ultrapure water up to 50 mL. Finally, 50 µL SDS (10%) is added.

The slides are washed in a dark, heated bath for 20 minutes at 48°C. They are then rinsed with ultra-pure water and left to dry in a dark place.

Slide Storage: 2-3 drops of anti-fading agent (Citifluor) are added, samples are covered with cover slips in low light, and stored at -20°C in special containers.

Observation-Counting: The slides are observed under a fluorescence microscope with the appropriate filter (Cy3 or TexasRed), which is compatible with the fluorophore of the probe, to

detect the specific target microorganisms (target group) and then with the DAPI filter to find all the microorganisms. About 20 pairs of photos (Cy3-DAPI or TexasRed-DAPI) were taken for each sample and used to measure the percentage of the genus or class we are targeting / total microorganisms (target group/DAPI) using the Image-Pro program.

Measurement Evaluation: For the evaluation of the results with the FISH method and the rejection of erroneous measurements, the following criteria are set:

1) The sum of bacteria and archaea should range between 80-120%. It is also important that bacteria and archaea are measured in samples of Gram-negative microorganisms (samples in a 4% w/v PFA/PBS solution), but some Gram-positive microorganisms (samples in pure ethanol) cannot be observed because the probe will not penetrate their cell wall.

2) The percentage of a subset (e.g., genus) or the sum of the subsets should be equal to or less than its larger category (e.g., class) with an acceptable error (+/-5%).

3) The standard deviation of the two measurements in one replicate cannot exceed 15%. An exception is when the percentage of the target group is less than 10% of the total microorganisms, as the error may be larger. In this case, no criterion was set, since the measurement is considered too low to be taken into account.

4) The standard deviation of two duplicates cannot exceed 20%.

The specific oligonucleotide probes used for this study along with their specific microbe identification and the DNA sequence are summarized in Table 3.6.

Samples were taken at each different HRT studied, with and without Iron addition to determine the changes on the microbial population.

Table 3. 6: Summary of oligonucleotide probes used on this study

A/A	Probe	Target Group	Sequence
1	EUB338	Eubacteria	5'- GCT GCC TCC CGT AGG AGT -3'
2	ARCH915	Archaea	5'- GTG CTC CCC CGC CAA TTC CT -3'
3	MSMX860	*Methanosarcina* & *Methanosaeta* spp.	5'-GGC TCG CTT CAC GGC TTC CCT-3'
4	MG1200	Methanomicrobiales	5'-CGG ATA ATT CGG GGC ATG CTG-3'
5	SRB687	*Desulfovibrio* spp.	5'- TAC GGA TTT CAC TCC T -3'

3.4 Model Setup

3.4.1 Description of the ADM1 model setup for AnMBR

✓ **Experimental data collection**

The lab-scale AnMBR implemented for the application of ADM1 was as delineated at the commencement of this chapter. This AnMBR was meticulously operated for approximately 3.5 years under the conditions previously described. This section reconvenes to succinctly outline the operational scenarios under which the AnMBR was scrutinized over these years. MATLAB Simulink was employed to apply the ADM1 model to the system, aiding in thorough analysis and simulation of the model's application to the real-world system.

The system underwent examination under six distinct scenarios, all of which are encapsulated in Table 3.7.

The model's calibration was performed during the winter period, with the first HRT set at two days, while validation was concurrently conducted across the other five scenarios. This calibration and validation under varying conditions enhanced the robustness of our model, ensuring its reliability and applicability across different operational scenarios.

Table 3. 7: Varied Operational Scenarios for the AnMBR Model

PARAMETERS	HRT 2days	HRT 1 day	HRT 12h
	Winter/summer	Winter/summer	Winter/summer
T (^{o}C)	18/23	19/24	19/24
Q (L/d)	20	40	80
HRT (d)	2	1	0.5
SRT (d)	50	50	50

Our investigation prominently focused on key outlet generic parameters such as Chemical Oxygen Demand (COD_out), gas flow rate (Q_gas), Volatile Suspended Solids (VSS), Total Nitrogen (TN), pH, and methane content (CH_4) were considered. Beyond that, a comprehensive approach was adopted to explore the subdivisions of COD within the system. Several additional parameters—total acetate (Sac), total butyrate (Sbut), total propionate (Spro), Valerate and

butyrate degraders (Xc4), Acetate degraders (Xac), and Hydrogen degraders (XH2)—were incorporated to analyze the subdivided COD with greater precision and detail. This meticulous analysis permitted the relative significance of various components to be discerned, enriching the understanding of the operational intricacies and variable influences within the AnMBR system.

✓ **Interface used**

The ADM1 was diligently implemented using MATLAB Simulink to accurately represent the intricate processes within the AnMBR system. Figure 3.10 illustrates the customized interface of Simulink, meticulously modified to cater to the specific needs and nuances of our research.
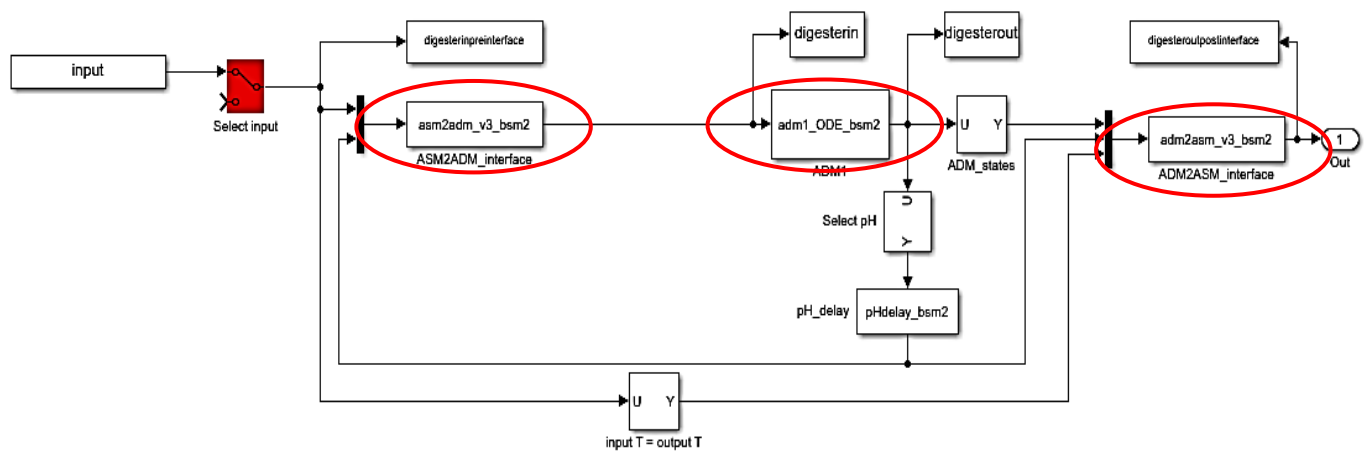
Figure 3. 10 Modelling methodology used for kinetic parameter calibration.

The following points of interaction were accentuated in Figure 3.10, marked in red, indicating the areas where interventions were made to simulate the lab-scale AnMBR accurately:

- Inlet Interface (ASM to ADM)
- ODE Code
- Outlet Interface (ADM to ASM)

✓ **The inlet interface**

It is important to note the inherent unit disparities between ASM1 and ADM1. Due diligence and meticulous attention to detail are crucial to circumvent potential conversion errors during the

integration of model interfaces. Figure 3.11 portrays the variances between the variables of ASM and ADM1.
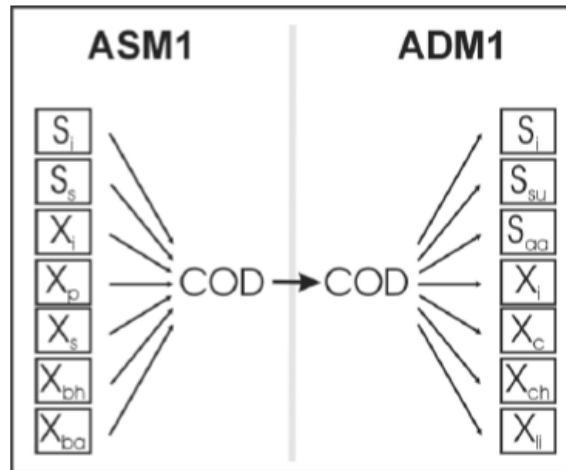
Figure 3. 11: ASM1 to ADM1 state variable conversions for COD[506]

In our specific context, COD was meticulously subdivided into ASM1 variables, following comprehensive experimental analysis to understand the different COD fractions.

✓ **The Outlet interface**

The conversion to ASM1 is somewhat simpler. In this conversion, the goal is to maximize X_s (slowly biodegradable substrate), S_s (readily biodegradable substrate), S_i (soluble inert COD) and X_i (particulate inert COD) with respect to the available COD and, S_{nh} (ammonia), X_{nd} (particulate organic nitrogen) and S_{nd} (soluble organic nitrogen) with respect to nitrogen. Figure 3.12 shows a schematic representation of the COD conversions.
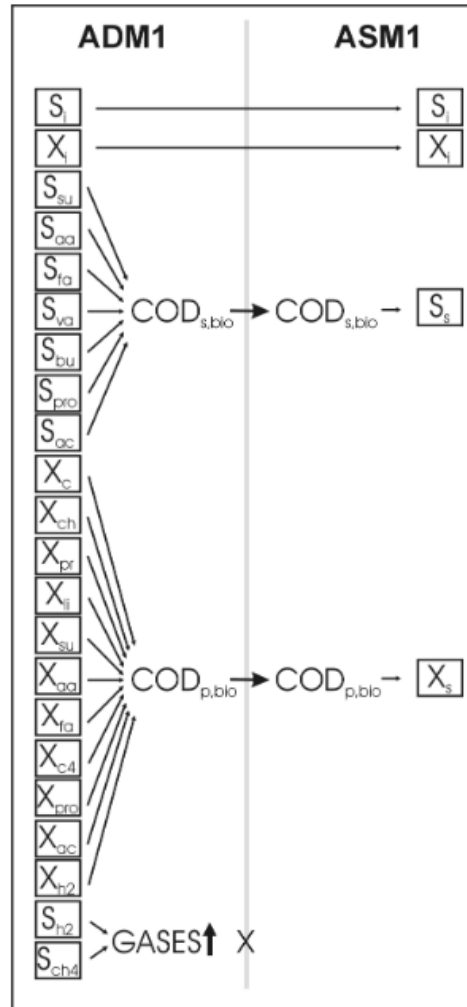
Figure 3. 12: ADM1 to ASM1 state variable conversions for COD[506]

In the effluent of the AnMBR system, only soluble constituents are present, with particulate elements being effectively sequestered by the membrane elements. This is identified as a critical feature of AnMBRs, as only soluble substances are allowed to permeate by the membranes, with particulates being retained. To align the model closely with experimental observations and ensure the accurate simulation of the AnMBR, the particulate variables in the outlet were systematically nullified within the Anaerobic Digestion Model No. 1 (ADM1)/Activated Sludge Model (ASM) interface code.

✓ **ODE CODE**

Modifications were also instituted within the ODE code to accurately depict the sludge removal process, based on the SRT. In this model, a specific amount of sludge must be removed daily, corresponding to 1/50 of the sludge, representing a removal rate of 1/SRT of the sludge. .

Each scenario incorporates a standard value, which is the ratio of HRT to SRT, and is subtracted at every step of the equations. For the first scenario, this value is 0.04. Below is an illustration of one such equation to elucidate the application of this standard value in the modeling process.

Metabolism of particulate fractions (Eq 3.17)

$$dX_c/dt = q_{in}/V_{liq} * (X_{c,in} - 0.04 * X_c) - \rho_1 + \sum_{i=13}^{19} \rho_i \qquad \text{Eq (3.17)}$$

The same intervention was made in the rate equations of all the particulate model components.

✓ **Model calibration/ validation**

The calibration of the model generally focuses on the kinetic parameters. Kinetic parameters are generally calibrated using the method described in Fig. 3.13. A large number of kinetic parameters are involved in the model, but only a limited number are contestable. The parameters are estimated by minimizing the error between the experimental and simulated data. The "trial and error" method is a simple manual calibration that is suitable for situations where a few parameters need to be calibrated or the simulated results are similar to the experimental data.
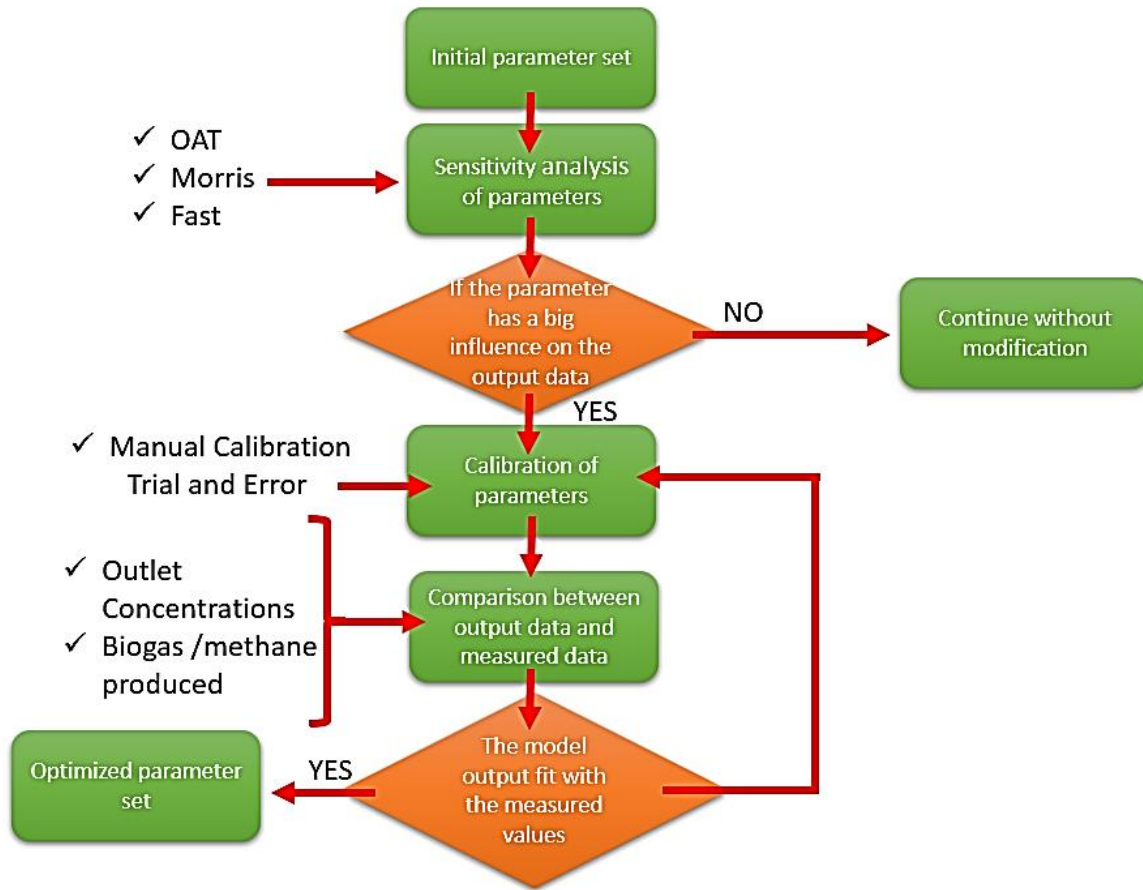
Figure 3. 13 Modelling methodology used for kinetic parameter calibration.

Calibration, as previously described, was carried out in a scenario with an HRT of 2 days during the winter period. In principle the default values suggested in ADM1 were used as reference. All these values refer practically to 35°C and have been appropriate for sludge treatment. The calibration process focused mainly on kinetic parameters which were adjusted for the working temperature of the pilot system by using the following temperature dependence equation:

$$Kx, T = Kx, 35 * e^{0.07 \ (Top-35)}$$ *Eq. (3.18)*

In this equation:

- ✓ $K_{X,35}$ represents the value of Kx at 35°C.
- ✓ 0.07 is the temperature coefficient sourced from the literature.
- ✓ Top is the operating temperature of the AnMBR bioreactor.

✓ **Sensitivity analysis of the system.**

In the pursuit of identifying critical parameters and analyzing their impact on key effluent values, three renowned methodologies were employed:

1) One at a Time (OAT) Analysis: This local sensitivity analysis technique scrutinizes the impact of individual parameters by altering them one at a time and observing the subsequent variations in model output.

2) Fourier Amplitude Sensitivity Test (FAST): FAST dissects the parameter space into various frequency bands, analyzing the amplitude of model responses to pinpoint influential parameters [457]

3) Morris Method: This approach evaluates the influence of parameters through elementary effect-based assessments, exploring the alterations in model output in response to minor modifications in each parameter [481,507].

It's imperative to note that within the applied OAT method, 41 parameters were selected. The GSA was carried out with 25 parameters to economize on simulation time, and the selection was based on their lack of influence on outlet values, as observed in OAT. Table 3.8 illustrates the chosen parameters for sensitivity analysis.

These methodologies of sensitivity analysis were meticulously applied to the revised ADM1 model to assess the sensitivity of parameters and to comprehend their consequential impact on the performance of the model.

Table 3. 8: Parameters applied for Local and Global sensitivity analysis

Parameters chosen for OAT	Parameters chosen for Fast, Morris
pH_UL_aa	Kdec_fa',
pH_UL_ac	Kdec_c4',
pH_LL_h2	'Kdec_pro',
pH_UL_h2	'Kdec_ac',
k_m_c4	Y_fa',
Y_fa	Y_c4'
k_m_ac	Y_pro'
Y_ac	Y_ac'
k_m_pro	Ks_c4',
Y_pro	Ks_pro',
K_S_c4	Ks_ac',
Y_c4	Km_su'
k_dec_Xfa	Km_c4'
K_S_ac	Km_pro'

Parameters chosen for OAT	Parameters chosen for Fast, Morris
K_S_pro	Km_ac',
k_dec_Xc4	Khyd_ch',
k_dec_Xac	Khyd_pr',
k_dec_Xpro	Khyd_li'
k_m_su	Kdec_su',
Y_su	Kdec_aa',
K_S_su	Y_su',
k_m_h2	Y_aa',
Y_h2	Km_aa',
k_m_aa	Km_h2'
k_dec_Xsu	
Y_aa	
pH_LL_ac	
K_S_h2	
K_S_aa	
k_dec_Xaa	
K_S_IN	
k_dec_Xh2	
K_Ih2_fa	
K_Ih2_pro	
K_I_nh3	
K_Ih2_c4	
pH_LL_aa	
k_dis	
k_hyd_pr	
k_hyd_li	
k_hyd_ch	

Chapter 4 Results

4.1 Introduction

Chapter 4 presents the experimental results derived from a comprehensive experimental evaluation of an AnMBR used for treating municipal wastewater at ambient temperatures. The study focuses on a range of operational parameters, aiming to both deepen the academic understanding of AnMBR systems and offer practical guidelines for optimizing their performance. More specifically, the objectives of the lab-scale experiments are as follows:

- ➢ The assessment of the effect of Hydraulic Retention Time (HRT), high organic as well as temperature on the performance of the AnMBR for municipal wastewater treatment.
- ➢ The evaluation of the effect of $FeCl_3$ addition, for controlling membrane fouling and phosphorus removal. The assessment relates to biogas production, COD removal, the elimination of nutrients, and the removal of selected organic micropollutants from the NSAID and EDC groups.

In Section 4.2, the initial start-up phase of the AnMBR is dissected. Special emphasis is placed on achieving steady state conditions. Section 4.3 delves into the overall performance of the AnMBR system, exploring the interplay of HRT and seasonal temperature variations. This section is further divided into sub-sections that offer comparative analyses of AnMBR efficiency at different HRTs during both winter and summer seasons. Section 4.4 focuses on a comprehensive analysis of the COD mass balance and how it relates to the overall system performance. This section aims to offer a holistic understanding of COD's role in AnMBR efficiency. Section 4.5 investigates the impact of adding iron (III) chloride to the AnMBR, assessing its role in affecting reactor performance. Each section commences with a detailed description of the experimental design, followed by the presentation and interpretation of the data within the context of existing research and theoretical frameworks.

The ultimate goal of this chapter is to identify the operational variables that have the most significant influence on the AnMBR system's performance. By achieving this, the chapter aims to contribute valuable insights for future academic research and practical applications in wastewater treatment systems.

4.2 AnMBR start-up

The start-up phase of AnMBR unit took approximately three months to be completed. One key observation during this phase was the significant time required to achieve steady-state conditions. This slower attainment of stable operation poses a disadvantage when compared to aerobic MBR systems, which generally reach steady-state conditions more rapidly.

During the start-up period, the operating temperature within the reactor ranged between 15 to 20°C. The treatment capacity of the unit was configured to handle 20L per day (L·d-1), and the organic loading rate was maintained at 0.25 kg of COD per cubic meter per day (kgCOD/m³/d). HRT was set at 2 days, which is critical for the reactor's performance and the digestion process. Excess sludge was not regularly removed from the reactor; it was only taken out for the purposes of sampling, thereby allowing for a more consistent internal environment.

In terms of operational parameters, the concentration of MLSS within the AnMBR tank stabilized at approximately 4 g·L-1, with a standard deviation of ± 45. The membrane flux, another critical parameter, averaged 1.6 L per square meter per hour (LMH).

All the operameters during the startup period are summarized in Table 4.1.

Table 4. 1: Key Operating Parameters During the Startup Phase of Anaerobic Membrane Bioreactors (AnMBRs)

Parameters	PHASE Start up
Days of operation	93
Operating temperature ($^{\circ}$C)	15-20
Q(L·d^{-1})	20
HRT(d)	2
SRT(d)	50
Flux (L/m^2 h)	1.6±0.2
OLR (KgCOD/m^3/d)	0.25±0.5
Waste Activated Sludge (L·d^{-1})	0.8

Figure 4.1 provides a comprehensive look at the organic carbon removal rates observed during the start-up phase. This includes data on influent COD, effluent COD, and VFAs, offering a temporal perspective on how the system's performance evolved throughout the start-up period.
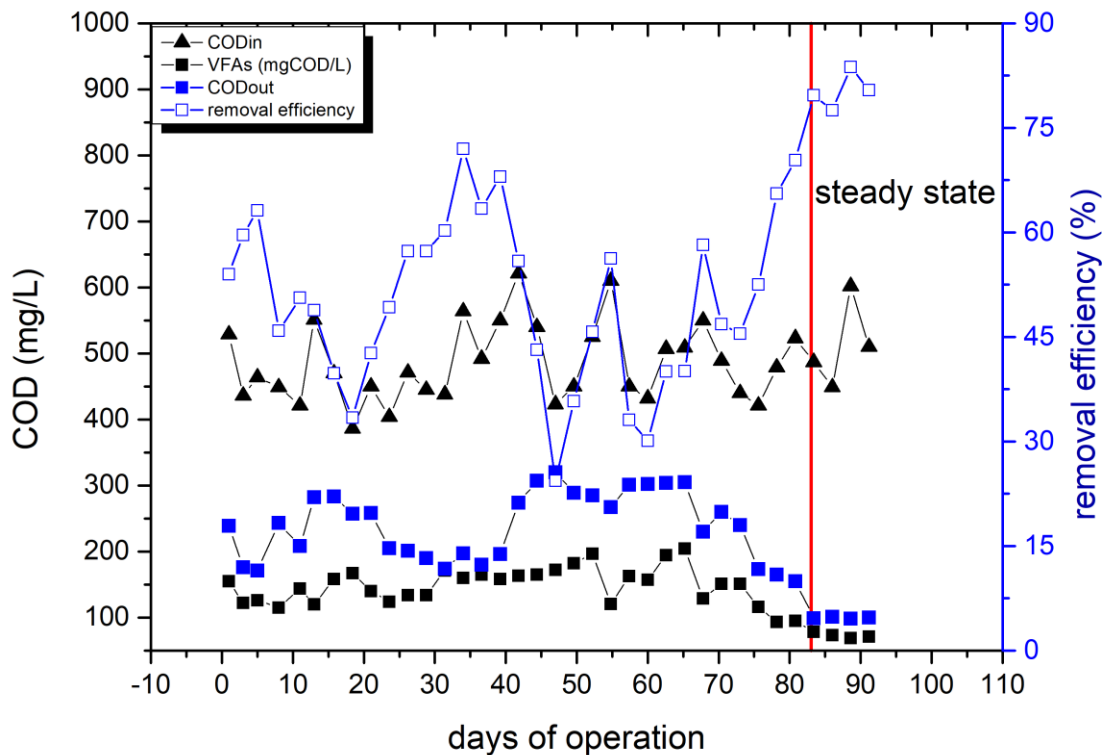
Figure 4. 1: Changes in COD Influent, Permeate Concentrations, Removal Efficiencies, and VFAs During the Start-Up Phase of AnMBR.

During the initial start-up phase, the unit demonstrated suboptimal performance with respect to COD removal. Specifically, the average effluent COD was measured at 241 ± 50 mg/L, translating to a COD removal efficiency of approximately 49%. Notably, the presence of VFAs was observed to accumulate during this period, signaling an imbalance between acetogenic and methanogenic microbial activities within the system. After the initial 80-day period, the system began to stabilize, reaching a consistent outlet value, which is indicated on the graph.

The observed VFA accumulation led to an unfavorable decrease in system pH, which was recorded at 6.9±0.3. This pH value is significantly lower than the pH range observed during subsequent operating phases, where methanogenic activity was more stabilized, thus indicating a more balanced microbial ecosystem.

Figure 4.2 provides a comprehensive analysis of the alkalinity variations during this start-up phase, including measurements for total, partial, and intermediate alkalinity. The data suggests

that the unit had not yet reached a steady-state equilibrium between acidogenic and methanogenic processes, resulting in suboptimal treatment efficiency.
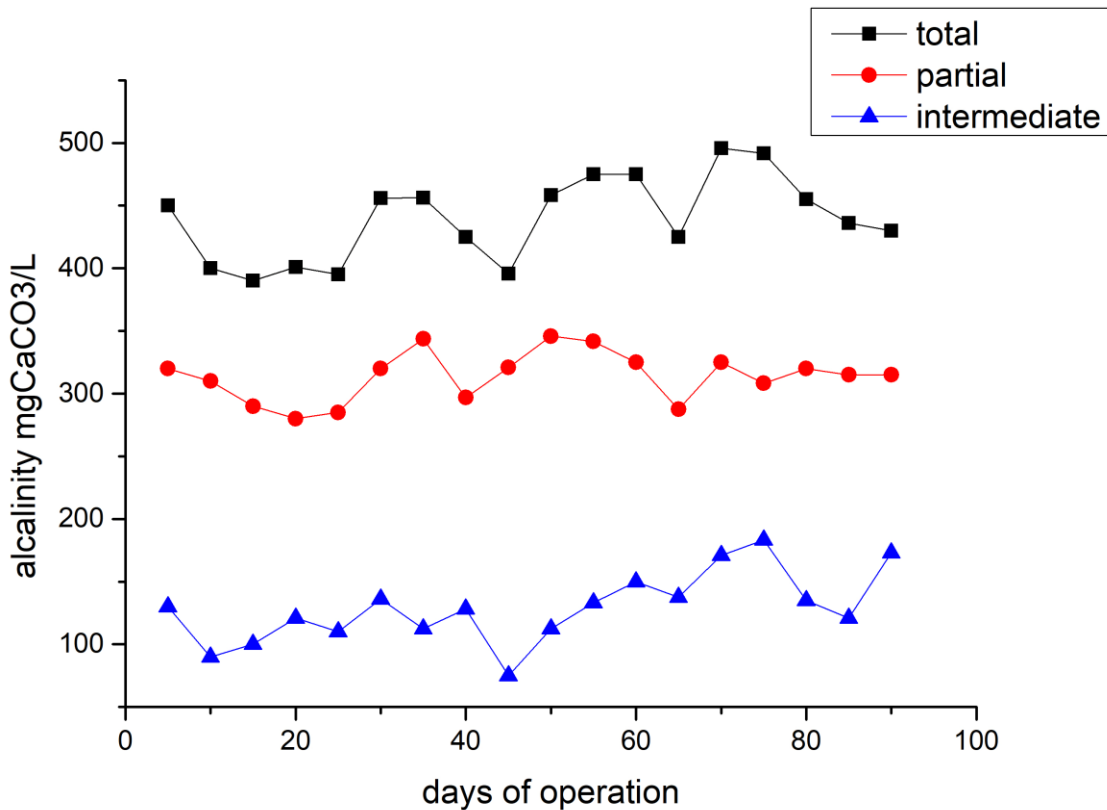
Figure 4. 2: Total, partial and Intermediate Alkalinity Levels During the Start-Up Phase

The determination of alkalinity in two stages enables the calculation of the ratio between intermediate alkalinity (IA) and partial alkalinity (PA). In the present study, the average IA/PA ratio was found to be relatively high, measuring 0.43 ± 0.1. According to research conducted by Ripley et al. (1986), such a value suggests an unstable methanogenesis process. In their study, Ripley and colleagues demonstrated that typical values for stable conditions are below 0.3. Conversely, IA/PA ratios exceeding 0.8 are indicative of process upsets, the accumulation of VFAs, and significant reductions in methanogenesis.

4.3 AnMBR overall performance

4.3.1 Exploring the Synergistic Effects of HRT and Ambient Temperature on Anaerobic Membrane Bioreactor Efficiency

This subchapter delves into a comprehensive, six-month-long systematic investigation of each HRT setting in the AnMBR. During this time, SRT was consistently maintained at 50 days across all AnMBR operations.

Four distinct HRTs—48 hours, 24 hours, 12 hours, and 6 hours—were systematically studied. Each HRT underwent an exhaustive six-month evaluation period, further divided into two separate three-month phases to mimic seasonal variations corresponding to summer and winter conditions. The rationale for this three-month subdivision lies in the SRT of 50 days; nearly two SRT cycles are completed in this span, thereby enhancing the reliability of the results.

Four discrete HRTs were methodically investigated, specifically 48 hours, 24 hours, 12 hours, and 6 hours It should be noted that after each HRT adjustment, the system required approximately one week to return to a steady state. The data pertaining to this stabilization period are not included in the present analysis.

The primary objectives of this in-depth study are to assess the feasibility of operating the AnMBR under ambient conditions at various HRTs; More specifically, to examine effluent water quality and membrane fouling rates, aiming to minimize the need for frequent cleaning and thus ensure a smooth system operation.

Through this rigorous methodology, valuable insights into the adaptability and efficiency of the AnMBR system under various operational conditions are intended to be provided. For each HRT setting, a table detailing the operational conditions is presented. Accompanying these tables, series of graphs are included to elucidate key parameters such as organic load removal, VFAs and alkalinity levels, biogas production rates, biomass concentrations, and occurrences of membrane fouling.

4.3.1.1 AnMBR, operating at a 2 days HRT and ambient temperatures: A Winter-Summer Comparative Study

Following the initial startup, the system achieved stability. The first HRT assessed was 2 days, with an SRT set at 50 days. Results below depict two different temperature variations during summer and winter period.

Table 4.2 showcases the aggregated operational characteristics for the specified period.

Table 4. 2:Aggerated operational characteristics for 2 days HRT

Parameters	HRT 2 days Winter period / Summer period
Days of operation	1-90/91-180
Operating temperature ($^{\circ}$C)	18±4/23 ±1
Q(L·d^{-1})	20
HRT(d)	2
SRT(d)	50
Flux (L/m^2 h)	1.6±0.2
OLR (KgCOD/m^3/d)	0.24 ±0.3/ 0.23 ± 0.02

- Organic Load

Figure 4.3 illustrates total COD of the inlet, the permeate and the removal efficiency. Average COD values of the permeate were doubled during the winter period, showing that temperature greatly influences AnMBR performance.
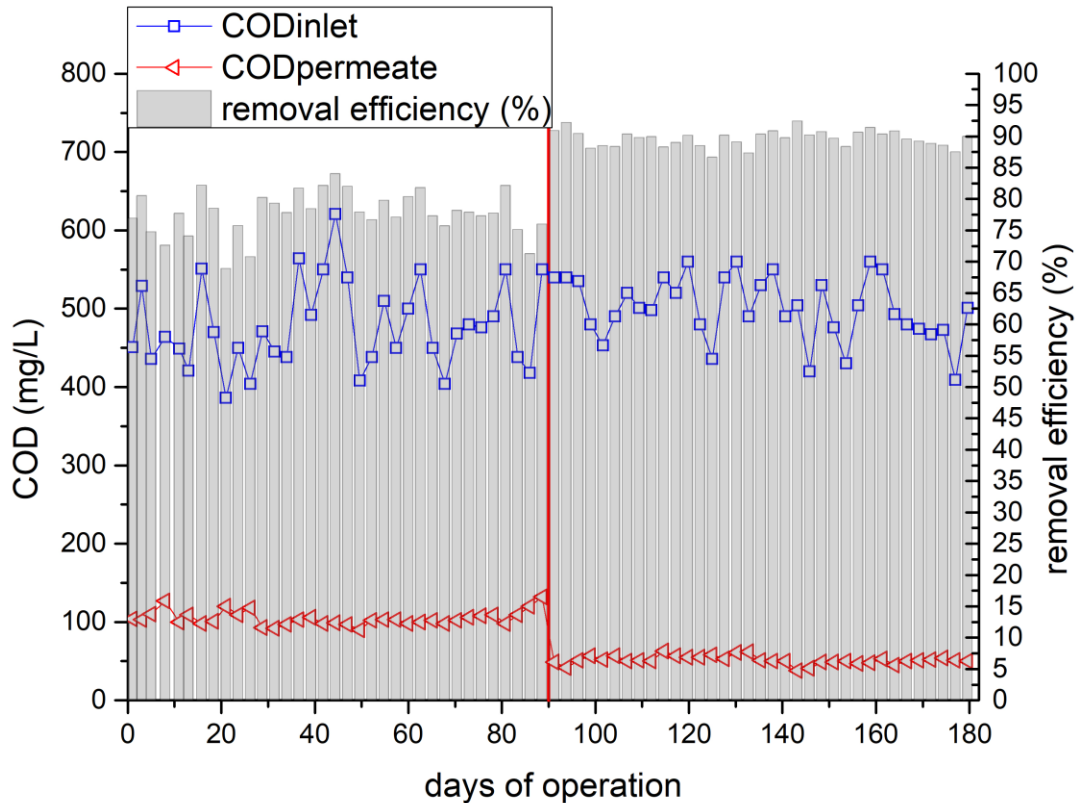
Figure 4. 3: AnMBR performance in terms of COD removal at 2 days HRT

As illustrated in Figure 4.3, average COD values for the permeate display significant seasonal variations. Specifically, during the winter period (days 90-180), the average COD values are 105 ± 9 mg/L, which is approximately twice as high as the values recorded during the summer period, at 51 ± 5 mg/L. This marked discrepancy underscores the substantial influence of temperature on AnMBR performance.

- VFAs / Alkalinity

Alkalinity and VFAs are important parameters for maintaining the buffering capacity of anaerobic systems. Figure 4.4 elucidates key performance indicators, including TA and VFAs, expressed in mg $CaCO_3$/L and mg COD/L, respectively. The figure also presents two critical ratios: VFAs/TA and IA/PA.
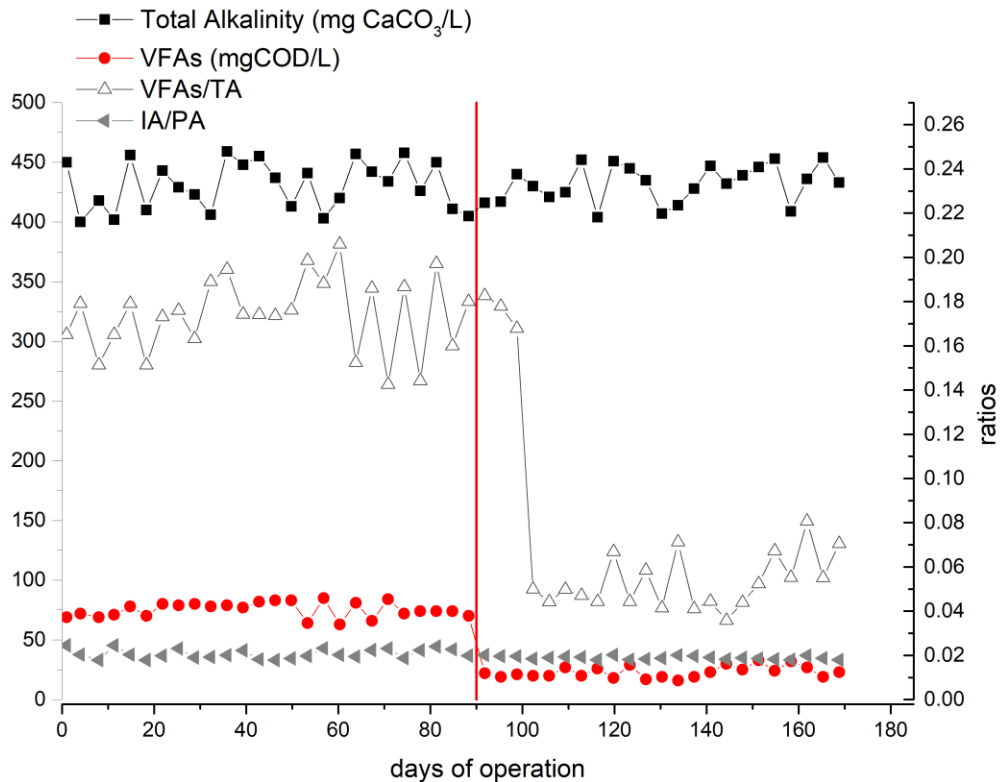
Figure 4. 4 Volatile Fatty Acids and the Three Phases of Alkalinity in a 2-Day HRT AnMBR

Figure 4.4 delineates variations in crucial parameters over two distinct temperature regimes: a winter phase from days 01 to 90, and a summer phase from days 91 to 180. The alkalinity determination in two stages leads to the ratio IA/PA. Castro et al. assert that a VFAs/TA ratio below 0.6 signifies adequate process stability, while Ripley et al. (1986) argue that an IA/PA ratio under 0.3 also indicates a stable process. In the scope of our study, TA remained consistent over the entire six-month observation period, conforming to these established stability benchmarks. In terms of ratios, although the VFAs/TA ratio consistently stayed below the 0.6 threshold, it exhibited higher values during the winter period. A similar trend was observed for the IA/PA ratio; while it remained below 0.3, it too was elevated during the winter period. AnMBR with 2-day HRT, VFAs exhibit no discernible accumulation, and interestingly, their concentrations are observed to be lower during the summer period. Elevated production of VFAs can have a dual impact on the microbial community involved in anaerobic digestion. On one hand, it serves as a stimulatory factor for acetogenic bacteria, accelerating their metabolic activities. On the other hand, it exerts an inhibitory effect on methanogenic microorganisms. This inhibition occurs because

methanogens are unable to metabolize the VFAs at the rate at which they are generated through acetogenesis. Such a kinetic disparity between acetogenic and methanogenic processes could potentially disrupt the overall stability of the anaerobic digestion system.

- pH

Figure 4.5 displays the pH values recorded during two distinct temperature periods: the winter season from days 90 to 180, and the summer season from days 180 to 270.
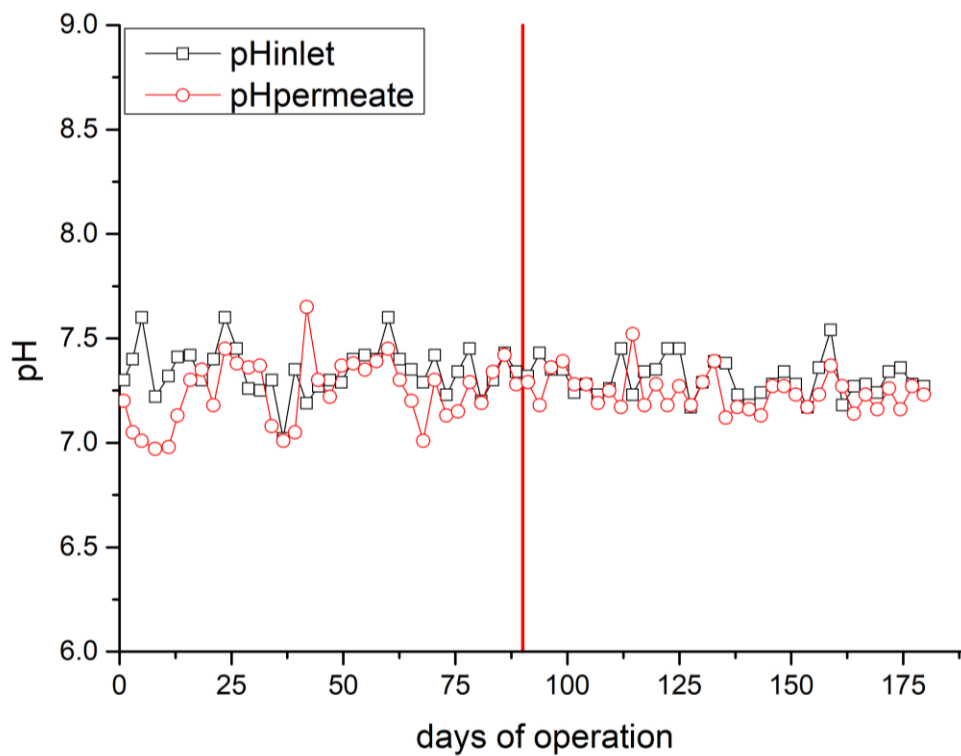
Figure 4. 5: Seasonal Variations in Inlet and Permeate pH Values at a 2-Day HRT

As illustrated in the graph, pH levels remained stable, which is conducive for the growth of methanogenic microorganisms. The average pH value for the inlet was 7.35 ± 0.12, while the permeate had an average pH of 7.28 ± 0.16. Notably, these values exhibited minimal fluctuations during both the winter and summer periods.

- Biomass concentrations

Figure 4.6 presents the concentrations of MLSS and MLVSS within the AnMBR reactor.
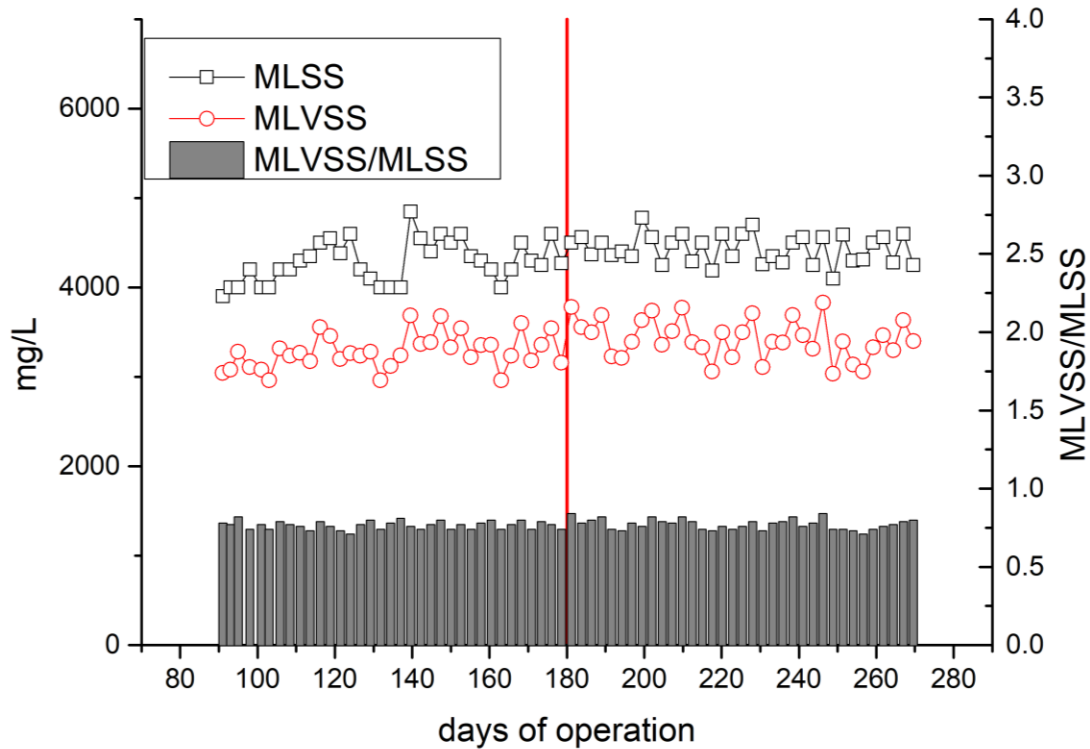
Figure 4. 6: MLSS and MLVSS concentrations inside the AnMBR reactor

No significant changes in MLSS and MLVSS concentrations were observed in response to temperature variations, suggesting thermal resilience of the microbial community within the AnMBR reactor. The average concentration of MLSS remained stable at 4359 ± 215 mg/L, while the MLVSS/MLSS ratio also displayed minimal variation with an average value of 0.77 ± 0.1. These findings may indicate robust process stability and effective biological treatment, irrespective of seasonal temperature changes.

- Biogas Production

An AnMBR offers the potential for biogas recovery. Theoretically, with 1 g of COD removal at 0°C and a pressure of 1 atm, approximately 0.350 L of methane can be produced. The biogas generated in an AnMBR contains various other components, mainly CO_2 and H_2S.

Figure 4.7 showcases the daily production of biogas during the winter period (0-90 days) and the summer period (91-180 days). Additionally, the theoretical biogas production (L/d) is also presented. It should be noted that the theoretical production range of biogas is between 0.50-0.70 L/g COD removed. The graph also includes the ratios of L biogas/day and L biogas/g COD inlet for further clarity.
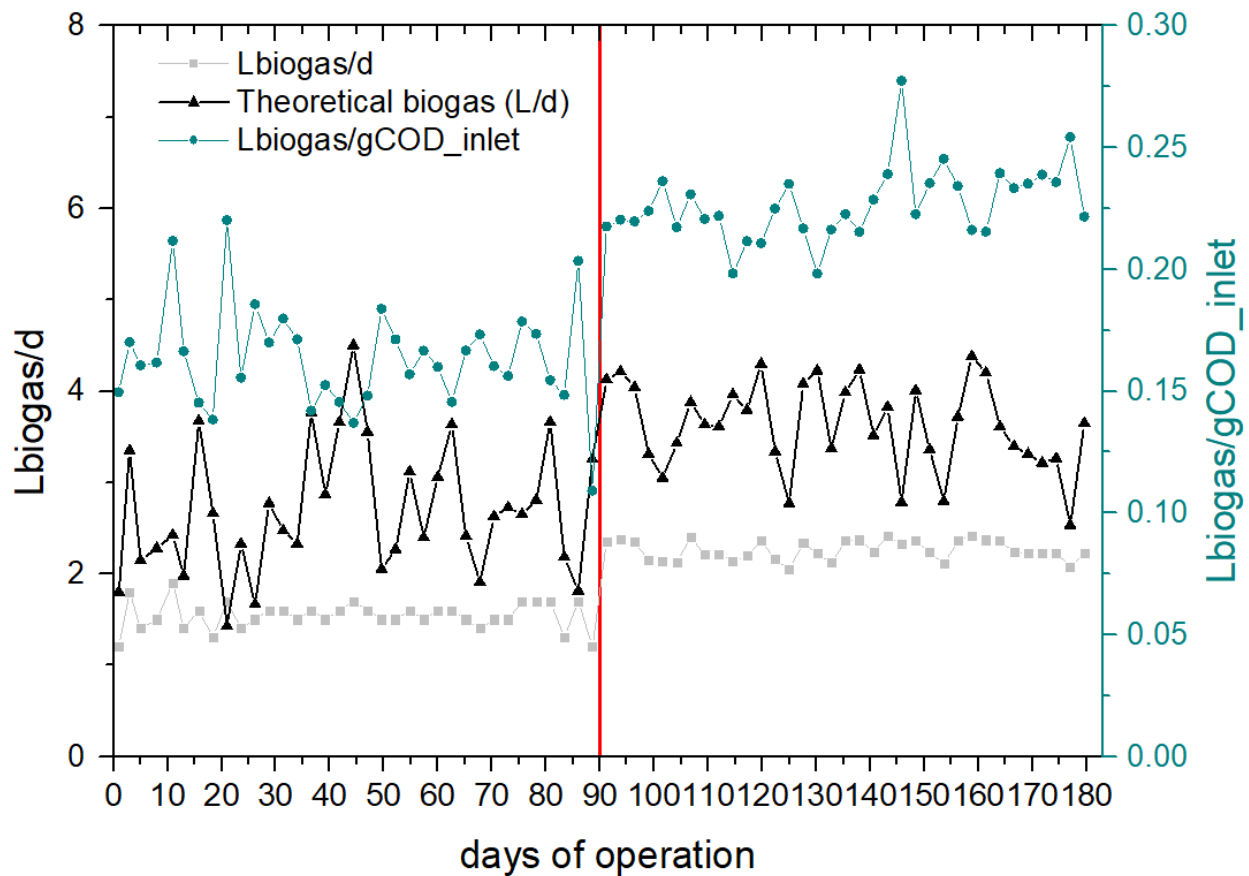
Figure 4. 7: AnMBR performance in terms of biogas production for 2 days HRT

As discerned from the graphical data, the biogas production exhibited distinct seasonal variations. Specifically, the empirical average daily biogas yield was calculated to be 1.45±0.15 L during the winter season and 2.06±0.1 L throughout the summer season. Furthermore, the rate of biogas production per g of COD inlet exhibited similar seasonal disparities. The empirical values were 0.16±0.1 L/g CODinlet for the summer season and 0.22±0.08 L/g CODinlet for the winter season. It is noteworthy that the performance related to biogas production was evidently better during the

summer season. Additionally, the system demonstrated greater stability in the summer, as evidenced by fewer fluctuations in biogas production. This seasonal variation in biogas yield and efficiency warrants further investigation to optimize system performance across different climatic conditions.

Figure 4.8 corroborates the findings illustrated in the preceding figure. In this instance, the data are normalized by the amount of COD removed from the process, thereby providing two key ratios: L CH$_4$/g COD removed and L biogas/g COD removed.
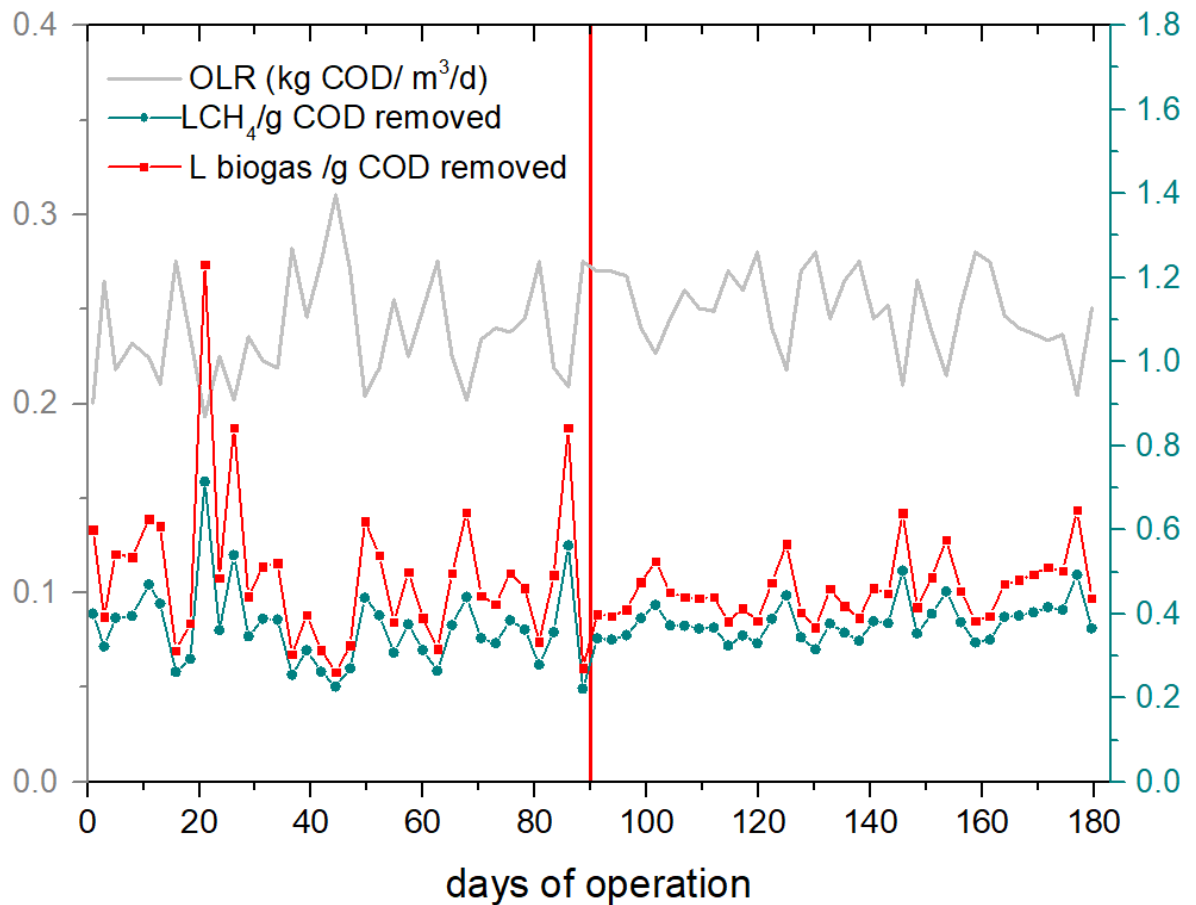
Figure 4. 8: Organic Load, methane and biogas ratios of the AnMBR operating in 2 days HRT

The observed average values for these metrics stood at 0.35±0.10 and 0.38±0.040 for L biogas/g COD removed and 0.27±0.07 and 0.29±0.06 for L CH$_4$/g COD removed during the winter and summer periods, respectively.

▪ Biogas composition

Figure 4.9 depicts the variations in biogas production, methane generation rates, and methane composition throughout both the summer and winter seasons.
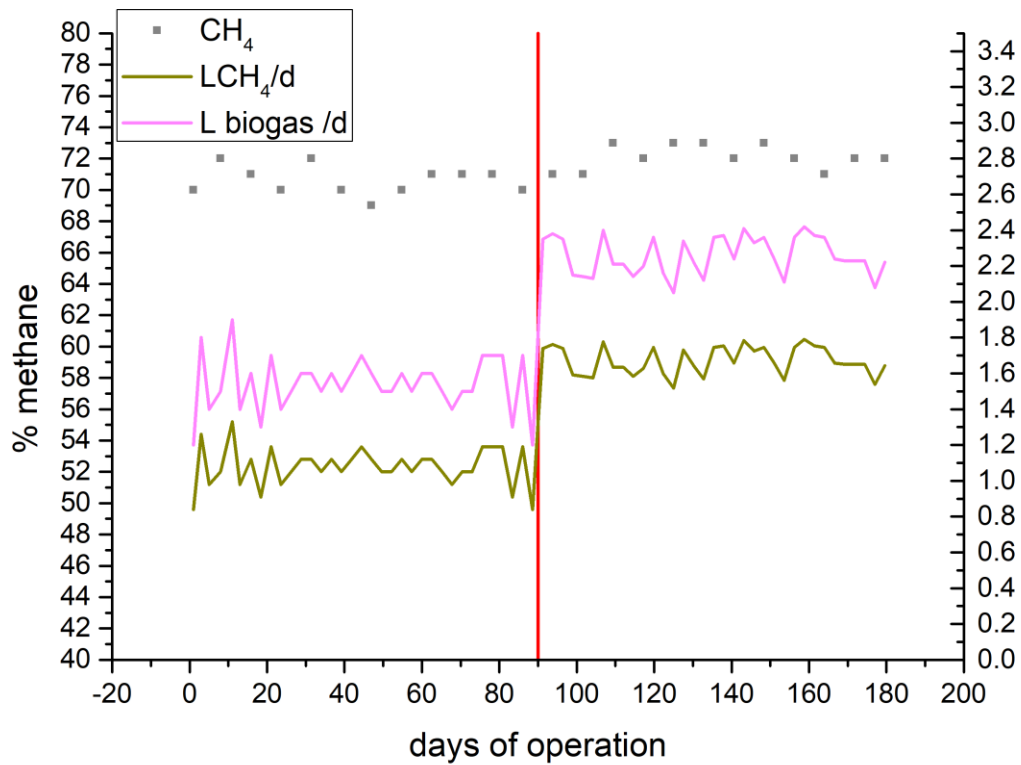
Figure 4. 9: Biogas, methane production and biogas composition for 2days HRT

Experimental results revealed that the biogas composition consisted of 70.6 ± 0.9 % methane during the winter period and 72 ± 0.8% methane during the summer period. This indicates a marginal improvement in methane concentration in the summer. Both percentages are within satisfactory ranges.

Additionally, Figure 4.10 illustrates how methane composition correlates with the operational temperature of the AnMBR reactor.
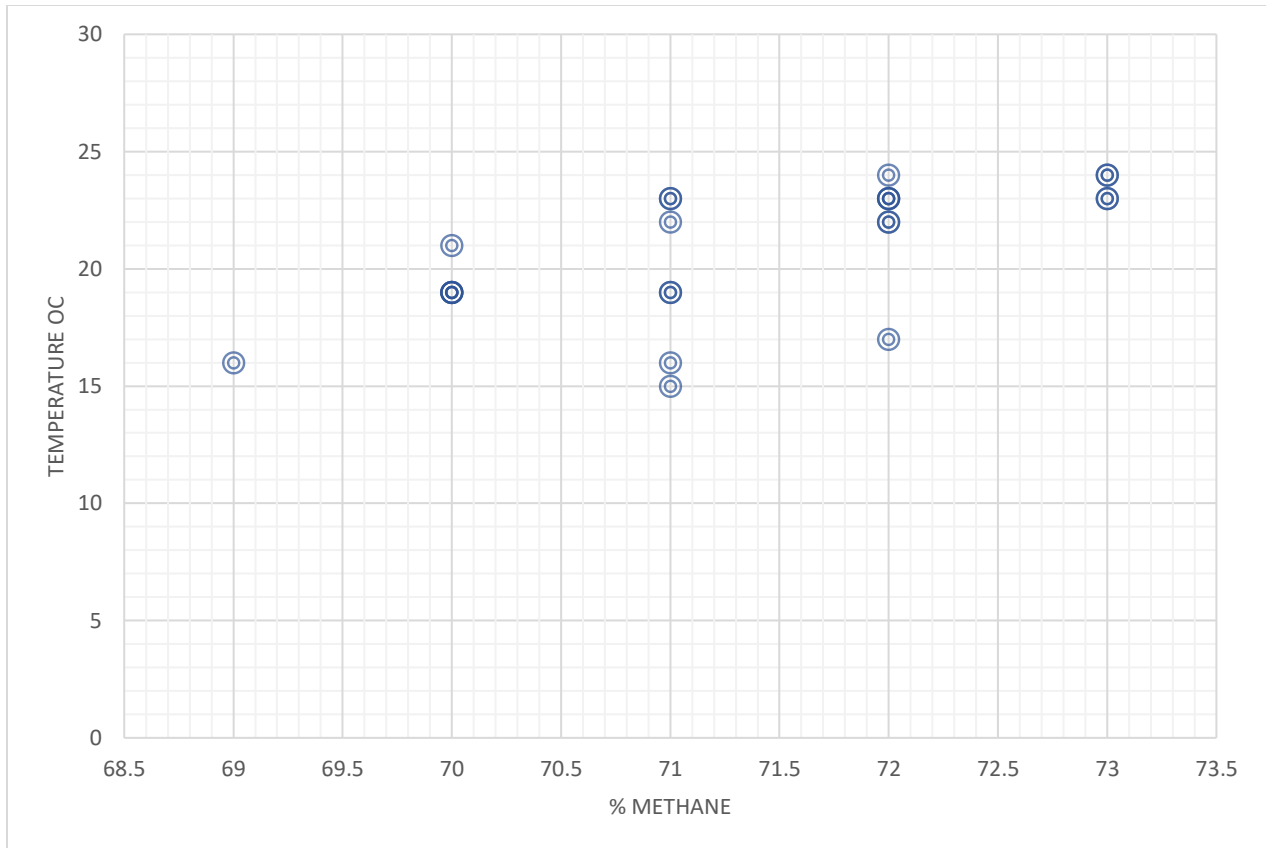
Figure 4. 10:Relation between methane percentage and temperature for both periods in 2 days HRT

From the graph, it can be concluded that when the temperature exceeds 20°C, the methane composition consistently remains above 70%.

- Membrane fouling

Figure 4.11 showcases the performance of the AnMBR with a focus on membrane fouling and the rate of increase in TMP.
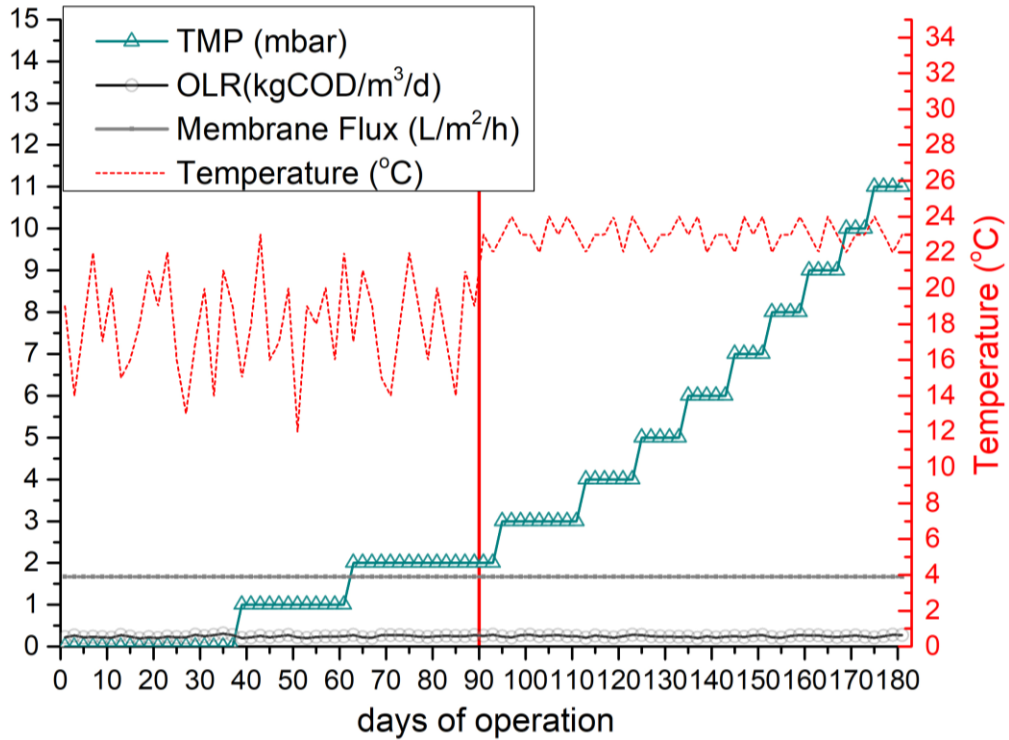
Figure 4. 11:AnMBR performance in 2 days HRT in terms of membrane fouling

Figure 4.11 illustrates various parameters, TMP, OLR membrane flux, and the temperature within the AnMBR throughout the operational period. The results indicate that the TMP experienced a minimal increase, rising from 0 mbar to 11 mbar over 180 days. This corresponds to an extremely low rate of approximately 0.0389 mbar/day. Due to these negligible TMP values, it was not feasible to assess potential seasonal variations between the summer and winter periods. The limited TMP increase suggests that there was no need for chemical cleaning of the membrane.

4.3.1.2 AnMBR, operating at 1 day HRT and ambient temperatures: A Winter-Summer Comparative Study

For the second HRT assessed, 1 day was employed, with the SRT remaining fixed at 50 days. As with the previous assessment, data were collected during both the summer and winter periods to evaluate seasonal variations. Table 4.3 illustrates the operational characteristics of the AnMBR when functioning at a 1-day HRT.

Table 4. 3: Operational characteristics of the AnMBR working at 1 day HRT

Parameters	HRT 1 day Winter period / Summer period
Days of operation	0-90/90-180
Operating temperature (ºC)	19±2/24±2
Q(L·d⁻¹)	40±7
HRT(d)	1
SRT(d)	50
Flux (L/m² h)	3.3±0.4
OLR (KgCOD/m³/d)	0.45± 0.04/0.49 ± 0.05

▪ Organic Load

Figure 4.12 delineates the total COD for the inlet, the permeate, and the removal efficiency.
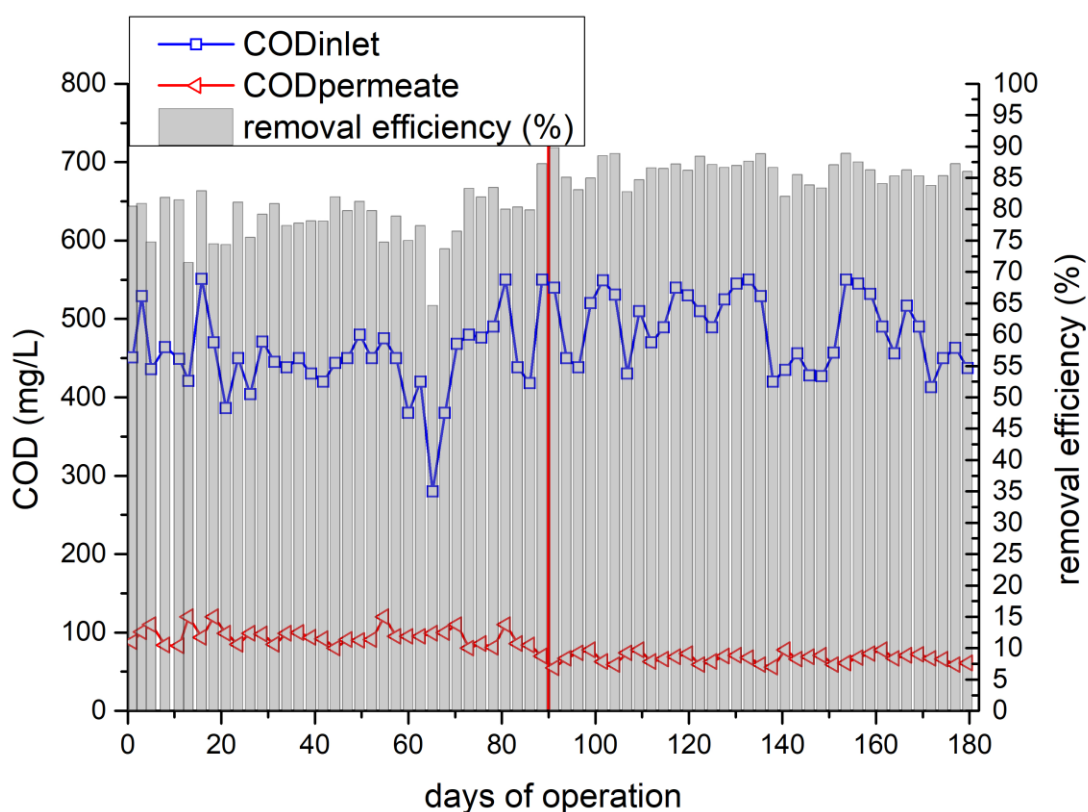
Figure 4. 12:AnMBR performance in terms of COD removal at 1 day HRT

More specifically, elucidates the seasonal disparities in the efficacy of organic matter removal within the AnMBR reactor during summer and winter timeframes. Notably, these seasonal

variances are less marked when compared to the fluctuations observed under a 2-day HRT regime. Quantitatively, the summer period exhibited a permeate concentration averaging 66 ± 5 mg/L, while the winter period yielded a higher average concentration of 95 ± 12 mg/L.

- VFAs /alkalinity

Figure 4.13 provides a comprehensive visualization of key performance indicators, including the concentration of VFAs in the permeate water, the overall alkalinity levels, and two critical ratios that serve as benchmarks for assessing the system's operational stability.
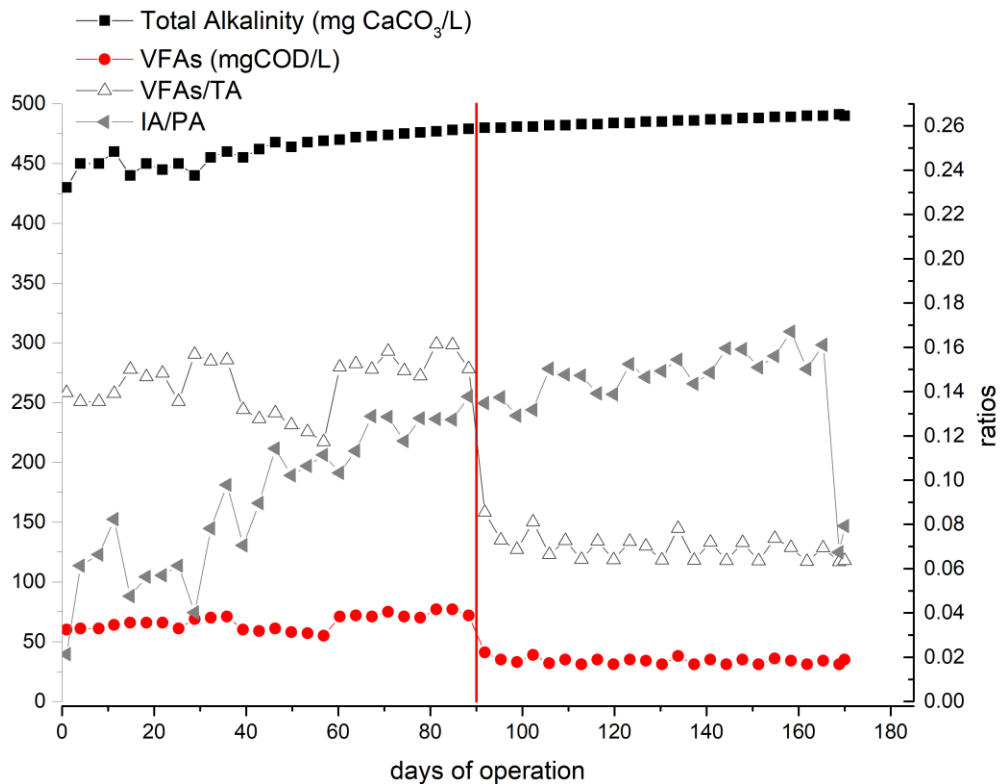
Figure 4. 13: VFAs and the Three Phases of Alkalinity in a 1-Day HRT AnMBR

Figure 4.13 illustrates that total alkalinity exhibits an increasing trend over the observed period for both winter and summer seasons. This suggests that despite initial minor fluctuations, total alkalinity tends to stabilize and demonstrate increased resilience, even during winter. In line with observations from a 2-day HRT. VFAs do not appear to accumulate and generally maintain low concentrations. The two examined ratios fall below the threshold indicative of system instability. However, the IA/PA ratio exhibits a distinct pattern compared to that obtained in a 2-day HRT; it

demonstrates an increasing trend throughout the operation. Notwithstanding, the consistently low values suggest that this is not a cause for concern.

- pH

Figure 4.14 displays the pH values recorded during two distinct temperature periods: the winter season from days 0 to 90, and the summer season from days 0 to 180.
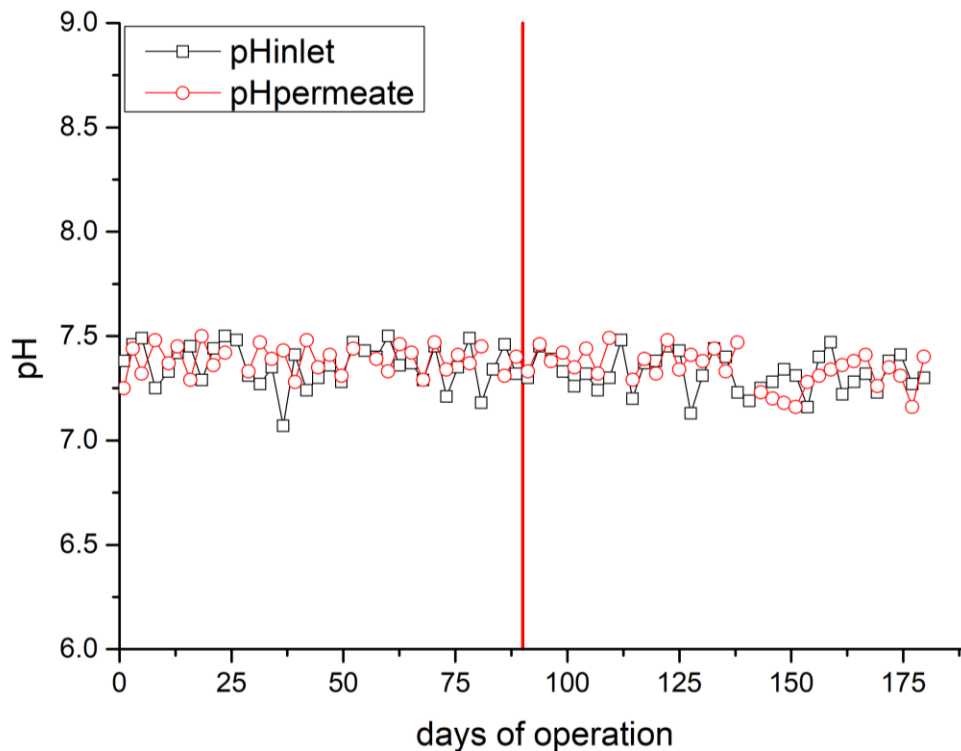
Figure 4. 14: pH variation for the inlet and the permeate for 1-day HRT

The graph compellingly illustrates a remarkable level of stability in pH values, an essential condition that fosters the growth of methanogenic microorganisms. For the inlet, the average pH was measured at 7.35, with a relatively low standard deviation of ± 0.09. The permeate followed suit, displaying an average pH of approximately 7.36 across both the winter and summer periods, and also accompanied by a standard deviation of ± 0.09. This consistent pH data further underscores the system's overall stability in this regard.

- Biomass concentrations

Figure 4.15 illustrates the concentration of MLSS within the AnMBR reactor. Notably, no significant fluctuations are observed between winter and summer periods, nor are there notable changes in relation to HRT.
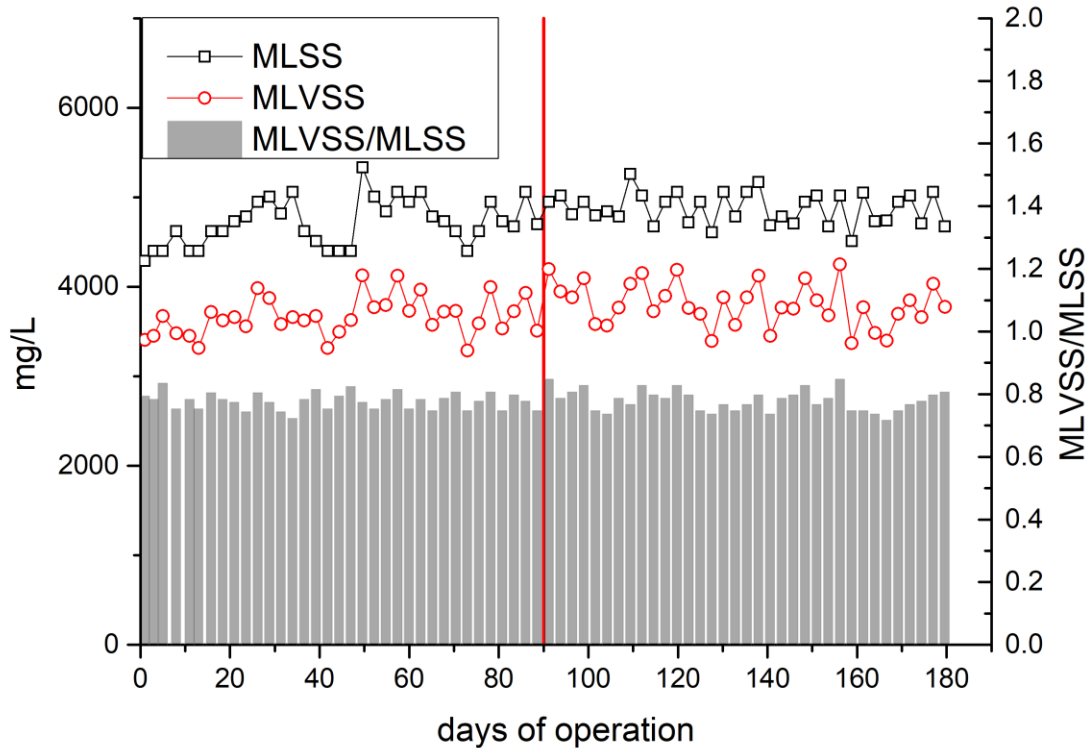
Figure 4. 15: MLSS and MLVSS concentration inside AnMBR reactor for 1day HRT

When compared to the HRT of 2 days, the graph shows only a modest increase in MLSS and MLVSS, amounting to approximately a 10% rise.

- Biogas production

Figure 4.16 displays the daily biogas output during both the winter (days 0-90) and summer (days 91-180) phases. The graph also includes projected values for theoretical biogas production, measured in L per day (L/d). Additionally, the graph elucidates the ratios of biogas produced per

day (L biogas/day) as well as per g of COD inlet (L biogas/g COD inlet) for enhanced understanding.
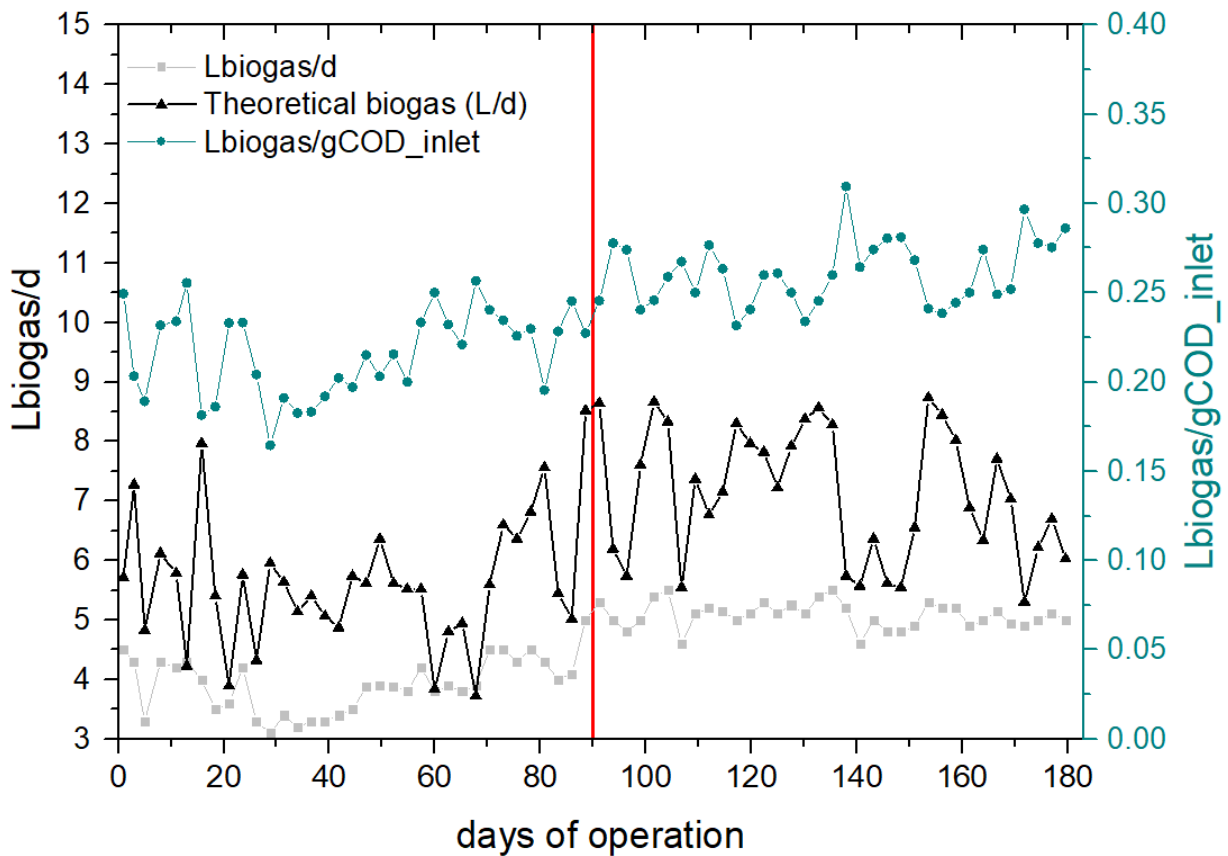
Figure 4. 16: AnMBR performance in terms of biogas production for 1 day HRT

As indicated by the graph, the system's biogas production displays some seasonal patterns. Specifically, the observed average daily biogas output was 3.79 ±0.5 L during winter and increased to 4.94 ±0.22 L in the summer. These observed values are lower than the theoretical estimations, which projected higher yields of 6.24 ± 1.1 L and 7.82 ± 1.1 L for the winter and summer periods, respectively.

Additionally, the rate of biogas production per g of COD in the influent did exhibit seasonal variations, albeit with modest differences. Specifically, the rate was recorded as 0.21±0.2 L biogas/g COD inlet during the summer months, increasing slightly to 0.26±0.03 L biogas/g COD inlet in the winter period. Notably, the efficiency of biogas production showed marginal improvement during the warmer months. However, unlike observations made during the 2-day

HRT, the data here did not suggest significant differences in system stability. That is, the rate of fluctuations remained relatively consistent across both summer and winter periods.

Figure 4.17 lends further support to the observations made in the previous figure. In this case, the data are adjusted for the quantity of COD removed from the process, resulting in two critical ratios: L CH_4/g COD removed and L biogas/g COD removed.
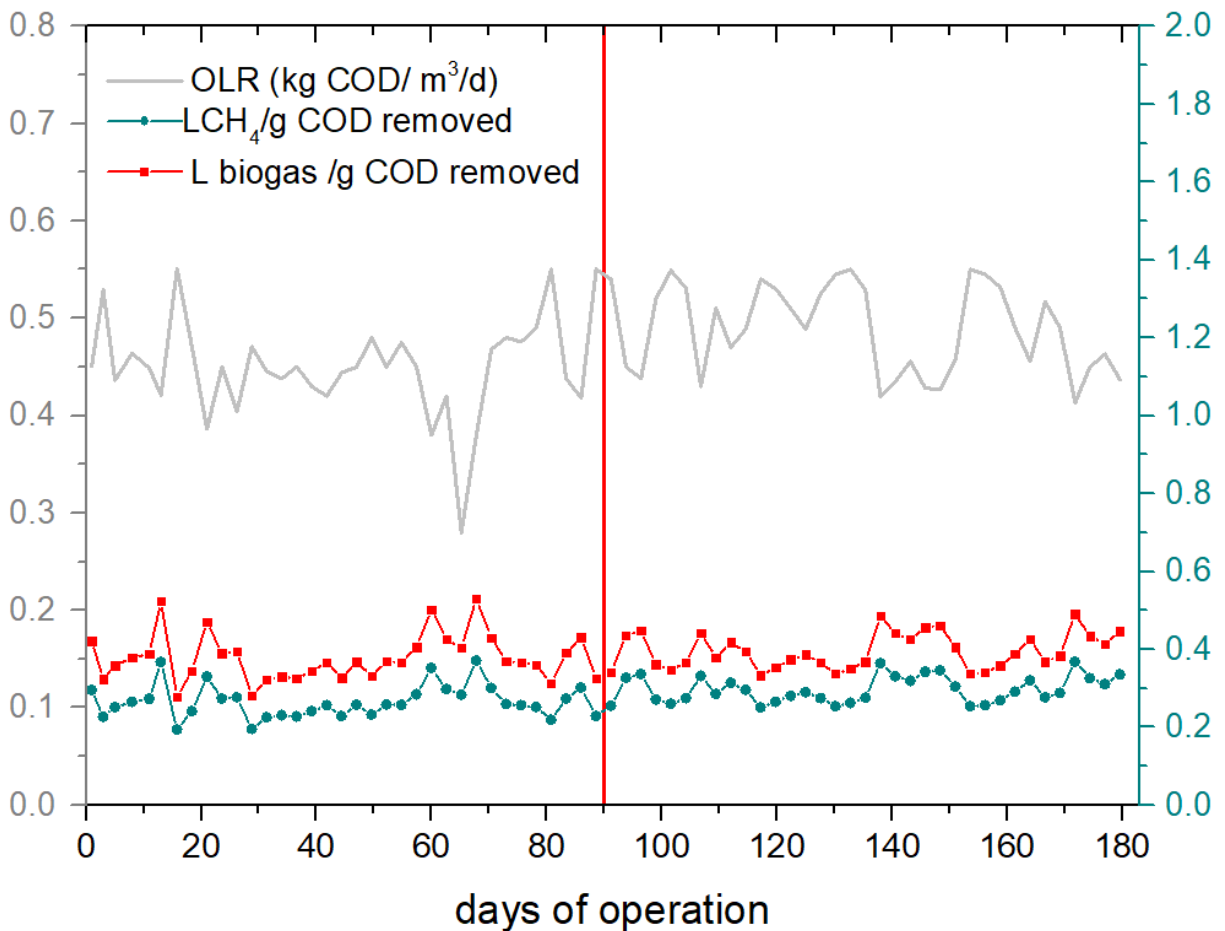
Figure 4. 17: Organic Load, methane and biogas ratios of the AnMBR operating in 1-day HRT

The collected average values for these parameters were 0.37±0.08 and 0.40±0.07 L biogas/g COD removed for winter and summer, respectively. Additionally, the observed values for L CH_4/g COD removed were 0.27±0.06 in winter and 0.30±0.05 in summer, values that are close to the theoretical value of 0.350 L of methane /g COD removed.

- Biogas composition

Figure 4.18 depicts the variations in biogas production, methane generation rates, and methane composition throughout both the summer and winter seasons.
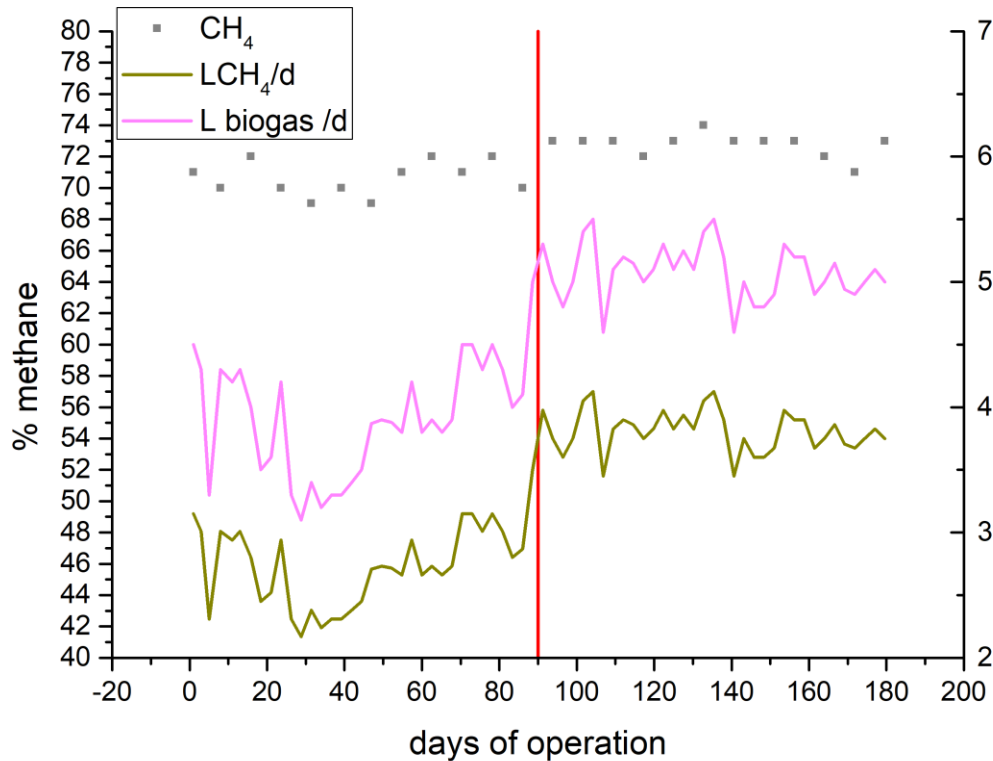
Figure 4. 18: Biogas, methane production and biogas composition for 1 day HRT

Experimental results demonstrate seasonal variations in the composition of biogas. In the winter months, the methane content was measured to be 70.5 ± 1% of the total biogas composition. This percentage showed a modest increase to 72.8 ± 0.8% during the summer months, pointing to a minor seasonal enhancement in methane concentration. When comparing these values at varying HRT, it was found that a 1-day HRT yielded nearly the same methane percentages as a 2-day HRT during the winter. However, during the summer, the 1-day HRT showed a slightly higher percentage of methane compared to the 2-day HRT

Additionally, Figure 4.19 illustrates how methane composition correlates with the operational temperature of the AnMBR reactor.
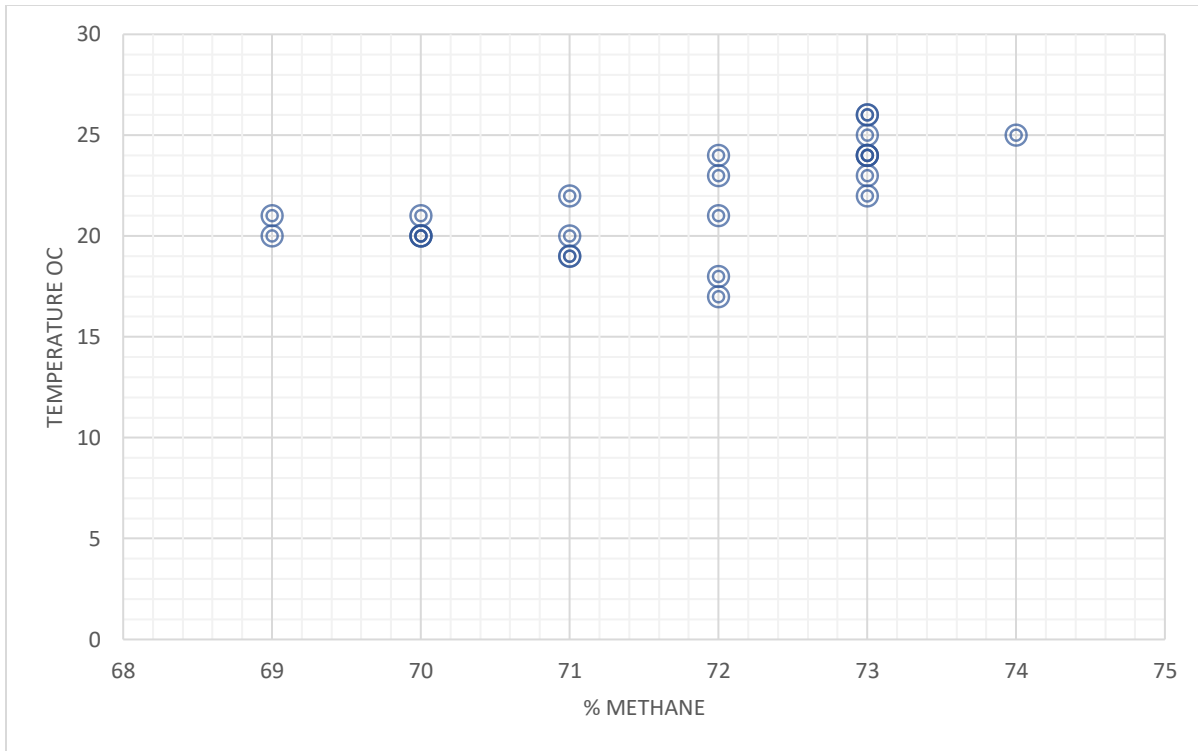
Figure 4. 19: Relation between methane percentage and temperature for both periods in 1 day HRT

- Membrane fouling

Figure 4.20 illustrates the performance of the AnMBR with a focus on membrane fouling and TMP increase.
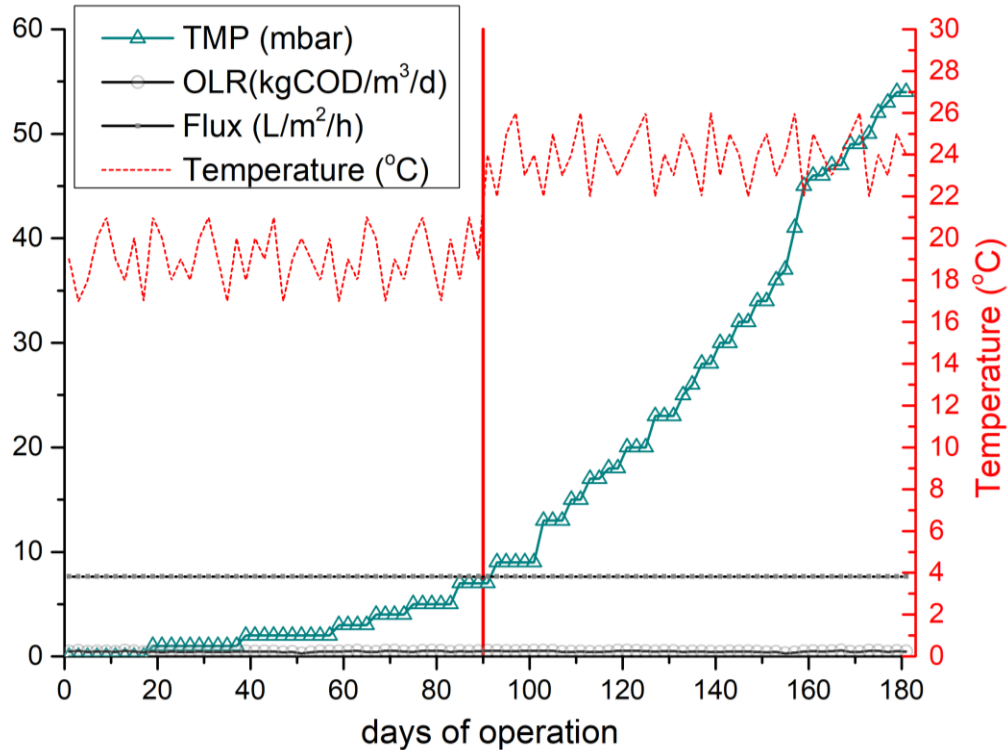
Figure 4. 20: AnMBR performance in 1 day HRT in terms of membrane fouling

From the graph 4.20, it is observed that the TMP showed a relatively stable trend for the initial part of the operational period before experiencing a noticeable increase. This increase in TMP can be marked from around day 100, where it climbs sharply from close to 0 mbar to slightly over 50 mbar by day 180. Despite this rise, the TMP still did not reach the threshold value of 300 mbar. Therefore, chemical cleaning was deemed unnecessary, and an analysis of temperature variations was not delved into.

4.3.1.3 AnMBR, operating at 12 h HRT and ambient temperatures: A Winter-Summer Comparative Study

The third HRT evaluated was 12 hours, operating under an SRT of 50 days. As with the previous assessment, data were collected during both the summer and winter periods to evaluate seasonal variations.

Table 4.4 illustrates the operational characteristics of the AnMBR when functioning at a 12 h HRT.

Table 4. 4: Operational parameters for the AnMBR operating at 12 h HRT

Parameters	HRT 12 h Winter period / Summer period
Days of operation	0-90/90-180
Operating temperature (ºC)	19±3/24±3
Q(L·d^{-1})	80±12
HRT(d)	0.5
SRT(d)	50
Flux (L/m^2 h)	6.6±0.7
OLR (KgCOD/m^3/d)	0.9±0.09 / 0.91±0.1

▪ Organic Load

Data presented in Figure 4.21 depict the variance in total COD for both the inlet and the permeate, as well as the corresponding removal efficiency. It was observed that the average COD values in the permeate doubled during winter months, highlighting the significant impact of temperature fluctuations on the performance of the AnMBR.
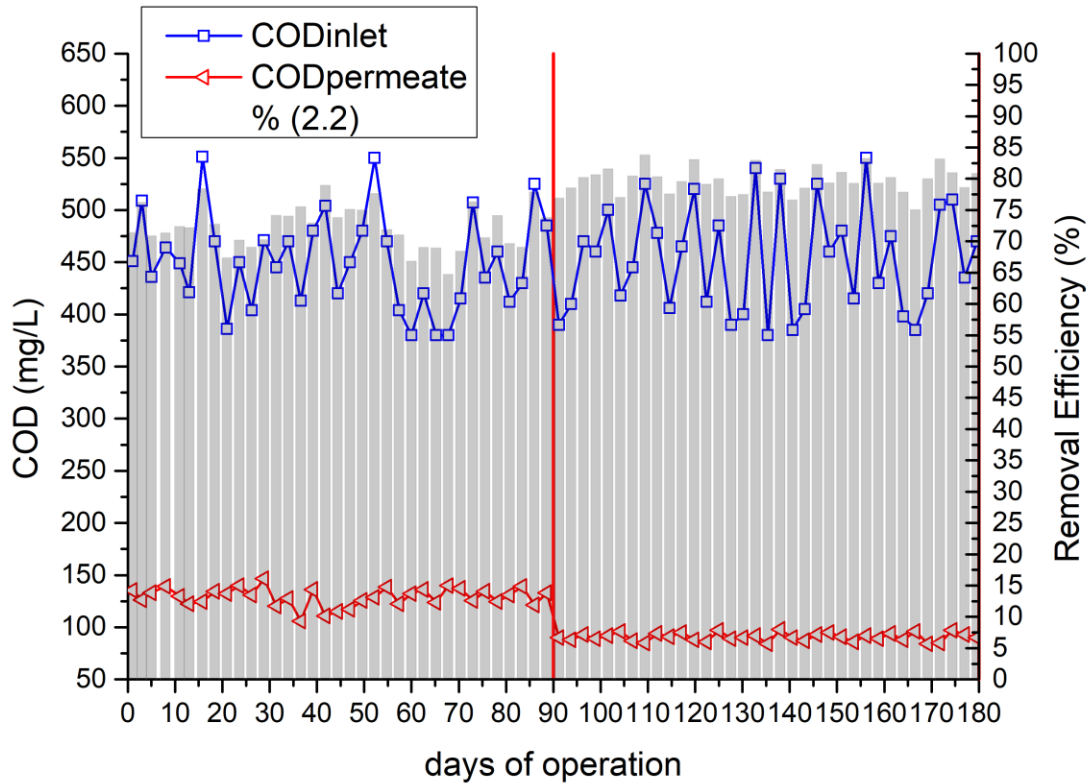
Figure 4. 21:AnMBR performance in terms of COD removal at 12 hours HRT

COD values for the permeate show considerable seasonal differences. Specifically, during the winter months (days 0-90), effluent COD values average 123mg/L, a standard deviation of 9, signifying a low level of fluctuation. In contrast, the summer period records an average COD of 91 mg/L with a remarkably stable standard deviation of 4. This contrast accentuates the profound effect of temperature variations on the AnMBR performance. Also that with lower temperatures, AnMBR appears to be slightly more unstable.

- VFAs / Alkalinity

Figure 4.22 provides a comprehensive visualization of key performance indicators, including the concentration of VFAs in the permeate water, the overall alkalinity levels, and two critical ratios that serve as benchmarks for assessing the system's operational stability.
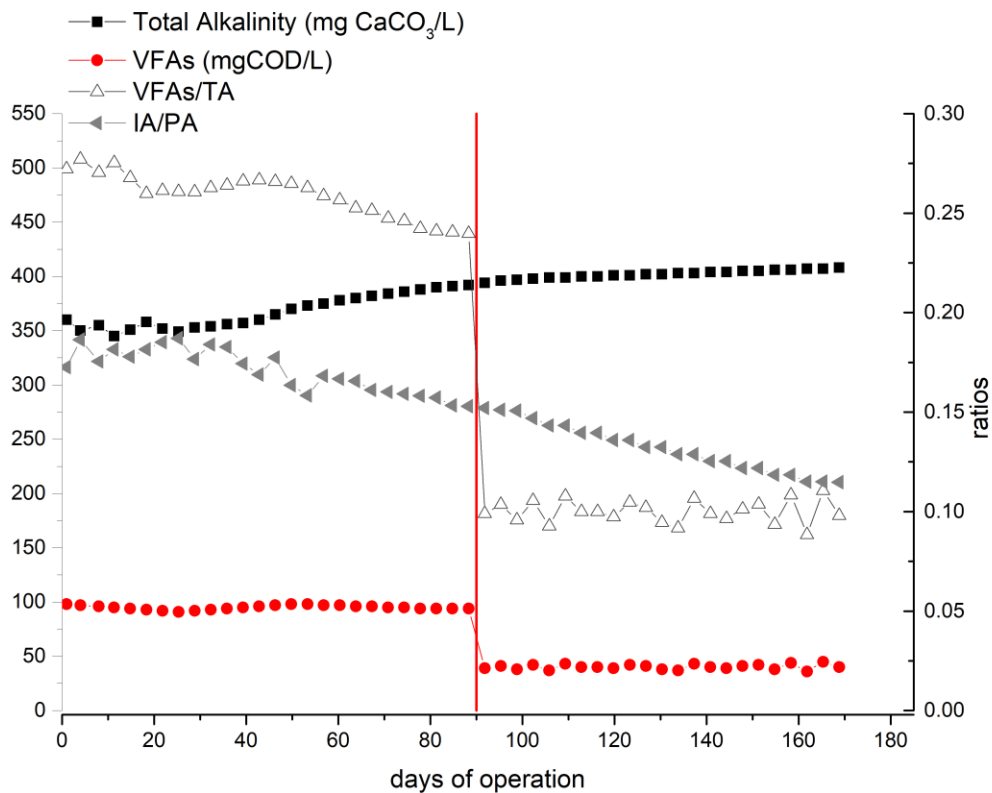
Figure 4. 22:VFAs and alkalinity in a 12 h HRT AnMBR

Figure 4.22 reveals a consistent upward trend in total alkalinity over the course of the operational period. Notably, these alkalinity levels remain relatively low when compared to those observed at other HRTs under study. Concurrently, the concentrations of VFAs are observed to be twice as high as those in 2 d HRT. However, this increase in VFAs is not necessarily indicative of system instability, as the associated ratios still fall below the critical threshold for instability. When it comes to seasonal variations, the graph demonstrates a downward trend in these ratios during the summer months. Interestingly, the summer values closely align with those observed at other HRTs, suggesting that a 12-hour HRT maintains system stability during both winter and summer months.

- ▪ pH

Figure 4.23 presents a detailed analysis of pH values, segmented by two distinct temperature regimes: the winter season spanning from Day 0 to Day 90, and the summer season extending

from Day 91 to Day 180. This breakdown allows for a nuanced understanding of how seasonal temperature variations may influence pH levels within the system.
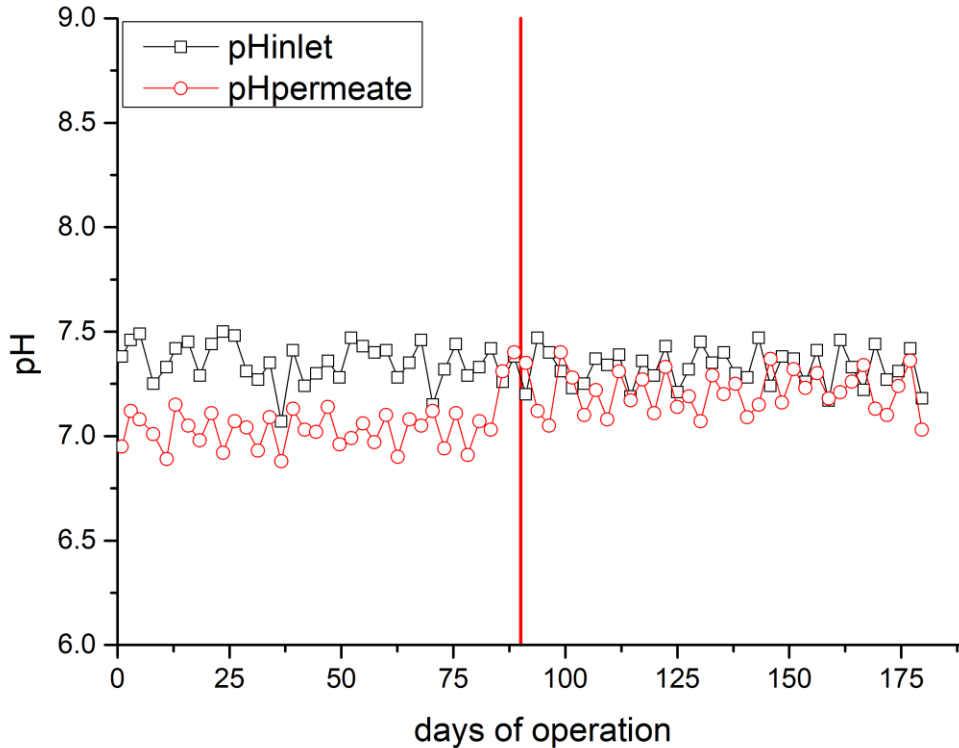
Figure 4. 23: Variation in pH Levels for Inlet and Permeate Streams at a 12 h HRT.

Graph highlights the seasonal variations in pH levels of the permeate, comparing winter and summer periods. In winter, the average pH is 7.05 with a standard deviation of ± 0.12. While this value does not adversely impact methanogenesis, lower pH levels could potentially be detrimental. This winter trend is largely attributed to higher VFA concentrations at a 12-hour HRT. Conversely, during the summer period, pH averages at 7.2 with a standard deviation of ± 0.1. This summer average closely aligns with both the inlet pH and the pH values observed at other HRTs studied. The data emphasizes the system's differing pH stability across seasons.

▪ Biomass concentrations

Figure 4.24 provides a detailed representation of MLSS concentrations within the AnMBR reactor. Significantly, the data demonstrates consistent stability across both winter and summer seasons, with no marked variations attributable to changes in HRT.
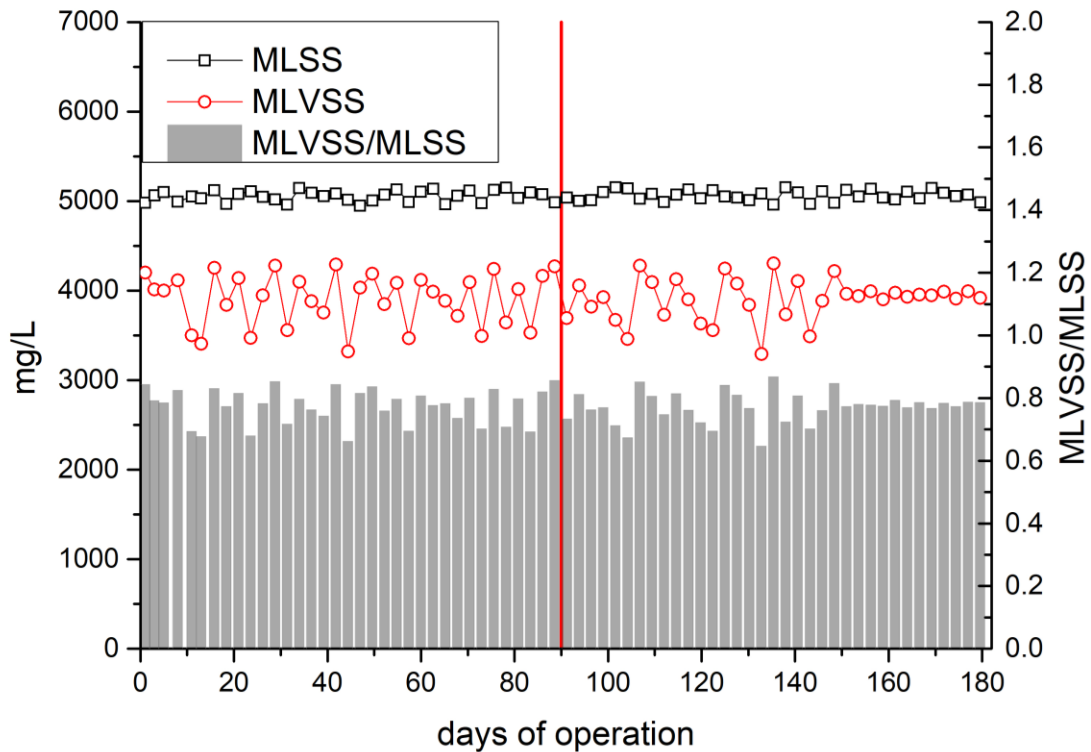
Figure 4. 24: MLSS and MLVSS concentrations inside the AnMBR reactor for 12 h HRT

Notably, VSS concentrations exhibit greater fluctuations when compared to the relatively stable MLSS levels. However, a trend toward stabilization is observed in the VSS concentrations during the most recent month. The average MLSS concentration in the AnMBR system stands at 5058 ± 58, whereas the MLVSS concentrations register an average of 3905 ± 269.

- ▪ Biogas production

Figure 4.25 elucidates the daily biogas output for two distinct seasonal phases: winter (Days 0-90) and summer (Days 91-180). Alongside the empirical data, the figure also includes calculated theoretical biogas yields, expressed in L per day (L/d). To enhance interpretive clarity, the graph

further delineates the ratios of daily biogas production in liters (L biogas/day) and biogas production per g of COD in the influent (L biogas/g COD inlet).
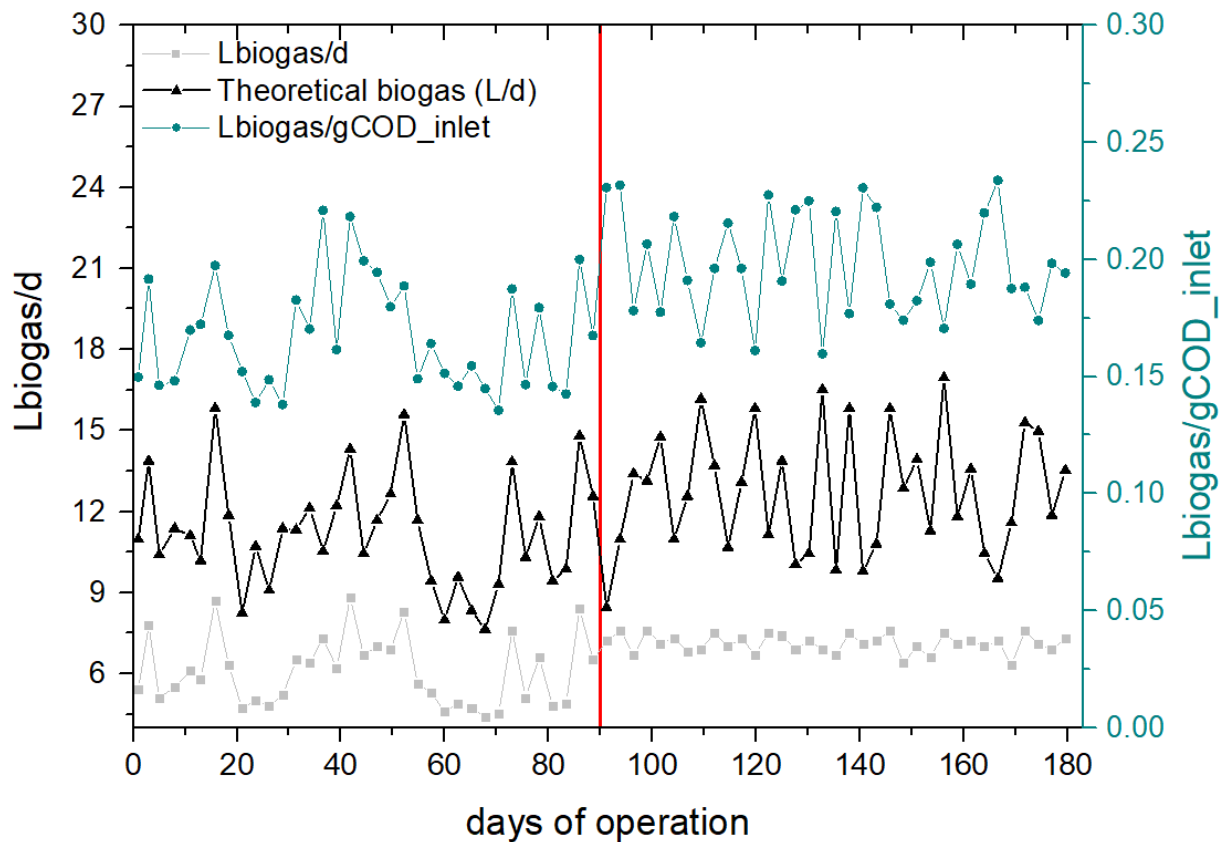
Figure 4. 25:AnMBR performance in terms of biogas production in 12 h HRT

As illustrated in the graph, the daily biogas production rates exhibited discernible seasonal variations. Specifically, the measured average daily biogas volume was 6.1±1.3 L during the winter season, elevating to 7.2 ±0.35 L during the summertime. These empirical observations diverge from the theoretical predictions, which estimated daily biogas yields of 11.2± 2 L and 12.7 ± 2.2 L for the respective winter and summer periods.

Moreover, the rate of biogas generation per gr of COD in the influent exhibited nuanced seasonal fluctuations. The recorded rate advanced from 0.21±0.02 L biogas/g COD inlet during the summer months to 0.26±0.02 L biogas/g COD inlet over the winter period. Importantly, the efficiency of the system's biogas production saw minor but discernible improvements during the warmer season. Intriguingly, these enhancements outperformed those observed in the 2-day and 1-day HRT

setups. However, lower ratios were displayed in the present dataset, indicating a greater likelihood of biogas loss from the system, a topic that will be delved into further subsequently.

These observed seasonal disparities in both the yield and efficiency of biogas production underscore the necessity for additional research to fine-tune the system's performance under different climatic conditions.

Figure 4.26 provides additional empirical evidence that complements the insights gained from the preceding figure. In this specific instance, the data have been normalized according to the amount of COD removed from the system. This normalization results in two pivotal metrics: the ratios of L CH$_4$/g COD removed and L biogas/g COD removed.
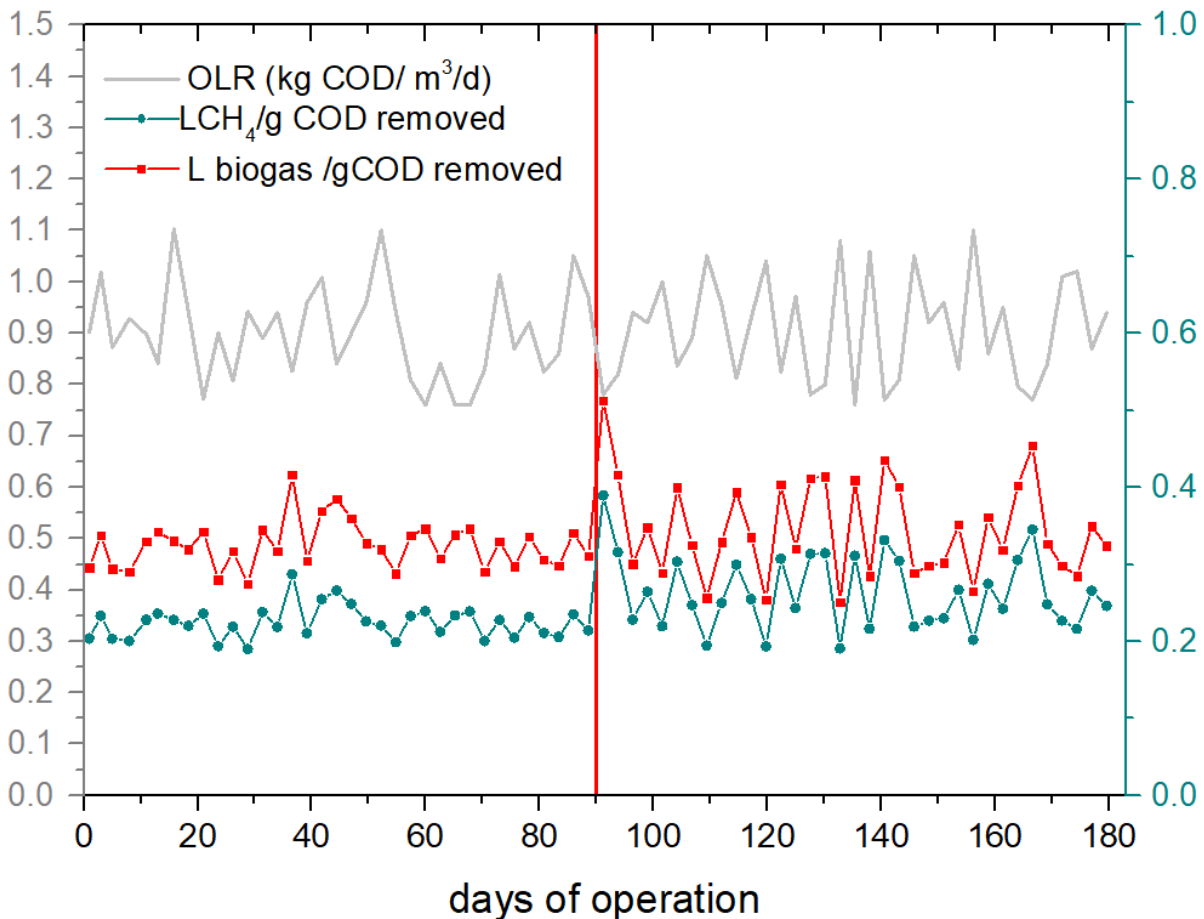
Figure 4. 26: Organic Load, methane and biogas ratios of the AnMBR operating in 12 h HRT

The average values for these ratios were found to be 0.32±0.03 L biogas/g COD removed during the winter months and 0.35±0.07 L biogas/g COD removed over the summer period. Furthermore, the ratios for L CH_4/g COD removed stood at 0.22±0.02 and 0.26±0.05 for the winter and summer seasons, respectively.

Figure 4.27 depicts the variations in biogas production, methane generation rates, and methane composition throughout both the summer and winter seasons.
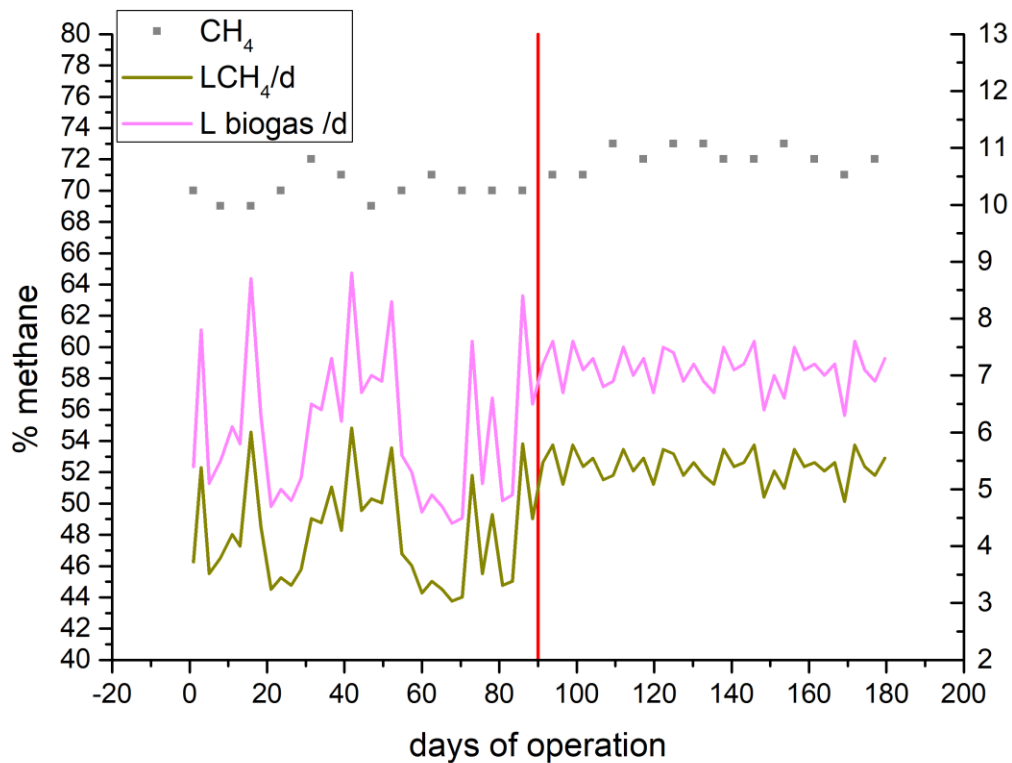
Figure 4. 27: Biogas, methane production and biogas composition for 12 h HRT

Experimental findings indicate that the methane content in the biogas composition varied seasonally, comprising 70.1 ± 0.9% during the winter and increasing slightly to 72.1 ± 0.8% during the summer. This marginal increase suggests a modest improvement in methane concentration during the warmer months. Furthermore, both percentages fall within the range considered satisfactory according to existing literature on anaerobic systems. When compared to other HRTs examined, the differences in methane percentages were minimal and barely noticeable.

Additionally, Figure 4.28 illustrates how methane composition correlates with the operational temperature of the AnMBR reactor.
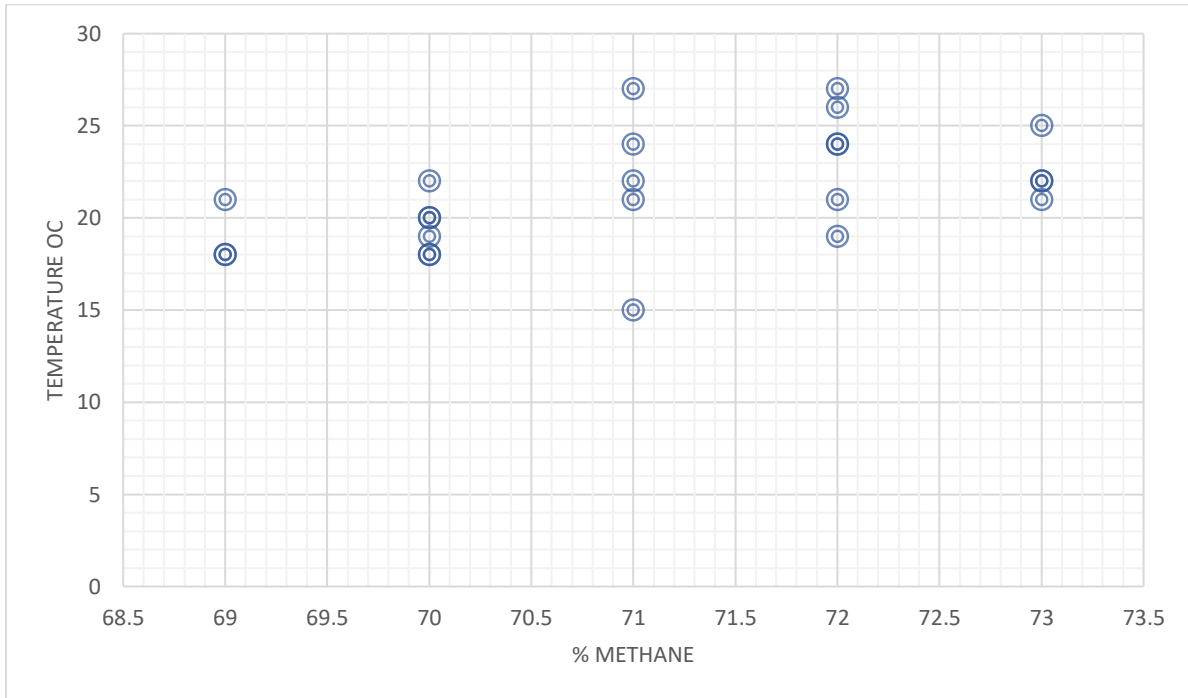
Figure 4. 28: Relation between methane percentage and temperature for both periods in 12 h HRT

- Membrane fouling

Figure 4.29 illustrates the performance of the AnMBR with a focus on membrane fouling and the rate of increase in TMP.
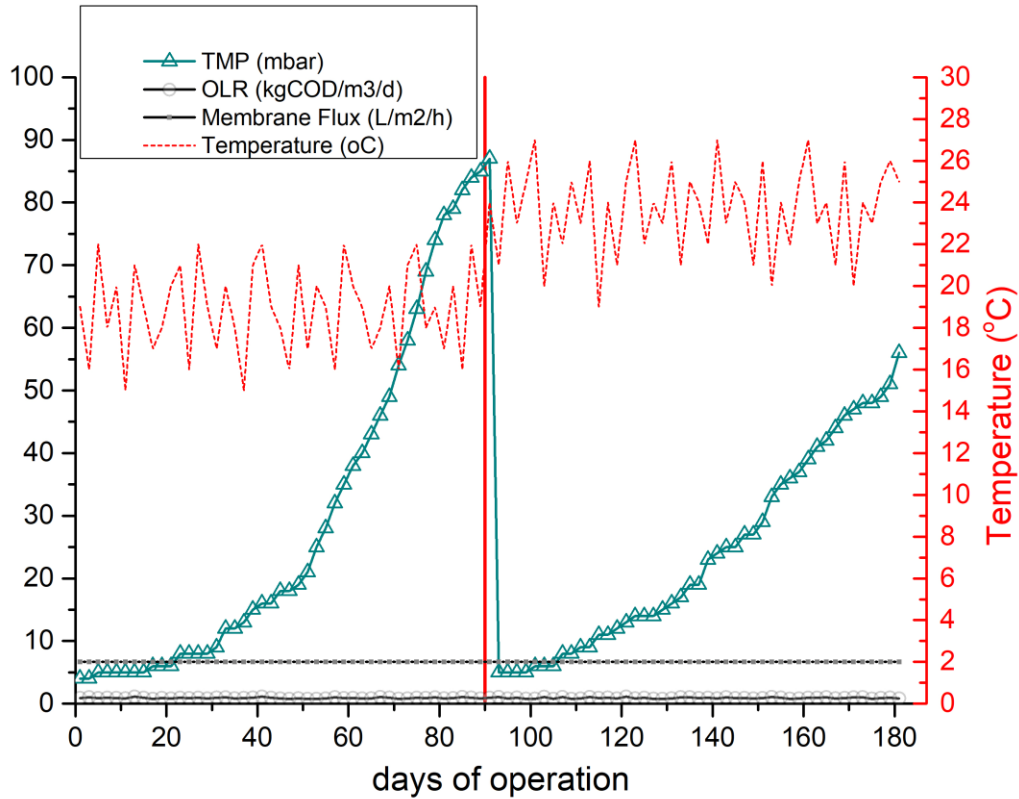
Figure 4. 29: AnMBR performance in12 h HRT in terms of membrane fouling

Figure 4.29 illustrates the behavior of membrane fouling in terms of TMP, along with other operational parameters such as operating temperature, OLR, and membrane flux. During the winter period, the AnMBR system saw an increase in TMP, rising from 5 mbar to 85 mbar over a 90-day period. This yielded a rapid rate of increase of approximately 0.8889 mbar/day. In contrast, the subsequent summer period exhibited a more moderate TMP increase, climbing from 5 mbar to 56 mbar over an identical 90-day span, at a rate of approximately 0.5667 mbar/day.

Despite these seasonal variations in TMP increase rates, the pressure never reached the critical threshold of 300 mbar, generally eliminating the need for chemical cleaning. However, chemical cleaning was performed after the first three months of operation, specifically to enable an examination of seasonal variations. The results indicated that the AnMBR system performed better in terms of membrane fouling during the summer, as evidenced by the lower rate of TMP increase.

4.3.1.4 AnMBR, operating at 6 h HRT and ambient temperatures: A Winter-Summer Comparative Study

In a subsequent HRT assessment, a six-hour HRT was employed, while maintaining the SRT at a constant 50 days. Consistent with the initial evaluation, data were collected during both the summer and winter seasons to investigate seasonal variations.

Table 4.5 illustrates the operational characteristics of the AnMBR when functioning at a 6 h HRT.

Table 4. 5:Operational parameters for the AnMBR operating at 6 h HRT

Parameters	HRT 6 h Winter period / Summer period
Days of operation	0-90/91-180
Operating temperature (°C)	18±3/23±2
Q(L·d⁻¹)	160
HRT(d)	0.25
SRT(d)	50
Flux (L/m² h)	13±0.7
OLR (KgCOD/m³/d)	2 ± 0.11/1.8 ±0.22

- Organic Load

Figure 4.30 depicts the total COD metrics for the inlet, the permeate, and the removal efficiency. In this case as well, the analysis spanned 180 days: the winter period accounted for days 0-90, while the summer period covered days 91-180.
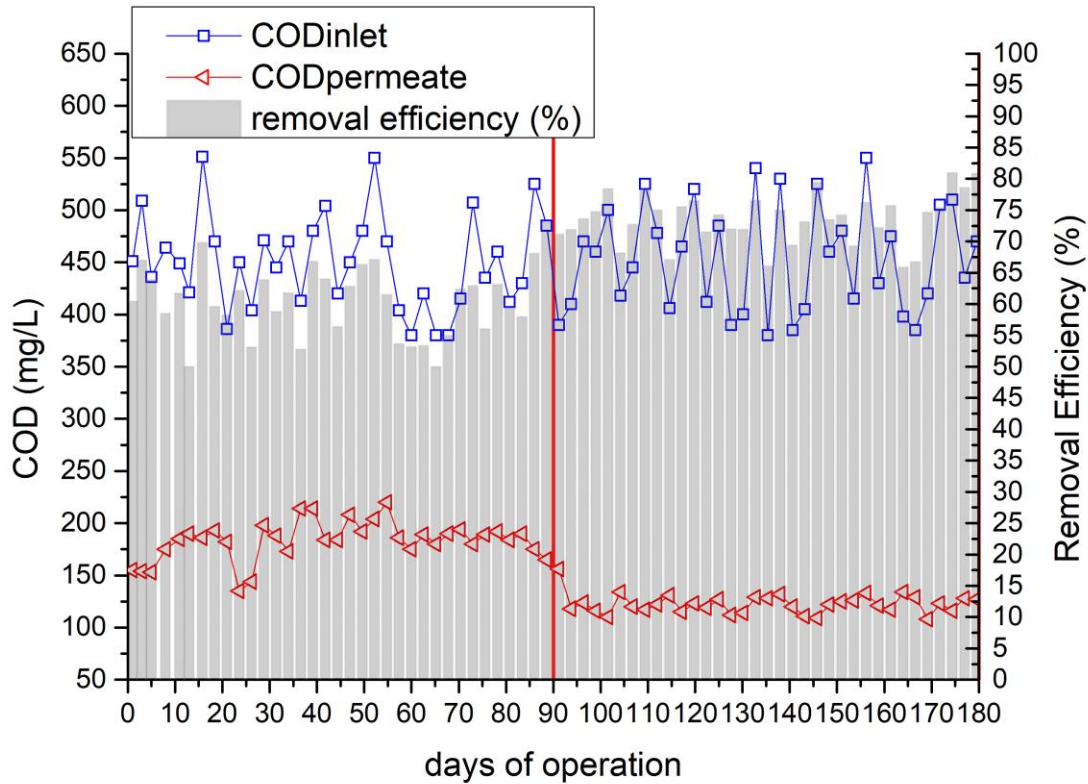
Figure 4. 30: AnMBR performance in terms of COD removal at 6h HRT

As depicted in Figure 4.30, the average COD values for the permeate in this evaluation show less pronounced seasonal variation compared to the previous HRT assessment. Notably, the removal efficiency improved during the summer months. In this instance, the COD values exceed 100 mg/L in both seasons. Specifically, for the winter period (days 90-180), the average COD values register at 177 ± 18 mg/L. In contrast, during the summer months, the values average 121 ± 8 mg/L. These results indicate that with a 6-hour HRT, the average removal efficiency stands at 60% for the winter period and 73% for the summer period.

- ▪ VFAs /Alkalinity

Figure 4.31 offers an in-depth graphical representation of essential performance metrics, such as the VFAs concentration in the permeate water, overall alkalinity levels, as well as two pivotal ratios that act as key indicators for evaluating the system's operational stability.
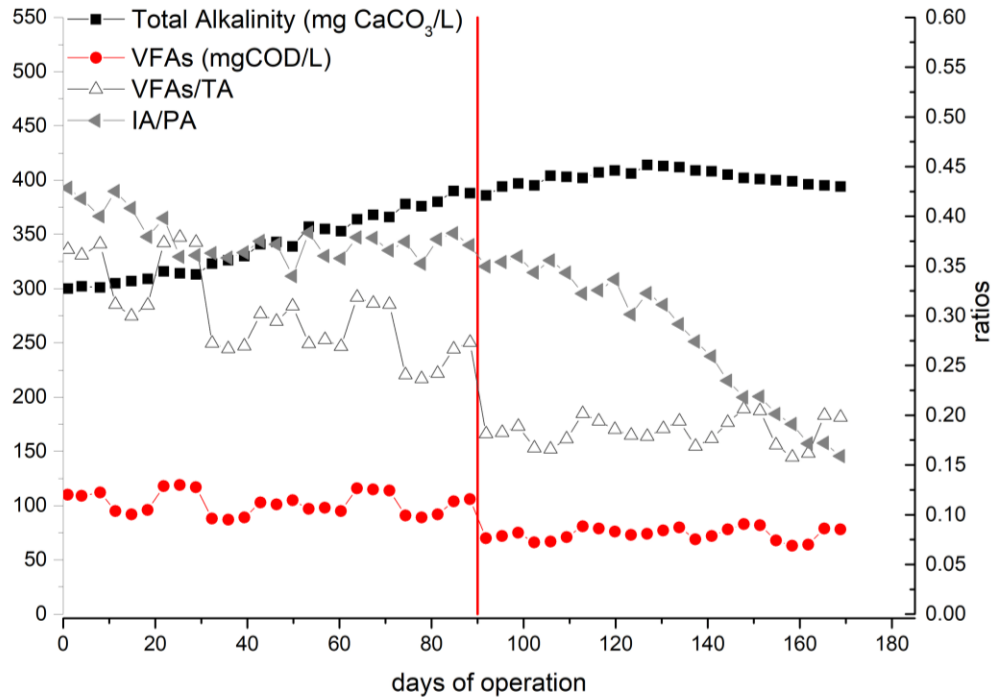
Figure 4. 31: VFAs and alkalinity in a 6 h HRT AnMBR

Figure 4.31 illustrates that the TA initiates at notably low levels—starting at 300—especially when compared to other HRTs. However, this metric begins to rise as the system operates, showing signs of stabilization around the midpoint of the summer period. In contrast, the concentration of VFAs maintains a level like that observed in the 12-d HRT assessment yet displays elevated values even during the summer. The critical ratios commence with high values, exceeding the threshold of 0.3. These ratios, however, gradually decline as the system continues to operate, and by the end of the summer period, they align more closely with the values observed in the 12-h HRT.

- ▪ pH

Figure 4.32 offers a comprehensive breakdown of pH levels, categorized by two separate thermal conditions: the winter period running from Day 0 to Day 90, and the summer period covering Day 91 to Day 180. This segmented analysis provides a more refined insight into the potential impact of seasonal temperature fluctuations on the system's pH levels.
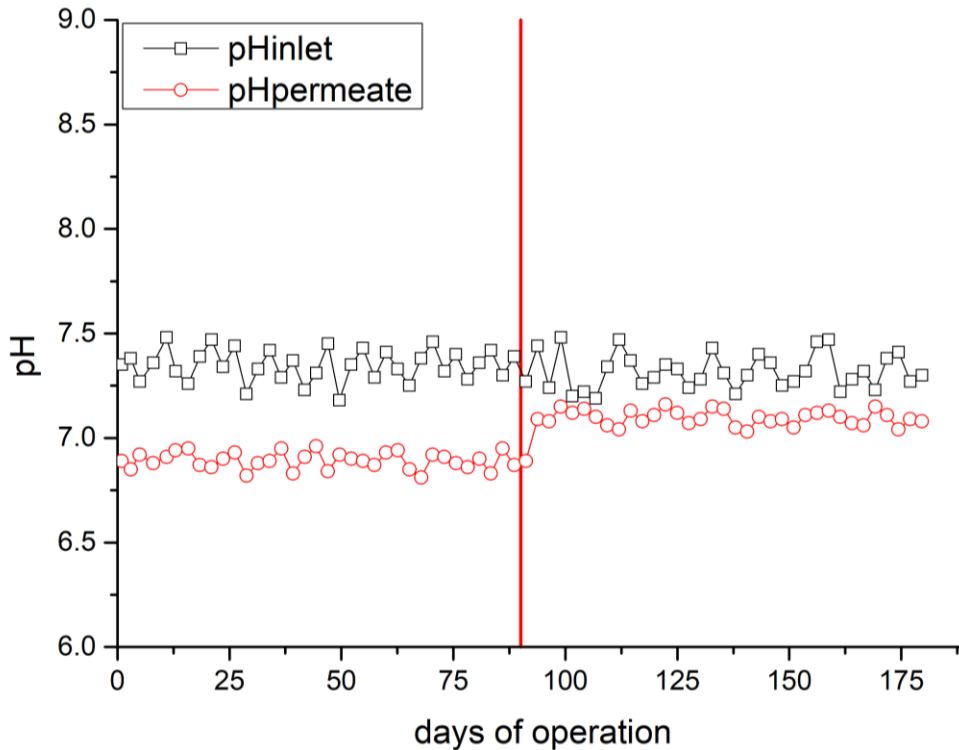
Figure 4. 32: pH of the Inlet and Permeate in AnMBR Operating at 6-Hour HRT

Figure 4.32 highlights the seasonal variations in pH levels of the permeate, comparing winter and summer periods. In winter, the average pH is 6.9 with a standard deviation of ± 0.08. This value is approaching a level at which concerns about its impact on methanogenic activity could begin to arise. This winter trend is largely attributed to higher VFA concentrations at a 6-hour HRT even during the summer period. During the summer period, the pH averages at 7.09 with a standard deviation of ± 0.04. This summer average closely aligns with both the inlet pH and the pH values observed at other HRTs studied.

- Biomass concentrations

Figure 4.33 provides a detailed representation of MLSS concentrations within the AnMBR reactor.
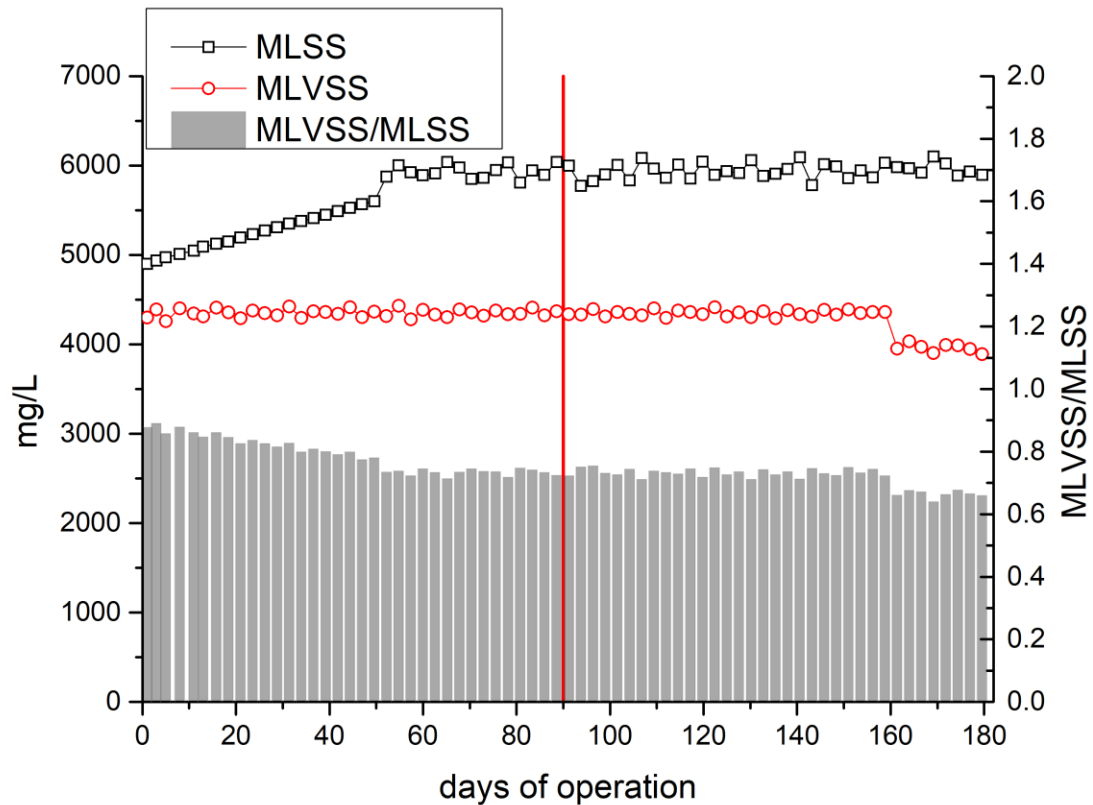
Figure 4. 33: MLSS and MLVSS concentrations inside AnMBR reactor working at 6 hours HRT

Importantly, the data corresponding to the 6-hour HRT reveals an increase in MLSS concentration. However, this increase is not observed in MLVSS. The MLVSS/MLSS ratio starts at values around 0.8, and as time progresses, it decreases to levels more commonly seen in anaerobic systems, nearing values close to 0.7. MLSS begins to stabilize after one month of operation.

- Biogas production

Figure 4.34 presents on the daily biogas production during two separate seasonal periods: winter, spanning Days 0-90, and summer, covering Days 91-180. In addition to the actual measured values, the figure incorporates theoretical estimates of daily biogas production in liters (L/d). To further aid in data interpretation, the graph also includes key ratios, specifically the daily biogas output in liters (L biogas/day) as well as the biogas yield per gram of COD present in the influent (L biogas/g COD inlet).
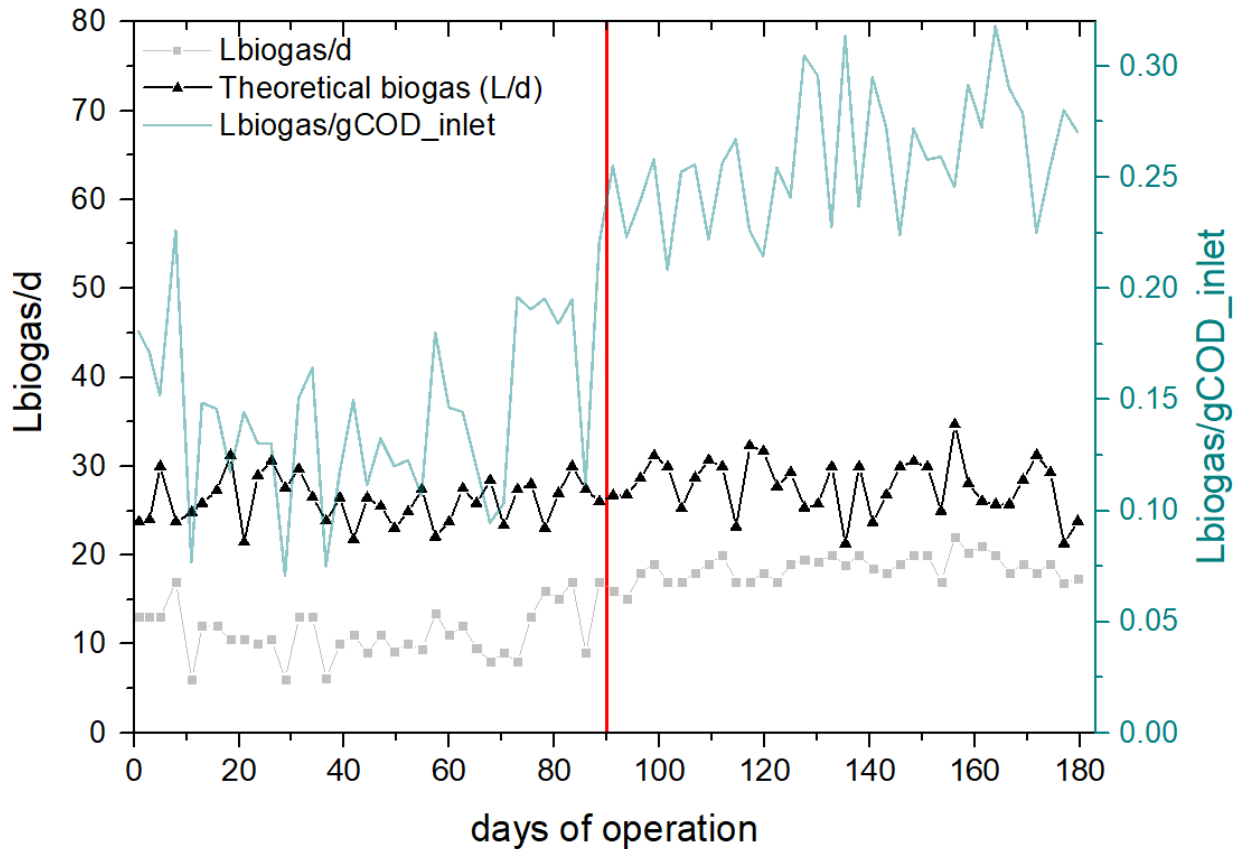
Figure 4. 34: AnMBR performance in terms of biogas production at 6 hours HRT

During the winter season, empirical data show an average daily biogas production of 11.4 ±3 L, which sees an uptick to 18.8 ± 1.4 L during the summer months. These observed values contrast with theoretical estimations, which forecast daily biogas yields of 25.11±2.8 L for winter and 28.8±3.1 L for summer. As the HRT decreases, the gap between real and theoretical data widens. Additionally, the rate of biogas generated per gr of COD inlet also shows subtle seasonal changes. Specifically, the summer period sees a measured rate of 0.14±0.04 L biogas/g COD inlet, increasing marginally to 0.25±0.03 L biogas/g COD inlet during the winter months. It's worth noting that the system exhibits gains in biogas production efficiency during the summer, similar to those observed with 2-day and 1-day HRTs. However, the data also reveal lower ratios at 12 h HRT, suggesting an increased likelihood of biogas loss within the system, a matter that warrants further exploration.

Figure 4.35 provides additional empirical evidence that complements the insights gained from the preceding figure. In this specific instance, the data have been normalized according to the amount of COD removed from the system. This normalization results in two pivotal metrics: the ratios of L CH_4/g COD removed and L biogas/g COD removed
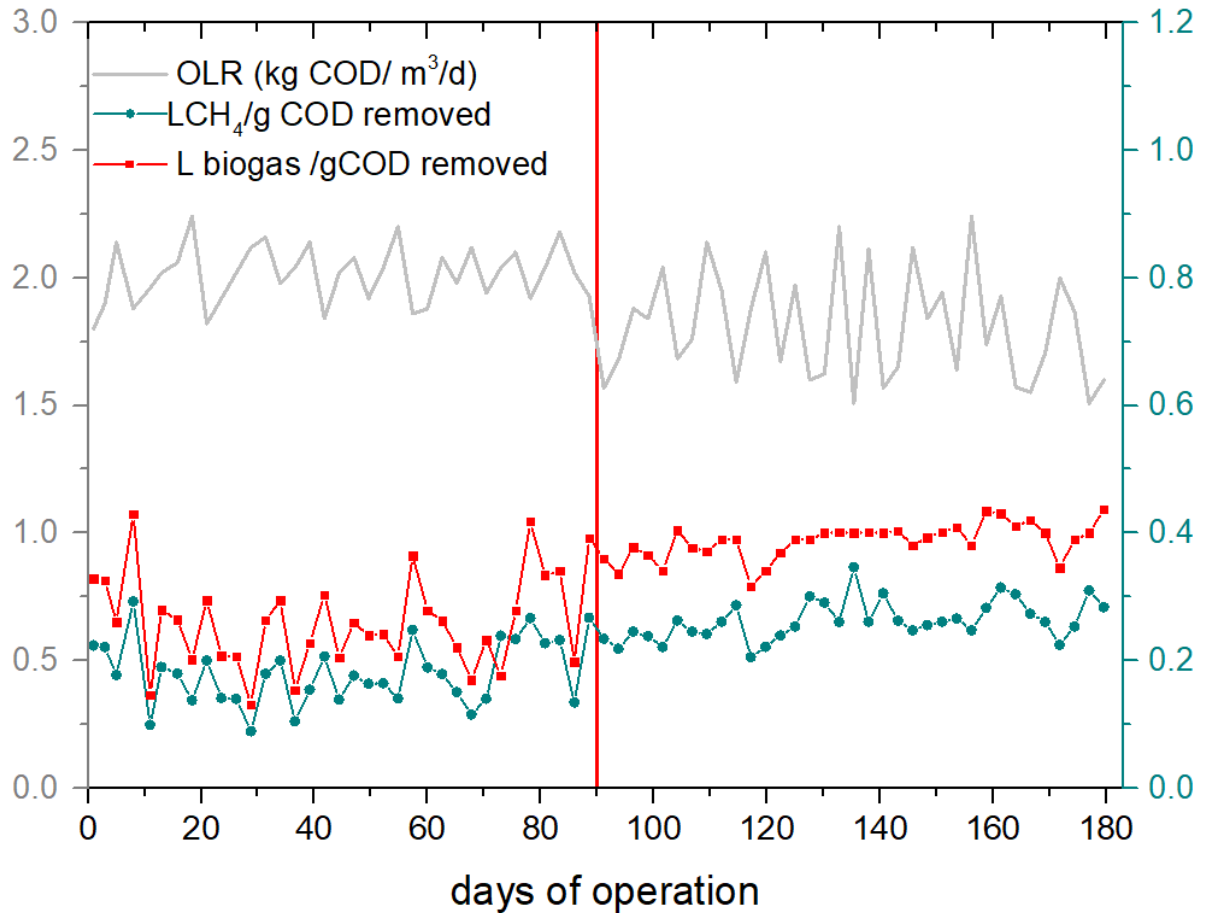
Figure 4. 35:Organic Load, methane yield and biogas ratios operating at 6 h HRT

The average values for these ratios were found to be 0.26±0.07 L biogas/g COD removed during the winter months and 0.37±0.04 L biogas/g COD removed over the summer period. Furthermore, the ratios for L CH4/g COD removed stood at 0.18±0.02 and 0.26±0.03 for the winter and summer seasons, respectively.

Figure 4.36 depicts the variations in biogas production, methane generation rates, and methane composition throughout both the summer and winter seasons.
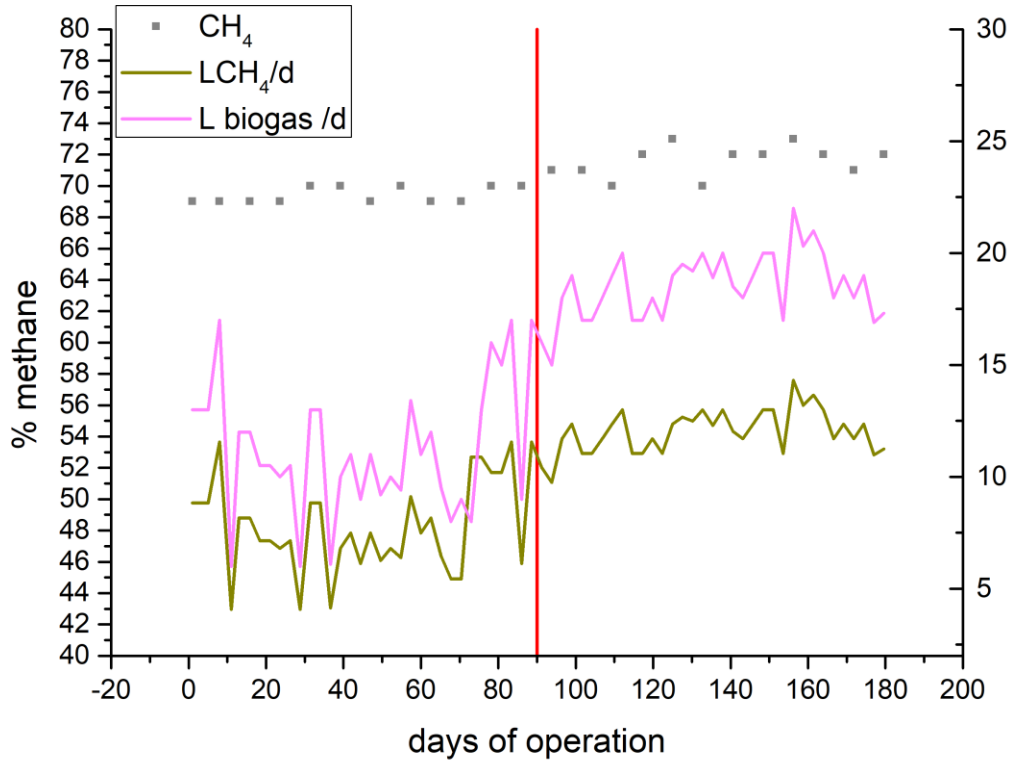
Figure 4. 36: Biogas, methane production and biogas composition in 6 hours HRT

Experimental data show that the biogas generated during the winter period had a methane content of 69.5 ± 0.5%, which increased to 71.5 ± 1% during the summer. Of all the HRTs examined, this HRT exhibited the lowest winter methane percentages.

Moreover, Figure 4.37 demonstrates the relationship between the methane composition and the operating temperature of the AnMBR reactor.
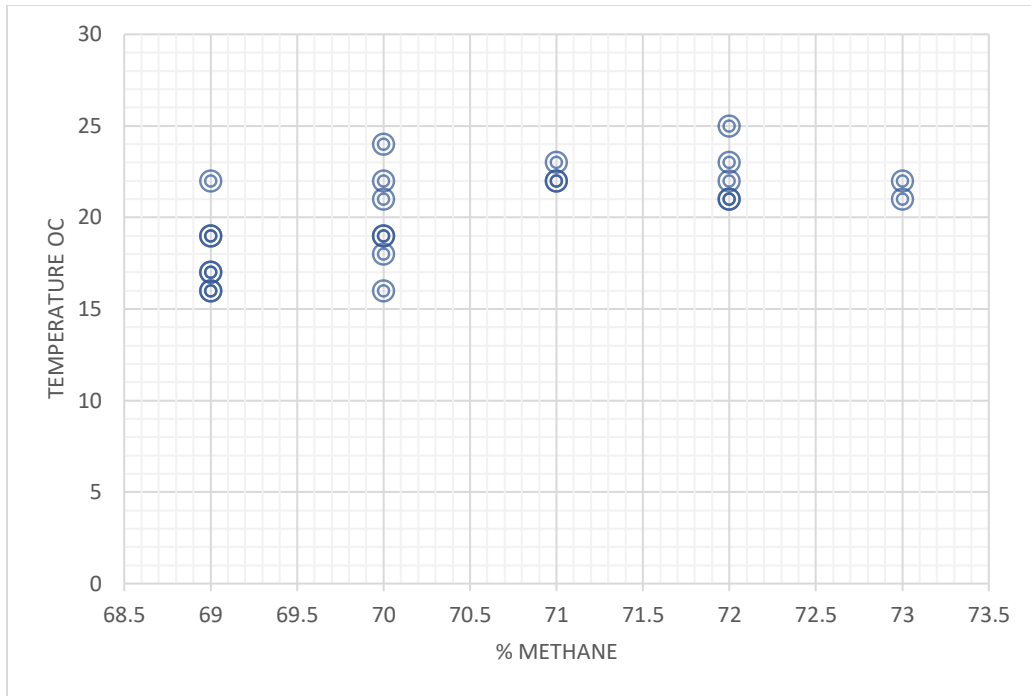
Figure 4. 37:Relation between methane percentage and temperature for both periods in 6 hours HRT

What can be concluded is that in this specific case, the majority of methane percentages cluster around 69% and 70%.

- Membrane fouling

Figure 4.38 illustrates the performance of the AnMBR with a focus on membrane fouling and the rate of increase in TMP.
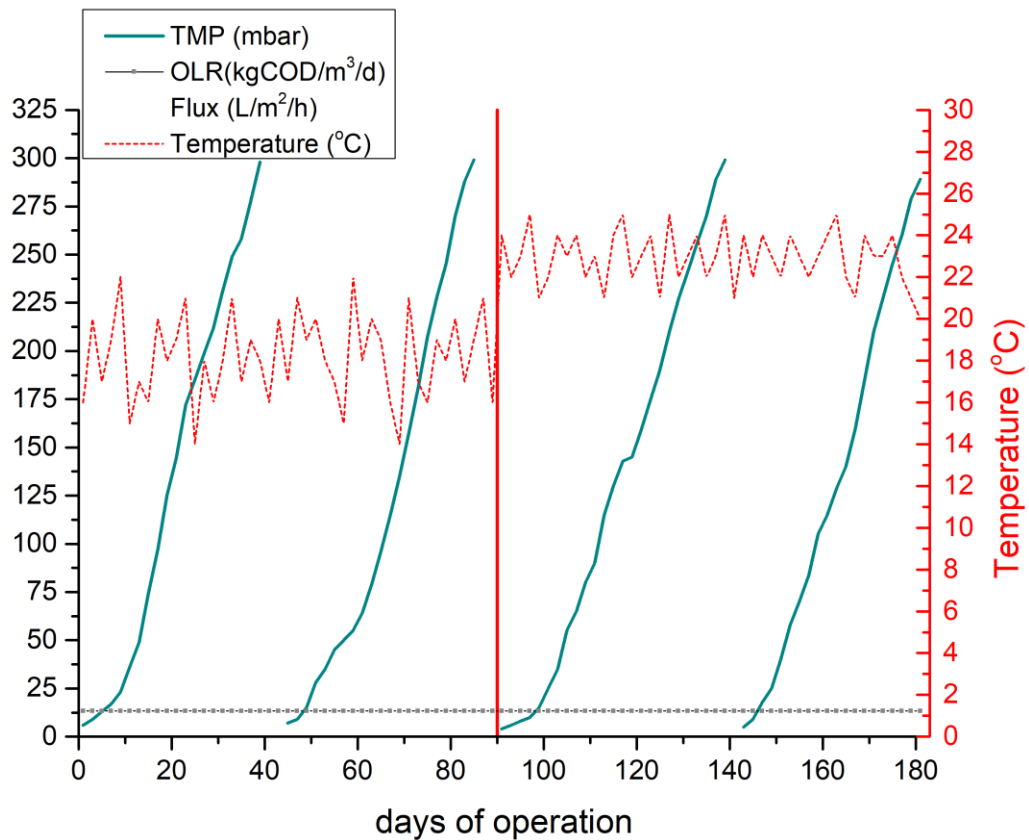
Figure 4. 38: AnMBR performance in6 h HRT in terms of membrane fouling

During a critical 38-day window in the winter, the AnMBR system witnessed a dramatic increase in TMP, soaring from an initial value of 5 mbar to a cleaning threshold of 300 mbar. This necessitated chemical cleaning, which significantly compromised the system's operational efficiency. This challenge prompted a new line of investigation, subsequently discussed in this thesis, focused on reducing membrane fouling and enhancing long-term operational sustainability without the need for frequent chemical cleaning.

In contrast, the situation improved slightly during the subsequent summer period. The TMP increased to 300 mbar, but the time required for chemical cleaning extended to 50 days. Although the rate of TMP increase was somewhat lower during the summer, the system still necessitated a single chemical cleaning intervention to maintain optimal performance.

4.3.2 Comparative evaluation of the HRTs examined.

The comparison of the results is based on the main parameters and the indicators of good AnMBR performance. The comparative analysis of the results is carried out for the main operating period and for all the different parameters that are examined.

In this context, Table 4.6 offers a comprehensive summary of the outcomes for the four distinct HRTs within the examined temperature ranges. Additionally, Figures 4.39 and 4.40 provide in-depth visual representations of the COD removal rates and biogas production across all operational phases.

Table 4. 6: Average results for AnMBR (± standard deviation) at different HRTs and temperatures

	unit	HRT 2 days		HRT 1 day		HRT 12h		HRT 6 h	
		Winter	Summer	Winter	Summer	Winter	Summer	Winter	Summer
COD inlet	mg·L^{-1}	477 ±62	451 ±48	486 ±46	488 ±45	455±46	442±51	475 ± 38	453 ± 55
COD permeate	mg·L^{-1}	105 ±9	51±5	95 ± 12	67±6	123 ±9	91±4	177 ± 18	121 ± 8
COD removal efficiency	%	76± 4	89±1	77±4	85±2	69±5	78±3	60 ± 3	73 ± 4
VFAs	mgCOD·L^{-1}	75±5	23±7.9	66±5	34± 8	95±3	40±1.4	102±11	74±7
Biogas production	L d^{-1}	1.45±0.15	2.06±0.1	3.79±0.5	4.94±0.22	6.13 ±1.3	7.18±0.35	11.4 ± 3	18.8 ± 1.4
Gaseous methane production	L d^{-1}	1.1 ± 0.11	1.7 ± 0.09	2.7 ± 0.3	3.8 ± 0.2	4.19 ±0.9	5.4 ± 0.26	7.8 ± 2	12 ± 1
Ratio for Gaseous Methane	LCH$_4$/gCOD removed	0.27±0.07	0.29±0.06	0.27±0.06	0.30±0.05	0.22±0.02	0.27±0.05	0.18±0.02	0.26±0.03
CH$_4$	%	70.6 ±0.9	72.1 ± 0.8	70.5 ± 1.1	72.8 ±0.8	70.1 ± 0.9	72.1 ± 0.8	69.4 ±0.5	71.5±1
Theoretical biogas production	L d^{-1}	2.7 ±0.7	3.5±0.38	6.24±1.1	7.82 ± 1.1	11.2±2.1	12.7±2.2	25.11± 2.8	28.8 ±3.1
Dissolved methane at the effluent	LCH$_4$ d^{-1}	0.75	0.56	1.57	1.12	3.14	2.24	6.27	4.5
Sum of biogas production and dissolved methane at the effluent	L d^{-1}	2.2	2.62	5.36	6.06	9.27	9.42	17.7	23.3
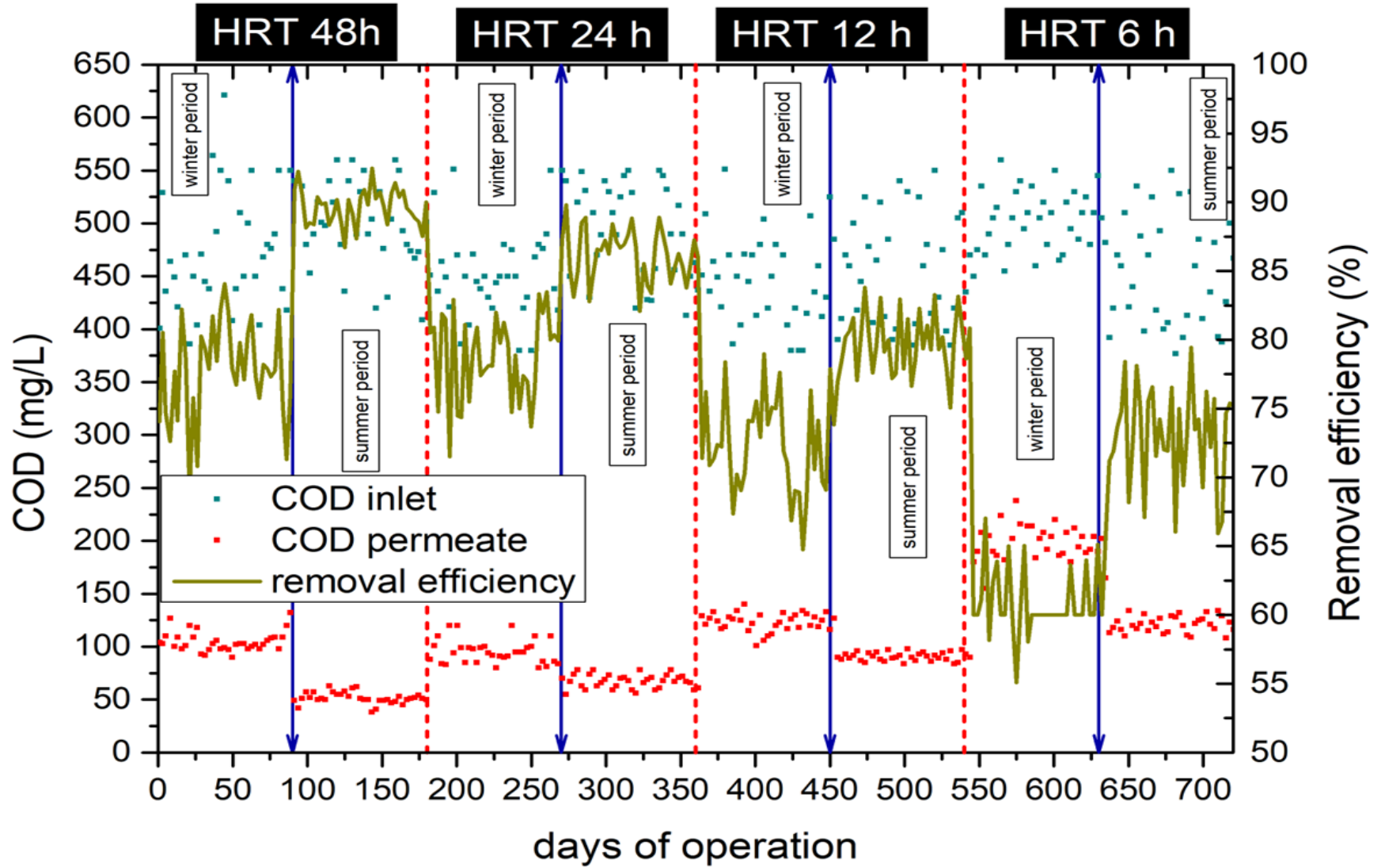
Figure 4. 39: AnMBR performance in terms of biogas production for all the HRTs examined.
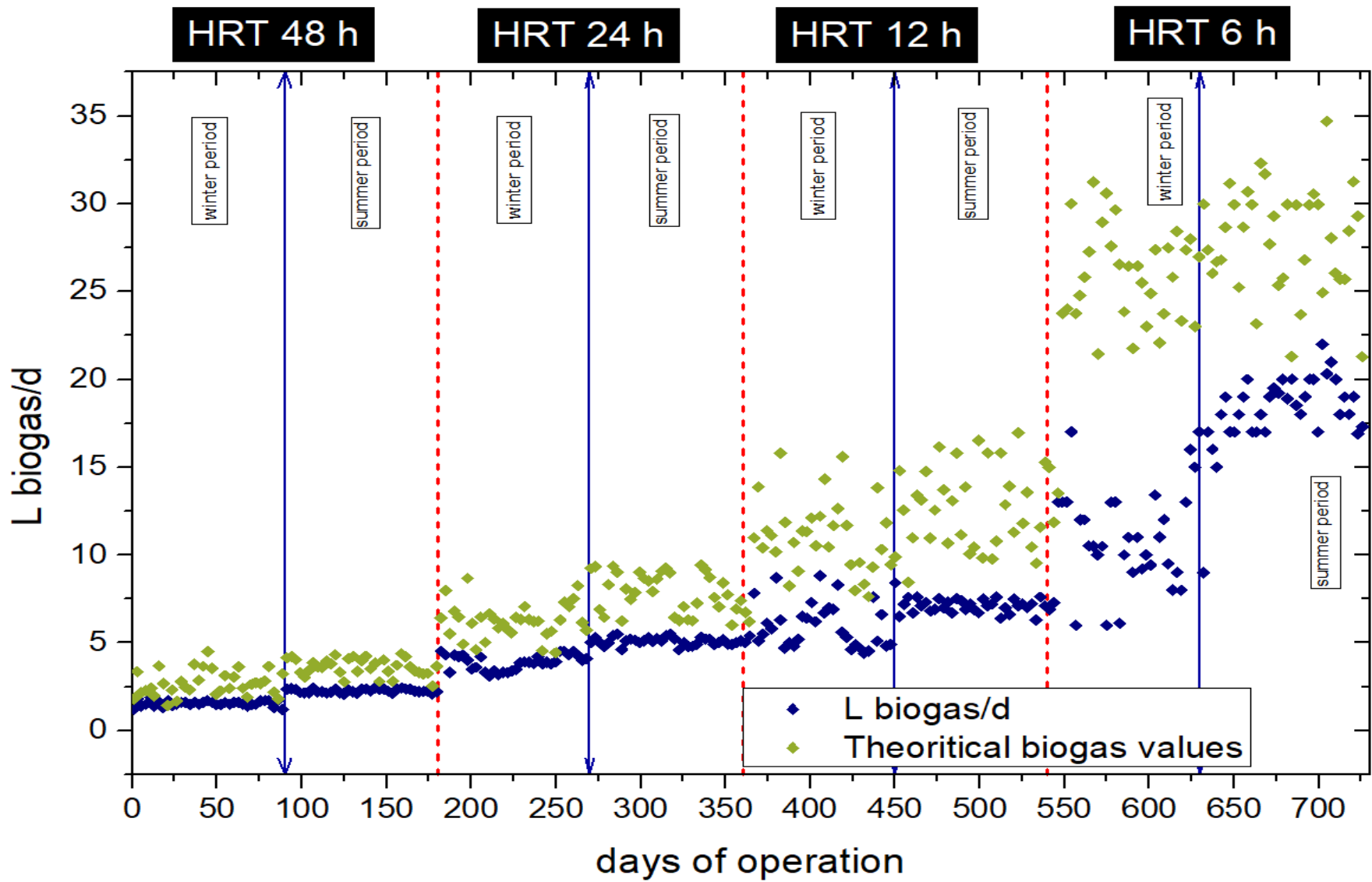
Figure 4. 40: AnMBR performance in terms of biogas production for all the HRTs examined.

More specifically, Figure 4.39 offers a detailed graphical depiction of both the influent and permeate COD concentrations, as well as COD removal efficiency, over the course of the entire experimental period. During the initial winter and summer phases at an HRT of 2 days, the AnMBR system yielded average effluent COD concentrations of 105 ± 9 mg L^{-1} and 51 ± 5 mg L^{-1}, respectively. In the subsequent winter period at an HRT of 1 day, the effluent COD averaged 95 ± 12 mg L^{-1}, closely mirroring the results of the prior winter phase. During the following summer phase average effluent COD was 67 ± 6 mg L^{-1}. These observations suggest a limited impact on permeate quality when reducing the HRT from 2 days to 1 day. During the third phase, at an HRT of 12 hours, the average effluent COD was 123 ± 9 mg L^{-1} in winter and 91 ± 4 mg L^{-1} in summer. Reducing the HRT to 6 hours reduced more the removal efficiency of organic load, effluent average COD was 177 ± 18 during the winter and 121 ± 8 during the summer period.

When comparing the results of this study with previous research, it is evident that the findings largely align with previous studies, despite most earlier works are utilizing synthetic wastewater. For instance, Ding et al. (2018) conducted an evaluation of an AnMBR system, operating on synthetic wastewater at ambient temperatures. They reported average effluent COD concentrations of 137 mg/L for a 1-day HRT and 110 mg/L for a 12-hour HRT. Similarly, Watanabe et al. (2017) observed elevated COD removal rates at temperatures comparable to those in this study. Specifically, they documented effluent COD concentrations of 18 mg/L and COD removal rates exceeding 95% at temperatures below 25°C. In contrast, they noted a decline in COD removal efficiency when the bioreactor temperature fell to 10°C. Furthermore, Dagnew et al. (2011) reported an average effluent COD of 47 mg/L and a COD removal rate of 79% at an ambient temperature of 22°C.

Figure 4.40 illustrates biogas production throughout the operation. The biogas production is standardized to specific conditions (temperature and pressure) so that it serves as a comparable metric for all reactors as well as with other systems. From Figure 4.40 is concluded that throughout the duration of the study, the observed biogas production in the AnMBR consistently fell below the theoretical biogas production values. Furthermore, a seasonally induced decrement in biogas production was discernible during the winter months, which can be attributed to the lower ambient temperatures.

The disparity between the empirical data and theoretical projections of biogas production can largely be ascribed to the loss of dissolved methane in the effluent, as confirmed by Table 4.7. This table delineates the theoretical values associated with dissolved methane concentrations. The aggregate of daily biogas production and the soluble methane lost in the effluent closely

approximates the theoretical estimates based on observed COD removal rates. It should be noted that the dissolved methane values presented in the table represent saturation concentrations. This was further verified by experimental data, which involved calculating the dissolved methane concentrations. The protocol for these calculations is detailed in the 'Materials and Methods' section.

Table 4.7 delineates the percentage deviation between the theoretical and the observed biogas production values. The equation employed to compute this deviation from the theoretical biogas yield is as follows:

$$deviation = \frac{Y_{theoritical} - Y_{average}}{Y_{theoritical}} \ (\%)$$

These benchmark values served as the basis for calculating the observed deviations, which are comprehensively detailed in Table 4.7.

Table 4. 7 Deviation (%) of biogas production from the theoretical value

	HRT 2days		HRT 1day		HRT 12h		HRT 6h	
	winter	summer	winter	summer	winter	summer	winter	summer
Biogas deviation*	45%	41%	30%	30.6%	45%	42%	54%	36%

*It is referred only to gaseous biogas without the dissolved methane lost in the effluent

As is observed, there are several deviations of the theoretical value from the actual value calculated in the system. However, the methane lost in the liquid is not considered in the above results. This is reflected in Table 4.7 as well as below, where the mass balance of the system is calculated. The percentage of deviation is greater during the winter months, which is logical since it is known that at low temperatures, the solubility of methane in the liquid phase increases, resulting in a higher biogas loss in the effluent.

Such findings are supported existing literature, such as the work of Smith et al. (2013), who reported that approximately 40–50% of the total methane generated in AnMBR systems was dissolved in the permeate and consequently discharged, rather than being collected. Moreover, while a reduction in HRT from 2 days to 1 day led to an increase in average biogas production, it simultaneously resulted in a decreased biogas yield—from 0.46 L biogas/g COD removed to 0.42 L biogas/g COD removed. These observations underscore that shorter HRTs are associated with

reduced biogas yields, aligning well with prior research. For example, Bornare et al. (2014) observed biogas yields ranging between 0.42 and 0.48 L biogas/g COD removed, while Ho and Sung (2009) indicated that a decrease in HRT from 12 hours to 6 hours led to a 13% decline in methane recovery.

- ***Membrane performance at different HRTs***

In AnMBRs, membranes serve as a crucial component for biomass retention and are instrumental in delivering high-quality effluent. However, these membranes are susceptible to fouling, a phenomenon that can occur either internally or externally, blocking or clogging the membrane pores. According to existing literature, fouling is influenced by various parameters, one of which is the operating flux passing through the membrane. This flux is directly related to the driving force behind the system, known as the TMP. The changes in TMP over time during membrane filtration at various HRTs are shown in Figure 4.41.
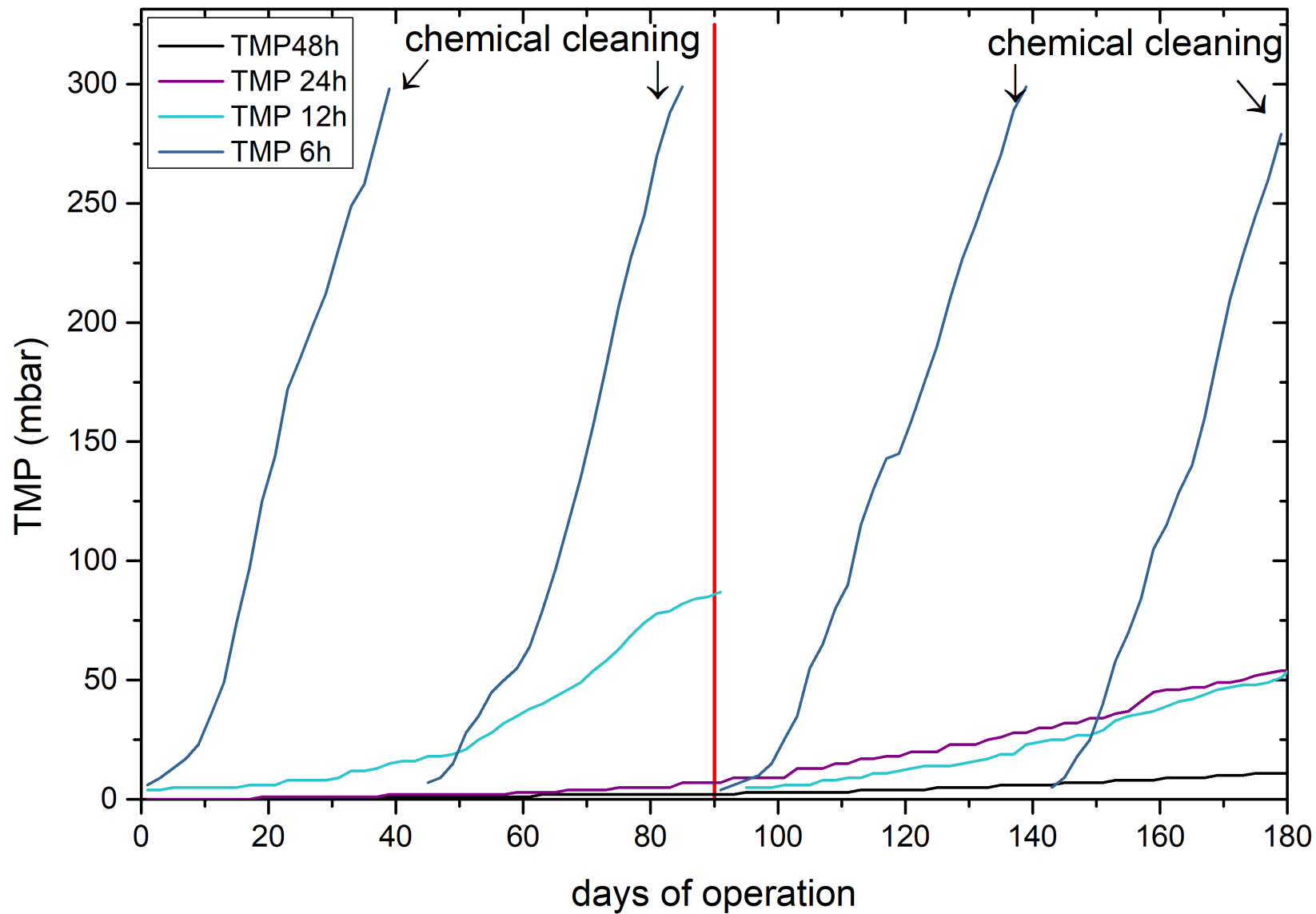
Figure 4. 41:AnMBR performance in terms of membrane fouling

From the TMP graph, it's clear that during the first two HRTs examined, chemical cleaning was not required. At an HRT of 2 days, TMP increase was negligible, while at an HRT of 1 day, TMP only increased to 50 mbar, well below the threshold value of 300 mbar. Due to the minimal increase, it wasn't possible to evaluate the impact of seasonal temperature variations between summer and winter.

In contrast, at an HRT of 12 hours, TMP reached 80 mbar during the first 90 days of operation and led to chemical cleaning before the summer period. During the subsequent summer period, TMP increased only to 50 mbar, showing better performance. However, upon further reducing the HRT, TMP showed a rapid increase, hitting the threshold of 300 mbar in approximately one month. During the summer, the membrane lasted for about 45 days. Despite these results, the scalability of AnMBR under these conditions is not feasible. Therefore, another chapter examines the addition of $FeCl_3$ to the system for phosphorus removal and potential mitigation of membrane fouling.

Figure 4.42 illustrates the AnMBR flat sheet membranes before and after chemical cleaning.

Figure 4. 42: Flat sheet membranes before (left) and after(right) chemical cleaning.

- ***VFAs concentration on different HRTs***

The major components of VFAs include acetic acid, propionic acid, butyric acid and iso-butyric acid. The components are mainly produced in the acidogenic phase of anaerobic digestion. Among these VFA components, acetic, propanoic and butyric acids are predominant during VFA production from the anaerobic process. According to literature, 65 to 95% of methane present in biogas is directly produced from butyric and acetic acid[304,508,509].
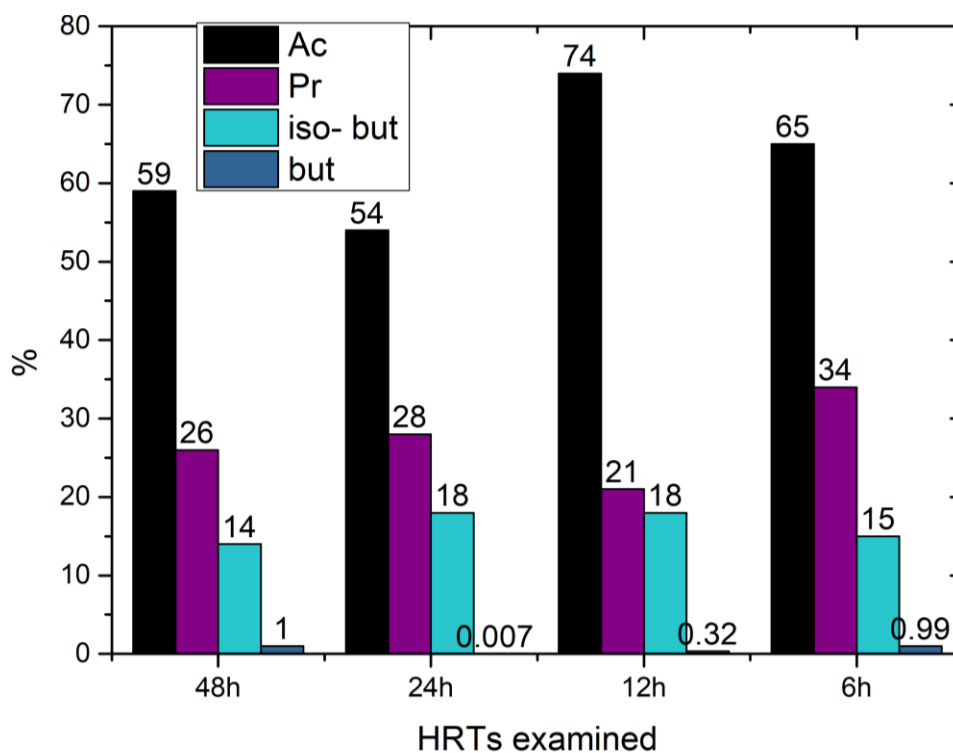
Figure 4. 43: VFAs concentration on different HRTs

During the experiment, it was noted that the concentration of the 4 VFAs measured, kept steady for the HRT of 48 h and 24 h and the 3 others (propionic isobutyric and butyric) also had very slow differences between the HRTs. However, concentration of acetic acid increased 20% more, at 12 hours HRT. At 6 hours it was still more but decreased a little. from, when the HRT was reduced from 48 hours to 24 hours. This shift in acetic acid concentration, particularly from 48 to 12 hours, suggests a change in microbial processes from methanogenesis to acidogenesis.

When the HRT was reduced from 48 hours to 6 hours, a progressive increase in the concentration of propionic acid was observed, with the only exception being at 12 hours. The peak concentration was recorded at the 6-hour HRT. Unlike acetic and butyric acids, propionic acid tends to remain in the final stages of anaerobic digestion due to its thermodynamically less favorable characteristics compared to the other two major VFAs [275]. Consequently, propionic acid accumulates in the bioreactor under conditions of high organic loading rates or shorter HRTs. Literature suggests that this specific VFA is a key factor in the rapid acidification observed in

anaerobic bioreactors, which can result in microbial stress, abrupt pH shifts, and reactor instability [510].

- ***Microbial communities on different HRTs and temperature variations***

The community structure of the microbial biocenosis was determined using fluorescence in situ hybridization (FISH). The specific oligonucleotide probes employed were EUB338 for Eubacteria (Cy3), ARC915 for Archaea (Cy3), MSMX860 for both *Methanosarcina and Methanosaeta,* MS821 specifically for *Methanosarcina,* and MG1200 for *Methanomicrobiales* (Cy3). The sequences for ten-methanogen group-specific probes, as well as those for two probes complementary to the 16S rRNAs of the Archaea (ARC915 and ARC344), are provided in Figure 4.44.

Probe	Sequence (5'–3')	Target site (E. coli numbering)	T_d (°C)
MC1109	GCAACATAGGGCACGGGTCT	1128–1109	55
MB314	GAACCTTGTCTCAGGTTCCATC*	335–314	
MB310	CTTGTCTCAGGTTCCATCTCCG	331–310	57
MB1174	TACCGTCGTCCACTCCTTCCTC	1195–1174	62
MG1200	CGGATAATTCGGGGCATGCTG	1220–1200	53
MSMX860	GGCTCGCTTCACGGCTTCCCT	880–860	60
MS1414	CTCACCCATACCTCACTCGGG	1434–1414	58
MS1242	GGGAGGGACCCATTGTCCCATT*	1263–1242	
MS821	CGCCATGCCTGACACCTAGCGAGC	844–821	60
MX825	TCGCACCGTGGCCGACACCTAGC	847–825	59
ARC915	GTGCTCCCCCGCCAATTCCT	934–915	56
ARC344	TCGCGCCTGCTGCICCCCGT	363–344	54

* underlined sequences indicate regions of internal complementarity

Figure 4. 44: Classification of methanogens (45) in relationship to the oligonucleotide probes characterized in this study. (Inset) Methanogenic- and Archaea-specific 16S rRNA probes with probe name, sequence, target site, and experimentally determined[511]

The structure of the microbial community is crucial for efficient methane production. Our research aims to understand the variations in the relative abundance of methanogenic communities across different HRTs and examined temperatures.

We selected these probes -described in Materials and Methods section- specifically to differentiate not just within the archaeal community, which comprises methanogens, but also to pinpoint the genus of these methanogens to determine if they are hydrogenotrophic or acetoclastic. Figures 4.45 and 4.46 depict the classification of methanogens/sulfate-reducing bacteria in relation to the oligonucleotide probes MSMX860 and SRB687.
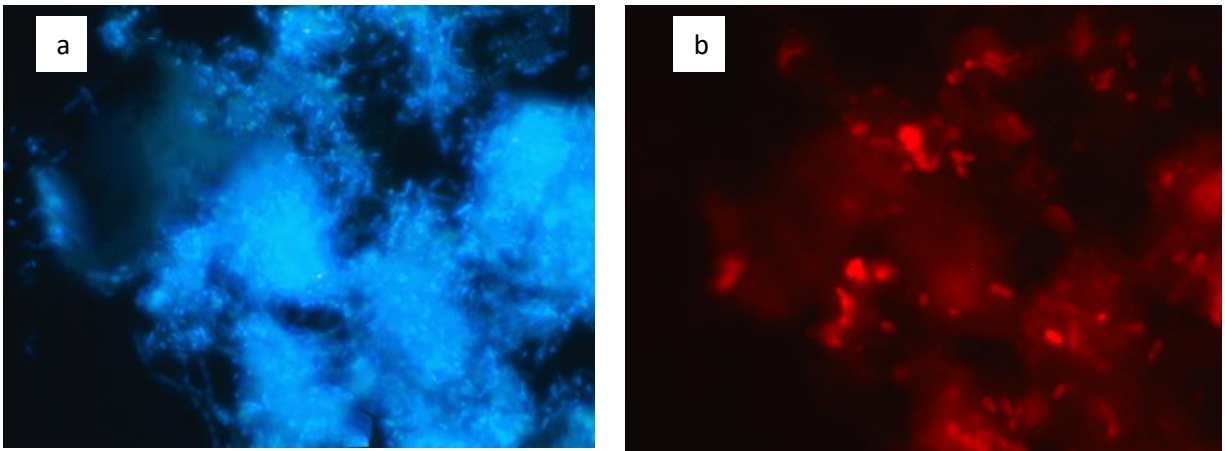
Figure 4. 45: FISH image of Methanosarcina & Methanosaeta for HRT 2 days, winter period (MSMX860) (a) DAPI and (b)Cy3
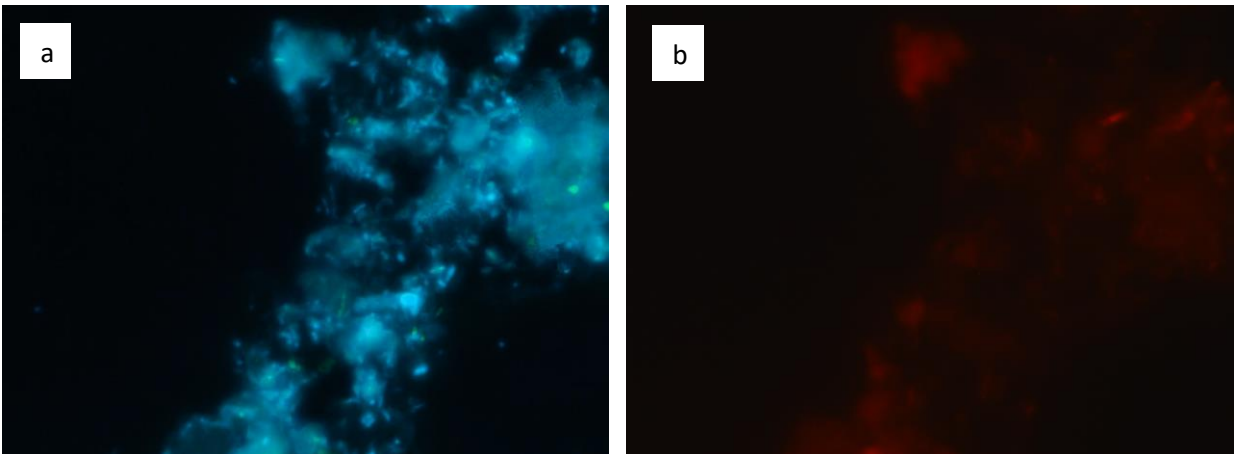
Figure 4. 46: FISH image of for sulphate reducing bacteria for HRT 2 days, winter period (SRB687) (a) DAPI and (b)Cy3

Results indicated minimal differences in microbial communities with variations in HRTs. However, a decrease in *Methanosaeta* was noted at a 6h HRT during the winter months. Specifically, the Archaea communities comprised 39 ± 6% of all microorganisms. Of this, 25% was attributed to both *Methanosarcina* and *Methanosaeta*. Given the probe specifically for *Methanosarcina* showed a very low percentage, this suggests that *Methanosaeta* was previously more dominant. Figure 4.47 below presents the relative abundance of specific methanogens within the archaeal communities.
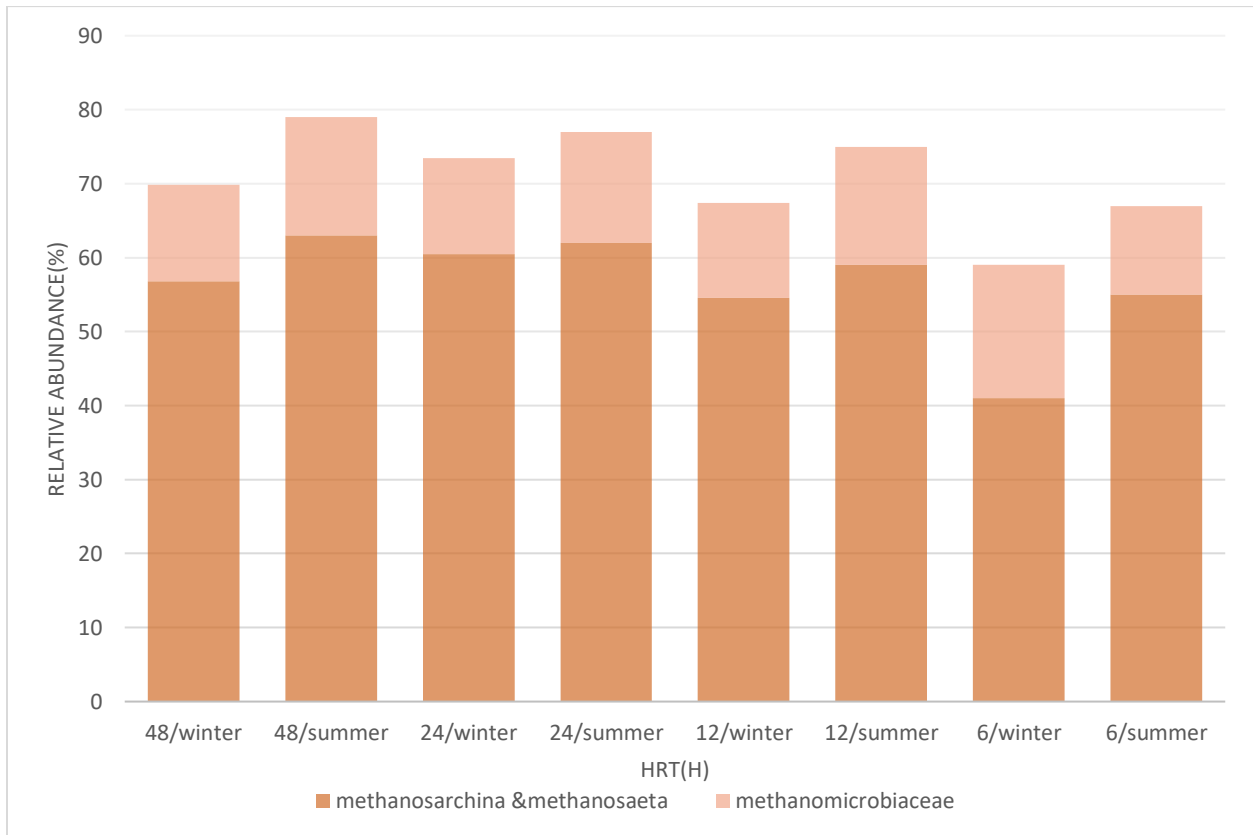
Figure 4. 47: Relative Abundance of Specific Methanogen Communities within Archaeal Communities.

The graph illustrates that the dominant genus within the archaeal community was *Methanosaeta,* followed closely by the hydrogenotrophic family, *Methanomicrobiaceae*. The proportion of acetotrophic methanogens, specifically *Methanosaeta*, decreased from an average of 59% ± 3 across all HRTs and temperatures, to 41% in winter at an HRT of 6 h. Regardless of changes in HRT, *Methanosaeta*, an acetotrophic methanogen, consistently emerged as the dominant

participant. Sulphate-reducing bacteria were present in such low percentages that they weren't accounted (Figure 4.46).

Methanosaeta, an acetotrophic methanogen, is capable of converting acetic acid into methane and CO_2, a process that accounts for approximately 70% of methane production[12]. The presence of *Methanosaeta* typically correlates with a higher methane yield, so an increased relative abundance of *Methanosaeta* suggests conditions conducive to methane production[12]. Furthermore, *Methanosaeta* often dominates over other acetoclastic methanogens, such as *Methanosarcina,* especially at particular temperatures, due to its competitive edge.

However, with decreasing temperatures, there's a shift in the dynamics of methanogenic dominance. Under psychrophilic conditions, generally below 20°C, the acetoclastic methanogenic pathway might become thermodynamically less preferred, leading hydrogenotrophic methanogens to potentially take a more dominant role.

4.4 Comprehensive Analysis of COD Mass Balance and System Performance

Figure 4.48 illustrates the COD mass balance for each HRT investigated, considering seasonal variations. The data presented in the graph are derived from calculations involving the COD levels at the system inlet and all the system outlets. These outlets include the permeate water, excess sludge, generated biogas, dissolved methane in the effluent, as well as the COD consumed by sulfate-reducing bacteria (SRBs). Below you can find the COD mass balance equation used:

$$COD\ in \cdot Qin = COD\ out\ \cdot Qout + COD\ biogas + COD\ sludge\ \cdot Q\ sludge + COD\ SO4\ \cdot Qout$$

Steps:

1. <u>Measure Influent and Effluent COD:</u> COD in x Qin and CODout × Qout
2. <u>Measure or Estimate Sludge COD:</u> CODsludge×Qsludge.
3. <u>Biogas Measurements:</u> Measure the biogas production rate and its composition (mainly methane CH_4 and carbon dioxide CO_2).

4. <u>Calculate Gaseous COD</u>: Convert the volume or energy content of the biogas to a COD equivalent.
5. <u>Calculate Dissolved Biogas</u>: In our system there was a lot of methane that was lost in the effluent. That's why this calculation is very important.
6. <u>Calculate COD SO_4</u> : From a stoichiometric standpoint, the relationship between COD and sulfate ion concentration can be defined as follows:

$$COD_{SO4} = 0.67 \cdot SO_4{}^{2-}$$
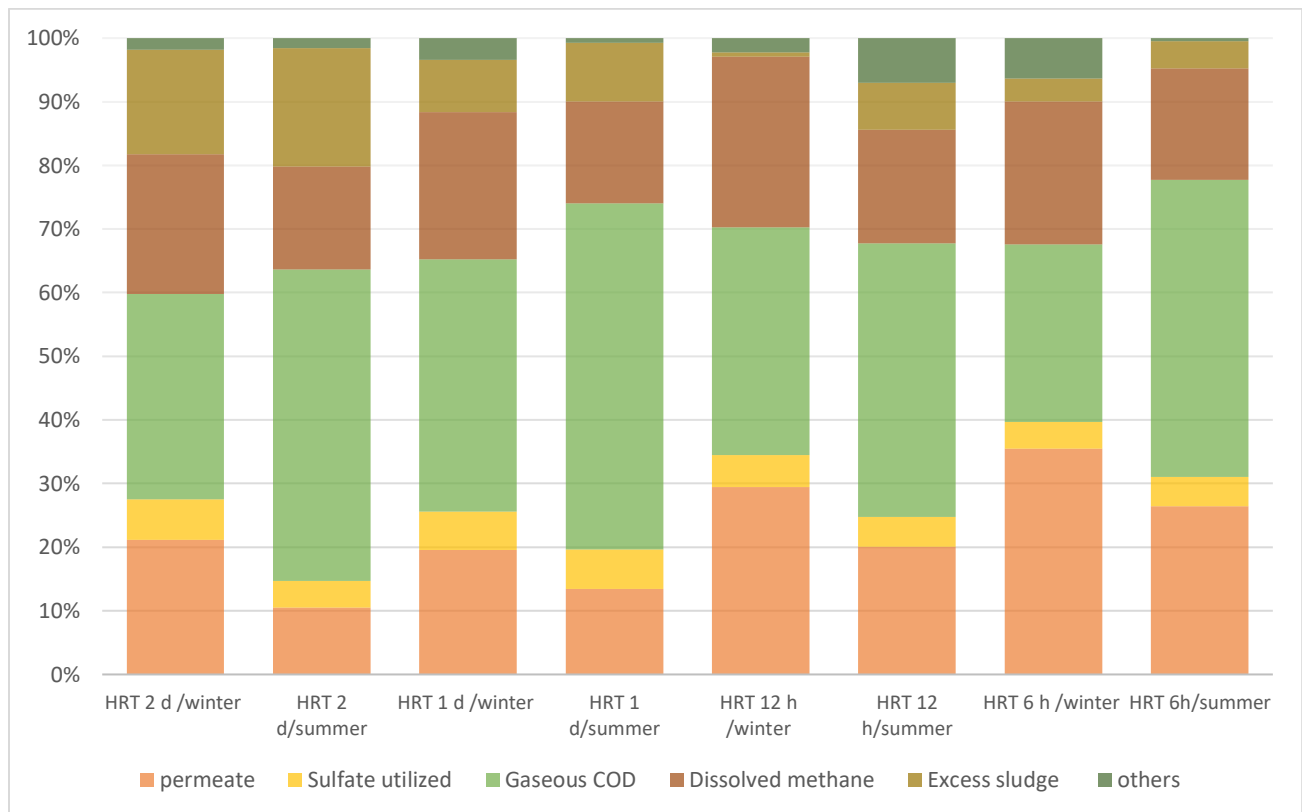
Figure 4. 48: Evaluating COD Mass Balance in the different HRTs examined.

It should be underlined that throughout the experiments the COD mass balances based on the average values, account for almost all the influent COD with a difference that varies between 1% - 9%. This finding indicates that the processes included in the mass balance are a very accurate approximation of the real conditions in the AnMBR.

In most scenarios examined, the COD mass balance demonstrates a close approximation to equilibrium. However, noteworthy small deviations are primarily observed during the winter

season with a HRT of 12 hours, and during the summer season when the HRT is configured to 6 hours.

In all winter scenarios examined, gaseous COD constitutes approximately 30% of the total. The sole exception occurs in the 6-hour HRT scenario, where it accounts for only 20% due to suboptimal organic removal. Additionally, dissolved CH_4 comprises a significant 20% in winter scenarios. This poses a critical consideration for effective AnMBR implementation, necessitating the development of strategies for the extraction of this substantial CH_4 fraction. Notably, during the summer period, dissolved CH_4 continues to represent an elevated proportion, exceeding.

- VFAs and COD correlation

The dynamic equilibrium of the system is evident from the concentration of VFAs in relation to the concentration of dissolved COD. Figures 4.49 and 4.50 present the concentrations of COD and VFAs for all the HRTs and the temperature ranges.
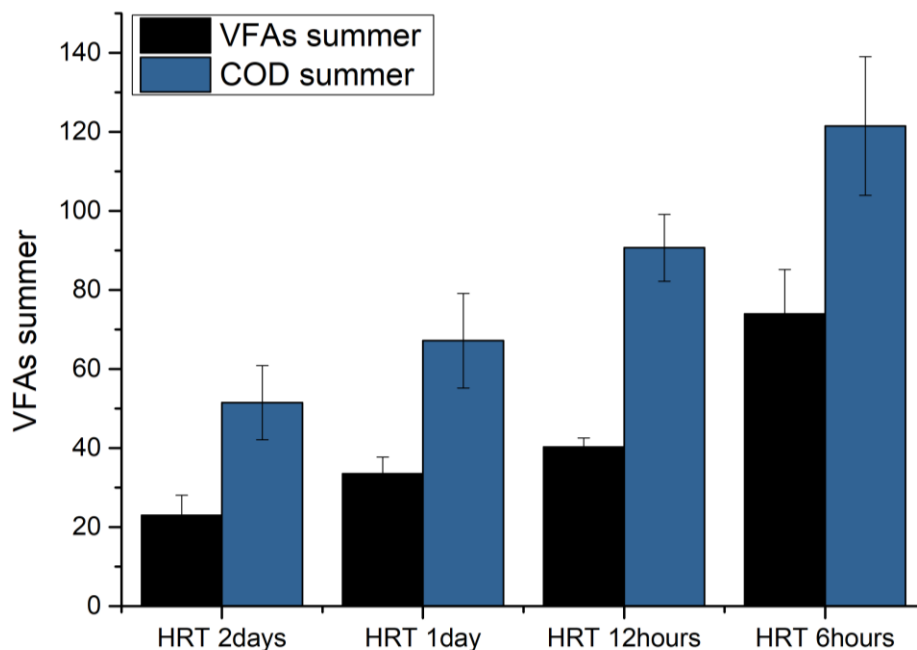
Figure 4. 49: VFAs and COD concentrations during summer period in all the HRTs examined.
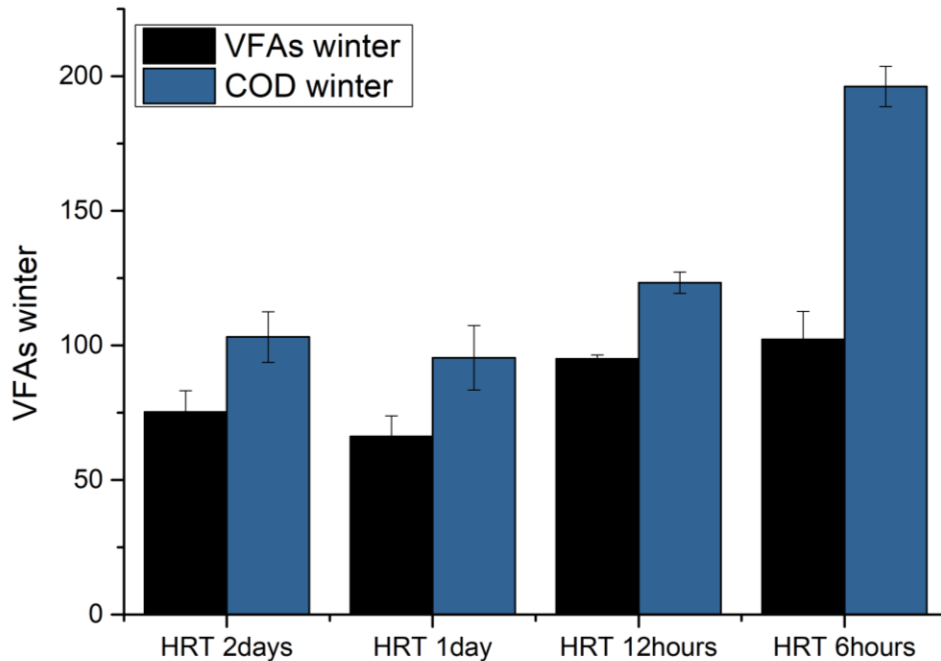
Figure 4. 50: VFAs and COD concentrations during winter period in all the HRTs examined.

The mean concentration of VFAs and its statistical correlation with dissolved COD in the control reactors serve as reliable indicators of a dynamically stable system. Specifically, this dynamic equilibrium in the production and consumption of VFAs suggests optimal reactor performance.

4.5 Water quality regulations for safe permeate disposal and potential water reuse.

Policy related information regarding existing water reuse and disposal regulation imposed in Greece and specifically in the reclaimed water, was collected. The objective was to ensure that all regulatory aspects will be recognized.

In May 2018, the European Commission put forward a proposal for a regulation setting EU-wide standards that reclaimed water would need to meet to be used for agricultural irrigation, with the aim of encouraging greater use of reclaimed water and contributing to alleviating water scarcity. The European Parliament adopted its first-reading position on 12 February 2019, and the Council agreed on a general approach on 26 June 2019. Trilogue negotiations concluded with a provisional agreement on 2 December. The agreed text, endorsed by the ENVI committee on 21 January 2020, was adopted at first reading by the Council on 7 April. It was then returned to the

Parliament for final adoption at second reading (EU 2020/7411). Until this Regulation, water reuse was identified and encouraged in provisions of two existing EU instruments, which however do not specify conditions for the reuse that are applied in the European Commission:

1. The Water Framework Directive (2000/60/EC, WFD2), which mentions water reuse as one of the possible supplementary measures to be included in the programmes of measures for each river basin; and

2. The Urban Wastewater Treatment Directive (91/271/EEC, UWWTD3) which provides that treated wastewater shall be reused whenever appropriate while the disposal routes shall minimize the adverse effects on the environment.

To evaluate adherence to UWWTD guidelines, Figure 4.51 extends the analysis by showcasing COD permeate concentrations during both winter and summer for the HRTs studied. The figure also plots these values against the 125 mg/L threshold specified by the UWWTD, offering a comprehensive view of regulatory compliance. It should be underlined that according to the Regulation (EU) 2020/741 of the European Parliament and of the Council (25 May 2020) on minimum requirements for water reuse, the same standards that are applied for wastewater disposal, are required for reclaimed wastewater quality class B, C and D.
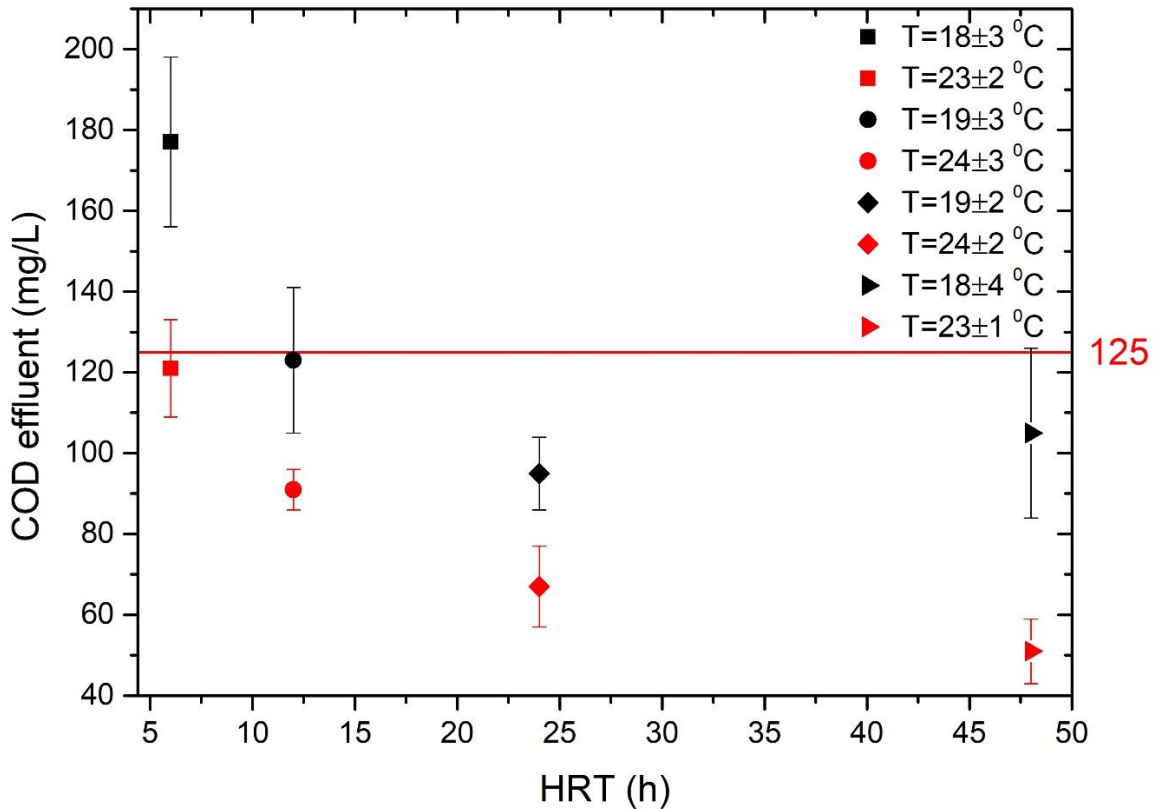
Figure 4. 51: COD Permeate Levels Across 4 HRTs examined: UWWTD Compliance

The findings presented in Figure 4.51 show that for the 24 h and 48 h HRTs, the effluent COD values were consistently below the UWWTD limit of 125 mg/L, and the requirements for wastewater reuse in agriculture, during both winter and summer periods. However, for the 12 - hour HRT during the summer season, the values met the required criteria, while during winter, some of the values exceeded the set limit. Moreover, for the 6-hour HRT, even during the summer period, some values exceeded the limit, and during the winter season, all values were considerably higher than the 125 mg/L threshold. Based on the findings discussed, it can be concluded that for future scaling up of this technology, the optimal HRT would be 12 h during the summer period and 24 h during the winter period. By operating under these conditions, the effluent COD values would meet the standards set by the UWWTD.

Throughout all operational periods, effluent concentrations of Total Nitrogen (TN) and Total Phosphorus (TP) remained largely consistent. In practice, nutrient removal was minimal and occurred solely due to sludge yield. As anticipated in anaerobic processes, nutrient removal is primarily constrained to biomass growth and falls short of meeting standard nutrient removal

requirements. Therefore, the permeate from the AnMBR requires additional treatment to achieve the regulatory limits of 10-15 mg/L for TN and 1-2 mg/L for TP.

4.6 Investigation of the effect of adding iron (III) chloride on the performance of the Membrane Anaerobic Bioreactor

4.6.1 AnMBR Performance with Iron Addition

The previously discussed findings highlighted the challenges encountered by the AnMBR system operating at a 6h HRT during the winter period, primarily characterized by inadequate organic load removal and elevated membrane fouling rates compared to other HRTs and the data from summer operations. To mitigate these issues, iron was introduced into the system in concentrations of 25 and 30 mg $FeCl_3$ L^{-1}.

Prior to the integration of iron, detailed lab-scale experiments were undertaken to study the influence of varied iron doses on the system. Biomass from the AnMBR was used for these investigative trials. The early set of experiments delved into the impacts of higher iron concentrations, namely 100 and 200 mg of $FeCl_3$/L, followed by another set exploring the repercussions of lower concentrations, 20 and 40 mg of $FeCl_3$/L. Figures 4.48 and 4.49 effectively encapsulate the outcomes of these series, shedding light on how different iron concentrations affect the system.

This series of preliminary experiments were instrumental in deciphering the optimal iron concentrations to counter the operational challenges faced by the AnMBR system during the colder months.
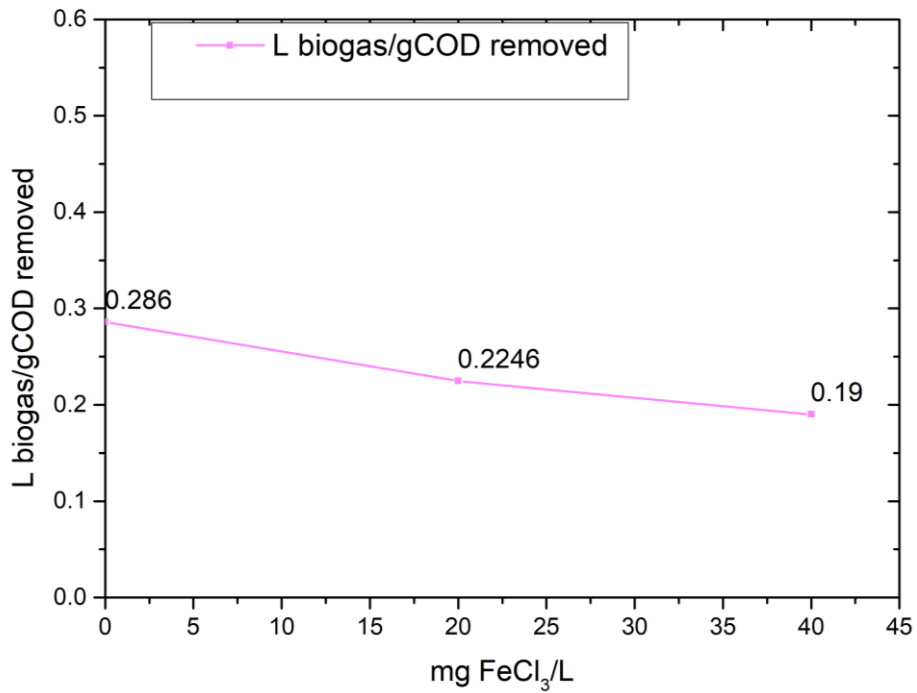
Figure 4. 52: Batch experiments with addiction of 20 and 40 mg FeCL3 /L
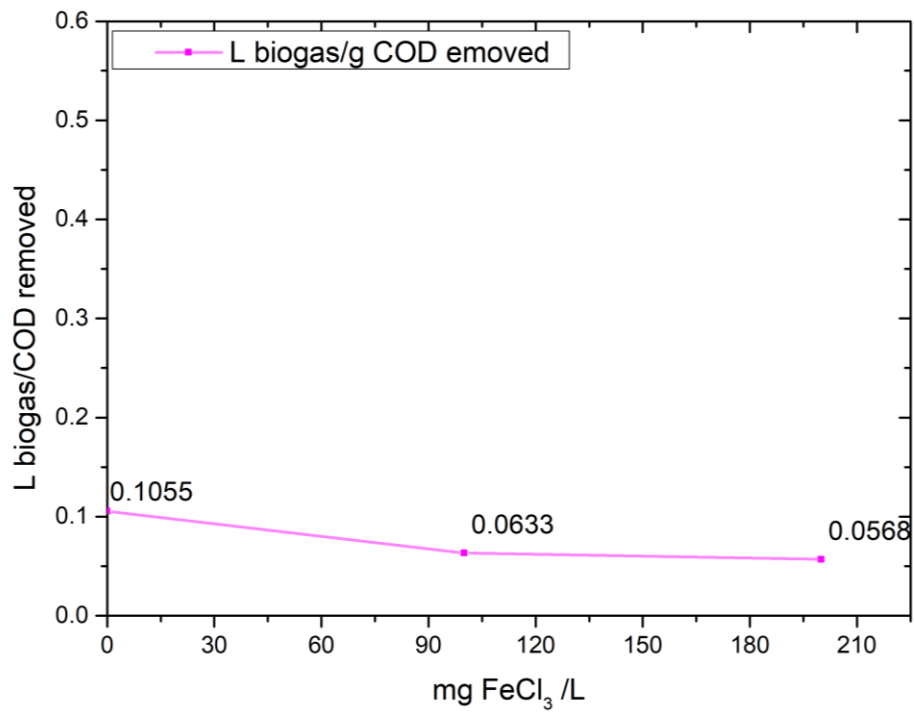
Figure 4. 53:Batch experiments with addiction of 100 and 200 mg FeCL3/L

Figure 4.49 delineates the diverse impacts of $FeCl_3$ concentrations on biogas production. A dose of 20 mg $FeCl_3$/L appeared to have no detrimental impact on biogas production, while 40 mg $FeCl_3$/L induced a slight reduction. When the concentrations were increased to 100 mg $FeCl_3$/L and 200 mg $FeCl_3$/L, biogas production experienced significant decrement, with the methanogenesis process particularly disrupted at these levels.

Due to the observed impacts of these varied concentrations, specific doses of 25 and 30 mg $FeCl_3$/L were selected for more focused examination on their effects on the system. The performance of the bioprocess was once more evaluated, focusing on effluent quality, membrane fouling, and biogas production. Table 4.8 consolidates the mean concentrations of COD, VFAs, biogas production, TN, and TP, along with the associated removal efficiencies in both untreated and treated effluent. These efficiencies provided crucial insights, helping to quantify the effect of $FeCl_3$ addition on the overall efficacy of the AnMBR system's treatment processes.

The average effluent concentration of COD was 177 mg/L without $FeCl_3$ addition, while with 25 mg $FeCl_3$ L^{-1} and 30 mg $FeCl_3$ L^{-1}, COD decreased to 147 mg/L and 149 mg/L, respectively (Figures 4.50, 4.51), still not complying with the respective UWWTD limit. Another noteworthy observation is that the addition of iron chloride resulted in a halving of the standard deviation in the effluent, indicating a more stable and consistent profile in the treatment process.

TP removal efficiencies obtained at 30 mg $FeCl_3$ L^{-1} and 25 mg $FeCl_3$ L^{-1} were 100% and 75%, respectively. The results suggest that the addition of $FeCl_3$ had a significant effect on the COD and P removal. It is anticipated that some of the soluble organic matter was coagulated and formed flocs that were retained by the membrane in the reactor.

Table 4. 8: Average concentrations (±SD) for influent and effluent quality parameters with and without $FeCl_3$ addition.

Parameter	HRT 6 h Winter Period Dose = 0	HRT 6 h Winter Period Dose = 25 Fe $^{3+}$/L	HRT 6 h Winter Period Dose = 30 Fe $^{3+}$/L
COD in (mg L^{-1})	490 ± 38	501 ± 44	485 ± 34
COD out (mg L^{-1})	177 ± 18	147 ± 8	149 ± 11
COD rem (%)	60 ± 4	69 ± 2	66 ± 3
Operating temperature	18.3 ± 3	18.7 ± 2	19.1 ± 3
VFAs (mgCOD L^{-1})	92 ± 7	80 ± 6	85 ± 8
MLSS (mg L^{-1})	6180	7050	7600
Biogas production (L day^{-1})	11.41 ± 3.1	10.7 ± 2.2	10.5 ± 2
TN in (mg L^{-1})	69 ± 46	71 ± 3	68 ± 2
TN out (mg L^{-1})	67 ± 5	72 ± 4	73 ± 3
TP in (mg L^{-1})	8.24 ± 2	8.35 ± 2.4	9.21 ± 3

Parameter	HRT 6 h Winter Period Dose = 0	HRT 6 h Winter Period Dose = 25 Fe $^{3+}$/L	HRT 6 h Winter Period Dose = 30 Fe $^{3+}$/L
TP out (mg L^{-1})	8.5 ± 1.7	2.25 ± 2.3	0.5 ± 0.7
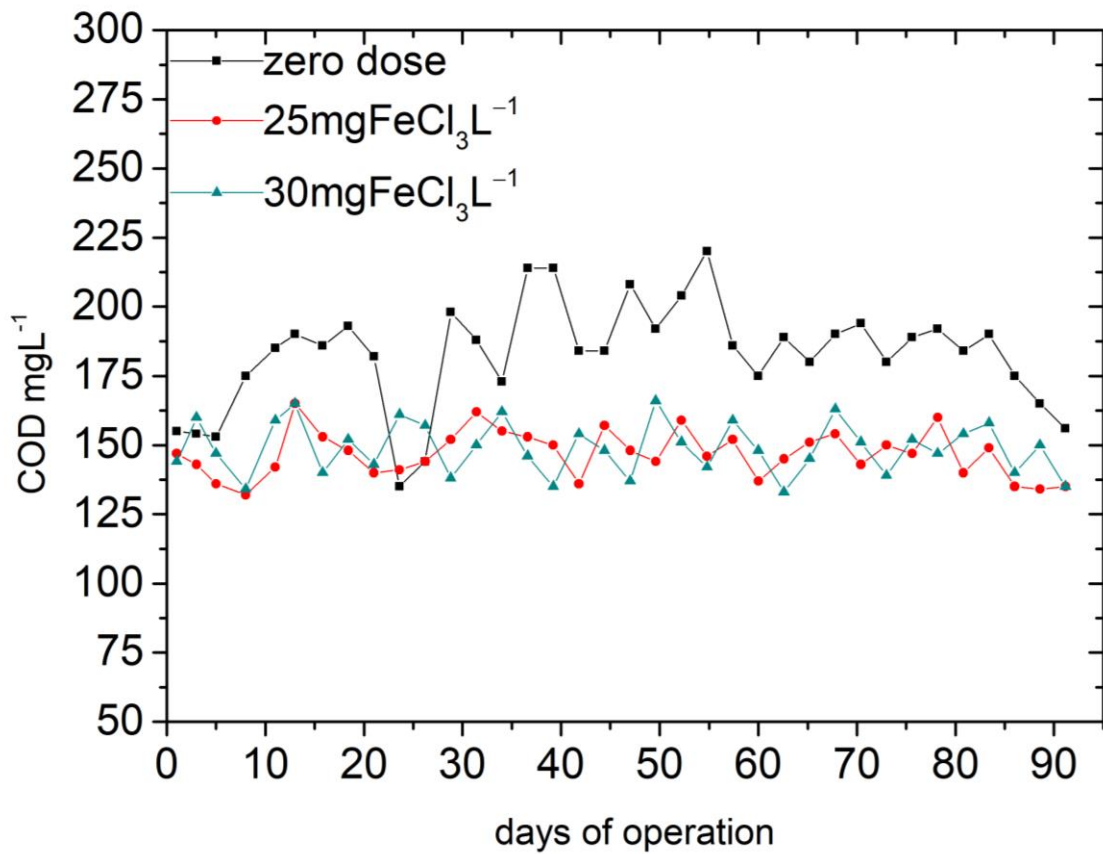
Figure 4. 54:COD permeate profile for the 2 iron doses examined.
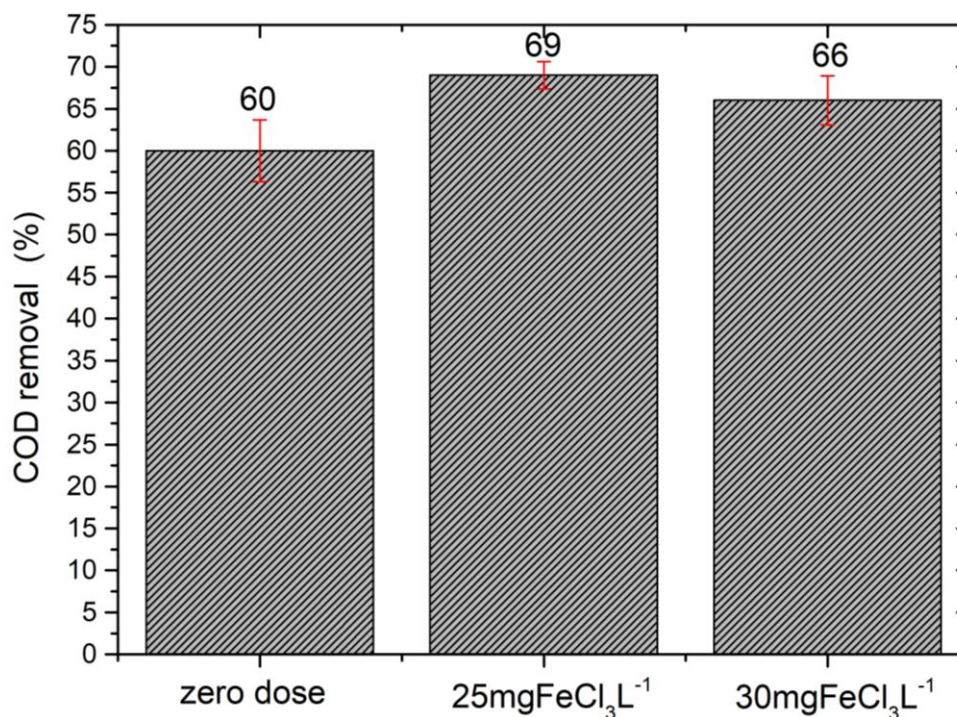
Figure 4. 55:COD percent removal for the two iron doses.

In addition, as shown in Table 4.8, iron addition resulted in increased MLSS concentrations due to chemical P removal and the formation of iron phosphate salts. The analysis revealed a 20% increase in the value of MLSS due to iron addition. This finding highlights a potential environmental problem regarding the formation of ferric-rich sludge, which could restrict disposal or reuse alternatives [512,513]. Furthermore, due to iron addition, membrane fouling was mitigated. As reported in [514,515], coagulant addition introduces positive charges, neutralizing the negative charge of activated sludge flocs and thus favoring flocculation and reduction of colloidal matter. The addition of ferric chloride concentrations of 25 and 30 mg $FeCl_3$ L^{-1} significantly lowered the biomass pH to 6.7 and 6.6, respectively. It is expected that higher ferric doses will require pH adjustment in order to avoid unacceptably low values that would inhibit bio-mass growth.

Biogas production decreased slightly with the addition of $FeCl_3$, while methane content also decreased from 69% to 67%. The energy and mixing needs of the AnMBR can be met by methane production and pumping, which may contribute to the sustainability of the AnMBR [514]. However, Fe^{3+} addition can theoretically reduce methane production by (i) binding organic material or (ii) acting as an external electron acceptor. In our case, bio-gas production decreased only slightly

due to FeCl$_3$ addition. It can be concluded that FeCl$_3$ addition, at the dosages studied, does not inhibit the activity of methanogens, or significantly reduce the availability of organic material.

Previous AnMBR studies have shown that methane yield decreased from 102 ± 29 mL CH$_4$/g COD to 91 ± 37.8 mL CH$_4$/g COD when fed with a dose of 26 mg/L FeCl$_3$ [351]. Therefore, no significant effect on biogas production occurred. However, at higher iron dosages, methane yield decreased from 0.167 ± 0.017 g CH$_4$ as COD/g COD feed to about 0.079 gCH$_4$ as COD/g COD feed with the addition of 43 mg/L FeCl$_3$ [351]. Therefore, FeCl$_3$ dosage should be carefully considered as it may affect biogas production.

4.6.2 Evaluation of Membrane Performance: Comparative Analysis with and without Iron Addition

The outcomes of this study are presented for the winter season, during which the operational temperature was maintained at 18 °C ± 3, utilizing two distinct dosages of iron. As is already said in previous chapter, membrane utilized in the AnMBR had a manufacturer-designated upper pressure limit of 300 mbar as a protective measure. The differences in the fouling rates of zero-iron dose, 25 mg FeCl$_3$ L^{-1} and 30 mg FeCl$_3$ L^{-1} iron dose were evaluated by monitoring the TMP changes over time. TMP values were employed to characterize fouling since the AnMBR was operated at a constant flux of 13 LMH.

TMP showed a slight improvement upon FeCl$_3$ addition, but no further improvement upon increasing iron dose (Figure 4.56) was observed. The TMP after approximately 40 days of operation with iron addition did not reach 300 mbar TMP (value initiating chemical cleaning), which means that membrane operation time can be extended without chemical cleaning, resulting in AnMBR operation improvement.

The analysis indicated that during the initial 15 days, the TMP experienced an increase at a rate of 10 mbar/day for the zero-iron dose, while the other two doses, with iron, manifested nearly identical rates of around 9 mbar/day. This demonstrates that the rates of increase for these two doses were comparable.

However, between days 20 and 40, the rates at which the TMP increased for both iron doses were substantially lower than the rate for the zero-iron dose. Post the chemical cleaning process, the TMP ascended at a reduced rate for all doses, including the zero-iron one, indicating a uniform

rate of increase across all doses. Nonetheless, in the concluding 20 days, the rate of increase for the zero-iron dose escalated significantly more than the iron doses.

These findings imply that the incorporation of iron does influence the rate at which TMP increases, with the zero-iron dose showing the most substantial rise throughout the duration of the study. Another critical observation is that augmented iron concentrations did not yield any additional improvements, revealing a saturation point beyond which increased iron levels do not enhance performance or efficiency.
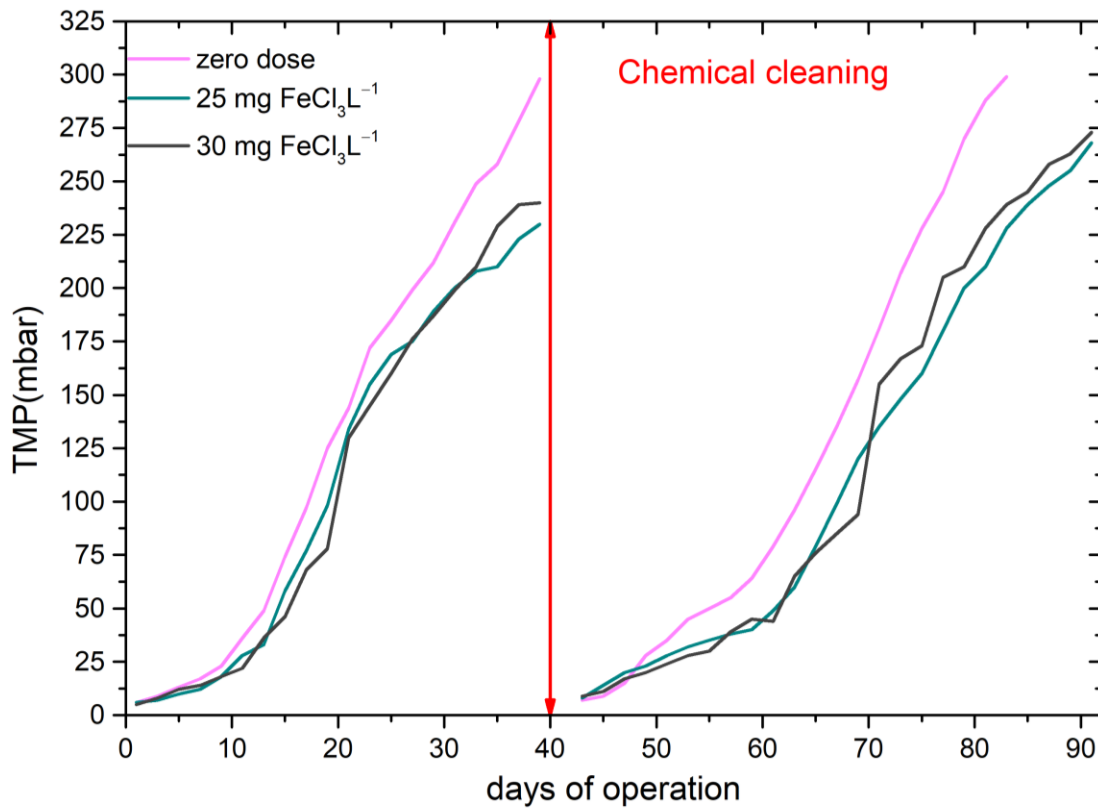
Figure 4. 56: Analysis of TMP Profiles with and without FeCl₃ Addition during the Winter Period

In another study, carried out with the addition of FeCl$_3$, there was again a reduction in the TMP value [516]. More specifically, the absence of FeCl$_3$ resulted in an initial TMP range of 5.7–6.3 kPa for 45 days, which subsequently increased to 21.5 kPa by day 91. In contrast, when FeCl$_3$ was added, TMP values were initially in the range of 1.5–5.1 kPa for 75 days, followed by an increase to 8.8 kPa on day 90.

4.6.3 Micropollutant removal with and without iron addition

Micropollutant removal investigation was conducted at a 25 mg $FeCl_3$ L^{-1} dose, as this dose provided the most satisfactory results regarding membrane fouling mitigation and organic load removal. The removal of micropollutants in wastewater treatment is mainly due to biosorption and biotransformation. In AnMBR systems, biotransformation removal outweighs sludge sorption, especially at long SRTs [277]. The high SRT increases the efficiency of the removal of micropollutants, as it increases the exposure time to the slowly growing anaerobic microbial populations [517].

In our study, the effect of iron addition on micropollutant removal in the AnMBR was investigated by monitoring influent and effluent micropollutant concentrations. Specifically, seven organic micropollutants—nonyphenol (NP), triclosan (TCS), and bisphenol A (BPA) from the EDC group and ibuprofen (IBU), naproxen (NPX), diclofenac (DCF), and ketoprofen (KTP) from the NSAID category—were measured with 25 $FeCl_3$ mg/L and without iron addition. The results of the removal efficiency for the target compounds are shown in Figure 4.57.
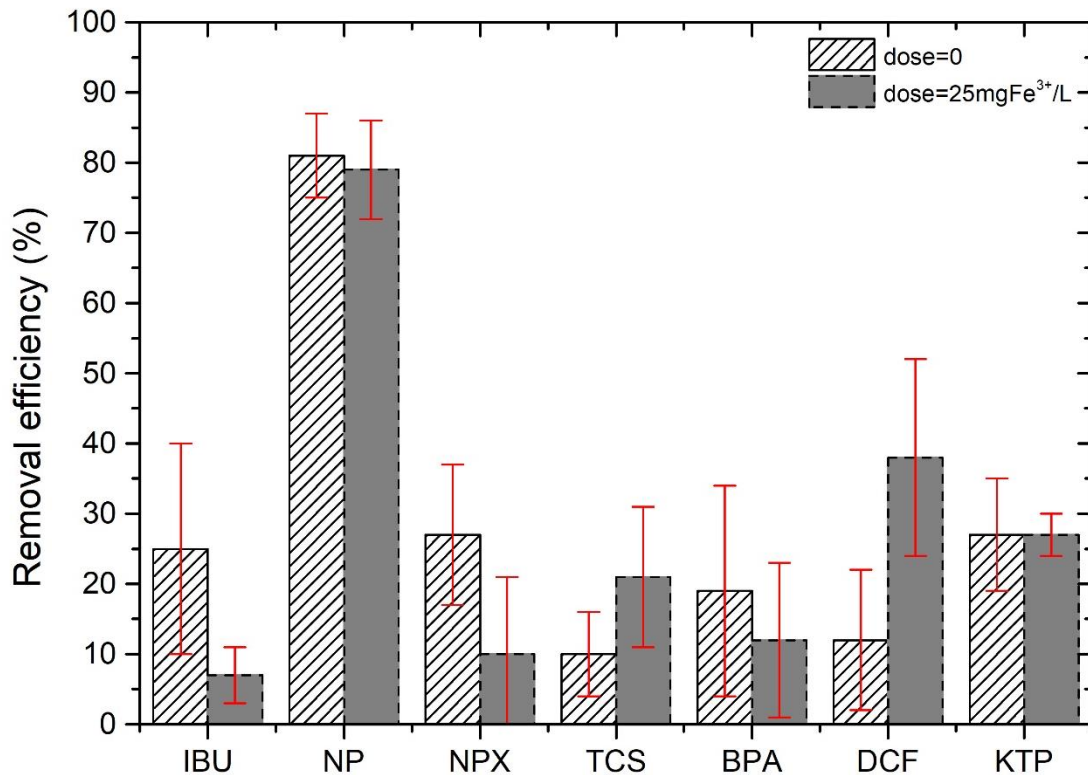
Figure 4. 57: Removal efficiencies of 7 micropollutants with and without iron addition.

The results revealed that iron addition enhanced the removal of TCS and DCF, while the removal of IBU, NPX, and BPA appeared to improve in the absence of iron. For the remaining compounds (NP, KTP) the effect of iron on their removal seems to be insignificant. The overall efficiency of the system is that it can achieve high nonylphenol removal efficiency with and without iron addition, while removal of other target compounds remains low to moderate. The high NP removal obtained can be associated with its high hydrophobic–lipophilic nature (logKow = 5.76) with a high affinity for sorption (logKoc = 3.1) and bioaccumulation. Thus, both the sorption into the sludge and the anaerobic degradation seem to play a crucial role in the eradication of NP [518], while iron seems not to have a significant effect. KTP removal was on average 27%, consistent with other removals recorded in the literature [318,519], while biotransformation was presented as the primary removal mechanism. The poor removal performance of AnMBR systems for ibuprofen and diclofenac has also been reported by others [318]. The enhanced removal of diclofenac in our system when $FeCl_3$ is supplied to the reactor could be attributed to sorption into ferric complexes formed in the presence of water molecules and hydroxyls under anaerobic conditions. These complexes are trapped in the reactor by precipitation or by retainment by the membrane. Other researchers claim that although the biodegradability of DCF under anaerobic conditions is low, it is the primary removal mechanism [277], while others [519] support that biodegradation is negligible and low adsorption on sludge occurs. According to the results of this study, it was confirmed that TCS degradation is low under anaerobic conditions and the observed removal can be attributed both to sorption and biodegradation, which remained low with iron addition. Others also report adsorption as the major removal mechanism in an AnMBR system, though only at the early stages of the experiments [277]. Accumulation in sludge has also been reported for target hydrophobic compounds (BPA, TCS, NP), but biodegradation is suggested as the main removal mechanism [520].

As aforementioned, the anaerobic treatment seemed less effective compared to aerobic, for most of the target compounds (BPA, TCS, IBU, KFN, DCF), which is also reported by others in the literature [277,318,521,522].Aerobic treatment (CAS, MBR) has been reported to be quite effective for the removal of almost all the target compounds (NP, BPA, TCS, IBU, NPX, KFN) [519,521–524]. Evidently, as far as DCF is concerned, it should be noted that even though its biodegradation is poor under aerobic and anaerobic environments, it could be enhanced through the combination of anoxic–oxic processes [521]. Even though the physiochemical properties, such as molecular weight, ring structure, and functional groups, influence biodegradability and govern the removal of each pollutant, especially for those with low hydrophobicity, the biotransformation of the

compounds is highly influenced by the redox conditions since the variety of microbial communities and metabolic pathways, as well as microbial activity, are driven by them [26,70]. As such, the rapid metabolism of aerobic bacteria and the short biodegradation pathway of organic matter during aerobic treatment are possible explanations for the enhanced removal, as reported in other studies [230]. In addition, the sorption mechanism is another factor to take into consideration, especially for the more hydrophobic CECs, because it results in a much higher retention time in the reactor. Therefore, according to the literature [318,523], the higher biodegradation obtained under aerobic conditions is partly attributed to increased sorption to biosolids due to smaller floc size which enhances mass transfer by diffusion.

4.7 Comparative Energy Consumption Analysis: AnMBR versus Traditional Aerobic Activated Sludge System

Wastewater treatment can contribute in the conservation of our freshwater resources and reduce the effects of climate change. It is essential to consider the energy use of WWTPs, as it affects both the environment and operating costs. This emphasis on energy-efficient wastewater treatment is highlighted by the proposal to revise the Urban Wastewater Treatment Directive (UWWTD) 91/271/EEC, which underscores the global shift towards energy-neutral urban wastewater treatment—a testament to our collective drive for a sustainable future ((https://environment.ec.europa.eu/publications/proposal-revised-urban-wastewater-treatment-directive accessed on 13 March 2023).

The data from Greek WWTPs provides insightful benchmarks in this realm. On average, these facilities consume electrical energy of around 38 kWh per Population Equivalent (PE) annually, with figures ranging from 15 to 86 kWh/PE. In terms of environmental impact, these plants emit between 61 and 161 kg CO_2 equivalent per PE annually. Between 40-70% of a plant's energy consumption is used for aeration, highlighting areas for potential energy savings. [107,433].

Given this context, there is a growing interest in AnMBRs. Due to their energy production and resource recovery capabilities, AnMBRs align well with the principles of circular economy. Figure 4.58 depicts the energy dynamics of a traditional activated sludge system in comparison to an AnMBR, with data sourced from the literature. On one hand, the traditional system, evident on the left, is particularly energy-intensive in its aerobic treatment phase, consuming 0.4 kWh/m³. In some cases energy is recoved only through the anaerobic digestion stage which produces energy, generating 0.15 kWh/m³ from biogas[166].

In contrast, the AnMBR system, depicted on the right, stands out with its energy efficiency. Utilizing a mere 0.23 kWh/m³ for its operational processes, it further underscores its energy-efficient profile by yielding 1 kWh/m³ of biogas. [525].
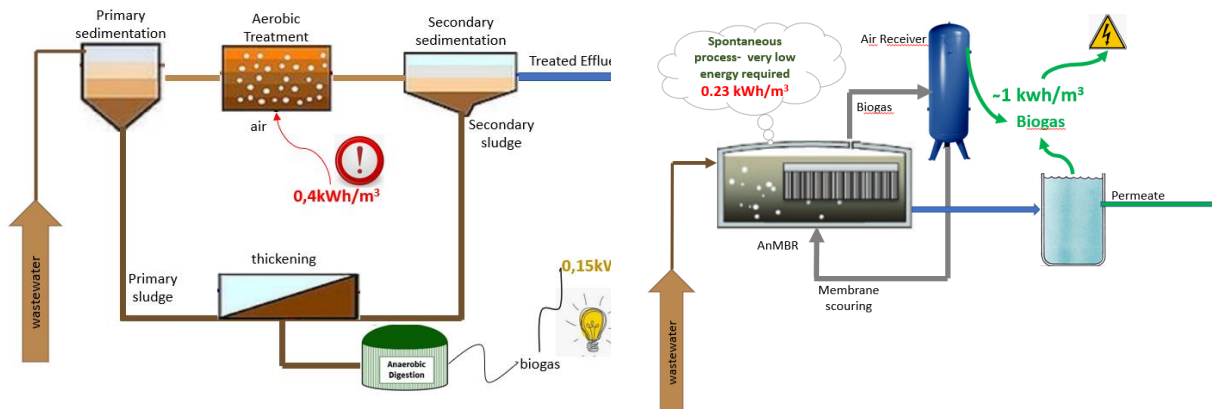
Figure 4. 58: Comparison of energy consumption and production between a)a conventional Wastewater Treatment Plant and b) an AnMBR system.

In order to further evaluate the energy efficiency of AnMBR, we conducted an energy balance according to the results obtained from the operation of the lab-scale AnMBR throughout this investigation. Table 4.9 and Figure 4.59 illustrates the energy production derived from methane generation in our lab-scale biogas system across all examined HRTs. The total energy content of CH_4 (both thermal and electrical) was computed utilizing a conversion factor of 0.222 kWh per mole of CH_4[526].

Table 4. 9: Analysis of Energy Production Based on HRTs examined and Season variations

	HRT 2 days	HRT 1 day	HRT 12h	HRT 6h
Winter				
Methane Production (L/d) *	1.1	2.7	4.19	7.8
Energy (kWh/day)	0.011	0.027	0.04	0.078
Energy (kWh/m³)	0.55	0.67	0.52	0.48
Total methane (L/d) **	1.85	4.27	7.31	14.07
Energy for total methane(kWh/m³) ***	0.92	1.09	0.66	0.68
Energy (kWh/KgCOD rem) ***	1.6	2.3	1.5	1.7
Summer				
Methane Production *(L/d)	1.7	3.8	5.4	12

	HRT 2 days	HRT 1 day	HRT 12h	HRT 6h
Energy (kWh/day)	0.017	0.038	0.053	0.12
Energy (kWh/m³)	0.84	0.94	0.67	0.74
*Total methane**(L/d)*	2.26	4.92	7.64	16.5
Energy for total methane(kWh/m³)	1.12	1.22	0.95	1.03
*Energy (kWh/KgCOD rem) ****	2	2.5	1.8	2.3

*Refers to gaseous methane production.

**Denotes the combined total of gaseous methane and the dissolved methane present in the effluent, highlighting the potential energy if the dissolved methane was captured and utilized.

*** Refers to the energy (thermal and electrical) from gaseous methane.
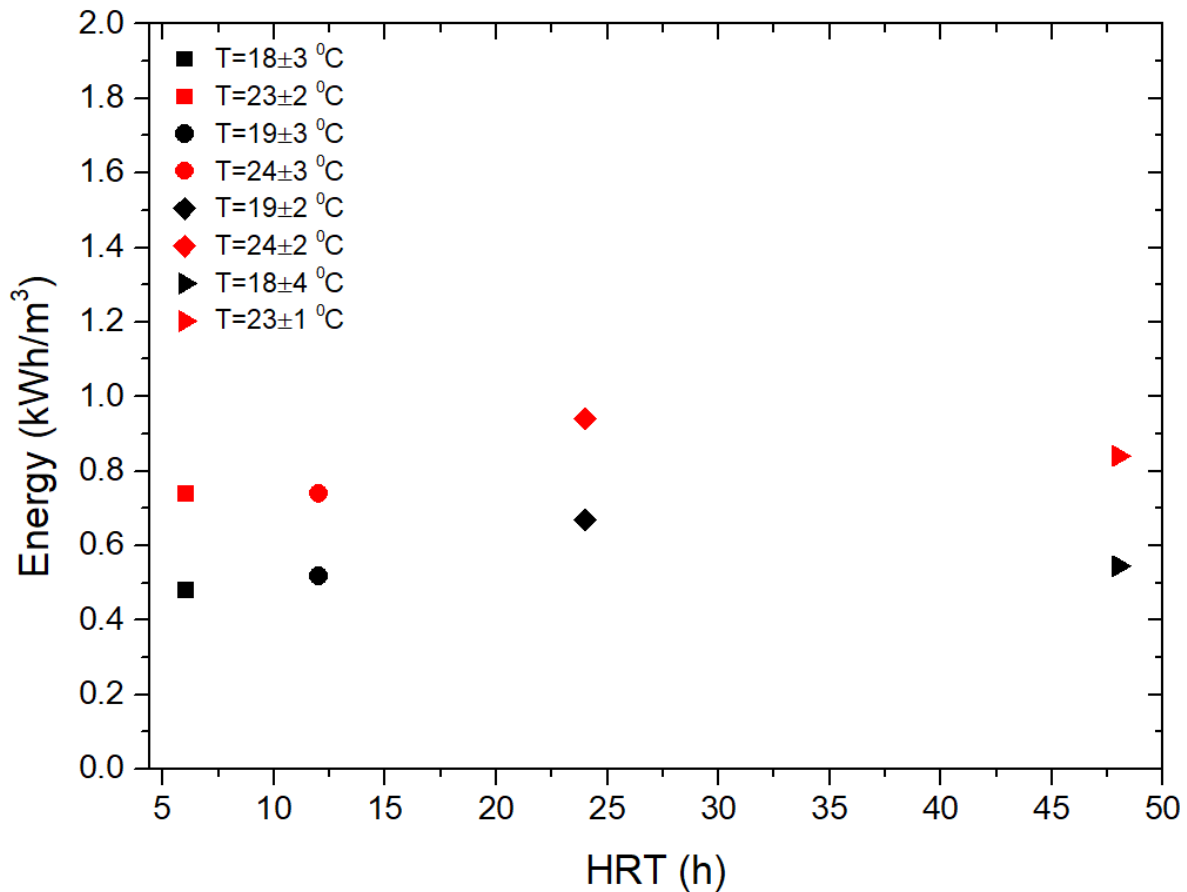
Figure 4. 59: Potential Energy Production from the Gaseous Methane Produced for All the HRTs Examined.

As shown in Table 4.9, for the winter season, energy derived from gaseous methane was found to range between 0.55 kWh/m³ and 0.67 kWh/m³. Consistent energy values across various HRTs were observed. For the summer season, the energy range derived from gaseous methane, was

determined to be between 0.67 kWh/m^3 and 0.94 kWh/m^3. Summer was identified as a more favorable period for energy production.

Upon comparison, it was noted that an HRT of 1 day during summer yielded the highest energy per m^3. However, when the daily treatment capacity was considered, it was seen that shorter HRTs could process larger volumes, potentially leading to a higher total energy output, even if the energy per m^3 was slightly reduced. Thus, the selection of the optimal HRT was understood to be a balance between energy yield per m^3 and the total volume treated per day, when the only criterion evaluated is energy production.

Figure 4.60 showcases the COD mass flow in a standard wastewater treatment plant where CAS acts as the central treatment module. Clearly, the majority of the energy that could be harnessed from this process originates from the anaerobic digestion of both primary and secondary sludges.
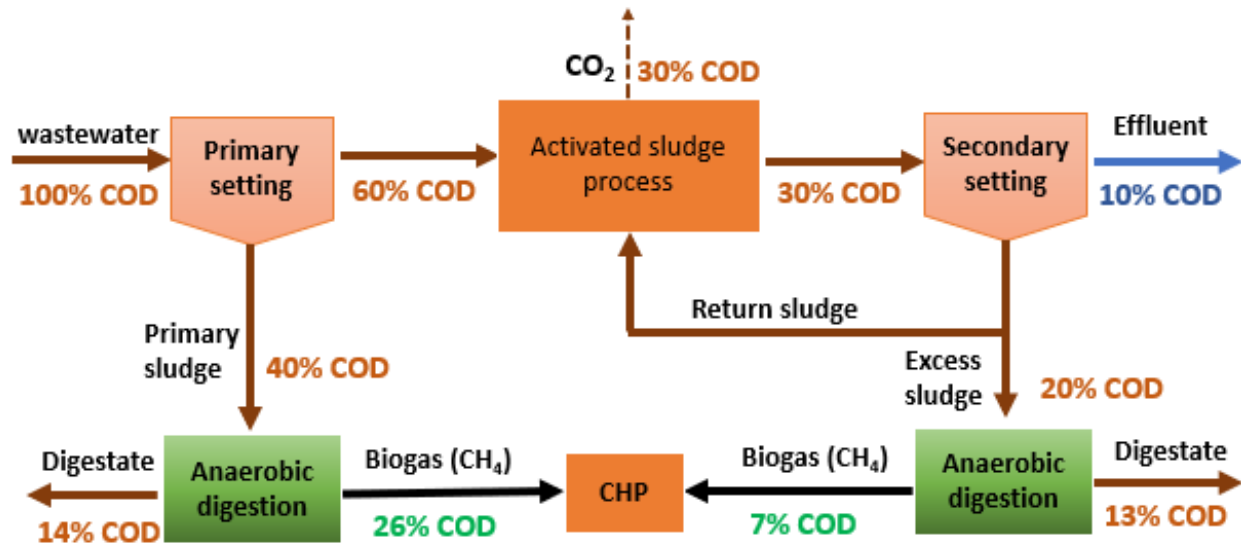
Figure 4. 60: COD mass flow through a conventional WWTP [109]

From the data in Figure 4.60, it's evident that 26% of the total COD from primary sludge and 7% from secondary sludge can be transformed into methane via anaerobic digestion. Given that the theoretical chemical energy from a gram of methane-COD is approximately 13.9 kJ, the cumulative recoverable chemical energy is derived by adding (13.9 × 0.26) from the primary sludge to (13.9 × 0.07) from the secondary sludge, which equals 4.58 kJ/g COD. It's important to recognize that only around 35% of methane's chemical energy can be turned into electricity when burned. Consequently, the upper limit of electrical energy that can be extracted from traditional

wastewater through anaerobic digestion in wastewater treatment plants stands at (4.58 × 0.35) = 1.60 kJ/g COD. This is half the energy required to remove a gram of COD, approximately 3.20 kJ/g COD. This indicates that the energy derived from wastewater can only compensate for up to 50% of the total energy expenditure for the operation of present-day wastewater treatment plants.

Figure 4.61 on the other hand depicts the COD mass flow on an AnMBR scheme.
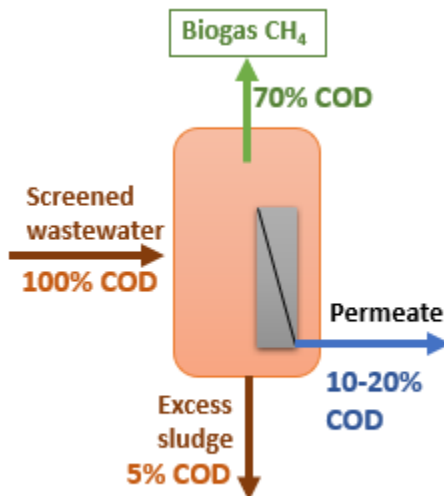
Figure 4. 61: COD mass flow through AnMBR

From the data in Figure 4.61, it's evident that 10-20% of the total COD is the permeate flow, 5% of the COD is leaving the system as excess sludge and 70% can be transformed into methane via anaerobic digestion. Specifically for our scenario, to determine the energy balance and ascertain whether the system yields a positive or negative outcome, Table 4.10 displays the energy derived from methane—specifically the 35% that can be converted to electricity.

Table 4. 10:Energy balance of the Lab scale AnMBR

	HRT 2days	HRD 1day	HRT 12h	HRT 6h
Winter				
Energy transferred to electricity (KWh/KgCODrem)	0.56	0.805	0.53	0.6
Total Energy consumption (KWh/KgCODrem)*	0.225	0.225	0.225	0.225
Energy Balance (KWh/KgCODrem)	+0.334	+0.58	+0.305	+0.375
Summer				
Energy transferred to electricity (KWh/KgCODrem)	0.7	0.88	0.63	0.805
Total Energy consumption (KWh/KgCODrem)*	0.225	0.225	0.225	0.225
Energy Balance (KWh/KgCODrem)	+0.475	+0.655	+0.405	+0.58

*refers to total energy consumption from AnMBRs, such as feeding, membrane scouring, sludge dewatering, reactor mixing, etc. [527]

According to the results shown in Table 4.10, energy balance is favorable for all the scenarios conducted through our investigation. The total electrical energy that can be extracted from AnMBR for the winter and the summer period is in the 0.3 – 0.58 KWh/KgCODrem and 0.4 – 0.66 KWh/KgCODrem range, respectively. Similar findings are reported in the literature for AnMBRs operating at ambient temperatures [527], where electric energy recovery ranges from 0.21 – 0.65 KWh/KgCODrem.

It's essential to note that the total energy consumption data of Table 4.10, was sourced from the literature, as calculating these consumptions for our lab-scale system wouldn't be accurate due to its small scale. Even excluding thermal energy, the electrical energy gives a positive balance. Compared to the CAS system, a positive energy balance is hard to achieve with conventional AS systems. In addition to mitigating climate change, this positive energy outcome aligns with the stricter energy criteria set to appear in the new directive scheduled for implementation in 2023. This directive, mentioned earlier in this chapter, emphasizes the goal of energy neutrality.

Chapter 5 Simulation Model of the AnMBR System

5.1 Introduction

Modifications to the ADM1 model by the IWA have yielded a model that adeptly simulates an An MBR, as detailed in the Materials and Methods section, which operates at ambient temperatures and processes municipal wastewater.

The model underwent extensive sensitivity analysis, utilizing methods such as Morris, Fast, and One-at-a-Time (OAT), and it has been thoroughly calibrated and validated. In applying this model, initial values were retained from the benchmark model, and two interfaces were established: inlet and outlet. Our exploration was principally concentrated on pivotal outlet parameters, namely Chemical Oxygen Demand (COD_out), gas flow rate (Q_gas), Volatile Suspended Solids (VSS), Total Nitrogen (TN), and methane content (CH_4).

Beyond this, a holistic approach was embraced to scrutinize the subdivisions of COD within the system. This included integrating numerous additional parameters—such as total acetate (Sac), total butyrate (Sbut), total propionate (Spro), valerate and butyrate degraders (Xc4), acetate degraders (Xac), and hydrogen degraders (XH2). This incorporation allowed for a more meticulous and detailed analysis of the subdivided COD, enabling a deeper understanding of the various components and their interactions within the system.

By maintaining a consistent focus on these critical parameters and their subdivisions, a comprehensive and precise exploration of the system has been ensured, contributing to the ongoing development and refinement of wastewater treatment processes.

5.2 Sensitivity Analysis

5.2.1 Sensitivity analysis methods applied.

As mentioned, sensitivity analysis is recognized as a powerful tool in the field of mathematical models and allows the impact of a disturbance of a model's input parameters on the corresponding results it produces to be assessed. [528]. So far, in the environmental field, models

mainly use local methods, with the primary one being "one-at-a-time," which does not allow for the quantification and identification of any interactions between the model's parameters. Regarding global methods, the Morris method has been used [481], as well as methods which quantify sensitivity through the calculation of variances (e.g., Extended FAST). Chapter 2 extensively analyzed the way and the categories in which the various methods are divided, as well as the advantages and disadvantages of each one.

In conclusion, pertaining to the selection of a method for sensitivity analysis, it must be conducted in alignment with certain criteria, several of which are universally applicable across all studies, such as computational cost. Simultaneously, the researcher must delineate the objective behind undertaking the sensitivity analysis, from which corresponding criteria emerge, such as parameter screening and ranking among others. Ultimately, the amalgamation of all these criteria facilitates the selection of the most apt method for sensitivity analysis.

In this dissertation, three methods of sensitivity analysis were strategically chosen with the objective to assess the most crucial input parameters, which are delineated in the subsequent sections. Taking into consideration the discussions about the methodologies in Chapter 2, it was resolved to implement the following four methods: 1) a local method, termed as "one-at-a-time", 2) a GSA method, known as FAST, and 3) a method that is a hybrid between local and global, the Morris method,

5.2.1.1 Local ''one a time method''

LSA methods are substantially more economical in terms of computational cost and time; however, their results are of a qualitative nature. Their primary limitation is that they are incapable of estimating any form of interaction amongst the parameters. The parameters engaged with in the sensitivity analysis were listed in Chapter 2. Based on the aforementioned factors, the initial form of analysis is chosen to be conducted with the local "one-at-a-time" method. This method has a relatively simple and quick implementation and qualitatively displays the significance of each parameter through numerical indicators. More specifically, for each simulation, one of the parameters is altered with a disturbance (e.g., +30%, -30%) while all the other parameters maintain the same value as the reference state, which had been initially calculated. Ultimately, an index emerges which essentially quantifies the alteration in the value of each output variable,

relative to the corresponding alteration of each parameter that was changed for that specific simulation. The method of calculating this index is presented in the Eq 5.1:

$$Spy_{ji} = \frac{\frac{\Delta yi}{yi,o}}{\frac{\Delta pj}{pj,o}}$$

Eq (5.1)

Where:

Δyi represents the difference between the value of the output variable in the reference state and its corresponding value due to the disturbance of the input parameter pj,

Δpj is the difference between the value of the input parameter in the reference state and its corresponding value after its disturbance,

Yi,0 denotes the value of the output variable in the reference state,

pj,0 represents the value of the input parameter in the reference state.

In this manner, a sensitivity-gravity index was calculated for each output variable y, for each one of the two disturbances (+30%, -30%) of every input parameter p. Subsequently, the maximum absolute value of the index was taken among the values due to the two different disturbances. Consequently, this value ultimately described the sensitivity of each variable to the respective input parameter. Based on the aforementioned, a preliminary view on the significance of the parameters can be obtained, on how much they affect the output variables, and also on how they are influenced (positive or negative variation). It is reminded that the method was applied with the disturbance of only one parameter at a time while all the others were kept constant. As is logical, no information is provided regarding any potential interactions among the input parameters.

This method was applied to all the output variables, which, are 4 in total. The value 0.1 is chosen as the limit for assessing the significance of a parameter, according to the literature [529]. In this way, a sorting between significant and non-significant parameters is carried out for each output variable. All of the above are presented in Figures 5.1-5.2. Out of the 41 parameters evaluated using the OAT method for COD in the effluent, eight were identified as significant. These are highlighted in red in Figure 5.1.
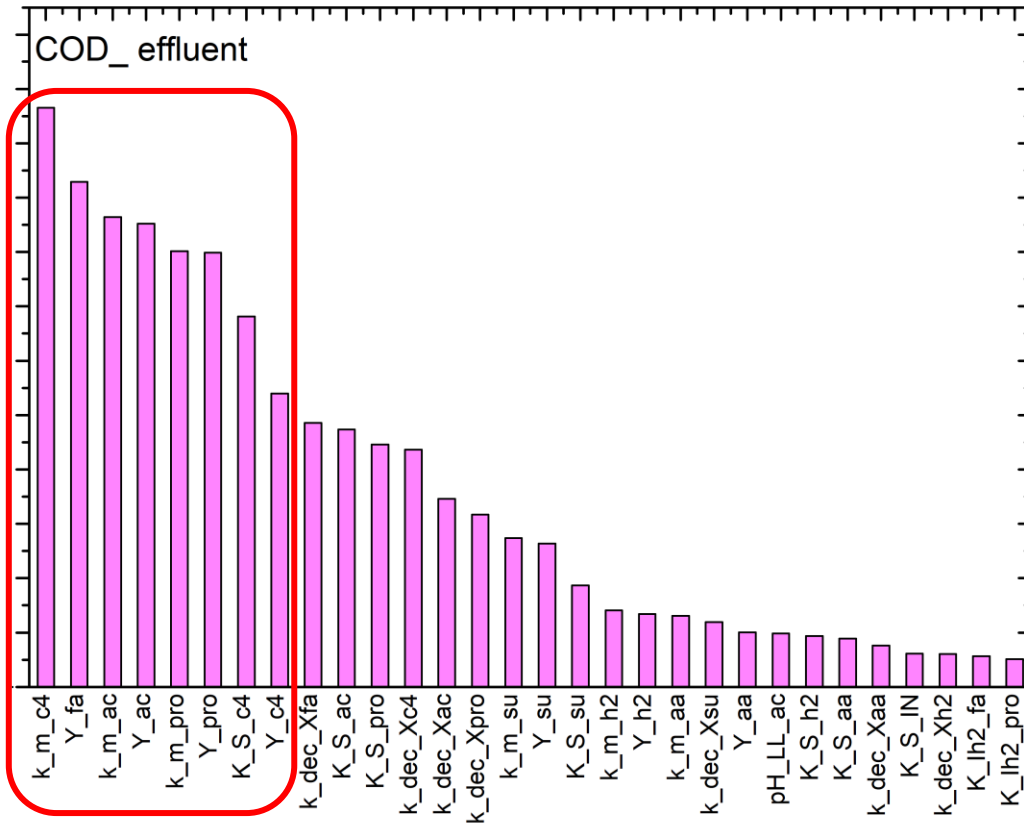
Figure 5. 1: Hierarchical Arrangement of Parameters for COD effluent via the 'One-at-a-Time' Method.
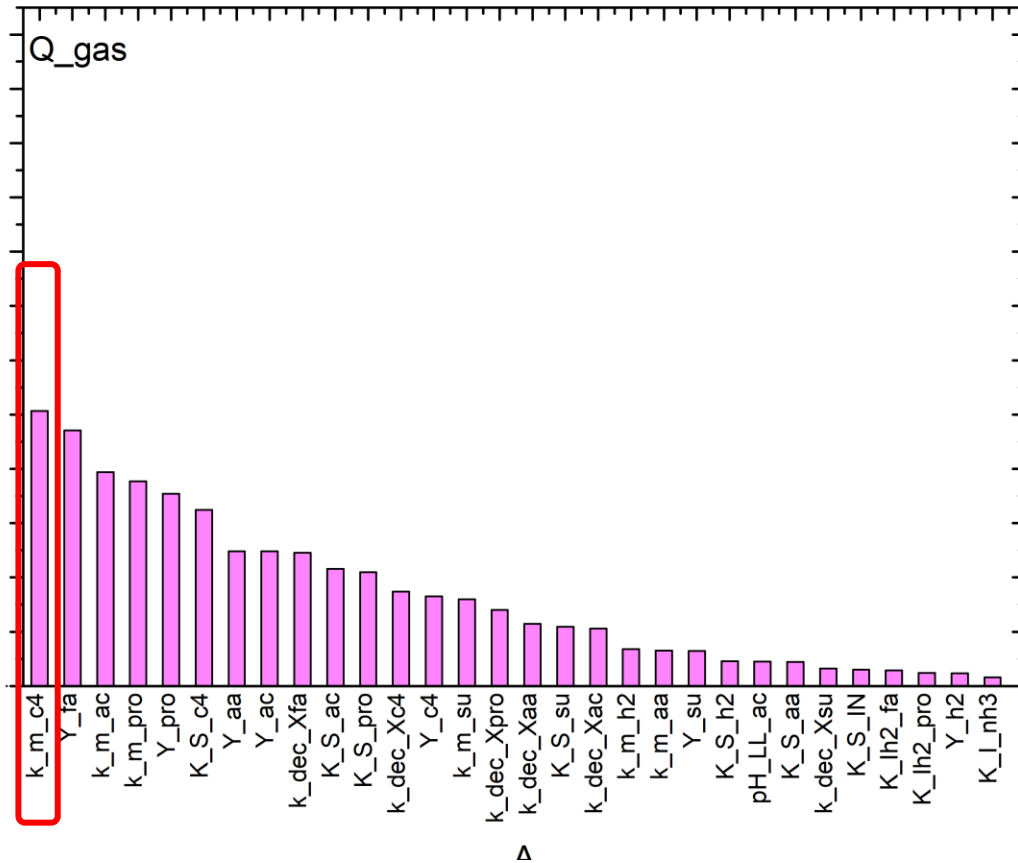
Figure 5. 2: Hierarchical Arrangement of Parameters for Q_gas via the 'One-at-a-Time' Method.

For TN and VSS, no significant parameters were identified, and as a result, no graphical representation is presented.

In summary, when categorizing parameters as significant or non-significant, our classification adhered to the threshold we established at 0.1. Notably, certain parameters were found to be significant for two of the four examined effluent parameters, whereas for Q_gas, only one parameter was deemed significant.

In the forthcoming chapter, a comparison will be conducted between the outcomes derived from all the analytical techniques, as well as a juxtaposition between the global and local methods. The local method was selected primarily because of its inherent simplicity and rapid implementation. Furthermore, it was used as an initial tool to streamline and reduce the parameters for subsequent GSA, ensuring a more efficient simulation process. However, it is important for the results of the local method to be verified against the universally accepted and comprehensive global

approaches. This will not only validate the findings but also determine its efficacy, especially when its potential limitations are taken into account.

5.2.1.2 GSA -FAST method

FAST method offers an alternative technique and approach to the traditional variance-based method for calculating sensitivity indices. While FAST requires significantly less computational resources and time, it is limited in its outcomes, as it only calculates indices for first-order effects of the respective parameters. Given this, it can be utilized for the two primary objectives of sensitivity analysis: ranking all parameters and segregating them into significant and non-significant categories. The foundation of this technique bears resemblance to variance-based methods. However, distinctions arise in the generation of random samples for parameter values and the numerical calculation of indices.

The general methodology and practice of the FAST method were presented in Chapter 2. Hence, in this section, details will not be delved into again, as the final formulas used for calculating the sensitivity indices were also described in that chapter.

As mentioned, the FAST method is a global method, so its results have greater accuracy. This happens because the parameters change simultaneously and randomly within their value range, resulting in them affecting each other. Therefore, the quantification of the interaction of the parameters among themselves is not provided by this method, however, it has been taken into account in the final calculation of their significance. The significance limit for the indices was set as 0.01, according to Cosenza et al., (2013), which means that there is the possibility of selection, as mentioned also for the "one-at-a-time" method. Below are the charts for the sensitivity indices for variables of the model in the form of vertical bar charts. The method also offers the possibility of precise classification of the parameters according to the values of their indices. The hierarchy of the parameters for each variable is presented below in the form of vertical bar charts.

When parameters were categorized as either significant or non-significant, the threshold set at 0.01 was adhered to. Notably, certain parameters were identified as significant across all variables. This contrasts with the results from the OAT method, where significant parameters were presented in only 2 out of the 4 variables.

More specifically, significant parameters include Km_ac, Kdec_ac and Ks_ac.

Figures 5.3-5.6 showcase the sensitivity indices for the key examined effluent parameters and provide a ranking based on these indices.
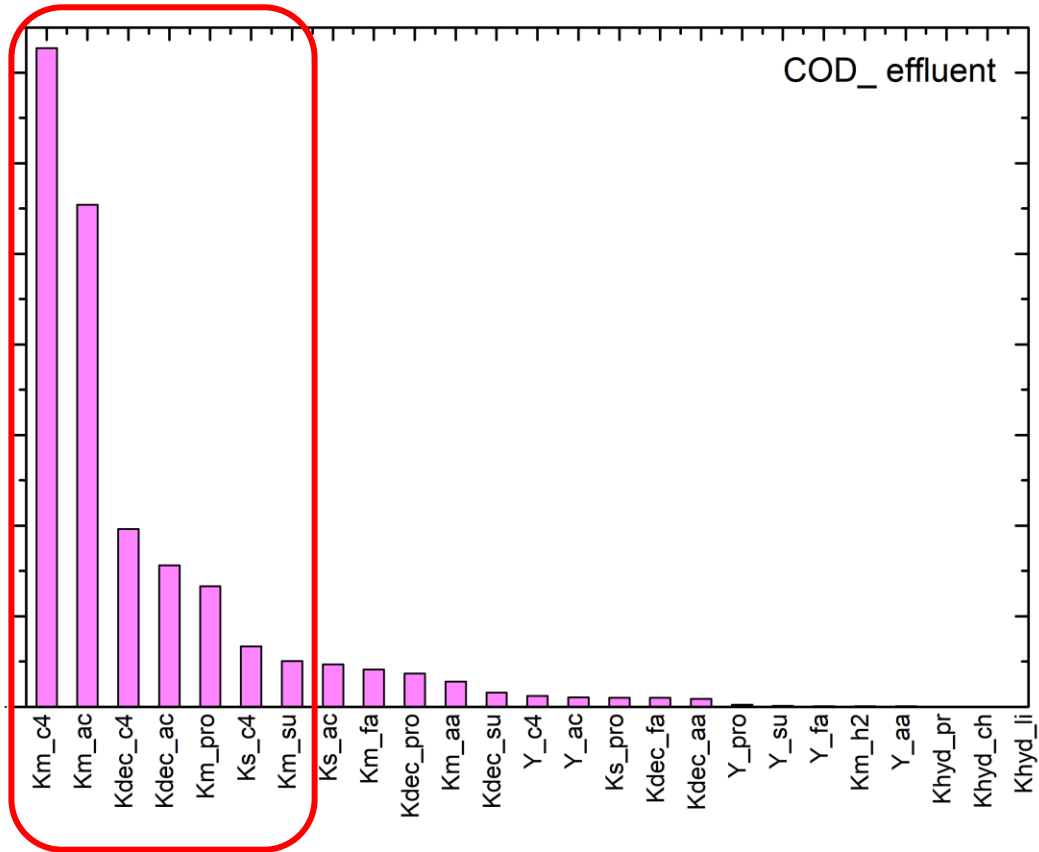
Figure 5. 3: Hierarchical Arrangement of Parameters for COD via the 'FAST' Method

Figure 5.3 highlights the significant parameters for COD effluent in red, with 7 being identified out of the 25 examined. Figure 5.4 illustrates the key parameters for Q_gas effluent, marking 8 significant ones out of the 25 evaluated in red. Notably, many of these overlap with those identified for COD effluent.
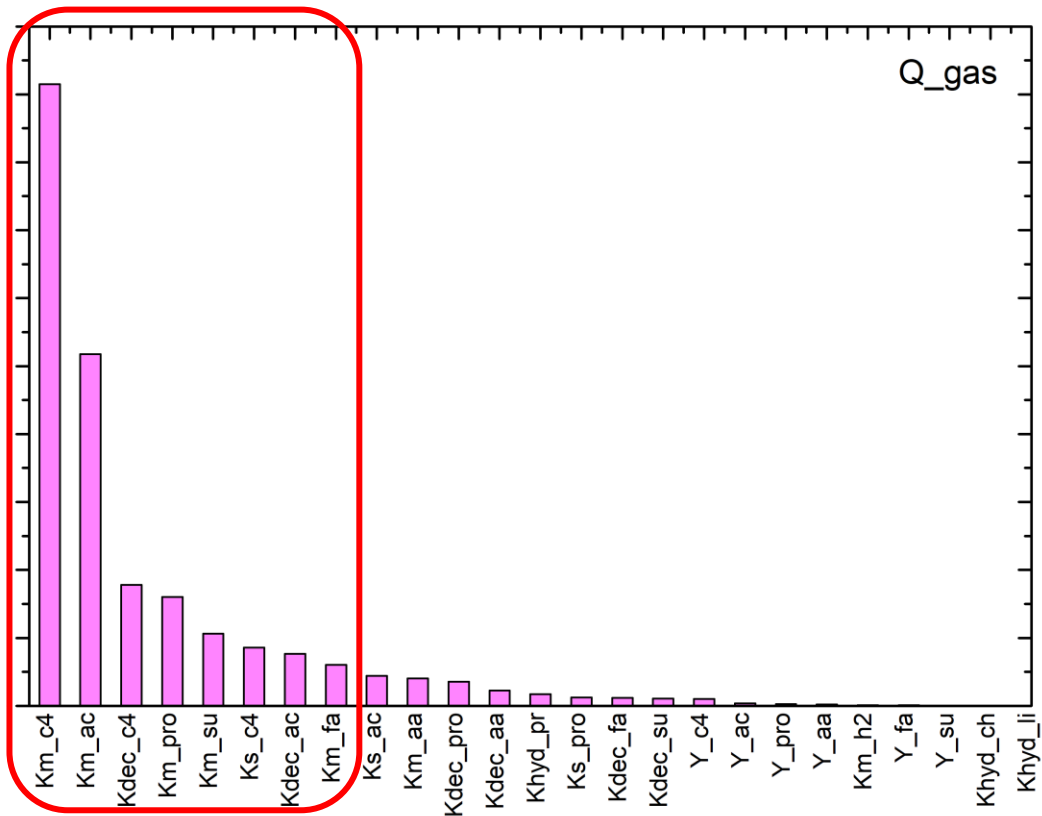
Figure 5. 4: Hierarchical Arrangement of Parameters for Q_gas via the 'FAST' Method

In Figure 5.5, the crucial parameters for VSS are delineated. Out of the 25 parameters assessed, seven were notably highlighted in red, signifying their significant influence. It is worth noting that there's a considerable overlap in these parameters with those pinpointed for COD effluent and Q_gas. A standout observation from the graph is the pronounced prominence of Kdec_aa. This parameter's value is substantially higher, being approximately four times greater than the other marked parameters.
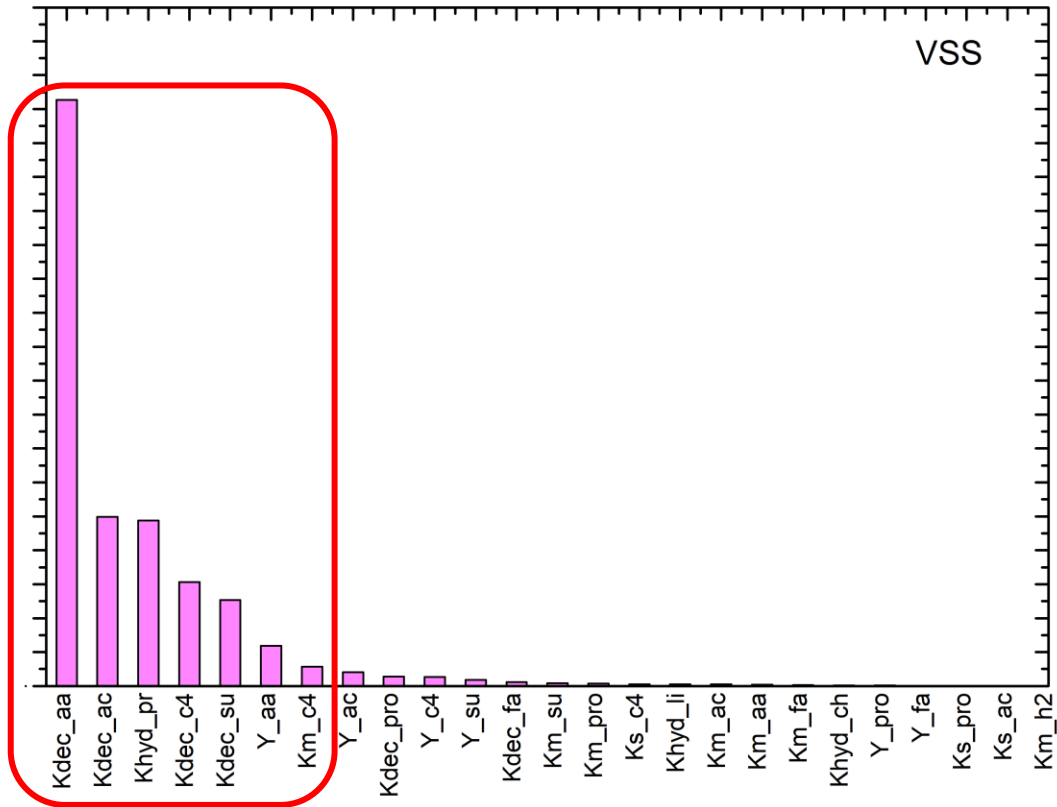
Figure 5. 5:Hierarchical Arrangement of Parameters for VSS via the 'FAST' Method

In Figure 5.6, the essential parameters for TN are depicted. Of the 25 parameters analyzed, 6 are distinctly marked in red, underscoring their paramount importance. Interestingly, many of these parameters exhibit a significant correlation with other parameters studied. A salient feature from the graph is the remarkable prominence of Km_aa. Its value is distinctly elevated, approximately twice as high as the other emphasized parameters.
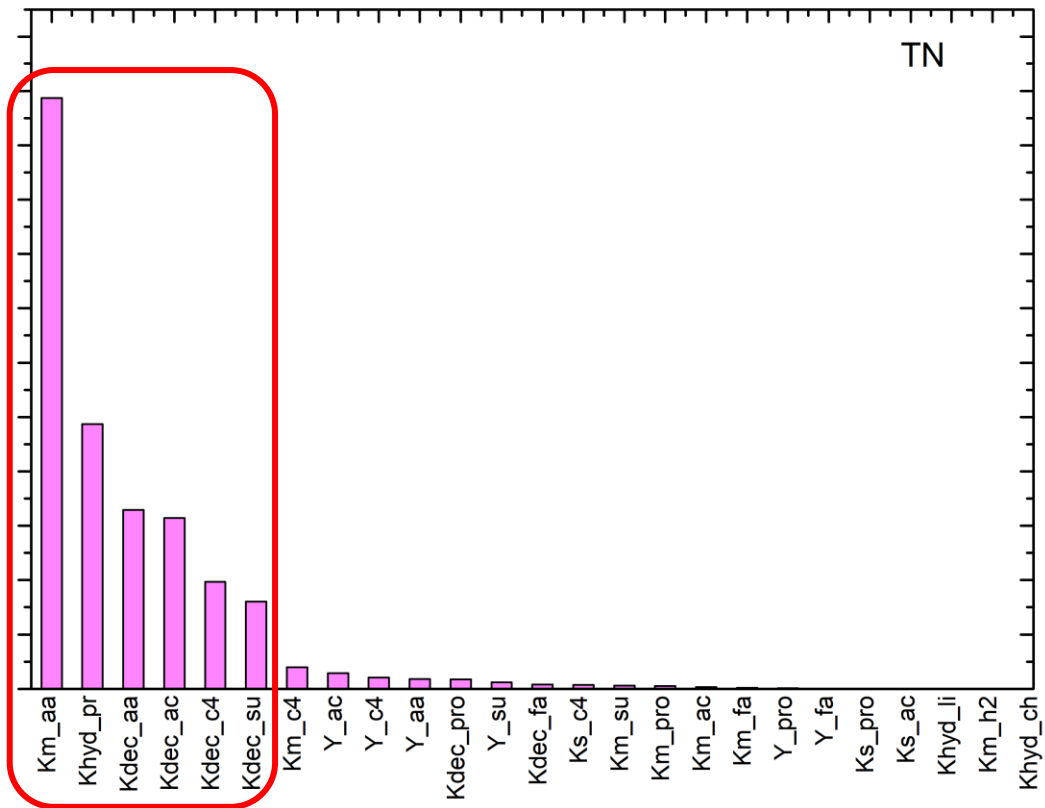
Figure 5. 6:Hierarchical Arrangement of Parameters for TN via the 'FAST' Method

In Figures 5.7 and 5.8, the graphical representations elucidate the fractions of COD. These visuals distinctly demarcate both the significant and non-significant parameters marked with red associated with soluble constituents. In a similar vein, Figures 5.9 and 5.10 provide a detailed portrayal of the parameters pertinent to particulate matters.
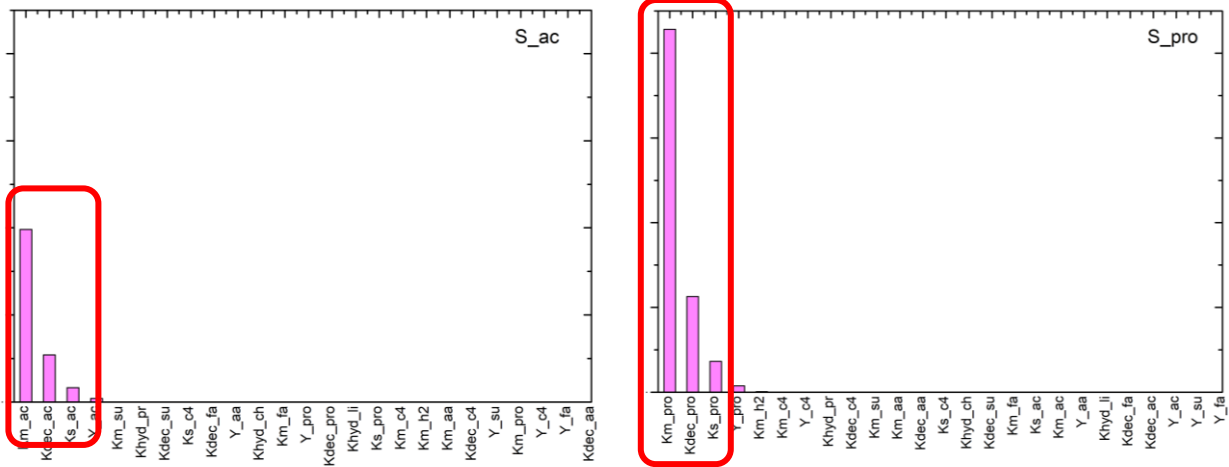
Figure 5. 7:Hierarchical Arrangement of Parameters for S_ac (left) and S _pro (right) via the 'FAST' Method
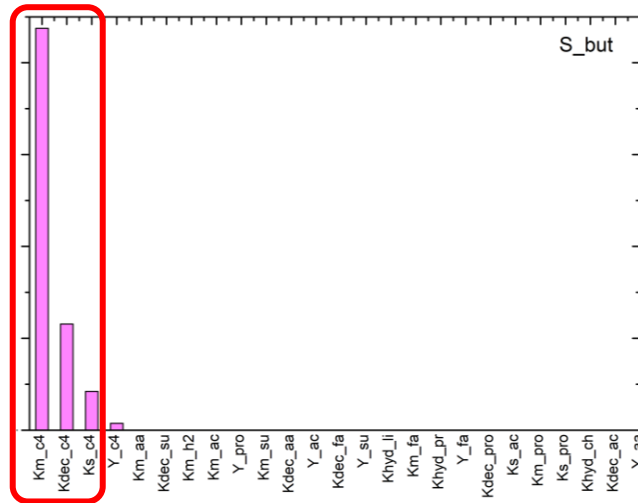
Figure 5. 8: Hierarchical Arrangement of Parameters for S_but via the 'FAST' Method

As it is depicted from the graphs, there are significant parameters in every parameter but the fractions are
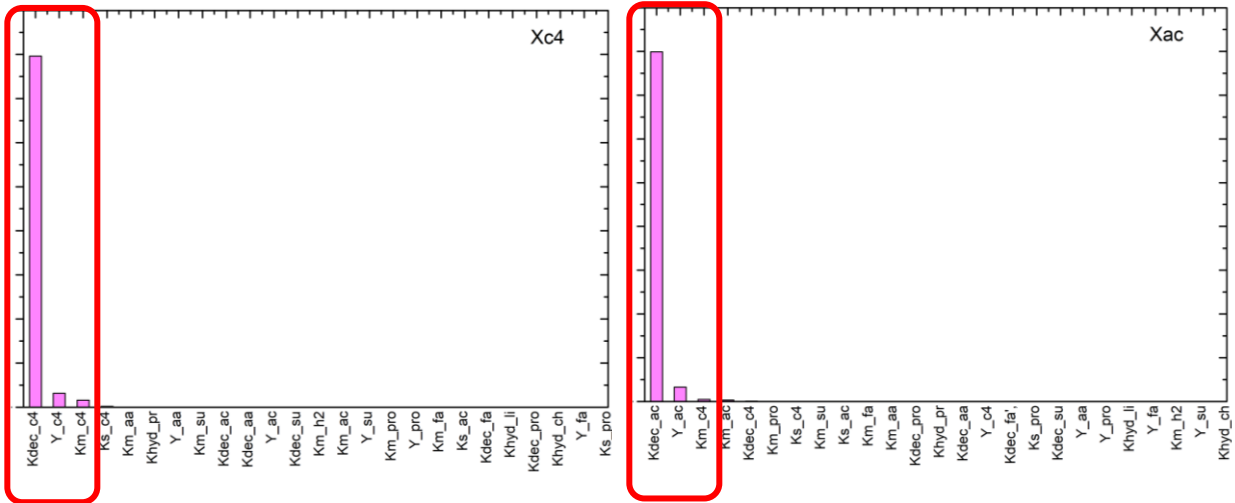
Figure 5. 9: Hierarchical Arrangement of Parameters for Xc4 (left) and Xac (right) via the 'FAST' Method
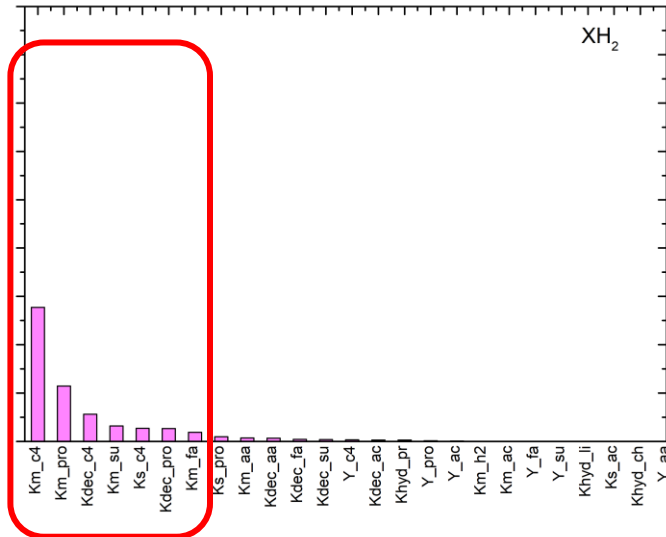
Figure 5. 10: Hierarchical Arrangement of Parameters for XH2 via the 'FAST' Method

For every variable under consideration, significant parameters are consistently present. Within these variables, certain parameters exhibit a predominant influence that varies from one variable to another. The notable exception is with Xh2, where the impactful parameters seem to be more uniformly distributed.

5.2.1.3 GSA -Morris method

Subsequently, the Morris method was applied, which is based on disturbances that occur simultaneously. In this way, relationships and interactions between the parameters are taken into account. Concurrently, the variations and variability of the model's output sizes are examined, consistent with all the parameters. The method is based on finite differences, and more specifically, the sensitivity indices are calculated based on the average value of these differences, according to the following formula presented in Eq 5.2.

$$Si = \frac{1}{r}\sum_{j=1}^{r} EE^j$$
Eq (5.2)

For each specific index j, the Elementary Effect (EE) quantifies the discrepancy between two scenarios: Firstly, the value of the model's output variable when subjected to a perturbation, represented as Δy(x1,…,xi−1,xi+Δ,xi+1,..,xn) and secondly, the intrinsic value of the output variable in the absence of such perturbation, denoted as y(x1,…,xn). This framework provides a nuanced understanding of how individual input parameters influence the overall behavior of the model(Eq 5.3).

$$EEi\ (x1,\dots,xn,\varDelta) = \frac{y(x_1,\dots,x_{i-1},x_i + \varDelta, \chi_{i+1},\dots,\chi_{n)} - y(x_1,\dots,x_n)}{\varDelta}$$
Eq (5.3)

In this context, the disturbance, denoted as Δ, assumes values within the interval {1/(p-1),…,1 − 1/(p-1)}, with p representing the number of levels, specifically set at 6 in this case. To gauge the relative importance of each parameter and to understand the intricacies of its interactions with other parameters, two key metrics are turned to: the mean value m and the variance S, which capture the central tendency and the spread of the EEs, respectively.

In the investigation, it was discerned that the Morris method, though comprehensive, demanded significantly more simulation time compared to FAST, presenting a considerable computational challenge. Nevertheless, the Morris analysis was conducted across all parameters to ensure thoroughness. However, for the scope of this thesis, our emphasis has been directed specifically towards 'Q gas'. This strategic focus arises from its crucial importance as a central parameter in the AnMBR system. While all the parameters were explored, highlighting 'q gas' was deemed

essential due to its significance and to offer a streamlined presentation, especially given the extensive nature of examining the other nine parameters in detail.

For the Morris method, a significance threshold of 0.1 was chosen, meaning the average value m of the EEs for each parameter must be greater than 0.1 for it to be considered significant. However, as mentioned, this method also takes into account interactions between the parameters. This is evident from the value of the standard deviation S of the EEs for each parameter, which indicates whether the parameter interacts with the others. Therefore, to identify the significant and non-significant parameters, both these values and their appropriate combination must be considered. Below, a scatter plot presents the values (m,S) of all parameters for Q_gas. Qualitatively, the farther to the right a point is on the plot, the more significant the corresponding parameter is. Similarly, the higher it is, the more it interacts with the other parameters. It should be noted that a m value lower than the significance threshold is not a sufficient condition to exclude a parameter because, if it interacts with others, it is naturally considered significant for the model.

In Figure 5.11, a scatter plot is presented showcasing the sensitivity indices of the 25 parameters for Q_gas. The method also offers the capability for precise ranking of the parameters based on their index values.
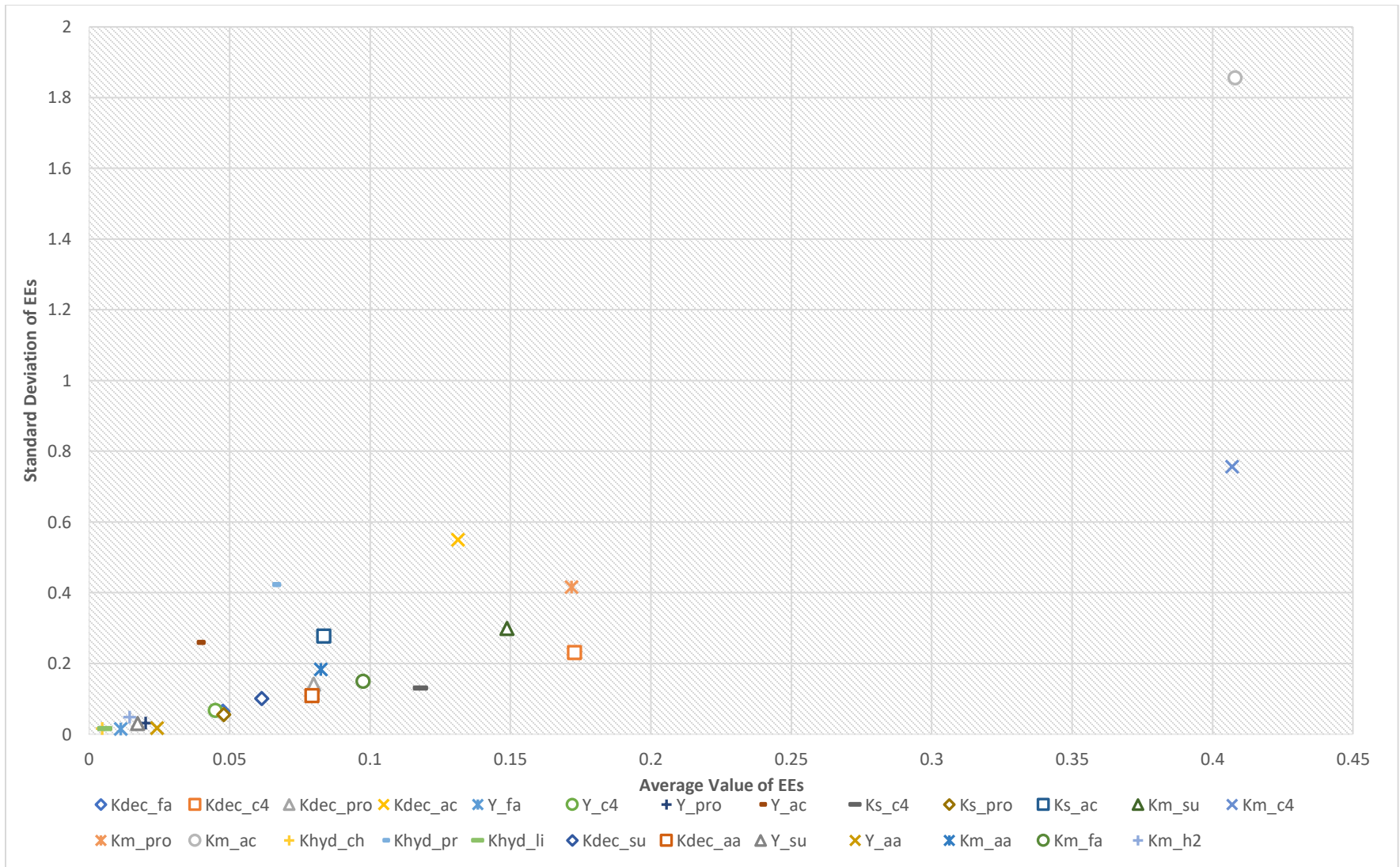
Figure 5. 11: Scatter plot (m, S), Morri's method for Q_gas for 25 parameters.

From the graph in Figure 5.12, the most significant parameters are Km_c4 and Km_ac. The ranking of parameters for the Q_gas is presented in Figure 5.12 in the form of a vertical bar chart.
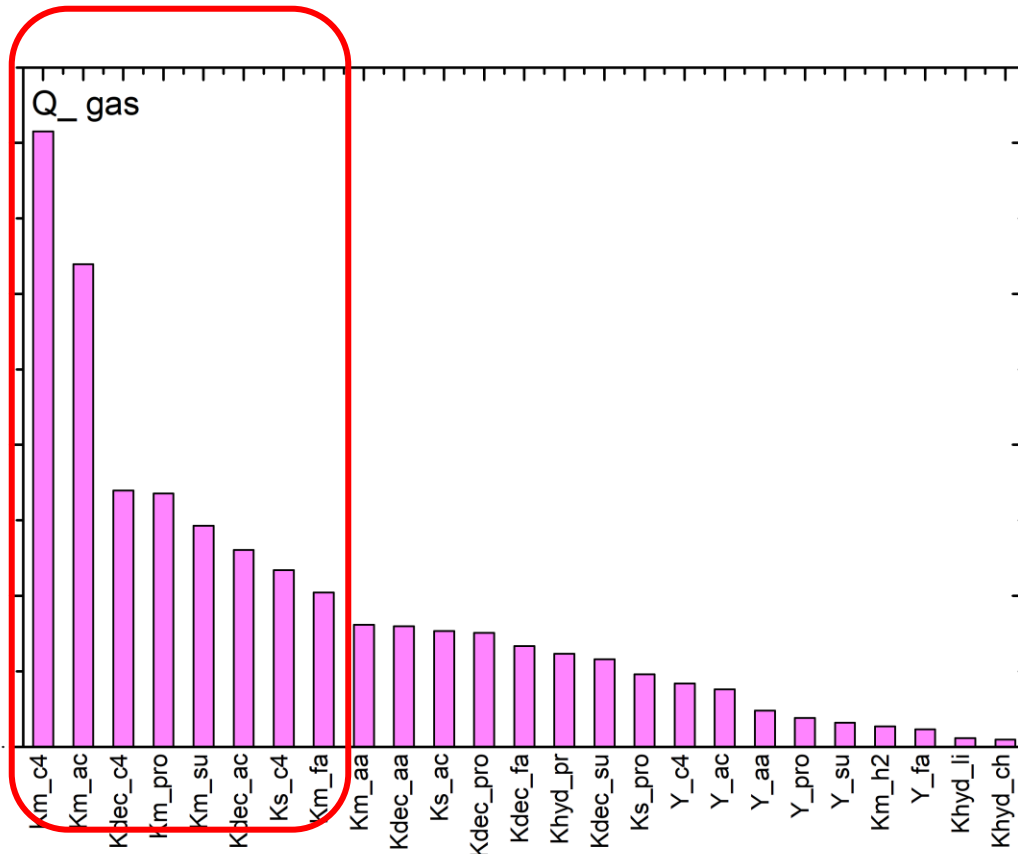
Figure 5. 12:Hierarchical Arrangement of Parameters for Q_gas via the 'Morris' Method

In Figure 5.12, the significant parameters affecting Q gas were identified using the Morris method. Out of the 25 parameters assessed, 8 were found to be significant and are highlighted in red.

5.2.2 Assessment of Sensitivity Analysis methods

5.2.2.1 Method convergence

Sensitivity analysis encompasses the generation of samples based on parameter values, derived through randomized procedures. The goal of such sampling is to replicate a broad array of random conditions, striving for an exhaustive and precise representation of natural events. Within the domain of sensitivity analysis, there's also the forecasting phase where statistical discrepancies and uncertainties come into play. A pivotal element in the sampling procedure is the sample's size N. In the context of sensitivity analysis, this size directly correlates with the number of iterations required for our model. Broadly speaking, a larger sample size results in the inclusion of a more diverse range of conditions within our simulation. This, in turn, enhances the quality of our predictions and optimizes the method's outcome convergence. The selection of the sample size N is influenced by various factors: the intrinsic nature of the phenomenon under simulation, the quantity of parameters M, the specific sensitivity analysis technique employed, and computational constraints. Consequently, every sensitivity analysis approach exhibits distinct convergence and predictive precision. As such, it's imperative that the method's inherent characteristics be evaluated in tandem with its outcomes.

One statistical technique employed in evaluating convergence in sampling methods is "bootstrapping". This approach offers a swifter way to assess the initial sample size since it can generate results without necessarily executing numerous additional simulations. The "bootstrapping" technique involves constructing new samples and recalculating values derived from them. Depending on the sensitivity analysis method used, these new samples might either be subsets of the original, thus smaller, or entirely new and larger in comparison to the original. Generally, a sample size is deemed effective when its derived results closely match those of a theoretically smaller or larger sample size. This method helps verify the convergence of the values arising from the chosen sample. As one might expect, the larger the sample size, the closer it gets to fully depicting the phenomenon that the model simulates. Therefore, computational constraints, both in terms of processing power and simulation times, play a critical role in deciding an appropriate initial sample size, and subsequently, in the application of the "bootstrapping" technique.

In terms of methodological convergence, three distinct metrics are employed. Firstly, the 'Stat indices' is utilized to gauge the convergence in the values associated with sensitivity indices. Secondly, the 'Stat ranking' is pivotal for the hierarchical classification of parameters. Lastly, 'Stat screening' serves to filter out parameters deemed non-significant. The primary convergence metric is established by determining the maximum disparity between the upper and lower bounds of confidence intervals pertaining to each parameter's sensitivity index. The specific formula for this calculation will be delineated below in Eq 5.4.

$$Stat_{indices} = \max_{i=1...M} (Si^{ub-}Si^{lb})$$ Eq (5.4)

Where Siub and Silb are the upper and lower bounds of the sensitivity index for parameter i, and M represents the number of parameters introduced into the method (Sarrazin et al., 2016). The smaller the value of this index, the better the convergence achieved in the method, with the convergence threshold set at 0.05.

The second convergence index pertains to the ranking order of the parameters and evaluates the accuracy of this order for the initial sample chosen. A modified Spearman coefficient is used, which places greater weight on the most significant parameters. Initially, the Si indices are calculated for all the different samples generated by bootstrapping. Subsequently, these parameters are ranked based on their importance. Their position after ranking is represented by the number Ri, while the exponents j,k indicate the corresponding samples from the bootstrapping. The modified coefficient assigns a greater importance to the differences in the ranking positions of the most crucial parameters, whereas, if there are variations in less significant parameters, their weight is diminished.

$$\rho_{s,j,k} = \sum_{i=1}^{M} |R_i^j - R_i^k| \frac{\max_{j,k}(S_i^j, S_i^k)^2}{\sum_{i=1}^{M} \max_{j,k}(S_i^j, S_i^k)^2}$$ Eq 5.5

For the ρs,j,k, the Ri and Si values are calculated for each possible pair between the samples j,k that have been created. Ultimately, the index for the convergence of parameter ranking is the value of the 95% confidence interval, derived from the ρs,j,k values that arise from all possible combinations [530]. The smaller the value of the index, the better the convergence achieved by the method, with the convergence limit set at 1 (Eq 5.6).

$$Stat_{ranking} = Q_{j,k}^{0.95}(\rho_{s,j,k})$$

Regarding the distinction of parameters into significant and non-significant, the indicator used is similar to the one for the convergence of sensitivity index values, known as Stat indices. The difference lies in the Si values, from which the differences between the upper and lower confidence limits are calculated, leading to the determination of the Stat screening index. Specifically, for the screening process, only the indices for parameters deemed non-significant based on the selected threshold T are used (Sarrazin et al., 2016). The smaller the value of the indicator, the better the convergence achieved in the method, with the convergence threshold set at 0.05 (Eq 5.7, 5.8).

$$X_o = \{x_i \ when \ S_i < T\}$$

$$Stat_{Screening} = \max_{xi \in Xo}(Si^{ub} - Si^{lb})$$

A. 'One-at-a-time' Method

The 'one-at-a-time' method is a local sensitivity analysis technique. Therefore, parameter values are not selected randomly, but through a consistent perturbation. As a result, it does not involve any sample generation process, and the issue of its convergence does not arise."

B. FAST Method

For the FAST method, a sample size of N_{FAST}=25,000 was chosen. For FAST, the 'bootstrapping' process was completed by constructing two samples smaller and three new samples larger than the original (15000,20000, 30000,35000, 40000). Table 5.1 indicates stat indicators examined (stat indices, stat screening and stat ranking).

Table 5. 1: Indicators examined, FAST method.

Variables	0.05 STAT indices	1 STAT ranking	0.05 STAT screening
COD	0.011	0.7	0.001
Qgas	0.011	0.4	0.001
Sac	0.003	15	0.000
Sbut	0.012	13.6	0.000
Spro	0.012	44.3	0.00013
TN	0.009	0.8	0.001
VSS	0.011	0.0	0.001
Xc4	0.001	9.6	0.000
Xac	0.002	0.8	0.001
Xh2	0.008	0.004	0.000

For all the variables studied, the statistical indices and screening indicators are almost negligible. This suggests that we've achieved convergence in the sensitivity values of the parameters. At the same time, this also effectively filters out parameters that aren't significant.

When it comes to ranking, most variables have reached convergence. However, some show an index that surpasses one, specifically within the subdivisions of COD: Sac, Sbut, Apro, and Xc4. This presents a challenge when drawing definitive conclusions about parameter ranking. Yet, it's worth noting two crucial points:

1. Since the sensitivity index values have been stabilized and won't shift further, and significant and non-significant parameters have been accurately differentiated, the ranking of the truly significant parameters—our primary concern—has likely been rendered unproblematic.
2. For the variables in question, there are minimal significant parameters (only three). Among these, one parameter stands out with a markedly higher sensitivity index value than the others. Given the formula used to compute the ranking statistic, this vast difference might cause the ranking convergence index to inflate.

Simply put, major ranking disparities only manifest for non-significant parameters. But because one parameter has such predominant significance, it tends to skew the convergence index. Thus, for parameters that genuinely matter, ranking discrepancies are minimal to non-existent.

To further refine our findings, increasing the number of iterations can potentially lead to full convergence in ranking.

In Figure 5.13, detailed insights are specifically centered around the Qgas parameter. This methodological choice was taken to ensure conciseness and focused elucidation, thereby refraining from an extensive exposition of the other nine parameters scrutinized within this research.
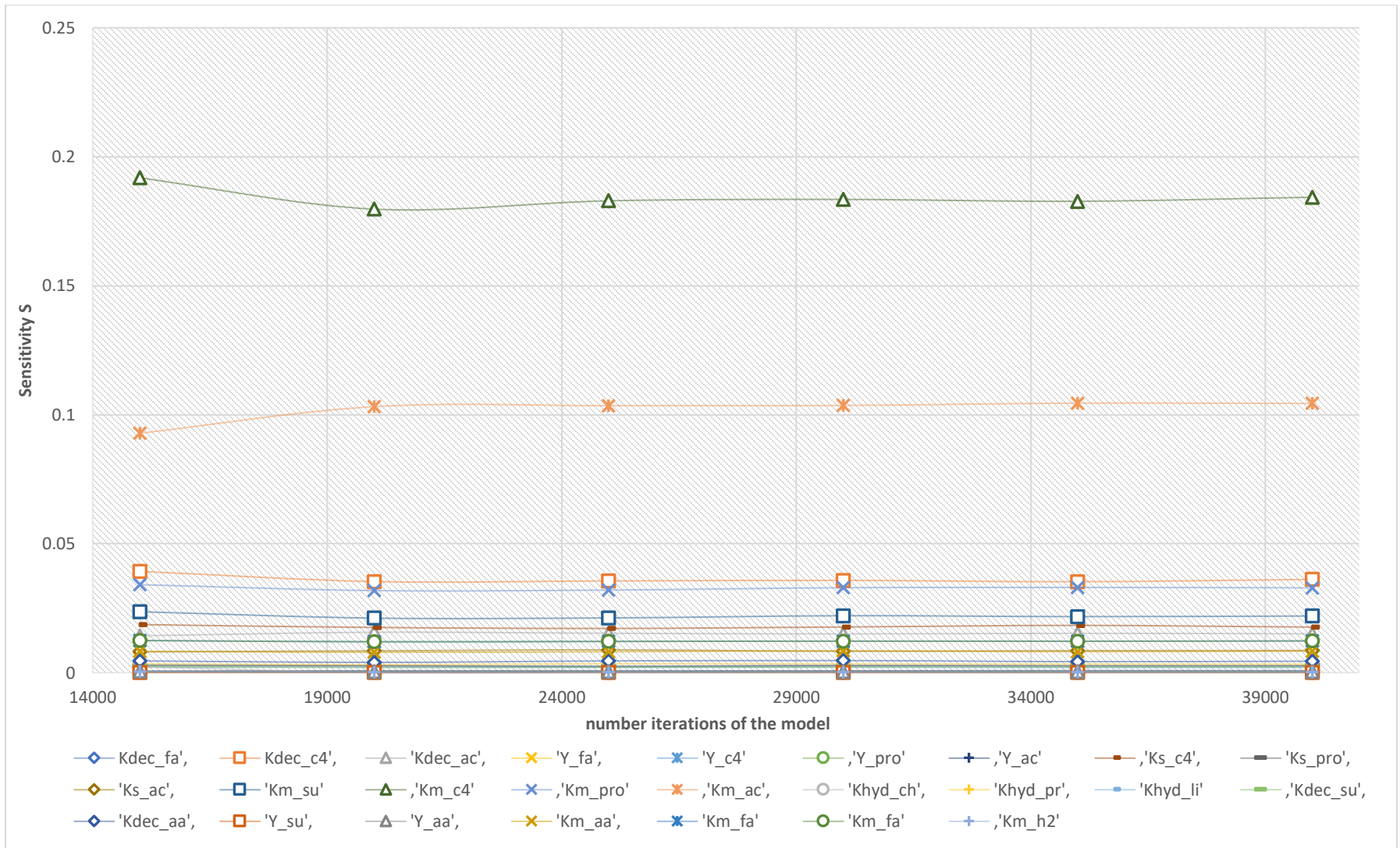
Figure 5. 13: Convergence diagram of parameters for Q_gas, Fast method

C. Morris method

For the Morris method, a sample size of N morris=39,000 was chosen. For Morris, the 'bootstrapping' process was completed by constructing two samples smaller and four new samples larger than the original (13000,26000,52000,65000,78000,156000). Table 5.2 indicates stat indicators examined (stat indices, stat screening and stat ranking).

Table 5. 2:Indicators examined, Morris method.

Variables	0.05 STATindices	1 STATranking	0.05 STATscreening
COD	18.5	0.27	0.001
Qgas	0.033	0.12	0.06
Sac	0.02	13.30	0.009
Sbut	0.005	3.13	0.001
Spro	0.004	4.55	0.001
TN	0.047	0.048	0.005
VSS	97.6	0.00	0.023
Xc4	0.017	0.93	0.017
Xac	0.026	0.054	0.003
Xh2	0.002	0.15	0.0006

In all the variables studied, the statistical indices and screening indicators have been found to be nearly negligible. This suggests that convergence in the sensitivity values for most of the parameters has been achieved. However, the values for two variables surpass the threshold of 0.05, and the VSS value is noted to be exceptionally high. Yet, when this value is juxtaposed with the STAT screening mean, it becomes evident that such discrepancies are not present for the significant parameters. This indicates that the values linked to this index have not yet fully converged. On the brighter side, a consistent convergence in both the categorization and ranking processes has been observed. This solidifies the reliability of the findings, ensuring that no unforeseen changes, such as previously deemed non-significant parameters suddenly becoming significant or major shifts in parameter values causing ranking adjustments, are likely to occur.

In terms of ranking, a majority of variables display convergence. However, as pointed out by the FAST method, some register an index beyond one, particularly in the COD subdivisions: Sac, Sbut, and Spro. This makes drawing unequivocal conclusions about parameter ranking

challenging. When these figures are cross-referenced with the FAST method, they align much closer to zero.

To summarize, while the Morris method provides valuable insights for sorting and ranking parameters, its occasional inability to converge, especially in the numerical values of sensitivity indices, should be factored in. For visual clarity, Figure 5.13 depicts convergence diagrams of the Q_gas for all parameters, correlated to the number of model iterations.
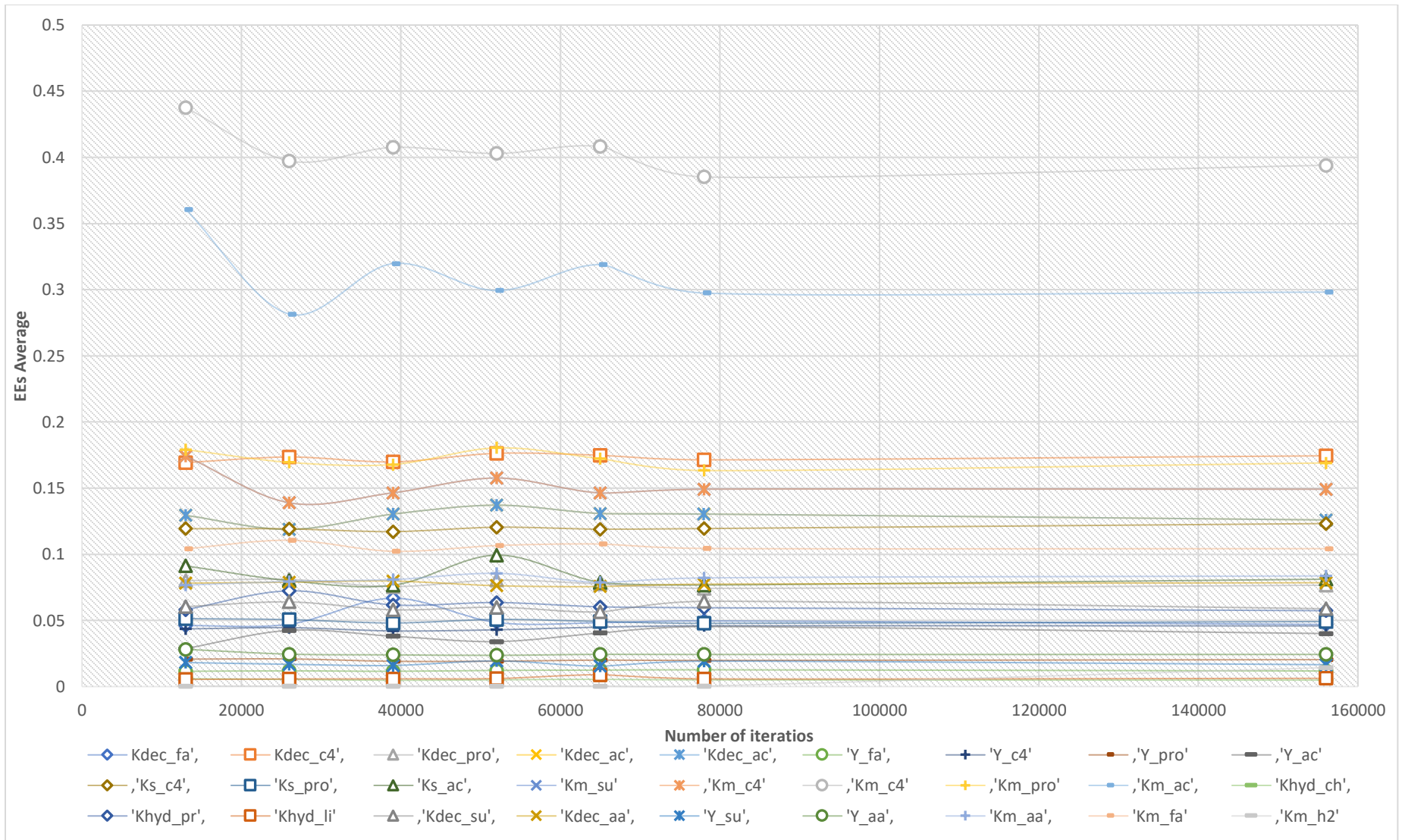
Figure 5. 14: Convergence diagram of parameters for Q_gas, Morris method

Figure 5.14 highlights a convergence process that is observed to be notably more challenging in comparison to the FAST method. Initially, the runs were limited to 78,000. However, further assessments indicated that convergence had not been achieved for all parameters. As a result, the analysis was broadened to encompass 156,000 runs to ensure a thorough examination. The graph clearly depicts numerous fluctuations in the Morris method, suggesting that the model has not yet reached convergence and requires many more runs to do so. This is seen as a significant drawback, especially when compared to the efficiency of the FAST method.

5.2.2.2 Method comparison

The "one-at-a-time" method is a local sensitivity analysis method, and thus, it comes with the corresponding advantages and disadvantages discussed in the preceding chapters. The FAST method is a global approach, while the Morris method is a hybrid between the two. Therefore, a comparison between these methods should be made based on suitable criteria that apply to all three methods. Specifically, the methods are compared based on:

The number of significant and non-significant parameters each method identifies,

- ✓ Their ranking order and the differences therein,
- ✓ Which parameters are deemed significant or not, and
- ✓ The number of iterations each method executed.

Regarding the distinction of parameters into significant and non-significant, Venn diagrams are created with the aim to qualitatively reveal which parameters are significant for each of them, as well as which ones are significant for both simultaneously.

Again, the Venn diagram that is presented is for Q_gas and is displayed in Figure. 5.15.
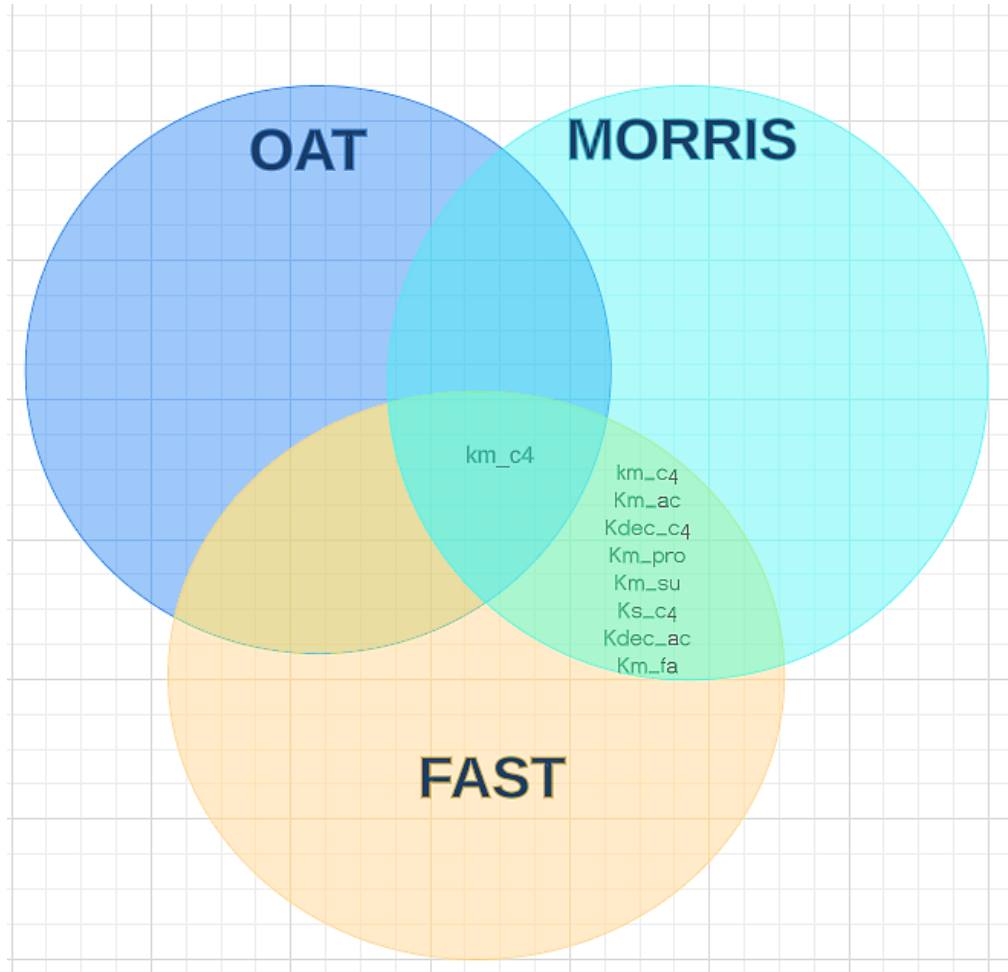
Figure 5. 15: Venn diagram for Q_gas

Figure 5.15 illustrates that for Q gas, both the Morris and FAST methods identify exactly the same significant parameters. In contrast, the OAT method underestimates the important ones. However, the singular parameter deemed significant by OAT is also recognized as significant by both the Morris and FAST methods. Notably, there are no parameters that are unique to just one method, which underscores a sense of stability and consistency across the methods.

➢ **PF indicator**

Regarding the order of classification for each method, a modified position factor (PF) is used, which is presented in Eq 5.9 [531].

$$PF = \sum_{k=1}^{n} \frac{|P_{k,i} - P_{k,j}|}{\mu_{Pk,i}, P_{k,j}}$$ Eq(5.9)

The formula is defined as follows: where n represents the total number of parameters, i and j are two distinct sensitivity analysis methods, $P_{k,I}$ and $P_{k,j}$ denote the ranking positions of the kth parameter for methods i and j respectively, and $\mu_{Pk,i, Pk,j}$ is the average of the two aforementioned values. This index quantifies the differences in ranking between the methods, with a smaller value indicating fewer discrepancies between them.

Values of the PF indicator for the three sensitivity analysis methods applied are presented in Table 5.3.

Table 5. 3: Pf indicator for the three sensitivity analysis methods applied

	OAT	FAST	MORRIS
OAT	-	13.37	15.10
FAST	13.37	-	6.04
MORRIS	15.10	6.04	-

In Table 5.3, the values represent the average measures derived from the four pivotal parameters examined across all three sensitivity methods: VSS, TN, COD, and Qgas.

Between the OAT and Morris methods, the PF is 15.1. This suggests a certain level of disparity in the ranking sequences of the two methods. A PF value closer to zero indicates a stronger alignment or agreement between the methods. In the comparison of FAST and OAT, the PF is slightly lower at 13.37, closely aligning with the 15.1 value from the OAT and Morris comparison.

Conversely, the PF between Morris and FAST is significantly lower at 6.04. This substantial reduction in PF value underscores a notably stronger agreement in the ranking sequences between these two methods compared to the other combinations.

➢ **Number of iterations**

Table 5.4 presents the number of iterations applied in each method.

Table 5. 4: Number of iterations for each method

Number of iterations	N
OAT	80
Morris	156,000
FAST	40,000

In the preceding chapter, the convergence of various methods prompted a detailed discussion on the number of iterations, denoted as N, each method requires. Subsequently, our current comparison primarily hinges on their respective numerical iteration counts.

The OAT method, distinct in its absence of a sampling process, necessitates two simulations for every parameter. These are characterized by alterations of -30% and +30% from their foundational values. An additional simulation is mandated for the reference state. Consequently, for the OAT method, a total of N OAT=80 iterations were executed.

When considering the FAST method, the number of iterations it demands for optimal functionality was ascertained to be 14,249. It's crucial to note that these iterations are pivotal in yielding results for one distinct model output variable. As an aggregate, the FAST method underwent N FAST=40,000 iterations.

Lastly, the Morris method witnessed a comprehensive count of N Morris=156,000 iterations.

5.3 Model calibration

The calibration procedure was thoroughly detailed in Chapter 3, where the analytical methods were delineated. For the calibration of the model, HRT 2days was employed, which represents the initial scenario during winter conditions with a temperature of 18°C.

To effectively calibrate the model to this scenario, a series of tests were undertaken. These were primarily influenced by the sensitivity analysis of the model that had been previously discussed, as well as insights gleaned from pertinent literature. Our adjustments were specifically targeted to fine-tune the model's responsiveness to seasonal temperature variations, from winter to summer, with the ultimate goal of maximizing its accuracy and performance. It is emphasized that

the calibration was implemented by adjusting the values of kinetic parameters (maximum rates and half saturation coefficients) at 35°C, while the partitioning factors of Xc where also changed to better represent typical wastewater rather than sewage sludge (that the default values of the model refer to). The respective values of the calibrated kinetic parameters for winter and summer conditions were calculated by using the temperature dependence equation (Eq. 3.18).

To provide a clear picture of this calibration, the parameter values will be presented as they were originally set by the model. Subsequently, the adjustments that were made tailored to both winter and summer conditions will be showcased. As a result of this systematic approach of tweaking and refining, two distinct parameter sets were derived, each uniquely suited for winter or summer scenarios. For a side-by-side comparison, Table 5.5 lists the newly adjusted parameter values next to the original, baseline values, facilitating a direct assessment of the changes implemented.

Table 5. 5: Modified parameter values.

Parameter	Unit	Benchmark] Value at 35°C	Calibrated value at 35°C	Winter	Summer
fsl,xc	-	0.1	-	0.05	0.05
fxl,xc	-	0.2	-	0.05	0.05
fch,xc	-	0.2	-	0.3	0.3
fpr,xc	-	0.2	-	0.3	0.3
Fli,xc	-	0.3	-	0.3	0.3
K,dis	d^{-1}	0.5	2	1.2	1.4
K,hyd	d^{-1}	10	-	10	10
Km,su	d^{-1}	30	60	20	28
KS,su	$KgCOD\ m^{-3}$	0.5	-	0.2	0.2
Km,aa	d^{-1}	50	80	26	37
KS,aa	$KgCOD\ m^{-3}$	0.3	-	0.1	0.1
Km,fa	d^{-1}	6	15	5	7
KS,fa	$KgCOD\ m^{-3}$	0.4	-	0.1	0.1
Km,c4	d^{-1}	20	30	10	14
Km,pro	d^{-1}	13	20	7	9
Km,ac	d^{-1}	8	16	5	7
Km,h2	d^{-1}	35	50	16	23

Parameter	Unit	Benchmark] Value at 35°C	Calibrated value at 35°C	Winter	Summer
Ks,c4	KgCOD m^{-3}	0.2	-	0.1	0.1
Ks,pro	KgCOD m^{-3}	0.1	-	0.05	0.05
Ks,ac	KgCOD m^{-3}	0.15	-	0.05	0.05

After the parameters were fine-tuned (Table 5.5), specific outcomes related to the target values were observed. These have been compiled in Table 5.6 for clarity: values from the experiments are highlighted in red, while those generated by the model are shown in black.

Table 5. 6: Model Predictions vs. Experimental Data for Calibration

SCENARIO HRT 2days, winter	COD out (mg/L)	Qgas (L/d)	VSS (mg/L)	pH	CH$_4$ (g/d) liquid+air
experiment	**105**	**1.45**	**3550**	**7.28**	**1.23**
model	94	1.68	3446	7.1	1.27

In calibration scenario, the model aligns well with the experimental results for all the parameters examined. The model predicts slightly lower values but mirrors the experimental behavior in Qgas.

5.4 Model validation

After the in-depth calibration of our model in the preceding section, the validation phase took place. Table 5.7presents a detailed comparison between the experimental data (in red) and the simulation results.

Table 5. 7:Model validation results in the 5 remaining research scenarios

SCENARIOS		COD eff (mg/L)	Q gas (L/d)	MLVSS (mg/L)	pH	CH$_4$ (g/d) liquid+air
HRT 2days Summer	**experiment**	**51**	**2.06**	**3530**	**7.18**	**1.44**
	model	77	1.98	3711	6.99	1.35
	experiment	**95**	**3.79**	**3950**	**7.3**	**2.92**

SCENARIOS		COD eff (mg/L)	Q gas (L/d)	MLVSS (mg/L)	pH	CH$_4$ (g/d) liquid+air
HRT 1 day winter	model	101	2.97	4102	7.12	2.27
HRT 1day summer	**experiment**	**67**	**4.94**	**4120**	**7.29**	**3.16**
	model	76	3.54	4266	6.98	2.35
HRT 12 hours winter	**experiment**	**123**	**6.13**	**4200**	**7.05**	**5.26**
	model	121	5.15	4150	6.89	4.01
HRT 12 hours summer	**experiment**	**91**	**7.18**	**4290**	**7.2**	**5.19**
	model	91	6.36	4302	6.97	4.42

Upon reviewing Table 5.7, the efficacy of the model during its validation phase is evident. The model's predictions align remarkably well with the experimental data across all variables studied. However, there's a discernible deviation when observing qgas, which showcases the most significant discrepancies.

To provide a more granulated insight into these deviations, Table 5.8 enumerates the disparities for each variable across different scenarios, offering a direct comparison between the model's predictions and the experimental outcomes.

Table 5. 8: Percentage deviation of model vs experimental results

SCENARIOS	COD eff (mg/L)	Q gas (L/d)	MLVSS (mg/L)	pH	CH$_4$ (g/d) liquid+air
HRT 2days Summer	50%	4%	5%	13%	6%
HRT 1 day winter	6%	21%	4%	2%	21%
HRT 1day summer	13%	28%	3.5%	4%	25%
HRT 12 hours winter	1.6%	16%	1.1%	2.3%	24%
HRT 12 hours summer	0%	11%	0.3%	3.2	14%

A notable observation is the substantial deviation in COD eff (mg/L) during the HRT of 2 days in summer, which stands out at 50%. This marks the highest deviation across all scenarios and parameters, pointing to a significant disparity in this instance.

In contrast, for scenarios with an HRT of 12 hours, both in winter and summer, the deviations are relatively minimal for all parameters, consistently hovering below 5%, showcasing the model's accuracy in shorter HRT durations.

Another point of interest is the Q gas and CH4 parameters. In a couple of scenarios, specifically with an HRT of 1 day, both winter and summer, their deviations exceed 20%. This parallel increase in both parameters suggests a potential linked behavior or sensitivity in the model to certain conditions.

In a broader context, these observed discrepancies are relatively modest, especially when considering the complexities associated with the AnMBR reactor operating under ambient temperatures and processing real wastewater. The inherent unpredictability of these conditions makes it challenging to precisely emulate experimental results. Such deviations, then, underscore the model's commendable accuracy in a real-world setting.

A visual representation highlighting the relationship between experimental results and simulation outputs for all scenarios is also presented. Figures 5.16-5.18 illustrate the three critical parameters: COD effluent, MLVSS, and Qgas (with CH_4 emphasized as the crucial component of biogas).
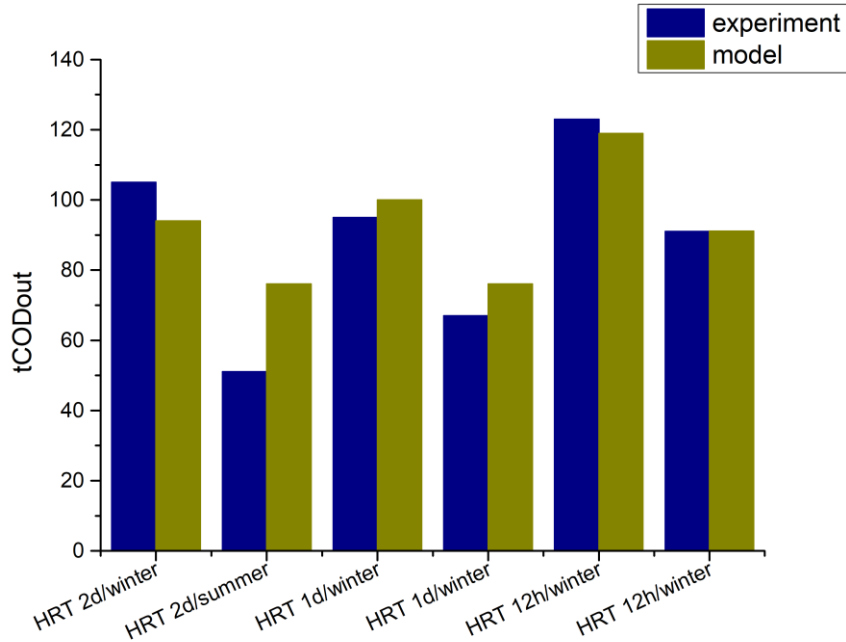
Figure 5. 16: Comparative Column Plots for COD out: Model vs. Experimental Results

As previously highlighted, the COD results for all scenarios align closely with the experimental findings, with the notable exception of the HRT 2-day scenario during the summer period, which exhibits a significant deviation.
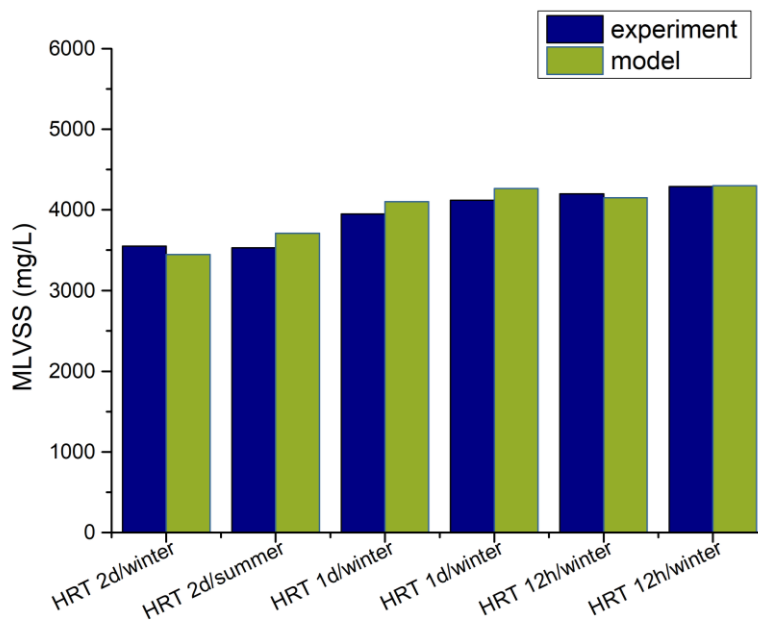
Figure 5. 17: Comparative Column Plots for MLVSS: Model vs. Experimental Results

Figure 5.16 illustrates the model's impressive accuracy in predicting the MLVSS levels within the bioreactor.
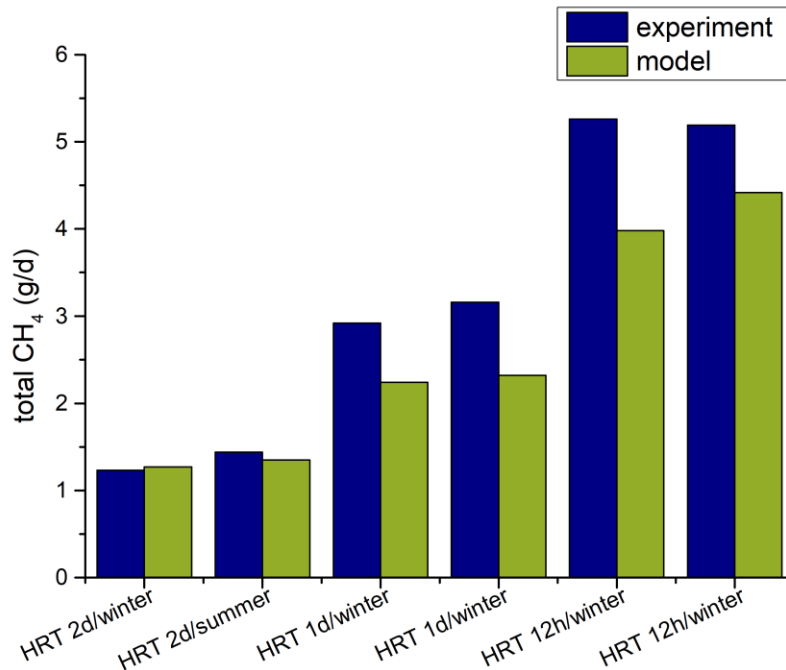
Figure 5. 18:Comparative Column Plots for total CH₄: Model vs. Experimental Results

Figure 5.18 depicts the total methane, which encompasses both liquid and gaseous methane captured from the bioreactor's top. A discernible trend is observed: as the HRTs decrease, the disparity between model predictions and actual measurements widens. The model's most accurate prediction aligns with the HRT of 2 days, which is the scenario where calibration was applied.

5.5 Exploring the Influence of HRT on an AnMBR System

In the AnMBR system model, the goal was to assess its performance across operational settings end examine the optimal operation ones for effluent quality and biogas production. Its behavior was evaluated by varying the HRT, from 3 h to 4 days by keeping all the other parameters constant. The assessment occurred for both summer and winter periods.

Tables 5.9 and 5.10 and Figures 5.19, 5.20 present the results for winter and summer period respectively, highlighting how key parameters evolved with the adjustments in HRT.

Table 5. 9: Data and Outcome Analysis for HRT Influence for winter period.

HRT WINTER	COD	Q gas	VSS	pH	TN
3h	315	0	3845	7.1	65
6h	251	1.7	3922	6.8	66
12h	156	4.08	3988	6.9	66
1 day	115	2.85	3896	6.9	66
2days	94	1.69	3740	6.9	67
4days	83	0.93	3853	6.9	67

Table 5. 10: Data and Outcome Analysis for HRT Influence for summer period.

HRT SUMMER	COD	Q gas	VSS	pH	TN
3h	306	0.00	3830	7.1	66
6h	184	6.51	3996	6.9	66
12h	117	5.79	4008	6.9	66
1 day	92	3.50	3882	6.9	66
2days	77	1.98	3711	6.9	67
4days	70	1.06	3818	6.9	67

Figures 5.19 and 5.20 elucidates the impact of HRT on both the COD and gas production (Qgas) for winter and summer scenarios respectively.
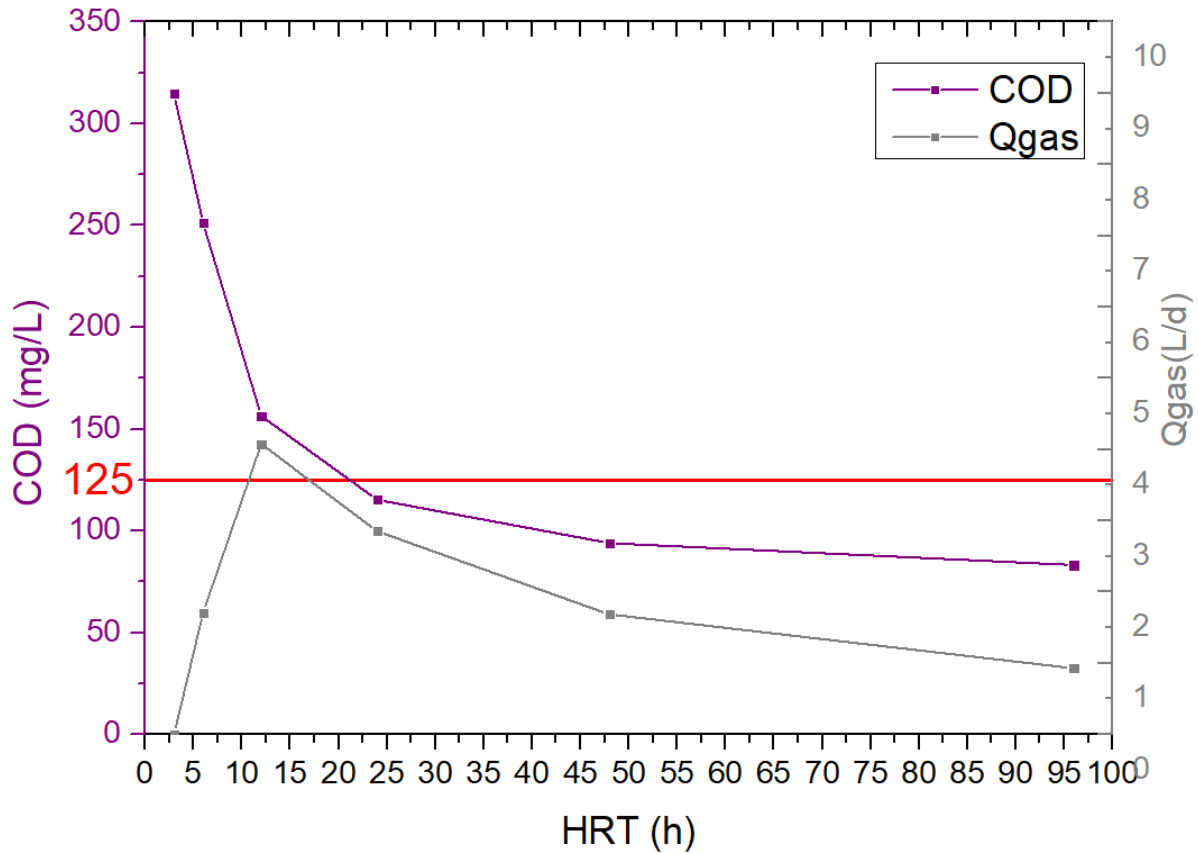
Figure 5. 19: Changes in COD Permeate and gas production with Varying HRTs Examined at winter period

A significant drop in COD is observed as HRT increases, with a sharp decrease evident from 0 to 15 h, before transitioning to a steadier reduction. Alongside, Qgas also exhibits a declining trend, although less pronounced than that of COD. An unusual pattern emerges for Qgas at HRTs below 12 h. This could be due to the slower growth rate of methanogens potentially not allowing methanogenesis to fully initiate. Interestingly, this pattern was absent in experimental results at the 6-hour HRT, though no data was available for a 3-h interval. The red line on the graph represents the legislative threshold for COD, set at 125 mg/L, highlighting the regulatory necessity to maintain COD levels beneath this benchmark. The combination of model and experimental findings offers crucial insights into waste treatment efficiency, gas production, and compliance, underscoring the importance of corroborating model predictions with real data.
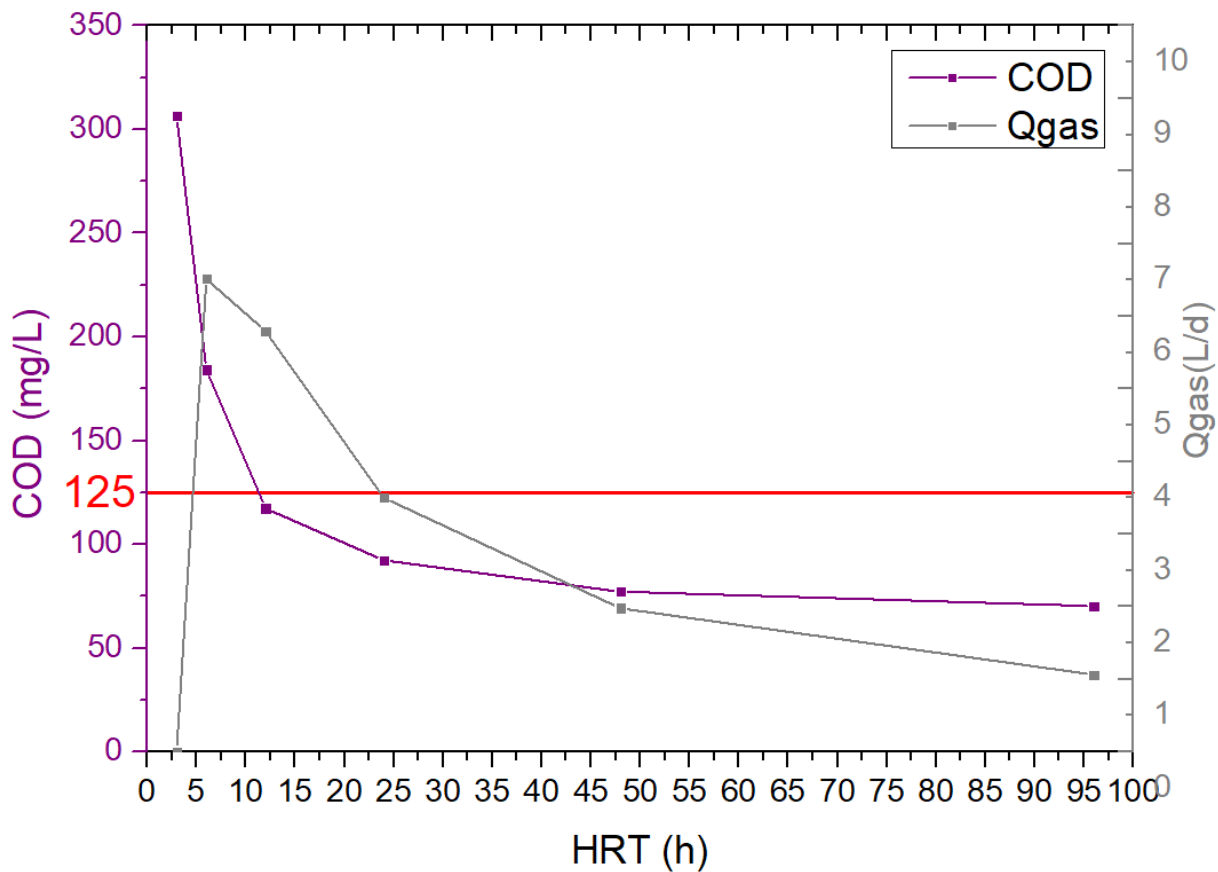
Figure 5. 20: Changes in COD Permeate and gas production with Varying HRTs Examined at summer period

Building on the winter data, Figure 5.20 graph depicts the reactor's performance in summer conditions. As with the winter graph, an increase in HRT is associated with a decrease in COD levels, with a significant reduction observed up to about 15 h. The Qgas similarly declines, but at a more gradual rate. A key difference between the summer and winter graphs is the Qgas behavior. During summer, Qgas shows an irregularity at an HRT of 6 hours, while in winter, this unusual pattern occurs at 12 h. This variation could be influenced by the warmer summer temperatures affecting the methanogens.

To explore the variations in Qgas at shorter HRTs, Figures 5.21 and 5.22 display the methane production in both gaseous and liquid forms.
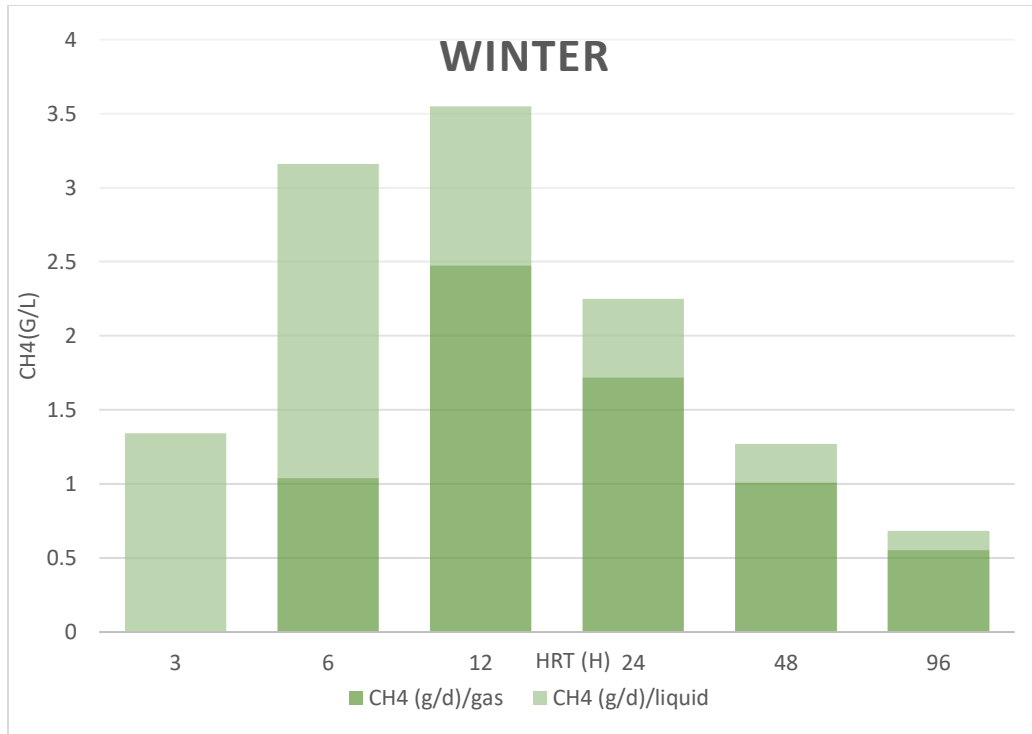
Figure 5. 21: Representation of methane (CH_4) production at both gaseous and liquid form at various HRTs during the winter period.

Figure 5.21 illustrates that as HRT decreases, there's an increase in methane loss in the effluent. This observation aligns with expectations, as more water is treated daily. Notably, at a 6-hour HRT, the anomalous behavior in Qgas, indicating a predominant loss of methane in the effluent in its liquid form. Furthermore, at an even shorter HRT of 3 h, the time appears insufficient for methane to be observed in its gaseous form, with methane predominantly present in the liquid phase.
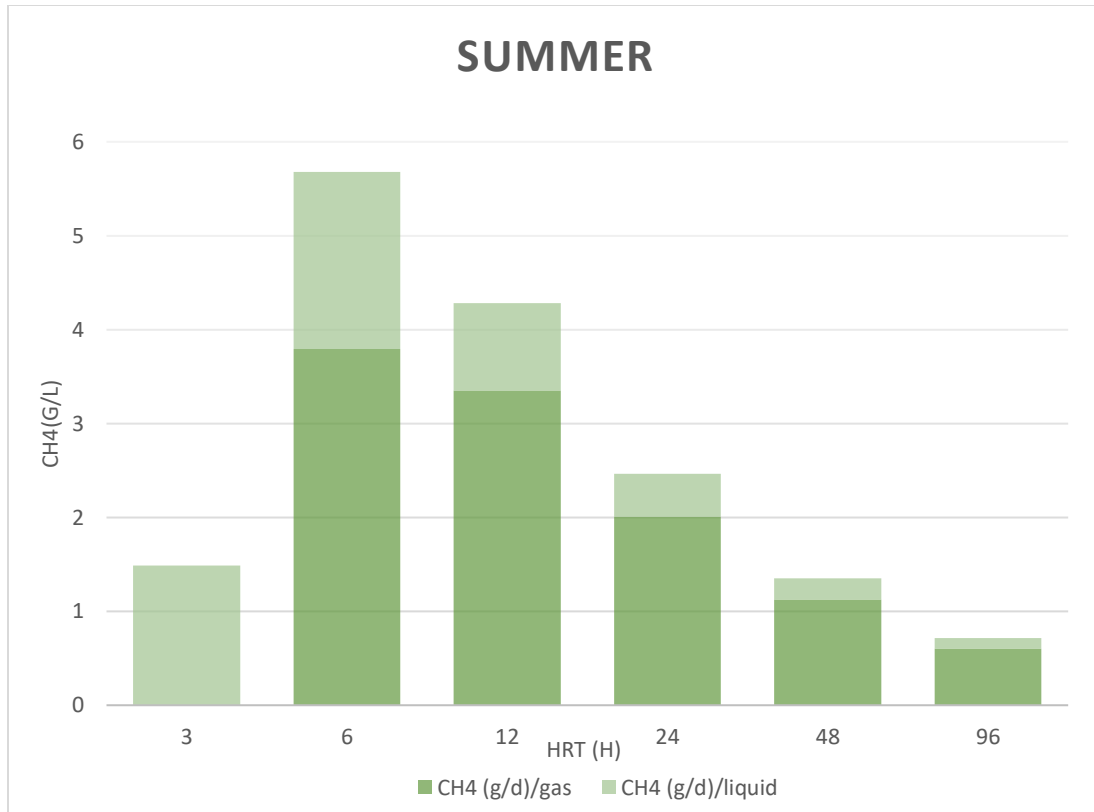
Figure 5. 22: Representation of methane (CH₄) production at both gaseous and liquid form at various HRTs during the summer period.

In the summer conditions, the quantity of liquid methane decreases in all HRTs, due to the temperature-dependent saturation levels of methane. At 6-h HRT, the gaseous form of methane is more prevalent than at a 12-hour HRT, which contrasts with its behavior during the winter.

Conclusively, based on the model's insights, the optimal operational durations are set at 12 hours for summer periods and range between 20 to 24 hours for the winter ones.

Chapter 6: Conclusions, Future Research and Recommendations

6.1 Conclusions

Wastewater treatment advancements have been observed, particularly in the expanded applicability of anaerobic processes. Originally utilized for high-strength wastewaters, these processes are now seen as suitable for low-strength municipal wastewater. In this study, a 40 L Anaerobic Membrane Bioreactor (AnMBR) with a submerged flat sheet membrane was studied. Over three years, the 40 L pilot-scale AnMBR was operated within the 14 – 26°C temperature range at four different HRTs. The main objective was to assess the performance of the AnMBR under psychrophilic temperatures. This conclusion section compiles the primary findings, highlighting the potential and limitations of AnMBR technology for Wastewater Treatment Plants in Mediterranean climates.

> ➤ <u>AnMBR Overall Performance:</u>

In the summer with an average Temperature 23±1, 24 ± 2, 24 ±3 and 23 ±2, removal rates of 89%±1, 85%±2, 78%±3, and 73±4 were achieved by the AnMBR, resulting in average permeate effluent COD concentrations of 51±5 mg/L, 67±6 mg/L, 91±4 mg/L, and 121±8 mg/L for HRTs of 2 d, 1 d, 12 h, and 6h, respectively. In the winter (with T=18±4°C, 19 ±2 , 19±3 and 18 ±3), removal rates were recorded at 76%±4, 77%±4, 69%±5, and 60%±3, with corresponding average permeate effluent COD concentrations of 105±9 mg/L, 95±12 mg/L, 123±9 mg/L, and 177±8 mg/L, respectively. Throughout the study, stability of the AnMBR operation was maintained. TMP values were observed to be low at the 2 d HRT but increased at 1 d HRT and a more significant increase was observed at 12 h HRT. At the 6 h HRT, a noticeable TMP growth rate was obtained during winter, leading to a need for chemical cleaning every 38 days, whereas in summer, this cleaning interval was extended to 50 days. It was found that AnMBR performance was most affected by temperature changes at the 12 h and 6h HRTs.

> ➤ Enhancement of AnMBR Operation with Iron Addition:

During winter at a 6 h HRT, $FeCl_3$ was introduced. When iron was added at concentrations of 25 mg $FeCl_3$/L and 30 mg $FeCl_3$/L, reductions in average effluent COD to 147 mg/L and 149 mg/L

were observed, down from 177 mg/L without FeCl$_3$. This indicates an improvement of COD removal. Total P removals of 75% and 100% were also obtained with FeCl$_3$ addition. The methane yield remained unchanged with the different iron doses. An average of 0.37 L biogas/g COD removed was produced during winter. Soluble methane in the permeate was found to be at saturation levels, accounting for 20.6% and 43.8% of the total methane in summer and winter, respectively. For large-scale applications of AnMBR, an effective dissolved methane recovery process is deemed necessary.

When 25 mg FeCl3/L was added, micropollutant removal was observed. Except for NP, the AnMBR was found to have limited efficacy in micropollutant removal. With or without iron, more than 70% NP removal efficiency was achieved. However, other micropollutants such as TCS, BPA, IBU, NPX, DCF, and KTP showed removal rates between 10% and 40%. From these observations, it was concluded that anaerobic conditions might not be optimal for the removal of most target CECs.

> ➤ Regulatory Compliance & Potential Reuse:

From the data, it can be inferred that AnMBR systems operating under psychrophilic temperatures common in Southern Europe during winter, appear to meet the standards of Directive 91/271/EEC for HRTs of 2 days, 1 day, and 12 h. The 12 h HRT performance observed in winter, was close to the set limit specified by the UWWTD, suggesting caution in its operation. While the addition of iron improved the process, it did not consistently achieved effluent values, below the effluent Standards. Despite these challenges, AnMBRs are considered a promising process for urban wastewater treatment, offering both energy generation and water suitable for fertigation.

> ➤ Energy production

Our research indicates that the lab-scale AnMBR system consistently achieved a balanced energy output across all examined scenarios. Specifically, the recorded energy outputs ranged from 0.3 – 0.9 KWh/KgCODrem during both winter and summer periods. When compared to conventional aerobic activated sludge systems, the AnMBR system aligns with the energy neutrality standard. Given the European Commission's recent proposal for the revision of the Urban Wastewater Treatment Directive (UWWTD) 91/271/EEC, which emphasizes the need for energy-neutral urban wastewater treatment plants), the optimization of AnMBR becomes even more pertinent, not just

in Europe but worldwide.(https://environment.ec.europa.eu/publications/proposal-revised-urban-wastewater-treatment-directive)

➢ AnMBR Modeling

The IWA ADM1 model was modified and adapted for the simulation of the AnMBR reactor using experimental data provided in Chapter 4. Sensitivity was assessed using the Morris, Fast, and One-at-a-Time (OAT) methods. Following this, a calibration of the model was performed based on empirical data. During validation, the model's reliability was confirmed. The code was modified to fit our data, and it was observed that the values of many kinetic parameters required were significantly higher than in the original model. This indicates that processes within the reactor were faster than anticipated. In five distinct scenarios, close alignment was found between the model's predictions and the experimental outcomes. The model was further employed to examine the optimal AnMBR operation in terms of effluent quality and biogas production. The model results, verified the experimental results and predicted optimum HRT for winter and summer, of 24 h and 12 h respectively.

➢ Broader Implications and Modeling Context

The dynamics of an AnMBR reactor, especially when treating real wastewater, are effectively mirrored by the model. Variations between the model's predictions and the actual experimental results, which can be attributed to real-world unpredictability, were noted. In scenarios with a 12-hour HRT for both seasons, a high degree of accuracy was exhibited by the model, with most parameters showing less than a 5% deviation. An exception was found with CH4 during winter, where a more pronounced variance was detected.

6.2 Future Research and Recommendations

➢ AnMBR performance

The Anaerobic Membrane Bioreactors (AnMBR) show potential for improved wastewater treatment. While the thesis provides insights, further exploration is necessary. For instance, our findings suggest a 50-day Sludge Retention Time (SRT) ensures quality permeate, but variations

in SRT durations might reveal more about system performance. Furthermore, Hydraulic Retention Times (HRT) under 12 hours have challenges, especially in winter, indicating the need for optimization.

In terms of membrane fouling, potential solutions such as the introduction of $FeCl_3$ show promise, but the effects of other flux enhancers like alum need further exploration. Understanding the relationship between HRT and membrane performance requires more advanced tools, and biogas sparging's role in reversible fouling deserves attention.

A gap remains between bench-scale studies and full-scale AnMBR applications. Bridging this divide is essential for broader industry acceptance. The potential of material addition in large scales and the feasibility of such operations should also be a focus.

Energy optimization, especially in biogas production and methane recovery, should be prioritized. Exploring energy potential in municipal wastewater can lead to more self-sufficient AnMBR systems. Additionally, there's potential in innovative AnMBR configurations to address challenges such as membrane fouling.

In conclusion, while AnMBRs have advantages, more extensive research is essential for their widespread adoption, aiming to develop mature technology for broader applications.

> AnMBR Modeling and Application

AnMBRs are emerging as effective wastewater treatment solutions. However, there's room for improvement. Our AnMBR model, particularly the ADM1, had limitations, especially at shorter HRTs. Addressing these is crucial for cost-effective operations. A comprehensive approach to sensitivity analysis in simulation models can ensure robustness and consistency.

Measuring more than just biogas flow can help in model calibration. For instance, our research introduced a cost-effective methane analyzer, showing promise for broader applications. A lack of consistent benchmarks and databases hampers current modeling efforts. Establishing a well-structured database, especially for less-explored temperatures like psychrophilic ones, can help.

Applying models to varied scenarios broadens AnMBR understanding. Increasing iterative cycles in research could align experimental and computational findings better.

In closing, as sustainable wastewater treatment becomes a priority, refining AnMBR models becomes essential. Through systematic tools and expanded databases, acceptance among industry professionals can grow

References

1. Van Lier, J. B. *et al. Anaerobic Wastewater Treatment*. *IWA Publishing* 415–457 (IWA Publishing, 2008).

2. Gerardi, M. H. The Microbiology of Anaerobic Digesters. *Microbiol. Anaerob. Dig.* (2003). doi:10.1002/0471468967

3. Samir Kumar Khanal. Anaerobic Biotechnology for Bioenergy Production: Principles and Applications. *Anaerob. Biotechnol. Bioenergy Prod. Princ. Appl.* (2008).

4. Abbasi, T., Tauseef, S. M. & Abbasi, S. A. Anaerobic digestion for global warming control and energy generation - An overview. *Renew. Sustain. Energy Rev.* **16**, 3228–3242 (2012).

5. Nayono, S. E. Anaerobic digestion of organic solid waste for energy production. (2010). doi:10.5445/KSP/1000015038

6. Parawira, W. Enzyme research and applications in biotechnological intensification of biogas production. *Crit. Rev. Biotechnol.* **32**, 172–186 (2012).

7. Ostrem, K. M., Millrath, K. & Themelis, N. J. Combining anaerobic digestion and waste-to-energy. *Proc. 12TH Annu. North Am. Waste to Energy Conf.* 265–271 (2004). doi:10.1115/NAWTEC12-2231

8. Botheju, D., Lie, B. & Bakke, R. Oxygen effects in anaerobic digestion - II. *Model. Identif. Control* **31**, 55–65 (2010).

9. Schlüter, A. *et al.* The metagenome of a biogas-producing microbial community of a production-scale biogas plant fermenter analysed by the 454-pyrosequencing technology. *J. Biotechnol.* **136**, 77–90 (2008).

10. Zeeman, G., Sanders, W. T. M., Wang, K. Y. & Lettinga, G. Anaerobic treatment of complex wastewater and waste activated sludge — Application of an upflow anaerobic solid removal (UASR) reactor for the removal and pre-hydrolysis of suspended COD. *Water Sci. Technol.* **35**, 121–128 (1997).

11. Lier, J. van, Mahmoud, N. & Zeeman, G. Anaerobic biological wastewater treatment. 415–511 (2008).

12. Gujer, W. & Zehnder, A. J. B. Conversion Processes in Anaerobic Digestion. *Water Sci. Technol.* **15**, 127–167 (1983).

13. Bilitewski, B., Hardtle, G. & Marek, K. *Waste management*. *Waste management* (Springer, 1997).

14. Speece, R. E. Anaerobic biotechnology for industrial wastewaters. 394 (1996).

15. Ma, J. *et al.* A simple methodology for rate-limiting step determination for anaerobic digestion of complex substrates and effect of microbial community ratio. *Bioresour. Technol.* **134**, 391–395 (2013).

16. McCarty, P. L. & Mosey, F. E. Modelling of Anaerobic Digestion Processes (A Discussion of Concepts). *Water Sci. Technol.* **24**, 17–33 (1991).

17. Xia, A., Cheng, J. & Murphy, J. D. Innovation in biological production and upgrading of methane and hydrogen for use as gaseous transport biofuel. *Biotechnol. Adv.* **34**, 451–472 (2016).

18. Lew, B., Lustig, I., Beliavski, M., Tarre, S. & Green, M. An integrated UASB-sludge digester system for raw domestic wastewater treatment in temperate climates. *Bioresour. Technol.* **102**, 4921–4924 (2011).

19. McKeown, R. M., Hughes, D., Collins, G., Mahony, T. & O'Flaherty, V. Low-temperature anaerobic digestion for wastewater treatment. *Curr. Opin. Biotechnol.* **23**, 444–451 (2012).

20. Batstone, D. J. *et al.* The IWA Anaerobic Digestion Model No 1 (ADM1). *Water Sci. Technol.* **45**, 65–73 (2002).

21. Azbar, N., Ursillo, P. & Speece, R. E. Effect of process configuration and substrate complexity on the performance of anaerobic processes. *Water Res.* **35**, 817–829 (2001).

22. Mata-Alvarez, J. *Biomethanization of the Organic Fraction of Municipal Solid Wastes*. *Water 21* (IWA Publishing, 2005). doi:10.2166/9781780402994

23. Killilea, J. E., Colleran, E. & Scahill, C. Establishing procedures for design, operation and maintenance of sewage sludge anaerobic treatment plants. *Water Sci. Technol.* **41**, 305–312 (2000).

24. Bouallagui, H., Ben Cheikh, R., Marouani, L. & Hamdi, M. Mesophilic biogas production from fruit and vegetable waste in a tubular digester. *Bioresour. Technol.* **86**, 85–89 (2003).

25. Verrier, D., Roy, F. & Albagnac, G. Two-phase methanization of solid vegetable wastes. *Biol. Wastes* **22**, 163–177 (1987).

26. Hwang, M. H., Jang, N. J., Hyun, S. H. & Kim, I. S. Anaerobic bio-hydrogen production from ethanol fermentation: The role of pH. *J. Biotechnol.* **111**, 297–309 (2004).

27. Liu, Y. & Tay, J. H. State of the art of biogranulation technology for wastewater treatment. *Biotechnol. Adv.* **22**, 533–563 (2004).

28. Molina, F., Castellano, M., García, C., Roca, E. & Lema, J. M. Selection of variables for on-line monitoring, diagnosis, and control of anaerobic digestion processes. *Water Sci. Technol.* **60**, 615–622 (2009).

29. Boe, K., Batstone, D. J., Steyer, J. P. & Angelidaki, I. State indicators for monitoring the anaerobic digestion process. *Water Res.* **44**, 5973–5980 (2010).

30. Rao, M. S. & Singh, S. P. Bioenergy conversion studies of organic fraction of MSW: kinetic studies and gas yield–organic loading relationships for process optimisation. *Bioresour. Technol.* **95**, 173–185 (2004).

31. Bouallagui, H., Lahdheb, H., Ben Romdan, E., Rachdi, B. & Hamdi, M. Improvement of fruit and vegetable waste anaerobic digestion performance and stability with co-substrates addition. *J. Environ. Manage.* **90**, 1844–1849 (2009).

32. Scherer, P. A., Vollmer, G. R., Fakhouri, T. & Martensen, S. Development of a methanogenic process to degrade exhaustively the organic fraction of municipal "grey waste" under thermophilic and hyperthermophilic conditions. *Water Sci. Technol.* **41**, 83–91 (2000).

33. Ahring, B. K. Status on science and application of thermophilic anaerobic digestion. *Water Sci. Technol.* **30**, 241–249 (1994).

34. Lettinga, G., Rebac, S. & Zeeman, G. Challenge of psychrophilic anaerobic wastewater treatment. *Trends Biotechnol.* **19**, 363–370 (2001).

35. Neczaj, E. & Grosser, A. Biogas production by thermal hydrolysis and thermophilic

anaerobic digestion of waste-activated sludge. *Ind. Munic. Sludge Emerg. Concerns Scope Resour. Recover.* 741–781 (2019). doi:10.1016/B978-0-12-815907-1.00031-3

36. Ge, H., Jensen, P. D. & Batstone, D. J. Pre-treatment mechanisms during thermophilic–mesophilic temperature phased anaerobic digestion of primary sludge. *Water Res.* **44**, 123–130 (2010).

37. Gebreeyessus, G. D. & Jenicek, P. Thermophilic versus Mesophilic Anaerobic Digestion of Sewage Sludge: A Comparative Review. *Bioeng. 2016, Vol. 3, Page 15* **3**, 15 (2016).

38. Lawrence, A. & McCarty, P. Kinetics of Methane Fermentation in Anaerobic Treatment on JSTOR. *Water Pollut. Control Fed.* **41**, R1–R17 (1969).

39. Switzenbaum, M. S. & Jewell, W. J. Anaerobic attached film expanded bed reactor for the treatment of dilute organic wastes. (1978). doi:10.2172/6085589

40. Huser, B. A., Wuhrmann, K. & Zehnder, A. J. B. Methanothrix soehngenii gen. nov. sp. nov., a new acetotrophic non-hydrogen-oxidizing methane bacterium. *Arch. Microbiol.* **132**, 1–9 (1982).

41. Svensson, B. H. Different temperature optima for methane formation when enrichments from Acid peat are supplemented with acetate or hydrogen. *Appl. Environ. Microbiol.* **48**, 389–394 (1984).

42. Lin, C. Y., Noike, T., Sato, K. & Matsumoto, J. Temperature characteristics of the methanogenesis process in anaerobic digestion. *Water Sci. Technol.* **19**, 299–310 (1987).

43. Westermann, P. *et al.* Temperature Compensation in Methanosarcina barkeri by Modulation of Hydrogen and Acetate Affinity. *Appl. Environ. Microbiol.* **55**, 1262 (1989).

44. Matsushige, K., Inamori, Y., Mizuochi, M., Hosomi, M. & Sudo, R. The effects of temperature on anaerobic filter treatment for low-strength organic wastewater. *http://dx.doi.org/10.1080/09593339009384942* **11**, 899–910 (2008).

45. Wu, W. M., Thiele, J. H., Jain, M. K. & Zeikus, J. G. Metabolic properties and kinetics of methanogenic granules. *Appl. Microbiol. Biotechnol.* **39**, 804–811 (1993).

46. Rebac, S. *et al.* High-rate anaerobic treatment of wastewater under psychrophilic conditions. *J. Ferment. Bioeng.* **80**, 499–506 (1995).

47.   Kettunen, R. H. & Rintala, J. A. The effect of low temperature (5-29 °C) and adaptation on the methanogenic activity of biomass. *Appl. Microbiol. Biotechnol.* **48**, 570–576 (1997).

48.   van den Berg, L. Effect of temperature on growth and activity of a methanogenic culture utilising acetate. *Can. J. Microbiol.* **23**, 898–902 (1977).

49.   Van Lier, J. B. *et al.* Anaerobic treatment of partly acidified wastewater in a two-stage Expanded Granular Sludge Bed (EGSB) system at 8°C. *Water Sci. Technol.* **36**, 317–324 (1997).

50.   Jiang, Y., Heaven, S. & Banks, C. J. Strategies for stable anaerobic digestion of vegetable waste. *Renew. Energy* **44**, 206–214 (2012).

51.   Angelidaki, I. & Sanders, W. Assessment of the anaerobic biodegradability of macropollutants. *Rev. Environ. Sci. Biotechnol.* **3**, 117–129 (2004).

52.   Angelidaki, I. *et al.* Defining the biomethane potential (BMP) of solid organic wastes and energy crops: A proposed protocol for batch assays. *Water Sci. Technol.* **59**, 927–934 (2009).

53.   Demirel, B. & Scherer, P. Trace element requirements of agricultural biogas digesters during biological conversion of renewable biomass to methane. *Biomass and Bioenergy* **35**, 992–998 (2011).

54.   Wan, C., Zhou, Q., Fu, G. & Li, Y. Semi-continuous anaerobic co-digestion of thickened waste activated sludge and fat, oil and grease. *Waste Manag.* **31**, 1752–1758 (2011).

55.   Hussain, A., Kumar, P. & Mehrotra, I. Nitrogen and phosphorus requirement in anaerobic process: A review. *Environ. Eng. Manag. J.* **14**, 769–780 (2015).

56.   Montusiewicz, A. Environmental factors affecting the biomethanization process. *Arch. Environ. Prot.* 265–279 (2008).

57.   Chen, Y., Cheng, J. J. & Creamer, K. S. Inhibition of anaerobic digestion process: A review. *Bioresour. Technol.* **99**, 4044–4064 (2008).

58.   Mcdonnell, G. & Russell, A. D. Antiseptics and disinfectants: activity, action, and resistance. *Clin. Microbiol. Rev.* **12**, 147–179 (1999).

59.   Fujishima, S., Miyahara, T. & Noike, T. Effect of moisture content on anaerobic digestion of dewatered sludge: ammonia inhibition to carbohydrate removal and methane production. *Water Sci. Technol.* **41**, 119–127 (2000).

60.   Angelidaki, I. *et al.* General rights Anaerobic Biodegradation, Activity and Inhibition (ABAI) . in *Proceedings of the ABAI Task Group Meeting* (2007).

61.   Mata-Alvarez, J., Macé, S. & Llabrés, P. Anaerobic digestion of organic solid wastes. An overview of research achievements and perspectives. *Bioresour. Technol.* **74**, 3–16 (2000).

62.   Wendland, C. Anaerobic Digestion of Blackwater and Kitchen Refuse. (Technical University Hamburg, 2009).

63.   Angelidaki, I. & Ahring, B. K. Thermophilic anaerobic digestion of livestock waste: the effect of ammonia. *Appl. Microbiol. Biotechnol.* **38**, 560–564 (1993).

64.   Kiely, G., Tayfur, G., Dolan, C. & Tanji, K. Physical and mathematical modelling of anaerobic digestion of organic wastes. *Water Res.* **31**, 534–540 (1997).

65.   Hansen, K. H., Angelidaki, I. & Ahring, B. K. ANAEROBIC DIGESTION OF SWINE MANURE: INHIBITION BY AMMONIA. *Water Res.* **32**, 5–12 (1998).

66.   Ramirez, I. *et al.* Modified ADM1 disintegration/hydrolysis structures for modeling batch thermophilic anaerobic digestion of thermally pretreated waste activated sludge. *Water Res.* **43**, 3479–3492 (2009).

67.   McCarty, P. Anaerobic waste treatment fundamentals. *Public Work.* **95**, (1964).

68.   Hobson, P. N. & Shaw, B. G. Inhibition of methane production by Methanobacterium formicicum. *Water Res.* **10**, 849–852 (1976).

69.   Sung, S. & Liu, T. Ammonia inhibition on thermophilic anaerobic digestion. *Chemosphere* **53**, 43–52 (2003).

70.   Procházka, J., Dolejš, P., MácA, J. & Dohányos, M. Stability and inhibition of anaerobic processes caused by insufficiency or excess of ammonia nitrogen. *Appl. Microbiol. Biotechnol.* **93**, 439–447 (2012).

71.   Fotidis, I. A., Karakashev, D., Kotsopoulos, T. A., Martzopoulos, G. G. & Angelidaki, I.

Effect of ammonium and acetate on methanogenic pathway and methanogenic community composition. *FEMS Microbiol. Ecol.* **83**, 38–48 (2013).

72. Kadam, P. C. & Boone, D. R. Influence of pH on Ammonia Accumulation and Toxicity in Halophilic, Methylotrophic Methanogens. *Appl. Environ. Microbiol.* **62**, 4486–4492 (1996).

73. Greben, H. A., Maree, J. P., Eloff, E. & Murray, K. Improved sulphate removal rates at increased sulphide concentration in the sulphidogenic bioreactor. *Water SA* **31**, 351–358 (2005).

74. Perkin, G. *et al.* Response of Methane Fermentation Systems to Industrial Toxicants on JSTOR. *J. (Water Pollut. Control Fed.* **55**, 44–53 (1983).

75. Yamaguchi, T., Harada, H., Hisano, T., Yamazaki, S. & Tseng, I. C. Process behavior of UASB reactor treating a wastewater containing high strength sulfate. *WatRe* **33**, 3182–3190 (1999).

76. Feijoo, G., Soto, M., Méndez, R. & Lema, J. M. Sodium inhibition in the anaerobic digestion process: Antagonism and adaptation phenomena. *Enzyme Microb. Technol.* **17**, 180–188 (1995).

77. Appels, L., Baeyens, J., Degrève, J. & Dewil, R. Principles and potential of the anaerobic digestion of waste-activated sludge. *Prog. Energy Combust. Sci.* **34**, 755–781 (2008).

78. Bashir, B. & Matin, A. Combined effect of potassium and magnesium on sodium toxicity in anaerobic treatment processes. *Electron. J. Environ. Agric. Food Chem.* **4**, (2005).

79. Bashir, B. & Matin, A. Combined effect of calcium and magnesium on sodium toxicity in anaerobic treatment processes. *Electron. J. Environ. Agric. Food Chem.* **4**, (2005).

80. Wu, D., Yang, Z. & Tian, G. Inhibitory effects of Cu (II) on fermentative methane production using bamboo wastewater as substrate. *J. Hazard. Mater.* **195**, 170–174 (2011).

81. Hao, H., Tian, Y., Zhang, H. & Chai, Y. Copper stressed anaerobic fermentation: biogas properties, process stability, biodegradation and enzyme responses. *Biodegradation* **28**, 369–381 (2017).

82. Zhang, Q., Sun, F., Dong, W., Zhang, G. & Han, R. Micro-polluted surface water treatment and trace-organics removal pathway in a PAC-MBR system. *Process Biochem.*

50, 1422–1428 (2015).

83.   Tian, Y. *et al.* Biogas properties and enzymatic analysis during anaerobic fermentation of Phragmites australis straw and cow dung: influence of nickel chloride supplement. *Biodegradation* **28**, 15–25 (2017).

84.   Andriamanohiarisoamanana, F. J. *et al.* Valorizing waste iron powder in biogas production: Hydrogen sulfide control and process performances. *J. Environ. Manage.* **208**, 134–141 (2018).

85.   Zhang, H., Tian, Y., Wang, L., Zhang, L. & Dai, L. Ecophysiological characteristics and biogas production of cadmium-contaminated crops. *Bioresour. Technol.* **146**, 628–636 (2013).

86.   Bourven, I. *et al.* Potential of DGT in a new fractionation approach for studying trace metal element impact on anaerobic digestion: the example of cadmium. *Int. Biodeterior. Biodegradation* **119**, 188–195 (2017).

87.   Chan, P. C., de Toledo, R. A., Iu, H. I. & Shim, H. Effect of Zinc Supplementation on Biogas Production and Short/Long Chain Fatty Acids Accumulation During Anaerobic Co-digestion of Food Waste and Domestic Wastewater. *Waste and Biomass Valorization* **10**, 3885–3895 (2019).

88.   Scalbert, A. Antimicrobial properties of tannins. *Phytochemistry* **30**, 3875–3883 (1991).

89.   Foxon, K. M. *et al.* The evaluation of the anaerobic baffled reactor for sanitation in dense peri-urban settlements Report to the Water Research Commission Evaluation of the Anaerobic Baffled Reactor for Sanitation in Dense Peri-urban Settlements. (2006).

90.   Arceivala, S. J. & Asolekar, D. S. R. *Wastewater Treatment for Pollution Control and Reuse. Rwanda Journal of Health Sciences* **1**, (McGraw-Hill Education, 2007).

91.   Muyzer, G. & Stams, A. J. M. The ecology and biotechnology of sulphate-reducing bacteria. *Nat. Rev. Microbiol.* **6**, 441–454 (2008).

92.   Madigan, M., Martinko, john & Brock, T. Brock biology of microorganisms | WorldCat.org. in *Pearson Prentice Hall,* (2006).

93.   Chartrain, M. & Zeikus, J. G. Microbial ecophysiology of whey biomethanation: characterization of bacterial trophic populations and prevalent species in continuous

culture. *Appl. Environ. Microbiol.* **51**, 188–196 (1986).

94. Uddin, M. M. & Wright, M. M. Anaerobic digestion fundamentals, challenges, and technological advances. *Phys. Sci. Rev.* (2022). doi:10.1515/PSR-2021-0068/MACHINEREADABLECITATION/RIS

95. Linke, B. Kinetic study of thermophilic anaerobic digestion of solid wastes from potato processing. *Biomass and Bioenergy* **30**, 892–896 (2006).

96. Sialve, B., Bernet, N. & Bernard, O. Anaerobic digestion of microalgae as a necessary step to make microalgal biodiesel sustainable. *Biotechnol. Adv.* **27**, 409–416 (2009).

97. Nijaguna, B. T. *Biogas Technology, New Age International*. (Limited Publishers, 2012).

98. Khoiyangbam, R. S., Gupta, N. & Kumar, S. Biogas technology: towards sustainable development. *Biogas Technol. Towar. Sustain. Dev.* (2011).

99. Abbasi, T., Tauseef, S. M. & Abbasi, S. A. Anaerobic digestion for global warming control and energy generation—An overview. *Renew. Sustain. Energy Rev.* **16**, 3228–3242 (2012).

100. Ergüder, T. H., Güven, E. & Demirer, G. N. The inhibitory effects of lindane in batch and upflow anaerobic sludge blanket reactors. *Chemosphere* **50**, 165–169 (2003).

101. Mulder, A., van de Graaf, A. A., Robertson, L. A. & Kuenen, J. G. Anaerobic ammonium oxidation discovered in a denitrifying fluidized bed reactor. *FEMS Microbiol. Ecol.* **16**, 177–183 (1995).

102. Peng, Y. & Zhu, G. Biological nitrogen removal with nitrification and denitrification via nitrite pathway. *Appl. Microbiol. Biotechnol.* **73**, 15–26 (2006).

103. Hao, X., Liu, R. & Huang, X. Evaluation of the potential for operating carbon neutral WWTPs in China. *Water Res.* **87**, 424–431 (2015).

104. Wang, H. *et al.* Comparative analysis of energy intensity and carbon emissions in wastewater treatment in USA, Germany, China and South Africa. *Appl. Energy* (2016). doi:10.1016/j.apenergy.2016.07.061

105. Santos, E., Albuquerque, A., Lisboa, I., Murray, P. & Ermis, H. Economic Assessment of Energy Consumption in Wastewater Treatment Plants: Applicability of Alternative Nature-

Based Technologies in Portugal. *Water 2022, Vol. 14, Page 2042* **14**, 2042 (2022).

106. Vaccari, M., Foladori, P., Nembrini, S. & Vitali, F. Benchmarking of energy consumption in municipal wastewater treatment plants – a survey of over 200 plants in Italy. *Water Sci. Technol.* **77**, 2242–2252 (2018).

107. Mamais, D., Noutsopoulos, C., Dimopoulou, A., Stasinakis, A. & Lekkas, T. D. Wastewater treatment process impact on energy savings and greenhouse gas emissions. *Water Sci. Technol.* **71**, 303–308 (2015).

108. Siatou, A., Manali, A. & Gikas, P. Energy Consumption and Internal Distribution in Activated Sludge Wastewater Treatment Plants of Greece. *Water 2020, Vol. 12, Page 1204* **12**, 1204 (2020).

109. Wan, J., Gu, J., Zhao, Q. & Liu, Y. COD capture: a feasible option towards energy self-sufficient domestic wastewater treatment. *Sci. Reports 2016 61* **6**, 1–9 (2016).

110. Zhou, Y., Zhang, D. Q., Le, M. T., Puah, A. N. & Ng, W. J. Energy utilization in sewage treatment - A review with comparisons. *J. Water Clim. Chang.* **4**, 1–10 (2013).

111. Jonasson, M. Energy Benchmark for Wastewater Treatment Processes-a comparison between Sweden and Austria. *Lund Univ.* (2007).

112. Monteith, H., Kalogo, Y. & Louzeiro, N. ACHIEVING STRINGENT EFFLUENT LIMITS TAKES A LOT OF ENERGY! *Proc. Water Environ. Fed.* **2007**, 4343–4356 (2012).

113. Mizuta, K. & Shimada, M. Benchmarking energy consumption in municipal wastewater treatment plants in Japan. *Water Sci. Technol.* **62**, 2256–2262 (2010).

114. McCarty, P. L., Bae, J. & Kim, J. Domestic wastewater treatment as a net energy producer-can this be achieved? *Environ. Sci. Technol.* **45**, 7100–7106 (2011).

115. Shizas, I. & Bagley, D. M. Experimental Determination of Energy Content of Unknown Organics in Municipal Wastewater Streams. *J. Energy Eng.* **130**, 45–53 (2004).

116. Heidrich, E. S., Curtis, T. P. & Dolfing, J. Determination of the internal chemical energy of wastewater. *Environ. Sci. Technol.* **45**, 827–832 (2011).

117. Lin, H. *et al.* A review on anaerobic membrane bioreactors: Applications, membrane fouling and future perspectives. *Desalination* **314**, 169–188 (2013).

118. An, Y., Wang, Z., Wu, Z., Yang, D. & Zhou, Q. Characterization of membrane foulants in an anaerobic non-woven fabric membrane bioreactor for municipal wastewater treatment. *Chem. Eng. J.* **155**, 709–715 (2009).

119. Show, K. Y. & Lee, D. J. *Anaerobic Treatment Versus Aerobic Treatment*. *Current Developments in Biotechnology and Bioengineering: Biological Treatment of Industrial Effluents* (Elsevier B.V., 2016). doi:10.1016/B978-0-444-63665-2.00008-4

120. Grady, C. P. L., Daigger, G. T., Love, N. G. & Filipe, C. D. M. Biological wastewater treatment: Third edition. *Biol. Wastewater Treat. Third Ed.* 1–963 (2011).

121. *Wastewater Engineering Treatment and Resource Recovery.* . (McGraw-Hill, 2014).

122. Young, J. C. Factors Affecting the Design and Performance of Upflow Anaerobic Filters. *Water Sci. Technol.* **24**, 133–155 (1991).

123. Lettinga, G., van Velsen, A. F. M., Hobma, S. W., de Zeeuw, W. & Klapwijk, A. Use of the Upflow Sludge Blanket (USB) reactor concept for biological wastewater treatment, especially for anaerobic treatment. *Biotechnol. Bioeng.* **22**, 699–734 (1980).

124. Tiwari, M. K., Guha, S., Harendranath, C. S. & Tripathi, S. Influence of extrinsic factors on granulation in UASB reactor. **71**, 145–154 (2006).

125. Chong, S., Sen, T. K., Kayaalp, A. & Ang, H. M. The performance enhancements of upflow anaerobic sludge blanket (UASB) reactors for domestic sludge treatment – A State-of-the-art review. *Water Res.* **46**, 3434–3470 (2012).

126. Seghezzo, L., Zeeman, G., van Lier, J. B., Hamelers, H. V. M. V. M. & Lettinga, G. A review: The anaerobic treatment of sewage in UASB and EGSB reactors. *Bioresour. Technol.* **65**, 175–190 (1998).

127. Tandukar, M., Ohashi, A. & Harada, H. Performance comparison of a pilot-scale UASB and DHS system and activated sludge process for the treatment of municipal wastewater. *Water Res.* **41**, 2697–2705 (2007).

128. Vlyssides, A., Barampouti, E. M. & Mai, S. Granulation mechanism of a UASB reactor supplemented with iron. *Anaerobe* **14**, 275–279 (2008).

129. Torres, P. & Foresti, E. Domestic sewage treatment in a pilot system composed of UASB and SBR reactors. *Water Sci. Technol.* **44**, 247–253 (2001).

130. Tiwari, M. K., Guha, S., Harendranath, C. S. & Tripathi, S. Enhanced granulation by natural ionic polymer additives in UASB reactor treating low-strength wastewater. *Water Res.* **39**, 3801–3810 (2005).

131. Hickey, R. F., Wu, W.-M., Veiga, M. C. & Jones, R. START-UP, OPERATION, MONITORING AND CONTROL OF HIGH-RATE ANAEROBIC TREATMENT SYSTEMS. *Wal. Sci. Tech* **24**, 207–255 (1991).

132. Weiland, P. & Rozzi, A. The Start-Up, Operation and Monitoring of High-Rate Anaerobic Treatment Systems: Discusser's Report. *Water Sci. Technol.* **24**, 257–277 (1991).

133. Zoutberg, G. R. & De Been, P. The Biobed® EGSB (Expanded Granular Sludge Bed) system covers shortcomings of the Upflow Anaerobic Sludge Blanket reactor in the chemical industry. *Water Sci. Technol.* **35**, 183–187 (1997).

134. Lettinga, G. & Pol, L. W. H. UASB Process design for various types of wastewaters. 87–109 (1991).

135. Lew, B., Lustig, I., Beliavski, M., Tarre, S. & Green, M. An integrated UASB-sludge digester system for raw domestic wastewater treatment in temperate climates. *Bioresour. Technol.* **102**, 4921–4924 (2011).

136. Heffernan, B., Van Lier, J. B. & Van Der Lubbe, J. Performance review of large scale up-flow anaerobic sludge blanket sewage treatment plants. *Water Sci. Technol.* **63**, 100–107 (2011).

137. Li, J., Hu, B., Zheng, P., Qaisar, M. & Mei, L. Filamentous granular sludge bulking in a laboratory scale UASB reactor. *Bioresour. Technol.* **99**, 3431–3438 (2008).

138. Ghangerekar, M. & Behera, M. Suspended Growth Treatment Processes. Comprehensive Water Quality and Purification,. *Compr. water Qual. Purif.* **3**, (2014).

139. Sarria, V., Kenfack, S., Guillod, O. & Pulgarin, C. An innovative coupled solar-biological system at field pilot scale for the treatment of biorecalcitrant pollutants. *J. Photochem. Photobiol. A Chem.* **159**, 89–99 (2003).

140. Hulshoff Pol, L. W., De Castro Lopes, S. I., Lettinga, G. & Lens, P. N. L. Anaerobic sludge granulation. *Water Res.* **38**, 1376–1389 (2004).

141. Liu, Y., Xu, H. Lou, Show, K. Y. & Tay, J. H. Anaerobic granulation technology for

wastewater treatment. *World J. Microbiol. Biotechnol.* **18**, 99–113 (2002).

142. Sarti, A. & Zaiat, M. Anaerobic treatment of sulfate-rich wastewater in an anaerobic sequential batch reactor (AnSBR) using butanol as the carbon source. *J. Environ. Manage.* **92**, 1537–1541 (2011).

143. Li, J., Wang, J., Luan, Z., Ji, Z. & Yu, L. Biological sulfate removal from acrylic fiber manufacturing wastewater using a two-stage UASB reactor. *J. Environ. Sci. (China)* **24**, 343–350 (2012).

144. Delforno, T. P., Moura, A. G. L., Okada, D. Y. & Varesche, M. B. A. Effect of biomass adaptation to the degradation of anionic surfactants in laundry wastewater using EGSB reactors. **154**, 114–121 (2014).

145. Luo, G. *et al.* Performance, kinetics behaviors and microbial community of internal circulation anaerobic reactor treating wastewater with high organic loading rate: Role of external hydraulic circulation. *Bioresour. Technol.* **222**, 470–477 (2016).

146. Chen, X., Wang, Y., Wang, Z. & Liu, S. Efficient treatment of traditional Chinese pharmaceutical wastewater using a pilot-scale spiral symmetry stream anaerobic bioreactor compared with internal circulation reactor. *Chemosphere* **228**, 437–443 (2019).

147. Wang, G., Liu, D., Fan, S., Li, Z. & Su, J. High- k erbium oxide film prepared by sol-gel method for low-voltage thin-film transistor. *Nanotechnology* **32**, (2021).

148. Hu, M. *et al.* Hierarchical dual-nanonet of polymer nanofibers and supramolecular nanofibrils for air filtration with a high filtration efficiency, low air resistance and high moisture permeation. *J. Mater. Chem. A* **9**, 14093–14100 (2021).

149. Muñoz Sierra, J. D., Oosterkamp, M. J., Wang, W., Spanjers, H. & van Lier, J. B. Comparative performance of upflow anaerobic sludge blanket reactor and anaerobic membrane bioreactor treating phenolic wastewater: Overcoming high salinity. *Chem. Eng. J.* **366**, 480–490 (2019).

150. Bhuyan, S. C., Swain, A. K., Sahoo, A. & Bhuyan, S. K. Nutrient (sulphate) removal from wastewater in inverse fluidized bed biofilm reactor. *Mater. Today Proc.* **33**, 5476–5480 (2020).

151. Foglia, A. *et al.* Long-term operation of a pilot-scale anaerobic membrane bioreactor

(AnMBR) treating high salinity low loaded municipal wastewater in real environment. (2019). doi:10.1016/j.seppur.2019.116279

152.   Holst, T. C., Truc, A. & Pujol, R. Anaerobic fluidized beds: ten years of industrial experience. *Water Sci. Technol.* **36**, 415–422 (1997).

153.   Zoutberg, G. R. & Frankin, R. Anaerobic treatment of chemical and brewery waste water with a new type of anaerobic reactor; the biobed® EGSB reactor. *Water Sci. Technol.* **34**, 375–381 (1996).

154.   Rebac, S. *et al.* Psychrophilic (6–15 °C) High-Rate Anaerobic Treatment of Malting Wastewater in a Two-Module Expanded Granular Sludge Bed System. *Biotechnol. Prog.* **14**, 856–864 (1998).

155.   Rinzema, A. Anaerobic treatment of wastewater with high concentrations of lipids or sulfate. *Environ. Technol.* (1988).

156.   Lu, Q. *et al.* Performance Comparison of EGSB and IC Reactors for Treating High-Salt Fatty Acid Organic Production Wastewater. *Process. 2022, Vol. 10, Page 1295* **10**, 1295 (2022).

157.   Van Lier, J. B., Van Der Zee, F. P., Tan, N. C. G., Rebac, S. & Kleerebezem, R. Advances in high-rate anaerobic treatment: Staging of reactor systems. *Water Sci. Technol.* **44**, 15–25 (2001).

158.   van Lier, J. B., Boersma, F., Debets, M. M. W. H. & Lettinga, G. High rate thermophilic anaerobic wastewater treatment in compartmentalized upflow reactors. *Water Sci. Technol.* **30**, 251–261 (1994).

159.   Tagawa, T., Takahashi, H., Sekiguchi, Y., Ohashi, A. & Harada, H. Pilot-plant study on anaerobic treatment of a lipid- and protein-rich food industrial wastewater by a thermophilic multi-staged UASB reactor. *Water Sci. Technol.* **45**, 225–230 (2002).

160.   Banik, G. C. & Dague, R. R. ASBR treatment of low strength industrial wastewater at psychrophilic temperatures. *Water Sci. Technol.* **36**, 337–344 (1997).

161.   Alves, M. M., Mota Vieira, J. A., Alvares Pereira, R. M., Pereira, M. A. & Mota, M. Effects of lipids and oleic acid on biomass development in anaerobic fixed-bed reactors. Part II: Oleic acid toxicity and biodegradability. *Water Res.* **35**, 264–270 (2001).

162. van Lier, J. B., van der Zee, F. P., Frijters, C. T. M. J. & Ersahin, M. E. Celebrating 40 years anaerobic sludge bed reactors for industrial wastewater treatment. *Rev. Environ. Sci. Biotechnol.* **14**, 681–702 (2015).

163. Malamis, S. & Andreadakis, A. Fractionation of proteins and carbohydrates of extracellular polymeric substances in a membrane bioreactor system. *Bioresour. Technol.* **100**, 3350–3357 (2009).

164. Malamis, S., Andreadakis, A., Mamais, D. & Noutsopoulos, C. Investigation of long-term operation and biomass activity in a membrane bioreactor system. *Water Sci. Technol.* **63**, 1906 (2011).

165. Robles, Á. *et al.* A review on anaerobic membrane bioreactors (AnMBRs) focused on modelling and control aspects. *Bioresour. Technol.* **270**, 612–626 (2018).

166. Pretel, R., Robles, A., Ruano, M. V., Seco, A. & Ferrer, J. Economic and environmental sustainability of submerged anaerobic MBR-based (AnMBR-based) technology as compared to aerobic-based technologies for moderate-/high-loaded urban wastewater treatment. *J. Environ. Manage.* **166**, 45–54 (2016).

167. Gao, W. J. *et al.* Performance of submerged anaerobic membrane bioreactor for thermomechanical pulping wastewater treatment. *J. Water Process Eng.* **13**, 70–78 (2016).

168. Ng, K. K., Shi, X., Tang, M. K. Y. & Ng, H. Y. A novel application of anaerobic bio-entrapped membrane reactor for the treatment of chemical synthesis-based pharmaceutical wastewater. *Sep. Purif. Technol.* **132**, 634–643 (2014).

169. Chen, H., Chang, S., Guo, Q., Hong, Y. & Wu, P. Brewery wastewater treatment using an anaerobic membrane bioreactor. *Biochem. Eng. J.* **105**, 321–331 (2016).

170. Yurtsever, A., Sahinkaya, E. & Çınar, O. Performance and foulant characteristics of an anaerobic membrane bioreactor treating real textile wastewater. *J. Water Process Eng.* (2020).

171. Szabo-Corbacho, M. A. *et al.* Impact of solids retention time on the biological performance of an AnMBR treating lipid-rich synthetic dairy wastewater. *https://doi.org/10.1080/09593330.2019.1639829* **42**, 597–608 (2019).

172. Ramos, C., Zecchino, F., Ezquerra, D. & Diez, V. Chemical cleaning of membranes from an anaerobic membrane bioreactor treating food industry wastewater. *J. Memb. Sci.* **458**, 179–188 (2014).

173. European Commission. The Joint Declaration of Intent for the INNOVATION DEAL on sustainable waste water treatment combining anaerobic membrane technology and water reuse. 1–14 (2017).

174. Giménez, J. B. B. *et al.* Experimental study of the anaerobic urban wastewater treatment in a submerged hollow-fibre membrane bioreactor at pilot scale. *Bioresour. Technol.* **102**, 8799–8806 (2011).

175. Smith, A. L., Skerlos, S. J. & Raskin, L. Psychrophilic anaerobic membrane bioreactor treatment of domestic wastewater. *Water Res.* **47**, 1655–1665 (2013).

176. Cookney, J. *et al.* Dissolved methane recovery from anaerobic effluents using hollow fibre membrane contactors. *J. Memb. Sci.* **502**, 141–150 (2016).

177. Grethlein, H. E. Anaerobic membrane domestic digestion separation wastewater. *J. (Water Pollut. Control Fed.* **50**, 754–763 (1978).

178. Kirmura, S. Japans Aqua Renaissance'90 Project. *Water Sci. Technol.* **23**, 1573–1592 (1991).

179. Minami, K., Okamura, K., Ogawa, S. & Naritomi, T. Continuous anaerobic treatment of wastewater from a kraft pulp mill. *J. Ferment. Bioeng.* **71**, 270–274 (1991).

180. Minami, K. A trial of high performance anaerobic treatment on wastewater from a kraft pulp mill. *Desalination* **98**, 273–283 (1994).

181. Kanai, M., Ferre, V., Wakahara, S., Yamamoto, T. & Moro, M. A novel combination of methane fermentation and MBR — Kubota Submerged Anaerobic Membrane Bioreactor process. *Desalination* **250**, 964–967 (2010).

182. Liao, B. Q., Kraemer, J. T. & Bagley, D. M. *Anaerobic membrane bioreactors: Applications and research directions*. *Critical Reviews in Environmental Science and Technology* **36**, (Taylor & Francis Group , 2006).

183. Aquino, S. F., Hu, A. Y., Akram, A. & Stuckey, D. C. Characterization of dissolved compounds in submerged anaerobic membrane bioreactors (SAMBRs). *J. Chem.*

Technol. Biotechnol. **81**, 1894–1904 (2006).

184. Lin, H. J. *et al.* Sludge properties and their effects on membrane fouling in submerged anaerobic membrane bioreactors (SAnMBRs). *Water Res.* **43**, 3827–3837 (2009).

185. He, Y., Xu, P., Li, C. & Zhang, B. High-concentration food wastewater treatment by an anaerobic membrane bioreactor. *Water Res.* **39**, 4110–4118 (2005).

186. Le-Clech, P., Chen, V. & Fane, T. A. G. Fouling in membrane bioreactors used in wastewater treatment. *J. Memb. Sci.* **284**, 17–53 (2006).

187. Brockmann, M. & Seyfried, C. F. Sludge activity and cross-flow microfiltration — A non-beneficial relationship. *Water Sci. Technol.* **34**, 205–213 (1996).

188. Choo, K. H. & Lee, C. H. Membrane fouling mechanisms in the membrane-coupled anaerobic bioreactor. *Water Res.* **30**, 1771–1780 (1996).

189. Ghyoot, W. R. & Verstraete, W. H. Coupling Membrane Filtration to Anaerobic Primary Sludge Digestion. *http://dx.doi.org/10.1080/09593331808616575* **18**, 569–580 (2010).

190. Kim, J., Lee, C. H. & Choo, K. H. Control of struvite precipitation by selective removal of NH(4)+ with dialyzer/zeolite in an anaerobic membrane bioreactor. *Appl. Microbiol. Biotechnol.* **75**, 187–193 (2007).

191. Spagni, A., Casu, S., Crispino, N. A., Farina, R. & Mattioli, D. Filterability in a submerged anaerobic membrane bioreactor. *Desalination* **250**, 787–792 (2010).

192. Sui, P., Wen, X. & Huang, X. Membrane fouling control by ultrasound in an anaerobic membrane bioreactor. *Front. Environ. Sci. Eng. China* **1**, 362–367 (2007).

193. Huang, Z., Ong, S. L. & Ng, H. Y. Feasibility of submerged anaerobic membrane bioreactor (SAMBR) for treatment of low-strength wastewater. *Water Sci. Technol.* **58**, 1925–1931 (2008).

194. Jeison, D., Telkamp, P. & van Lier, J. B. Thermophilic Sidestream Anaerobic Membrane Bioreactors: The Shear Rate Dilemma. *Water Environ. Res.* **81**, 2372–2380 (2009).

195. Jeong, E., Kim, H. W., Nam, J. Y., Ahn, Y. T. & Shin, H. S. Effects of the hydraulic retention time on the fouling characteristics of an anaerobic membrane bioreactor for treating acidifi ed wastewater. **18**, 251–256

196. Wijekoon, K. C., Visvanathan, C. & Abeynayaka, A. Effect of organic loading rate on VFA production, organic matter removal and microbial activity of a two-stage thermophilic anaerobic membrane bioreactor. *Bioresour. Technol.* **102**, 5353–5360 (2011).

197. Lin, H., Chen, J., Wang, F., Ding, L. & Hong, H. Feasibility evaluation of submerged anaerobic membrane bioreactor for municipal secondary wastewater treatment. *Desalination* **280**, 120–126 (2011).

198. Saddoud, A., Hassaïri, I. & Sayadi, S. Anaerobic membrane reactor with phase separation for the treatment of cheese whey. *Bioresour. Technol.* **98**, 2102–2108 (2007).

199. Kim, M. S., Lee, D. Y. & Kim, D. H. Continuous hydrogen production from tofu processing waste using anaerobic mixed microflora under thermophilic conditions. *Int. J. Hydrogen Energy* **36**, 8712–8718 (2011).

200. Stamatelatou, K., Kopsahelis, A., Blika, P. S., Paraskeva, C. A. & Lyberatos, G. Anaerobic digestion of olive mill wastewater in a periodic anaerobic baffled reactor (PABR) followed by further effluent purification via membrane separation technologies. *J. Chem. Technol. Biotechnol.* **84**, 909–917 (2009).

201. Torres, A., Hemmelmann, A., Vergara, C. & Jeison, D. Application of two-phase slug-flow regime to control flux reduction on anaerobic membrane bioreactors treating wastewaters with high suspended solids concentration. *Sep. Purif. Technol.* **79**, 20–25 (2011).

202. Gao, W. J. J. J. J., Lin, H. J. J., Leung, K. T. T. & Liao, B. Q. Q. Influence of elevated pH shocks on the performance of a submerged anaerobic membrane bioreactor. *Process Biochem.* **45**, 1279–1287 (2010).

203. Van Zyl, P. J., Wentzel, M. C., Ekama, G. A. & Riedel, K. J. Design and start-up of a high rate anaerobic membrane bioreactor for the treatment of a low pH, high strength, dissolved organic waste water. *Water Sci. Technol.* **57**, 291–295 (2008).

204. Baêta, B. E. L., Ramos, R. L., Lima, D. R. S. & Aquino, S. F. Use of submerged anaerobic membrane bioreactor (SAMBR) containing powdered activated carbon (PAC) for the treatment of textile effluents. *Water Sci. Technol.* **65**, 1540–1547 (2012).

205. Beaubien, A., Bâty, M., Jeannot, F., Francoeur, E. & Manem, J. Design and operation of anaerobic membrane bioreactors: development of a filtration testing strategy. *J. Memb. Sci.* **109**, 173–184 (1996).

206. Herrera-Robledo, M., Morgan-Sagastume, J. M. & Noyola, A. Biofouling and pollutant removal during long-term operation of an anaerobic membrane bioreactor treating municipal wastewater. *https://doi.org/10.1080/08927010903243923* **26**, 23–30 (2009).

207. Lew, B., Tarre, S., Beliavski, M., Dosoretz, C. & Green, M. Anaerobic membrane bioreactor (AnMBR) for domestic wastewater treatment. *Desalination* **243**, 251–257 (2009).

208. Baek, S. H., Pagilla, K. R. & Kim, H.-J. J. Lab-scale study of an anaerobic membrane bioreactor (AnMBR) for dilute municipal wastewater treatment. *Biotechnol. Bioprocess Eng.* **15**, 704–708 (2010).

209. Nagata, N., Herouvis, K. J., Dziewulski, D. M. & Belfort, G. Cross-flow membrane microfiltration of a bacteriol fermentation broth. *Biotechnol. Bioeng.* **34**, 447–466 (1989).

210. Verstraete, W. & Vandevivere, P. New and broader applications of anaerobic digestion. *Crit. Rev. Environ. Sci. Technol.* **29**, 151–173 (1999).

211. Zhang, X. *et al.* Formation of dynamic membrane in an anaerobic membrane bioreactor for municipal wastewater treatment. *Chem. Eng. J.* **165**, 175–183 (2010).

212. Gao, D. W. & Tao, Y. Versatility and application of anaerobic ammonium-oxidizing bacteria. *Appl. Microbiol. Biotechnol.* **91**, 887–894 (2011).

213. Nghiem, L. D., Tadkaew, N. & Sivakumar, M. Removal of trace organic contaminants by submerged membrane bioreactors. *Desalination* **236**, 127–134 (2009).

214. Ifelebuegu, A. O. The fate and behavior of selected endocrine disrupting chemicals in full scale wastewater and sludge treatment unit processes. *Int. J. Environ. Sci. Technol.* **8**, 245–254 (2011).

215. Czajka, C. P. & Londry, K. L. Anaerobic biotransformation of estrogens. *Sci. Total Environ.* **367**, 932–941 (2006).

216. Sundararaman, S. & Saravanane, R. Effect of loading rate and HRT on the removal of cephalosporin and their intermediates during the operation of a membrane bioreactor treating pharmaceutical wastewater. *Water Sci. Technol.* **61**, 1907–1914 (2010).

217. Lin, H. *et al.* Membrane Bioreactors for Industrial Wastewater Treatment: A Critical Review. *https://doi.org/10.1080/10643389.2010.526494* **42**, 677–740 (2012).

218. Côté, P., Masini, M. & Mourato, D. Comparison of membrane options for water reuse and reclamation. *Desalination* **167**, 1–11 (2004).

219. Verrecht, B., Maere, T., Nopens, I., Brepols, C. & Judd, S. The cost of a large-scale hollow fibre MBR. *Water Res.* **44**, 5274–5283 (2010).

220. Grundestam, J. & Hellström, D. Wastewater treatment with anaerobic membrane bioreactor and reverse osmosis. *Water Sci. Technol.* **56**, 211–217 (2007).

221. Baek, S. H. & Pagilla, K. R. Aerobic and anaerobic membrane bioreactors for municipal wastewater treatment. *Water Environ. Res.* **78**, 133–140 (2006).

222. Shahid, M. K. *et al.* A brief review of anaerobic membrane bioreactors emphasizing recent advancements, fouling issues and future perspectives. **270**, 110909 (2020).

223. Seco, A. *et al.* Exploring the limits of anaerobic biodegradability of urban wastewater by AnMBR technology. *Environ. Sci. Water Res. Technol.* **4**, 1877–1887 (2018).

224. Vinardell, S., Astals, S., Jaramillo, M., Mata-Alvarez, J. & Dosta, J. Anaerobic membrane bioreactor performance at different wastewater pre-concentration factors: An experimental and economic study. *Sci. Total Environ.* **750**, 141625 (2021).

225. Gouveia, J., Plaza, F., Garralon, G., Fdz-Polanco, F. & Peña, M. Long-term operation of a pilot scale anaerobic membrane bioreactor (AnMBR) for the treatment of municipal wastewater under psychrophilic conditions. **185**, 225–233 (2015).

226. Ferrer, J. *et al.* Design methodology for submerged anaerobic membrane bioreactors (AnMBR): A case study. *Sep. Purif. Technol.* **141**, 378–386 (2015).

227. Balcıoğlu, G., Yilmaz, G. & Gönder, Z. B. Evaluation of anaerobic membrane bioreactor (AnMBR) treating confectionery wastewater at long-term operation under different organic loading rates: Performance and membrane fouling. *Chem. Eng. J.* **404**, 126261 (2021).

228. Kong, Z. *et al.* Sludge yield and degradation of suspended solids by a large pilot-scale anaerobic membrane bioreactor for the treatment of real municipal wastewater at 25 °C. *Sci. Total Environ.* **759**, 143526 (2021).

229. Hu, Y., Cheng, H., Ji, J. & Li, Y. Y. A review of anaerobic membrane bioreactors for municipal wastewater treatment with a focus on multicomponent biogas and membrane fouling control. *Environ. Sci. Water Res. Technol.* **6**, 2641–2663 (2020).

230. Liu, W. *et al.* Comparison between aerobic and anaerobic membrane bioreactors for trace organic contaminant removal in wastewater treatment. *Environ. Technol. Innov.* **17**, 100564 (2020).

231. Yue, X., Koh, Y. K. K. & Ng, H. Y. Effects of dissolved organic matters (DOMs) on membrane fouling in anaerobic ceramic membrane bioreactors (AnCMBRs) treating domestic wastewater. *Water Res.* **86**, 96–107 (2015).

232. Lee, S. J. & Kim, J. H. Differential natural organic matter fouling of ceramic versus polymeric ultrafiltration membranes. *Water Res.* **48**, 43–51 (2014).

233. Jeong, Y., Hermanowicz, S. W. & Park, C. Treatment of food waste recycling wastewater using anaerobic ceramic membrane bioreactor for biogas production in mainstream treatment process of domestic wastewater. *Water Res.* **123**, 86–95 (2017).

234. Shoener, B. D. *et al.* Design of anaerobic membrane bioreactors for the valorization of dilute organic carbon waste streams. *Energy Environ. Sci.* **9**, 1102–1112 (2016).

235. Cath, T. Y., Childress, A. E. & Elimelech, M. Forward osmosis: Principles, applications, and recent developments. *J. Memb. Sci.* **281**, 70–87 (2006).

236. Silva, A. F. R., Ricci, B. C., Koch, K., Weißbach, M. & Amaral, M. C. S. Dissolved hydrogen sulfide removal from anaerobic bioreactor permeate by modified direct contact membrane distillation. *Sep. Purif. Technol.* **233**, 116036 (2020).

237. Xie, M., Lee, J., Nghiem, L. D. & Elimelech, M. Role of pressure in organic fouling in forward osmosis and reverse osmosis. *J. Memb. Sci.* **493**, 748–754 (2015).

238. Rezania, B., Oleszkiewicz, J. A. & Cicek, N. Hydrogen-driven denitrification of wastewater in an anaerobic submerged membrane bioreactor: potential for water reuse. *Water Sci. Technol.* **54**, 207–214 (2006).

239. Zeigler, S. Treatment of Low Strength Wastewater Using Bench-Scale Anaerobic Membrane Bioreactor. *J. New Engl. Water Environ. Assoc.* **41**, 9207–9218 (2007).

240. Gao, D. W. *et al.* Membrane fouling in an anaerobic membrane bioreactor: Differences in relative abundance of bacterial species in the membrane foulant layer and in suspension. *J. Memb. Sci.* **364**, 331–338 (2010).

241. Wong, K. *et al.* Removal of Viruses and Indicators by Anaerobic Membrane Bioreactor

Treating Animal Waste. *J. Environ. Qual.* **38**, 1694–1699 (2009).

242. Padmasiri, S. I. *et al.* Methanogenic population dynamics and performance of an anaerobic membrane bioreactor (AnMBR) treating swine manure under high shear conditions. *Water Res.* **41**, 134–144 (2007).

243. Trzcinski, A. P. & Stuckey, D. C. Continuous treatment of the organic fraction of municipal solid waste in an anaerobic two-stage membrane process with liquid recycle. *Water Res.* **43**, 2449–2462 (2009).

244. Xu, M., Wen, X., Huang, X. & Li, Y. Membrane fouling control in an anaerobic membrane bioreactor coupled with online ultrasound equipment for digestion of waste activated sludge. *Sep. Sci. Technol.* **45**, 941–947 (2010).

245. Jeison, D., Van Betuw, W. & Van Lier, J. B. Feasibility of Anaerobic Membrane Bioreactors for the Treatment of Wastewaters with Particulate Organic Matter. *http://dx.doi.org/10.1080/01496390802221659* **43**, 3417–3431 (2008).

246. Vallero, M. V. G., Lettinga, G. & Lens, P. N. L. High rate sulfate reduction in a submerged anaerobic membrane bioreactor (SAMBaR) at high salinity. *J. Memb. Sci.* **253**, 217–232 (2005).

247. Kim, J. O. & Jung, J. T. Performance of membrane-coupled organic acid fermentor for the resources recovery form municipal sewage sludge. *Water Sci. Technol.* **55**, 245–252 (2007).

248. Ji, J. *et al.* Anaerobic membrane bioreactors for treatment of emerging contaminants: A review. *J. Environ. Manage.* **270**, (2020).

249. Hagos, K., Zong, J., Li, D., Liu, C. & Lu, X. Anaerobic co-digestion process for biogas production: Progress, challenges and perspectives. *Renew. Sustain. Energy Rev.* **76**, 1485–1496 (2017).

250. Nakamura, K., Suda, T. & Matsumoto, K. Characterization of pore size distribution of non-woven fibrous filter by inscribed sphere within 3D filter model. *Sep. Purif. Technol.* **197**, 289–294 (2018).

251. Meng, F. *et al.* Recent advances in membrane bioreactors (MBRs): Membrane fouling and membrane material. *Water Res.* **43**, 1489–1512 (2009).

252. Li, N., Hu, Y., Lu, Y. Z., Zeng, R. J. & Sheng, G. P. In-situ biogas sparging enhances the performance of an anaerobic membrane bioreactor (AnMBR) with mesh filter in low-strength wastewater treatment. *Appl. Microbiol. Biotechnol.* **100**, 6081–6089 (2016).

253. Maaz, M. *et al.* Anaerobic membrane bioreactors for wastewater treatment: Novel configurations, fouling control and energy considerations. *Bioresour. Technol.* **283**, 358–372 (2019).

254. Grossman, A. D. *et al.* Effect of ultrafiltration membrane material on fouling dynamics in a submerged anaerobic membrane bioreactor treating domestic wastewater. *Environ. Sci. Water Res. Technol.* **5**, 1145–1156 (2019).

255. Zin, G. *et al.* Modification of hydrophobic commercial PVDF microfiltration membranes into superhydrophilic membranes by the mussel-inspired method with dopamine and polyethyleneimine. *Sep. Purif. Technol.* **212**, 641–649 (2019).

256. Wen, C., Huang, X. & Qian, Y. Domestic wastewater treatment using an anaerobic bioreactor coupled with membrane filtration. *Process Biochem.* **35**, 335–340 (1999).

257. Cheng, H., Li, Y., Li, L., Chen, R. & Li, Y. Y. Long-term operation performance and fouling behavior of a high-solid anaerobic membrane bioreactor in treating food waste. *Chem. Eng. J.* **394**, 124918 (2020).

258. Sethunga, G. S. M. D. P., Karahan, H. E., Wang, R. & Bae, T. H. Wetting- and fouling-resistant hollow fiber membranes for dissolved methane recovery from anaerobic wastewater treatment effluents. *J. Memb. Sci.* **617**, (2021).

259. Zhang, S. *et al.* Performance of a metallic membrane bioreactor treating simulated distillery wastewater at temperatures of 30 to 45°C. *Desalination* **194**, 146–155 (2006).

260. Li, L. *et al.* A comparative long-term operation using up-flow anaerobic sludge blanket (UASB) and anaerobic membrane bioreactor (AnMBR) for the upgrading of anaerobic treatment of N, N-dimethylformamide-containing wastewater. *Sci. Total Environ.* **699**, (2020).

261. Arévalo, J., Ruiz, L., Pérez, J., Moreno, B. & Gómez, M. Removal performance of heavy metals in MBR systems and their influence in water reuse. *Water Sci. Technol.* **67**, 894–900 (2013).

262. Liu, Z. *et al.* Distinction between polymeric and ceramic membrane in AnMBR treating municipal wastewater: In terms of irremovable fouling. *J. Memb. Sci.* **588**, 117229 (2019).

263. Bai, L. *et al.* Cellulose nanocrystal-blended polyethersulfone membranes for enhanced removal of natural organic matter and alleviation of membrane fouling. *Chem. Eng. J.* **382**, 122919 (2020).

264. Mahmood, Z., Cheng, H. & Tian, M. A critical review on advanced anaerobic membrane bioreactors (AnMBRs) for wastewater treatment: advanced membrane materials and energy demand. *Environ. Sci. Water Res. Technol.* **8**, 2126–2144 (2022).

265. Cheng, H., Hiro, Y., Hojo, T. & Li, Y. Y. Upgrading methane fermentation of food waste by using a hollow fiber type anaerobic membrane bioreactor. *Bioresour. Technol.* **267**, 386–394 (2018).

266. Zhen, G. *et al.* Anaerobic membrane bioreactor towards biowaste biorefinery and chemical energy harvest: Recent progress, membrane fouling and future perspectives. *Renew. Sustain. Energy Rev.* **115**, 109392 (2019).

267. Pacheco-Ruiz, S., Heaven, S. & Banks, C. J. Effect of mean cell residence time on transmembrane flux, mixed-liquor characteristics and overall performance of a submerged anaerobic membrane bioreactor. *Environ. Technol.* **38**, 1263–1274 (2017).

268. Ho, J. & Sung, S. Anaerobic membrane bioreactor treatment of synthetic municipal wastewater at ambient temperature. *Water Environ. Res.* **81**, 922–928 (2009).

269. Huang, Z., Ong, S. L. & Ng, H. Y. Submerged anaerobic membrane bioreactor for low-strength wastewater treatment: Effect of HRT and SRT on treatment performance and membrane fouling. *Water Res.* **45**, 705–713 (2011).

270. Dereli, R. K. *et al.* Potentials of anaerobic membrane bioreactors to overcome treatment limitations induced by industrial wastewaters. *Bioresour. Technol.* **122**, 160–170 (2012).

271. Maleki, E. Psychrophilic anaerobic membrane bioreactor (AnMBR) for treating malting plant wastewater and energy recovery. *J. Water Process Eng.* **34**, (2020).

272. Yeo, H. & Lee, H. S. The effect of solids retention time on dissolved methane concentration in anaerobic membrane bioreactors. *Environ. Technol. (United Kingdom)* **34**, 2105–2112 (2013).

273. Ho, J. & Sung, S. Anaerobic Membrane Bioreactor Treatment of Synthetic Municipal Wastewater at Ambient Temperature. *Water Environ. Res.* **81**, 922–928 (2009).

274. Weiland, P. Biogas production: Current state and perspectives. *Appl. Microbiol. Biotechnol.* **85**, 849–860 (2010).

275. Yu, J. *et al.* Accelerated acidification by inoculation with a microbial consortia in a complex open environment. *Bioresour. Technol.* **216**, 294–301 (2016).

276. Ersahin, M. E. *et al.* Impact of anaerobic dynamic membrane bioreactor configuration on treatment and filterability performance. *J. Memb. Sci.* **526**, 387–394 (2017).

277. Xiao, Y., Yaohari, H., De Araujo, C., Sze, C. C. & Stuckey, D. C. Removal of selected pharmaceuticals in an anaerobic membrane bioreactor (AnMBR) with/without powdered activated carbon (PAC). *Chem. Eng. J.* **321**, 335–345 (2017).

278. Yee, T. L., Rathnayake, T. & Visvanathan, C. Performance Evaluation of a Thermophilic Anaerobic Membrane Bioreactor for Palm Oil Wastewater Treatment. *Membranes (Basel).* **9**, (2019).

279. Narihiro, T., Nobu, M. K., Kim, N. K., Kamagata, Y. & Liu, W. T. The nexus of syntrophy-associated microbiota in anaerobic digestion revealed by long-term enrichment and community survey. *Environ. Microbiol.* **17**, 1707–1720 (2015).

280. Babaee, A. & Shayegan, J. Effect of Organic Loading Rates (OLR) on Production of Methane from Anaerobic Digestion of Vegetables Waste. *Proc. World Renew. Energy Congr. – Sweden, 8–13 May, 2011, Linköping, Sweden* **57**, 411–417 (2011).

281. Seo, H. *et al.* Linking process performances and core microbial community structures in anaerobic membrane bioreactor with rotatory disk (ARMBR) system fed with high-strength food waste recycling wastewater. *Bioresour. Technol.* **291**, (2019).

282. Chen, L., Hu, Q., Zhang, X., Cai, Z. & Wang, Y. Effects of ZnO nanoparticles on the performance of anaerobic membrane bioreactor: An attention to the characteristics of supernatant, effluent and biomass community. *Environ. Pollut.* **248**, 743–755 (2019).

283. Ganesh Saratale, R. *et al.* A critical review on anaerobic digestion of microalgae and macroalgae and co-digestion of biomass for enhanced methane generation. *Bioresour. Technol.* **262**, 319–332 (2018).

284. Ozgun, H. *et al.* Impact of temperature on feed-flow characteristics and filtration performance of an upflow anaerobic sludge blanket coupled ultrafiltration membrane treating municipal wastewater. *Water Res.* **83**, 71–83 (2015).

285. Ferrari, F., Balcazar, J. L., Rodriguez-Roda, I. & Pijuan, M. Anaerobic membrane bioreactor for biogas production from concentrated sewage produced during sewer mining. *Sci. Total Environ.* **670**, 993–1000 (2019).

286. Watanabe, R., Nie, Y., Wakahara, S., Komori, D. & Li, Y. Y. Investigation on the response of anaerobic membrane bioreactor to temperature decrease from 25 °C to 10 °C in sewage treatment. *Bioresour. Technol.* **243**, 747–754 (2017).

287. Kwak, W., Rout, P. R., Lee, E. & Bae, J. Influence of hydraulic retention time and temperature on the performance of an anaerobic ammonium oxidation fluidized bed membrane bioreactor for low-strength ammonia wastewater treatment. *Chem. Eng. J.* **386**, (2020).

288. Cho, K. *et al.* Effects of changes in temperature on treatment performance and energy recovery at mainstream anaerobic ceramic membrane bioreactor for food waste recycling wastewater treatment. *Bioresour. Technol.* **256**, 137–144 (2018).

289. Dolejs, P. *et al.* Effect of psychrophilic temperature shocks on a gas-lift anaerobic membrane bioreactor (Gl-AnMBR) treating synthetic domestic wastewater. *J. Water Process Eng.* **16**, 108–114 (2017).

290. Jeison, D. & van Lier, J. B. Cake layer formation in anaerobic submerged membrane bioreactors (AnSMBR) for wastewater treatment. *J. Memb. Sci.* **284**, 227–236 (2006).

291. Trzcinski, A. P. & Stuckey, D. C. Treatment of municipal solid waste leachate using a submerged anaerobic membrane bioreactor at mesophilic and psychrophilic temperatures: Analysis of recalcitrants in the permeate using GC-MS. *Water Res.* **44**, 671–680 (2010).

292. Martinez-Sosa, D., Helmreich, B. & Horn, H. Anaerobic submerged membrane bioreactor (AnSMBR) treating low-strength wastewater under psychrophilic temperature conditions. *Process Biochem.* **47**, 792–798 (2012).

293. Yao, M. *et al.* Volatile fatty acids and biogas recovery using thermophilic anaerobic membrane distillation bioreactor for wastewater reclamation. *J. Environ. Manage.* **231**,

833–842 (2019).

294. Burman, I. & Sinha, A. Performance evaluation and substrate removal kinetics in an up-flow anaerobic hybrid membrane bioreactor treating simulated high-strength wastewater. *Environ. Technol.* **41**, 309–321 (2020).

295. Ho, J. & Sung, S. Effects of solid concentrations and cross-flow hydrodynamics on microfiltration of anaerobic sludge. *J. Memb. Sci.* **345**, 142–147 (2009).

296. Narra, M. *et al.* Performance evaluation of anaerobic hybrid reactors with different packing media for treating wastewater of mild alkali treated rice straw in ethanol fermentation process. *Bioresour. Technol.* **152**, 59–65 (2014).

297. Jiang, M., Westerholm, M., Qiao, W., Wandera, S. M. & Dong, R. High rate anaerobic digestion of swine wastewater in an anaerobic membrane bioreactor. *Energy* **193**, 116783 (2020).

298. Jeong, Y., Kim, Y., Jin, Y., Hong, S. & Park, C. Comparison of filtration and treatment performance between polymeric and ceramic membranes in anaerobic membrane bioreactor treatment of domestic wastewater. *Sep. Purif. Technol.* **199**, 182–188 (2018).

299. Santos, F. S., Ricci, B. C., França Neta, L. S. & Amaral, M. C. S. Sugarcane vinasse treatment by two-stage anaerobic membrane bioreactor: Effect of hydraulic retention time on changes in efficiency, biogas production and membrane fouling. *Bioresour. Technol.* **245**, 342–350 (2017).

300. Yang, Y., Zang, Y., Hu, Y., Wang, X. C. & Ngo, H. H. Upflow anaerobic dynamic membrane bioreactor (AnDMBR) for wastewater treatment at room temperature and short HRTs: Process characteristics and practical applicability. *Chem. Eng. J.* **383**, (2020).

301. Emmanuel Alepu, O. & Li, Z. Effect of Hydraulic Retention Time on Anaerobic Digestion of Xiao Jiahe Municipal Sludge. *Int. J. Waste Resour.* **6**, (2016).

302. Chen, C. *et al.* Challenges in biogas production from anaerobic membrane bioreactors. *Renew. Energy* **98**, 120–134 (2016).

303. Aslam, M. & Kim, J. Investigating membrane fouling associated with GAC fluidization on membrane with effluent from anaerobic fluidized bed bioreactor in domestic wastewater

treatment. *Environ. Sci. Pollut. Res.* **26**, 1170–1180 (2019).

304.   Khan, M. A. *et al.* Optimization of process parameters for production of volatile fatty acid, biohydrogen and methane from anaerobic digestion. *Bioresour. Technol.* **219**, 738–748 (2016).

305.   Ahring, B. K., Sandberg, M. & Angelidaki, I. Volatile fatty acids as indicators of process imbalance in anaerobic digestors. *Appl. Microbiol. Biotechnol.* **43**, 559–565 (1995).

306.   Ji, J. Y., Wang, H., Zheng, P., Xing, Y. J. & Zheng, X. L. Early-warning on the performance of novel high-rate anaerobic bioreactor. *Sep. Purif. Technol.* **156**, 103–107 (2015).

307.   Ngo, H. H., Khan, M. A., Guo, W., Pandey, A. & Lee, D. J. Non-conventional Anaerobic Bioreactors for Sustainable Wastewater Treatment. *Energy, Environ. Sustain.* 265–295 (2019). doi:10.1007/978-981-13-3259-3_13

308.   Borja, R., Banks, C. J., Wang, Z. & Mancha, A. Anaerobic digestion of slaughterhouse wastewater using a combination sludge blanket and filter arrangement in a single reactor. *Bioresour. Technol.* **65**, 125–133 (1998).

309.   Callaghan, F. J., Wase, D. A. J., Thayanithy, K. & Forster, C. F. Continuous co-digestion of cattle slurry with fruit and vegetable wastes and chicken manure. *Biomass and Bioenergy* **22**, 71–77 (2002).

310.   Debik, E. & Coskun, T. Use of the Static Granular Bed Reactor (SGBR) with anaerobic sludge to treat poultry slaughterhouse wastewater and kinetic modeling. *Bioresour. Technol.* **100**, 2777–2782 (2009).

311.   Vyrides, I. & Stuckey, D. C. Saline sewage treatment using a submerged anaerobic membrane reactor (SAMBR): Effects of activated carbon addition and biogas-sparging time. *Water Res.* **43**, 933–942 (2009).

312.   Wu, H., Yang, D., Zhou, Q. & Song, Z. The effect of pH on anaerobic fermentation of primary sludge at room temperature. *J. Hazard. Mater.* **172**, 196–201 (2009).

313.   Smith, A. L. L. ., Dorer, H. ., Love, N. G. G. ., Skerlos, S. J. J. . & Raskin, L. Role of Membrane Biofilm in Psychrophilic Anaerobic Membrane Bioreactor for Domestic Wastewater Treatment. *84th Annu. Water Environ. Fed. Tech. Exhib. Conf.* **2011**, 4948–

4952 (2011).

314. Kim, J. *et al.* Anaerobic Fluidized Bed Membrane Bioreactor for Wastewater Treatment. *Environ. Sci. Technol.* **45**, 576–581 (2011).

315. Liu, Y., Zhang, K., Bakke, R., Li, C. & Liu, H. Membrane installation for enhanced up-flow anaerobic sludge blanket (UASB) performance. *J. Biosci. Bioeng.* **116**, 357–361 (2013).

316. Gao, D. W., Hu, Q., Yao, C. & Ren, N. Q. Treatment of domestic wastewater by an integrated anaerobic fluidized-bed membrane bioreactor under moderate to low temperature conditions. *Bioresour. Technol.* **159**, 193–198 (2014).

317. Prieto, A. L., Futselaar, H., Lens, P. N. L., Bair, R. & Yeh, D. H. Development and start up of a gas-lift anaerobic membrane bioreactor (Gl-AnMBR) for conversion of sewage to energy, water and nutrients. *J. Memb. Sci.* **441**, 158–167 (2013).

318. Monsalvo, V. M., McDonald, J. A., Khan, S. J. & Le-Clech, P. Removal of trace organics by anaerobic membrane bioreactors. *Water Res.* **49**, 103–112 (2014).

319. Dutta, K. *et al.* Removal of pharmaceuticals and organic matter from municipal wastewater using two-stage anaerobic fluidized membrane bioreactor. *Bioresour. Technol.* **165**, 42–49 (2014).

320. Chen, L. *et al.* Performance of a submerged anaerobic membrane bioreactor with forward osmosis membrane for low-strength wastewater treatment. *Water Res.* **50**, 114–123 (2014).

321. Wei, C. H., Harb, M., Amy, G., Hong, P. Y. & Leiknes, T. O. Sustainable organic loading rate and energy recovery potential of mesophilic anaerobic membrane bioreactor for municipal wastewater treatment. *Bioresour. Technol.* **166**, 326–334 (2014).

322. Ozgun, H. *et al.* Impact of membrane addition for effluent extraction on the performance and sludge characteristics of upflow anaerobic sludge blanket reactors treating municipal wastewater. *J. Memb. Sci.* **479**, 95–104 (2015).

323. Gu, Y. *et al.* Development of anaerobic osmotic membrane bioreactor for low-strength wastewater treatment at mesophilic condition. *J. Memb. Sci.* **490**, 197–208 (2015).

324. Seib, M. D., Berg, K. J. & Zitomer, D. H. Low energy anaerobic membrane bioreactor for municipal wastewater treatment. *J. Memb. Sci.* **514**, 450–457 (2016).

325. Seib, M. D., Berg, K. J. & Zitomer, D. H. Reduced energy demand for municipal wastewater recovery using an anaerobic floating filter membrane bioreactor. *Environ. Sci. Water Res. Technol.* **2**, 290–297 (2016).

326. Wei, C. H., Hoppe-Jones, C., Amy, G. & Leiknes, T. O. Organic micro-pollutants' removal via anaerobic membrane bioreactor with ultrafiltration and nanofiltration. *J. Water Reuse Desalin.* **6**, 362–370 (2016).

327. Chen, C. *et al.* Impact of reactor configurations on the performance of a granular anaerobic membrane bioreactor for municipal wastewater treatment. *Int. Biodeterior. Biodegradation* **121**, 131–138 (2017).

328. Chen, C. *et al.* Evaluation of a sponge assisted-granular anaerobic membrane bioreactor (SG-AnMBR) for municipal wastewater treatment. *Renew. Energy* **111**, 620–627 (2017).

329. Nie, Y., Tian, X., Zhou, Z. & Li, Y. Y. Impact of food to microorganism ratio and alcohol ethoxylate dosage on methane production in treatment of low-strength wastewater by a submerged anaerobic membrane bioreactor. *Front. Environ. Sci. Eng.* **11**, 6- (2017).

330. Wang, X. *et al.* Development of a novel anaerobic membrane bioreactor simultaneously integrating microfiltration and forward osmosis membranes for low-strength wastewater treatment. *J. Memb. Sci.* **527**, 1–7 (2017).

331. Cheng, H. & Hong, P. Y. Removal of Antibiotic-Resistant Bacteria and Antibiotic Resistance Genes Affected by Varying Degrees of Fouling on Anaerobic Microfiltration Membranes. *Environ. Sci. Technol.* **51**, 12200–12209 (2017).

332. Cheng, H., Cheng, D., Mao, J., Lu, T. & Hong, P. Y. Identification and characterization of core sludge and biofilm microbiota in anaerobic membrane bioreactors. *Environ. Int.* **133**, (2019).

333. Ding, Y. *et al.* The Performance and Microbial Community Identification in Mesophilic and Atmospheric Anaerobic Membrane Bioreactor for Municipal Wastewater Treatment Associated with Different Hydraulic Retention Times. *Water 2019, Vol. 11, Page 160* **11**, 160 (2019).

334. Wei, C. H. *et al.* Removal and biotransformation pathway of antibiotic sulfamethoxazole from municipal wastewater treatment by anaerobic membrane bioreactor. *J. Hazard. Mater.* **380**, 120894 (2019).

335. Lim, M. *et al.* Removals of micropollutants in staged anaerobic fluidized bed membrane bioreactor for low-strength wastewater treatment. *Process Saf. Environ. Prot.* **127**, 162–170 (2019).

336. Khan, M. A. *et al.* Selective production of volatile fatty acids at different pH in an anaerobic membrane bioreactor. *Bioresour. Technol.* **283**, 120–128 (2019).

337. Kim, M., Lam, T. Y. C., Tan, G. Y. A., Lee, P. H. & Kim, J. Use of polymeric scouring agent as fluidized media in anaerobic fluidized bed membrane bioreactor for wastewater treatment: System performance and microbial community. *J. Memb. Sci.* **606**, (2020).

338. Burman, I. & Sinha, A. Anaerobic hybrid membrane bioreactor for treatment of synthetic leachate: Impact of organic loading rate and sludge fractions on membrane fouling. *Waste Manag.* **108**, 41–50 (2020).

339. Gao, T., Zhang, H., Xu, X. & Teng, J. Integrating microbial electrolysis cell based on electrochemical carbon dioxide reduction into anaerobic osmosis membrane reactor for biogas upgrading. *Water Res.* **190**, (2021).

340. Guo, Y. *et al.* The first pilot-scale demonstration of the partial nitritation/anammox-hydroxyapatite process to treat the effluent of the anaerobic membrane bioreactor fed with the actual municipal wastewater. *Sci. Total Environ.* **807**, 151063 (2022).

341. Zhang, X., Gu, J. & Liu, Y. Necessity of direct energy and ammonium recovery for carbon neutral municipal wastewater reclamation in an innovative anaerobic MBR-biochar adsorption-reverse osmosis process. *Water Res.* **211**, 118058 (2022).

342. Ho, J. & Sung, S. Methanogenic activities in anaerobic membrane bioreactors (AnMBR) treating synthetic municipal wastewater. *Bioresour. Technol.* **101**, 2191–2196 (2010).

343. Martinez-Sosa, D. *et al.* Pilot-scale anaerobic submerged membrane bioreactor (AnSMBR) treating municipal wastewater: The fouling phenomenon and long-term operation. *Water Sci. Technol.* **64**, 1804–1811 (2011).

344. Dagnew, M. *et al.* Pilot Testing of an AnMBR for Municipal Wastewater Treatment. *Proc. Water Environ. Fed.* **2011**, 4931–4941 (2011).

345. Robles, A., Ruano, M. V., García-Usach, F. & Ferrer, J. Sub-critical filtration conditions of commercial hollow-fibre membranes in a submerged anaerobic MBR (HF-SAnMBR)

system: The effect of gas sparging intensity. *Bioresour. Technol.* **114**, 247–254 (2012).

346. Giménez, J. B., Martí, N., Ferrer, J. & Seco, A. Methane recovery efficiency in a submerged anaerobic membrane bioreactor (SAnMBR) treating sulphate-rich urban wastewater: Evaluation of methane losses with the effluent. *Bioresour. Technol.* **118**, 67–72 (2012).

347. Shin, C., McCarty, P. L., Kim, J. & Bae, J. Pilot-scale temperate-climate treatment of domestic wastewater with a staged anaerobic fluidized membrane bioreactor (SAF-MBR). *Bioresour. Technol.* **159**, 95–103 (2014).

348. Yoo, R. H., Kim, J. H., McCarty, P. L. & Bae, J. H. Effect of temperature on the treatment of domestic wastewater with a staged anaerobic fluidized membrane bioreactor. *Water Sci. Technol.* **69**, 1145–1150 (2014).

349. Pretel, R. *et al.* Designing an AnMBR-based WWTP for energy recovery from urban wastewater: the role of primary settling and anaerobic digestion. *Sep. Purif. Technol.* **156**, 132–139

350. Gouveia, J., Plaza, F., Garralon, G., Fdz-Polanco, F. & Peña, M. A novel configuration for an anaerobic submerged membrane bioreactor (AnSMBR). Long-term treatment of municipal wastewater under psychrophilic conditions. *Bioresour. Technol.* **198**, 510–519 (2015).

351. Dong, Q., Parker, W. & Dagnew, M. Impact of FeCl3 dosing on AnMBR treatment of municipal wastewater. *Water Res.* **80**, 281–293 (2015).

352. Mei, X., Wang, Z., Miao, Y. & Wu, Z. Recover energy from domestic wastewater using anaerobic membrane bioreactor: Operating parameters optimization and energy balance analysis. *Energy* **98**, 146–154 (2016).

353. Cerón-Vivas, A. & Noyola, A. Fouling membrane in an anaerobic membrane bioreactor treating municipal wastewater. *Water Pract. Technol.* **12**, 314–321 (2017).

354. Ruigómez, I., Vera, L., González, E. & Rodríguez-Sevilla, J. Pilot plant study of a new rotating hollow fibre membrane module for improved performance of an anaerobic submerged MBR. *J. Memb. Sci.* **514**, 105–113 (2016).

355. Mei, X., Quek, P. J., Wang, Z. & Ng, H. Y. Alkali-assisted membrane cleaning for fouling

control of anaerobic ceramic membrane bioreactor. *Bioresour. Technol.* **240**, 25–32 (2017).

356. Mei, X., Wang, Z., Miao, Y. & Wu, Z. A pilot-scale anaerobic membrane bioreactor under short hydraulic retention time for municipal wastewater treatment: performance and microbial community identification. *J. Water Reuse Desalin.* **8**, 58–67 (2017).

357. Hu, Y., Yang, Y., Yu, S., Wang, X. C. & Tang, J. Psychrophilic anaerobic dynamic membrane bioreactor for domestic wastewater treatment: Effects of organic loading and sludge recycling. *Bioresour. Technol.* **270**, 62–69 (2018).

358. Wang, K. M. *et al.* Identification of gas sparging regimes for granular anaerobic membrane bioreactor to enable energy neutral municipal wastewater treatment. *J. Memb. Sci.* **555**, 125–133 (2018).

359. Peña, M. *et al.* Anaerobic submerged membrane bioreactor (AnSMBR) treating municipal wastewater at ambient temperature: Operation and potential use for agricultural irrigation. *Bioresour. Technol.* **282**, 285–293 (2019).

360. Rongwong, W., Goh, K., Bae, T.-H. & Bae, T. H. Energy analysis and optimization of hollow fiber membrane contactors for recovery of dissolve methane from anaerobic membrane bioreactor effluent.

361. Evans, P. J. *et al.* A comparative pilot-scale evaluation of gas-sparged and granular activated carbon-fluidized anaerobic membrane bioreactors for domestic wastewater treatment. *Bioresour. Technol.* **288**, (2019).

362. Ji, J. *et al.* Application of two anaerobic membrane bioreactors with different pore size membranes for municipal wastewater treatment. *Sci. Total Environ.* **745**, (2020).

363. Inaba, T. *et al.* Microbial community in an anaerobic membrane bioreactor and its performance in treating organic solid waste under controlled and deteriorated conditions. *J. Environ. Manage.* **269**, (2020).

364. Cong Nguyen, N. *et al.* Water and nutrient recovery by a novel moving sponge-Anaerobic osmotic membrane bioreactor-Membrane distillation (AnOMBR-MD) closed-loop system. (2020). doi:10.1016/j.biortech.2020.123573

365. Chen, C. *et al.* Robustness of granular activated carbon-synergized anaerobic membrane

bioreactor for pilot-scale application over a wide seasonal temperature change. *Water Res.* **189**, 116552 (2021).

366. Plevri, A., Mamais, D. & Noutsopoulos, C. Anaerobic MBR technology for treating municipal wastewater at ambient temperatures. *Chemosphere* **275**, 129961 (2021).

367. Ji, J. *et al.* One-year operation of a 20-L submerged anaerobic membrane bioreactor for real domestic wastewater treatment at room temperature: Pursuing the optimal HRT and sustainable flux. *Sci. Total Environ.* **775**, (2021).

368. Kong, Z. *et al.* Large pilot-scale submerged anaerobic membrane bioreactor for the treatment of municipal wastewater and biogas production at 25 °C. *Bioresour. Technol.* **319**, (2021).

369. Rong, C. *et al.* Seasonal and annual energy efficiency of mainstream anaerobic membrane bioreactor (AnMBR) in temperate climates: Assessment in onsite pilot plant and estimation in scaled-up plant. *Bioresour. Technol.* **360**, 127542 (2022).

370. Robles, Á. *et al.* A semi-industrial scale AnMBR for municipal wastewater treatment at ambient temperature: performance of the biological process. *Water Res.* **215**, 118249 (2022).

371. Ji, J. *et al.* Submerged anaerobic membrane bioreactor applied for mainstream municipal wastewater treatment at a low temperature: Sludge yield, energy balance and membrane filtration behaviors. *J. Clean. Prod.* **355**, 131831 (2022).

372. Rong, C. *et al.* Pilot plant demonstration of temperature impacts on the methanogenic performance and membrane fouling control of the anaerobic membrane bioreactor in treating real municipal wastewater. *Bioresour. Technol.* **354**, 127167 (2022).

373. Li, G. *et al.* Application of deep learning for predicting the treatment performance of real municipal wastewater based on one-year operation of two anaerobic membrane bioreactors. *Sci. Total Environ.* **813**, 151920 (2022).

374. Du, R., Hu, Y., Nitta, S., Ji, J. & Li, Y. Y. Material mass balance and elemental flow analysis in a submerged anaerobic membrane bioreactor for municipal wastewater treatment towards low-carbon operation and resource recovery. *Sci. Total Environ.* **852**, 158586 (2022).

375. Kong, Z. *et al.* Insights into the carbon neutrality for the treatment process engineering of municipal wastewater by anaerobic membrane bioreactor integrated with partial nitritation-anammox: CO2 reduction and energy recovery. *J. Water Process Eng.* **49**, 102996 (2022).

376. An, Y., Yang, F., Bucciali, B. & Wong, F. Municipal Wastewater Treatment Using a UASB Coupled with Cross-Flow Membrane Filtration. *J. Environ. Eng.* **135**, 86–91 (2009).

377. Smith, A. L., Stadler, L. B., Love, N. G., Skerlos, S. J. & Raskin, L. Perspectives on anaerobic membrane bioreactor treatment of domestic wastewater: A critical review. *Bioresour. Technol.* **122**, 149–159 (2012).

378. Andrade, L. H. de, Mendes, F. D. dos S., Espindola, J. C. & Amaral, M. C. S. Internal versus external submerged membrane bioreactor configurations for dairy wastewater treatment. *Desalin. Water Treat.* **52**, 2920–2932 (2014).

379. Meng, F. *et al.* Morphological visualization, componential characterization and microbiological identification of membrane fouling in membrane bioreactors (MBRs). *J. Memb. Sci.* **361**, 1–14 (2010).

380. Di Bella, G. *et al.* The role of fouling mechanisms in a membrane bioreactor. *Water Sci. Technol.* **55**, 455–464 (2007).

381. Choo, K.-H. & Sainbayar, A. Approaches to membrane fouling control in anaerobic membrane bioreactors WaterEnergyNEXUS-Taste the future-International Conference Series View project Quorum quenching membrane bioreactors View project. (2000). doi:10.2166/wst.2000.0681

382. YOON, S. H., KANG, I. J. & LEE, C. H. Fouling of Inorganic Membrane and Flux Enhancement in Membrane-Coupled Anaerobic Bioreactor. *Sep. Sci. Technol.* **34**, 709–724 (1999).

383. Sun, Y., Wang, Y. & Huang, X. Relationship between sludge settleability and membrane fouling in a membrane bioreactor. *Front. Environ. Sci. Eng. China* **1**, 221–225 (2007).

384. Meng, F. & Yang, F. Fouling mechanisms of deflocculated sludge, normal sludge, and bulking sludge in membrane bioreactor. *J. Memb. Sci.* **305**, 48–56 (2007).

385. You, H. S. *et al.* A novel application of an anaerobic membrane process in wastewater

treatment. *Water Sci. Technol.* **51**, 45–50 (2005).

386. Jeison, D. & van Lier, J. B. Cake formation and consolidation: main factors governing the applicable flux in anaerobic submerged membrane bioreactors (AnSMBR) treating acidified wastewater. *Sep. Purif. Technol.* **56**, 71–78 (2007).

387. Hwang, B. K. *et al.* Correlating TMP increases with microbial characteristics in the bio-cake on the membrane surface in a membrane bioreactor. *Environ. Sci. Technol.* **42**, 3963–3968 (2008).

388. Cho, B. D. & Fane, A. G. Fouling transients in nominally sub-critical flux operation of a membrane bioreactor. *J. Memb. Sci.* **209**, 391–403 (2002).

389. Charfi, A. *et al.* Analysis of fouling mechanisms in anaerobic membrane bioreactors. *Water Res.* **46**, 2637–2650 (2012).

390. Lin, H. *et al.* New insights into membrane fouling in a submerged anaerobic membrane bioreactor based on characterization of cake sludge and bulk sludge. *Bioresour. Technol.* **102**, 2373–2379 (2011).

391. Zhang, J., Chua, H. C., Zhou, J. & Fane, A. G. Factors affecting the membrane performance in submerged membrane bioreactors. *J. Memb. Sci.* **284**, 54–66 (2006).

392. Chen, J. *et al.* Osmotic pressure effect on membrane fouling in a submerged anaerobic membrane bioreactor and its experimental verification. *Bioresour. Technol.* **125**, 97–101 (2012).

393. Bruus, J. H., Nielsen, P. H. & Keiding, K. On the stability of activated sludge flocs with implications to dewatering. *Water Res.* **26**, 1597–1604 (1992).

394. Matthew Higgins, B. J., Member, A. & Novak, J. T. Characterization of Exocellular Protein and Its Role in Bioflocculation. *J. Environ. Eng.* **123**, 479–485 (1997).

395. Martin-Garcia, I. *et al.* Impact of membrane configuration on fouling in anaerobic membrane bioreactors. *J. Memb. Sci.* **382**, 41–49 (2011).

396. Pollice, A., Brookes, A., Jefferson, B. & Judd, S. Sub-critical flux fouling in membrane bioreactors — a review of recent literature. *Desalination* **174**, 221–230 (2005).

397. Salazar-Peláez, M. L., Morgan-Sagastume, J. M. & Noyola, A. Influence of hydraulic

retention time on UASB post-treatment with UF membranes. *Water Sci. Technol.* **64**, 2299–2305 (2011).

398. Xie, K. *et al.* Performance and fouling characteristics of a submerged anaerobic membrane bioreactor for kraft evaporator condensate treatment. *https://doi.org/10.1080/09593330903527898* **31**, 511–521 (2010).

399. Jeison, D., Telkamp, P. & van Lier, J. B. Thermophilic sidestream anaerobic membrane bioreactors: the shear rate dilemma. *Water Environ. Res.* **81**, 2372–2380 (2009).

400. Lin, H. J. *et al.* Factors affecting sludge cake formation in a submerged anaerobic membrane bioreactor. *J. Memb. Sci.* **361**, 126–134 (2010).

401. Salazar-Peláez, M. L., Morgan-Sagastume, J. M. & Noyola, A. Influence of hydraulic retention time on fouling in a UASB coupled with an external ultrafiltration membrane treating synthetic municipal wastewater. *Desalination* **277**, 164–170 (2011).

402. Akram, A. & Stuckey, D. C. Flux and performance improvement in a submerged anaerobic membrane bioreactor (SAMBR) using powdered activated carbon (PAC). *Process Biochem.* **43**, 93–102 (2008).

403. Lin, H. J., Gao, W. J., Leung, K. T., Liao, B. Q. & Lin, H. J. Characteristics of different fractions of microbial flocs and their role in membrane fouling. *Water Sci. Technol.* **63**, 262–269 (2011).

404. Chung, Y. C., Jung, J. Y., Ahn, D. H. & Kim, D. H. Development of two phase anaerobic reactor with membrane separation system. *J. Environ. Sci. Heal. - Part A Toxic/Hazardous Subst. Environ. Eng.* **33**, 249–261 (1998).

405. Shen, X., Gao, B., Guo, K. & Yue, Q. Application of composite flocculants for removing organic matter and mitigating ultrafiltration membrane fouling in surface water treatment: the role of composite ratio. *Environ. Sci. Water Res. Technol.* **5**, 2242–2250 (2019).

406. Yang, Z., Hou, J. & Miao, L. Harvesting freshwater microalgae with natural polymer flocculants. *Algal Res.* **57**, 102358 (2021).

407. Koshani, R., Tavakolian, M. & Van De Ven, T. G. M. Cellulose-based dispersants and flocculants. *J. Mater. Chem. B* **8**, 10502–10526 (2020).

408. Sohn, W. *et al.* A review on membrane fouling control in anaerobic membrane bioreactors

by adding performance enhancers. *J. Water Process Eng.* **40**, 101867 (2021).

409. Cruz Viggi, C. *et al.* Magnetite particles triggering a faster and more robust syntrophic pathway of methanogenic propionate degradation. *Environ. Sci. Technol.* **48**, 7536–7543 (2014).

410. Li, J. *et al.* Biochar from microwave pyrolysis of biomass: A review. *Biomass and Bioenergy* **94**, 228–244 (2016).

411. Abbas, Y. *et al.* Recent advances in bio-based carbon materials for anaerobic digestion: A review. *Renew. Sustain. Energy Rev.* **135**, 110378 (2021).

412. Yun, S. *et al.* Use of bio-based carbon materials for improving biogas yield and digestate stability. *Energy* **164**, 898–909 (2018).

413. Chiappero, M. *et al.* Review of biochar role as additive in anaerobic digestion processes. *Renew. Sustain. Energy Rev.* **131**, 110037 (2020).

414. Ng, C. A. *et al.* Investigation on the performance of hybrid anaerobic membrane bioreactors for fouling control and biogas production in palm oil mill effluent treatment. *Water Sci. Technol.* **76**, 1389–1398 (2017).

415. Charfi, A., Aslam, M., Lesage, G., Heran, M. & Kim, J. Macroscopic approach to develop fouling model under GAC fluidization in anaerobic fluidized bed membrane bioreactor. *J. Ind. Eng. Chem.* **49**, 219–229 (2017).

416. Bani-Melhem, K. & Elektorowicz, M. Development of a novel submerged membrane electro-bioreactor (SMEBR): Performance for fouling reduction. *Environ. Sci. Technol.* **44**, 3298–3304 (2010).

417. Moussa, D. T., El-Naas, M. H., Nasser, M. & Al-Marri, M. J. A comprehensive review of electrocoagulation for water treatment: Potentials and challenges. *J. Environ. Manage.* **186**, 24–41 (2017).

418. Guo, P., Yan, N., Wang, L. & Zou, X. Database mining of zeolite structures. *Cryst. Growth Des.* **17**, 6821–6835 (2017).

419. Cheng, H., Li, Y., Kato, H. & Li, Y. Y. Enhancement of sustainable flux by optimizing filtration mode of a high-solid anaerobic membrane bioreactor during long-term continuous treatment of food waste. *Water Res.* **168**, 115195 (2020).

420. Peng, H. *et al.* Roles of magnetite and granular activated carbon in improvement of anaerobic sludge digestion. *Bioresour. Technol.* **249**, 666–672 (2018).

421. Song, X. *et al.* Enhanced electron transfer and methane production from low-strength wastewater using a new granular activated carbon modified with nano-Fe3O4. *Chem. Eng. J.* **374**, 1344–1352 (2019).

422. Baek, G., Kim, J., Cho, K., Bae, H. & Lee, C. The biostimulation of anaerobic digestion with (semi)conductive ferric oxides: their potential for enhanced biomethanation. *Appl. Microbiol. Biotechnol.* **99**, 10355–10366 (2015).

423. Wang, J., Liang, J., Sun, L. & Gao, S. PVA/CS and PVA/CS/Fe gel beads' synthesis mechanism and their performance in cultivating anaerobic granular sludge. *Chemosphere* **219**, 130–139 (2019).

424. Düppenbecker, B., Engelhart, M. & Cornel, P. Fouling mitigation in Anaerobic Membrane Bioreactor using fluidized glass beads: Evaluation fitness for purpose of ceramic membranes. *J. Memb. Sci.* **537**, 69–82 (2017).

425. Christian, S. *et al.* The First Two Years of Full-Scale Anaerobic Membrane Bioreactor (Anmbr) Operation Treating a High Strength Industrial Wastewater at Kens Foods Inc. *Proc. Water Environ. Fed.* **2010**, 4019–4033 (2012).

426. Judd, S. *MBR Book- EditionPrinciples and applications of membrane bioreactors in water and wastewater treatment.* (2006).

427. Judd, S. J. Membrane technology costs and me. *Water Res.* **122**, 1–9 (2017).

428. Martin, I., Pidou, M., Soares, A., Judd, S. & Jefferson, B. Modelling the energy demands of aerobic and anaerobic membrane bioreactors for wastewater treatment. **32**, 921–932 (2011).

429. Butcher, G. J. Experiences with anaerobic digestion of wheat starch processing waste. *Int. Biodeterior.* **25**, 71–77 (1989).

430. Herrera-Robledo, M., Cid-León, D. M., Morgan-Sagastume, J. M. & Noyola, A. Biofouling in an anaerobic membrane bioreactor treating municipal sewage. *Sep. Purif. Technol.* **81**, 49–55 (2011).

431. Robles, A., Ruano, M. V., Ribes, J. & Ferrer, J. Factors that affect the permeability of

commercial hollow-fibre membranes in a submerged anaerobic MBR (HF-SAnMBR) system. *Water Res.* **47**, 1277–1288 (2013).

432. Fetting Constaze. *The European Green Deal, ESDN Report, .* (2020).

433. Goliopoulos, N., Mamais, D., Noutsopoulos, C., Dimopoulou, A. & Kounadis, C. Energy Consumption and Carbon Footprint of Greek Wastewater Treatment Plants. *Water 2022, Vol. 14, Page 320* **14**, 320 (2022).

434. Theuerl, S. *et al.* The Future Agricultural Biogas Plant in Germany: A Vision. *Energies 2019, Vol. 12, Page 396* **12**, 396 (2019).

435. Jimenez, J. *et al.* Instrumentation and control of anaerobic digestion processes: a review and some research challenges. *Rev. Environ. Sci. Bio/Technology 2015 144* **14**, 615–648 (2015).

436. Batstone, D. J. Mathematical Modelling of Anaerobic Reactors Treating Domestic Wastewater: Rational Criteria for Model Use. *Rev. Environ. Sci. Bio/Technology 2006 51* **5**, 57–71 (2006).

437. Kleinstreuer, C. & Poweigha, T. Dynamic simulator for anaerobic digestion processes. *Biotechnol. Bioeng.* **24**, 1941–1951 (1982).

438. Weinrich, S. & Nelles, M. Systematic simplification of the Anaerobic Digestion Model No. 1 (ADM1) – Model development and stoichiometric analysis. *Bioresour. Technol.* **333**, 125124 (2021).

439. Mo, R., Guo, W., Batstone, D., Makinia, J. & Li, Y. Modifications to the anaerobic digestion model no. 1 (ADM1) for enhanced understanding and application of the anaerobic treatment processes – A comprehensive review. *Water Res.* **244**, 120504 (2023).

440. Mottet, A. *et al.* New fractionation for a better bioaccessibility description of particulate organic matter in a modified ADM1 model. *Chem. Eng. J.* **228**, 871–881 (2013).

441. Rajagopal, R., Massé, D. I. & Singh, G. A critical review on inhibition of anaerobic digestion process by excess ammonia. *Bioresour. Technol.* **143**, 632–641 (2013).

442. Zheng, Z. *et al.* The effects of C/N (10–25) on the relationship of substrates, metabolites, and microorganisms in "inhibited steady-state" of anaerobic digestion. *Water Res.* **188**,

116466 (2021).

443. Shang, Y., Johnson, B. R. & Sieger, R. Application of the IWA Anaerobic Digestion Model (ADM1) for simulating full-scale anaerobic sewage sludge digestion. *Water Sci. Technol.* **52**, 487–492 (2005).

444. Elmitwalli, T., Feng, Y., Behrendt, J. & Otterpohl, R. Anaerobic digestion potential for ecological and decentralised sanitation in urban areas. *Water Sci. Technol.* **53**, 45–54 (2006).

445. Derbal, K., Bencheikh-lehocine, M., Cecchi, F., Meniai, A. H. & Pavan, P. Application of the IWA ADM1 model to simulate anaerobic co-digestion of organic waste with waste activated sludge in mesophilic condition. *Bioresour. Technol.* **100**, 1539–1543 (2009).

446. Lohani, S. P. *et al.* ADM1 modeling of UASB treating domestic wastewater in Nepal. *Renew. Energy* **95**, 263–268 (2016).

447. Ozgun, H. Anaerobic Digestion Model No. 1 (ADM1) for mathematical modeling of full-scale sludge digester performance in a municipal wastewater treatment plant. *Biodegradation* **30**, 27–36 (2019).

448. Baquerizo, G., Fiat, J., Buffiere, P., Girault, R. & Gillot, S. Modelling the dynamic long-term performance of a full-scale digester treating sludge from an urban WRRF using an extended version of ADM1. *Chem. Eng. J.* **423**, 128870 (2021).

449. Normak, A. *et al.* Improving ADM1 model to simulate anaerobic digestion start-up with inhibition phase based on cattle slurry. *Biomass and Bioenergy* **80**, 260–266 (2015).

450. Pandey, P. K., Ndegwa, P. M., Alldredge, J. R., Pitts, M. & Soupir, M. L. Modeling effects of granules on the start-up of anaerobic digestion of dairy wastewater with Langmuir and extended Freundlich equations. *Bioprocess Biosyst. Eng.* **33**, 833–845 (2010).

451. Zhao, B. H. *et al.* Dynamic modeling the anaerobic reactor startup process. *Ind. Eng. Chem. Res.* **49**, 7193–7200 (2010).

452. Jabłoński, S. J. & Łukaszewicz, M. Mathematical modelling of methanogenic reactor start-up: Importance of volatile fatty acids degrading population. *Bioresour. Technol.* **174**, 74–80 (2014).

453. Shi, E., Li, J., Leu, S. Y. & Antwi, P. Modeling the dynamic volatile fatty acids profiles with

pH and hydraulic retention time in an anaerobic baffled reactor during the startup period. *Bioresour. Technol.* **222**, 49–58 (2016).

454. Guellout, Z., Clion, V., Benguerba, Y., Dumas, C. & Ernst, B. Study of the dark fermentative hydrogen production using modified ADM1 models. *Biochem. Eng. J.* **132**, 9–19 (2018).

455. Oliveros-Muñoz, J. M. *et al.* Luus-Jaakola method and ADM1 based optimization of hydrogen sulfide in anaerobic digestion of cow manure. *Biochem. Eng. J.* **171**, 108012 (2021).

456. Pianosi, F. *et al.* Sensitivity analysis of environmental models: A systematic review with practical workflow. *Environ. Model. Softw.* **79**, 214–232 (2016).

457. Saltelli, A., Tarantola, S. & Chan, K. P. S. A quantitative model-independent method for global sensitivity analysis of model output. *Technometrics* **41**, 39–56 (1999).

458. Devenish, B. J., Francis, P. N., Johnson, B. T., Sparks, R. S. J. & Thomson, D. J. Sensitivity analysis of dispersion modeling of volcanic ash from Eyjafjallajökull in May 2010. *J. Geophys. Res. Atmos.* **117**, 0–21 (2012).

459. Paton, F. L., Maier, H. R. & Dandy, G. C. Relative magnitudes of sources of uncertainty in assessing climate change impacts on water supply security for the southern Adelaide water supply system. *Water Resour. Res.* **49**, 1643–1667 (2013).

460. Sieber, A. & Uhlenbrook, S. Sensitivity analyses of a distributed catchment model to verify the model structure. *J. Hydrol.* **310**, 216–235 (2005).

461. Harper, E. B., Stella, J. C. & Fremier, A. K. Global sensitivity analysis for complex ecological models: a case study of riparian cottonwood population dynamics. *Ecol. Appl.* **21**, 1225–1240 (2011).

462. Nossent, J., Elsen, P. & Bauwens, W. Sobol' sensitivity analysis of a complex environmental model. *Environ. Model. & Softw.* **26**, 1515–1525 (2011).

463. Kelleher, C. *et al.* Identifiability of transient storage model parameters along a mountain stream. doi:10.1002/wrcr.20413

464. Butler, M. P., Reed, P. M., Fisher-Vanden, K., Keller, K. & Wagener, T. Identifying parametric controls and dependencies in integrated assessment models using global

sensitivity analysis. *Environ. Model. Softw.* **59**, 10–29 (2014).

465. Hamm, N. A. S., Hall, J. W. & Anderson, M. G. Variance-based sensitivity analysis of the probability of hydrologically induced slope instability. *Comput. Geosci.* **32**, 803–817 (2006).

466. Pastres, R., Chan, K., Solidoro, C. & Dejak, C. Global sensitivity analysis of a shallow-water 3D eutrophication model. *CoPhC* **117**, 62–74 (1999).

467. Nguyen, T. G. & de Kok, J. L. Systematic testing of an integrated systems model for coastal zone management using sensitivity and uncertainty analyses. *Environ. Model. Softw.* **22**, 1572–1587 (2007).

468. Singh, R., Wagener, T., Crane, R., Mann, M. E. & Ning, L. A vulnerability driven approach to identify adverse climate and land use change combinations for critical hydrologic indicator thresholds: Application to a watershed in Pennsylvania, USA. *Water Resour. Res.* **50**, 3409–3427 (2014).

469. Anderson, B., Borgonovo, E., Galeotti, M. & Roson, R. Uncertainty in climate change modeling: can global sensitivity analysis be of help? *Risk Anal.* **34**, 271–293 (2014).

470. Howard, R. A. Decision analysis: practice and promise. *Manage. Sci.* **34**, 679–695 (1988).

471. Powell, S. G. & Baker, K. R. Management science : the art of modeling with spreadsheets. 519

472. Beven, K., Beven & Keith. Prophecy, reality and uncertainty in distributed hydrological modelling. *AdWR* **16**, 41–51 (1993).

473. Kleijnen, J. P. C. & Helton, J. C. Statistical analyses of scatterplots to identify important factors in large-scale simulations, 1: Review and comparison of techniques. *Reliab. Eng. Syst. Saf.* **65**, 147–185 (1999).

474. Saltelli, A. & Marivoet, J. Non-Parametric Statistics in Sensitivity Analysis for Model Output. A Comparison of Selected Techniques. *Reliab. Eng. Syst. Saf.* **28**, 229–253 (1990).

475. Freer, J., Beven, K. J. & Ambroise, B. Bayesian estimation of uncertainty in runoff prediction and the value of data : an application of the GLUE approach. (1996).

476. Werkhoven, K. van, Wagener, T., Reed, P. & Tang, Y. Sensitivity-guided reduction of parametric dimensionality for multi-objective calibration of watershed models. *Adv. Water Resour.* **32**, 1154–1169 (2009).

477. Spear, R. C. *et al.* Parameter uncertainty and interaction in complex environmental models. *WRR* **30**, 3159–3169 (1994).

478. Baroni, G. & Tarantola, S. A General Probabilistic Framework for uncertainty and global sensitivity analysis of deterministic models: A hydrological case study. *Environ. Model. Softw.* **51**, 26–34 (2014).

479. Helton, J. C. Uncertainty and sensitivity analysis techniques for use in performance assessment for radioactive waste disposal. *Reliab. Eng. Syst. Safety; (United Kingdom)* **42:2**–**3**, 327–367 (1993).

480. Borgonovo, E. A new uncertainty importance measure. *Reliab. Eng. Syst. Saf.* **92**, 771–784 (2007).

481. Morris, M. D. Factorial Sampling Plans for Preliminary Computational Experiments. *Technometrics* **33**, 161–174 (1991).

482. Campolongo, F. & Saltelli, A. Sensitivity analysis of an environmental model: an application of different analysis methods. *Reliab. Eng. & Syst. Saf.* **57**, 49–69 (1997).

483. Sobol', I. M. & Kucherenko, S. Derivative based global sensitivity measures and their link with global sensitivity indices. *Math. Comput. Simul.* **79**, 3009–3017 (2009).

484. Rakovec, O. *et al.* Distributed Evaluation of Local Sensitivity Analysis (DELSA), with application to hydrologic models. *Water Resour. Res.* **50**, 409–426 (2014).

485. Iman, R. L. & Helton, J. C. Investigation of uncertainty and sensitivity analysis techniques for computer models. *Risk Anal.; (United States)* **8:1**, 71–90 (1988).

486. Minunno, F., van Oijen, M., Cameron, D. R. & Pereira, J. S. Selecting parameters for bayesian calibration of a process-based model: A methodology based on canonical correlation analysis. *SIAM-ASA J. Uncertain. Quantif.* **1**, 370–385 (2013).

487. Spear, R. C., Hornberger, G. M., Spear, R. C. & Hornberger, G. M. Eutrophication in peel inlet-II. Identification of critical uncertainties via generalized sensitivity analysis. *WatRe*

14, 43–49 (1980).

488. Norton, J. An introduction to sensitivity assessment of simulation models. *Environ. Model. Softw.* **69**, 166–174 (2015).

489. Wagener, T. *et al.* A framework for development and application of hydrological models. *Hydrol. Earth Syst. Sci.* **5**, 13–26 (2001).

490. Tang, Y., Reed, P., Wagener, T. & Van Werkhoven, K. Comparing sensitivity analysis methods to advance lumped watershed model identification and evaluation. *Hydrol. Earth Syst. Sci.* **11**, 793–817 (2007).

491. Saltelli, A. & D'Hombres, B. Sensitivity analysis didn't help. A practitioner's critique of the Stern review. *Glob. Environ. Chang.* **20**, 298–302 (2010).

492. Kucherenko, S., Tarantola, S. & Annoni, P. Estimation of global sensitivity indices for models with dependent variables. *Comput. Phys. Commun.* **183**, 937–946 (2012).

493. Cukier, R. I., Fortuin, C. M., Shuler, K. E., Petschek, A. G. & Schaibly, J. H. Study of the sensitivity of coupled reaction systems to uncertainties in rate coefficients. I Theory. *J. Chem. Phys.* **59**, 3873–3878 (1973).

494. Oakley, J. E. & O'Hagan, A. Probabilistic sensitivity analysis of complex models: a Bayesian approach. *J. R. Stat. Soc. Ser. B* **66**, 751–769 (2004).

495. Wang, J., Li, X., Lu, L. & Fang, F. Parameter sensitivity analysis of crop growth models based on the extended Fourier Amplitude Sensitivity Test method. *Environ. Model. Softw.* **48**, 171–182 (2013).

496. Kolb, B. & Ettre, L. S. Static headspace-gas chromatography : theory and practice. 349 (2006).

497. Gossett, J. M. Measurement of Henry's Law Constants for C1 and C2 Chlorinated Hydrocarbons. *Environ. Sci. Technol.* **21**, 202–208 (1987).

498. Samaras, V. G., Thomaidis, N. S., Stasinakis, A. S. & Lekkas, T. D. An analytical method for the simultaneous trace determination of acidic pharmaceuticals and phenolic endocrine disrupting chemicals in wastewater and sewage sludge by gas chromatography-mass spectrometry. *Anal. Bioanal. Chem.* **399**, 2549–2561 (2011).

499. Luo, Z., Chen, H., Wu, S., Yang, C. & Cheng, J. Enhanced removal of bisphenol A from aqueous solution by aluminum-based MOF/sodium alginate-chitosan composite beads. *Chemosphere* **237**, 124493 (2019).

500. Mahmad, A. *et al.* Response surface methodology and artificial neural network for prediction and validation of bisphenol a adsorption onto zeolite imidazole framework. *Groundw. Sustain. Dev.* **21**, 100925 (2023).

501. Müller, S. & Schlatter, C. Oestrogenic potency of nonylphenol in vivo - A case study to evaluate the relevance of human non-occupational exposure. *Pure Appl. Chem.* **70**, 1847–1853 (1998).

502. Crini, G. *et al.* Advanced Treatments for the Removal of Alkylphenols and Alkylphenol Polyethoxylates from Wastewater. *Environ. Chem. a Sustain. World* **2**, 305–398 (2021).

503. PubChem. Available at: https://pubchem.ncbi.nlm.nih.gov/. (Accessed: 13th March 2023)

504. Petrie, B., Barden, R. & Kasprzyk-Hordern, B. A review on emerging contaminants in wastewaters and the environment: Current knowledge, understudied areas and recommendations for future monitoring. *Water Res.* **72**, 3–27 (2015).

505. Madikizela, L. M. & Ncube, S. Occurrence and ecotoxicological risk assessment of non-steroidal anti-inflammatory drugs in South African aquatic environment: What is known and the missing information? *Chemosphere* **280**, 130688 (2021).

506. Copp, J. B., Jeppsson, U. & Rosen, C. TOWARDS AN ASM1 – ADM1 STATE VARIABLE INTERFACE FOR PLANT-WIDE WASTEWATER TREATMENT MODELING. *Proc. Water Environ. Fed.* 498–510 doi:10.2175/193864703784641207

507. Campolongo, F., Cariboni, J. & Saltelli, A. An effective screening design for sensitivity analysis of large models. *Environ. Model. Softw.* **22**, 1509–1518 (2007).

508. Mamimin, C., Prasertsan, P., Kongjan, P. & O-Thong, S. Effects of volatile fatty acids in biohydrogen effluent on biohythane production from palm oil mill effluent under thermophilic condition. *Electron. J. Biotechnol.* **29**, 78–85 (2017).

509. Morgan-Sagastume, F. *et al.* Production of volatile fatty acids by fermentation of waste activated sludge pre-treated in full-scale thermal hydrolysis plants. *Bioresour. Technol.* **102**, 3089–3097 (2011).

510. Wang, Q., Kuninobu, M., Ogawa, H. I. & Kato, Y. Degradation of volatile fatty acids in highly efficient anaerobic digestion. *Biomass and Bioenergy* **16**, 407–416 (1999).

511. Raskin, L., Stromley, J. M., Rittmann, B. E. & Stahl, D. A. Group-specific 16S rRNA hybridization probes to describe natural communities of methanogens. *Appl. Environ. Microbiol.* **60**, 1232 (1994).

512. Strasser, H., Brunner, H. & Schinner, F. Leaching of iron and toxic heavy metals from anaerobically-digested sewage sludge. *J. Ind. Microbiol.* **14**, 281–287 (1995).

513. Sotero-Santos, R. B., Rocha, O. & Povinelli, J. Toxicity of ferric chloride sludge to aquatic organisms. *Chemosphere* **68**, 628–636 (2007).

514. Smith, A. L. *et al.* Navigating wastewater energy recovery strategies: a life cycle comparison of anaerobic membrane bioreactor and conventional treatment systems with anaerobic digestion. *Environ. Sci. Technol.* **48**, 5972–5981 (2014).

515. Malamis, S., Andreadakis, A., Mamais, D. & Noutsopoulos, C. Comparison of alternative additives used for the mitigation of membrane fouling in membrane bioreactors. **52**, 5740–5747 (2014).

516. Hawash, H. B. *et al.* Occurrence and spatial distribution of pharmaceuticals and personal care products (PPCPs) in the aquatic environment, their characteristics, and adopted legislations. *J. Water Process Eng.* **52**, 103490 (2023).

517. Lim, M., Patureau, D., Heran, M., Lesage, G. & Kim, J. Removal of organic micropollutants in anaerobic membrane bioreactors in wastewater treatment: critical review. *Environ. Sci. Water Res. Technol.* **6**, 1230–1243 (2020).

518. Azizi, D. *et al.* A comprehensive review on current technologies for removal of endocrine disrupting chemicals from wastewaters. *Environ. Res.* **207**, 112196 (2022).

519. Wijekoon, K. C. *et al.* The fate of pharmaceuticals, steroid hormones, phytoestrogens, UV-filters and pesticides during MBR treatment. *Bioresour. Technol.* **144**, 247–254 (2013).

520. Wijekoon, K. C. *et al.* Development of a predictive framework to assess the removal of trace organic chemicals by anaerobic membrane bioreactor. *Bioresour. Technol.* **189**, 391–398 (2015).

521. Behera, S. K., Kim, H. W., Oh, J. E. & Park, H. S. Occurrence and removal of antibiotics, hormones and several other pharmaceuticals in wastewater treatment plants of the largest industrial city of Korea. *Sci. Total Environ.* **409**, 4351–4360 (2011).

522. Kim, J. Y. *et al.* Degradation of bisphenol A and nonylphenol by nitrifying activated sludge. *Process Biochem.* **42**, 1470–1474 (2007).

523. Tadkaew, N., Hai, F. I., McDonald, J. A., Khan, S. J. & Nghiem, L. D. Removal of trace organics by MBR treatment: The role of molecular properties. *Water Res.* **45**, 2439–2451 (2011).

524. Gurung, K., Ncibi, M. C. & Sillanpää, M. Assessing membrane fouling and the performance of pilot-scale membrane bioreactor (MBR) to treat real municipal wastewater during winter season in Nordic regions. *Sci. Total Environ.* **579**, 1289–1297 (2017).

525. Zielińska, M. & Ojo, A. Anaerobic Membrane Bioreactors (AnMBRs) for Wastewater Treatment: Recovery of Nutrients and Energy, and Management of Fouling. *Energies 2023, Vol. 16, Page 2829* **16**, 2829 (2023).

526. Pfluger, A. *et al.* Energy-generating potential of anaerobically enhanced primary treatment of domestic wastewater using multiple-compartment bioreactors. *Environ. Sci. Water Res. Technol.* **6**, 117–131 (2019).

527. Jiménez-Benítez, A. *et al.* Life cycle costing of AnMBR technology for urban wastewater treatment: A case study based on a demo-scale AnMBR system. *J. Environ. Chem. Eng.* **11**, 110267 (2023).

528. Campolongo, F. *et al.* Sensitivity Anaysis as an Ingredient of Modeling. *Stat. Sci.* **15**, 377–395 (2000).

529. Cosenza, A., Bella, G. Di, Mannina, G., Torregrossa, M. & Viviani, G. Biological Nutrient Removal and Fouling Phenomena in a University of Cape Town Membrane Bioreactor Treating High Nitrogen Loads. *J. Environ. Eng.* **139**, 773–780 (2013).

530. Sarrazin, F., Pianosi, F. & Wagener, T. Global Sensitivity Analysis of environmental models: Convergence and validation. *Environ. Model. Softw.* **79**, 135–152 (2016).

531. Ruano, M. V., Ribes, J., Seco, A. & Ferrer, J. An improved sampling strategy based on trajectory design for application of the Morris method to systems with many input factors.

Environ. Model. Softw. **37**, 103–109 (2012).